GEOLOGICA ULTRAIECTINA

Mededelingen van de
Faculteit Aardwetenschappen
Universiteit Utrecht

No. 237

Structural evolution of the Marble Bar Domain, Pilbara granite-greenstone terrain, Australia: the role of Archaean mid-crustal detachments

Armelle Kloppenburg

Promotor:

Prof. Dr S.H. White
Faculteit Aardwetenschappen
Universiteit Utrecht, The Netherlands

Co-promotor:

Dr J.R. Wijbrans
Afdeling Isotopen Geochemie
Vrije Universiteit Amsterdam, The Netherlands

Members of the dissertation committee:

Prof. P. Dirks
University of the Witwatersrand
South Africa

Dr. K.A.A. Hein
Faculteit Geowetenschappen
Universiteit Utrecht, The Netherlands

Prof. H.N.A. Priem
Van Breestraat 64
1071 ZR Amsterdam, The Netherlands

Prof. R.L.M. Vissers
Faculteit Geowetenschappen
Universiteit Utrecht, The Netherlands

Prof. M. de Wit
Department of Geological Sciences
University of Cape Town, South Africa

Cover illustration: Archaean pillow basalts at Marble Bar Pool, Western Australia

ISBN: 90-5744-096-2

Structural evolution of the Marble Bar Domain, Pilbara granite-greenstone terrain, Australia: *the role of Archaean mid-crustal detachments*

Structurele evolutie van het Marble Bar Domein, Pilbara graniet-groensteen terrein, Australië: *de rol van Archaeische décollements in de middenkorst*

(met een samenvatting in het nederlands)

proefschrift

Ter verkrijging van de graad van doctor aan de Universiteit Utrecht
Op gezag van de Rector Magnificus Prof Dr W.H. Gispen
Ingevolge het besluit van het College voor Promoties in het openbaar te verdedigen op

3 November 2003, 10:30

door

Armelle Kloppenburg

Geboren op 23 april 1970 te 's-Gravenhage

Aan mijn ouders
en Rob, natuurlijk..

Contents

Samenvatting voor niet-geologen in het nederlands 7

Abstract 10

Chapter 1
Introduction 13

Chapter 2
Structural evolution of the Warrawoona Greenstone Belt and adjoining granitoid complexes, Pilbara Craton, Australia: implications for Archaean tectonic regimes 35

Chapter 3
Structural history and SHRIMP U–Pb zircon chronology of an Archaean mid-crustal detachment, Pilbara Craton, Australia 79

Chapter 4
The Mid Archaean 'Salgash Dyke Swarm': implications for tectonismduring its emplacement 127

Chapter 5
^{40}Ar-^{39}Ar chronology constraints for the structural development of the eastern Pilbara granite-greenstone terrain, Australia 159

Chapter 6
Synthesis, discussion and conclusions 191

Appendix 1
Analytical procedures and conditions using SHRIMP 211

Appendix 2
Common-lead corrected data from SHRIMP analysis 213

Appendix 3
Processed ^{40}Ar-^{39}Ar incremental heating data 221

References 233

Acknowledgements / Dankbetuiging 251

Curriculum Vitae 255

Samenvatting voor niet-geologen in het nederlands

De Aarde is ongeveer 4600 miljoen jaar oud. De meeste gesteenten die de aardkorst vormen zijn echter veel jonger, omdat de korst continue gerecycled wordt. Recycling gebeurt als onderdeel van het proces 'plaattectoniek', het bewegen van de continenten ten opzichte van elkaar.

Plaattectoniek zorgt ervoor dat vandaag de dag gesteente wordt gevormd, onder andere bij het uit elkaar trekken van de continentale platen en het vormen van oceanische korst, zoals dit gebeurt langs de Mid Atlantische Rug. Een deel daarvan ligt boven water bij IJsland. Ook worden gesteenten gevormd bij het botsen van continenten, in bijvoorbeeld de Alpen en de Andes. Het is de vraag of de vroege gesteentevormende processen vergelijkbaar waren met die van nu, omdat de aarde mogelijk warmer was in het vroege begin van haar bestaan.

Het onderzoeksgebied van deze studie, het Pilbara graniet-groensteen terrein in noordwest Australië, is één van de grootste bewaard gebleven oude stukken aardkorst. De Pilbara bevat voornamelijk granitische en vulkanische gesteenten van tussen de 2800 en 3600 miljoen jaar oud, ontstaan in tijdvak 'het Archaeicum'. De Pilbara is sinds 2800 miljoen jaar geleden haast onveranderd bewaard gebleven, afgezien van wat erosie, en geeft dus een unieke kans om te bestuderen hoe dit gebied destijds gevormd is.

Tijdens deze studie is met behulp van veldwerk in de Pilbara onderzocht of de gesteenten en de geologische geschiedenis van dit gebied vergelijkbaar zijn met die van jongere gebieden op aarde, ofwel: is deze archaeische korst gevormd door plaattectoniek of door een typisch archaeisch proces? Er is een archaeisch proces bedacht waarbij, in tegenstelling tot horizontale bewegingen, vertikale verplaatsingen in de korst ontstaan door een verschil in gewicht. Bij dit proces bewegen lichtere gesteenten omhoog en zakken zwaardere gesteenten en vormen daarbij breukzones tussen de twee. Dit proces wordt 'diapirisme' genoemd. Het gebied dat centraal staat in deze discussie is het Marble Bar Domein, met de relatief zware voornamelijk vulkanische gesteenten van de Warrawoona groensteen gordel en de naastgelegen lichtere granieten en gneissen van de Mount Edgar en Corunna Downs graniet complexen. Vooral de gneissen kwamen van diep in de korst, en deze zijn naast de vulkanische gesteenten komen te liggen door beweging langs breukzones. Om te achterhalen wat de drijvende kracht hiervoor is geweest is een reconstructie van de geschiedenis noodzakelijk. Hiervoor is gedetailleerde kennis nodig van de verschillende gesteenten in dit gebied en van het gedrag van de breukzones. Ook bij

plaattectonische processen kunnen vertikale bewegingen in de korst voorkomen, echter deze vertikale bewegingen zijn een gevolg van de horizontale bewegingen. De vraag voor dit gebied is nu: zijn de vertikale bewegingen het gevolg van de breukvorming of andersom?

Behalve voor het beantwoorden van deze puur wetenschappelijke vraag helpt kennis van de vorming en ontwikkeling van de Archaeïsche gebieden bij de exploratie van metalen zoals goud. Archaeïsche gebieden staan bekend om hun goud en ook diamant voorkomens in breukzones.

Tijdens het veldwerk zijn, naast het in kaart brengen van verschillende soorten gesteenten en de relatie met kilometers lange breukzones, ook monsters genomen om de ouderdom te kunnen bepalen, van de gesteente zelf, maar ook van de breukzones waaraan het monster is gerelateerd. De ouderdommen zijn bepaald in het laboratorium op basis van halfwaardetijden van radioactieve elementen. Twee soorten ouderdommen zijn bepaald. Enerzijds zijn kristallisatie-ouderdommen van granietachtige stenen bepaald door het meten van onder andere uranium- en loodisotopen in zirkoon kristallen. Dit is gedaan met behulp van de Scanning High Resolution Ion Microprobe (SHRIMP) in Perth, Australië. Anderzijds zijn afkoelingsouderdommen bepaald, door het meten van onder andere argon isotopen in het gas dat vrijkomt bij het verhitten van bepaalde mineralen met behulp van de VULKAAN laser probe op de Vrije Universiteit in Amsterdam. Beide dateringstechnieken kunnen worden gebruikt om activiteit van breukzones te dateren.

Het resultaat van dit onderzoek heeft geleid tot inzicht in het type en de tijdsduur van verschillende gesteentevormende processen gedurende ontwikkeling van de Pilbariaanse korst.

Er zijn vier belangrijke bevindingen gedaan.

Allereerst zijn er deformatie-strukturen geïdentificeerd, die bewijs leveren voor vijf deformatie fasen gedurende 700 miljoen jaar. De structuren en de deformatie geschiedenis, vooral in de grotere regionale context, geven aan dat de drijvende kracht - voor de stapeling alswel voor het uit elkaar trekken van de korst - het werk is van grootschalige drijvende krachten, en dat het lokaal diapirisme van de granieten een secundair fenomeen is. Diapirisme is één van de gevolgen van regionale deformatie, en niet de oorzaak van alle deformatie.

De belangrijkste deformatie fase was gedurende 3.47 tot 3.42 miljard jaar geleden (Ga). Deze fase heeft onder andere geleid tot het vormen van de Mount Edgar Shear Zone, een steilstaande 70 km lange, 2 tot 5 km brede breukzone. Deze is oorspronkelijk gevormd op circa 15 km diepte, maar ligt nu aan de oppervlakte. Deze breukzone is vaak geïnfiltreerd geweest door vloeibaar gesteente, de resten van dit gesteente zijn te vinden als dunne lensen. Deze lensen op hun beurt hebben ervoor gezorgd dat de zone zwak bleef en dat deformatie hierin localiseerde. De Mount Edgar Shear Zone is ten minste vijf keer actief geweest. De oudst herkenbare activiteit was gerelateerd aan een fase waarin de korst uit elkaar werd getrokken en de Mount Edgar Shear Zone als een subhorizontale breukzone ontwikkelde terwijl het geïntrudeerd werd door vloeibaar

magmatische gesteente.

Een tweede belangrijke deformatie fase gebeurde circa 100 miljoen jaar later, rond 3.32-3.31 miljard jaar geleden. Gedurende deze fase werd wederom de Mount Edgar Shear Zone geïntrudeerd door vloeibare granitische gesteenten. Deze tweede fase resulteerde zowel in opstapeling van aardlagen en steilstelling van de Mount Edgar Shear Zone. Deze steilstelling wordt toegeschreven aan de stapeling van de korst welke zou kunnen hebben geresulteerd in het opwarmen, gedeeltelijk opsmelten, instabiliteit en extensie van de korst. Deze opwarming en extensie van de korst zou ook veroorzaakt kunnen zijn door een 'mantle plume', een grootschalige magmapijp onder de korst. Een mantle plume echter, kan niet makkelijk een stapeling van de korst verklaren.

De derde en vierde deformatiefase gingen gepaard met respectivelijk NE-SW en ENE-WSW gericht samendrukken van de korst, welke voornamelijk resulteerde in semi-brosse structuren en kleine breuken. In het studiegebied was geen vulkanische activiteit tijdens deze fasen waardoor ze moeilijk te dateren zijn. Vergelijkbare structuren met die van de vierde deformatiefase zijn net buiten het studiegebied gedateerd op 2.93 – 2.91 miljard jaar geleden.

Geconcludeerd is dat - op basis van de geobserveerde deformatiestructuren en de herleide geologische geschiedenis van dit gebied - de deformatie een regionale oorzaak heeft, en niet door diapirisme is veroorzaakt. Een regionale oorzaak voor deformatie zou door een proces kunnen zijn dat niet veel anders is dan het hedendaagse proces van plaattectoniek.

Abstract

The eastern Pilbara granite-greenstone terrain in Western Australia contains rocks that are largely Early to Mid Archaean in age, from ca 3.6 to 2.9 Ga. The area has been stable since 2.77 Ga and as such provides an opportunity to study the tectonic processes that were involved in the earliest part of the Earth's development. The specific aim of this study was to determine the relationship between horizontal and vertical tectonics during the development of the Early to Mid Archaean structural architecture of the Marble Bar Domain in the eastern Pilbara granite-greenstone terrain, by identifying the main structures, and understanding the deformation history and the role of associated magmatism.

Lithological and structural mapping and analysis focussed on the Warrawoona Greenstone Belt, the adjacent Mt Edgar Granitoid Complex and selected parts of the surrounding greenstone belts, which is an area that has been central in the discussion on Archaean tectonics. Time constraints for magmatic, tectonic and metamorphic events were obtained from geochronological study that involved SHRIMP U-Pb zircon chronology and ^{40}Ar-^{39}Ar Ar isotope chronology (VULKAAN laser-probe).

It was found that the main deformation structures in the Mt Edgar Granitoid Complex and selected parts of the surrounding greenstone belts include: i) the Mt Edgar Shear Zone, an originally mid-crustal detachment, now a 2-5 km wide, steeply dipping shear zone complex, mainly preserved along a ~70 km long outcrop on the SW half margin of the Mt Edgar Granitoid Complex; ii) the Beaton Well Zone, which acted as a transfer zone to the Mt Edgar Shear Zone within high-grade gneisses of the Mt Edgar Granitoid Complex; iii) the Central Warrawoona Shear Zone with a complex deformation history, located along the central axis of the Warrawoona Greenstone Belt; iv) the Brockman Hay and Fieldings Find Shear Zones that dominantly show W-vergent thrusting, and v) regional foliations, crenulations and minor thrusts that indicate (N)NE-(S)SW compression.

The mid-crustal Mt Edgar Shear Zone has recorded a complex structural history. The centre of this zone displays an intricate relationship between shear localisation and intrusions ranging from ultramafic to mafic to felsic. Most significant is the uni-directional pattern of well developed stretching lineations in combination with kinematics that show initial layer parallel extension followed by dominantly NE-tectonic transport. Structures and kinematics of the Mt Edgar Shear Zone indicated that if diapirism played a role in the development of the domes it was a minor one.

The Mt Edgar Shear Zone was found to have been active during five deformation phases (D_{X+1} to D_{X+5}), but most of its development was associated with extension and magmatic intrusions dated at 3.47-3.42 Ga (D_{X+1}) and 3315-3309 Ma (D_{X+2E}) by determining the crystallization age of syn- and post-tectonic granitoids, using SHRIMP U-Pb zircon chronology.

The period preceding the 3.32-3.31 Ga granitoid genesis and doming of the Mt Edgar Granitoid Complex involved regional (N)NE-(S)SW extension and intrusion of multiple mafic to

ultramafic dyke suites. ^{40}Ar-^{39}Ar isotope chronology on hornblende from two upper crustal dykes in the Kelly Greenstone Belt yielded minimum ages of 3440 ± 58 Ma and 3356 ± 21 Ma: they potentially form the oldest dyke swarm yet recorded on Earth and are associated with deposition of the Salgash Subgroup. The original orientation and the timing of the dykes indicate that they were emplaced during regional (N)NE-(S)SW extension, around the time that the Mt Edgar Shear Zone was active as a mid-crustal extensional detachment. This was followed by regional E-W compression, possibly as part of a prolonged deformation period from 3.34 to 3.20 Ga (D_{X+2C}).

The period following the 3.32-3.31 Ga granitoid genesis and doming of the Mt Edgar Granitoid Complex involved a phase of (N)NE-(S)SW compression and (N)NE-vergent thrusting (D_{X+3}) that caused regional brittle-ductile fracture cleavages, crenulation cleavages and local thrusts. This phase post-dates 3.32-3.31 Ga granitoid intrusions, but the absolute age is not clear (see chapters 2 and 5).

Pre-2.77 Ga dextral transcurrent shearing, largely localised on the Central Warrawoona Shear Zone which is situated along the axis of the Warrawoona Belt (D_{X+4}), is attributed to a phase of regional WNW-ESE compression at 2.95-2.93 Ga.

The Mt Edgar Shear Zone shows similar structures and kinematics compared to the Split Rock Shear Zone, a detachment zone along the adjacent granitoid complex to the west, identified by Zegers (1996). Both may be remnants of an Early Archaean detachment system that was widespread within the mid-crust of the eastern Pilbara.

The relationship between horizontal and vertical tectonics in the development of the Marble Bar Domain as seen from the structures and kinematics of regionally recognised mid-crustal detachments, such as the Mt Edgar Shear Zone and the Split Rock Shear Zone, and the tectonomagmatic history of the Mt Edgar Granitoid Complex and adjoining greenstone belts, indicate that doming was the consequence of horizontal deformation involving extension and compression. That is, the doming is a consequence of regional deformation, not the cause. Solid-state diapirism only played a minor role in the development of the Mt Edgar Granitoid Complex.

Mid-crustal detachments such as the Mt Edgar Shear Zone and the Split Rock Shear Zone played a central role in doming of the granitoid complexes. Intrusive sheets of ultramafic, mafic and felsic rocks exploited the mid-crustal Mt Edgar Shear Zone, facilitated deformation and may have enhanced doming, possibly by inflating the structure and by heating and weakening the crust.

Ages obtained from ^{40}Ar-^{39}Ar isotope chronology method on hornblende, muscovite and biotite from intrusive and extrusive rocks, some of which are sheared and/or metamorphosed, ranged from 3.44 to 2.8 Ga. Some ages show that part of the upper crustal sequence, namely the volcanic units of the Kelly Greenstone Belt, has remained at upper crustal levels throughout the history of the area, whereas others, namely the Mt Edgar Shear Zone, may not have reached upper-crustal levels until 3.32 Ga. Additionally, the obtained range in ^{40}Ar-^{39}Ar ages in the Marble Bar Domain suggests strongly that the area has not been subjected to a regional thermal resetting event in the Late Archaean and subsequent eras.

For the eastern Pilbara granite-greenstone terrain, the role of magmatic thickening of the crust and possibly 'vertical tectonics' is considered to have been the main probable mechanism for the

formation of the Early Archaean mafic crust and the first main Tonalite-Trondhjemite-Granodiorite suites at 3.46 Ga, possibly by a combination of mantle plumes and lower crustal delamination. From the development of the upper Salgash Subgroup onwards, the structural history of the Marble Bar Domain provides indications for 'horizontal tectonics', with the first regional compressional phase between 3.34 Ga and 3.20 Ga, indicating regionally imposed stresses, suggesting some form of plate-interaction.

Chapter 1

Introduction

1.1 Preamble

Since the development and the acceptance of the plate-tectonic hypothesis, the question has been raised as to whether plate tectonics has operated throughout Earth's history, particularly in the earliest part of Earth's history, the Archaean, i.e. from 4000 to 2500 Ma (see for discussions: Condie, 1981; Kröner, 1981; Windley, 1984; Nisbet, 1987; Condie, 1994; De Wit and Ashwal, 1997). It is generally accepted that the internal heat production of the Earth in the Archaean was higher than today (O'Nions et al., 1978; Richter, 1984; Jackson and Pollack, 1984; Davies, 1993). However, the temperature profile of the Earth, the mechanisms by which the Earth dissipated heat, the rate of crustal growth, and the ways of recycling of crustal materials remain as subjects of discussion (e.g. Taylor and McLennan, 1995; Condie, 2000). As is further discussed below, theoretical thermal models that are based on the rheological behaviour of the mantle as a function of its assumed temperature predict that plate tectonics, as we know it, cannot operate in an Earth with a hotter mantle (Vlaar, 1986; Hoffman and Ranalli, 1988; Davies, 1992; Vlaar et al, 1994). In contrast, geochemical crustal growth models indicate that some form of recycling has occurred from the Early Archaean onwards (for a discussion see: Taylor and McLennan, 1995; Vervoort et al., 1996; De Wit and Ashwal, 1997; Green et al., 2000). At present, plate tectonics efficiently cools the Earth. If plate tectonics was not operative in the Archaean, then the question arises as to how the Earth lost its heat (for a discussion see Nisbet, 1987).

Archaean terrains are special in that they may host a combination of granitoid batholiths, greenstone belts, high-grade gneisses and rock-types uncommon in Proterozoic and Phanerozoic terrains. The terrains are found as part of most continents throughout the world (see figure 1.1). A distinction can be made between Early and Mid Archaean terrains (4000–3000 Ma) and terrains of Late Archaean age (3000–2500 Ma), the most striking difference being the outcrop pattern. That is, where the older terrains show a pattern of ovoid granitoids enveloped by greenstone belts, the younger terrains generally have a linear outcrop pattern (see Myers, 1995; De Wit and Ashwal, 1997). Whereas observations in Late Archaean linear terrains, such as the Yilgarn Craton and the Superior Province, led to actualistic models in which terrane accretion and subduction play a role (Myers, 1995; Jackson and Cruden, 1995), the circular outcrop pattern of Archaean granite-greenstone terrains has led to the initial and to the recurring comparison of their structural development with solid-state diapirism (McGregor, 1951; Collins, 1989; Jelsma and Van Der Beek, 1993; Choukroune et al., 1995; Chardon et al., 1998; Collins et al., 1998; Blewett, 2002).

Solid-state diapirism is a model that describes vertical, gravity driven rise of relatively light

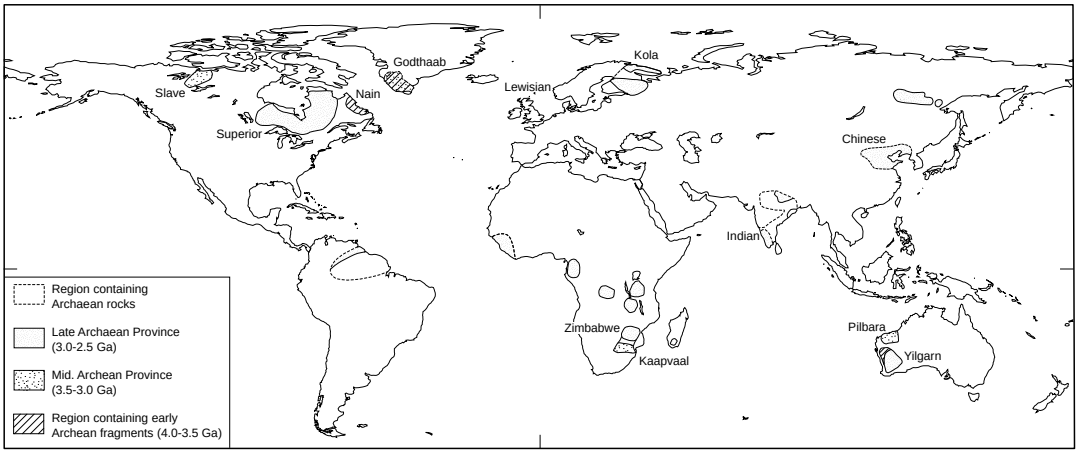

Figure 1.1 Map showing the distribution of the main Early, Mid and Late Archaean terrains (after Zegers, 1996).

material through denser material on top as the main cause for deformation. It is referred to as passive as it requires no plate tectonic forces to operate. With the development of mantle plume models (e.g. Fyfe, 1978; Campbell et al., 1989; Campbell and Griffiths, 1992; Hill et al., 1992a), passive, gravity driven diapirism was readily explained as the crustal response of a mantle plume-head below an Archaean continental crust (Choukroune et al., 1995; Chardon et al., 1998; Collins et al., 1998). The combination of mantle plumes and solid-state diapirism would provide an alternative mechanism for crustal development in the absence of plate tectonics. However, even though the mantle plume model explains upwelling of material, it does not provide a mechanism for recycling of crustal material back into Early Earth's mantle, and by itself cannot replace plate-tectonics as a mechanism.

Theoretical considerations that would prevent subduction of hotter and more buoyant oceanic crust, have led workers to propose alternative models for the development of continental crust and recycling of crustal material into Early Earth's mantle. These theoretical models are dominated by obduction/flake-tectonics (e.g. Hoffman and Ranalli, 1988), delamination of the mantle root and lower crust (A-subduction) (Kröner, 1981, 1984; Davies, 1992; Vlaar et al., 1994), and delamination of the lower crust leaving the mantle root intact (Zegers and Van Keken, 2000).

Geological observations in Archaean cratons world-wide indicating that (some form) of plate interaction and 'horizontal tectonics' of rigid crust occurred in the Early and Mid Archaean include: km-scale overthrust and nappe structures and ophiolite components in the Barberton Greenstone Belt (De Wit, 1982, De Wit et al., 1987a), accretionary orogens in Greenland (Nutman et al., 1993), continental dyke swarms (McGregor, 1973), cratonic sediments and continental rifts (Eriksson and Fedo, 1994). These suggest that plate tectonic theory may be applicable to the Early to Mid Archaean and make it controversial to reject plate tectonics on theoretical grounds (for a discussion see Condie, 1994). Nevertheless, the presence, in Mid Archaean but also in Late Archaean terrains, of komatiites, the abundance of heavy REE-depleted Tonalite-Trondhjemite-Granodiorite (TTG) suites, and anorthosites, which are rocks not commonly found in modern, Phanerozoic terrains,

suggests that if plate tectonics operated, it was in a modified form (see Condie, 1994 and references therein). As subduction of oceanic lithosphere is one of the cornerstones of modern-day plate tectonic theory, and as long as no unequivocal evidence has been presented for lithosphere-scale subduction in Early to Mid Archaean terrains, Archaean tectonics remains a subject of controversy.

The present study is concerned with a part of the Early to Mid Archaean eastern Pilbara granite-greenstone terrain in northwestern Australia. This granite-greenstone terrain, which is known for its ovoid outcrop pattern, developed largely between 3.66 Ga and 2.85 Ga and has been part of a stable craton since ca. 2.77 Ga. As this terrain is one of the two largest best preserved and exposed Early-Mid Achaean terrains, it forms one of the few natural laboratories in which it is possible to study Early to Mid Archaean structural processes.

The traditional structural model for the eastern Pilbara granite-greenstone terrain is that of solid-state diapirism (Hickman, 1983). This model predicts vertical, gravity-driven diapiric rise of a relatively light, granitic lower crust, and downward movement of denser upper crustal greenstone sequences, as the dominant cause for deformation. In this model horizontal transport, such as passive sliding off the diapiric dome, is a relatively small-scale, secondary feature. In contrast, other studies have emphasised the role of horizontal tectonics, advocating both extensional and compressional tectonic settings (Bickle et al., 1980, 1985; Krapez, 1984; Boulter et al., 1987; Krapez and Barley, 1987; Krapez, 1993; Zegers et al., 1996, 1998a; Van Haaften and White, 1998; Van Kranendonk and Collins, 1998; Barley and Pickard, 1999; Blewett, 2002) and some have recognised that extension and compression may have been the cause for passive rise of granitoid domes (Bickle et al., 1980, 1985, Zegers et al., 1996).

If crustal development in the Pilbara, and by inference all other Early to Mid Archaean terrains, could be explained in terms of diapirism, then a form of plate-interaction need not be inferred (Choukroune et al., 1995). Recently, for the Pilbara granite-greenstone terrain, diapiric rise of granitoids and inter-diapir greenstone sagging was combined in the model of partial convective overturn of the continental crust in response to the thermal effects of a mantle plume below the lithosphere (Collins et al., 1998). The process by which the ovoid granitoids have developed thus has become central in the discussion on the tectonic and geodynamic processes that formed and differentiated the first continents.

Proponents of solid-state diapirism have used field observations from the Mt Edgar Granitoid Complex and the surrounding greenstone belts, situated in the Marble Bar Domain, of the eastern Pilbara granite-greenstone terrain, as proof for their theories of crustal development (Hickman, 1983; Collins, 1989; Collins et al., 1998). Key observations, including a circular outcrop pattern, a steep shear zone on the margin of the Mt Edgar Granite and the greenstones, the occurrence of a gneissic 3.45 Ga basement and a suite of 3.31 Ga TTGs (Collins, 1989; Williams and Collins, 1990), have lent support to a model in which solid-state diapirism may have been active from 3.45 Ga onwards, culminating in one main activity at ca. 3.31 Ga (Collins, 1989; Collins et al., 1998; Van Kranendonk et al., 2002). This is a model in which the development of this area is explained exclusively by solid-state diapirism and vertical motion and that appears to conflict with models that emphasise horizontal tectonics (deformation of rigid crust by far-field forces potentially caused by plate-interaction) for the development of the Marble Bar Domain (Bickle et al., 1980, 1985; Krapez,

1984; Boulter et al., 1987; Krapez and Barley, 1987; Krapez, 1993; Zegers et al., 1996, 1998a; Van Haaften and White, 1998; Barley and Pickard, 1999; Blewett, 2002).

1.2 Introduction to the thesis

1.2.1 Aims and Approach

The objective of the present study is to provide insight into the relative importance of horizontal tectonic processes and diapiric processes in the development of Early and Mid Archaean terrains. The specific aim of this study was to determine the relationship between horizontal and vertical tectonics, and the role of associated magmatism, in the Early to Mid Archaean development of the structural architecture of the Marble Bar Domain. This aim was achieved by:

Identifying and understanding the main deformation structures in the Mt Edgar Granitoid Complex and selected parts of the surrounding greenstone belts by detailed structural mapping and kinematic analyses.

Constructing a structural, kinematic and magmatic framework for the study area, particularly from the main structure: the shear zone on the margin of the Mt Edgar Granitoid Complex.

Constraining the timing of activity of this shear zone by dating the crystallization of magmatic components, both syn- and post-tectonic, using SHRIMP U-Pb zircon chronology (SHRIMP-II, Perth, Western Australia).

Investigating the cause for the 3.32–3.31 Ga granitoid genesis and the domal development of the Mt Edgar Granitoid Complex, by studying the tectonic history of the preceding period, stratigraphically represented by the Salgash Subgroup of the Warrawoona Group.

Quantifying the thermal history of the Mt Edgar Granitoid Complex and in particular its margin applying ^{40}Ar-^{39}Ar isotope chronology (VULKAAN laser-probe, Amsterdam, The Netherlands) to investigate the timing of denudation, and to determine the role of late deformation and/or granites in obtaining its current steep geometry.

The thus derived temporally constrained, structural and magmatic framework, leads to a geological model of the development of the area through time. This model forms the basis for a discussion on the relative importance of horizontal and vertical tectonics throughout the ~800 m.y. history of the Marble Bar Domain. This history is then discussed in terms of models for Archaean crustal growth, interaction and recycling.

This thesis concentrates on the tectonic evolution of the Marble Bar Domain and to a lesser extent on the eastern part of the Pilbara granite-greenstone terrain, because this domain is the area quoted as having largely developed by solid-state diapirism. The western part of the Pilbara granite-greenstone terrain is generally younger, has a more linear outcrop pattern, and is regarded to have largely developed by plate tectonic processes (see for an overview e.g. Krapez and Eisenlohr, 1998),

and consequently was not considered in this study. It formed the research of Beintema (2003).

This study is part of the multi-disciplinary Utrecht Pilbara Research Project, which focuses on the thermo-tectonic evolution of the Pilbara Craton and the relationship to Early Earth metallogenic processes and basin development. Field studies have been financially supported by the Dr. Schürmann Foundation for Precambrian Research.

1.2.2 Organisation of the thesis

The thesis contains six chapters, one with an introductory overview, four presenting new data and conclusions based on these data, a chapter in which the combined results are discussed in terms of a model for the development of the area, and with a summation of the main findings.

The first chapter provides an introduction to the thesis, an introduction to Archaean geology and to the geological setting of the study area, the Pilbara granite-greenstone terrain.

Chapter 2 presents results from detailed structural and kinematic mapping and analyses of parts of the Warrawoona Greenstone Belt and the adjacent part of the Mt Edgar Granitoid Complex. The results indicate that the area has experienced a complex structural history of at least five deformation phases, including compression, extension and strike-slip deformation, and some of which are closely associated with magmatism. The southwestern margin of the Mt Edgar Granitoid Complex is found to have developed as a 2-5 km wide, complex detachment zone between the granitoid complex and the structurally overlying supracrustal sequence and is called the Mt Edgar Shear Zone. The centre of this zone displays an intricate relationship between deformation and intrusions of various composition. This chapter was published as *Kloppenburg, A., White, S. and Zegers, T., 2001. Structural evolution of the Warrawoona greenstone Belt and adjoining granitoid complexes, Pilbara Craton, Australia: implications for Archaean tectonic processes. Precambrian Research 112, 107-147.*

Chapter 3 reports on a detailed structural and kinematic study of the Mt Edgar Shear Zone (MESZ) in which the timing of its development is constrained by SHRIMP U-Pb zircon geochronology. The results show that the MESZ has developed as a mid-crustal detachment zone with a history of tectonic and magmatic activity from at least 3.46 Ga to 3.31 Ga. The history of the MESZ is consistent with an interpretation that the Mt Edgar Granitoid Complex has initially developed as an extensional dome at 3.46 Ga. The MESZ may be part of an Early Archaean detachment system within the mid-crust of part of the eastern Marble Bar Domain.

Chapter 4 focuses on the tectonic history of the Marble Bar Domain between 3.46 Ga and 3.31 Ga, during development of the Salgash Subgroup. A collection of generally NW-SE trending suites of mafic to ultramafic dykes, the 'Salgash Dyke Swarm' were found to have been emplaced post 3.47 Ga and pre-3.31 Ga. They potentially form the oldest dyke swarm recorded on Earth to date. It is concluded that the dykes were emplaced in the upper crust during regional (N)NE-(S)SW extension, around the time that the Mt Edgar Shear Zone was active as a mid-crustal extensional detachment. The dyke swarm comprises feeder dykes for basaltic units of the upper Warrawoona Group that were deposited on a generally submerged continental basement.

Chapter 5 documents the time constraints on the thermal history of the study area, particularly of the Mt Edgar Shear Zone. These were obtained using the ^{40}Ar-^{39}Ar isotope chronology method

on hornblende, muscovite and biotite from intrusive and extrusive rocks, some of which are sheared or otherwise metamorphosed. The resulting argon cooling ages largely fall in the 3.44 to 2.80 Ga range. Two upper crustal dykes of the Salgash Dyke Swarm yielded minimum ages of 3440 ± 58 Ma and 3356 ± 21 Ma. The results indicate that part of the upper crustal sequence, namely the volcanic units of the Kelly Greenstone Belt, has remained at upper crustal levels throughout the history of the area, whereas others, namely the Mt Edgar Shear Zone, may not have reached upper-crustal levels until 3.32 Ga. Additionally, the obtained range in ^{40}Ar-^{39}Ar ages in the Marble Bar Domain suggests strongly that the area has not been subjected to a regional thermal resetting event in the Late Archaean and subsequent eras.

In chapter 6 the results are integrated to refine the tectonic history of the study area. A new tectonic model for the Mt Edgar granitoid Complex and the surrounding greenstone belts is presented. In this model horizontal tectonics play a major role in the evolution of the area from ca. 3.45 Ga onwards, whilst vertical (diapiric) tectonics can have played a subsidiary role only. This is subsequently integrated with the geological history of the other areas of the Marble Bar Domain. The implication from the overall development of the Marble Bar Domain for the Early Earth tectonics is then discussed. The main conclusions are listed as well as indications for future research.

1.2.3 Conventions, methods and list of abbreviations

The names of the greenstone belts and granitoid complexes follow Hickman (1983), however, 'Granitoid Complex' is used for the granitoid complexes rather than 'Batholith' to reflect their internal heterogeneity. With the type-sections of the stratigraphic formations within the Marble Bar Domain, names of stratigraphic units follow the lithostratigraphic system (Hickman, 1983, 1990; Van Kranendonk and Morant, 1998) with recent amendments by Van Kranendonk et al. (2002), rather than the sequence-stratigraphic system (Krapez, 1993). Although the pre-fix 'meta-' is not used, most rocks in the study area are metamorphosed. Terminology of magmatic rocks follows Streckeisen (1974, 1976a), apart from the terms 'monzogranite' and 'adamellite' frequently used in the literature of the Pilbara, referring to Streckeisen's quartz-monzonite and plagio-granite, respectively. The term granitoid refers to felsic and intermediate plutonic rocks in general. The term 'gneiss' is used for compositionally banded felsic rock, and does not apply to foliated granitoids. A rock is referred to as being migmatitic when it shows macroscopic evidence of partial melting. Stereoplot 3.06 written by N. Mancktelow is used for stereographic projections and rotations. Nomenclature for kinematic indicators follows the convention of White et al. (1986). The term 'terrain' is used in a geographical sense, whilst 'terrane' refers to a tectonostratigraphically defined area. A zircon date is a number reflecting the age of a single spot measurement. A zircon age is a number reflecting the age of an intrusive component based on more than three statistically grouped zircon dates. Ages, if not indicated otherwise, are SHRIMP U-Pb zircon ages that represent the time of crystallization of the rock. A particular moment in time is expressed in Ma (10^6 years) when it can be estimated to within ± 10 m.y., otherwise Ga (10^9 years) is used. Time spans and the duration of processes are quoted in millions of years (m.y.).

The following abbreviations and meanings of words are applied:

m.y. = million years
Ma = million years ago
Ga = billion years ago
CWSZ = Central Warrawoona Shear Zone
MESZ = Mt Edgar Shear Zone
BWZ = Beaton Well Zone
FFSZ = Fieldings Find Shear Zone
HBSZ = Hilly Basalt Shear Zone
WGB = Warrawoona Greenstone Belt
MEGC = Mt Edgar Granitoid Complex
CDGC = Corunna Downs Granitoid Complex
CPA = Carbana Pool Adamellite
TTGs = Tonalite-Trondhjemite-Granodiorite suites

1.3 Introduction to Archaean geology

1.3.1 Introduction

A brief introduction to Archaean geology and the Archaean rock record on Earth is presented here. It includes an overview of constraints and arguments for, and a summary of, the main tectonic/geodynamic models proposed for the Early to Mid Archaean crustal development. The present introduction aims to provide a context for the work undertaken in this study and forms a basis for the discussion on the structural development of the eastern Pilbara granite-greenstone terrain.

1.3.2 Archaean cratons and their characteristics

1.3.2.1 The Archaean era

The Archaean era is defined as the period from 4000 to 2500 million years ago. With the oldest rocks recognised on Earth dated at ca. 4.0-3.9 Ga (see Nutman et al, 1996), the Archaean spans nearly 40% of the Earth's (recorded) history. Rocks of this age are the product of the processes that were active during that period, and are our only direct means to study the Archaean. Despite the nature of the Earth to recycle its crustal rocks, Archaean rocks have been preserved and form small parts of most continents today (see Nisbet, 1987). These areas show both similarities and differences with modern areas, and hold clues to the nature of Archaean processes. An introduction to the nature of Archaean terrains is given below, for extensive overviews and discussions, refer to work by Condie (1981, 2000), Kröner (1981, 1982, 1984, 1991), Windley (1984), Nisbet (1987) and De Wit and Ashwal (1997).

1.3.2.2 Archaean provinces and terrains

Archaean provinces are generally divided into Early (4000–3500 Ma), Mid (3500–3000 Ma) or Late Archaean (3000–2500 Ma), depending on the age of the dominant rock forming events.

The oldest, Early Archaean, provinces occur as fragmented remnants in small regions throughout the continents. They are dominated by high-grade gneisses of mixed composition, predominantly granodioritic and tonalitic, but also minor granite, gabbro, supracrustal and ultramafic rocks. The oldest rocks among them are granitoid gneisses that form part of the Itsaq Gneiss in Greenland and of the Acasta Gneiss and Nain Province in Canada (see Nutman et al., 1996 for an overview of the oldest rocks). Although high-grade gneisses form the main component of the older terrains, and have been referred to as a separate type of terrain, they are also observed as an integral part of granitoid complexes in Mid and Late Archaean granite-greenstone terrains as described below.

Mid Archaean provinces are rare and are largely represented by the Kaapvaal (Africa) and Pilbara Provinces (Australia). They are largely composed of granite-greenstone terrains, which contain ovoid granitoid complexes and belts of encompassing volcano-sedimentary sequences. The characteristics of granite-greenstone terrains are described below.

Late Archaean provinces are the most common and overall the largest provinces, the best known being the Superior Province in Canada (see Jackson and Cruden, 1995) and the Yilgarn Province in Western Australia (see Myers, 1995). They are generally composed of granite-greenstone terrains. Whereas for the Mid Archaean granite-greenstone terrains the outcrop patterns are generally ovoid, for the Late Archaean terrains a more linear structural trend is seen.

On top of both Mid and Late Archaean granite-greenstone terrains kilometers thick sedimentary sequences of Late Archaean to Early Proterozoic age are found (e.g. Mt Bruce Supergroup in the Pilbara; Witwatersrand Supergroup in South Africa). The development of these basins is taken to reflect rifting and the development of stable shelf conditions at the end of the Archaean era (Eriksson and Fedo, 1994).

Granite-greenstone terrains range in age from Mid to Late Archaean. These terrains comprise multi-component granitoid complexes that are encompassed by dominantly volcanic supracrustal sequences that form the greenstone belts. The oldest granite-greenstone terrains are those of the Pilbara and Kaapvaal provinces, the development of which dates back to at least ca 3.5 Ga (Nelson et al., 1999).

The granitoid complexes in general comprise high-grade gneisses and variably deformed intrusions of tonalitic, trondhjemitic, and granodioritic composition (TTG) as well as plutons of K-rich monzogranite/adamellite, generally interpreted to be post-tectonic (Condie, 1982). The composition of granitoids, particularly of the early TTG suites is an important part of the puzzle of Archaean tectonic processes, as is further discussed below. The greenstone belts generally consist of basaltic and felsic volcanic units, as well as minor ultramafic rocks and sediments. The metamorphic grade of greenstone belts is typically low-grade, greenschist facies: greenstones generally lack evidence of regional HP/LT metamorphism. Remarkable in greenstone belt sequences is the general lack of intermediate volcanism: andesites are relatively rare. An additional remarkable observation is the occurrence of komatiites (high-Mg rocks with spinifex textures first described by

Viljoen and Viljoen, 1969). Even though komatiites form only a small percentage of the greenstone sequence, their occurrence implies special geodynamic processes and/or mantle conditions, which is further discussed below.

1.3.2.3 Lithospheric and crustal structure of Archaean provinces

Archaean provinces have a typical lithospheric and crustal structure. Seismological data has indicated that the present-day mantle lithosphere below Archaean provinces is generally 260–300 km, which is generally thicker than that below Proterozoic provinces (240–280 km) (Beghoul and Meren, 1992) and dramatically thicker than that below Phanerozoic areas (ca. 70 km). Those parts of the lithosphere are stable at present, and are therefore generally referred to as cratonic shields, or cratons. The continental *crust* of Archaean provinces, in contrast, is generally thinner (27–40 km) than Proterozoic crust (40–55 km) and lacks the basal high velocity zone that is common in modern crust, as was shown by a review of seismological data world-wide (Durrheim and Mooney, 1991, 1994). These observations were consistent with those for the Australian continent by Drummond and Collins (1986), Drummond (1988) and Drummond et al. (1993), and for the Superior Province in Canada (Calvert et al., 1995).

These characteristic lithospheric and crustal thicknesses have been attributed to a higher Archaean mantle temperature by Durrheim and Mooney (1994). In their model a higher mantle temperature leads to a higher degree of partial melting at Archaean MORs, leaving an ultra-depleted lithosphere that is relatively light compared to the non-depleted surroundings. This lithosphere is relatively stable which protects the area from subsequent modification by events such as mafic underplating of the crust or subduction (Durrheim and Mooney, 1994). However, the internal structure of the earth has been and still is the subject of debate that is centred around the discussion on Archaean mantle temperature, as outlined below.

1.3.2.4 Temperature of the Archaean Earth

Archaean mantle temperatures, dissipation of heat within the Archaean earth, the internal structure of the mantle, the lithosphere, and (oceanic) crust and the nature of early mantle convection are related subjects, and have been the topic of much discussion (see Nisbet, 1987; Taylor and McLennan, 1995, and Condie, 2000 and references therein). Geodynamical models that are based on the rheological behaviour of the mantle as a function of its temperature predict that plate tectonics, as we know it, cannot operate in an Earth with a hotter mantle (Vlaar, 1986; Hoffman and Ranalli, 1988; Davies, 1992; Vlaar et al, 1994).

Estimates for the Archaean mantle temperature have been based on the general acceptance that the earth's radioactive heat production may have been two to six times higher than today (Davies, 1993; Jackson and Pollack, 1984; O'Nions et al., 1978; O'Nions and Pankhurst, 1978; Richter, 1984; Pollack, 1997 and references therein). This in combination with the stored heat from initial accretion and formation of the core has led people to conclude that the mantle was hotter.

Observational evidence in support of a hotter mantle in the Archaean exists in the form of komatiites. Komatiites are ultramafic rocks that are indicative of high degrees of partial melting of a deep mantle source (see Arndt and Nisbet, 1982; Arndt, 1994). As most komatiites occur in

Archaean terrains, and as a high degree of partial melting is more likely in a hotter mantle, the occurrence of komatiites has been used as an argument for a mantle temperature in the Archaean of 400-500°C hotter than today if komatiites represent the overall mantle (Sleep, 1997; Nisbet and Fowler, 1983 and Vlaar, 1986), to 100-300°C if they represent partial melts due to hotspots (Sleep and Windley, 1982; McKenzie, 1984; Campbell and Griffiths, 1992). However, Campbell et al. (1989) proposed that Archaean komatiites formed in central plume-axes that tap into lower, hotter, parts of the mantle. Therefore, if komatiites are a typical product of plumes, the temperatures in the subcontinental mantle may have been similar as today (Boyd et al, 1985; Richardson; 1985). If komatiites were formed by melting of a hydrous mantle, then elevated mantle temperatures need not be inferred (Grove and De Wit, 1995).

Thermal modelling has indicted that in a hotter mantle decompression melting starts at a deeper level, producing more melt at spreading ridges, which would result in a thicker oceanic crust and a strongly depleted mantle lithosphere (Sleep and Windley, 1982; Vlaar, 1986; McKenzie and Bickle, 1988). In addition, a hotter mantle would have a lower viscosity and behave more vigorous (Karato and Wu, 1993). Calculations indicate that a hotter mantle would require increased spreading activity to dissipate the extra heat, either by a greater total mid-oceanic ridge length, or by an average higher spreading rate (Bickle, 1978; Nisbet and Fowler, 1983; Hargraves, 1986). The combination of a thicker, stable oceanic crust, faster convection and hence less time to cool for oceanic crust have been the main arguments for the concept that the oceanic crust was too buoyant to subduct in the Archaean (Hoffman and Ranalli, 1988; Davies, 1992; Vlaar et al., 1994). Subduction of oceanic crust, however, would be theoretically possible at that time if the oceanic crust generated was largely komatiitic (Nisbet and Fowler, 1983). Archaean oceanic crust has been predicted to have been similar to present-day oceanic plateaus (Condie, 1997; Kuski and Kidd, 1992; Polat et al., 1998).

Whether a hotter mantle and a thicker oceanic crust would indicate a hotter continental crust is uncertain. If the continental crust was thicker at that time, it may have had a geothermal gradient that is higher than today, as heat producing elements (K, Th and U) that concentrate in the crust would have led to a higher crustal heat production (Sandiford, 1989). A hotter geotherm would affect the strength profile of the crust in that the brittle-ductile transition would be shallower (Marshak, 1999). This in turn would affect the style of deformation of the crust in that the amount of crustal thickening is limited by more readily occurring gravitation collapse (Bailey, 1999; Dewey, 1988).

1.3.2.5 Geochemical constraints

Additional constraints for Early Earth tectonics come from (theoretical) models that have focussed on the geochemical development of the Earth, including the timing of separation of the crust from the mantle, the rate of crustal growth and the amount and mechanism of crustal recycling.

Models for crustal growth and recycling are largely based on the Sm and Nd isotopic record. Nd model ages reflect the age of mantle extraction of the source rock. Based on this it was concluded that at least 50-60% of the continental crust existed at ca. 2.6 Ga (Taylor and McLennan, 1995).

Additional models that predict slow initial growth from 4.0 Ga onwards, with increased growth in the Mid to Late Archaean include those of Hurley (1968) and Veizer and Jansen (1979) and are based on the available geological record. Alternatively, earlier and more rapid initial crustal growth from ca. 4.5 Ga to 4.0 Ga, with a steady state (equal growth / recycling) from the Early to Mid Archaean onwards was proposed by Fyfe (1978), Armstrong (1981) and Reymer and Schubert (1986) based on Sm/Nd isotopic measurements and freeboard constraints. Agreement on a model for crustal growth and amount of recycling throughout the Earth's history has not been reached (for a discussion see Taylor and McLennan, 1995; Vervoort et al., 1996; De Wit and Ashwal, 1997; Green et al., 2000).

Based on geochemical similarities of Early to Mid Archaean granitoids and volcanic rocks and those formed in modern (back) arc basins, subduction has been proposed as a mechanism of continental crust reworking (Barley, 1984; Barley and Pickard, 1999; Nisbett, 1987; Hoffman, 1991; Spray, 1985; Windley, 1984; Sleep and Windley, 1982; Condie, 1989; Ludden et al., 1986; Taylor and McLennan, 1995).

1.3.3 Tectonic models and structural settings for Early-Mid Archaean terrains

The various observations in Archaean terrains, in combination with theoretical views on Archaean mantle temperatures, (oceanic) crustal thickness, sizes of plates and the vigour of recycling, and the nature of the early MORs, and the indications from geochemical data for crustal growth and crustal recycling, have led to various geodynamic models for the development of the early Earth's mantle, and various tectonic models for crustal formation and crustal development for the Early to Mid Archaean terrains.

1.3.3.1 Models for formation of primary mafic crust

Two different settings have been proposed for the formation of Early to Mid Archaean mafic crust. In favour of a MOR-type setting are greenstones that were recognised as ophiolites in the Early-Mid Archaean Barberton Greenstone Belt in South Africa (De Wit et al., 1987). Alternatively, an implied high mantle plume activity in the Archaean combined with the role of mantle plumes in the formation of Phanerozoic Large Igneous Provinces (LIPs), such as the 20 km thick Kerguelen Plateau and the southwest Pacific Ontong Java Plateau (Coffin and Eldholm, 1994) has led workers to propose that parts of greenstone belt sequences have been deposited as oceanic plateau's (Kusky and Kidd, 1992; Condie, 1997; Polat et al., 1998). Shared features include high eruption rates, thick sequences, large lateral extent of the volcanism, bimodal, but dominantly (ultra)mafic rocks, relatively uniform sequences, with upper felsic units (Reymer and Schubert, 1986; Desrocher et al., 1993; Krapez, 1993; Eriksson, 1994; Kerr et al., 1996; Kent et al., 1996; Arndt et al., 1997). Differences between greenstone sequences and LIPs, such as more komatiites, and thicker greenstone sequences, would be explained by the proposed higher mantle temperatures. (Arndt and Nisbett, 1982; Storey et al., 1991; Campbell and Griffiths, 1992; Kusky and Kidd, 1992).

1.3.3.2 Models for reworking of mafic crust to form continental crust

Central in the discussion on the mechanism of modification of mafic (oceanic) crust to continental crust is the constraint that this process must have formed the earliest tonalite-trondhjemite-granodiorite suites (TTGs). TTGs can be produced by reworking of a mafic crust through partial melting of amphibolite/hornblende-eclogite, leaving garnet ± hornblende in the residue (Martin, 1994; Rapp and Watson, 1995; Wyllie et al., 1997). But, to produce eclogites, a thick relatively thick and cool crust is necessary. TTGs can then be formed by partial melting of these eclogites at the base of that crust (Hill, 1991; Abbott and Mooney, 1995; Arndt, 1992: cf. Martin, 1994). The proposed models to establish an overthickened Archaean crust either invoke magmatic thickening or tectonic stacking.

Tectonic stacking of mafic crust has been proposed to be the result of either ocean-ocean obduction (De Wit and Hart, 1993; De Wit, 1998), or by ocean-ocean subduction (Sylvester et al., 1987). Both models would readily explain a thickened crust. *Obduction* and preservation of the primary mafic crust is proposed to have been triggered by 'drowning of the MORs': eruption of lava below sea-level allows interaction with seawater and hydrated Archaean oceanic crust at convergent margins would have interacted by stacking through obduction, rather than recycling through subduction (see De Wit et al., 1987; De Wit and Hynes, 1995). *Subduction* may have occurred in a form that promotes the melting of the subducted slab itself: Archaean TTG suites have been likened to Adakite, a typical granitoid that forms due to modern-day shallow subduction of hot (young) oceanic crust (see for an overview: Defant and Kapezhiskas, 2001; cf. Smithies, 2000). A combination of partial obduction and partial subduction of slices of thick oceanic crust, referred to as 'flake tectonics', has been proposed by Hoffman and Ranalli (1988).

After thickening of a basaltic crust the TTG suites form by partial melting. An elegant model for the formation of TTG has recently been presented by Zegers and Van Keken (2000). Their 'in-situ differentiation and delamination' model proposes delamination of the base of a thick crust after a phase-change to dense eclogite or garnet-rich granulite. This phase change may involve partial melting and the formation of melt with high-Al TTG composition. The dense eclogite or garnet granulite of the lower crust would subsequently sink through the relatively less dense depleted mantle (Vlaar, 1994). The removal of the lower crust causes upwelling of the replacing mantle, which causes heating and partial melting of the basaltic crust that is still in place to produce a second pulse of TTG melts. This model is consistent with geophysical observations of a preserved thick lithospheric mantle, and with the general absence of a lower crustal high-velocity zone associated with Archaean cratons (Drummond and Collins, 1986). This delamination model differs from 'A-subduction' (Kröner, 1981, 1984; Davies, 1992; Vlaar et al., 1994) in that it preserves the mantle root (Zegers and Van Keken, 2000).

A model that does not require a thick basaltic crust to form TTGs is the Lunar maria model, which proposes that the energy of meteorite impacts caused large melt fractions (Green, 1972; Glikson, 1999). Evidence for meteorite impact has been found in the form of spherulites in a ca. 3240 Ma unit in the Kaapvaal Craton (Kyte et al., 1992).

In all the above models TTG formation is modelled by a two-stage melting process: extraction of magma from the mantle to form a basaltic crust (either MOR or igneous plateau-type) followed

by partial melting of mafic crust to form TTGs. However, geochemical modelling of Evans and Hanson (1992) has showed that a two stage model is not necessary, and that TTGs could be produced from melts that are derived directly from the mantle.

1.3.3.3 Models for reworking of continental crust

Mechanisms for reworking of Archaean continental crust comprise both actualistic models and those typical for the Archaean. Similarities between chemical signatures of Archaean granitoids and volcanic rocks and those found in modern subduction related settings (see above) have formed the basis to propose this mechanism for crustal recycling as early as the Early to Mid Archaean (Barley, 1984; Barley and Pickard, 1999; Nisbett, 1987; Hoffman, 1991; Spray, 1985; Windley, 1984; Sleep and Windley, 1982; Condie, 1989; Ludden et al., 1986; Taylor and McLennan, 1995). In addition, field observations have led to interpretations in which greenstone belts are relics of marginal rift basins squeezed between ancient continental margins (Anhaeusser, 1975; Tarney et al., 1976; Groves et al., 1978; Drury et al., 1984), and back-arc basins (Windley, 1984). Regional compression and resulting extensional collapse has been proposed particularly in relation to the genesis and emplacement of granitoids (James and Mortensen, 1992; Kuski, 1993; Marshak et al., 1997).

An alternative model for the reworking of Archaean continental crust ascribes partial melting of the base of continental crust and crustal anatectic granites to heating by dominantly mafic magmatism due to mantle plume activity for the 2.7 Ga development of the Yilgarn (Campbell and Hill, 1988) and for the 3.3 Ga development of the Pilbara granite-greenstone terrain (Collins et al., 1998).

The crustal response to heating by a mantle plume has been proposed to be solid-state diapirism (Gee, 1981; Hickman, 1984; Choukroune, 1995, Chardon, 1999; Jelsma et al., 1993; Bouhallier et al., 1993; Byerly et al., 1996; Chardon et al., 1996), which for the Pilbara granite-greenstone terrain has also been referred to as 'crustal partial convective overturn', that involved partial melting an mobilisation of an existing gneissic basement at ca. 3.31 Ga (Collins et al., 1998). Even though solid-state diapirism is an elegant model to explain the generally circular outcrop patterns of Mid Archaean terrains, most of these terrains have now been recognised to have more complex structural histories that involve compression, extension and strike-slip deformation (Zegers, 1996; Zegers et al., 1998; Blewett, 2002). In addition, a plume model poses a problem for the Pilbara because it predicts a mafic underplate (Durrheim and Mooney, 1994), for which there is no evidence in the Pilbara (Drummond, 1988).

1.3.3.4 Models for destabilisation of continental crust, rifting

In the concept of plate tectonics, recycling of crust is driven by plate tectonic forces of ridge-push, slab-pull and mantle drag, forces which have been considered to have operated during rifting and oceanization of Archaean terrains (Henderson, 1981, 1985; Easton, 1985; Park, 1982; Williams and Wittaker, 1993, Windley, 1977).

An alternative mechanism for the destabilisation of cratons is proposed to have involved A-subduction (Kröner, 1981), also referred to as mantle-root drop-off, or 'drip-tectonics', driven by

conversion of the lower part of the lithosphere to garnet-granulite and eclogite (Campbell et al., 1989; Vlaar, 1994; Vlaar, 2000). As mentioned before, problematic with this 'drip' model is that at present all cratons have thick lithospheric roots, which suggests that it was not possible to survive without one, and which renders it unlikely that drop-off of this root caused events in the history of those granite-greenstone terrains that have survived (De Wit, 1998).

A model that requires neither plate interaction, nor mantle-root drop off for the de-stabilisation of Archaean crust is the model of lower crust delamination, as described above (Zegers and Van Keken, 2000). This model predicts weakening of crust by delamination of the lower crust, thinning and partial melting and upwelling of mantle material. This may lead to continental rifting.

Mantle plumes have been widely used to explain the break-up of modern continents. This has led to models in which plumes caused the break-up of Archaean cratons (Hill, 1989, Campbell and Hill, 1988; Campbell et al., 1989; Nisbet et al., 1993; McDonough and Ireland, 1993; Abbott, 1996). However, whether modern mantle plumes are the *cause* or the *consequence* of rifting (re-active versus active rifting) has been the subject of discussion. Plume and plate-induced continental rifting should theoretically be distinguishable by the relative timing of extension and the onset of magmatic activity (Wilson, 1989). Plume-induced continental rifting initially causes uplift, then extension by forced doming and stretching of the crust above the plume, then mafic volcanism. This is followed by ultramafic volcanism and rifting (see e.g. Richards et al., 1989; Campbell and Griffiths, 1989; Hill, 1991; Hill et al., 1992). In contrast, plate-induced continental rifting progressively causes thinning of the crust, subsidence, rifting and uplift of the rift shoulders, followed by mafic volcanism (see e.g. White and McKenzie 1989). Despite these theoretical differences, even for the development of Phanerozoic terrains this is a subject of ongoing discussion (see Courtillot et al., 1999; Sheth, 1999a, 199b). McKenzie and Bickle (1988) noted that a mantle plume is not a prerequisite for mafic magmatism, particularly not in the Archaean, as limited extension and adiabatic rise in hotter mantle is sufficient to cause melting.

1.4 Geology of the eastern Pilbara Granite-greenstone terrain

1.4.1 Introduction

The Pilbara Craton is situated in the northwest of Western Australia (see Figure 1.2). It is about 600 x 550 km in extent (Wellman, 2000). The northern regions of the craton are formed by the Pilbara granite-greenstone terrain (3.66-2.85 Ga), which to the south is unconformably overlain by Late Archaean volcano-sedimentary rocks of the ca 2.77-2.41 Ga Mt Bruce Supergroup that was deposited in the Hamersley Basin (Griffin, 1990).

The Pilbara granite-greenstone terrain is one of the two largest and best exposed Mid Archaean provinces in the world. The classic work on the geological history of the Pilbara granite-greenstone terrain is that of Hickman (1983), which describes an all-encompassing Pilbara-wide model for the structural and stratigraphic development. That model was based on a compilation of a Pilbara-wide mapping project of the Geological Survey of Western Australia, that led to the first 1:250 000

geological maps of the area. Hickman (1983, 1984) explained the evolution of this area in terms of typical Archaean, multi-stage, solid-state diapirism that describes gravity driven 'passive' rise of granitoids domes to pierce the overlying denser supracrustal greenstone sequence. This model was recently viewed in the broader context of 'convective overturning of the crust' that emphasises downward motion of the dense crust (Collins et al., 1998). In either model, deformation is the result of a density inversion within the crust. Over the last 20 years, this geological history has been further refined (see Van Kranendonk et al., 2002).

Studies in the Pilbara granite-greenstone terrain since 1983 have included structural, sedimentological, geochemical and geochronological work, as will be described below. An overview of these has been presented by Zegers (1996) as part of her Ph.D. thesis, the first of this Utrecht Pilbara Research Project. A wider overview of the Pilbara Craton as a whole has been provided by Barley (1997) in the book 'Greenstone Belts' by Ashwal and De Wit (1997). The most recent new data has been reported based on mapping, geochronological, geochemical and geophysical studies undertaken as part of the National Geoscience Mapping Accord by the Australian Geological Survey Organization and the Geological Survey of Western Australia. A summary of these main findings has been published by Van Kranendonk et al. (2002) and Blewett (2002). A large number of U-Pb zircon SHRIMP ages have been obtained throughout the Pilbara granite-greenstone terrain (Nelson, 1995, 1996, 1997, 1998, 1999, 2000, 2001, 2002), which are summarised in Van Kranendonk et al. (2002). These ages have led to a better understanding of the tectonomagmatic history and to a revision of the stratigraphic sequence (see Van Kranendonk et al., 2002). In addition, regional gravity and magnetic anomaly coverage (Wellman, 1999, 2000) has provided insight into the shape of the granitoids and greenstone belts with depth. It was found that part of the greenstone sequences must largely have steepened after ca. 3250 Ma, which is the age of the main magnetic marker (see Blewett et al., 2000, 2002).

An alternative all-encompassing model for the Pilbara as a whole is that of Krapez (1993) and Krapez and Eisenlohr (1998). These workers took a uniformitarian, sequence stratigraphic approach, that assumes plate tectonic activity. This led to a genetic-stratigraphic interpretation of the stratigraphy with two plate-tectonic cycles of ~380 and 340 m.y., for the history of the eastern and western Pilbara granite-greenstone terrain, respectively, with the last stages of the second cycle represented by rifting at 2.77 Ga. Additional models for the development of the eastern Pilbara granite greenstone terrain have focussed on parts of the terrain and on parts of the history as will be further discussed below.

A recent compilation and structural study by Blewett (2002) led to a 6-fold deformation history for the Pilbara granite-greenstone terrain. It confirmed that polyphase horizontal tectonics, both compression and extension, occurred at least after 3.2 Ga. As for the older history, it was noted that the observed regional framework for the timing of the deformation suggests that doming was the consequence of deformation, rather than the cause.

The Pilbara granite-greenstone terrain is divided by craton-scale structures into six domains (Krapez and Barley, 1987; Krapez, 1993; Krapez and Eisenlohr, 1998; Smith, 1998), which in turn are grouped into three Superdomains, namely the Eastern, Central and Western Pilbara (see Blewett, 2002). The Eastern Pilbara comprises domains 1, 2 and 3 (Figure 1.2). Domain 2 is referred

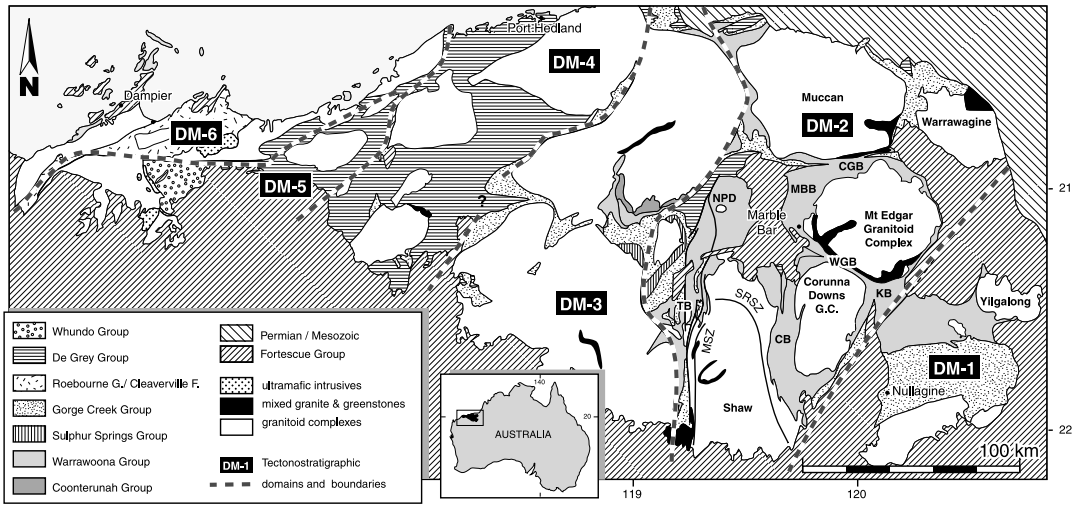

Figure 1.2 Location, generalised geological map and structural elements of the Pilbara granitoid-greenstone terrain showing the distribution of the ovoid granitoid complexes, the distribution of the seven stratigraphic groups that constitute the greenstone belts, the overlying Fortescue Group and the Phanerozoic cover (after Hickman, 1983; Van Kranendonk and Morant, 1998; Buick et al., 1995). Subdivision into six tectonostratigraphic domains is after Krapez and Barley (1987); Krapez (1989); Krapez (1993) and Smith et al., (1998). TB=Tambourah Belt, CB=Coongan Belt, NPD=North Pole Dome, MGB=Marble Bar Belt, WGB=Warrawoona Belt, CGB=Coppin Gap Belt and KB=Kelly Belt. MSZ=Mulgandinah Shear Zone, SRSZ=Split Rock Shear Zone.

to as the Marble Bar Domain. As this study focuses on the Marble Bar Domain, the overview of the geological history presented below is limited to this and adjacent domains.

1.4.2 Geological history of the eastern Pilbara granite-greenstone terrain

The ca 800 m.y. of tectonomagmatic development of the eastern Pilbara granite-greenstone terrain, from crystallization of the oldest recognised gneissic component at 3.66 Ga to the intrusion of post-tectonic granitoids at 2.85 Ga, involved an intricate relationship between deformation and at least four main rock forming episodes (see Nelson et al., 1999; Barley and Pickard, 1999; Van Kranendonk et al. 2002 and references therein). These rock forming episodes have been named the Warrawoona episode (3470-3450 Ma), the Wyman episode (3325-3310 Ma), the Roebourne episode (3260-3240 Ma) and the Millindinna episode (2950-2930 Ma) (Nelson et al., 1999) (see figure 1.3). The relationship between development of the stratigraphic succession, intrusive events and deformation is here described, in relation to these four episodes. More detailed accounts on parts of the history are presented in chapters 2, 3, 4 and 5. For location names refer to figure 2.1.

1.4.2.1 The pre-Warrawoona history (> ca. 3.47 Ga)

The pre-Warrawoona history is in part represented by the oldest stratigraphic sequence in the Pilbara granite-greenstone terrains, the Coonterunah Succession. It occurs in a single but ~80 km

long outcrop of dominantly tholeiitic basalts and minor felsic volcanic units on the north-western margin of the Marble Bar Domain, a felsic unit of which was dated at ca 3515 Ma (Buick et al., 1995). Geochemical studies have indicated that the basalts are crustally contaminated (Green et al., 2000) suggesting the existence of pre-existing crustal material, as is also indicated by existence of 3.66 Ga granite gneisses in the Eastern Pilbara. The succession has recently been upgraded to a stratigraphic group (Van Kranendonk, 1998) (See figure 1.3). The depositional environment of the Coonterunah has been regarded as a deep water one based on sedimentological evidence (Buick et al., 1995).

A lateral equivalent of the Coonterunah Group has been proposed to be the Talga Talga Subgroup (Zegers, 1996), based on ca. 3.51 Ga ^{40}Ar-^{39}Ar cooling ages of rocks from the Talga Talga Subgroup in the Coongan Greenstone Belt and north of the Shaw Batholith (Davids et al., 1997; Zegers et al., 1999). The base of this subgroup, the North Star Basalt, has not been dated with the SHRIMP U-Pb method because the unit contains dominantly mafic and ultramafic rocks. A Sm/Nd extraction age has yielded a date of 3560 ± 32 Ma (Hamilton et al., 1981), which, if the rocks were extracted directly from the mantle, would indicate that the North Star Basalt is older than the Coonterunah Formation.

Granitoid protoliths for gneisses of the Warrawagine Batholith were recently dated at >3576 ± 6 Ma, and are possibly as old as ca. 3660-3640 Ma (Nelson et al., 1999). Other pre-Coonterunah rocks are the 3578 ± 4 Ma anorthosite and gabbro enclaves in gneiss of the Shaw Granitoid Complex (McNaughton et al., 1988). Xenocrystic zircons found in the Marble Bar Domain range back in age from ca 3500 Ma to ca. 3725 Ma (Thorpe et al., 1992, Nelson, 2000, see also the summary of available geochronological data in figure 3.2, and see Van Kranendonk et al., 2002 p. 705, for an overview of evidence of ancient crust in the Pilbara). These observations support the findings of Green (2000) that a continental crust existed prior to the deposition of the Coonterunah Formation.

1.4.2.2 Development during the Warrawoona episode (3.49-3.42 Ga)

The development of the area after deposition of the Coonterunah Group is represented by the rocks attributed to the Warrawoona Group, the upper part of which locally lies unconformably on the Coonterunah Succession (Buick et al., 1995). They form the two dominantly basaltic Talga Talga and Salgash subgroups, separated by the largely felsic 3.47-3.45 Ga Duffer Formation (See figure 1.3).

The Talga Talga Subgroup comprises the North Star Basalt at the base which is of uncertain age (see above). It is overlain by the strongly deformed McPhee Formation, situated on top of which is the Mt Ada Basalt (Hickman, 1983). SHRIMP U-Pb zircon ages from a foliated chert from the McPhee Formation in the Marble Bar Greenstone Belt have been dated at 3477 ± 2 Ma (Nelson, 2000) and a felsic volcanic unit or subvolcanic unit in the Mt Ada Basalt has been dated at 3469 ± 3 Ma (Nelson, 1999). This indicates that there is no major hiatus between deposition of the upper part of the Talga Talga Subgroup and the Duffer Formation. Van Kranendonk et al. (2002) propose to group the Duffer Formation with the Talga Talga Subgroup.

The depositional environment of the *upper* Talga Talga Subgroup has been regarded in terms of a shallow marine marginal setting (Barley et al, 1979). The *lower* units, of the North Star Basalt, have

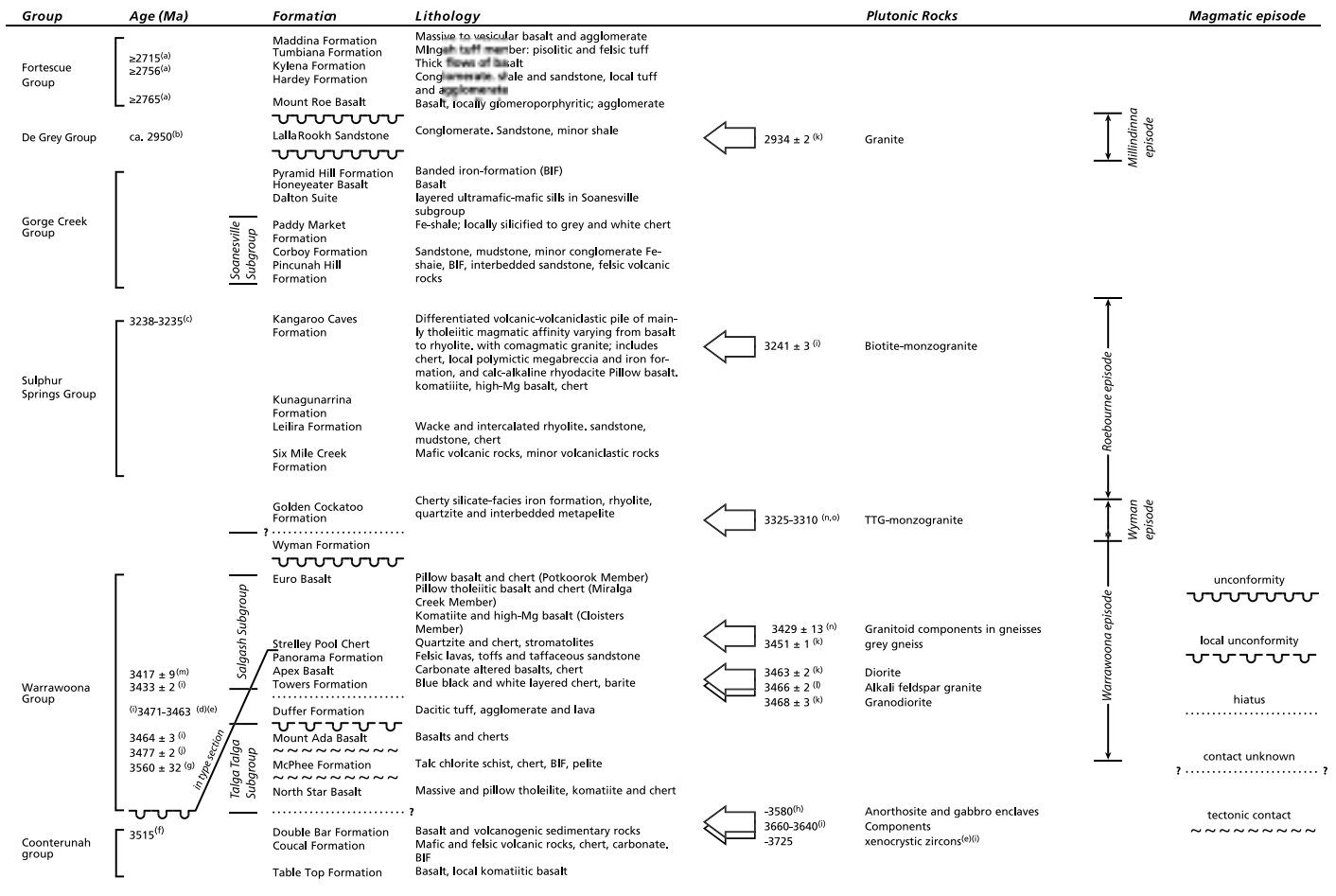
Group
Age (Ma)
Formation
Lithology
Plutonic Rocks
Magmatic episode
Fortescue Group
≥2715(a)
≥2756(a)
≥2765(a)
Maddina Formation
Tumbiana Formation
Kylena Formation
Hardey Formation
Mount Roe Basalt
Massive to vesicular basalt and agglomerate
Mingah tuff member: pisolitic and felsic tuff
Thick flows of basalt
Conglomerate, shale and sandstone, local tuff and agglomerate
Basalt, locally glomeroporphyritic; agglomerate
De Grey Group
ca. 2950(b)
Lalla Rookh Sandstone
Conglomerate. Sandstone, minor shale
2934 ± 2 (k)
Granite
Millindinna episode
Gorge Creek Group
Soanesville Subgroup
Pyramid Hill Formation
Honeyeater Basalt
Dalton Suite
Paddy Market Formation
Corboy Formation
Pincunah Hill Formation
Banded iron-formation (BIF)
Basalt
layered ultramafic-mafic sills in Soanesville subgroup
Fe-shale; locally silicified to grey and white chert
Sandstone, mudstone, minor conglomerate Fe-shale, BIF, interbedded sandstone, felsic volcanic rocks
Sulphur Springs Group
3238-3235(c)
Kangaroo Caves Formation
Kunagunarrina Formation
Leilira Formation
Six Mile Creek Formation
Differentiated volcanic-volcaniclastic pile of mainly tholeiitic magmatic affinity varying from basalt to rhyolite. with comagmatic granite; includes chert, local polymictic megabreccia and iron formation, and calc-alkaline rhyodacite Pillow basalt. komatiiite, high-Mg basalt, chert
Wacke and intercalated rhyolite. sandstone, mudstone, chert
Mafic volcanic rocks, minor volcaniclastic rocks
3241 ± 3 (i)
Biotite-monzogranite
Roebourne episode
Golden Cockatoo Formation
Wyman Formation
Cherty silicate-facies iron formation, rhyolite, quartzite and interbedded metapelite
3325-3310 (n,o)
TTG-monzogranite
Wyman episode
Warrawoona Group
Salgash Subgroup
Talga Talga Subgroup
in type section
Euro Basalt
Strelley Pool Chert
Panorama Formation
Apex Basalt
Towers Formation
Duffer Formation
Mount Ada Basalt
McPhee Formation
North Star Basalt
3417 ± 9(m)
3433 ± 2 (i)
(i)3471-3463 (d)(e)
3464 ± 3 (i)
3477 ± 2 (j)
3560 ± 32 (g)
Pillow basalt and chert (Potkoorok Member)
Pillow tholeiitic basalt and chert (Miralga Creek Member)
Komatiite and high-Mg basalt (Cloisters Member)
Quartzite and chert, stromatolites
Felsic lavas, toffs and taffaceous sandstone
Carbonate altered basalts, chert
Blue black and white layered chert, barite
Dacitic tuff, agglomerate and lava
Basalts and cherts
Talc chlorite schist, chert, BIF, pelite
Massive and pillow tholeiiite, komatiite and chert
3429 ± 13 (n)
3451 ± 1 (k)
3463 ± 2 (k)
3466 ± 2 (l)
3468 ± 3 (k)
Granitoid components in gneisses
grey gneiss
Diorite
Alkali feldspar granite
Granodiorite
Warrawoona episode
Coonterunah group
3515(f)
Double Bar Formation
Coucal Formation
Table Top Formation
Basalt and volcanogenic sedimentary rocks
Mafic and felsic volcanic rocks, chert, carbonate. BIF
Basalt, local komatiitic basalt
-3580(h)
3660-3640(i)
-3725
Anorthosite and gabbro enclaves
Components
xenocrystic zircons(e)(i)
unconformity
local unconformity
hiatus
contact unknown
tectonic contact

been proposed to have developed as an oceanic island or plateau (Krapez, 1993; Eriksson et al., 1994). The 50-200 metre thick McPhee Formation, largely occupied by a shear zone (Van Haaften and White, 1998). Deformation along this zone involved pre-3.31 Ga extension, followed by E-vergent thrusting which was in turn followed by NE-tectonic transport, which may have led to early duplication of stratigraphy (Van Haaften and White, 1998).

The 3.47-3.45 Ga Duffer Formation comprises dacites, andesite, volcanoclastic and clastic sedimentary rocks (Barley et al., 1984). Deposition of these volcanic rocks and volcanoclastic sediments of the Duffer Formation may have occurred in half-grabens bounded by extensional growth faults in the Coongan Greenstone Belt (Zegers et al., 1996) and the Coppin Gap Greenstone Belt (Nijman et al., 1998a), but the extent of the halfgraben development is not clear (comments by A. Hickman and by S.White at 4th IAS Conference, Perth 2001). Coeval ENE-WSW extension may have caused development of a kms-wide detachment zone at the interface between the Shaw Granitoid Complex and the supracrustal sequence of the Coongan Belt, the Split Rock Shear Zone (Zegers, 1996; Zegers et al., 1998). The structures and kinematics of this shear zone indicated that solid-state diapirism cannot have been the sole mechanism for development of the Shaw Granitoid Complex and that doming was associated with crustal scale, uni-directional extension. Extension in the upper crustal sequences caused growth faulting and deposition of the Duffer Formation in the Coongan Belt (Zegers, 1996; Zegers et al., 1998). These workers have related extension to regional unidirectional far-field stresses, whereas Nijman and co-workers (1998a) envisaged the growth faults to have formed in a caldera collapse type setting.

Based on the calc-alkaline geochemistry of the felsic volcanic rocks of the Duffer Formation and coeval TTG suites in the Shaw Granitoid Complex, the petrogenetic process has been related to either subduction of mafic crust, or melting at the base of a thickened crust (Barley et al., 1984; Bickle et al., 1993; Smithies, 2000). Based on this geochemical character, and in combination with the nature of the volcanoclastic sediments, these rocks are proposed to have formed near volcanic centres similar to those observed in and around present day volcanic arcs, or back-arc settings (Hickman, 1983; Barley et al., 1984; DiMarco and Lowe, 1989a). A continental rift setting, either induced by plate-interaction or by collapse, or a back-arc basin setting, has been considered (Zegers, 1996), based on the (i) uni-directional extension on the Split Rock Shear Zone, (ii) extension of continental crust, (iii) syn-extensional deposition, and (iv) the geochemical signature of the Duffer Formation. Smithies (2000), however, has emphasised that the composition of the 3.45 Ga TTG suites from the Shaw Granitoid Complex does not provide evidence for modern-style subduction processes, and that, in general, melting at the base of a thickened crust may be more appropriate than subduction to form Archaean TTG suites.

After deposition of the Duffer Formation, a 4-5 km thick, dominantly mafic but overall bimodal

Figure 1.3 Overview of the stratigraphic units, plutonic rocks, and an indication of their age constraints for the Marble Bar Domain after Hickman (1983) and Van Kranendonk and Morant (1998). See also figure 4.1 for more detail on the Salgash Subgroup. See figure 3.2 for more chronological data. Ages are SHRIMP U-Pb zircon ages (Ma) if not otherwise indicated. References to ages are: (a) Arndt et al. (1991), (b) Van Kranendonk and Collins (1998), (c) Buick, unpubl. data, in: Van Kranendonk 1998), (d) McNaughton et al. (1993), (e) Thorpe et al. (1992), (f) Buick et al. (1995), (g) Sm-Nd, Hamilton et al. (1981), (h) McNaughton et al. (1988), (i) Nelson (2000), (j) Nelson (1999), (k) Zegers (1996), (l) Nelson (1998), (m) Barley et al. (1998), (n) Williams and Collins (1990), (o) Barley and Pickard (1999).

sequence of the Salgash Subgroup was deposited (See figure 1.3). The base comprises the dominantly sedimentary units of the Towers Formation. Superposed is the largely basaltic Apex Basalt, overlain by the Strelley Pool Chert. The latter is overlain by the Panorama Formation of dacites and rhyodacites, in the Kelly Belt dated at 3417 ± 9 Ma and 3433 ± 2 Ma (Barley et al., 1998a; Nelson, 2000). Geochemical data from the Panorama Formation has shown that it was generated by partial melting of garnet-bearing mafic rocks, possibly by melting of subducted mafic crust (Barley et al., 1984; Barley et al., 1998a). The Panorama Formation is overlain by the Euro Basalt, a sequence of alternating basaltic units and thin cherts. A recent finding of a 3346 Ma zircon population (together with smaller populations of 3363, 3659 and 3311 Ma) in a silicified felsic tuff or volcaniclastic sandstone one kilometer from the top of the Euro Basalt in the Kelly Belt (Nelson, 2001) was interpreted to represent the eruptive age of the tuff (M. Van Kranendonk and L. Bagas, Geological Survey of Western Australia, unpubl. data. In: Van Kranendonk et al., 2002). This, in combination with the age of xenocrystic zircons in overlying units (Nelson, 1998, 1999) led Van Kranendonk et al. (2002) to suggest that deposition of the Euro Basalt has occurred over a period from at least ca. 3395 to possibly 3325 Ma.

The Salgash Subgroup has been proposed to have developed in an extensional, dominantly subaqueous setting, possibly a submerged continental platform (Barley, 1993; Krapez, 1993; Eriksson et al., 1994).

1.4.2.3 Development during the Wyman episode (3.32 -3.29 Ga)

The tectonomagmatic development after deposition of the Salgash Subgroup is represented by rocks of the Wyman episode (Nelson et al., 1999), ranging in age from ca. 3325 Ma to 3290 Ma. It involved deposition of the felsic volcanic rocks of the Wyman Formation at 3325-3315 Ma (Thorpe et al., 1992; McNaughton et al., 1993; Barley and Pickard, 1999). On the basis of their interpretation of the above dates, Van Kranendonk et al. (2002) have recently assigned the Wyman Formation and the Euro Basalt to the newly defined Kelly Subgroup to form the upper Warrawoona Group. Intrusions of TTG suites of Wyman age constitute up to 75% of the Mt Edgar Granitoid Complex (Williams and Collins, 1990) and the larger part of the Corunna Downs Granitoid Complex to the south. Granitoids in the Mt Edgar Granitoid Complex may have formed by partial melting of older TTG suite rocks at a range of crustal depths, possibly represented by the 3.46-3.43 Ga Central Gneiss Complex in the Mt Edgar Granitoid Complex (Collins and Gray, 1990; Collins, 1993; Barley and Pickard, 1999).

The structural development of the Marble Bar Domain at ca. 3.32-3.31 Ga has traditionally been explained in terms of gravity driven solid-state diapirism of the granitoid complexes and inter-diapir sinking of greenstone keels, i.e. partial convective overturn of the crust (Hickman, 1983; Collins, 1989; Collins et al., 1998). Diapirism is believed to be the result of heating of the crust caused by a mantle plume: the sequence of events in the eastern Pilbara have been proposed to equal those associated with mantle plume impingement at the base of a continental crust (Collins et al., 1998). High-grade metamorphic assemblages (kyanite/sillimanite) that were found along the margin of the Warrawoona Greenstone Belt (Délor et al., 1991) were attributed the increased metamorphic conditions that occur in a sinking greenstone keel (Collins and Van Kranendonk, 1999).

Results from structural studies throughout the eastern Pilbara have shown that the structural development in the period associated with the Wyman episode, and possibly before, has involved compression. The associated compressional structures are briefly described below and further summarised in figure 2.6. A phase of generally E-W compression has caused regional metamorphism to amphibolite facies in the Tambourah Greenstone Belt (Bettenay et al., 1981; Bickle et al., 1985; Boulter et al., 1987). ^{40}Ar-^{39}Ar chronology has indicated that cooling occurred prior to ca. 3.20 Ga (Wijbrans and McDougall, 1987). Pre-3200 Ma deformation has been related to two phases of folding and thrusting causing an Alpine-style thickening of the crust, and development of high-pressure (kyanite/sillimanite-bearing) assemblages (Bickle et al., 1980, 1985; Boulter et al., 1987). A minimum age for folding and thrusting in the Coongan Greenstone Belt of ca. 3200 Ma was provided by ^{40}Ar-^{39}Ar chronology, but the exact timing for the onset and ending of this phase remained unclear (Zegers, 1996; Zegers et al, 1999). Additional evidence for E-W compression include: i) the ca. 3.34 Ga Warrery Shear Zone along the margin of the Coongan Greenstone Belt and the Corunna Downs Granitoid Complex (Zegers, 1996; Zegers et al., 1999), ii) inversion due to E-W compression of the extensional growth faults in the Coppin Gap Greenstone Belt prior to 3314 ± 13 Ma (Nijman et al., 1998a), iii) post-growth faulting, pre-doming, compressional folding of rocks of the Warrawoona Group around the North Pole Dome (Nijman et al., 1998b), iv) E and W-vergent movement along the Duffada and the McPhee Shear Zone (Van Haaften and White, 1998), and v) structures that formed during horizontal compression prior to ca. 3320 Ma have been observed in the overturned and brecciated cherts of the Towers Formation at the type-locality at Marble Bar Pool (Oliver and Cawood, 2001).

1.4.2.4 Development during the Roebourne episode (3.26-3.24 Ga)

The Roebourne episode involved extrusion of felsic volcanic units of the Sulphur Springs Group dated at ca. 3260-3240 Ma (Vearncombe et al., 1998) (See also figure 3.2 and references therein). Vearncombe et al. (op cit.) recognised a sub-marine extensional fault array in the volcanic rocks of the Strelley Belt. Coeval monzogranite intrusions were found in the nearby Strelley Granite and in most of the larger granitoid complexes. In the Mt Edgar Granitoid Complex this episode is represented by 3241 ± 3 Ma and 3243 ± 4 Ma monzogranites (Nelson, 1999). Biotite-monzogranites of this age are also found in the Muccan and Warrawagine Granitoid Complex (Nelson, 1998a, 1999). Structures within these granites and the relationship with the extension associated with deposition of the Sulphur Springs Group are unknown.

Barley and Pickard (1999) have suggested that the development of the sub-marine extensional fault array in the volcanic rocks of the Strelley Belt may be the continuation of extension at 3.32-3.31 Ga and may be related to back-arc extension.

1.4.2.5 Development during the Millindinna episode (2.95-2.93 Ga)

The first record of activity after the Roebourne episode is the intrusion of 2.95-2.93 Ga granitoids. Intrusion of these granitoids is associated with craton-wide transcurrent fault systems that have developed during regional WNW-ESE compression across the Pilbara granite-greenstone terrain, including the Marble Bar Domain (Van Kranendonk and Collins, 1998; Zegers et al.,

1998a). This phase was called the Millindinah episode (Nelson et al., 1999). This phase is held responsible for the development of the Lalla Rookh Basin and Whim Creek Greenstone Belt (Krapez and Barley, 1987). One of these craton-wide transcurrent fault systems, the Mulgandinah Shear Zone, defines the western margin of the Marble Bar Domain, and was active during sinistral shearing and granitoid intrusion at ca. 2.93 Ga attributed to a phase of regional (W)NW-(E)SE compression (Van Kranendonk and Collins, 1998; Zegers 1996). Pawley (2002) reported on the intricate relationship between shear and syntectonic sheet intrusion in the Mulgandinah Shear Zone.

Krapez and Barley (1987) noted that craton-wide strike-slip deformation requires externally imposed subhorizontal stresses at a regional scale (see also Sleep, 1992). The movement along bounding shears has been argued to reflect minor intra-craton reorganisation during cratonization, rather than interaction of (micro)plates and terrane accretion (Krapez and Barley, 1987).

1.4.2.6 The onset of the Fortescue episode

The Black Range dyke swarm forms a regional suite of mafic dykes throughout the Pilbara granite-greenstone terrain. These dykes have been associated with deposition of the Mt Roe flood basalts at the base of the Fortescue Group at ca. 2.80-2.75 Ga (Arndt et al., 1991; Wingate, 1999). At the time of intrusion of the Black Range dyke swarm, the main tectonomagmatic development of the Pilbara granite-greenstone terrain was completed.

Chapter 2

Structural evolution of the Warrawoona Greenstone Belt and adjoining granitoid complexes, Pilbara Craton, Australia: implications for Archaean tectonic processes

Published as: A. Kloppenburg, S.H. White and T.E. Zegers, 2001. Structural evolution of the Warrawoona Greenstone Belt and adjoining granitoid complexes, Pilbara Craton, Australia: implications for Archaean tectonic processes. Precambrian Research, 112, p. 107-147.

At the time of publication the isotopic ages reported in this thesis were not yet available

2.1 Abstract

The Pilbara granite-greenstone terrain (3.6-2.8 Ga), Australia, is quoted as the key area formed by passive, gravity-driven solid-state diapirism. But, contrasting views have recently been reported, which led us to re-examine the key area: the Warrawoona Greenstone Belt and the adjoining Mt Edgar and Corunna Downs granitoid complexes.

We found (i) an asymmetric, non-synclinal distribution of metamorphic grade and deformation intensity across the Warrawoona Greenstone Belt; (ii) a major shear zone on the margin of the Mt Edgar Granitoid Complex with a unidirectional stretching lineation pattern; (iii) a NE-trending transcurrent shear zone within the central gneiss complex of the Mt Edgar Granitoid Complex; (iv) coeval magmatic activity and doming of the granitoid complexes, and (v) the loss of about 9 km of stratigraphic units in the Warrawoona Greenstone Belt.

The area has had a prolonged history with at least four deformation phases between ca. 3.47 Ga and 2.8 Ga. The main domal geometry of the Mt Edgar Granitoid Complex was obtained during active NE-SW extension at 3.31 Ga (D_{X+2}), which appears to been in response to E-W compression. Possibly, the E-W compression resulted in crustal thickening and partial melting, probably of a 3.46-3.43 Ga granitic basement, causing crustal weakening, collapse and extrusion of

the 3.31 Ga granitoids. Extension at 3.31 Ga was accommodated by the Mt Edgar Shear Zone, a mid-crustal detachment, and by the associated Beaton Well Zone, which acted as a transfer zone within the gneissic basement. Doming of the Mt Edgar Granitoid Complex is interpreted to have occurred in an active, extensional core complex-type mode. An indication for deformation prior to 3.32 Ga comes from syntectonically intruded gabbro/diorite and dolerite sills within the Mt Edgar Shear Zone, which intruded possibly as early as 3.46-3.45 Ga (D_{X+1}). Ultramafic schistose xenoliths within the gabbro/diorite intrusions are the oldest observed deformed rocks, formed during D_x. Post-doming deformation involved NE-SW compression, D_{X+3}, followed by dextral transcurrent deformation, D_{X+4}, during NW-SE compression. The latter may be related to the regional phase of deformation at 2.93 Ga, during which the eastern and western Pilbara were amalgamated. Comparison of this deformation sequence to others within the Marble Bar Domain, suggests a common tectonic history from 3.46 Ga onward. Our structural and kinematic data, especially the 3.31 Ga unidirectional stretching lineation pattern, lead us to reject solid-state diapirism due to convectional overturn as the main cause for doming of the Mt Edgar Granitoid Complex. We suggest that the cause lies in a plate tectonic process.

2.2. Introduction

During the Archaean, radiogenic heat production is presumed to have been significantly higher than today (e.g. O'Nions et al., 1978; Richter, 1984; Jackson and Pollack, 1984; Davies, 1993) and, consequently, the mantle may have been hotter (e.g. Sleep, 1979; Nisbet and Fowler, 1983; Jackson and Pollack, 1984; Bickle, 1986; Pollack, 1986; Nisbet et al., 1993). If so, mechanically incoherent oceanic crust and the stable stratification of the upper mantle/lithosphere may have prevented modern-day plate-tectonic type processes (e.g. Vlaar, 1986; Hoffman and Ranalli, 1988; Davies, 1992; Vlaar et al., 1994) and the early tectonic development may have been dominated by mantle plumes (e.g. Fyfe, 1978; Campbell et al., 1989; Campbell and Griffiths, 1992; Hill et al., 1992). Solid-state diapirism has been proposed to be the crustal expression of a mantle plume (Choukroune et al., 1995, Chardon et al., 1998, Collins et al., 1998). Hence, if the crustal development of all Archaean terrains can be explained solely in terms of solid-state diapirism, then plate-tectonics, or a form of plate tectonics, need not be inferred.

The Pilbara Craton in NW Australia contains one of the oldest and best exposed Archaean granite-greenstone terrains, with a history of thermo-tectonic activity from at least 3.6 Ga to circa 2.8 Ga (e.g. Hickman, 1984; Barley, 1993; Krapez, 1993; Buick et al., 1995; Zegers et al., 1996; Krapez and Eisenlohr, 1998; Barley and Pickard, 1999; Nelson et al., 1999). This terrain, in particular the eastern part, is characterised by an outcrop pattern of ovoid granitoid complexes and skirting greenstone belts (Figure 2.1). Traditionally, the development of this area has been regarded in terms of solid-state diapirism associated with convective overturning of the crust (Hickman, 1983, 1984; Collins, 1989; Collins et al., 1998). In this model, density inversion within the crust causes 'passive' or body-force driven deformation, which does not require rigid plates and plate boundary stresses, and therefore the Pilbara has been quoted as field evidence for a non-plate tectonic

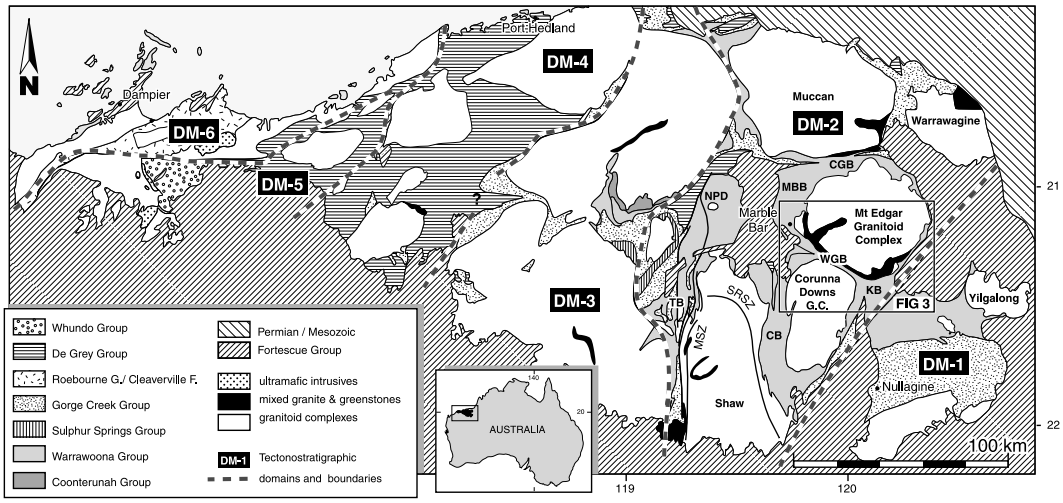

Figure 2.1 Generalised geological map of the Pilbara granitoid-greenstone terrain showing the distribution of the ovoid granitoid complexes, the distribution of the seven stratigraphic groups that constitute the greenstone belts, the relatively undeformed rocks of the Fortescue Group and the Phanerozoic cover rocks (after Hickman, 1983; Van Kranendonk and Morant, 1998; Buick et al., 1995). Subdivision into six tectonostratigraphic domains is after Krapez and Barley (1987); Krapez (1989); Krapez (1993) and Smith et al., (1998). The study area is situated in Domain 2, the Marble Bar Domain. The greenstone belts of this domain are: TB=Tambourah Belt, CB=Coongan Belt, NPD=North Pole Dome, MGB=Marble Bar Belt, WGB=Warrawoona Belt, CGB=Coppin Gap Belt and KB=Kelly Belt. MSZ=Mulgandinah Shear Zone, SRSZ=Split Rock Shear Zone.

behaviour of the Earth during the Archaean (Choukroune et al., 1995, Collins et al., 1998). However, results from geochemical, sedimentological and structural studies (e.g. Bickle et al., 1980, 1985; Krapez, 1984; Boulter et al., 1987; Krapez and Barley, 1987; Krapez, 1993; Zegers, 1996; Zegers et al., 1996; Van Haaften and White, 1998; White et al., 1998; Barley and Pickard, 1999), are more compatible with a development in which regional horizontal tectonics, involving both extension and compression, are the dominant cause for deformation, consistent with a plate-tectonic interpretation, which raises the question: can these models be reconciled?

In previous studies, structures in, and kinematics of, the Warrawoona Greenstone Belt and the adjoining Mt Edgar and, to a lesser extent, Corunna Downs Granitoid Complexes, are proposed to be similar to those predicted by numerical and analogue models of passive, gravity driven, solid-state diapirism (Collins, 1989; Collins et al., 1998). These models predict a characteristic combination of structures, including a concentric shear zone at the diapir margins, with radiating stretching lineations plunging away from the diapir centre and diapir-up kinematics (Dixon, 1975; Schwerdtner and Tröeng, 1977; Schwerdtner et al., 1978; Dixon and Summers, 1983; Cruden, 1988). Structures within the greenstones of the western Warrawoona Belt are explained to have formed as part of an inter-diapir 'plunging synform', with a strong linear fabric in the area of maximum sinking (Collins, 1989; Collins and Teyssier, 1990). An alternative model was proposed for doming of the Shaw Granitoid Complex and deformation of the adjoining Coongan Greenstone Belt (Figure 2.1), a model which has been likened to that of a metamorphic core complex (Zegers,

1996; Zegers et al., 1996). This model, like solid-state diapirism, predicts a shear zone on the margin of the dome. The structures within a shear zone related to a core complex, however, are distinctly different from those of solid-state diapirism; most importantly, the stretching lineations show a uni-directional pattern.

The question arises whether there is a fundamental difference between the origin of the structures as reported by Collins (1989) and Collins et al. (1998) for the Warrawoona Greenstone Belt and the adjacent granitoid complexes, and those from neighbouring areas, or, how the relative roles of vertical and horizontal tectonics may have been different in different areas. To answer this question we have re-investigated the structures in, and kinematics of, the Warrawoona Belt and its margins with the bounding batholiths. The results are presented and discussed below.

2.3 Geological setting of the Warrawoona Belt and adjacent granitoid complexes

2.3.1 Introduction

The supracrustal sequence that constitutes the Pilbara greenstone belts, has traditionally been described as forming a 'layer cake stratigraphy', the Pilbara Supergroup, that can be correlated throughout the craton (Hickman, 1983). This stratigraphy has since then been extended and refined (Hickman et al., 1990; Horwitz, 1990; Buick et al., 1995; Van Kranendonk and Morant, 1998). Subsequent geochronological, sedimentological and structural studies, have reported inconsistencies in the correlation of stratigraphic units, due to lateral facies changes and stratigraphic repetition. More recently, workers have advocated a tectono-stratigraphic approach, in which the Pilbara granite-greenstone terrain is divided into six tectono-stratigraphic domains (Figure 2.1), each with a specific tectonic history and stratigraphic record (Krapez and Barley, 1987; Barley, 1993; Krapez, 1993; Barley et al., 1998a; Krapez and Eisenlohr, 1998; Smith et al.,1998). Our study area forms the central part of Domain 2, the Marble Bar Domain.

In the Marble Bar Domain the supracrustal units belong to the lithostratigraphic Warrawoona, Gorge Creek, De Grey and Fortescue Groups (Hickman, 1983, 1990). Because the type-sections of the individual lithostratigraphic formations and subgroups that constitute the supracrustal sequence of the studied area (Warrawoona and Gorge Creek Groups) are located in the Marble Bar Domain, we will use the lithostratigraphic nomenclature (Figures 2.1 and 2.2). The base of the supracrustal sequence is formed by the >4.1 km thick Talga Talga Subgroup, which is overlain by the Duffer Formation (about 5 km) and the Salgash Subgroup (>5.5 km). These are unconformably overlain by the Wyman Formation (1 km), which is in turn unconformably overlain by the Gorge Creek Group. Only near the margin with Domain 3, the Sulphur Spring Group crops out (Van Kranendonk and Morant, 1998; Van Kranendonk, 1998, 1999). This group is stratigraphically situated above the Salgash Group and below the Gorge Creek Group. Only the units that are dominated by felsic volcanic rocks (Duffer and Wyman Formation) have been reliably dated. They have SHRIMP crystallization ages of 3470-3450 (Pidgeon, 1978a; Thorpe et al., 1992;

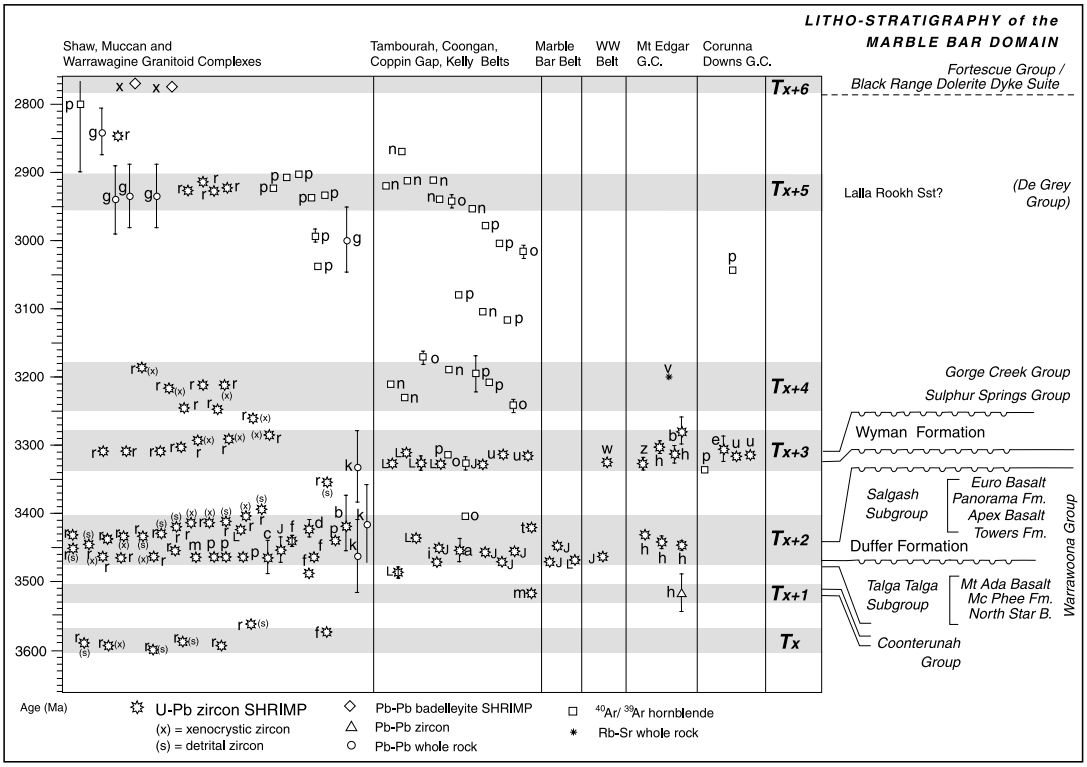

Figure 2.2 Published geochronological data for the Marble Bar Domain (Domain 2). Seven thermo(tectonic) events are recognised in this domain and are marked Tx to TX+6. See text for explanation. Lithostratigraphy after Hickman (1983); Buick et al. (1995); Van Kranendonk and Morant (1998). Geochronology after a=Pidgeon (1978a), b=Pidgeon (1978b), c=Williams et al. (1983), d=Froude et al. 1984, e=Pidgeon (1984), f=McNaughton et al. (1988), g=Bickle et al. (1989), h=Williams and Collins (1990), i=Thorpe et al. (1990), j=Thorpe et al. (1992), k=Bickle et al. (1993), l=Mc Naughton et al.(1993), m=Buick et al. (1995), n=Wijbrans and McDougall (1987), o=Davids et al. (1997), p=Zegers (1996), q=Nelson (1999), r=Nelson (1998a), s=Nelson (2000), t=Barley et al., (1998a), u=Barley and Pickard (1999), v=Collins and Gray (1990), w=Buick et al., in press, x=Wingate (1999), z=Collins et al. (1998).

McNaughton, 1993; Barley et al., 1998a) and 3325-3315 Ma (Thorpe et al., 1992; McNaughton et al., 1993; Barley and Pickard, 1999; Buick et al, in press), respectively. The Sulphur Springs Group is dated at ca. 3240 Ma (Buick et al, in press), which provides a maximum age for the Gorge Creek Group. A thin felsic intercalation within the dominantly basaltic Salgash Subgroup in the Coppin Gap Belt has been dated at 3454 ± 1 Ma (Thorpe et al., 1992). In the North Pole Dome (Figure 2.1), the Panorama Formation at the base of the Salgash Subgroup is dated at 3458 ± 2 Ma (Thorpe et al., 1992). This indicates that the Salgash Subgroup is only slightly younger than the Duffer Formation.

Components in the five granitoid complexes and in the North Pole Dome in the Marble Bar Domain (see figure 2.1) dominantly have TTG affinity and are generally similar in age to the aforementioned two felsic volcanic sequences (3.47-3.45 and 3.32-3.31 Ga, Figure 2.2). Components of different age and without extrusive equivalent are found in the Marble Bar

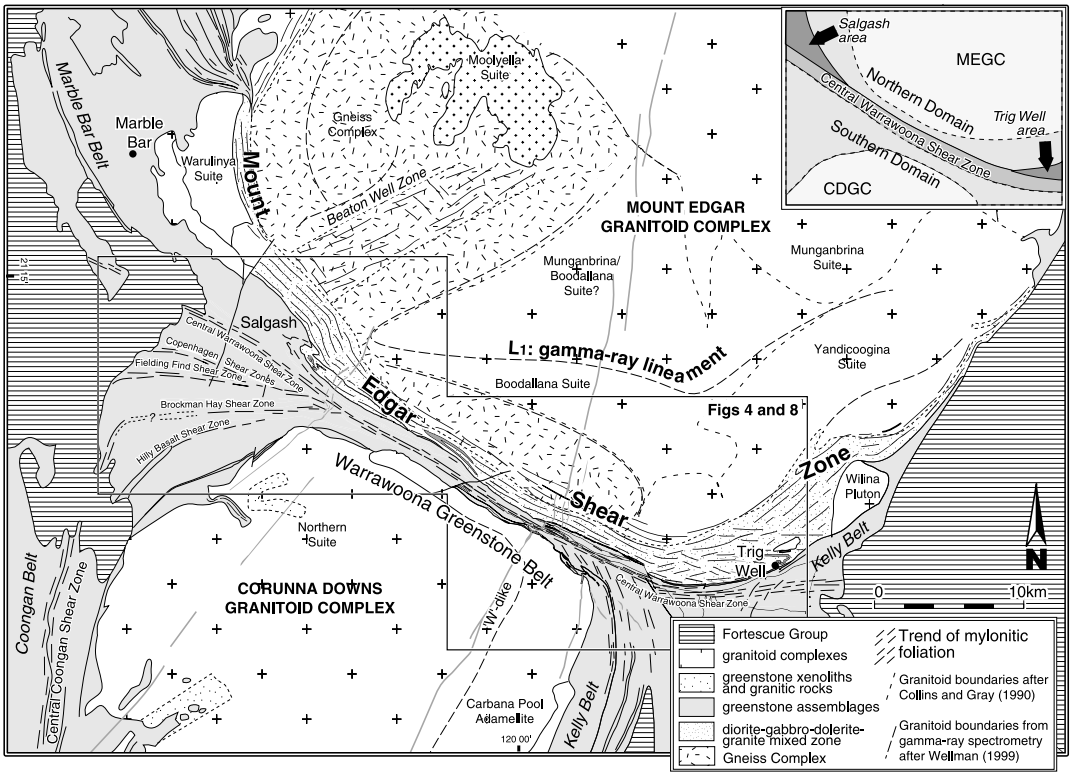

Figure 2.3 Overview map of the studied area with the trend of the main shear zones and the area of detailed mapping indicated. The Central Warrawoona Shear Zone divides the Warrawoona Belt into a Northern and Southern Domain (see inset). The Trig Well and the Salgash Areas are bound between the Mt Edgar Shear Zone and the Central Warrawoona Shear Zone in the east and west, respectively. The outlines of the individual granitoid components that constitute the Mt Edgar and Corunna Downs Granitoid Complexes as determined by geochemistry (Collins and Gray, 1990) and by gamma-ray spectrometry (Wellman, 1999) are marked.

Domain. The Warrawagine Granitoid Complex comprises grey gneisses, whose ca. 3600 Ma protolith age is amongst the oldest in the Pilbara (Nelson et al., 1999). In the Muccan Granitoid Complex, 3.25-3.20 Ma granites are found (Nelson, 1998a) and although supracrustal rocks with a similar age, the Sulphur Springs Group, have been identified on the margin with Domain 3, in the rest of the Marble Bar Domain these have not been observed. But, similar ^{40}Ar-^{39}Ar cooling ages were found in the Marble Bar, Tambourah and Coongan Belts (Wijbrans and McDougall, 1987; Davids et al., 1997; Zegers et al., 1999). Those ages have been interpreted to reflect cooling after a regional tectonic event. Interestingly, a similar age (ca 3200 Ma) is reflected by the Rb-Sr isotope systematics of the 3.4 and 3.3 Ga Mt Edgar Granitoid Complex components (Collins and Gray, 1990), an age which was interpreted to reflect either slow cooling and late closure or disturbance and resetting of the system (Williams and Collins, 1990). An additional component is recognised in the orthogneisses of the Mt Edgar Gneiss Complex (Figure 2.3), which yield ca. 3450-3430 Ma protolith ages (see figure 2.4a). Granitoids with similar ages have been in the Shaw Granitoid

Complex (Nelson, 1999). This is younger than the 3470–3450 Ma age of the Duffer Formation which cannot be its extrusive equivalent (Williams and Collins, 1990). However, the 3450–3430 Ma ages are similar to the ages of zircons from felsic volcanic rocks (mapped as Duffer Formation) in the McPhee Dome (Domain 1) and the Kelly Belt, dated by Barley et al. (1998a).

Seismic refraction data of the Pilbara Craton show a two-layered crust with a major discontinuity at 14 km depth, interpreted to be the base of the granite-greenstone layer (Drummond, 1983). Recent magnetic and gravity anomaly data were used to determine the shape, slope and depth of the granitoid bodies and greenstone belts. Most granitoid complexes comply to a starting model, in which the granitoids are assumed to be 14 km deep cylindrical bodies with subvertical sides (Wellman, 1999), but, with diameters of 40 to 60 km, the granitoid complexes should be regarded as oblate complexes, or discs, rather than vertical cylinders.

The available ages in the Marble Bar Domain show at least seven time-clusters which reflect thermal events, including thermo-tectonic events as will be discussed below, within the 800 million year time span from 3.6 to 2.77 Ga. We have labelled them T_x to T_{X+6}, (Figure 2.2) (cf. Barley, 1999; Blewett and Huston, 1999a, 1999b).

2.3.2 The Warrawoona Greenstone Belt

The greenstone sequence of the Warrawoona Greenstone Belt consists mainly of ultramafic, mafic and felsic volcanic rocks. SHRIMP U-Pb zircon ages indicate ages similar to the Duffer Formation, Salgash Subgroup and Wyman Formation (Barley and Pickard, 1999; McNaughton et al., 1993; Thorpe et al., 1992). A felsic volcanic unit in the Kelly Belt, traditionally correlated to the Duffer Formation, has been dated at 3417 ± 9 Ma (Barley et al., 1998a), raising doubt concerning the regional correlation. Units, corresponding the Talga Talga Subgroup have not been identified in this belt. Generally, the rocks are much more intensely deformed and attenuated than those of the neighbouring belts and deformation has resulted in steeply dipping bedding orientations and tectonic contacts between all lithological units. Rock distribution and younging directions in the least deformed volcanic rocks indicate a synclinal geometry (Collins and Teyssier, 1990; Hickman and Lipple, 1978).

2.3.3 The Mt Edgar and Corunna Downs Granitoid Complexes

The Mt Edgar and Corunna Downs Granitoid Complexes (Figure 2.3) contain various granitoid components. The Mt Edgar Granitoid Complex is dominated by trondhjemite-tonalite-granodiorite (TTG) intrusions, geochemically subdivided into six suites (Collins and Gray, 1990). Two of these, the Coppin Gap and Boodallana Suite, were dated at circa 3310 Ma (Williams and Collins, 1990) (Figure 2.5). An older, highly deformed, gneiss complex was identified in the southwestern part, with ca. 3430–3460 Ma protolith ages (Williams and Collins, 1990). Geochemical studies showed that this gneiss complex could be the source of TTG suites within the Mt Edgar Granitoid Complex (Davy and Lewis, 1981; Collins and Gray, 1990; Barley and Pickard, 1999). The relatively undeformed Moolyella Adamellite Suite in the centre of the gneiss complex and Wilina

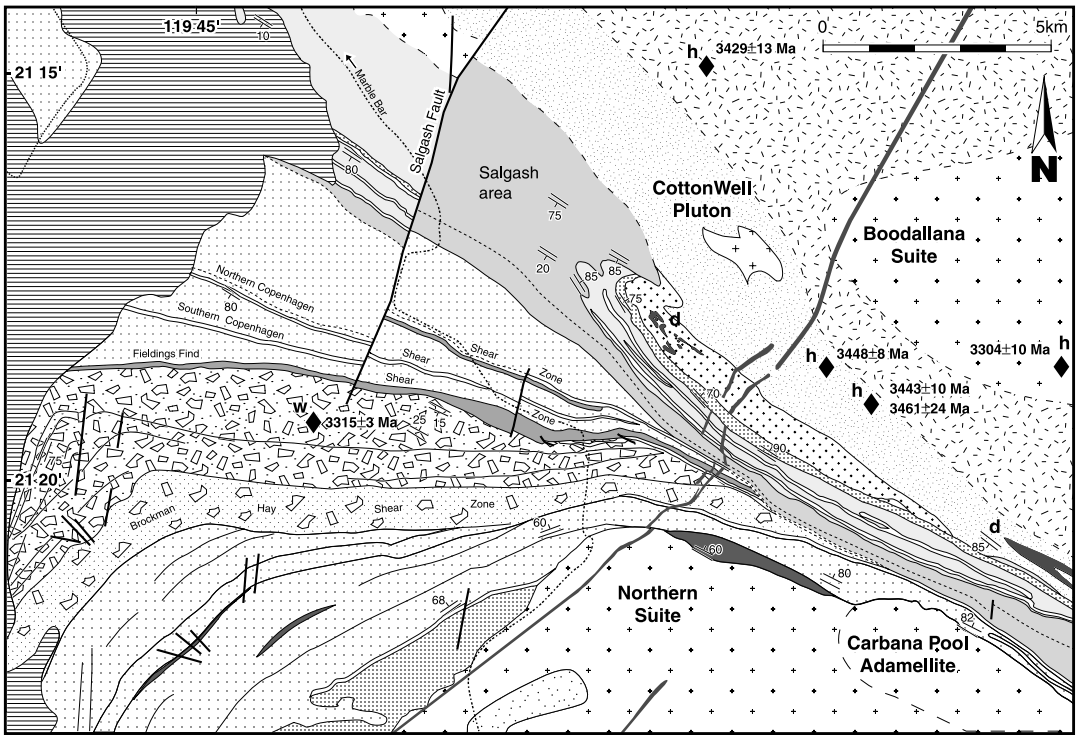

Figure 2.4a Lithological map of the western Warrawoona Greenstone Belt. Sites of published geochronological data are marked (for references see figure 2.2). See Figure 2.4b for legend.

Pluton on the margin of the Mt Edgar Granitoid Complex (Figure 2.5) are dated at <3240 ± 11 Ma and 3324 ± 6 Ma, respectively (Collins et al., 1998; Nelson, 2000). Recently, a gamma-ray spectrometry study of the Mt Edgar Granitoid Complex (Wellman, 1998) has largely confirmed Collins' subdivision, but identified an additional boundary, marked L_1 in figure 2.3, which separates the Boodallana Suite from the Munganbrina Suite. The Munganbrina Suite now appears to constitute more than half of the Mt Edgar Granitoid Complex. The crystallization age of the Munganbrina Suite is unknown.

The eastern and southern Corunna Downs Granitoid Complex mainly comprises 3.31 Ga granodiorite and biotite-monzogranite (Pidgeon, 1984; Barley and Pickard, 1999). The 3313 ± 9 Ma (Barley and Pickard, 1999) Carbana Pool Adamellite intruded at the contact with the Warrawoona and Kelly Belts (Figure 2.3). Older granitoids may occur in the western part, where no crystallization ages are available, and where contact-metamorphic hornblendes yield 3400 and 3340 Ma ^{40}Ar-^{39}Ar cooling ages (Davids et al., 1997; Zegers et al., 1999). The northern part of the Corunna Downs Granitoid Complex comprises a granodiorite suite, the Northern Suite, of unknown age.

2.3.4 Deformation

The Warrawoona Belt and the adjacent Mt Edgar Granitoid Complex have formed the key area for solid-state diapirism (Collins, 1989; Collins et al., 1998; Collins and Van Kranendonk, 1999). These workers relate structures such as recumbent folds, thrusts, and extensional faults within the Warrawoona Belt to the early stages of solid-state diapiric uplift of the Mt Edgar and Corunna Downs Granitoid Complexes (D_1), which initiated possibly as early as 3460 Ma (see figure 2.6). Ongoing doming and steepening of the supracrustal cover (D_2) was followed by the main stages of progressive diapirism at 3325-3315 Ma (D_4), during which a concentric shear zone developed around the Mt Edgar Granitoid Complex. A lineament within the Mt Edgar Granitoid Complex was explained as a non-diapiric structure (D_3 in Collins, 1989). Radial stretching lineations and an associated granitoid-up sense of shear were reported for this marginal shear zone (Collins, 1989; Collins et al., 1998).

Teyssier (1988) questioned diapirism as the dominant deformation model for the Warrawoona Belt and Mt Edgar Granitoid Complex, because the proposed model could not account for an observed change in deformation style 'from a 5 km thick mylonite zone to a few narrow detachment zones' along the marginal shear zone. Other studies within the Marble Bar Domain

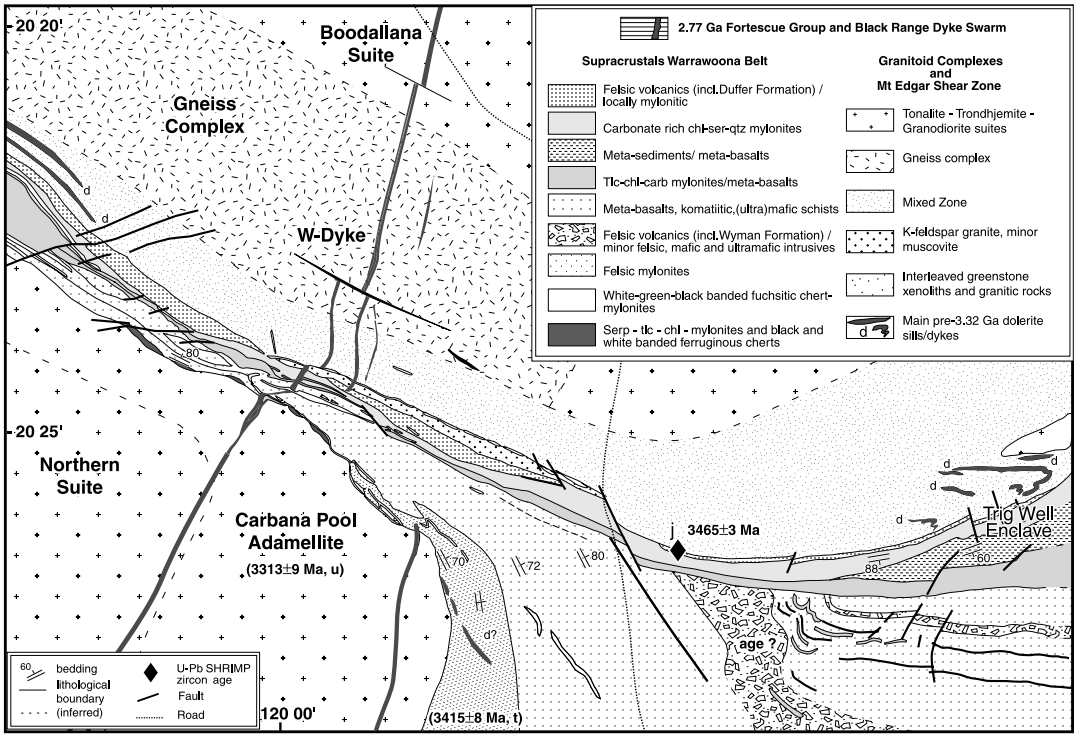

Figure 2.4b Lithological map of the eastern Warrawoona Greenstone Belt. Sites of published geochronological data are marked (for references see figure 2.2).

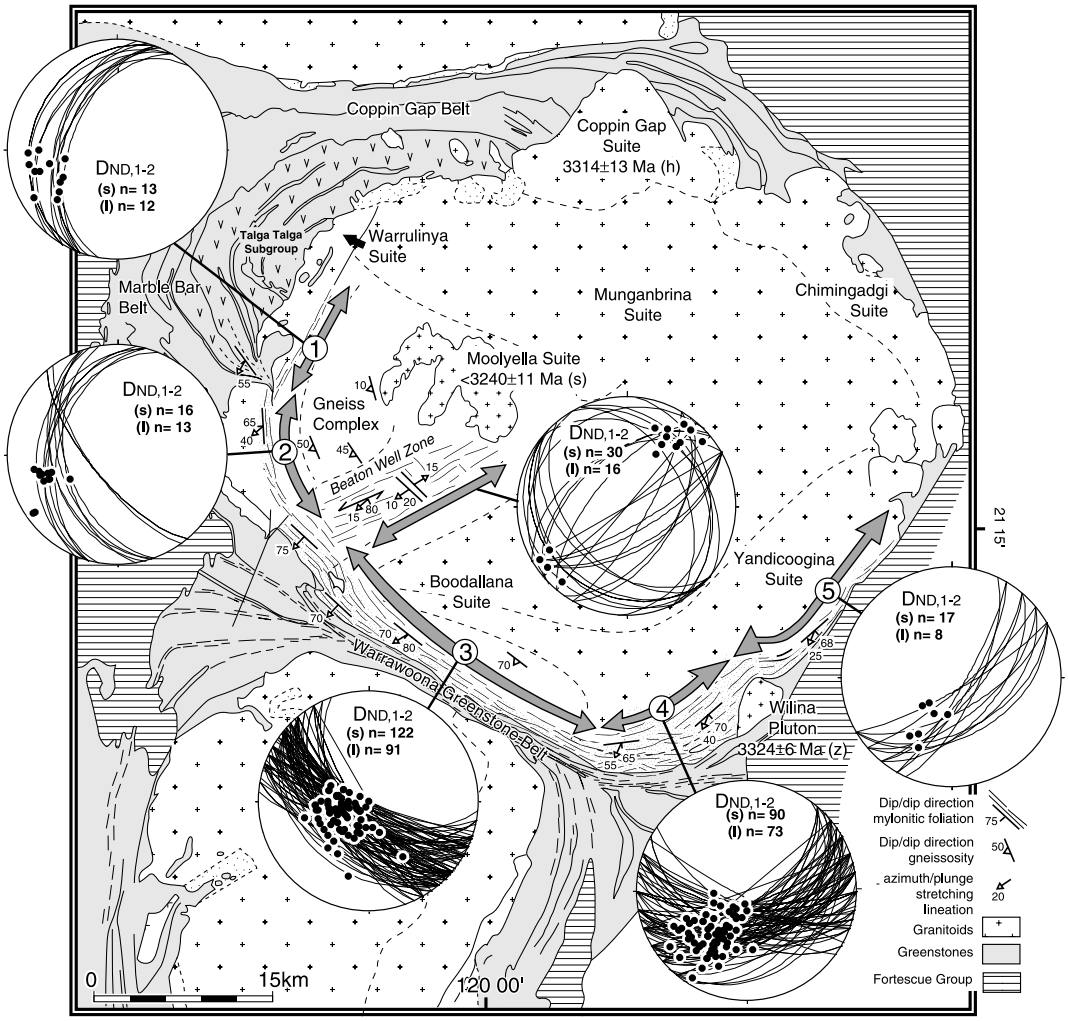

Figure 2.5 Structural trend map and stereographic projections (equal area) of the pre- and syn-3.31 Ga structures of the Northern Domain ($D_{ND,\,1}$ and $D_{ND,\,2}$). Stretching lineations, (l), show a constant SW azimuth, despite the variable orientation of the mylonitic foliations, (s), within the five sections of the Mt Edgar Shear Zone (1-5) and the Beaton Well Zone (6). References for geochronological data are in figure 2.2. Granitoid boundaries after Collins and Gray (1990) and Wellman (1999), see also figure 2.3.

reported non-diapiric structures, which are listed in figure 2.6. These include a metamorphic core complex-type dome, formed during active extension at 3.47-3.46 Ma in the Shaw Granitoid Complex area (Zegers, 1996; Zegers et al., 1996); an Alpine-style fold and thrust belt in the Tambourah Belt developed before deposition of the (<3240 Ma, Van Kranendonk and Morant, 1998) upper Gorge Creek Group sediments (Bickle et al., 1980, 1985; Boulter et al., 1987); and pan-cratonic strike-slip zones formed during craton-wide NW-SE compression at 2.95-2.93 Ga (Krapez and Barley, 1987; Zegers et al., 1998a; Van Kranendonk and Collins, 1998).

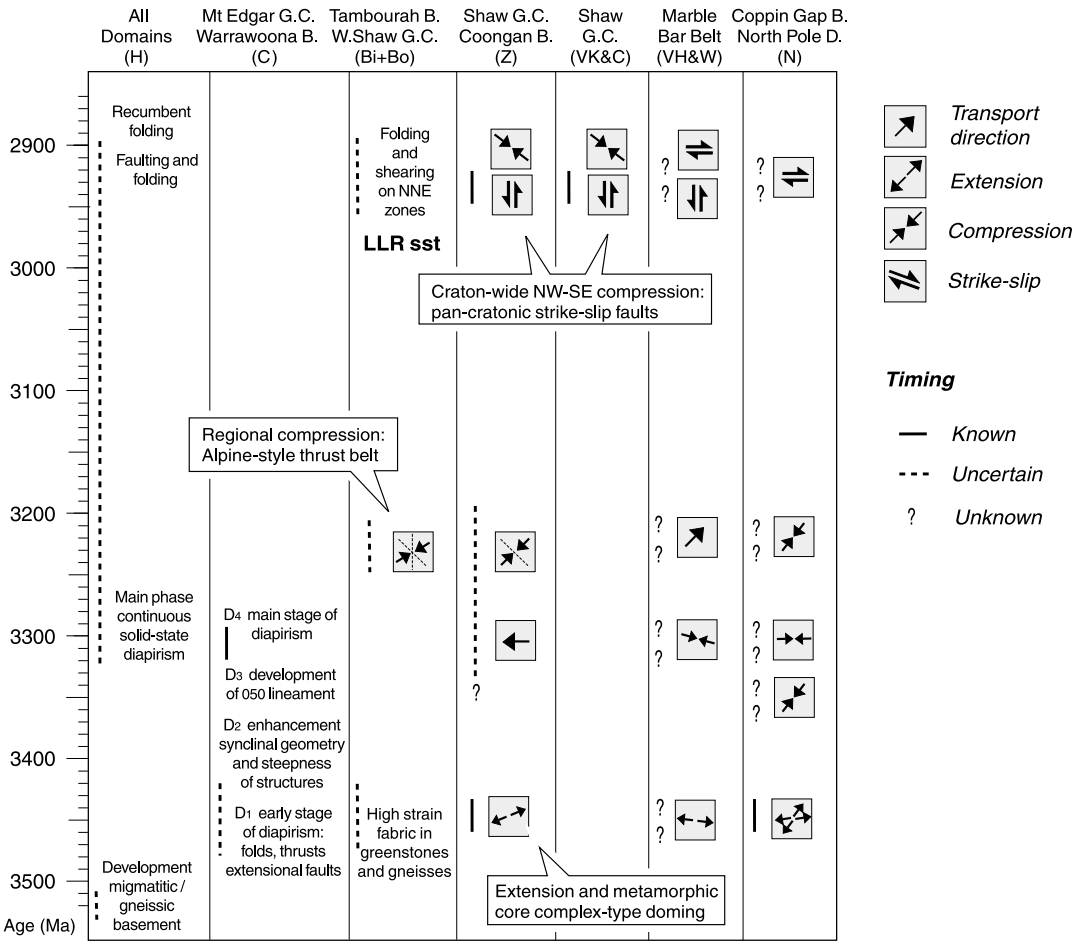

Figure 2.6 Overview of published structural studies within the Marble Bar Domain, see figure 2.1 for locations of greenstone belts (B.) and granitoid complexes (G.C.). Letters refer to references of structural studies: H=Hickman (1983); C=Collins (1989), Collins et al. (1998); Bi=Bickle et al. (1980, 1985); Bo=Boulter et al. (1987); Z=Zegers (1996), Zegers et al. (1996); VK&C=Van Kranendonk and Collins (1998); VH&W=Van Haaften and White (1998); N=Nijman et al. (1998).

2.3.5 Metamorphism

Metamorphism of supracrustal assemblages of the Marble Bar Domain is generally low-grade, greenschist facies, but may reach amphibolite facies adjacent to granitoid complexes (Hickman, 1983). High-pressure assemblages are scarce and have been reported for two areas only. On the highly deformed northern margin of the Warrawoona Belt, pre-, syn- and post-tectonic kyanite was interpreted to be the result of solid-state diapirism (Collins and Van Kranendonk, 1999). In this area, kyanite is overprinted by sillimanite and subsequent andalusite (Délor et al., 1991). In contrast, kyanite-bearing assemblages in the Tambourah Belt and western Shaw Granitoid Complex have

been interpreted to have formed, after crustal thickening, at the base of an Alpine-style orogenic belt (Bickle et al., 1985).

2.4 Structural and kinematic analysis within the Warrawoona Belt and its environs: Results

2.4.1 General statement

Because the supracrustal sequences of the Warrawoona Greenstone Belt are strongly deformed and attenuated, and geochronological data are insufficient to relate them to the stratigraphy, lithological rather then stratigraphic names are used for mapping (Figures 2.4a and 2.4b).

Deformation within the Warrawoona Belt is found to be strongly partitioned into shear zones, which are unevenly distributed across the belt (Figures 2.7, 2.8a and 2.8b). A major shear zone, the Central Warrawoona Shear Zone (CWSZ), which has been previously described as the synclinal axis of the belt (Collins, 1989; Collins and Teyssier, 1990), was found to mark the boundary between two areas with a different tectono-thermal history: the Northern and Southern Domain (Figure 2.3). We will present our results for the CWSZ first, followed by those of the Northern and Southern Domain, respectively.

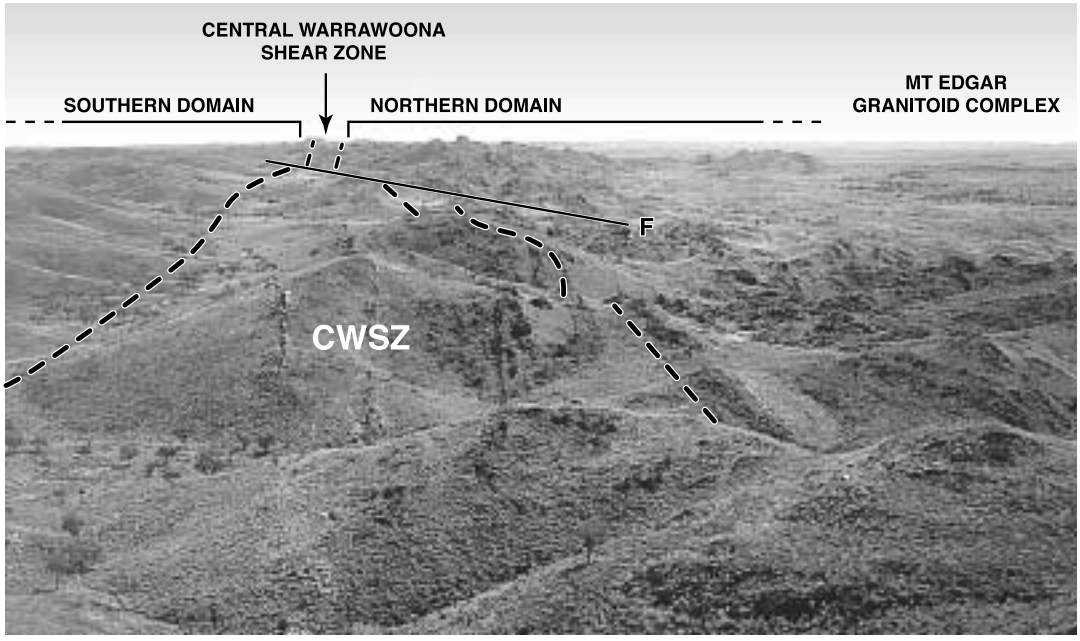

Figure 2.7 View to the NW along the Warrawoona Greenstone Belt. The Central Warrawoona Shear Zone forms the contact between the rocky, strongly deformed Northern Domain and the rounded hills of the moderately deformed, basalt dominated unit of the Southern Domain.

2.4.2 The Central Warrawoona Shear Zone (CWSZ)

The CWSZ is a subvertical shear zone which varies from 100 to 300 metres in width and is traceable for at least 50 km (see figures 2.3, 2.8a and 2.8b). The mylonites that define the CWSZ consist predominantly of highly altered and foliated talc-carbonate and chlorite rocks, but also comprise minor felsic mylonites and finely laminated chert. The foliation hosts two types of boudin: relatively undeformed metre-scale ankeritic and dolomitic boudins locally containing pseudomorphosed spinifex textures, and 10–100 metre scale boudins of diverse rock types, which are also mylonitised and contain a complex set of structures. The host mylonites and the boudins exhibit different structures, which are attributed to six groups (1–6) based on overprinting relations, schematically illustrated in figure 2.9. The CWSZ truncates the shear zones of the Southern Domain and overprints part of the Mt Edgar Shear Zone (MESZ) in the most attenuated part of the belt.

The oldest structures are found in larger boudins throughout the CWSZ (Figure 2.9). Mafic schists and chert bands define metre-scale upright folds, which are refolded by steeply reclined folds both have a sub-vertical to steeply SW dipping axial planar foliation. The axial planar foliation commonly transposes the initial mafic schistosity, which we assume is an earlier metamorphic fabric. The resultant complex fold interference pattern is particularly well developed in thin mylonitised chert bands because of competence contrasts between rock types, especially in the strongly attenuated part of the Warrawoona Belt [locality 1]*, see figure 2.8b). Strongly developed intersection and stretching lineations are preserved parallel to the axes of both the upright and steeply reclined folds, but those associated with the reclined folds are dominant. The intensity of the axial planar foliation increases in those boudins closer to the northern edge of the CWSZ [locality 2], where it becomes parallel to the dominant mylonitic foliation of the Mt Edgar Shear Zone (see §2.3.3). Therefore, both groups of fold, and possibly also the pre-existing mafic schists, are interpreted to have formed in relation to the Mt Edgar Shear Zone and are designated to $D_{CWSZ,1}$ (see figure 2.10).

The above complex fold structures and associated foliations are overprinted by two sets of cm-wide shear zones, which display sinistral (Figure 2.11a) and dextral displacement [locality 3]. The subvertical orientation of these shear zones and the asymmetry of the displaced foliations indicate a transcurrent displacement, but related stretching lineations are not common. An overprinting relationship between the sinistral and dextral shears has not been recorded. Therefore, it is not clear if these two sets of shears record two separate events or if they are conjugate sets formed during a single episode of flattening across the CWSZ, in which case they may be related to the later stages of the above folding. We attribute these structures to $D_{CWSZ,2}$ (see figure 2.10). Closer to the northern margin of the CWSZ, boudins with a well-developed mylonitic foliation and stretching lineation have preserved an S-C fabric, indicating SW-up movement. These mylonites are neither folded nor overprinted by the aforementioned dextral and sinistral shear bands and are tentatively attributed to $D_{CWSZ,3}$ (Figure 2.10).

---

* *Bracketed numbers in the text refer to illustrative outcrops marked in the form surface maps of figures 2.8a and 2.8b.*

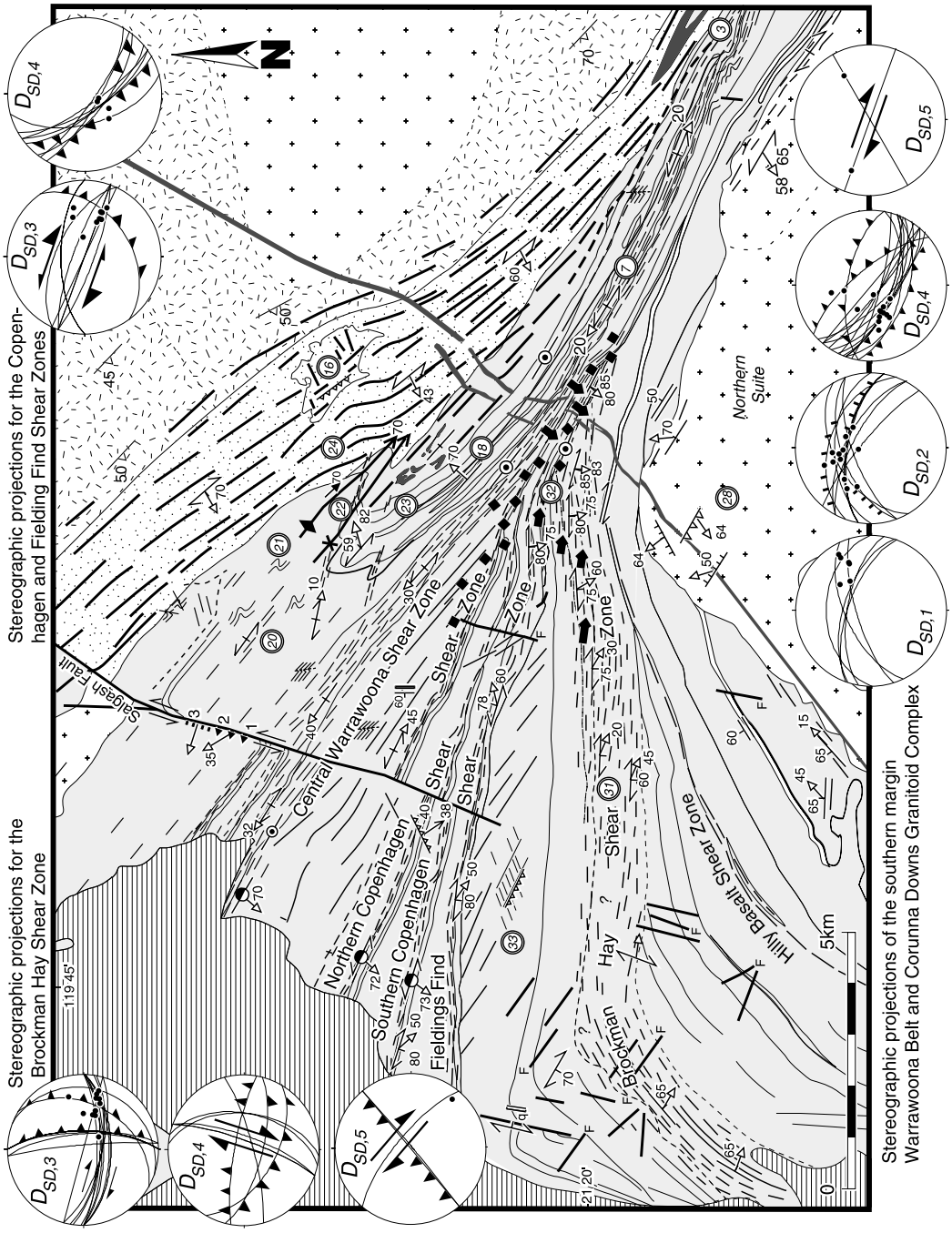

Figure 2.8 Form surface map of the Warrawoona Greenstone Belt and margins with the bounding granitoid complexes (a) northwestern part (b) southeastern part. The stereographic projections (equal area) contain the main foliations and

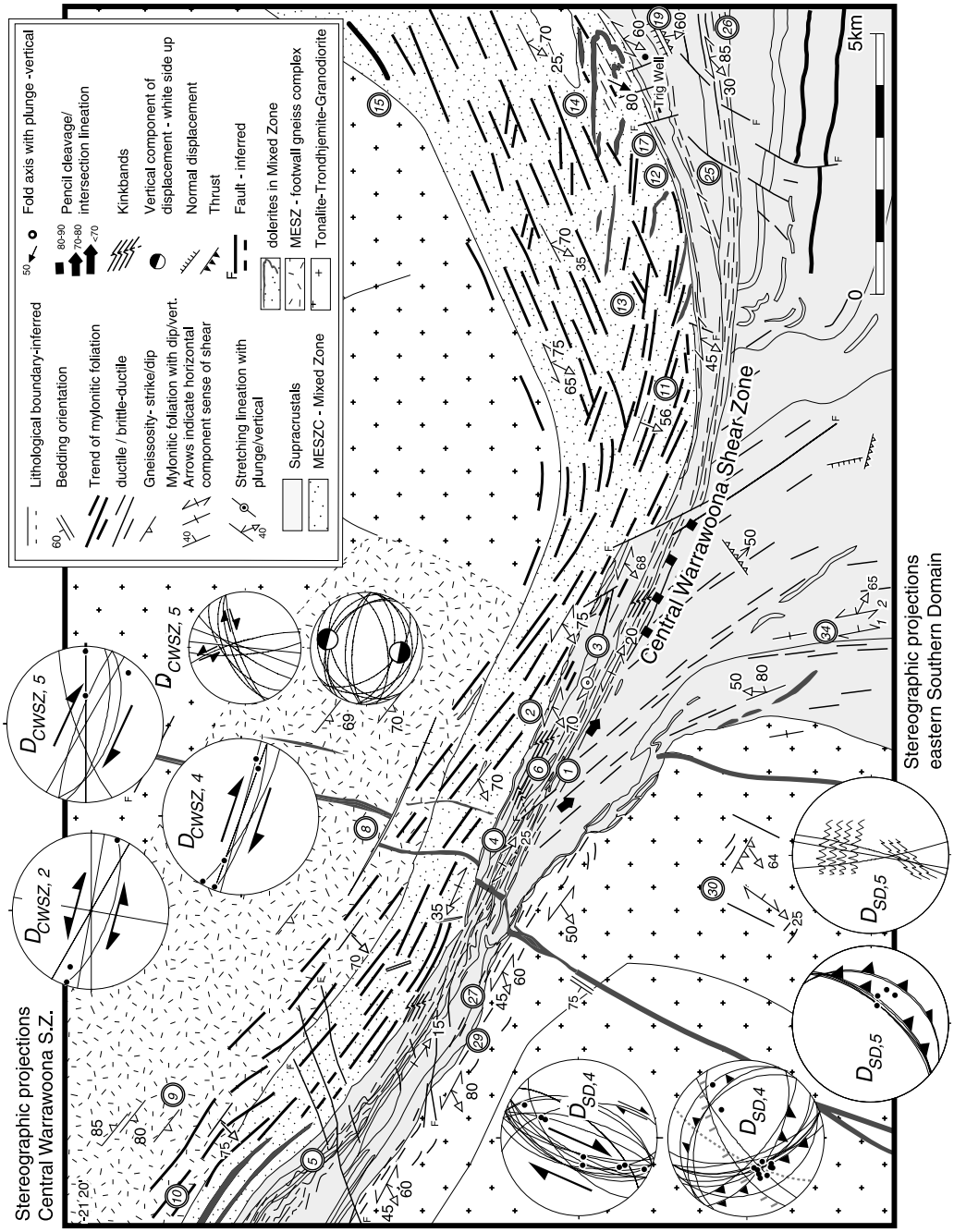

stretching lineations. Numbers refer to local deformation phases, referred to in the text. Legends apply to both 2.8a and 2.8b.

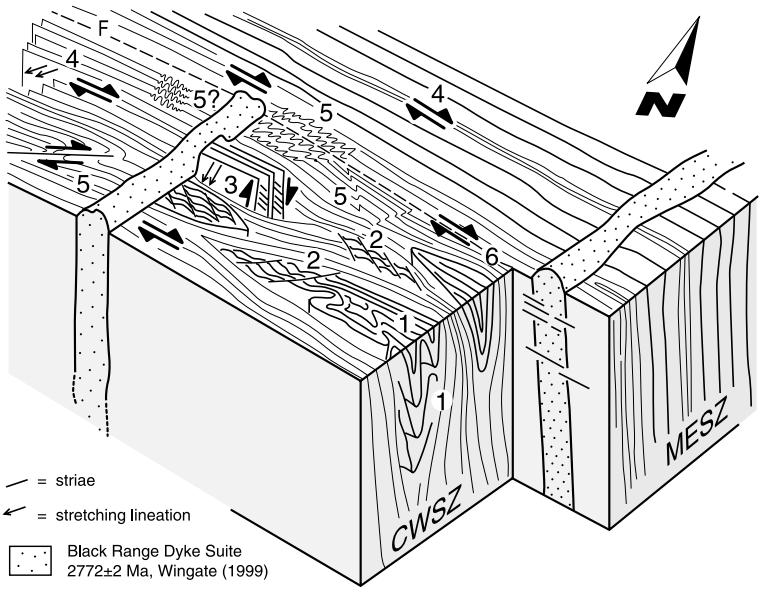

Figure 2.9 Schematic 3D illustration of structures, kinematics and overprinting relation within the Central Warrawoona Shear Zone. Numbers refer to the ordering of deformation phases within the shear zone. See text for explanation.

The WNW trending mylonitic foliation of the CWSZ, which hosts the above boudins, is subvertical and is dominated by chlorite and albite, indicating a greenschist facies metamorphic grade. A well-developed stretching and/or mineral lineation, formed by elongated chlorite pods, carbonates, quartz and, locally, elongated tremolite pods, pitches 15-30°, mainly to the west. The most widespread kinematic indicators associated with this lineation are asymmetric carbonate or quartz boudins, S-C fabrics, shear bands (C-C' fabrics) and cm-scale asymmetric folds with axes perpendicular to the associated stretching lineation [locality 4]. They all indicate an oblique dextral sense of shear (designated $D_{CWSZ,4}$, see figure 2.10). Where shear bands are well developed in the host mylonite, they give rise, locally, to an intense, steeply SW-plunging intersection lineation and rodding sub-parallel to the older steep stretching lineations in the MESZ boudins. On the northern margin of the CWSZ, especially in the finely foliated felsic mylonites of the MESZ, an ENE to E-W, striking foliation is seen. Locally, this foliation is found to be axial planar to dextral asymmetric folds in the more competent layers of the felsic mylonites ([locality 5], and see figure 2.11b). We interpret the fabric as an S-foliation, formed during the main phase of dextral shearing on the CWSZ ($D_{CWSZ,4}$, see figure 2.10).

Semi-brittle structures comprise conjugate sub-vertical ENE-trending dextral and NNW- to NNE-trending sinistral kinks and crenulations, which overprint the CWSZ host foliation ([locality 6], and see figure 2.11c). These structures, like those of the host mylonitic foliation, imply a NW-SE compressional setting, but the overprinting relationship and the more brittle nature has led us to assign them to a separate phase ($D_{CWSZ,5}$, see figure 2.10). Locally, N- to NNE-trending subvertical crenulations are observed [locality 7], which suggest a more WNW-ESE directed shortening, and which may indicate a separate deformation phase, or may be related to $D_{CWSZ,5}$. Narrow cataclasite zones with sub-horizontal slickensides have displaced the 'W' Dyke, member of the doleritic 2772 ±

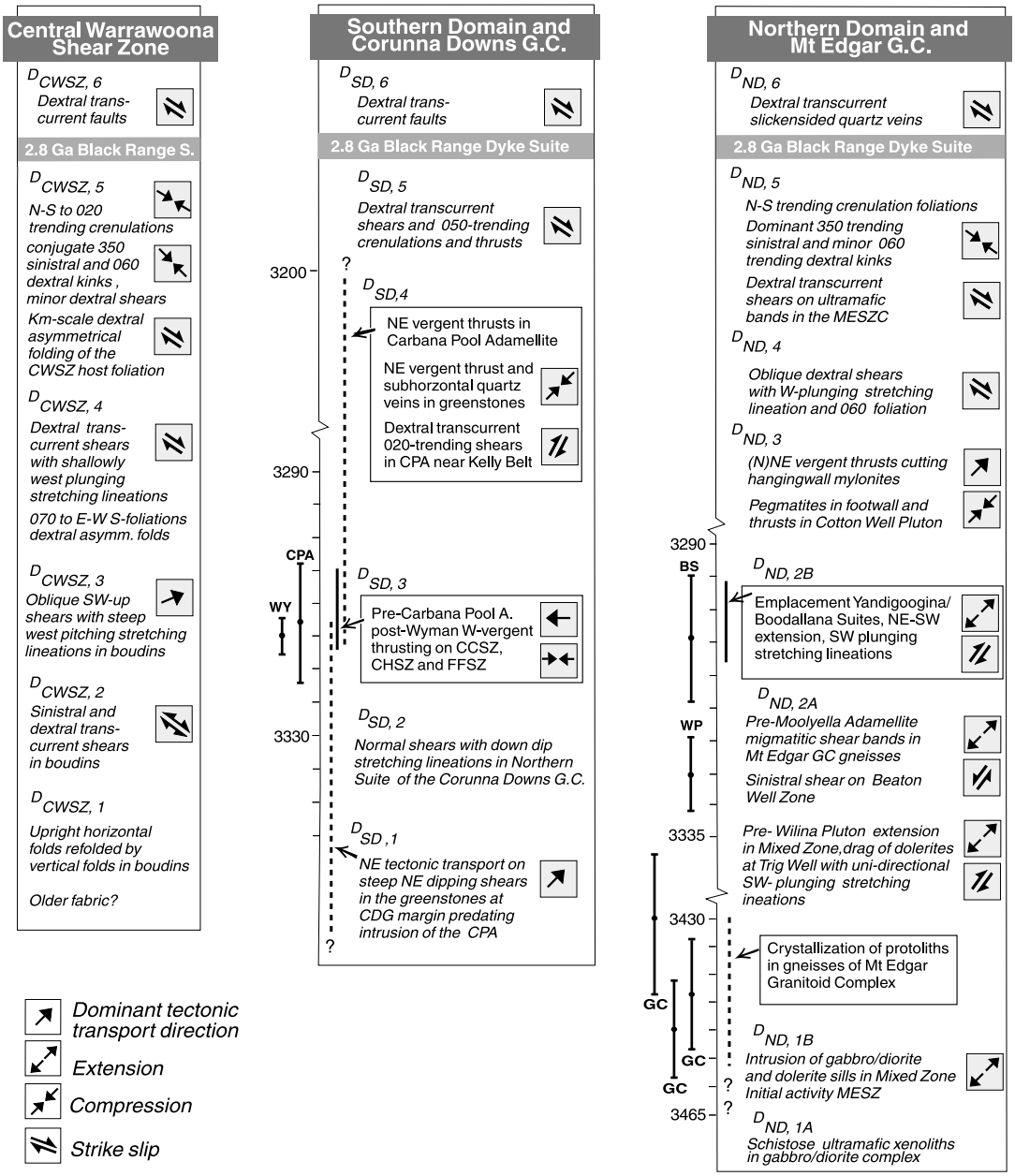

Figure 2.10 Summary of deformation events for each of the Domains within the Warrawoona Belt and for the Central Warrawoona Shear Zone. Structures with absolute time constraints are marked in squares, otherwise only relative ages apply. The age of constraining rock units are all SHRIMP, zircon ages. See figure 2.2 for references to geochronology. WY=Wyman felsic unit, CPA=Carbana Pool Adamellite, GC=Gneiss Complex protolith age, WP=Wilina Pluton, BS=Boodallana Suite, MA=Moolyella Adamellite.

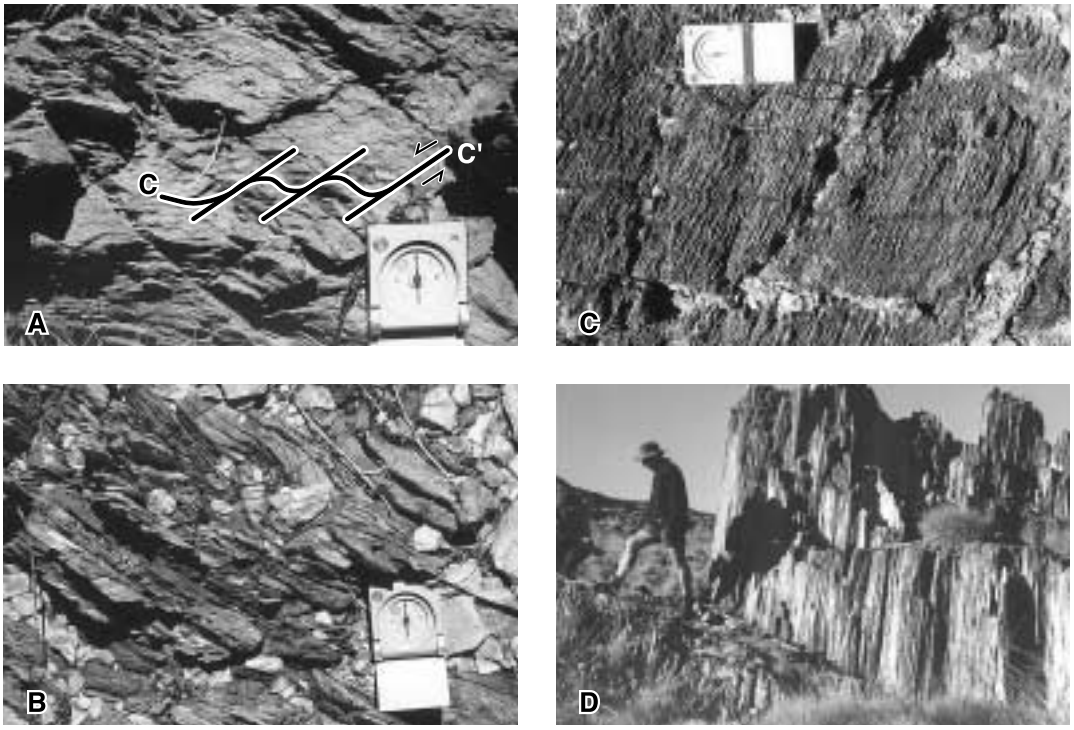

Figure 2.11 Structures within the Central Warrawoona Shear Zone. (a) Sinistral 070 trending R-shears in boudins within the CWSZ. View is to the north. (b) Northward view of dextral S-C relations and asymmetric folding indicating dextral transcurrent shearing, reactivating steeply dipping MESZ mylonites. (c) N-S to 020 trending sinistral kinks related to (W)NW-(E)SE compression, cross cutting strongest foliated dextral shears of the CWSZ, north is to the left. (d) Pencil cleaved felsics of the Wyman Formation near the central axis of the Warrawoona Greenstone Belt. Geologist facing north.

2 Ma Black Range Dyke Swarm (Wingate, 1999), dextrally [locality 8], marking a final phase of reactivation of the CWSZ ($D_{CWSZ,6}$, see figure 2.10).

The main structures and kinematics we found within the CWSZ are ordered based on overprinting relationships and are summarised in figure 2.10. This sequence summarises the main deformation events in the CWSZ. However, we recognise that the CWSZ has been a zone of weakness and we can not rule out a more complex deformational history than the one presented in figure 2.10.

2.4.3 The Northern Domain including the Mt Edgar Shear Zone

Deformation in the Northern Domain is concentrated in the Mt Edgar Shear Zone (MESZ), which forms the contact between the Warrawoona Greenstone Belt and the Mt Edgar Granitoid Complex. This 2 to 5 km wide shear zone can be traced to the northwest along the contact with the Marble Bar Greenstone Belt and to the northeast along the northern Kelly Belt (Figure 2.3). It partly coincides with the previously recognised 'Agmx' unit of mixed granite and greenstones

(Hickman and Lipple, 1978), and with the diapiric D_4 zone of Collins (1989). It comprises three subzones, each with distinctive lithological and structural characteristics: the gneissic footwall, the greenstone-dominated hangingwall and a Mixed Zone between the two, which comprises dominantly mylonitised intrusive rocks, and which approximately corresponds to the 'Agmx' above. The mylonitic foliation in the MESZ dips away from the Mt Edgar Granitoid Complex and generally decreases from subvertical in the hangingwall mylonites, to 70-80° in the Mixed Zone, and from 45° in the footwall gneisses, to subhorizontal towards the centre of the granitoid complex. A change in deformation behaviour from brittle-ductile (hangingwall mylonite) to ductile (Mixed Zone) and ductile with accompanying migmatism (footwall gneisses) is seen. Stereographic projections of these mylonitic foliations and of accompanying stretching lineations are presented in figure 2.5 and are discussed below.

Near the central, most attenuated part of the Warrawoona Greenstone Belt, the MESZ and the Central Warrawoona Shear Zone merge (Figure 2.3). To the west and east, less deformed greenstone belt sequences occur in between these shear zones: in the Salgash and Trig Well areas respectively, which are described after the MESZ.

2.4.3.1 The Mt Edgar Shear Zone footwall gneisses

The footwall gneisses are largely restricted to the SW quadrant of the Mt Edgar Granitoid Complex (Figure 2.3). Its oldest recognised components comprise banded grey gneisses with a SHRIMP protolith age of 3.46-3.43 Ga (Figure 2.4a) (Williams and Collins, 1990), which is similar to, or slightly younger than, the Duffer Formation (see §2.2.1). The banded gneisses are intruded by 1) grey granodiorite bodies, discordant with respect to the gneissosity, and locally by 2) granitoid sills, of unknown age, which have become an integral component of the gneisses. The gneisses locally contain ultramafic and mafic xenoliths. In places, both the banded gneisses and later granodiorites are migmatised. In the east the 3304 ± 10 Ma Boodallana Suite(Williams and Collins, 1990) (see figure 2.3) forms the footwall to the gneisses. The undeformed Moolyella Suite (see figure 2.3) discordantly intruded the gneisses. Its crystallization age (<3240 ± 11 Ma, Nelson, 2000) provides a minimum age for the gneissic fabric.

The orientation of the gneissosity follows a domal shape. It is generally parallel to the steep margins of the granitoid complex. Towards the centre of the Mt Edgar Granitoid Complex the gneissosity is subhorizontal (Figure 2.5). An important structural feature in the gneisses are dm- to m- scale extensional shear bands, which are widespread throughout the gneiss complex. They occur as a (W)NW-(E)SE trending conjugate set on outcrop-scale and cut across the gneissosity (Figure 2.12a) and are schematically illustrated in figure 2.13. In the centre of the gneiss complex, where the gneissosity is subhorizontal, shear bands dip to the (N)NE and (S)SW, with displacements indicating layer parallel extension. Towards the Mixed Zone, the orientation of the conjugate set with respect to the gneissosity has not changed, but both the shear bands and the gneissosity are tilted [locality 9]. The shear bands are the loci for partial melting and melt segregation of granitic composition. Melting occurred syntectonically because melt pockets which formed along the shear bands also show evidence of shearing, as indicated by small offsets of the melt veins (Figure 2.12a). The age of the migmatites is not known. The possible absolute age for this extensional phase and the formation

Figure 2.12 Rock types and structures of the Mt Edgar Marginal Shear Zone (a) NE dipping migmatitic shear bands, cutting across subhorizontal banded gneisses of the footwall Gneiss Complex, looking westward. (b) Mylonitisation of the gabbro/diorite complex and exploitation by dolerite and subsequent granitoid sills in the Mixed Zone, indicating strong interaction between intrusion and deformation in this part of the Mt Edgar Shear Zone. Warrawoona Belt supracrustals in the background, view to the SE. (c) Northwest view of a granitoid sill within the 050-trending section of the MESZ mixed zone, with oblique, SW-plunging Bi-Chl stretching lineation. (d) Tremolite bearing foliation plane (local S_2), cross cutting older mylonitic foliation (local S_1) in the upper Mixed Zone. An intersection lineation between S_1 and S_2 is well visible and is at an angle to the actinolite bearing stretching lineations (L2) associated with S_2.

of the gneissic fabric has a wide span, pre-dating intrusion of the Moolyella Adamellite Suite (<3240 ± 11 Ma, Nelson, 2000), but post-dating the crystallization of the protolith of the gneisses.

2.4.3.2 The Beaton Well Zone in the footwall gneisses

A structure associated with the above gneisses is a subvertical, NE-SW trending zone, the Beaton Well Zone (BWZ) (Figure 2.3). It was mapped by Hickman and Lipple (1978) as a 5-7 km wide, unnamed gneissic zone rich in greenstone xenoliths. The trend of the zone, and of the gneissosity within it, is oblique to the general domal trend of the Mt Edgar Granitoid Complex, and is almost at right angle to the contact with the Warrawoona Belt. Despite its orientation it has had no major effect on the overlying supracrustal assemblage (see also Collins (1989).

The rocks in the BWZ are characterised by a strong linear fabric, defined by elongated plagioclase/hornblende crystals and hornblende/biotite aggregates, which have a subhorizontal plunge and trend parallel to the zone. Foliations are generally gneissic, commonly banded, and are

locally mylonitic. On the outcrop scale, these foliations can be either subhorizontal, dipping shallowly to the NE or SW, or are subvertical with a NE-SW trend (see stereographic projection in figure 2.5). Mutually overprinting relationships indicate that these foliations had a coeval development. Both subhorizontal and subvertical foliations have the above linear fabric which, irrespective of the orientation of the foliation, plunges consistently and shallowly to the NE or SW (Figure 2.5). Conjugate shear bands are associated with both steep and flat gneissosity in the BWZ. Those in the subhorizontal gneisses are generally subhorizontal, whereas in the subvertical gneisses, both subhorizontal and subvertical shear bands occur. The subhorizontal shear bands, although commonly seen in conjugate sets, are dominated by those indicating tectonic transport to the SW. The displacement of the mylonitic foliations on NE-trending subvertical shear bands indicates a sinistral transcurrent motion (Figure 2.13).

2.4.3.3 The Mixed Zone of the Mt Edgar Shear Zone

The Mixed Zone forms the central part of the MESZ. Locally, this zone is about 4 km wide in its most complete section, but may be less than 2 km in more attenuated parts (Figures 2.4a and 2.4b). It consists of granite, diorite, dolerite and gabbro and their mylonitised equivalents. Multiple phases of intrusions have preferentially intruded shears containing mylonites derived from earlier intrusions and also the host mylonites.

The oldest identified intrusive component is a coarse-grained gabbro/diorite complex, which can be traced along the length of the Mixed Zone. The complex is enclosed in the mylonites of the Mixed Zone, but contains internal shears which preserve a memory of multiple phases of shear activity and intrusion. These internal shears are firstly intruded by gabbros and diorites which are themselves sheared, suggesting a syntectonic origin of the gabbro/diorite complex. Evidence for older deformation is found in the form of metre-scale xenoliths with foliated and strongly contact-metamorphosed ultramafic and mafic schists, within undeformed parts of the gabbro/diorite complex. Their existence suggests that the gabbro/diorite complex intruded into a pre-existing tectonised zone. Secondly, the shear zones within the gabbro/diorite complex are commonly exploited by dolerite sills, which are also strongly deformed. These are, in turn, the loci for hornblende-granitoid intrusions (Figure 2.12b), partly belonging to the 3304 ± 10 Ma (Williams and Collins, 1990) Boodallana Suite, which were subsequently mylonitised [locality 10]. The above mafic components are all discordantly intruded by the undeformed 3325 ± 6 Ma Wilina Pluton (Collins et al., 1998), which provide a minimum age for the development of this part of the Mixed Zone. Parts of the Mixed Zone have been active after intrusion of the Wilina Pluton, as is indicated by the structures in the Boodallana Suite, suggesting strain partitioning in the hotter base of the Mixed Zone. The age of the oldest intrusions would constrain the initial activity, but the gabbro/diorite has not been dated. A maximum age for the gabbro/diorite is the age of the host rock. The oldest dated rocks in the hangingwall are the ~3465 Ma Duffer felsic volcanic succession (see §2.2.1), which is similar in age to the oldest recognised component within the gneiss complex. This allows the Mixed Zone to have developed as early as ~3465 Ma. The relative age from intrusive relationships with the protoliths of the Gneiss Complex, especially the youngest component of 3420 Ma (see §2.2.2), is difficult to obtain, because of the strongly tectonised

concordant contact. Sills of alkali-feldspar rich granite (10-100 m thick) are found along the upper margin of the Mixed Zone at the contact with the hangingwall greenstones. The sills may be partly mylonitised, but are generally less deformed than the other components of the Mixed Zone. They are intruded by dolerites. A similar alkali-feldspar rich sheet, east of Marble Bar, was dated at 3466 ± 2 Ma (Nelson, 1998a), suggesting syn-Duffer tectonic activity in the Mixed Zone.

Internal structures and kinematics of the Mixed Zone are similar for all of the intrusion-derived mylonites, indicating that all have been exposed to the same kinematic framework. Stretching lineations are well developed, consistently plunging to the SW, irrespective of the orientation of the mylonitic foliation (Figures 2.5 and 2.12c). Conjugate mm-scale shear bands, which particularly occur in the dolerite sills, indicating layer parallel extension. In the alkali-feldspar granite sills shear bands dominantly indicate NE transport [locality 11]. Metamorphic assemblages stable during deformation are hornblende and plagioclase in the gabbro/diorite and hornblende and plagioclase (and garnet) in the dolerite sills, indicating amphibolite facies conditions. Greenschist facies shears overprint the amphibolitic fabric of the mafic sills, particularly on their margins. Elongated chlorite aggregates are sub-parallel to the regional SW plunging lineation [locality 12]. Hornblende-bearing granitoid sills display stretched hornblende-rich clots which are, in most places, altered to a biotite and chlorite stretching lineation. These relationships indicate that shearing in the Mixed Zone started under amphibolite grade conditions and continued to greenschist conditions, especially near the hangingwall. The pattern of consistently SW plunging stretching lineations is not restricted to the Mixed Zone, it is also found in the hangingwall, indicating a common deformation history, which will be described below.

The Mixed Zone generally follows the margin with the greenstone belt. However, a more complex pattern is observed in the Trig Well area ([locality 13] in figure 2.8b). In this area the internal structures show a complex interplay of 290° and 060°-trending mylonitic foliations, both of amphibolite grade. Mutual overprinting relationships suggests they were formed during one deformation phase. Dolerite and granite sills intruded parallel to both the 290° and 060°-trending mylonites The sills contain both 290° and 060°-trending mylonitic foliations, indicating that intrusion was intimately related to shearing. The fabric in the dolerite sills displays conjugate shear bands and SW plunging stretching lineations, irrespective of the orientation of the foliations with which they are associated, indicating layer parallel NE-SW extension.

2.4.3.3.1 Localised normal movement on the margins of the Mixed Zone

Evidence for localised normal movement is seen on the margins of the Mixed Zone in the eastern MESZ. Near the contact with the hangingwall sequence, the 290°-trending mylonitic foliation and parallel sills of the Mixed Zone show a km-scale fold pattern with a dextral asymmetry near the 060°-trending margin with the hangingwall [locality 14]. A finely spaced mm-scale mylonitic foliation parallel to the sills, has stable hornblende and plagioclase indicating amphibolite metamorphic facies. It is overprinted by an 060°-trending, wider spaced brittle-ductile mylonitic foliation, which is axial planar to the folds and parallel to the margin of the Mixed Zone. The latter foliation contains SW plunging chlorite pods and an S-C fabric which indicates a granitoid-up sense of shear with a dextral horizontal component. We interpret the dextral asymmetry of the older

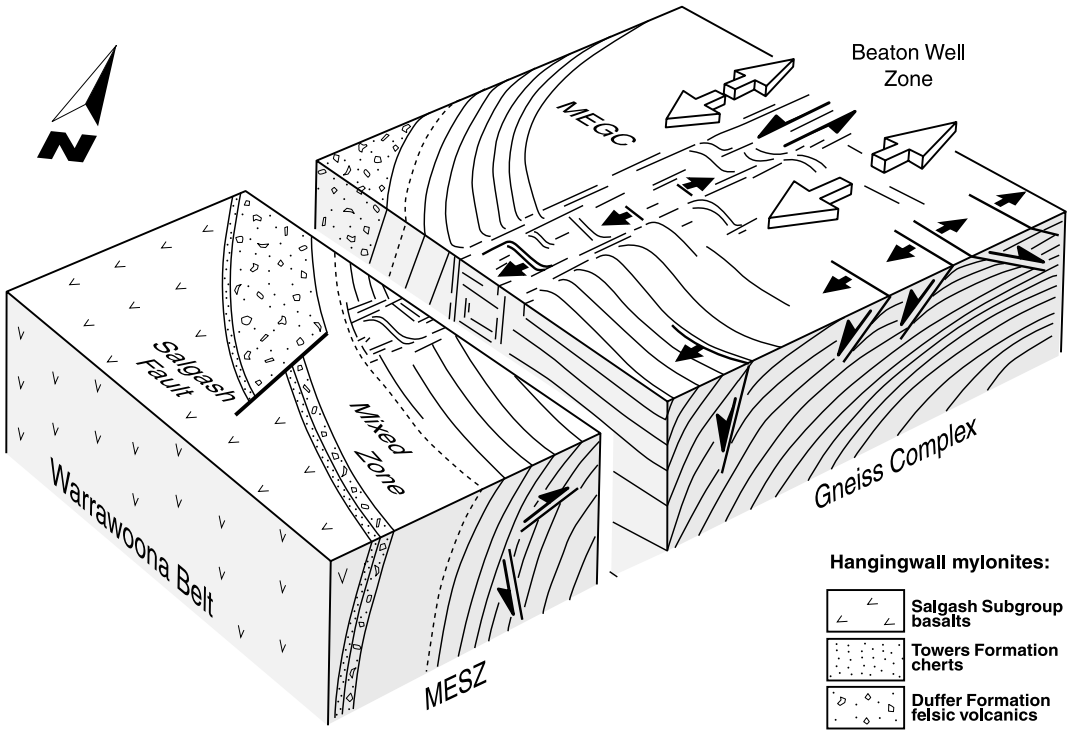

Figure 2.13 Schematic 3D illustration of the relationship between the gneissosity and shear bands within the Mt Edgar Granitoid Complex and Beaton Well Zone.

structures to be the result of normal movement on this 060°-trending system.

In the eastern MESZ, the Yandigoogina Suite of the ~3310 Ma TTG Suites (Collins and Gray, 1990) forms the footwall of the Mixed Zone [locality 15]. In this outcrop, a weak planar fabric throughout the granitoid is defined by parallel, locally chloritised, biotite grains, and has a N-S trend and dips shallowly to the east. No pervasive mylonitic foliation is developed, but NE-trending, SE-dipping 'diffuse' shear bands with weakly developed elongated SW plunging biotite aggregates show a dextral offset of the general fabric. This also indicates normal, granitoid-up, movement with a dextral oblique sense.

2.4.3.3.2 Late NE transport in the Mixed Zone

Mylonites of the Mixed Zone were intruded by late-stage plutons, including the Wilina and Cotton Well Plutons (Figures 2.4a and 2.5). The mylonites and the plutons are both cut by late-stage brittle-ductile shear zones [locality 16]. The Cotton Well Pluton consists of coarse-grained muscovite granite. It shows a well developed, subvertical, widely spaced 320-330°-trending foliation, marked by cm-size muscovite flakes. Throughout the pluton, cm-wide SW dipping (40-50°) brittle-ductile shear zones, and a locally developed S-C fabric, indicate a SW-up sense of shear. In their current orientation these structures are thrusts, indicating tectonic transport to the NE.

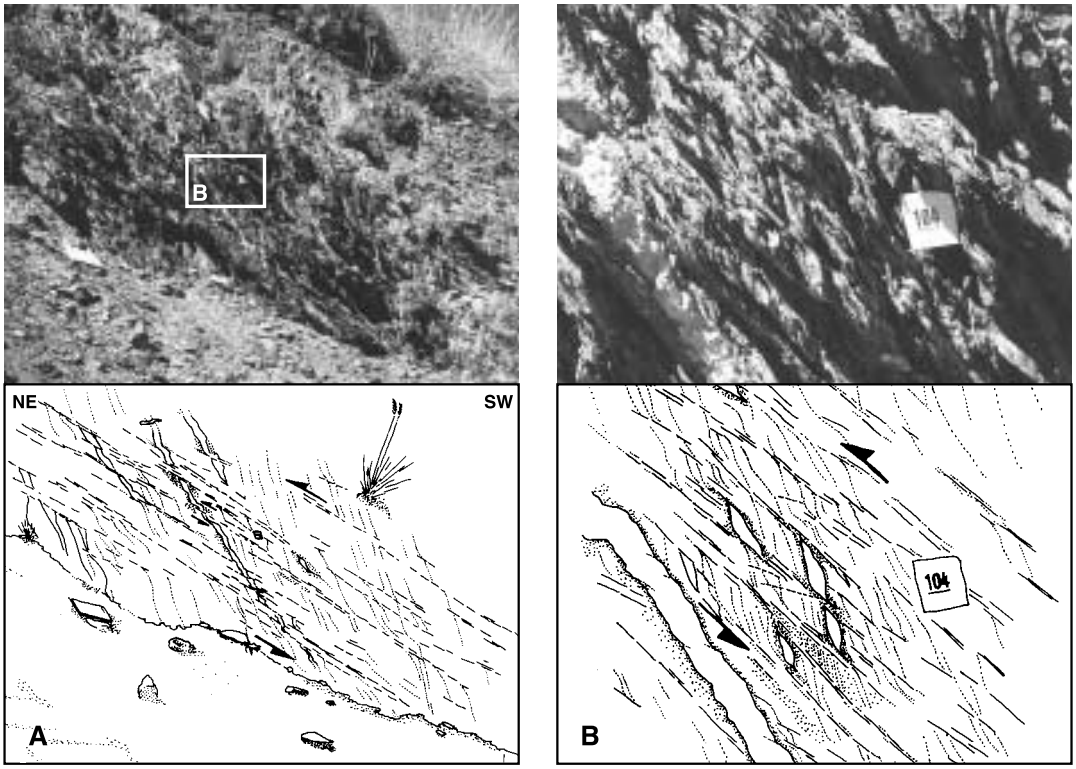

Figure 2.14 (a) Photograph and interpretative sketch of overprinting relation showing brittle-ductile NE-vergent thrusts cutting across the main mylonitic foliation in the MESZ hangingwall. Field notebook for scale (b) Enlargement of detail, showing the top-to-the-NE asymmetry of the fabric and the displacement of the quartz veins.

Subhorizontal pegmatite veins also preserve these structures, and fit a thrusting model. Similar structures are seen within the base of the Mixed Zone near Trig Well, where subhorizontal, metre-wide mica-bearing pegmatite dykes intrude the gabbroic, doleritic and granitoid mylonites. These pegmatites have a WNW strike (290°), but are generally less steep than the shears they have intruded. On the pegmatite margins, a WNW-trending, steeply dipping, brittle fracture cleavage, down-dip slickensides and poorly developed S-C fabrics, small offsets, and subhorizontal quartz veins indicate NNE tectonic transport during compressive deformation. Near the contact with the supracrustal sequence [locality 17], greenschist facies shears cut across the steeper amphibolite facies mylonites. Tremolite-bearing stretching lineations associated with these shears plunge to the SW (Figure 2.12d). Drag of the older foliation indicates SW block-up, or tectonic transport to the NE.

2.4.3.4 The hangingwall to the Mt Edgar Shear Zone

The hangingwall mylonites consist mainly of fuchsitic cherts, quartz-mica-chlorite and chlorite mylonites (Figure 2.4). The mylonites contain boudins that indicate that their protoliths were, respectively, fine-grained chert bands, pelitic schists, felsic extrusives, and basalt. Tracing the mylonites to the less deformed areas in the nearby belts indicates that they were derived from the

Duffer Formation, Towers Formation and other Salgash Subgroup lithologies.

The trend of the mylonitic foliation in this subzone is generally parallel to the margin of the Mt Edgar Granitoid Complex. The dip is subvertical or steep away from the margin. Kinematic indicators, including both S-C and C-C'-fabrics, dominantly indicate a SW-up sense of shear, or tectonic transport to the NE [locality 18]. Locally, however, the reverse is seen with brittle-ductile SW dipping thrusts overprinting the above mylonitic foliation and consistently indicating tectonic transport to the NE ([locality 19] and figure 2.14). The best developed mylonitic foliations are overprinted locally by N-S to 020-trending, subvertical mm- to cm-spaced, brittle-ductile crenulations. Throughout the zone, semi-brittle ~350° and ~050°-trending subvertical kinks form a conjugate set indicating WNW-ESE shortening.

2.4.3.5 The Salgash Area

The Salgash Area (Figure 2.4a) is part of the hangingwall to the MESZ. Its northeastern margin is formed by a series of continuous 10-100 metre thick cherts and mafic schists, which are strongly deformed and are part of the MESZ. The southern margin is marked by the CWSZ. To the west, the area is bounded by the NNE-trending Salgash Fault. In contrast to its strongly deformed margins, internally it displays the least deformed greenstones of the Northern Domain.

The cherts on the northeastern margin can be traced to the type-section of the Towers Formation in the Marble Bar Belt, and are part of the lower Salgash Subgroup. Overlying the cherts are isolated exposures of ultramafic intrusions, (pillowed) meta-basalts of the Salgash Subgroup and metasedimentary rocks, formerly sandstone, black shale and boulder conglomerate of unknown age; the last two have not been identified elsewhere in the hangingwall.

Throughout the area, a subvertical schistosity is developed parallel to the trend of the Warrawoona Belt. Locally, 300-310°-trending and steeply NE-dipping metre-wide shears are observed; they contain an S-C fabric and steeply east-pitching elongated chlorite aggregates, indicating a sinistral oblique sense of shear [locality 20]. Isolated exposures of the metasediments preserve steeply dipping bedding planes with a variable strike. The meta-conglomerates contain strongly stretched boulders, plunging ~70° to the SE [locality 21]. An 060°-trending steep talc-chlorite-carbonate foliation is developed locally in the ultramafic rocks and rotates into 1-10 metre wide ~290°-trending shears with subhorizontal quartz-chlorite stretching lineations, the drag indicating a dextral sense of shear [locality 22].

The most characteristic structures of this area are found along the northeastern boundary, within the MESZ hangingwall and Mixed Zone. There, the cherts of the Towers Formation form km-scale steeply inclined and steeply reclined folds with fold hinges plunging 70-80° (E)SE to NE (see also Collins, 1989). Underlying felsic mylonites are parallel to the chert units and are also folded. It is only in this area that their dip is to the NE, that is, towards the Mt Edgar Granitoid Complex [locality 23]. Both the cherts and, in particular, the felsic mylonites contain well developed stretching lineations marked by quartz and pyrite rods in the former and by elongated quartz phenocrysts, white mica and Al-silicates in the latter. The stretching lineations plunge constantly to the ENE, parallel to the aforementioned fold axes. The NE-dipping mylonitic foliation comprises quartz and kyanite, and has shear band and S-C relationships that indicate a batholith-up sense of

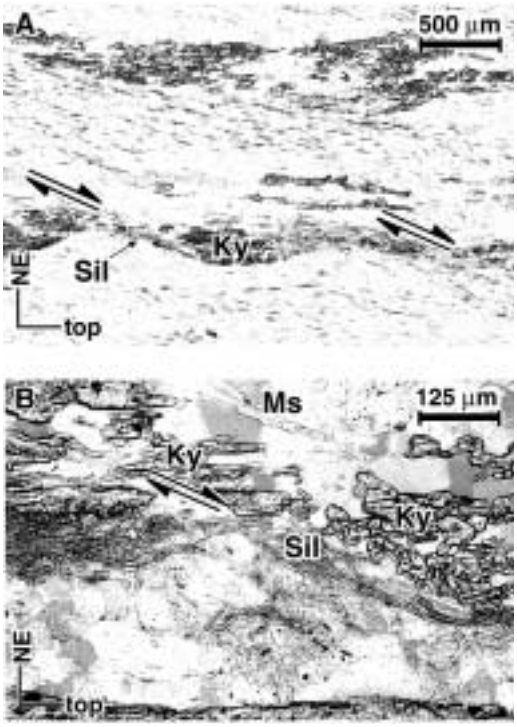

Figure 2.15 Microphotographs of subvertical to steeply NE-dipping mylonites from the Mt Edgar Shear Zone hangingwall near the Salgash Area. (a) The offset of kyanite-rich bands indicates NE-up kinematics. (b) Kyanite is overprinted by sillimanite.

shear (Figure 2.15a), with kyanite being replaced by sillimanite within the overprinting mylonitic foliation (Figure 2.15b). Both kyanite and sillimanite are overprinted by muscovite and andalusite towards the hangingwall greenstones (See also Délor et al., 1991). The mylonitic foliation becomes steeper to the NE, from a NE dip in the rocks close to the Warrawoona Belt, to subvertical in the Mixed Zone. In this part of the Mixed Zone, granitoid intrusions show a dominantly linear quartz-feldspar fabric, parallel to the dominant stretching lineations and fold axes [locality 24]. From the Mixed Zone further to the NE, the foliation becomes less steep, from subvertical to a 60-70° SW dip in the footwall gneisses. We interpret these structures to have formed during the same deformation event and to have been passively (over)steepened.

Summarising for the Salgash Area and the nearby MESZ, we order the structures into three groups on the basis of overprinting relationships, geometry and kinematics. The oldest structures comprise the main, NE-dipping mylonites. We interpret these to be the local, passively steepened, equivalents of the generally SW-dipping MESZ mylonites. The constant pitch of the lineations (90-70°E) within both the NE and SW dipping mylonitic foliation supports this interpretation. Steepening and local oversteepening of the foliation explains the variation in lineation azimuth from (E)NE to ESE. A similar orientation of the linear fabric of the granitoids on the upper margin of the Mixed Zone and the lineated boulders within the area, suggests their fabric is related to the development of the MESZ mylonites. The second group comprises the 300°-trending, oblique sinistral greenschist facies shears with steeply west-plunging lineations. The third and youngest group, contains the 1-10 metre-wide dextral shear zones and 060°-trending foliations.

2.4.3.6 The Trig Well Area

The Trig Well Area (Figure 2.4b), like the Salgash Area, is underlain by the MESZ and is cross-cut by the CWSZ in the south. It is overlain by the Fortescue Group to the east. The rock types of this area are similar to those elsewhere in the hangingwall, but here they are much less deformed, comprising schistose felsic rocks, carbonate-rich chlorite-quartz-sericite schist, talc-chlorite-carbonate schist and meta-basalt, with bands of chert and BIF, indicating low grade greenschist

facies conditions.

Internal structures of the Trig Well Area are dominated by NE-trending subvertical faults [locality 25]. Towards the Mt Edgar Granitoid Complex, these faults splay into a subvertical, carbonate-rich zone, parallel to the MESZ. No kinematic indicators were observed within the faults, but offset of the lithologies along the faults suggests a sinistral horizontal component of movement. Shear bands within the carbonate-rich shear zone indicate dominantly sinistral transcurrent movement, consistent with the sinistral movement on the faults, suggesting that these are related. Semi-brittle thrusts (~080/45S) overprint the NE-trending faults. They contain quartz rods plunging 30-60° to S-SW, indicating a N-NE vergence [locality 26]. An overprinting crenulation foliation (060/70NW) throughout the area indicates a later phase of WNW-ESE compression.

2.4.3.7 Kinematic interpretation and summary for the Northern Domain

The oldest deformation structures within the Northern Domain are found in the ultramafic schists within the gabbro/diorite complex of the Mixed Zone. Whether they reflect an individual deformation phase is unclear. Their occurrence suggests that the gabbro/diorite intruded into a tectonised zone. We refer to them as formed during $D_{ND,\,1A}$ (see figure 3.10).

The gabbro/diorite complex and dolerite sills are among the oldest intrusive components of the MESZ. The intrusion of gabbro/diorite sills into sheared parts of the complex implies a syntectonic timing ($D_{ND,1B}$). Despite the complex overprinting relationships of 290° and 060°-trending shears and sills in the Mixed Zone near the Trig Well area, the stretching lineations plunge constantly to the SW (Figure 3.5). These complex structures, in combination with the unidirectional amphibolite facies layer-parallel extension, are interpreted to be the effect of NE-SW extension. We suggest that active extension caused doming, for reasons similar as those for core-complex formation (further discussed below) and caused steepening of the MESZ during ongoing deformation. In the Mixed Zone near Trig Well, doming caused steepening of the marginal shear zone which resulted in a local 060° trend (Figure 3.16a). Because this trend is oblique to the extension direction, new amphibolite facies NW-trending mylonites formed (at a more energetically favourable angle to extension), and overprinted the 060° foliation (Figure 3.16b). This foliation was in turn intruded by gabbro/diorite and dolerite sills. Later extension and further steepening of the dome reactivated the 060°-trending foliations in this area (Figure 3.16c) ($D_{ND,2A}$?).

The localised normal movement on the margins of the Mixed Zone in the Trig Well area, is interpreted to have formed in the later stages of extension, possibly coeval with ~3.31 Ga granitoid emplacement in the footwall ($D_{ND,\,2B}$).

We consider the Beaton Well Zone to be an integral part of the MESZ, because of the similarity of its internal structures and kinematics, particularly with those of the footwall gneisses. The dominantly horizontal movement of this zone indicates that it accommodated differential NE-SW extension on the MESZ. The sinistral sense of shear suggests that extension to the SE of the BWZ was greater than to the NW. The timing of deformation on this zone is constrained by the $<3240 \pm 11$ Ma (Nelson, 2000) Moolyella Suite, which intruded across this zone and has remained undeformed.

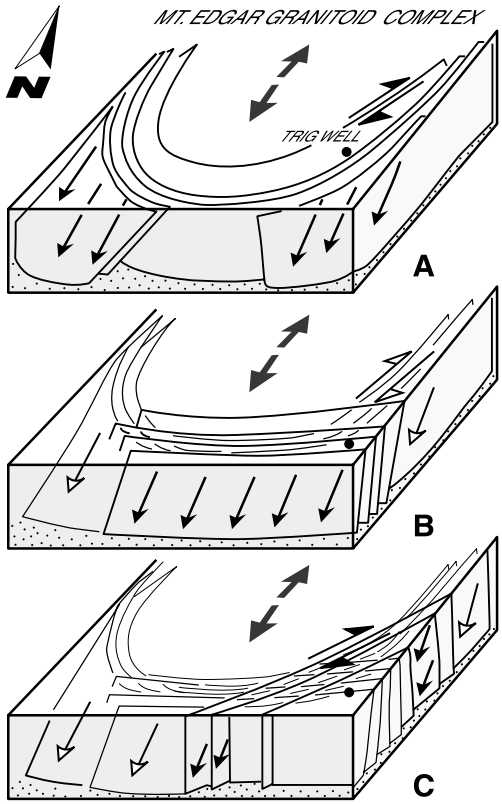

Figure 2.16 Model for development of complex overprinting relations in the Mixed Zone during progressive extension, sill intrusion and doming of the Mt Edgar Shear Zone.

Younger structures throughout the Northern Domain comprise (N)NE verging thrusts and local backthrusts. The structures indicate (N)NE-vergent thrusting in their current position, but they could also indicate NE-SW extension, depending on the orientation of the MESZ at the time of deformation. The above structures cross-cut the amphibolite facies mylonitic foliation of the MESZ, indicating they formed after the main development of the MESZ. They also post-date intrusion of the discordant plutons in the MESZ, which provides a maximum age for deformation. The brittle-ductile nature of the structures implies that they formed at lower temperatures, after the main phase of intrusion into the MESZ and after doming of the Mt Edgar Granitoid Complex. Therefore, we conclude that they formed in their current geometrical position, and reflect a (N)NE-(S)SW compressional deformation phase. In the sequence of events in the Northern Domain, we attribute these structures to $D_{ND,3}$. Dextral transcurrent shear zones locally reactivated the 300°-trending shears, with a west-pitching stretching lineation ($D_{ND,4}$). The youngest structures, two conjugate kink sets, also indicate NW-SE compression, but because they overprint the above dextral shears and because of their much more brittle nature, we relate them to a separate phase ($D_{ND,5}$).

2.4.4 The Southern Domain

The Southern Domain comprises a basaltic greenstone sequence (see figures 2.4a and 2.4b), which forms a relatively undeformed rim around the northern margin of the Corunna Downs Granitoid Complex. It contains lava flows ranging from komatiitic basalts to Fe-rich basalts, (ultra-) mafic sills, minor volcanic breccias and chert horizons, and is correlated to the Salgash Subgroup. Metamorphic assemblages are low grade and original igneous textures, such as spinifex and pillow structures, are well preserved. A felsic volcanic unit in the central western part of the belt (see figure 2.4a and 2.4b) was mapped as Wyman Formation (Hickman and Lipple, 1978). We found it to also contain mafic and ultramafic volcanic rocks with interlayered sedimentary rocks and to be intruded

by felsic sills and dykes. In a recent SHRIMP study, the felsic rocks yielded a Wyman age (3315 ± 3 Ma, Buick, in press), however, it is not clear whether the sampled rocks are from an extrusive or intrusive component. A second felsic volcanic unit occurs at the eastern margin of the Corunna Downs Granitoid Complex (Figure 2.4b). It was dated at 3415 ± 8 Ma (Barley and Pickard, 1999) Deformation within the Southern Domain is dominated by prominent shear zones within the greenstones and remnants of shears are found on the margin with the Corunna Downs Granitoid Complex (Figures 2.8a and 2.8b). The contact between the greenstones and the Corunna Downs Granitoid Complex is mainly intrusive, largely formed by the rapakivi-textured Carbana Pool Adamellite (CPA) (3313 ± 9 Ma, Barley and Pickard, 1999) and by the Northern Suite of unknown age (Figure 2.3). The narrow contact-metamorphic aureole of both indicates that their intrusion was at a high crustal level.

2.4.4.1 Structures associated with the margin of the Corunna Downs Granitoid Complex

Structures along the margin of this complex can be divided into four sets (Figure 2.8a). The oldest set comprises a mylonitic foliation within remnants of (ultra)mafic greenstones near the margin of the granite [locality 27]. The shears are parallel to the contact, generally subvertical or steeply dipping away from the Corunna Downs Granitoid Complex, and contain a serpentine-talc stretching lineation with a constant NE azimuth. Shear bands indicate a south side-up, slightly oblique movement ($D_{SD,1}$). These structures are intruded by the CPA, and are not observed within the CPA, indicating that they are older than this granitoid and were not related to its emplacement. A younger set of structures overprints these shears and are also found in the CPA. This set comprises a moderate to steeply SW dipping foliation (50-75°) with biotite stretching lineations plunging towards the WSW. Asymmetric clasts, S-C fabrics and shear bands, especially well preserved in the CPA granite, indicate a SW-up, oblique sense of shear with a sinistral component of horizontal displacement. An equigranular fine grained hornblende-biotite granodiorite occurs further west along the margin [locality 28] This granitoid also contains shears which generally indicate N(NW) verging sense of shear. These are not found in the CPA and are regarded to have formed during $D_{SD,2}$. Narrow brittle-ductile subvertical 010-020°-trending dextral shears within the eastern CPA, towards the Kelly Belt, contain stretching lineations/striae plunging ~30-40° towards the SSW [locality 30]. In between these shears a weakly developed, 320-330°-trending, sub-vertical foliation is recorded with local, metric scale, southwest dipping thrusts and SW plunging striae. These structures fit the NE-SW compressional stress field of $D_{SD,3}$. A fourth set of structures is well developed in the greenstones adjacent to the granitoids, but it also reactivated the oblique thrusts in the CPA. It comprises an 060°-trending crenulation foliation and 300°-trending dextral brittle-ductile transcurrent shears which can be related to NW-SE compression ($D_{SD,4}$) [locality 29].

2.4.4.2 Structures in the greenstones of the western Southern Domain

Deformation of the greenstones is localised in five main shear zones restricted to the western part of the belt (Figures 2.3 and 2.8a). The two most prominent shears are the 100-300 metre wide Fieldings Find Shear Zone (FFSZ), which marks the northern margin of the felsic Wyman unit (Figure 2.4a) and the kilometer wide Brockman Hay Shear Zone (BHSZ), which marks an oblique

contact with the Wyman unit and the (tectonically) overlying series of meta-basalt and ultramafic units to the south. The Hilly Basalt Shear Zone (HBSZ) is situated between two mafic units and is located in ultramafic schists. The thickness of the basaltic sequence increases to the west, south of the BHSZ, discussed below. The Northern and Southern Copenhagen Shear Zones have a trend parallel to that of the lithological units (Figure 2.4a) and are marked by carbonated talc-chlorite mylonites with cores of fuchsitic chert boudins which locally preserve sedimentary structures. Deformation is most intense along the sides of the cherts.

The Brockman Hay Shear Zone is an anastomosing zone in which the mylonitic foliation is subvertical near the axis of the Warrawoona Greenstone Belt (WGB) and dips steeply SE closer to the Coongan Belt (Figure 2.8a), where it swings into a N-S trend and can be traced into the Central Coongan Shear Zone (Figure 2.3). The mylonitic foliation of the Central Coongan Shear Zone dips steeply to the east, and contains down-dip stretching lineations (Zegers, 1996). Where they meet, the NE-trending foliation of the BHSZ and the N-S trending foliation of the Central Coongan Shear Zone mutually overprint. R-shears and asymmetric feldspar clasts in felsic mylonites indicate tectonic transport to the west. Undeformed NE-trending felsic sills intrude parallel to the BHSZ and cut across the N-S trending Central Coongan Shear Zone. Stretching lineations throughout the BHSZ are marked by elongate ocelli in the meta-mafic rocks, carbonate rods in the ultramafic rocks and quartz and feldspars rods in the meta-felsic rocks derived from the Wyman Formation. The azimuth of the stretching lineations is east, irrespective of orientation of the mylonitic foliation. Throughout most of the BHSZ, the plunge is about 45°, but near the margin with the felsic volcanic rocks, where the mylonite foliation is more platy, carbonatized and silicified, the plunge decreases to 20°E [locality 31]. Kinematics of S-C and C-C' fabrics indicate oblique west-vergent transpression, with a larger dextral component where the trend of the shear zone is more E-W. We interpret these structures to have developed during a phase of E-W compression ($D_{SD,3}$). Towards the Central Warrawoona Shear Zone, the pitch of the stretching lineation on the mylonitic foliation increases to 70-80°E and further steepens to finally become 60-70°W, subparallel to the stretching lineations in the MESZ (see above) [locality 32]. No overprinting relationship was found between the E and the W pitching lineations; rather one appears to rotate into the other. All felsic rocks are strongly deformed, no felsic sills like those near the Coongan Belt are observed. Where the BHSZ meets the Fieldings Find and Copenhagen Shear Zones, a steeply plunging pencil cleavage is developed due to the mutual intersection between their individual foliations. The resulting pencil cleavage produces rods that become thinner and more elongated in appearance closer to the CWSZ, where a single pencil/intersection rod may have a width of only 5 cm but may be over 1 metre in length (Figure 2.11d). These pencils/rods are parallel to stretching lineations marked by elongated K-feldspar clasts and to subvertical isoclinal folds within the felsic unit of the Wyman Formation. The area of the most intense penciling and intersection rodding, due to the shear zone interaction, geographically corresponds to the supposed area of maximum sinking of the plunging syncline (Collins and Teyssier, 1990; Collins et al., 1998).

In the Fieldings Find and the two Copenhagen Shear Zones, the mylonite foliation is subvertically to steeply south-dipping. Distinct pyrite and carbonate stretching lineations in the talc mylonites and fuchsitic cherts as well as quartz stretching lineations in the cherts, like in the BHSZ,

pitch 30–70°E at the edge of the zone, but have a flatter pitch (about 20°E) in the more platy and altered interior. Asymmetric clasts and pulled-apart pyrite cubes give a dextral oblique sense of shear. The two Copenhagen Shear Zones merge with the FFSZ before they are truncated by the CWSZ. Towards the CWSZ the stretching lineations rotate to subvertical.

A 315° to 330°-trending foliation is found in the thrust slices between the above shears, including the 3315 ± 3 Ma felsic rocks, mapped as the Wyman Formation[locality 33]. This foliation also overprints the shear zones, forming a fracture cleavage in the cherts. S-C fabric and en échelon sub-horizontal quartz veins indicate NE-vergent and locally minor SW-vergent thrusts (backthrusts) in a NE-SW compressional setting ($D_{SD,4}$).

A localised, but widely developed, 060°-trending steep foliation forms a crenulation cleavage in the highly foliated parts of the shears and a fracture cleavage in other areas. The chert ridges within the shear zones are cross-cut locally by 060°-trending NW verging brittle thrusts. We interpret these cleavages and thrusts to be related to NW-SE compression ($D_{SD,5}$).

2.4.4.3 Structures in the greenstones of the eastern Southern Domain

In the eastern part of the Southern Domain (Figure 2.8b), localised shears as described above are absent and deformation occurs in anastomosing chlorite schists and mylonites, leaving less deformed boudins on a 100 metre scale that form the rounded hills characteristic of this unit (see figure 2.7). In the mylonites, two sets of mutually overprinting sub-vertical foliations (290° and 330°) form a poorly developed pencil cleavage. Both foliations are cut by discrete 290°-trending sub-vertical metre-wide sinistral shears which are parallel to the main trend of the CWSZ. Locally, structures indicating a brittle dextral transcurrent reactivation are seen in the 290°-trending shears.

The most important shear in the eastern Southern Domain is about 20 metres wide, and is hosted in ultramafic rocks between the Hilly Basalts and felsic agglomerates and breccias near the Kelly Belt [locality 34]. The shear dips steeply to the E or ENE, and is intensely carbonatised. This zone has a complex history of early, approximately down dip, normal movement, indicated by both sigma clasts and shear bands ($D_{SD,1,2}$?). These are overprinted by brittle structures including tension gashes indicating top to the W thrusting with a minor sinistral component ($D_{SD,3}$). Later 060°-trending thrusts indicate a NW-SE compressional phase ($D_{SD,5}$). Quartz ridges on the margin of the Carbana Pool Adamellite and the Warrawoona Belt contain brittle structures, including tension gashes and slickensides, which, taken together, are indicative of dextral transcurrent movement along the margin ($D_{SD,6}$).

2.4.4.4. Kinematic interpretation and summary for the Southern Domain

In summary for the Southern Domain, we order the structures into six groups, which we relate to six deformation phases, $D_{SD,1\text{-}6}$ (Figure 2.10). The oldest structures are the steeply dipping shear zones in the ultramafic remnants on the margin with the Corunna Downs Granitoid Complex. In the current orientation, the kinematics of these shear zones, with steep E-pitching stretching lineations, indicate (extensional) tectonic transport to the NE, but their original attitude is not known. The shears and lineations pre-date the intrusion of the CPA and can therefore not be related to the later phase of NE-vergent thrusting. We attribute them to $D_{SD,1}$. The minor shears

with a normal sense of displacement within the Northern Suite may be related to its emplacement ($D_{SD,2}$). The west-verging thrusts in the Coongan Belt and dextral transcurrent shearing in the greenstones of the Southern Zone, including the 3315 ± 3 Ma Wyman Fm, are attributed to a phase of E-W compression ($D_{SD,3}$). This phase pre-dated the emplacement of the CPA, indicating a narrow time span for its activity (post-3315 ± 3 Ma to pre-3313 ± 9 Ma). All of the above structures and the CPA are overprinted by the NE-verging oblique thrusts, and local SW-vergent backthrusts, due to NE-SW compression ($D_{SD,4}$). Oblique dextral movement under greenschist facies and an 050° compressional crenulation were caused by subsequent NW-SE compression ($D_{SD,5}$). This phase was followed by brittle dextral slip on quartz veins parallel to the trend of the WGB ($D_{SD,6}$).

The progressive rotation of the stretching lineation in the BHSZ into the orientation of the steeply SW plunging lineation associated with the MESZ suggests that W-vergent thrusting preceded NE-SW extension on the MESZ. However the situation is complicated by the later phase of NE-SW compression ($D_{SD,4}$), which may have reactivated part of the MESZ and passively rotated parts of the BHSZ.

2.5 Reconstruction of the structural history

The events for each sub-area (the Central Warrawoona Shear Zone, Northern and Southern Domain) which were ordered internally by structural or intrusive relationships (Figure 2.10), are cross-correlated by comparing the ages of the constraining granitoids and the depositional age of the Wyman Formation. This results in a local structural history which involved four main deformation phases, D_{X+1} to D_{X+4}, before the intrusion of the 'W' Dyke of the 2.77 Ga Black Range Dyke Swarm and one subsequent phase D_{X+5} (Figure 2.17). The nature of each tectonic phase, the related structures and the available time constraints are discussed below.

2.5.1 D_X The oldest deformation structures

The oldest deformation structures are preserved in schistose ultramafic xenoliths within the undeformed parts of the oldest recognised intrusive component of the MESZ; that is, the gabbro-diorite complex. Within the Northern Domain they are attributed to the deformation phase $D_{ND,1A}$. The age of the gabbro-diorite would provide the best estimate for the minimum age of the oldest deformation structures. However, the gabbro-diorite is not dated. The oldest, dated, intrusive rock in the MESZ is the 3324 ± 6 Ma Wilina Pluton (Collins et al., 1998). This is then the minimum age of the schistosity within the xenoliths. The kinematic framework of the structures within the xenoliths is not known because remnants are small and scattered and may not have been preserved in their original orientation.

2.5.2 D_{X+1} NE-SW extension pre-3324 ± 6 Ma

After the schistosity in the ultramafic xenoliths, the second oldest structures are those preserved

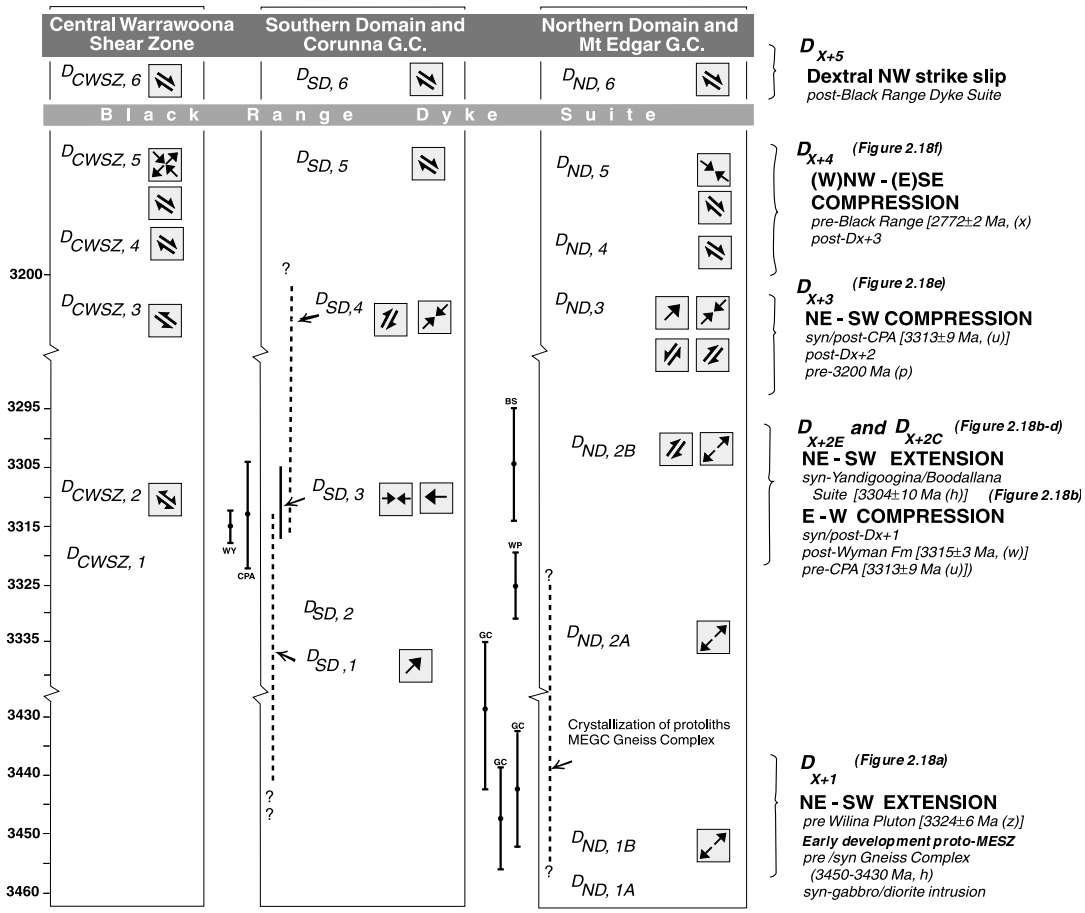

Figure 2.17 Cross-correlation of the observed deformation histories of the Northern and Southern Domains and the Central Warrawoona Shear Zone. Four main deformation phases, D_{X+1} to D_{X+4}, are recognised before intrusion of the ca. 2.77 Ga Black Range Dyke Swarm. These phases are discussed in the text, and are illustrated in figure 3.18. Letters in parentheses relate to references for geochronological data shown in figure 2.2.

within the gabbro/diorite complex and associated dolerite sills, which are the oldest identified intrusive components of the MESZ. The timing of the deformation is based on the observation that the gabbro/diorite complex and dolerite sills intruded syntectonically and on the assumption that they are all co-magmatic with the complex itself. The associated kinematics indicate NE-SW layer parallel extension, a phase referred to as $D_{ND,1B}$. The timing of this stage of extension is uncertain, because the ages of the gabbro/diorite and dolerites are unknown. A minimum age is provided by the crystallization age of the discordant Wilina Pluton (3324 ± 6 Ma, Collins et al., 1998). We suggest that NE-SW extension occurred at the time of the intrusion of gabbro/diorite and dolerite sills and caused the initial dome shape of what developed subsequently as the Mt Edgar Granitoid Complex. We attribute this part of the development to D_{X+1} (see figure 2.17).

2.5.3 D_{X+2} E -W compression and NE-SW extension at 3.32-3.30 Ga

Field data and geochronological constraints indicate that the structural development at 3.32-3.30 Ga involved both E-W extension ($D_{ND,2A-B}$ and ($D_{SD,1-2}$) and NE-SW compression ($D_{SD,3}$) (Figure 2.10).

Compression related structures comprise the W-vergent thrusts, the Brockman Hay and the Hilly Basalt Shear Zone, and the transpressional Fieldings Find and Copenhagen Shear Zones in the greenstones of the Southern Domain ($D_{SD,3}$). Geochronological constraints indicate a narrow time span for this phase, which occurred after deposition of the Wyman Formation, generally dated at ca. 3325 Ma, but dated at 3315 ± 3 Ma in the Warrawoona Belt (Buick et al., in press.) and before intrusion of the 3313 ± 9 Ma (Barley and Pickard, 1999) Carbana Pool Adamellite, which intruded the upper thrust slice and contains no E-W compressional structures.

Evidence for extension at this stage is seen in the upper and lower margins of the Mixed Zone. On the lower margin, structures within the Boodallana and Yandigoogina Suites indicate an NE-SW extensional setting for their emplacement at 3304 ± 10 Ma ($D_{ND,2B}$).

Although the available geochronological constraints indicate a narrow, overlapping time-span for thrusting and extension (Figure 2.10), the absence of E-W compressional structures (3315 ± 3 Ma to 3313 ± 9 Ma) in the syn-extensional 3304 ± 10 Ma Boodallana Suite (Williams and Collins, 1990) suggests E-W compression occurred before granitoid intrusion and extension. We refer to the compressional and extensional structures as formed during D_{X+2C} and D_{X+2E}, respectively, (Figure 2.17) and their relationship will be discussed further below.

2.5.4 D_{X+3} NE-SW compression

The best developed structures of this phase are found in the Carbana Pool Adamellite (CPA) where it intrudes the southern margin of the WGB (Figures 2.8a and 2.8b). They are the small SSW dipping brittle-ductile shears within the CPA and greenstones with oblique NE-vergent thrust sense ($D_{SD,4}$). The steep NNE-trending brittle-ductile shears in the CPA near the margin with the Kelly Belt, which show a dextral displacement (Figure 2.8b), are related to this phase. The age of the CPA (3313 ± 9 Ma, Barley and Pickard, 1999) provides a maximum age for these structures. NW-trending foliations and NE-vergent thrusts and subhorizontal quartz veins are found, cutting across the Brockman Hay, Fieldings Find and Copenhagen Shear Zones as well as the felsic volcanic units of the Wyman Formation ($D_{SD,4}$). In the CWSZ, the oblique SW-up shears fit a NE-SW compressional setting ($D_{CWSZ,3}$). In the Northern Domain, the greenschist facies shear zones that, in particular, cross-cut the well developed, amphibolite facies, mylonitic foliation of the hangingwall and the top of the Mixed Zone, and that show thrust-kinematics ($D_{ND,3}$), fit a NE-SW compressional setting. The NE-verging thrusts in the Cotton Well Pluton and the subhorizontal granitoid veins cutting the steep footwall mylonites of the MESZ are tentatively related to this phase.

2.5.5 D_{X+4} Dextral transcurrent shearing and NW-SE compression

The main structures of this phase are found in the CWSZ ($D_{CWSZ,4}$). They comprise dextral transcurrent to slightly oblique well-developed greenschist facies shears with consistently west-plunging stretching lineations. Parts of the MESZ and of the Southern Domain contain similar structures ($D_{ND,4}$ and $D_{SD,5}$) which we attribute to a phase of NW-SE compression, D_{X+4} (Figure 2.17). Brittle-ductile to brittle structures, including the dominantly 060° to 070°-trending crenulation cleavages, conjugate kink sets and km-scale dextral 070°-080°-trending faults and asymmetric folds overprint the above dextral greenschist facies shears ($D_{CWSZ,5}$ and $D_{ND,5}$), but fit the same NW-SE compressional framework. We interpret these structures to have developed during one continuous phase of NW-SE compression. Absolute age constraints for this phase are not available, but it predates intrusion of the dolerites of the 2.77 Ga Black Range Dyke Swarm.

The N-S to 020°-trending crenulation, that can be observed locally, formed late in the development of the Warrawoona Belt. It may indicate an ESE-WNW to E-W directed shortening, possibly related to the last stage of transcurrent shearing, or may be related to a phase that caused N-S trending crenulations regionally (Blewett and Huston, 1999a, 1999b).

2.5.6 D_{X+5} Post 2.77 Ga dextral strike-slip deformation

Faults with dextral strike-slip displacement have been recorded along quartz veins parallel to the WGB, mainly within the greenstones but also within the granitoid complexes . They dextrally offset the NNE-trending dolerite dykes of the 2772 ± 2 Ma (Wingate, 1999) Black Range Suite, which provides a maximum age for these structures ($D_{CWSZ,6}$; $D_{SD,6}$; $D_{ND,6}$). We attribute these structures to D_{X+5} (Figure 2.17).

2.6 Tectonic interpretation and discussion

A model for the evolution of the Warrawoona Greenstone Belt and adjacent granitoid complexes must integrate all five recognised tectonic phases (D_{X+1} - D_{X+5}, Figure 2.17). It must also explain: (i) the asymmetric, non-synclinal distribution of metamorphic grade and deformation intensity across the Warrawoona Greenstone Belt (Figures 2.8a and 2.8b); (ii) the Mt Edgar Shear Zone, its kinematics and the geometry of its structures (Figure 2.5); (iii) complex intrusive and geometric relationships in the Mixed Zone and the domal development of the granitoid complexes (Figure 2.16); (iv) the steep dip in the hangingwall of the Mt Edgar Shear Zone and the steep metamorphic gradient across the zone; (v) the loss of about 10 km of stratigraphy in the hangingwall; (vi) the occurrence of the Beaton Well Zone as a transfer zone to the MESZ (Figure 2.13); (vii) the occurrence of kyanite-bearing mylonites, overprinted by sillimanite and andalusite, also in the hangingwall of the MESZ (Figure 2.15). Additionally, a model must also explain the overall disk-like geometry of the granitoid complexes, indicated by geophysical models (Wellman, 1999).

2.6.1 Proposed model for the evolution of the Warrawoona Greenstone Belt and adjacent granitoid complexes

Our structural data and deformation sequence indicate that the Warrawoona Greenstone Belt and the adjacent granitoid complexes have undergone a multi-phase evolutionary history that is spread over a prolonged period, at least from deposition of the Duffer Formation at circa 3.46 Ga to after the Black Range Dyke Swarm at 2.77 Ga. The most prominent structures resulted from a phase of NE-SW extension during, and prior to, emplacement of the granitoid suites at 3.31 Ga. The MESZ and the Beaton Well Zone were active at 3.31 Ma and the Mt Edgar and Corunna Downs Granitoid Complexes were emplaced into the upper crust. We will argue later that not all intrusions in the MESZ were related to this 3.31 Ga event, and that some may have intruded during an earlier phase of activity on the (proto-)MESZ (see D_{X+1}). We will discuss the 3.31 Ga event first and then the deformation phases that preceded and followed it.

2.6.2 Deformation during the emplacement of the 3.31 Ga granitoids, D_{X+2}

Our data indicate that the Mt Edgar Shear Zone played an important role in the emplacement of the 3.31 Ga TTG suites in the Mt Edgar and Corunna Downs Granitoid Complexes during a NE-SW extensional tectonic event. The near orthogonal, E-W crustal shortening D_{X+2C} may have led to this event, as discussed below.

An important finding of our study is that in spite of the semi-circular outcrop pattern of the MESZ, it displays a uni-directional stretching lineation pattern (Figure 2.5), formed during NE-SW extension. This is different from the radial pattern predicted by the solid-state diapiric model (Dixon, 1975; Schwerdtner and Tröeng, 1977; Schwerdtner et al., 1978; Dixon and Summers, 1983; Cruden, 1988). In addition, we find, as described in §2.3.2 and as shown in figure 2.8a, that the supposedly interdiapiric, doubly plunging syncline in the WGB (characterised by a progressive increasing plunge of the stretching lineations towards the centre of the syncline) corresponds to an area in which shear zones merge and mutually interact to produce pencil rods through the intersection of oblique foliations. Consequently, especially because of the lineation pattern within the MESZ, we reject solid-state diapirism as the major cause of the emplacement of the Mt Edgar and Corunna Downs Granitoid Complex.

The rapid change in metamorphic grade from migmatitic gneisses to greenschists which occurs across the MESZ, the change in deformation mechanism from ductile in the footwall to brittle-ductile in the hangingwall during the domal event, together with the uni-directional stretching lineation is similar to what is seen in mid-crustal detachments formed around metamorphic core-complexes (e.g. Spencer, 1984; Reynolds and Lister, 1990; Dokka, 1993; Lister and Baldwin, 1993). The important role of plutonism in triggering doming, and the role of syntectonic sills in localizing strain within the mylonitic marginal zone has been emphasised by Lister and Baldwin (1993) and Pavlis (1996). Hence, intrusion of dolerite sills and sills of granitoids into the MESZ during NE-SW extension is also consistent with active extensional doming.

The model we propose for the 3.32 -3.31 Ga crustal thickening and extension is illustrated in

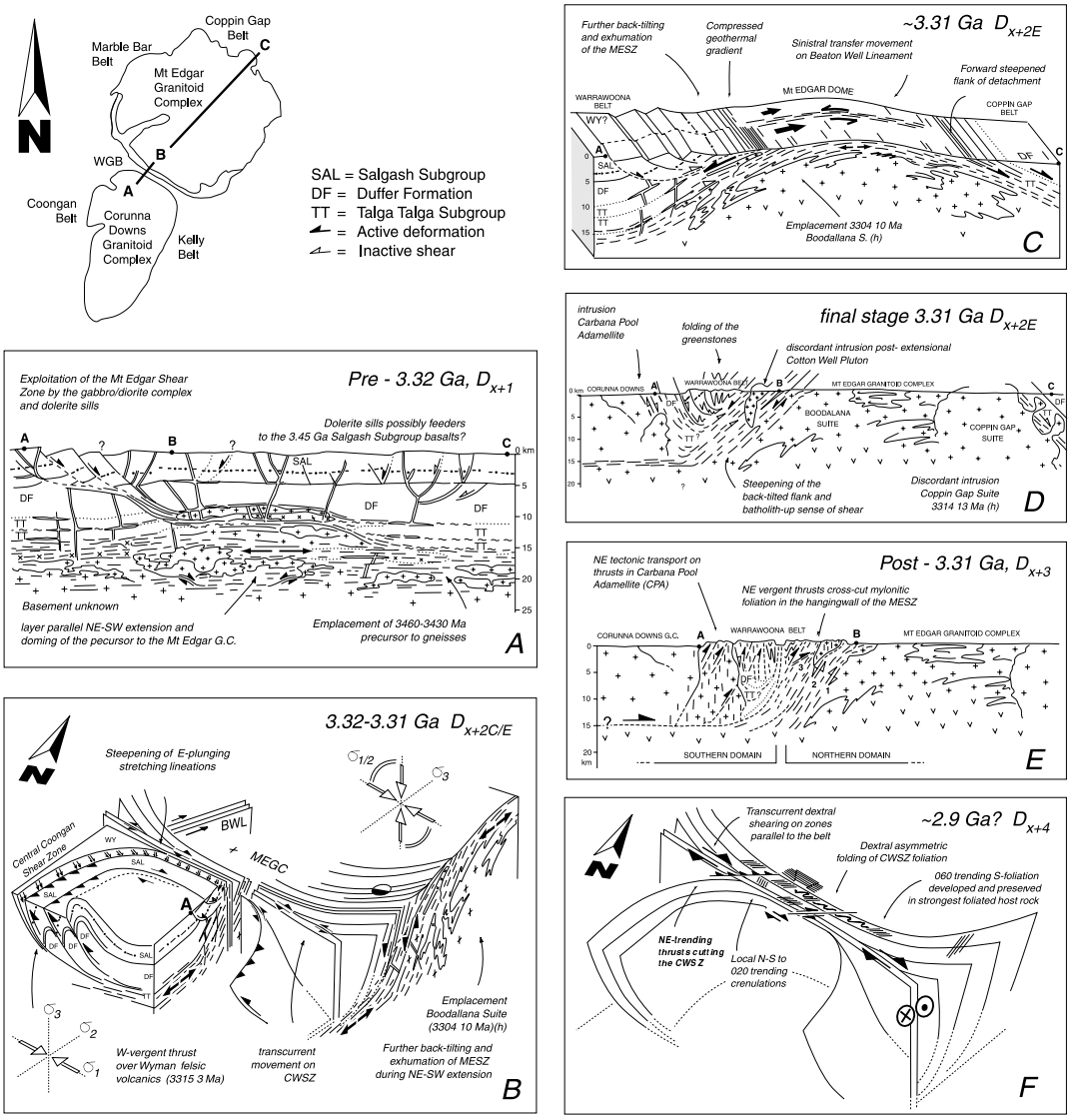

Figure 2.18 Cartoons summarizing the tectonic and magmatic development of the Warrawoona Belt and bounding granitoid complexes from ca. 3.47 to 2.9 Ga. (a) Pre-3.33 Ga gabbro/diorite and dolerite intrusions in the Mixed Zone, coeval NE-SW extension and doming of the MEGC. (b) Schematic representation of the W-vergent thrusting in the upper crustal sequences of the Southern Domain and concomitant NE-SW extrusion of 3.31 Ga granitoids at mid-crustal levels (c) Further development of the MESZ, with differential extension on the MESZ accommodated by transfer movement on the Beaton Well Zone (d) Final localised normal movement and further steepening of the MESZ followed by discordant intrusions of post-extensional plutons. (e) NE-verging thrusts reactivating the MESZ, the CWSZ and the margin of the Carbana Pool Adamellite. (f) Dextral transcurrent shearing, reactivation of the CWSZ as a transfer zone, NE trending thrusts and crenulations formed during regional NW-SE compression.

figure 2.18. This phase corresponds to the thermal event T_{X+3} in figure 2.2. Our observations indicate that E-W shortening immediately preceded the NE-SW extension, but may also have continued concomitantly with the extension (Figure 2.18b). The structural data within the Marble Bar Domain (see figure 2.6), are in accord with E-W compression preceding NE-SW extension at 3.31 Ga. In the Coppin Gap Belt, early, syn-Duffer (3460-3470 Ma) extension was followed by E-vergent thrusting, both of which occurred before steepening of the greenstone sequence and emplacement of the 3314 ± 13 Ma (Williams and Collins, 1990) Coppin Gap Suite (Nijman et al., 1998a). In the Tambourah Belt, thickening of the crust was proposed to have caused heating and the 'apparent diapiric rise' of granitoids (Bickle et al., 1980; Bickle et al, 1985; Boulter et al., 1987). Compression in this area may have led to mobilization, doming and partial melting of the ca. 3450 Ma gneissic basement of the Shaw Granitoid Complex at 3.3 Ga. However, only minor ~3310 Ma granitoid components occur in the Shaw Granitoid Complex (Chocolate Hill Suite, 3338 ± 52 Ma, Pb-Pb, whole rock, Bickle et al., 1993). The timing of compression in that area was at least ongoing till after ca. 3240 Ma, the recently determined maximum age of the basal Gorge Creek Group (Van Kranendonk and Morant, 1998), which was caught up in the compressional structures. The Coongan Belt is structurally dominated by folds and thrusts formed during E-W compression between deposition of the Wyman Formation and ca. 3200 Ma (Zegers et al., 1999). For the Marble Bar Belt, a sequence of deformation phases involved pre-3.31 Ga extension, followed by E-vergent thrusting which was in turn followed by NE-tectonic transport (Van Haaften and White, 1998).

The geochemistry of the 3.31 Ga granitoid suites in the Mt Edgar and Corunna Downs Granitoid Complex indicates they are derived from a felsic crustal source, possibly by partial melting of the 3.45 Ga gneissic basement (Collins, 1993; Barley and Pickard, 1999). The above model, in which partial melting was caused by crustal thickening and consequent heating of the crust, is consistent with the geochemical data. We suggest that the kyanite formed during this phase of crustal shortening and associated extension, and that the later generation of sillimanite and andalusite, preferentially in structures related to NE-SW extension, reflects exhumation during the extension, related to doming of, and magmatism within, the Mt Edgar Granitoid Complex. This relationship between compressional and extensional tectonic phases is similar to that found in modern collapsed orogens (Dewey, 1988) and has been described for the development of the Late-Archaean Zimbabwe Craton (Dirks and Jelsma, 1998).

In the studied area, compressional structures are preferentially preserved in the upper crustal sequences, whereas the extensional structures are best developed in the deeper crustal MESZ. This difference in structural level indicates that thinning of the thickened crust occurred dominantly at midcrustal levels, by sideways expulsion of rocks (Figure 2.18b). This difference in transport direction was accommodated by the MESZ, which would have decoupled the upper crustal levels from those below. This is unlike what is described for the majority of modern collapse-terrains, where upper crustal sections generally are described as having slid off the overthickened crust (Dewey, 1988). Rather, it is similar to that described for the Archaean Wawa gneiss domain, of the Superior Province, where regional compression caused duplication at upper crustal levels, and where at deeper crustal levels magma genesis and sideways extrusion of granitoids occurred. This happened within a period of 10-25 million years from initiation of the crustal thickening (Moser,

1994; Moser et al., 1996). A similar relationship between extensional and compressional structures during syncollisional extension at a mid-crustal level is described for the Palaeoproterozoic development of the Nagsuggtoquidian Gneiss Belt in West Greenland (Manatschal et al., 1998).

Our model infers that the MESZ would have tectonically eroded its way into upper crustal rocks as the Mt Edgar Granitoid Complex domed (Figure 2.18c). We see evidence for this in the current distribution of stratigraphic units (see Hickman and Lipple, 1978). When the stratigraphic assemblages of the western flank of the Mt Edgar Granitoid Complex (Marble Bar Belt) are compared with those of the southwestern flank (Warrawoona Belt), all of the Talga Talga Subgroup is missing and only 200 metres of strongly tectonised Duffer Formation is preserved. This indicates that possibly up to 9 km of the stratigraphic sequence has been removed. Similarly, when the western flank of the Mt Edgar Granitoid Complex is compared to the dominantly intrusive, northeastern flank, Coppin Gap Belt, (see Hickman and Lipple, 1978), a similar amount of stratigraphic section is missing. The preferential removal of stratigraphic units by tectonic erosion during active extensional doming in the direction of tectonic transport along the MESZ is predicted by a core complex model.

The Beaton Well Zone corresponds to a geophysically observed change in depth of the base of the Mt Edgar Granitoid Complex (Wellman, 1998), which suggests that it continues to depth. In our model, the Beaton Well Zone acted as a transfer zone, that accommodated differential extension on the MESZ, and to which the MESZ was the roof shear (Figures 2.18b and 2.18c). Similar structures, referred to as transverse zones, are described in the mid-Miocene core complexes of the D' Entrecasteaux Islands (Hill, 1994). Its dominantly sinistral transcurrent movement indicates that NE-directed extension was larger in the SE block than in the NW block. This is also reflected by the greater loss of stratigraphic units, when the supracrustal rocks in the SE block are compared to those in the NW block (Figure 2.3). Additional indications for differential extension are seen in when comparing the parts of the MESZ on either side of the Beaton Well Zone. The Mixed Zone of the MESZ is wider in the SE block (Figure 2.3). Also, the metamorphic grade of the hangingwall in the SE block is higher; kyanite and sillimanite-after-kyanite assemblages only occur in the SE block (see also Collins and Van Kranendonk, 1999; Délor et al., 1991). Finally, when comparing the NW to the SE block, the geophysically observed decrease in thickness of the Mt Edgar Granitoid Complex (Wellman, 1998), is consistent with an interpretation of greater extension in the SE block.

During active extension and doming of the detachment, the (north)northeastern margin of the Mt Edgar Granitoid Complex was tilted to the NE, and developed as the 'forward-tilted' part of the MESZ (see figure 2.18d). We envisage that the 'back-tilted', SW side of the MESZ became locked, but that the forward tilted part remained active during further extension. This would provide the space for the late- to post-tectonic intrusions, such as the 3314 ± 13 Ma Coppin Gap Suite (Williams and Collins, 1990) in the Mt Edgar Granitoid Complex (Figure 2.18d).

A prime feature of the studied area that is left unexplained by a core complex type model is the steep orientation of the MESZ. Both the forward- and back-tilted parts of the MESZ (see above) are approximately subvertical, which is steeper than the steepest (40-50°) maximum tilt described for traditional core complexes of the Basin and Range (e.g. Guérin et al., 1990). Marshak et al. (1997) have argued that steep marginal shear zones are an integral feature of extensional core-

complex formation in pre-Phanerozoic times. In their model, detachments and core complexes developed as a consequence of crustal-scale unidirectional extension similar to a modern-day metamorphic core complex (Figure 2.19-1). But, in pre-Phanerozoic times the crust may have been hotter and more mobile, and may have had an inverted density profile, that would make it less stable than the modern crust (see also Marshak, 1999). This, in combination with emplacement of granitoid plutons in the footwall of the detachments, will enhance the inverted density profile and the rheological contrast within the crust, and will trigger vertical rise of these granitoids through the basement (Figure 2.19-2). This would reactivate and steepen part of an original subhorizontal detachment towards the subvertical (Figure 2.19-3).

2.6.3 Pre-3.31 Ga deformation on the Mt Edgar Shear Zone, D_{X+1}

Evidence for activity on the MESZ prior to the NE-SW extension at 3.31 Ga is preserved in the Mixed Zone. The complicated overprinting relationships within the gabbro/diorite complex and dolerite sills, especially in the parts of the MESZ that are oblique to the transport direction (see figure 2.16), were developed prior to the intrusion of the Wilina Pluton, quoted at 3324 ± 6 Ma (Collins et al., 1998). It is not clear how much older the development of these structures in the Mixed Zone is. We tentatively relate this part of the development of the MESZ to the thermal event T_{X+2}, at circa 3.45 Ga (Figure 2.2) for the reasons outlined below.

In the Marble Bar Domain, pre-3.31 Ga igneous activity resulted in the 3.46-3.43 Ga granitoid components in the gneisses and the 3466 ± 2 Ma (Nelson, 1998a) alkali-feldspar granite on the western margin of the Mt Edgar Granitoid Complex, both corresponding to T_{X+2}. These intrusions formed coevally with deposition of the Duffer Formation, found in the greenstone belts surrounding the Mt Edgar Granitoid Complex (see §2.2.2). It is possible that the gabbro/diorite and dolerite intrusions are related to this phase of magmatic activity. They could be related to the syn-Duffer phase of extension that has been identified in the Coppin Gap and Marble Bar Belt (Nijman et al., 1998a; Van Haaften and White, 1998), which is thought to have produced the early doming in the North Shaw area (Zegers et al., 1996) and which is related to T_{X+2} in the Marble Bar Domain (Figures 2.2 and 2.6). Extension at 3.46 Ga was in an ENE-WSW to NE-SW direction, which could make distinction on geometrical grounds, between preserved 3.46 Ga structures and those formed at 3.31 Ga, difficult. We cannot rule out that the proto-MESZ may have been part of an earlier mid-crustal detachment system, related to that now seen exposed in the North Shaw area. This phase of tectonic activity (D_{X+1}) is illustrated in figure 2.18a. We show that crustal thinning in the studied area was limited, with slight doming of the lower crust into the upper, that is, the MESZ remained at mid-crustal levels until doming at 3.31 Ga (D_{X+2}). Alternatively, early extension and doming may have been significant, in which case the MESZ returned to mid-crustal levels prior to subsequent extension during D_{X+2}.

2.6.4 Deformation post-3.31 Ga granitoid emplacement

2.6.4.1 NE-SW compression, D_{X+3}

Structures of this phase, generally thrusts, crenulation foliations and fracture cleavages, have a constant NW trend in the granitoid complexes as well as in the Warrawoona Greenstone Belt, indicating that these structures formed after the main doming of the Mt Edgar Granitoid Complex. This phase may have steepened the domal structure of the MESZ and the structures of the Warrawoona Belt (Figure 2.18e). A maximum age is provided by the occurrence of related structures in the Carbana Pool Adamellite. A minimum age could be reflected by the widespread resetting of the Rb-Sr system of the Mt Edgar Granitoid Complex at ca. 3200 Ma (Collins and Gray, 1990) and similar ^{40}Ar-^{39}Ar cooling ages in the Coongan Belt (Zegers, 1996; Davids et al., 1997; Zegers et al., 1999)

A 3.20 Ga thermal event is widespread in the Marble Bar Domain (T_{X+4}, Figure 2.2), which suggests NE-SW compression may be regional. In the western Shaw Granitoid Complex and Tambourah Belt, post-Sulphur Springs, isoclinal recumbent folds, pre-dating the Lalla Rookh Sandstone, show a N to NW-trend (Bickle et al., 1980; Boulter, 1987), and may have formed during this phase. In the Marble Bar Belt, NE tectonic transport was observed in the Duffada Shear Zone (Van Haaften and White, 1998). Although an absolute age is not available, it was found to post date a phase of E-W compression in this area, and similar structures were found in the Warrulinya Suite, identified as one of the 3.31 Ga TTG suites of the Mt Edgar Granitoid Complex (Williams and Collins, 1990). In the Coppin Gap Belt and in the North Pole area, a phase of NE-SW compression caused folding, thrusting and steepening of early extensional and E-W compressional structures (Nijman et al., 1998). The widespread occurrence of NE-SW compressional structures indicates that it was a major deformation phase. We relate this phase of NE-SW compression to the thermal event, T_{X+4} (Figure 2.2).

2.6.4.2 Regional crustal-scale transcurrent shearing, D_{X+4}

This last main deformation phase resulted in dextral strike-slip reactivation of shear zones parallel to the Warrawoona Belt, especially the CWSZ, indicating NW-SE compression. NE-trending compressional foliations are widely developed, especially in the most intensely foliated parts of the WGB. The Southern Domain was less affected. These (crenulation) foliations are cut and dextrally offset by strike-slip deformation in the CWSZ. Later faults, thrusts and kinks (see §2.3.2) fit the same stress field and are interpreted to have been formed during this deformation phase (Figure 2.18f). The locally observed N-S to 020°-trending crenulation foliation may indicate an additional, more WNW-ESE directed, compressional phase, but its relationship with the main dextral phase, and its regional significance is unclear. The CWSZ as seen in present outcrops is dominantly a D_{X+4} structure. It cuts through the MESZ in the most attenuated part of the WGB and it preserves boudins with structures that are kinematically related to the MESZ. It is not clear if the CWSZ first developed during an earlier deformation phase, namely D_{X+2}.

On the western margin of the Marble Bar Domain, NW-SE compression caused major sinistral strike-slip movement on the N-S-trending Mulgandinah Shear Zone Complex (Zegers, 1996; Van

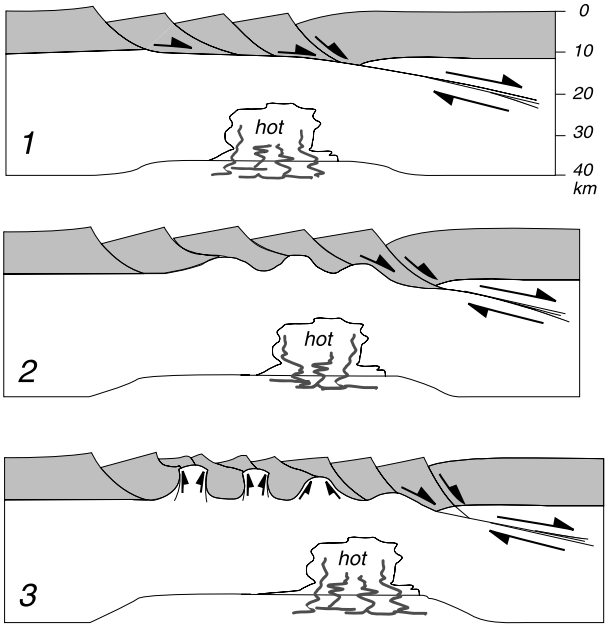

Figure 2.19 Schematic model for the development of dome-and-keel provinces formed in pre-Phanerozoic times (after Marshak et al., 1997). The steep-sided domes are not solid-state diapirs, but resemble steepened metamorphic core complex-type, which have formed as a result of active crustal extension. The steepness may reflect a different rheological state of the pre-Phanerozoic crust. Supracrustals are shaded, basement is white. 1: Initial extension. 2: Initial dome formation. 3: Late stage of dome formation.a

Kranendonk and Collins, 1998; Zegers et al., 1998a). The late phase of folding and shearing on NNE-trending shear zones in the Tambourah Belt and Western Shaw Granitoid Complex (Bickle et al., 1985; Boulter, 1987) may be related to this phase (Figure 2.6). In the Talga Talga area of the Marble Bar Belt, brittle N-S and E-W faults show sinistral and dextral displacement, respectively, indicating NW-SE compression (Van Haaften and White, 1998). In the E-W-trending Coppin Gap Belt, NW-SE compression resulted in dextral transcurrent shearing parallel to the trend of the belt. Regionally this phase is temporally constrained to circa 2950–2930 Ma (Zegers, 1996; Zegers et al., 1999) and corresponds to T_{X+5} (Figures 2.2 and 2.6). It has been related to the accretion of the eastern and western Pilbara (Smith et al., 1998) and to the strike-slip basins hosting the Lalla Rookh Sandstone (Krapez and Barley, 1987; Krapez and Eisenlohr, 1998).

2.6.5 Implications for Archaean geodynamics

The history of the Warrawoona Belt and bounding granitoid complexes involved a sequence of four main deformation events, before 2.77 Ga, which involved extension, compression and strike-slip deformation. All phases can be related to events recognised within the larger area of Marble Bar Domain, suggesting a common tectonic history, possibly from 3.47 Ga onwards. This indicates that the scale of the driving force for deformation is larger than the size of the domain and fits a plate-tectonic type interpretation in which regional stresses are caused by plate interaction. Although an accretionary complex has been recognised in the West Pilbara (Kiyokawa and Taira, 1998), many characteristics of plate tectonics, or more precisely, many characteristics of subduction related processes, have not been recognised in the Pilbara Craton (e.g. linear trending orogens, abundant high-pressure metamorphic assemblages, remnants of oceanic crust). The lack of such typical characteristics of subduction zones may be a preservation effect, or it may indicate that a different

mode of plate-type tectonics was operative (see review of Hamilton, 1998).

Models for cooling of the Archaean Earth have two end-members: plume dominated tectonics and plate tectonics. Recently, the role of mantle plumes has been emphasised for the early tectonic development of the Pilbara, driving crustal, solid-state diapirism at 3.45-3.3 Ga (Collins et al., 1998). Although we have shown that solid-state diapirism is not sufficient to explain the crustal development of the eastern Pilbara granite-greenstone terrain, we do not oppose the role of mantle plumes in Archaean geodynamics, but see it as subsidiary to plate interaction-type processes.

2.7 Conclusions

1. The Warrawoona Greenstone Belt and adjacent Mt Edgar and Corunna Downs Granitoid Complexes have had a prolonged history with at least four main deformation phases (D_{X+1} to D_{X+4}) between ca. 3.46 and 2.77 Ga.

2. An important doming phase occurred during active NE-SW extension and granitoid emplacement in the Mt Edgar Granitoid Complex at 3.31 Ga (D_{X+2}). Extension may have been the result of an earlier phase of E-W compression at ca. 3.32 Ga. This may have caused crustal thickening and resulted in partial melting, possibly of the 3.46-3.43 Ga granitic basement, causing crustal weakening, collapse and the emplacement of the 3.31 Ga granitoids.

3. NE-SW extension within the Mt Edgar Granitoid Complex at 3.31 Ga was accommodated by the Mt Edgar Shear Zone, a reactivated mid-crustal detachment, and the associated Beaton Well Zone, which acted as a transfer zone to the Mt Edgar Shear Zone.

4. Indications for an older doming phase, of unknown age, but prior to 3.32 Ga, come from the syntectonically intruded gabbro/diorite and dolerite sills in the Mt Edgar Shear Zone, which may have intruded as early as 3.46-3.45 Ga (D_{X+1}).

5. After the main development of the Mt Edgar and Corunna Downs Granitoid Complexes and their emplacement in the crust at 3.31 Ga, a phase of NE-SW compression (D_{X+3}) formed NW-SE trending brittle-ductile foliations and thrusts.

6. A phase of NW-SE compression (D_{X+4}) caused dextral transcurrent deformation on the Central Warrawoona Shear Zone. It is possibly related to a Pilbara-wide compressional deformation phase at 2.95-2.93 Ga.

7. The stretching lineation pattern, formed during doming of the Mt Edgar Granitoid Complex, is uni-directional, not radial. Consequently, we reject the hypothesis that passive, solid-state diapirism or crustal convective overturn was the major underlying geodynamic process, and consequently we rather seek an answer in plate-interaction type processes.

Chapter 3

Structural history and SHRIMP U–Pb zircon chronology of an Archaean mid-crustal detachment, Pilbara Craton, Australia

3.1 Abstract

The 2-5 km wide Mt Edgar Shear Zone forms the dome-shaped contact between supracrustal greenstone and variably deformed granitic rocks along the southern and southwestern margin of the Mt Edgar Granitoid Complex of the northeastern part of the Archaean Pilbara Craton of Western Australia. This structure has played a key role in the domal development of the Mt Edgar Granitoid Complex: it has formed the detachment that facilitated the emplacement of granitoids at ca. 3315-3309 Ma during NE-SW extension (See chapter 2). Older, coarse-grained mafic intrusive rocks were found to have intruded as syntectonic sheets in the detachment. This suggests that the Mt Edgar Shear Zone originated as a mid-crustal detachment prior to ca. 3315 Ma, and indicates that the development of the Mt Edgar Granitoid Complex at ca. 3315-3309 Ma exploited an earlier structure, the age of which was unknown.

Detailed mapping of deformational and intrusive relationships, combined with Sensitive High Resolution Ion MicroProbe (SHRIMP) U–Pb zircon geochronology has identified a pre-3.31 Ga history of the Mt Edgar Shear Zone. It was found that at least six syntectonic components intruded the proto-Mt Edgar Shear Zone during the period 3.47-3.42 Ga: (1) hornblende gabbro/diorite sills intruded during crustal scale layer-parallel NE-SW extension (D_{X+1A}) at 3462 ± 3 Ma (sample CTW-36), (2) phenocrystic dolerite sills, (3) alkali-feldspar granite, (4) granodiorite, diorite and tonalite sills, (5) syn-extensional intrusion of dolerite sills and dykes, and (6) leucogranite sills emplaced at 3447 ± 6 Ma (sample P95-gran).

An intricate relationship between structures, kinematics and overall retrograde metamorphic conditions are consistent with progressive doming of the Mt Edgar Granitoid Complex as a result of ENE-WSW extension prior to intrusion of the leucogranite at 3447 ± 6 Ma. A pattern of SW to SSW-plunging lineations are observed throughout the dome shaped detachment. In the central part

of the complex, subhorizontal 3426 ± 4 Ma granodiorite sheets (sample A94-22) intruded banded gneisses and provide a younger limit for the onset of development of the gneissic footwall (D_{X+1}).

Biotite-granodiorite sills that intruded the Mt Edgar Shear Zone at the margin with the footwall were dated at 3315 ± 5 Ma (sample ME-28). This confirms that the shear zone was active during a complex deformation phase of NE-SW extension and associated compression at ca. 3.32-3.31 Ga, attributed to D_{X+2} (see chapter 2). A discordant, late-tectonic muscovite-rich granite, the Cotton Well Pluton, was dated at 3309 ± 4 Ma (sample CTW-1A). This age provides a minimum age for the development of the Mixed Zone.

3.2 Introduction

An outcrop pattern of ovoid granitoid complexes and skirting greenstone belts is characteristic of mid-Archaean (3.5-3.0 Ga) granite-greenstone terrains such as in the Pilbara (Western Australia), Kaapvaal (South Africa) and Dharwar (India) cratons. The domal profile of granitoid complexes forms the basis for models that advocate crustal-scale solid-state diapirism (Hickman, 1983) or, convective overturn of the crust caused by heating of the crust due to mantle plumes (Choukroune et al., 1995; Chardon et al., 1998; Collins et al., 1998). Archaean non-diapiric structures, however, were recognised in the eastern part of the Pilbara granite-greenstone terrain (e.g. Bickle et al., 1980, 1985; Krapez, 1984; Boulter et al., 1987; Krapez and Barley, 1987; Krapez, 1993; Van Kranendonk and Collins, 1998; Zegers et al., 1996, 1998a; Van Haaften and White, 1998, 2001; Chapter 2). These structures have mostly been interpreted as the result of either active compression, extension and strike-slip deformation during formation and assembly of the granite-greenstone terranes of the Pilbara Craton.

One of the most studied granitoid complexes in the eastern Pilbara is the Mt Edgar Granitoid Complex (MEGC). This granitoid complex and the adjacent Warrawoona Greenstone Belt and Corunna Downs Granitoid Complex have had a prolonged history with at least four main deformation phases (D_{X+1} to D_{X+4}) between ca. 3.46 and 2.77 Ga, as has been shown in chapter 2. A key element in the development of this domal complex is the Mt Edgar Shear Zone (MESZ) (chapter 2). This shear zone is a 2-5 km wide structure that, along with the supracrustal units, geometrically defines the domal architecture of the Mt Edgar Granitoid Complex. The MESZ has previously been described as a circum-diapiric shear zone formed as the result of passive, solid-state diapirism of the MEGC (Collins, 1989; Collins et al., 1998). In chapter 2, however, it was found that the MESZ is a shear zone with a central core of mylonites and intrusions, that suggested a longlived and complex history. Most significant was the uni-directional pattern of well developed stretching lineations in the MESZ. It was concluded that the main doming was related to active NE-SW extension and granitoid emplacement in the Mt Edgar Granitoid Complex at 3.31 Ga (D_{X+2}). Indications for older deformation in the MESZ, of unknown age, but pre-dating 3.32 Ga, come from the syntectonically intruded gabbro/diorite and dolerite sills of unknown age in the Mt Edgar Shear Zone. To identify an older deformation phase in the MEGC and MESZ would be important in the reconstruction of the deformation history of the area, particularly for the discussion

on the cause and mechanism of doming

The aim of the study described in this chapter is to constrain the timing of activity of the MESZ. This is achieved by determining the age of magmatic components with a known spatial and temporal relationship to deformation structures in the MESZ using Sensitive High-Resolution Ion Microprobe (SHRIMP) U-Pb zircon geochronology. The samples were selected based on detailed lithological and (micro)structural mapping. Detailed mapping of the MESZ focussed on the Mixed Zone, as that is where the intricate relationships between deformation and intrusions are best developed. It is found that the MESZ was active during at least two tectono-magmatic phases, one at ca 3.31 Ga (D_{X+2}) and one at >3447 ± 6 Ma. This forms a basis for a discussion on the emplacement mechanisms of Early-Mid Archaean granitoid complexes.

3.3 Geological setting

The Pilbara granite greenstone terrain has been divided into six fault bounded domains (Krapez and Barley, 1987; Krapez, 1993; Krapez and Eisenlohr, 1998; Smith, 1998). The eastern part of the

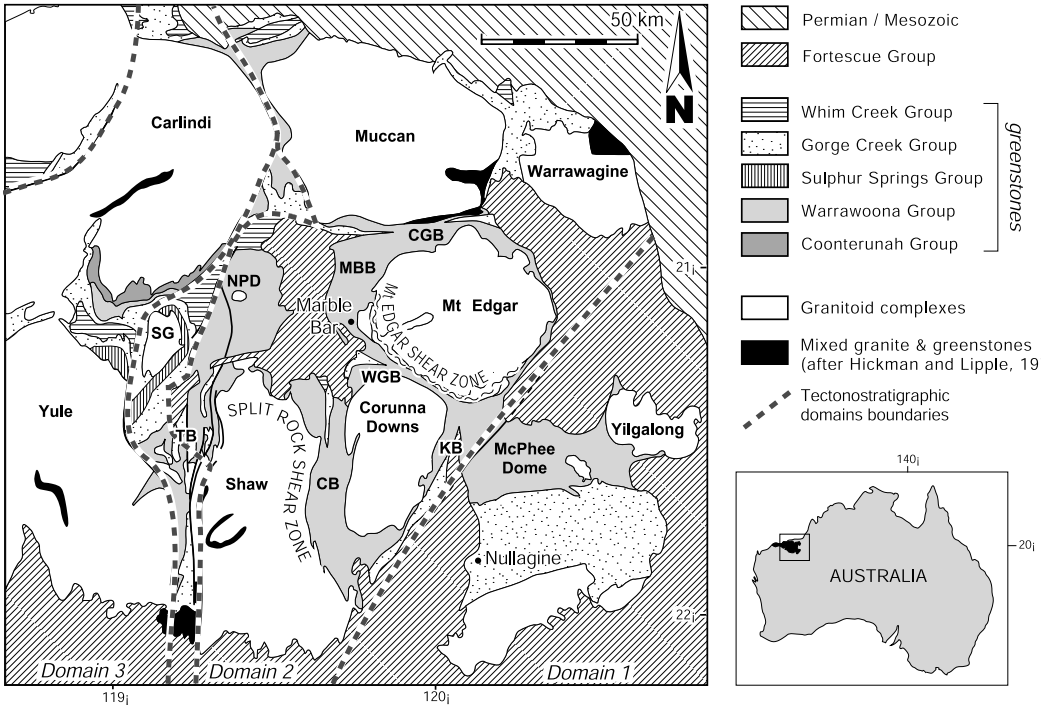

Figure 3.1 The eastern Pilbara, showing Domain 1, 2 and part of Domain 3. Stratigraphy is after Hickman (1983), Van Kranendonk and Morant (1998), Barley and Pickard (1999) and Buick et al. (1995). SG= Strelley Granite, TB= Tambourah Belt, CB= Coongan Belt, NPD= North Pole Dome, MBB= Marble Bar Belt, WGB= Warrawoona Belt, CGB= Coppin Gap Belt and KB= Kelly Belt. The Split Rock Shear Zone and the Mt Edgar Shear Zone along the margins of the Shaw and the Mt Edgar Granitoid Complex, respectively, are marked. Subdivision of tectonostratigraphic domains is after Krapez and Barley (1987), Krapez (1989, 1993), Krapez and Eisenlohr (1998) and Smith et al. (1998).

granite-greenstone terrain comprises Domain 1, 2 and 3 (Figure 3.1). Domain 2 is referred to as the Marble Bar Domain. It contains five main granitoid complexes which are surrounded by greenstone belts that predominantly consist of supracrustal rocks. The contact between the Marble Bar Domain and Domain 3 to the west is formed by an zone that includes the Tambourah Belt, Strelley Granite and the Lalla Rookh Basin, and is referred to as the Lalla Rookh Strike-Slip orogen (Krapez and Eisenlohr, 1998).

3.3.1 The Marble Bar Domain

The Marble Bar Domain comprises granitoid complexes and supracrustal rocks that were formed during at least five episodes of igneous activity, some of which were craton-wide and some of which were restricted to the eastern part of the Pilbara, from ca. 3650 to 2750 Ma (Figure 3.2, c.f. Blewett and Huston, 1999; Nelson et al., 1999 and references therein). The stratigraphy of the Marble Bar Domain has been defined by Hickman (1983), Buick et al., (1995), Van Kranendonk and Morant (1998) and is briefly summarised in figure 3.3. A short chronological overview is presented of igneous episodes, stratigraphic sequences and related deformation phases in the Marble Bar Domain. Ages, if not indicated otherwise, are SHRIMP U-Pb zircon ages that represent the time of crystallization of the rock.

3.3.1.1 Igneous episodes and deformation phases of the Marble Bar Domain

The oldest supracrustal rocks in the eastern Pilbara are those of the Coonterunah Group, dated at ca. 3515 Ma (Buick et al., 1995). They are dominantly basaltic and are found in a ~80 km long but narrow outcrop just to the west of the Marble Bar Domain. In the Marble Bar Domain itself, the oldest well defined volcanic episode is the Warrawoona episode (3490-3420 Ma) (Nelson et al., 1999), during which the Warrawoona Group was deposited (See figure 3.3). The Warrawoona Group comprises the lower Talga Talga Subgroup, the Duffer Formation, and the upper Salgash Subgroup. The Duffer Formation was deposited during the development of an extensional growth fault system at 3.47-3.46 Ma, caused by either regional extension as a result of plate-induced far-field stresses (Zegers et al., 1996) or caldera collapse (Nijman et al., 1998a). The tectonic setting of the Salgash Subgroup is the subject of chapter 4. A felsic unit of the upper Salgash Subgroup, the Panorama Formation, was dated at 3457 ± 3 Ma in the type section at Panorama Ridge in the North Pole Dome (See figure 3.1), using thermal ionisation mass spectrometry (TIMS) U-Pb zircon (Thorpe et al., 1992), but was recently found to be 3434 ± 5 Ma (Nelson, 2000).

The second oldest igneous episode in the Marble Bar Domain (the Wyman episode, Nelson et al., 1999) ranges from ca. 3325 Ma to 3290 Ma. It involved felsic volcanism of the Wyman Formation at 3325-3315 Ma (Thorpe et al., 1992; McNaughton et al., 1993; Barley and Pickard, 1999). Granitoid suites coeval with the Wyman Formation have been reported to constitute up to 75% of the MEGC (Williams and Collins, 1990). These granitoids may have formed by partial melting of older TTG suite rocks at a range of crustal depths, possibly from a 3.46-3.43 Ga Central Gneiss Complex in the MEGC (Collins, 1993; Barley and Pickard, 1999). This episode has been proposed to be the result of either partial convective overturn, including granitoid diapirism due to

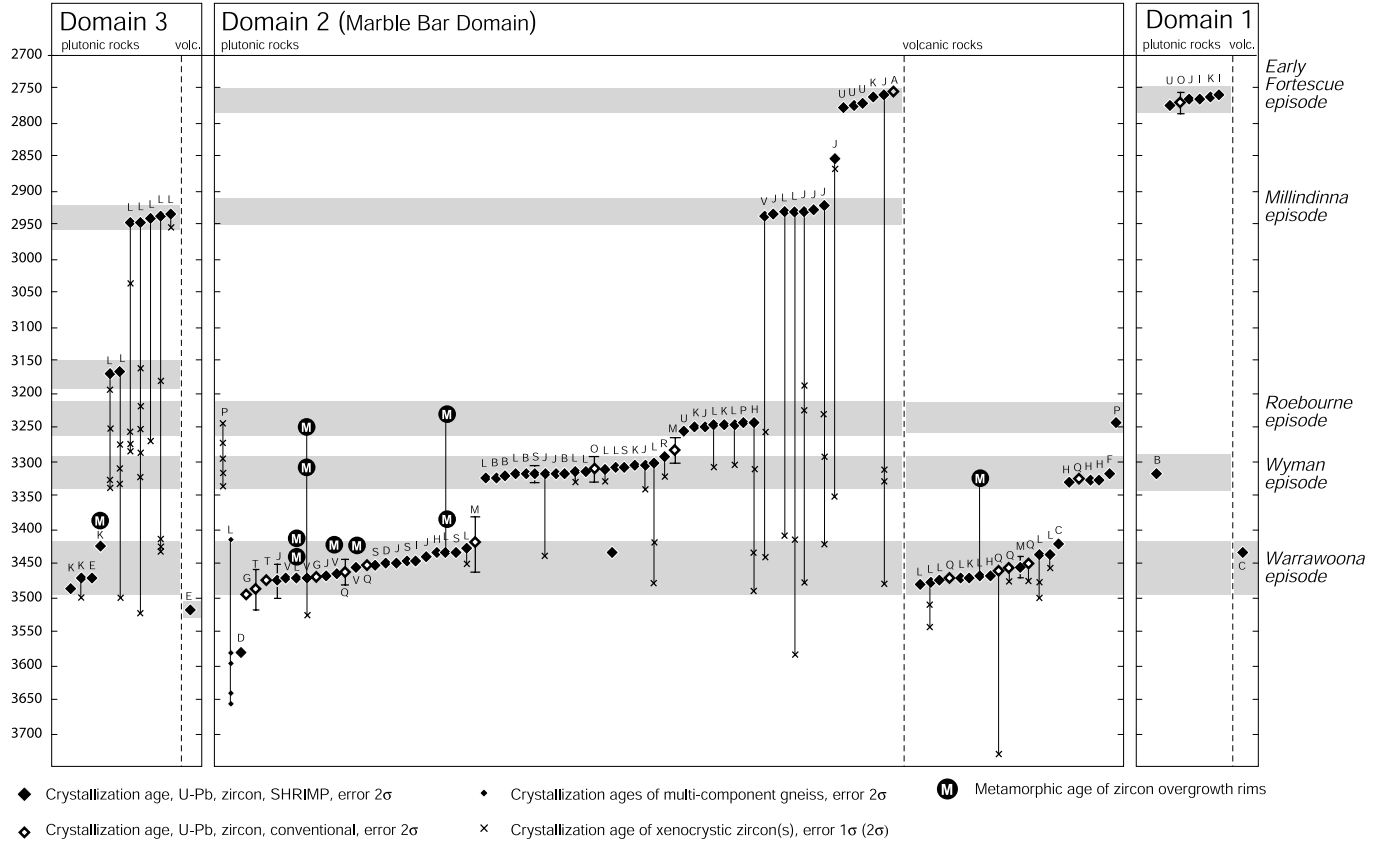

Figure 3.2 Available SHRIMP and conventional U-Pb zircon geochronological data for plutonic and volcanic rocks are plotted for Domains 1, 2 and 3. Five main episodes of igneous activity are recognised in domain 2, ranging in age from 3.5 to 2.8 Ga. Some of these episodes are absent in the adjacent domains, but correlate in age with xenocrystic zircons. The oldest zircons are found in magmatic components within gneiss. Their age ranges between 3650 and 3600 Ma, a poorly defined episode collectively referred to as Ix. Metamorphic zircon growth events are marked 'M'. The implications of metamorphic zircon growth events is discussed in the text. A= Arndt et al. (1991), B= Barley and Pickard (1999), C= Barley et al. (1998), D= Bettenay et al (subm. 1988), E= Buick et al. (1995), F= Buick et al. (subm.), G= McNaughton et al. (1988), H= McNaughton et al. (1993), I= Nelson (1996), J= Nelson (1998b), K= Nelson (1999), L= Nelson (2000), M= Pidgeon (1978a), O= Pidgeon (1984), P= R. Buick unpubl. data in: V. Kranendonk (1998), Q= Thorpe et al. (1992a), S= Williams and Collins (1990), T= Williams et al. (1983), U= Wingate (1999), V= Zegers (1996), W= Van Kranendonk, unpubl. data in: Collins et al., 1998).

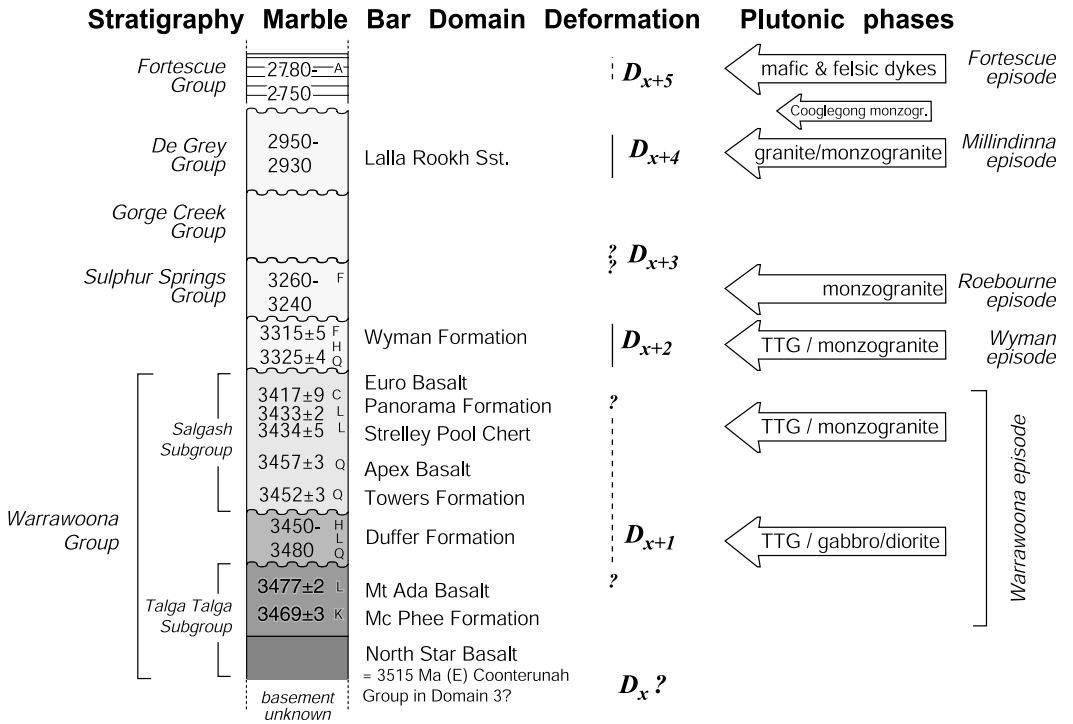

Figure 3.3 Showing the stratigraphy for the Marble Bar Domain after Hickman (1983) and Van Kranendonk and Morant (1998), Buick et al. (1995). The igneous episodes and the references to geochronological data refer to (Nelson et al., 1999) and those in figure 3.2 Deformation phases are as described in chapter 2.

mantle plume activity (Collins et al., 1998), or to a phase of E-W compression and NE-SW extension (See chapter 2).

A third igneous episode (the Roebourne episode, Nelson et al., 1999) is dominantly present as felsic volcanic units of the Sulphur Springs Group dated at ca. 3260-3240 Ma (See figure 3.2 and references therein). Coeval monzogranite intrusions were found in the nearby Strelley Granite and in most of the larger granitoid complexes, including the MEGC (Nelson et al., 1999). Barley and Pickard (1999) suggested that the development of a sub-marine extensional fault array in the volcanic rocks of the Strelley Belt at 3260-3240 Ga (Vearncombe et al., 1998) may be the continuation of extension at 3.32-3.31 Ga and may be related to back-arc extension.

The age of the dominantly sedimentary Gorge Creek Group is not constrained. Only a minimum age is provided by the De Grey Group, which is deposited during the Millindinna episode (Nelson et al., 1999) at 2930-2950 Ma. The latter is coeval with intrusion of granite and monzogranite associated with craton-scale strike slip zones related to regional WNW-ESE compression (Zegers, 1996; Van Kranendonk and Collins, 1998; Zegers et al, 1998a).

With the intrusion of the 2851 ± 2 Ma tin-bearing Cooglegong monzogranite in the Shaw Granitoid Complex (Nelson, 2000), and with deposition of the flood basalts of the Fortescue Group and intrusion of the basaltic Black Range Dyke Swarm at ca. 2.80-2.75 Ga (Arndt et al., 1991;

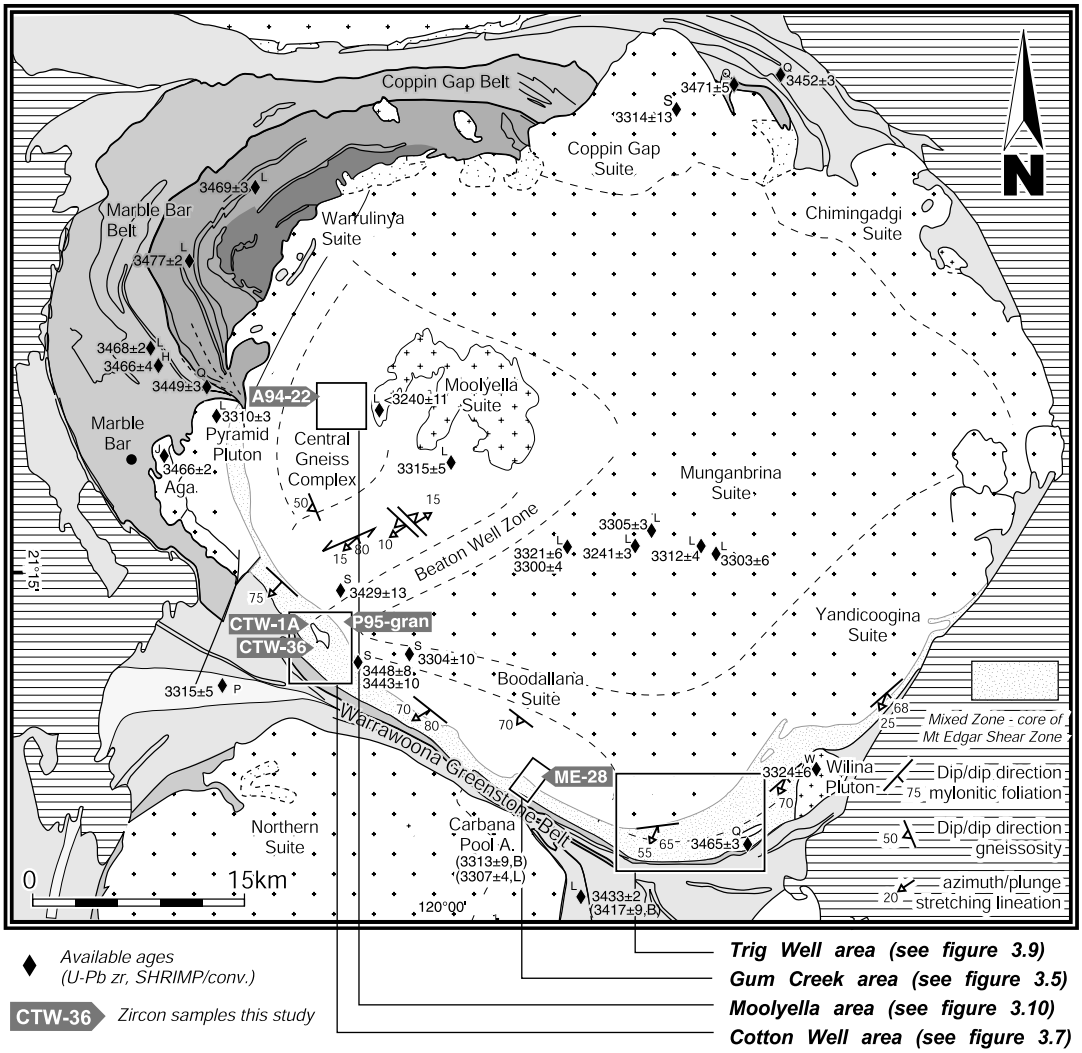

Figure 3.4 A generalised map of the Mt Edgar Granitoid Complex and the surrounding greenstone belts showing the trend of the Mt Edgar Shear Zone by marking its intrusion-dominated central core: the Mixed Zone (See chapter 2). The localities of the areas of interest for this study are marked. The outline of the granitoid suites within the MEGC is after Wellman (1999). See figure 3.2 for references to geochronological data. See figure 3.2 for legend of the stratigraphic units.

Wingate, 1999), the main structural development of the Pilbara Granite-greenstone terrain was completed.

3.3.2 The Mt Edgar Granitoid Complex and the Warrawoona Greenstone Belt

The Mt Edgar Granitoid Complex is located in the eastern part of the Marble Bar Domain (See figure 3.1). It comprises a Central Gneiss Complex with granitoid components ranging in age from 3.46 Ga to 3.42 Ga (Williams and Collins, 1990). These gneisses are intruded by TTG suites dated at 3.32-3.31 Ga, a monzogranite dated at ca. 3241 ± 3 Ma, and the post tectonic Moolyella Adamellite dated at <3240 Ma (possibly ~2850 Ma, Nelson 2000) (See figure 3.4 for locations and references to ages). These intrusive rocks are attributed to the Warrawoona, Wyman and Roebourne igneous episodes (See above and see Nelson et al., 1999).

The Warrawoona Greenstone Belt is a strongly deformed and attenuated supracrustal belt situated in between the Mt Edgar Granitoid Complex and the Corunna Downs Granitoid Complex (See figure 3.4). It contains rocks from the Duffer Formation, the Salgash Subgroup and the Wyman Formation (Hickman, 1983). A felsic volcanic unit in the southeastern part of the belt was previously lithostratigraphically correlated with the Duffer Formation (Hickman, 1983), but it was recently dated at 3417 ± 9 and 3433 ± 2 Ma by Barley et al. (1998a) and Nelson (2000), respectively, and hence is here referred to as Panorama Formation (See figure 3.3).

The main structure between the MEGC and the Warrawoona Belt is the Mt Edgar Shear Zone, which separates the granitoids from the greenstone sequence along the southern and southwestern margin. The MESZ has been active during the five deformation phases (D_{X+1} to D_{X+5}) (See chapter 2).

3.3.3 The Mt Edgar Shear Zone

The MESZ is an arcuate 2-5 km wide complex shear zone structure that runs along the steep margin between the MEGC and the Warrawoona Belt (See figure 3.4). As is outlined in chapter 2 the MESZ has a central core that is dominated by intrusive sills ranging from gabbro and dolerite through diorite and granodiorite to granite sills. This central core is referred to as the 'Mixed Zone'. The Mixed Zone separates a granite/granite-gneiss dominated footwall from a hangingwall dominated by metamorphic volcanic rocks. The MESZ was active during at least five deformation phases from pre-3.32 to post 2.77 Ga (See chapter 2). An overview of the relative timing of the main deformation phase of the MESZ in relation to the stratigraphic and magmatic development of the Marble Bar Domain is presented in figure 3.3.

3.4 Methodology

The structural and magmatic evolution of the ~75 km long MESZ was studied by investigating the structural and magmatic history of three selected areas. Each area is focussed on the central core of the MESZ, the Mixed Zone. These areas were mapped on scales varying from 1:1000 to 1:40 000 to derive the relationship between deformation and magmatism. These local relationships allowed SHRIMP U-Pb zircon geochronology to determine the timing of deformation. Figure 3.4 shows

the location of the selected areas.

In the Gum Creek area a 1400 m x 150 m segment across the Mixed Zone was mapped at a 1:1000 scale to establish intrusive relationships. Deformation in the area, however, was found to have obliterated many primary features. Therefore, two less deformed areas were selected to provide additional information on primary rock-types and intrusive relationships. The Cotton Well area is situated in the central southwestern part of the MESZ, and the Trig Well area is located in the southeastern part of the MESZ (See figure 3.4), some 20 km SE of Cotton Well. An additional reason to select the Trig Well area was to further investigate the syn-extensional doming structures described in chapter 2 and relate them to the magmatic history of the Mixed Zone. A fourth area comprises a well exposed part of the central Gneiss Complex west of the Moolyella Adamellite (See figure 3.4). It was selected to study the development of the footwall to the MESZ.

3.5 Results

3.5.1 Magmatic and structural history of the selected areas

3.5.1.1 The Gum Creek area

The centre of the Mixed Zone comprises coarse to medium-grained gabbroic to dioritic sills that form a 450 m thick sheeted complex (~450-1050m, figure 3.5). Anastomosing zones occur throughout the complex, but particularly in section 600-950m (Figure 3.5). In these zones the grain size is generally smaller and rocks show a well developed hornblende mineral lineation. Some of these aligned hornblende crystals are internally undeformed, suggesting a local magmatic origin of the fabric. Locally, a further reduction in grain-size and stretched hornblende and plagioclase crystals marks a mylonitic to ultra-mylonitic fabric in the hornblende-gabbro/diorite complex. Hornblende-gabbro/diorite sills were found to have intruded these anastomosing zones and contain a generally medium grained foliated and lineated fabric parallel to that of the host-rocks, suggesting syntectonic emplacement. The latter intrusions are referred to as sills because their orientation is parallel to the structure of the host rock (Philpotts, 1990). Both the mylonitic foliation and the sills dip steeply to the SW (Figure 3.6a). This unit is here referred to as the hornblende-gabbro/diorite complex (unit 'hg').

A suite of dolerite sills (unit 'd', figures 3.5 and 3.6b) have intruded into the mylonitic foliated zones in the hornblende-gabbro/diorite complex and into a sill of pink alkali-feldspar granite (600-950 m). Most dolerite sills show an aligned fabric defined by hornblende. Some dolerite sills contain a chlorite bearing mylonitic foliation.

Metre-wide leucogranite sills (unit 'lg', e.g. at 550-750 m, figure 3.5) locally intruded the margins of the dolerite sills in the hornblende-gabbro/diorite complex and alkali-feldspar granite and along the fabric of the gneissic 'gdt' near the footwall (e.g. at 50-150 m, figures 3.5 and 3.6c). The leucogranite sills are generally sheared, in both the Mixed Zone and the gneisses, with a mylonitic foliation and stretching lineation that is parallel to those in the hornblende-gabbro complex and dolerite sills.

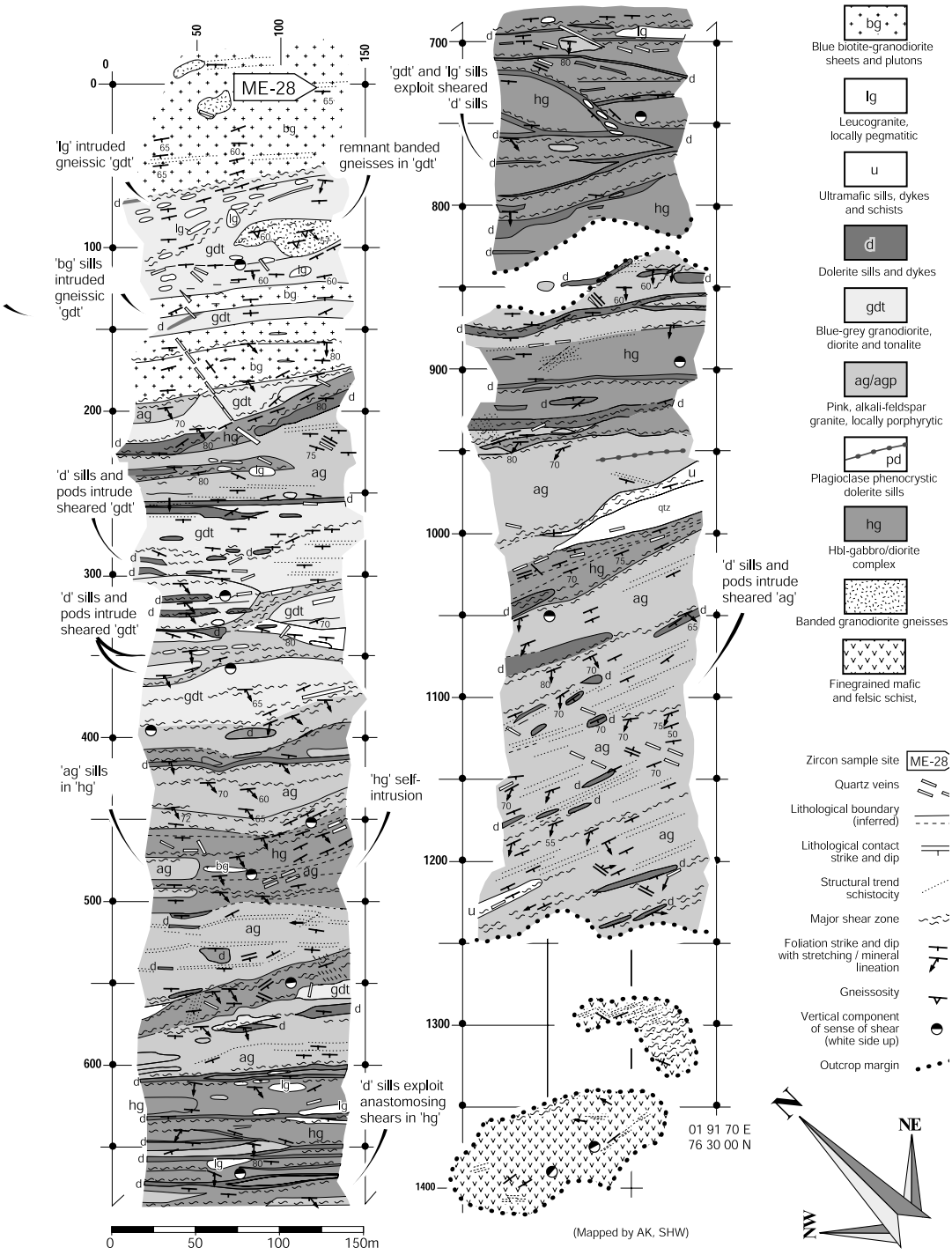
ME-28
'lg' intruded gneissic 'gdt'
remnant banded gneisses in 'gdt'
'bg' sills intruded gneissic 'gdt'
'd' sills and pods intrude sheared 'gdt'
'd' sills and pods intrude sheared 'gdt'
'ag' sills in 'hg'
'hg' self-intrusion
'd' sills exploit anastomosing shears in 'hg'
'gdt' and 'lg' sills exploit sheared 'd' sills
'd' sills and pods intrude sheared 'ag'
0 50 100 150m
(Mapped by AK, SHW)
01 91 70 E
76 30 00 N
Blue biotite-granodiorite sheets and plutons
Leucogranite, locally pegmatitic
Ultramafic sills, dykes and schists
Dolerite sills and dykes
Blue-grey granodiorite, diorite and tonalite
Pink, alkali-feldspar granite, locally porphyritic
Plagioclase phenocrystic dolerite sills
Hbl-gabbro/diorite complex
Banded granodiorite gneisses
Finegrained mafic and felsic schist,
Zircon sample site
Quartz veins
Lithological boundary (inferred)
Lithological contact strike and dip
Structural trend schistocity
Major shear zone
Foliation strike and dip with stretching / mineral lineation
Gneissosity
Vertical component of sense of shear (white side up)
Outcrop margin
N
NE
NW

Alkali-feldspar granite (unit 'ag') crops out as a 300 metre thick sheet near the contact with the hangingwall of the MESZ (950-1250 m) and as sills within the hornblende-gabbro/diorite complex. It contains metre-wide shears, which were intruded by dolerite sills (Figure 3.5). A mafic sill with distinct cm-scale plagioclase phenocrysts intruded the alkali-feldspar sheet southwest of the hornblende-gabbro/diorite complex. Ultramafic sills and schists of unknown origin occur near the MESZ hangingwall. Metre-wide alkali-feldspar granite sills, similar in appearance to 'ag' intruded the hornblende-gabbro/diorite complex (450-500 m).

A suite of 10-30 metre wide blue-grey granodiorite, diorite and tonalite sills occur over a 300 metre-wide zone (50-400 m) NE of the main hornblende-gabbro/diorite complex. These are collectively classified as unit 'gdt'. Small 'gdt' intrusions were locally observed to have intruded sheared alkali-feldspar granite 'ag' (~350 m), but the contact of the larger sills is generally strongly sheared. The larger 'gdt' sills were intruded by dolerite sills, leucogranite sills and pods, and by sills of blue biotite-granodiorite 'bg'. Sills of the 'gdt' suite are gneissic in appearance towards the footwall of the MESZ.

Metre-thick sheets of blue biotite-granodiorite (unit 'bg') have intruded the blue-grey granitoids, unit 'gdt', where it is gneissic in the footwall of the Mixed Zone (~130 m). Biotite-granodiorite sheets typically crop out as meter-high ridges and tors. These sheets have developed a steeply SW-dipping foliation, defined by biotite and chloritized biotite, parallel to their margins and the trend of the gneisses. Flattened and elongated cm-size biotite/chlorite xenoliths mark an elongation lineation that plunges to the SSW (Figure 3.5). The fabric in unit 'bg' is parallel to that in the older components of the area. Although no direct intrusive relationship has been recorded, the absence of dolerite sills, particularly along the sheets of the blue biotite-granodiorite 'bg', suggests that unit 'bg' is younger. The relationship of component 'bg' with unit 'ag' is not clear. Component 'bg' possibly belongs to the 3.31 Ga Boodallana or Yandigoogina TTG Suites (Collins and Gray, 1990; Williams and Collins, 1990). Gneissic xenolithic rafts occur within the unit 'gdt' and 'bg' near the hangingwall.

An intrusive sequence for the Gum Creek area, based on the aforementioned intrusive relationships, is proposed (in order of intrusion): hornblende-gabbro/diorite complex, alkali-feldspar granite, granodiorite-diorite-tonalite suite, dolerite sills and dykes, leucogranite and biotite-granodiorite. The age of the phenocrystic dolerite and ultramafic sill post-dates the alkali-feldspar granite, but the relationship with other components is unclear. Section 3.3.2 discusses the intrusive relationships in this area in the context of those observed in the other areas.

3.5.1.2 The Cotton Well area

The 4 km x 5 km Cotton Well area is situated on the southwestern margin of the MEGC (See Figure 3.4). In this area, the Mixed Zone is 3-4 km wide in outcrop. A lithological structural map is presented in figure 3.7. This is based on aerial photo interpretation and field checking.

Figure 3.5 Detailed lithological and structural map of the Mixed Zone in the area near Gum Creek (See figure 3.4 for location). SHRIMP sample ME-28 was collected from a biotite-granodiorite sill near the footwall gneisses.

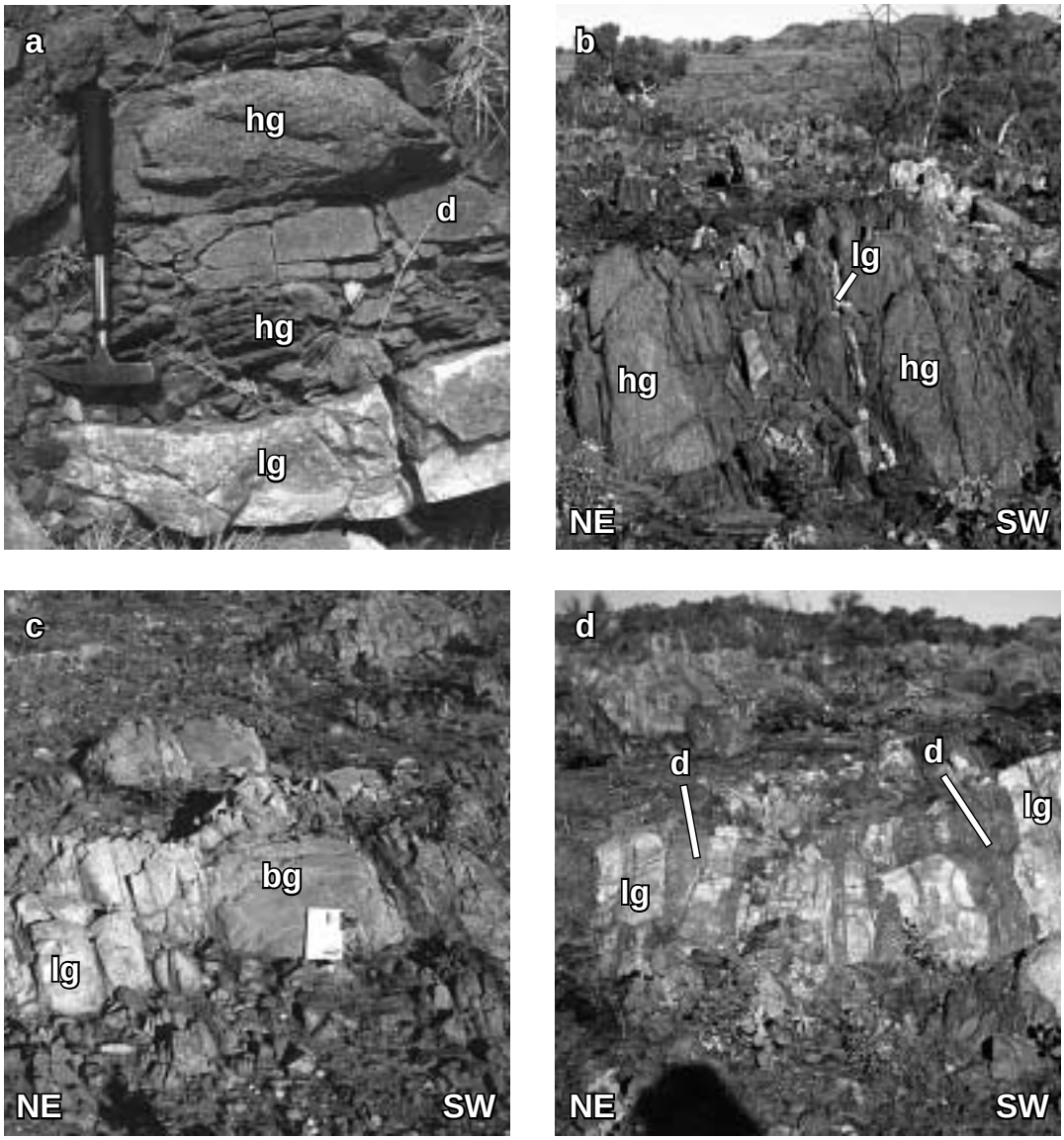

Figure 3.6 Field photographs of intrusive relationships within the Mixed Zone NW of the Gum Creek area (^{08}06.3E-^{76}36.0N). Photographs are taken towards the SE. Field notebook for scale. (a) Sheared hornblende-gabbro/diorite 'hg' is intruded by a dolerite sil 'd' and by a sill of leucogranite 'lg' (b) Coarse grained hbl-gabbro/diorite boudins 'hg' and sheared hbl-gabbro/diorite (darker). The shears are the preferential loci for intrusions such as the leucogranite sill 'lg' (c) Biotite-granodiorite sills 'bg' intruded leucogranite sills 'lg'. (d) Sheared dolerite sills 'd' are intruded by leucogranite sills 'lg'

Figure 3.7 Generalised lithological map of the Mt Edgar Shear Zone in the Cotton Well area (see figure 3.4 for location). Sample locations for zircon samples CTW1A, CTW-36, P95-gran are marked. See text for further discussion.

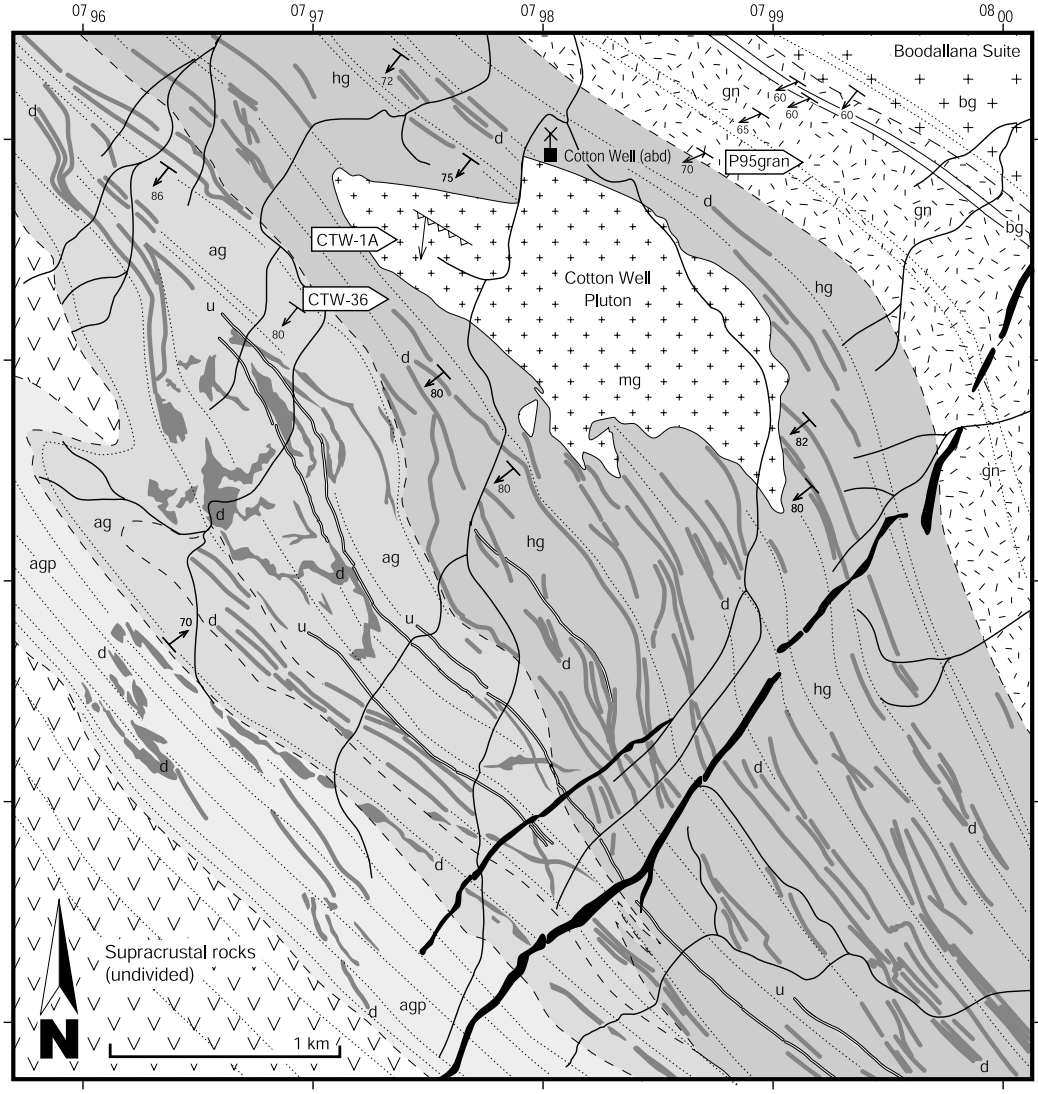

LEGEND COTTON WELL AREA

CTW-36 Zircon sample site

Black Range Dyke Suite 2.77 Ga (undivided)

mg Muscovite granite, locally pegmatitic

bg Blue biotite-granodiorite sheets and plutons

u Ultramafic sills and dykes

d Dolerite sills and dykes

ag / agp Pink, alkali-feldspar granite Dominantly porphyrytic (agp)

hg Hornblende-gabbro/diorite complex

gn Gneiss Complex incl. leucogranite sills, locally garnet bearing, locally pegmatitic

Quartz veins

Lithological boundary (inferred)

Lithological contact strike and dip

Structural trend of foliations (mylonitic and schistosity)

Mylonitic foliation strike and dip with stretching lineation

Gneissosity

Outcrop margin

The area largely consists of the hornblende-gabbro/diorite complex (unit 'hg'), which is particularly wide in this part of the MESZ. Available spectrometric images (Fig. 8 in Wellman, 1998) indicate that the hornblende-gabbro/diorite complex has a distinct low gamma-ray signal which can be traced from the Cotton Well area to the Gum Creek and Trig Well areas to the SE. Deformation in the hornblende-gabbro/diorite complex is generally localized in anastomosing, metre-scale mylonitic zones that are parallel to the general trend of the MESZ.

Multiple intrusions, including dolerite (unit 'd') and ultra-mafic sills (unit 'u', figure 3.7) have intruded into the shears in both the hornblende-gabbro/diorite complex and alkali-feldspar granite. Most of these intrusions have mylonitic foliations that are generally parallel to the margins of the shears in which they intrude. Intrusions also occur at an angle to the structural and lithological 'grain' of the Mixed Zone. These are here referred to as dykes following the definition of Philpotts (1990). Mafic and ultramafic intrusions show mutual intrusive relationships. Shearing on the MESZ has locally resulted in transposition of these dykes (See along the contact between 'ag' and 'agp' in figure 3.7), but discordant dolerites and doleritic 'pods' have been preserved, particularly in the alkali-feldspar granite unit 'ag' (Figure 3.7).

The Cotton Well Pluton is a discordant, coarse grained muscovite-bearing granite (unit 'mg') that intruded the hornblende-gabbro/diorite complex and truncates the dolerites. This pluton contains a foliation defined by alkali-feldspar, plagioclase and by cm-scale interstitial muscovite crystals. This foliation is interpreted to be magmatic. The foliation has been cut by brittle NNE-vergent thrusts related to compressional event D_{X+3} (See chapter 2).

The contact of the Mixed Zone and gneisses of the footwall of the MESZ, north of the Cotton Well Pluton, is strongly deformed, masking intrusive relationships and thus the relative age of the igneous components in this area. The gneisses contain boudins of coarse grained hornblende-gabbro (See figure 3.11c), which suggests that the gabbro/diorite complex is older than at least (part of) the gneissosity. Components of the gneisses have been dated in nearby localities at 3429 ± 13 Ma, 3443 ± 10 Ma and 3448 ± 8 Ma (Williams and Collins, 1990) (See figure 3.4). In addition the footwall contains components of the 3304 ± 10 Ma Boodallana Suite (Williams and Collins, 1990) (See also figure 3.7).

Leucogranite sills (unit 'lg') have intruded the footwall gneisses and are generally strongly mylonitised (Figure 3.8a) with a well developed stretching lineation (Figure 3.8c). North of the Cotton Well Pluton, mylonitised leucogranite sills can be traced across the gneissic fabric into pegmatite dykes that were locally affected by the mylonitic foliation (Figure 3.8b). This is interpreted to indicate that the intrusion of the leucogranite is syntectonic.

Sills of biotite-granodiorite, generally two to three metre wide but locally up to 10 metre wide, intruded the gneisses and the leucogranite. They are presumably part of the 3310 ± 4 Ma Boodallana Suite.

An intrusive sequence for the Cotton Well area, based on the above intrusive relationships, is (in order of intrusion): hornblende-gabbro/diorite complex, alkali-feldspar granite, mafic and ultramafic sills and dykes, leucogranite followed by biotite-granodiorite. Intrusion of the Cotton Well Pluton post-dates the hornblende-gabbro/diorite complex and dolerites, and therefore must be younger than the alkali-feldspar granite and ultramafic sills, but its relationship with the 3310 ± 4

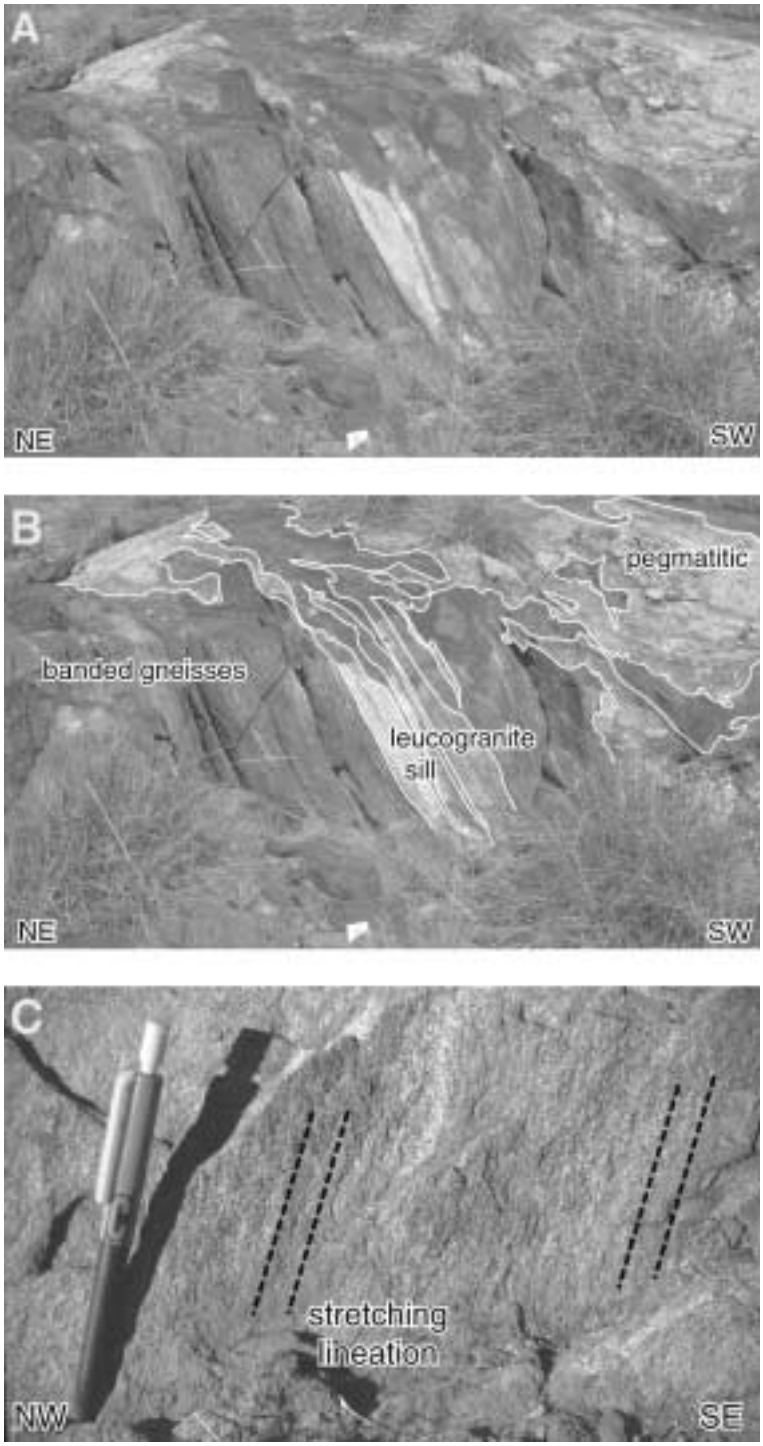

Figure 3.8 (a) Field photograph and (b) interpretation of the syntectonic, mylonitised leucogranite intrusion, unit 'lg', (component 6) at the margin of the Mixed Zone near the granodiorite footwall gneisses northeast of the Cotton Well Pluton. The leucogranite sill is largely parallel to the mylonitic foliation and it is sheared. However, locally the leucogranite intruded across the mylonitic foliation. There, it is more pegmatitic. The foliation also locally offset the leucogranite intrusion, which suggests that the leucogranite has been emplaced during deformation. SHRIMP sample P95-gran was collected from the top of the outcrop.

Ma Boodallana Suite (Williams et al., 1990) is unclear. Section 3.3.2 discusses the intrusive relationships in this area in the context of those observed in the other areas.

3.5.1.3 The Trig Well area

The location of the studied area near Trig Well is shown in figure 3.4. The results of numerous traverses and an aerial photograph interpretation is presented in figure 3.9.

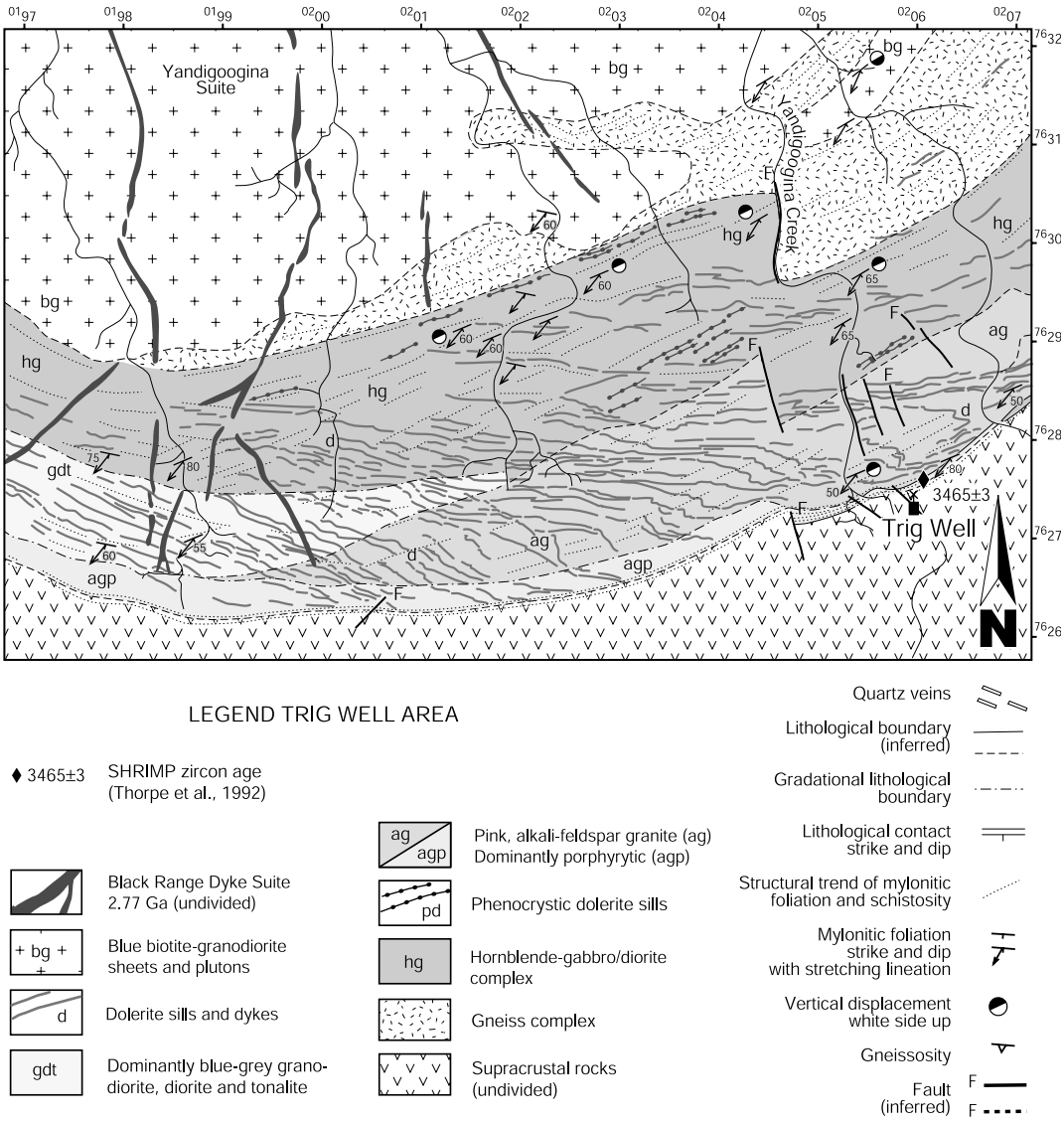

Figure 3.9 Lithological and structural map of the Mt Edgar Shear Zone in the Trig Well area. (see figure 3.3 for location). See text for further discussion.

The core of the Mixed Zone in the Trig Well area is largely occupied by the hornblende-gabbro/diorite complex (unit 'hg') and the pink to white alkali-feldspar granite (unit 'ag') (Figure 3.9). The generally medium-grained alkali-feldspar granite (unit 'ag') is porphyritic (unit 'agp') towards the contact with the supracrustal hangingwall, where it is also more schistose. Felsic schists on the hangingwall margin of the Mixed Zone were dated at 3465 ± 3 Ma (Figure 3.9) (TIMS U-Pb zircon, Thorpe et al., 1992) and were assigned to the Duffer Formation. This suggests that the 'ag' and 'agp' units may be intrusive equivalents of the Duffer Formation, like the 3466 ± 2 Ma (Nelson, 1998a) alkali-feldspar granite 'Aga' on the western margin of the MEGC near Marble Bar (Hickman, 1983). Towards the footwall, the alkali-feldspar granite 'ag' gradually changes to a granodioritic, dioritic and locally tonalitic composition, (unit 'gdt', see figure 3.9).

Three types of dolerite dykes have intruded the hornblende-gabbro/diorite complex and the alkali-feldspar granite in the Trig Well area. One type intruded parallel to shear zones in the gabbro/diorite complex. This type is characterised by a fine-grained matrix and cm-size plagioclase phenochrysts (unit 'pd'). They generally show a strong, hornblende- and plagioclase-bearing mylonitic foliation that is parallel to the margins of the sills. These sills are parallel to hornblende-gabbro/diorite sills in the complex. The alignment of hornblende marks a mineral lineation that plunges to the SSW, and that is parallel to those in the mylonites within the hornblende-gabbro/diorite complex.

A second type (unit 'd') comprises medium to fine-grained dolerites. These dolerites have intruded the hornblende-gabbro/diorite complex, the phenocrystic dolerite sills, the alkali-feldspar granite and the granodiorite-diorite-tonalite unit 'gdt'. A few of these dolerites are recognised in the greenstones of the hangingwall, for example in the 3465 ± 3 Ma felsic schist (unit 'agp'). Overall, these dolerites could be regarded as a roughly WNW to E-W trending dyke swarm, but in detail the pattern is more complicated. In the extreme western part of the Trig Well area, most of these dolerites are parallel to the WNW trend of the MESZ and therefore qualify as sills. Towards the east, however, as the overall trend of the Mixed Zone changes to ENE, a more complex pattern is observed: dolerites have intruded parallel to a structural trend that has overprinted the older structural and lithological 'grain' of the MESZ, but which was also locally offset by it (See figure 3.9 and see also §2.4.3.3, Chapter 2). This pattern is further complicated by the local folds along the margin with the hangingwall (See chapter 2). Despite these complex relationships, most dolerites contain a SW-plunging stretching lineation. This, in combination with the dolerite geometry, and cross-cutting relationships, was taken to indicate that the dolerites intruded during progressive doming of the MEGC (See figure 2.16). This dolerite swarm must be younger than the 3465 ± 3 Ma felsic schists that it has intruded, and since the dolerites were not observed in the biotite-granodiorite of the footwall (Yandigoogina Suite, one of the 3.31 Ga TTG suites, Williams and Collins, 1990), they are interpreted to have been emplaced between 3.46 and 3.31 Ga.

A third group of dykes comprises N to NNE- and locally NNW-trending felsic and mafic dykes that discordantly intruded the MESZ and adjacent units. This swarm can be distinguished from the older two because it has remained largely undeformed and unmetamorphosed. These dykes are related to the Fortescue Group (Hickman and Lipple, 1978).

3.5.1.4 The Moolyella Gneiss area

The ~2 km x 2 km area of interest is indicated in figure 3.4. The results of aerial photograph interpretation and structural mapping along numerous traverses are presented in figure 3.10. The observed relationship between the structural history and emplacement of magmatic components is

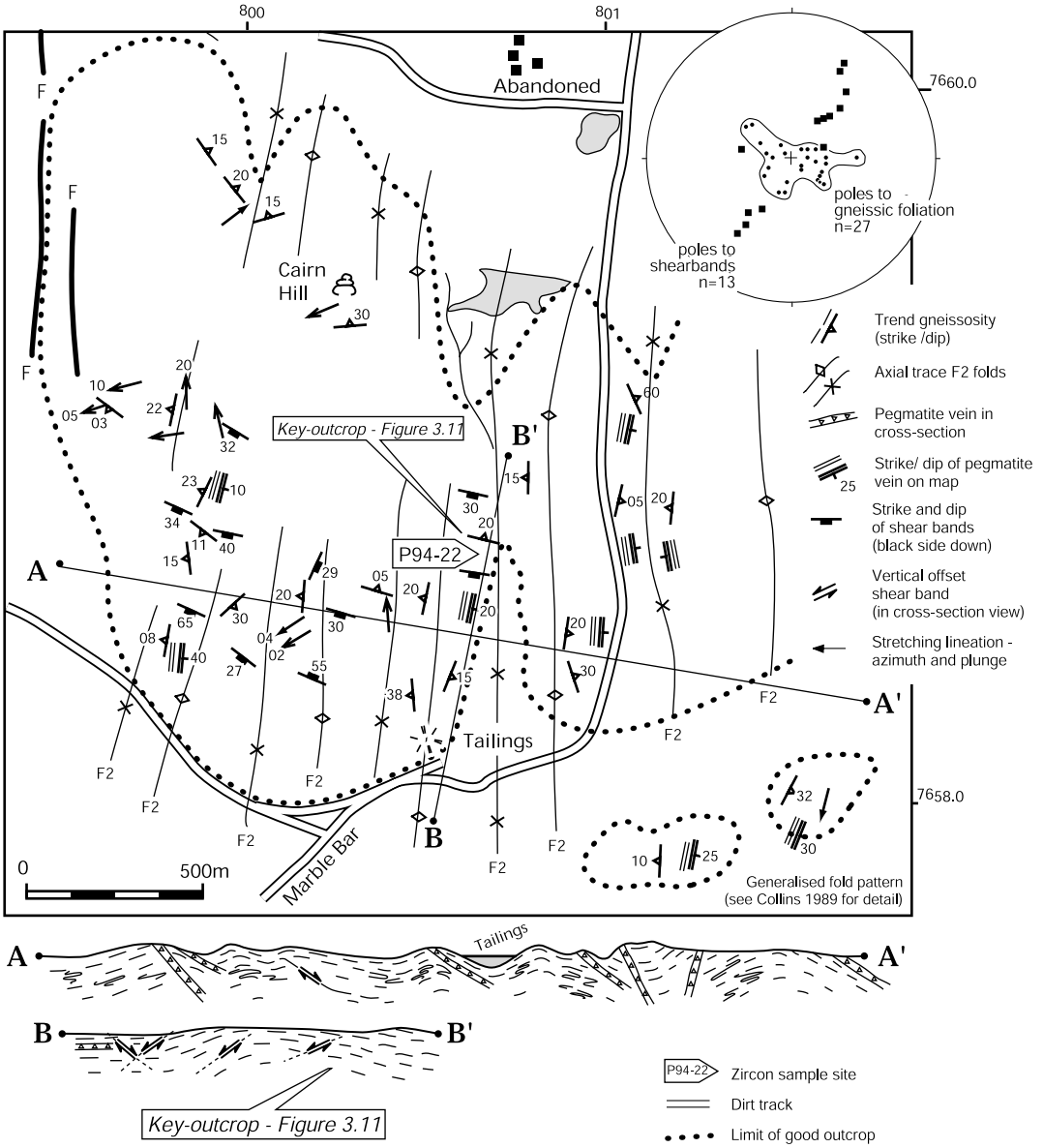

Figure 3.10 Generalised structural map and cross sections of the Central Gneiss Complex outcrop near Moolyella Tin Fields in the Mt Edgar Granitoid Complex (see figure 3.4 for location). Section A-A' illustrates the gneissosity that shows open, NNE-trending folds (F2). See text for discussion.

illustrated by the outcrop in figure 3.11. A more detailed lithological map can be found in figure 6 of Collins (1989). Collins (op.cit.) recognised a history of at least three deformation phases prior to the diapiric development during D_4. Structures attributed to the oldest deformation phase comprise a subhorizontal gneissosity (S_1) associated with intrafolial folds and syntectonic granite sheets parallel to the gneissosity. A second phase (F_2) caused subhorizontal, NNE-SSW trending open folds in the gneissosity on a 100-metre scale. A third deformation phase (F_3) caused NE-SW trending folds associated with the NE-trending 'D_3 lineament' (Collins, 1989). In chapter 2 the 'D_3 lineament' is proposed to have acted as a sinistral transfer zone that accommodated differential NE-SW extensional movement on the MESZ (See §2.4.3.2) and is referred to as the Beaton Well Zone. Hence, the Central Gneiss Complex is here regarded as part of the footwall of the MESZ. The

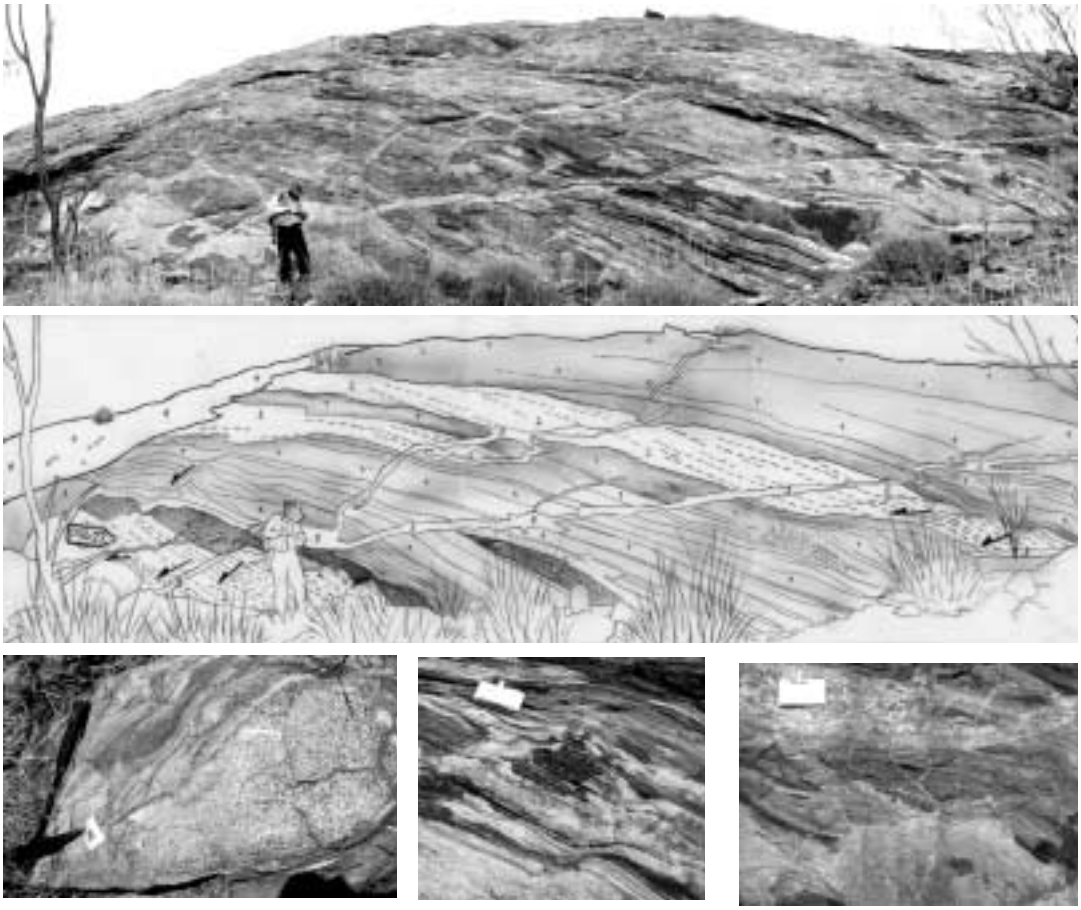

Figure 3.11 (a) Field photograph of a illustrative outcrop within the Central Gneiss Complex, marked in figure 3.10, looking WNW. (b) Interpretative sketch of the identified intrusive components. An interpretation of the intrusive order in relation to the structural development is discussed in the text. Sample location of zircon sample A94-22 is marked. (c). Hornblende-diorite boudin of unknown age within the banded gneisses (c) Black and white banded gneisses cut by SW-dipping shear bands. (e) Grey granodiorite sheet 'gn-2' that intruded generally parallel to the banded gneisses, but is locally discordant. Shear bands also cross-cut this sheet (See 3.11b).

Beaton Well Zone was geometrically related to migmatitic conjugate NE-SW extensional shear bands in the gneisses that surround the lineament.

The observed relationships between the structural history of the Moolyella Gneiss Area and the emplacement of the magmatic components are illustrated in figure 3.11. Black and white banded gneiss (component *Gn-1)* comprises biotite-rich melanosomes and feldspar/quartz leucosomes that define the subhorizontal gneissosity S_1 (See figures 3.11a and b). Other structures are complex ptygmatic, partially migmatitic and intrafolial folds, indicating high temperature conditions (See also Collins, 1989). Additionally, the banded gneisses contain metre-scale boudins of fine- to coarse-grained amphibolite, gabbro and diorite (Figure 3.11c). Equigranular grey granodiorite and tonalite sheets *(Gn- 2)* have intruded sub-parallel to the banded gneissosity, but have locally intruded discordantly to this fabric (Figure 3.11d). A biotite (partly chloritized) foliation occurs parallel to these sheets and the banded gneissosity. This foliation, the sheets and the banded gneisses were folded into 10-100 metre scale, subhorizontal open folds (F_2, F_3, Collins, 1989).

In addition to the aforementioned structures described by Collins (1989), metre-scale NE-SW extensional shear bands were observed to cross-cut both the S_1 gneissosity and the grey-granodiorite sheets throughout the area, but were predominantly seen in the latter (See figures 3.11b and 3.11e). Stereographic projection of the poles to the shear bands form two clusters on an 045-225°-trending girdle (Figure 3.10). This orientation and the offset along them suggests that these shear bands formed as a conjugate set during NE-SW extension. This is a similar orientation to that observed near the Beaton Well Zone (See above). The shear band orientation does not show evidence of F_2 or F_3 folding, suggesting that the folding occurred prior to NE-SW extension.

White to yellowish, fine-grained leucosome dykes *(Gn-3)* have intruded the banded gneisses and the grey granodiorite sheets (Centre of figure 3.11d). These locally follow the shear bands but are not offset by them, suggesting that they were intruded after NE-SW extension. Metre-wide and hundreds of metres long pegmatite dykes *(Gn-4*, see figure 3.11a*)* have intruded the above components. In the Moolyella area, they have a consistent N-S trend and a shallow eastward dip (Figure 3.10), suggesting that they intruded after F_2 and F_3 folding. The pegmatites intruded across the gneissosity and shearbands, indicating that they intruded after NE-SW extension.

Based on the above intrusive and structural relationships, the following development of the

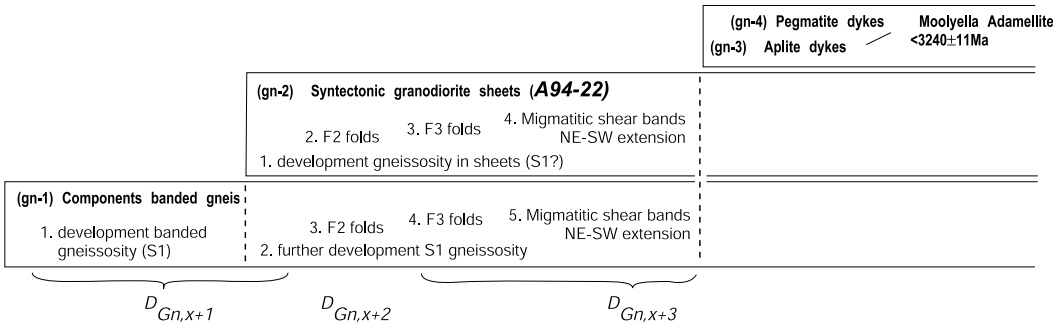

Figure 3.12 Proposed scheme for the structural and magmatic development of the Central Gneiss Complex near the Moolyella Tin Fields.

Moolyella Gneiss area is proposed (See figure 3.12). Development of the earliest banded gneissosity ($D_{Gn,X+1}$) was followed by the intrusion of the equigranular grey granodiorite sheets and development of a gneissic foliation within these sheets, parallel to the banded gneissosity. The banded gneisses, and probably also the granodiorite sheets, were folded during the NNE-SSW trending, open F_2 folding event ($D_{Gn,X+2}$). The F_3 folds have a similar trend, namely NE-SW, to the nearby Beaton Well Zone, the transfer zone to NE-SW extension on the MESZ. Note that folds may form parallel to an extension direction if there is a compressional component at right angles to extension. The overprinting migmatitic NE-SW extensional shear bands temporally and kinematically fit NE-SW extension, therefore they are tentatively related to NE-SW extension on the MESZ (See also chapter 2)($D_{Gn,X+3}$). Development of the shear bands was followed by intrusion of the aplite and pegmatite dykes *(Gn-3 and Gn-4)*.

3.5.1.5 Summary of the intrusive history of the Mixed Zone

A generalised intrusive sequence for the Mixed Zone is here proposed by integrating the intrusive relationships observed in the Gum Creek, the Cotton Well and Trig Well areas (See figure 3.13).

The oldest recognised intrusive component is the hornblende-gabbro/diorite (unit 'hg', component 1). This was intruded by the largely concordant alkali-feldspar granite ('ag', component 2). Both components were intruded by sills of phenocrystic dolerite sills (component 3), particularly in the Trig Well Area (See figure 3.9). Granodiorite/tonalite sills ('gdt', component 4) intruded the alkali-feldspar granite (See figure 3.5). All of the aforementioned components have been intruded by an extensive suite of dolerite sills and dykes, and ultramafic sills (units 'd' and 'u' see figures 3.5, 3.7 and 3.9). The dolerite and ultramafic intrusions display mutual intrusive relationships (See figure 3.7) suggesting coeval intrusion, and are therefore ordered as components 5a and 5b, respectively. Both have also been intruded by the leucogranite sills ('lg', component 6) (See figures 3.5 and 3.6), which in turn have been intruded by sills of biotite-granodiorite ('bg') (See figure 3.5) and by the

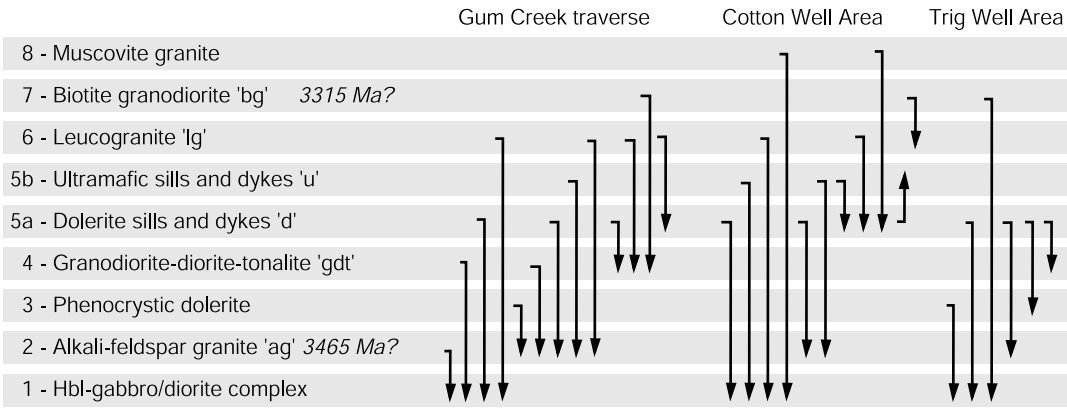

Figure 3.13 Proposed intrusive sequence for the Mixed Zone, based on the intrusive relationships in the Gum Creek traverse, the Cotton Well and Trig Well areas.

muscovite-rich granite of the Cotton Well Pluton (See figure 3.7). Intrusive relationships between the latter two components have not been recorded. Nevertheless, the concordant nature of the biotite-granodiorite sills contrasts with the discordant shape of the Cotton Well Pluton, suggesting that the latter is younger (See figures 3.5 and 3.7). The biotite-granodiorite sills and Cotton Well Pluton are therefore marked as components 7 and 8 respectively (Figure 3.13).

3.5.2 Microstructural analyses

Microstructural analyses of intrusive components of the Mixed Zone were undertaken to investigate the kinematics related to the SW-plunging lineations, particularly in relation to the metamorphic grade. The observed structures are illustrated in figure 3.14 and schematically ordered in figure 3.15.

Samples were collected from the two oldest recognised syntectonically emplaced components: the hornblende-gabbro/diorite complex (component 1) and the dolerite sills (component 5). Thin sections of samples of the hornblende-gabbro/diorite and dolerite sills that contained a macroscopic aligned fabric show a locally preserved fabric with subhedral to euhedral hornblende crystals (Figures 3.14a, b and c). Most of these crystals are internally strain-free and generally lack inclusions. Locally, hornblende crystals are imbricated (Figure 3.14a). These structures are similar to those described for magmatic textures in syntectonic granitoids (Paterson et al., 1991), suggesting that the lineation (partly) developed before the sills had fully crystallized. This is consistent with the observed syntectonic intrusion of the hornblende-gabbro/diorite complex and the dolerites of unit 'd'.

Samples from shear zones in the hornblende-gabbro/diorite complex generally show a hornblende and plagioclase-bearing foliation with associated conjugate shear bands (Figures 3.14c and d). These amphibolite facies conjugate sets have locally boudinaged larger hornblende crystals (Figure 3.14d), indicating thin-section scale layer-parallel extension and/or flattening.

The amphibolite facies mylonitic foliation in samples from the shear zones within the hornblende-gabbro/diorite complex is overprinted by hornblende, chlorite and epidote-bearing shear bands, indicating high temperature greenschist facies conditions. A prevalence of NE-vergent shear bands over those with SE-vergent asymmetry suggest a dominant NE-tectonic transport (Figures 3.14e, f and g). Shear bands that indicate NE-directed transport also occur within the mylonites in the alkali-feldspar granite and leucogranite (components 2 and 6). These shear bands contain quartz+biotite(±chlorite) and chloritized biotite (Figure 3.14h), which suggests retrograde conditions during NE transport. Most samples from the mafic dykes contain an ultra-mylonitic foliation (chlorite+epidote+albite) without kinematic indicators, but some show shear bands that indicate NE-tectonic transport (Figure 3.14i).

Undeformed, randomly-orientated hornblende porphyroblasts were locally found to have overgrown chlorite-bearing shear bands in the hornblende-gabbro/diorite complex 'gd' (Figure 3.14j) and dolerite sills of component 'd'. White-mica porphyroblasts have also overgrown the NE-vergent shear bands in the alkali-feldspar granite, and the MEGC-up shear bands in the leucogranite sills. These undeformed blasts are interpreted to reflect a contact metamorphic event that post-dates

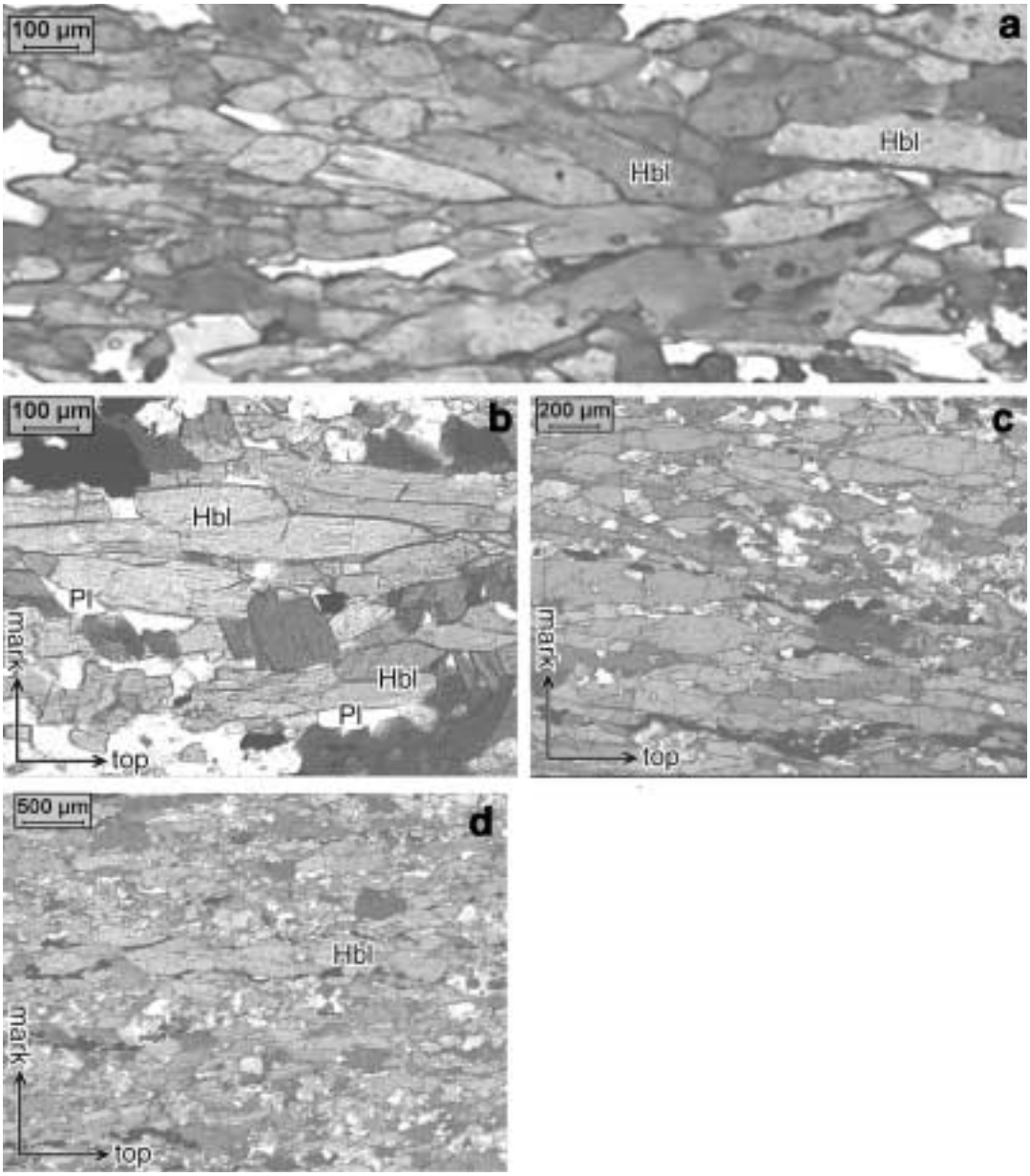

Figure 3.14 Microphotographs representing the main structures within components of the MESZ. T= top of sample. M= side of sample facing up. (a) Internally undeformed hornblende crystals generally without inclusion, with an overall alignment parallel to the foliation in the hbl-gabbro/diorite complex. Some crystals are imbricated. (b) Detail of aligned hornblende fabric. (c) Alignment of hornblende crystals in the dolerite sill, sample P96-167. (d) Mylonitic fabric and boudinaged hornblende indicating layer parallel extension in the hbl-gabbro/diorite complex.

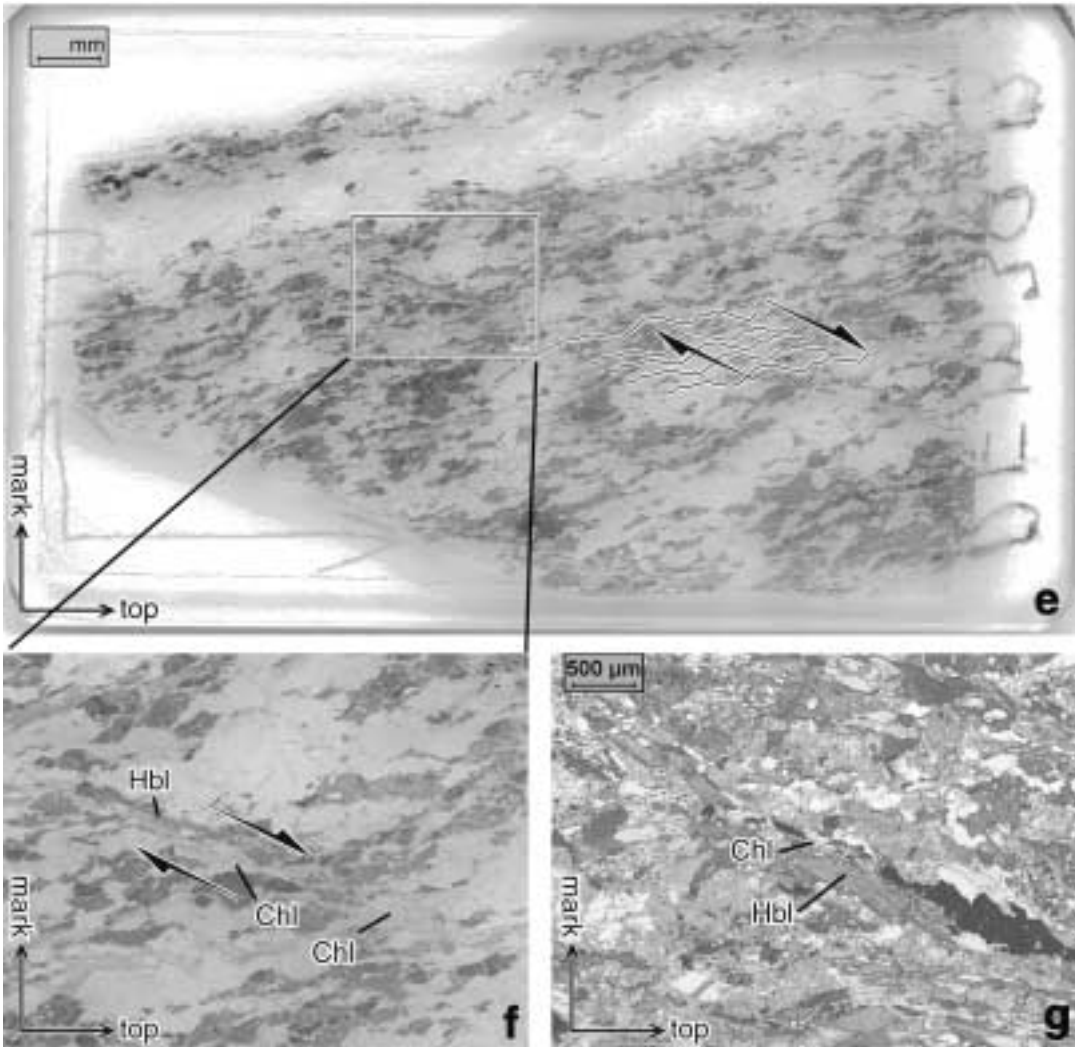

Figure 3.14 (e) NE-vergent shear bands in the hbl-gabbro/diorite complex. Thin section is 4.5 cm wide. (f) Detail of figure 3.14e showing hornblende, chlorite, epidote within the shear band foliation. (g) Mylonitic fabric with hornblende, actinolite, and minor chlorite and epidote. Shear bands dominantly indicate NE-tectonic transport are overgrown by late to post-tectonic actinolite blasts. (h) Chloritised biotite and chlorite-bearing NE-vergent shear bands in the alkali-feldspar granite. (i) NE-vergent shear band cutting across ultramylonitic fabric in a dolerite sill (j) Hornblende blasts overprint greenschist facies fabric in the hbl-gabbro. (k) Poorly developed, conjugate shears in the biotite-granodiorite.

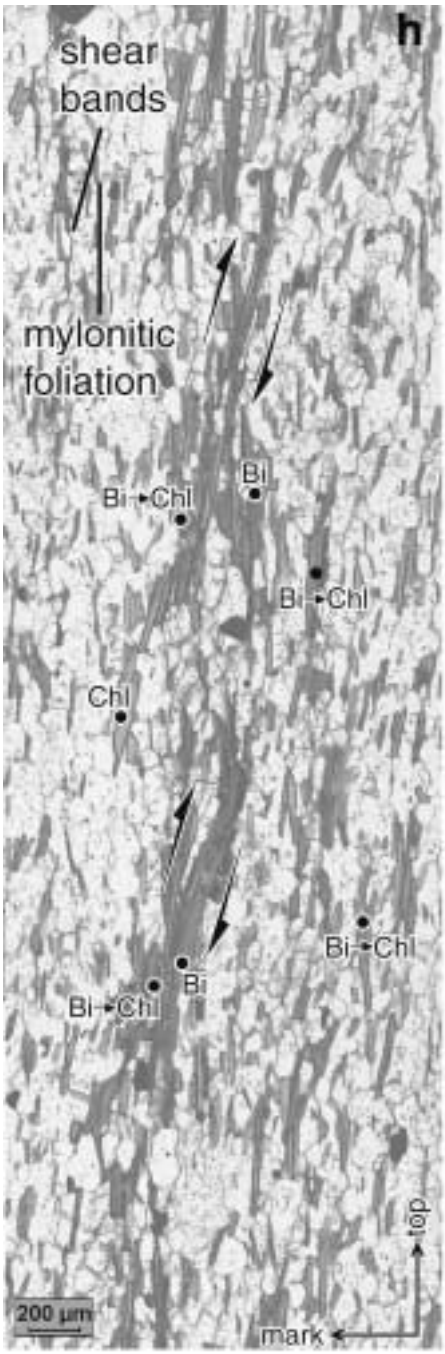
h
shear bands
mylonitic foliation
Bi
Bi→Chl
Chl
200 µm
mark
top

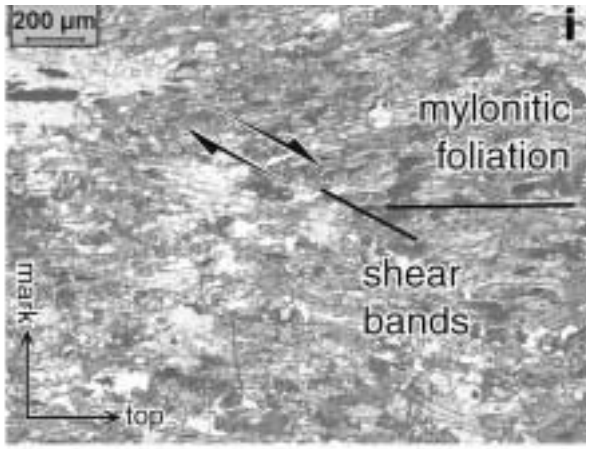
i
200 µm
mylonitic foliation
shear bands
mark
top

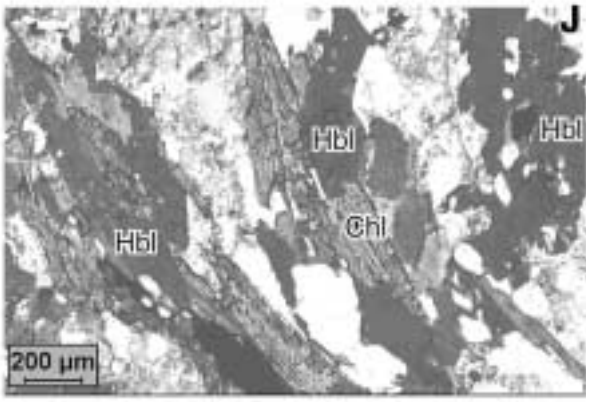
J
Hbl
Chl
200 µm

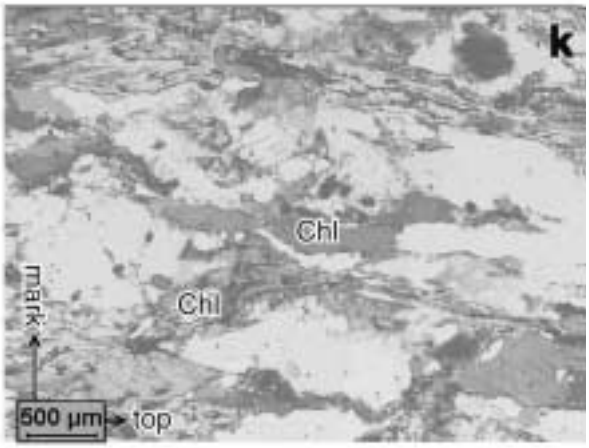
k
Chl
mark
500 µm
top

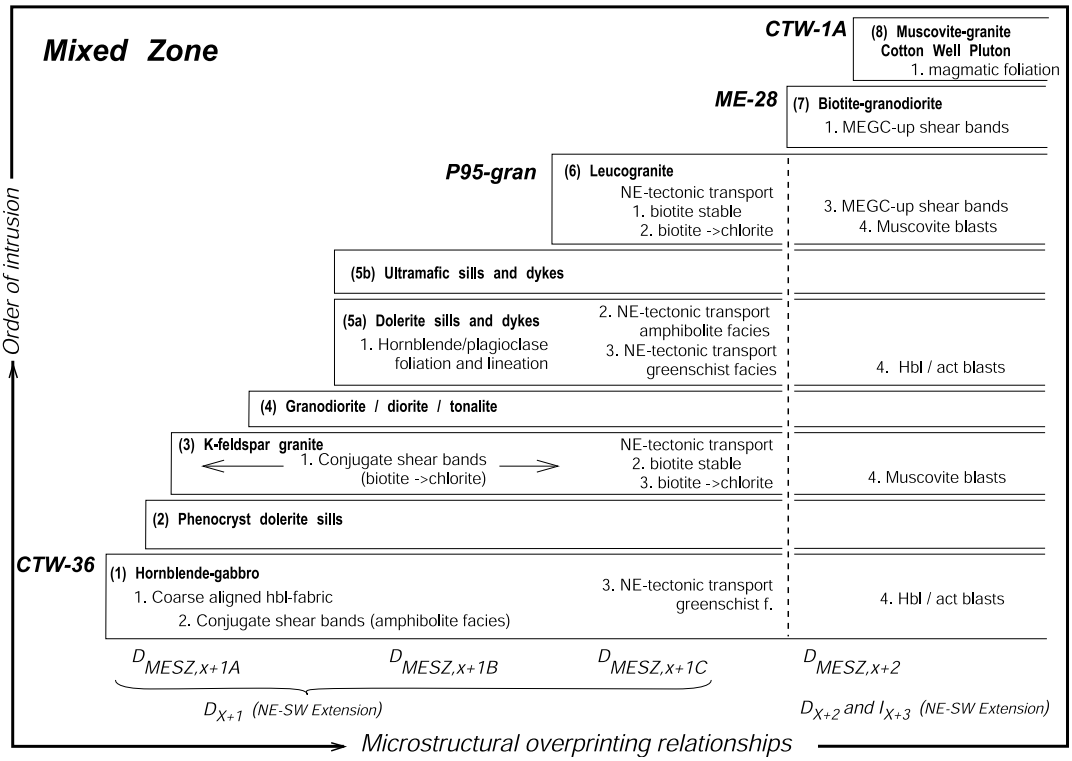

Figure 3.15 Interpreted magmatic history and microstructural/metamorphic development of the Mt Edgar Shear Zone (MESZ).

the development of both the amphibolite and greenschist facies mylonitic foliation.

The foliation in the biotite-granodiorite sills (component 7) along the MESZ footwall is defined by biotite and chloritised biotite, and has developed parallel to the margins of the granite sheets and the trend of the gneisses. Re-crystallized flattened feldspar clasts are surrounded by a chloritised biotite foliation, indicating flattening (Figure 3.14k).

3.5.3 Development of the Mt Edgar Shear Zone

In reconstructing the tectonomagmatic development of the MESZ, six main observations must be considered; (i) the intrusive sequence, (ii) the regional pattern of dominantly SW to SSW plunging stretching and mineral lineations, (iii) the syntectonic intrusion of the hornblende-gabbro/diorite complex and the dolerite sills, (iv) the magmatic and mylonitic fabric, that in most components predominantly indicates layer-parallel extension and/or flattening, but which has been overprinted by structures indicating NE-tectonic transport, (v) decreasing metamorphic conditions during layer-parallel extension and NE-tectonic transport, and (vi) the post-tectonic growth of hornblende and muscovite porphyroblasts.

Figure 3.15 list the intrusive components of the Mixed Zone and the available microstructures.

In the reconstruction of the tectono-magmatic history of the MESZ, it has been assumed that intrusive and deformation events are uniform in time and space on the scale of the Mixed Zone. This approach allows an interpretation in which the absence of a particular deformation structure in an intrusive component indicates that the deformation phase responsible for similar structures in the surrounding rocks occurred prior to intrusion of this component.

3.5.3.1 Pre-3.32 Ga development of the Mt Edgar Shear Zone

The deformation that occurred during or immediately after intrusion of hornblende-gabbro/diorite is here interpreted as the first stage of development of the Mixed Zone, and referred to as $\mathbf{D_{MESZ,X+1A}}$ (Figure 3.15). The only older deformation structures in the MESZ have been found in the form of schistose xenoliths within relatively undeformed parts of the hornblende-gabbro/diorite complex (See chapter 2). These schistose xenoliths are interpreted as remnants of deformed host rock. Their schistosity suggests older deformation, but whether this is caused by a separate phase, or is related to the early stages of $D_{MESZ,X+1A}$ is unclear. This schistosity is attributed to $\mathbf{D_{MESZ,X}}$. The intrusion of the alkali-feldspar granite and granodiorite/diorite/tonalite (unit 'gdt') is considered to be related to $D_{MESZ,X+1A}$ because of their general concordance with the gabbro complex (See figures 3.7 and 3.9). An age for this deformation phase may be provided by the crystallization age of the hornblende-gabbro/diorite complex. The complex has been sampled for SHRIMP U-Pb zircon geochronology (zircon sample CTW-36, see § 3.6.1).

A second phase of mafic magmatism resulted in dolerite intrusions (component 5a), and occurred during layer parallel extension and doming of the MESZ (See chapter 2). This stage is referred to as $\mathbf{D_{MESZ,X+1B}}$ (Figure 3.15). A minimum age for this stage may be provided by the crystallization age of component 6, the leucogranite. The leucogranite has been sampled for SHRIMP U-Pb zircon geochronology (zircon sample P95-gran, see § 3.6.1).

A decrease in metamorphic conditions is accompanied by a change in dominant kinematics from layer parallel extension to NE-tectonic transport. NE-vergent shear bands occur in all components older than the biotite-granodiorite (component 7). These structures are assigned to stage $\mathbf{D_{MESZ,X+1C}}$ (Figure 3.15). A minimum age for these structures may be provided by the crystallization age of the Cotton Well Pluton (zircon sample CTW-1A, see § 3.6.1) that discordantly intruded the mylonitic foliation of the MESZ.

The parallel orientation of the oldest structures of the MESZ (formed during $\mathbf{D_{MESZ,X+1A}}$ and $\mathbf{D_{MESZ,X+1B}}$) and those formed during NE-tectonic transport ($\mathbf{D_{MESZ,X+1C}}$) suggests a similar tectonic phase. But, whereas the kinematics of the older two stages were associated with extension, the top-to-the-NE transport on the MESZ is more consistent with NE-SW compression (that is, in the current position of the MESZ). The observed retrograde metamorphic conditions during NE-tectonic transport, however, are not compatible with such an interpretation as thrusting would cause stacking and burial of the footwall and MESZ, which leads to their increased metamorphic conditions rather than decreased.

We propose that the structures indicating NE-tectonic transport formed as part of the system that developed during NE-SW extension. Whereas the layer parallel structures are formed in the

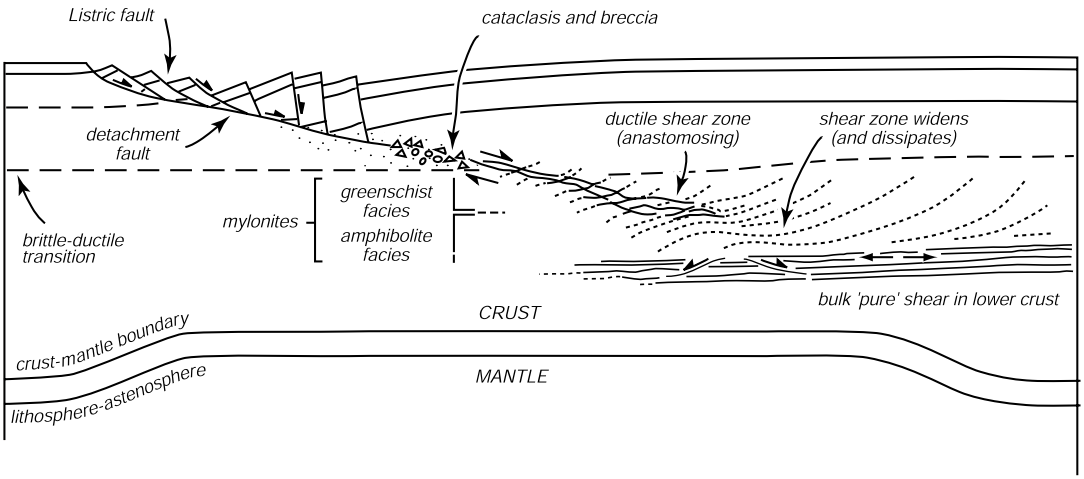

Figure 3.16 Model for continental extension by a crustal detachment shear zone (after Lister and Davis, 1989). The shear zone widens with depth and the deformation style changes with increasing depth and metamorphic grade. The various deformation styles throughout the detachement may be observed in one part of the MESZ that is transported upwards.

mid-crust, the NE-vergent structures may have formed in that part of the crust that would have been dominated by mylonitic 'simple shear': above the crustal level dominated by high-grade layer parallel flow, yet, still below the upper crustal level of brittle faulting, illustrated in figure 3.16 (e.g. Lister and Davis, 1989). The above overprinting relationships reflect the change of the MESZ, which moved from mid-crustal levels to shallower levels of the crust developed as it developed as a domal structure.

The amphibolite and greenschist facies NE-verging structures in the MESZ, attributed to D_{X+1C}, are unlikely to have developed during the post-3.31 Ga (N)NE-(S)SW compressional phase D_{X+3} (See chapter 2). Despite a similar compression direction, this phase generally caused brittle-ductile structures, such as a regional fracture cleavage, strike-slip faults, kinks and local thrusts such as those observed in the Cotton Well Pluton (See chapter 2). This pluton discordantly intruded the mylonitic foliation and the Mixed Zone of the MESZ, indicating that it intruded after the main development of the MESZ. Hence, not only the related metamorphic grade but also the timing of D_{X+3} is wrong. An additional compressional phase at ca. 3.29 – 3.27 Ga has recently been recognised to have caused km-scale folding and trusting in Domain 1 (S.White, J.Wijbrans, pers.comm.). An effect of this phase on the MESZ cannot be ruled out.

3.5.3.2 Syn to post 3.32-3.31 Ga development of the Mt Edgar Shear Zone

Emplacement of the 3.31 TTG suites during NE-SW extension caused MEGC-up kinematics dominantly within biotite-granodiorite sills, component 7 (See chapter 2). This stage is here referred to as DMESZ,X+2 (Figure 3.15). The timing is expected to be obtained by the crystallization age of the biotite granodiorite sill (zircon sample ME-28, see § 3.6.1).

Zircon sample **CTW-36**	Location (E-N of Australian Metric Grid zone 51)	Field relationships	Structural relationship
Hbl-gabbro/ diorite complex **P95-gran**	^{07}97.3-^{76}43.3 Central Mixed Zone in the Cotton Well Area (Figure 3.7)	Oldest, syntectonic intrusive component in the Mixed Zone. Pre to syn-NE-SW layer parallel extension.	Syn- $D_{MESZ,x+1A}$
Leucogranite **A94-22**	^{07}99.2-^{76}43.7 Footwall gneisses in the Cotton Well Area (Figure 3.7).	Syntectonic intrusive dyke in the gneisses of the MESZ footwall.	Post- $D_{MESZ,x+1A}$ Pre- $D_{MESZ,x+1C}$
Grey granodiorite **ME-28**	^{08}00.6-^{76}58.8 Gneiss Complex near Moolyella Tin Field (Figures 3.10 and 3.11).	Largely concordant sill in banded gneiss, with minor gneissic fabric. Cut by shear bands indicating NE-SW extension.	Pre- $D_{Gn,x+2}$ Post- $D_{Gn,\ x+1}$
Biotite-granodiorite **CTW-1A**	^{01}91.6-^{76}30.6 Mixed Zone in Gum Creek Area (Figure 3.4).	Sill near MESZ footwall, parallel to mylonitic foliations, with MEGC-up kinematics (Boodallana Suite?)	Syn- $D_{MESZ,x+2}$
Muscovite-granite	^{07}97.5-^{76}43.5 Cotton Well Pluton in Cotto Well area (Figure 3.7).	Discordant pluton, post-dates main development of Mixed Zone. Cut by NNE-vergent thrusts.	Post- $D_{MESZ,x+2}$ Pre- $D_{MESZ,x+3}$

Table 3.1 SHRIMP samples, sample locality, field relationships and relationship to the structural hisotry of the MESZ.

A late to post-tectonic increase in temperature is indicated by the undeformed hornblende and muscovite porphyroblasts that have overgrown the foliations in the older components. This may be due to the emplacement of the biotite-granodiorite sills (component 7), or to the emplacement of 3.24 Ga monzogranites that were recently dated near the centre of the MEGC (See Figure 3.4). The thermal history of the MESZ is the subject of chapter 5.

A comparison of the development of the footwall Gneiss Complex in the Moolyella Tin Field (Figure 3.10) and that of the Mixed Zone requires absolute age constraints, because the strong deformation along the contact with the Mixed Zone obliterated intrusive relationships. Sample A94-22 from a subhorizontal granodiorite sheet was selected for dating because of the intrusive relationships with the main structures in the Gneiss Complex. The crystallization age may provide absolute age constraint for these structures (zircon sample A94-22, see § 3.6.1).

3.6 SHRIMP U-Pb zircon geochronology

Five igneous components were sampled for SHRIMP U-Pb zircon geochronology to provide time constraints for the structural development of the MESZ. The samples and sample locations are described below. Table 3.1 summarises the coordinates of sample localities, the location and the relationship with the structural history of the MESZ.

Morph. group	Zircon colour and transparency	Zircon size (μm)	Zircon shape and surface features	Zircon 'Stratigraphy'
CTW-36				
19 (29x)	Semi-transparent	250 x 250	Equidimens., faces (fragm)	1)Oscill./sector/lamin. Zoned c+r 2)Fracturing. 3)High-CL r
20 (>50)	Semi-transparent, metamict tips	200 x (200-250)	Stubby, faces (incl. fragm.)	1)Oscill./sector/lamin. Zoned c+r 2)Fracturing. 3)High-CL r
P95-gran				
1 (30x)	Metamict/light pink	100 x 250	Long-prismatic, pitted	1) Oscill. c 2) IMP 3) Str.less c+r 4)Patchy c+r 5) High-CL r
2 (40x)	Colourless/light pink	60 x 250	Long-prismatic, faces	1) Oscill. c 4) Str.less and partly patchy c+r
3 (13x)	Pink, metamict	200 x 250	Equidim. rounded, pitted	1) Oscill. c 4) Str.less and partly patchy c+r
A94-22				
8 (37x)	Transparent	60 x 250	Long-prismatic.	3) Low-CL, patchy c+r
9 (>50)	Metamict (tips)	125 x (300-350)	Prismatic, pitted .	1) Lam/sector z. c 2) Oscill.r/str.less.c 3) Low-CL, str.less/patchy r
10 (>50)	Metamict (tips)	(200-250) x 300	Equidim. to prismatic, pitted	2) Oscill./struct.less c+r 3) Low-CL str.less. and patchy c+r
ME-28				
4 (>50)	dark-brown/red	125x (250-300)	Idiomorphic, prismatic.	3) Oscill. c+r 4) Patchy c+r 5) High-CL outer r
5 (>50)	hazelbrown/pink	50 x 250	Equidimensional.	3) Oscill. c+r 4) Struct.less/patchy c+r
6 (>50)	dark-brown/red	(200-250) x 400	Long-prismatic, idiomorphic.	1) Sector z. c. 2) Oscill. c. 3) Discordant oscill.r. 5) High-CL r.
7 (13x)	dark-brown/red	250 x 350	Idiomorphic, prismatic, pitted	?) Laminar zoned /patchy c. 3) Oscill. c+r 5) High-CL r.
CTW-1A				
16 (45x)	Hazelbrown	60 x 250	Long-prismatic, faces.	1) Str.less c 2) Low-CL oscill. c+r
17 (>50)	Dark pink/brown	(75-200) x 200	Long to short, rounded	1) Oscill./lamin/sector.z. c 3) High-CL oscill.r 4) IMP 5) str.less r.
18 (>50)	Pink-brown (mt.tips)	100 x (200-250)	Prismatic, idiomorphic, faces	1) Oscill./lamin/str.less cores. 3) High-CL oscill. r 6) Patchy c+r

Table 3.2 Zircon populations for the five SHRIMP samples, with morphological characteristics, size and shape each zircon population. A 'CL-stratigraphy' for each sample is based on CL-images, representative grains of which presented in figure 3.18, and is further discussed in the text.

3.6.1 Zircon samples and sample locations

Sample ***CTW-36*** is from a relatively undeformed part of the hornblende-gabbro/diorite complex (unit 'hg', component 1) within the MESZ near the Cotton Well Pluton (See figure 3.7). This sample was taken away from foliated zones and sills. The crystallization age of this sample provides the time of early activity of the MESZ (D_{X+1}, figure 3.15).

Sample ***P95-gran*** was collected from a syntectonic, mylonitised leucogranite intrusion, unit 'lg', component 6, of the margin of the Mixed Zone near the granodiorite footwall gneisses northeast of the Cotton Well Pluton (See figures 3.7, 3.8a and 3.8b). The leucogranite intrusion is largely parallel to, but has locally intruded across the mylonitic foliation in the granodiorite footwall. The foliation also locally offsets the leucogranite intrusion (Figure 3.8c), which suggests that the leucogranite has been emplaced during deformation.

Sample ***A94-22*** was taken from the gneissic granodioritic sheet in the Central Gneiss Complex (*Gn-2*), indicated in figure 3.11. The crystallization age of this sample provides a minimum age for the banded gneisses, a maximum age for F_2 and F_3 folding phases, and a maximum age for the NE-SW extension phase that caused the conjugate shear bands within this sheet ($D_{Gn,X+3}$). This sample has no direct intrusive relationship with the components of the Mixed Zone, but the age of this sample may facilitate a direct comparison between the development of the MEGC and the Mixed Zone based on absolute ages.

Sample ***ME-28*** was collected from the foliated biotite-granodiorite (unit 'bg', component 7) of the 3304 ± 10 Ma Boodallana Suite, near the footwall margin of the Mixed Zone, indicated in figure 3.5. The date obtained for this sample should indicate whether emplacement was related to regional deformation phase D_{X+2}, at 3.32-3.31 Ga.

Sample ***CTW-1A*** was taken from an outcrop of muscovite granite (component 8), free of pegmatites and thrusts, in the western part of the Cotton Well Pluton (See figure 3.6). As this pluton has intruded the Mixed Zone discordantly, the crystallization age of this sample will provide a minimum age for the shear zone development of the MESZ, and hence for most of the magmatic components of the Mixed Zone.

3.6.2 Zircon preparation and selection

Zircons were separated at the mineral separation laboratory of the Vrije University, Amsterdam, using methods described by Zegers (1996). All samples were taken from igneous rocks that had intruded into a multiply active shear zone, all samples were likely to contain zircon xenocrysts, along with zircons affected by various later magmatic, metamorphic and/or deformation phases (e.g. Van Breemen and Hanmer, 1986). Xenocrystic zircons may have distinctive morphologies. Therefore, zircons were selected based on shape, size, colour and transparency. Up to four morphological zircon types were recognised in each sample. Representative zircons from each morphological type were selected for investigation (Table 3.2).

The zircons were mounted in epoxy-resin and the mount was polished to expose the cores of the crystals. Internal zircon structures were investigated using cathodoluminescence (CL) and secondary electron (SE) imaging using a Philips XL-30 Scanning Electron Microscope. A 'zircon growth stratigraphy' (Vavra et al., 1994) was derived for some morphological groups by interpreting different internal structures, including remnant cores, magmatic and/or metamorphic overgrowths, partially resorbed zircon and inclusions, in terms of their relative timing (Table 3.2). This formed the basis for the selection of SHRIMP analyses sites. Representative CL-images of zircons from each sample are shown in figure 3.17. Transparent and reflected light images of the mounted zircons were used to identify cracks and inclusions, which were to be avoided during analysis. Analyses were done during a period of one month in 1996, at the SHRIMP laboratory located at Curtin University of Technology in Perth, Western Australia. Analytical procedures using SHRIMP and analytical conditions during analysis are described in appendix 1.

3.6.3 Results and interpretation of SHRIMP U-Pb zircon analyses

U-Th-Pb results are listed in appendix 2. Individual analysis labels refer to morphological group, zircon number and spot number listed in table 3.2. A concordia diagram for each rock sample is presented in figures 3.17a, b, c, d and e. All analyses are also listed according to age in figure 3.19, where they have been labelled according to the CL-characteristics of the analysed domains (oscillatory/laminar/sector zoned, structureless, or patchy). Relationships between the date obtained for each analysis site and the U and Th content and Th/U ratio is also illustrated in figures 3.19. The CL characteristics and U and Th contents of each domain have been considered in the interpretation of the data, as is discussed below. Dates for individual analyses have a $\pm 1\sigma$ error, whereas dates for grouped analyses are $\pm t\sigma$ (where 't' is 'students t'), corresponding to 95% confidence.

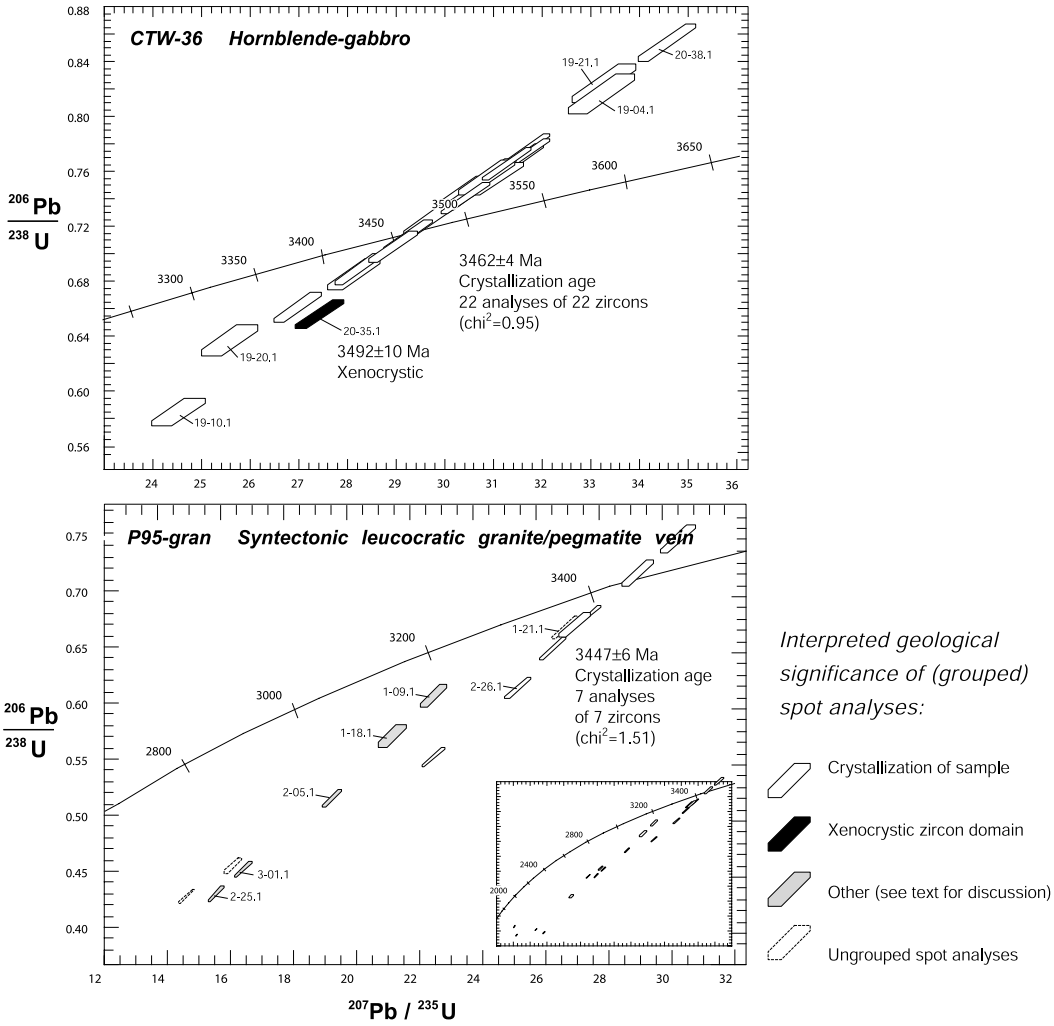

Figure 3.17

3.6.3.1 Hornblende-gabbro/diorite (CTW-36)

Sample CTW-36 yielded a small amount of relatively large, equidimensional zircons and zircon fragments. All zircons from this sample have a sector, laminar or fine, concentric, oscillatory zoning (See appendix 2 and figure 3.18a), indicative of a magmatic origin (e.g. Pidgeon and Aftalion, 1978). Twenty-three measurements were obtained from 23 zircons. The results are illustrated in the concordia plot of figure 3.17a. Many analyses are concordant, but analyses 19-10.1 and 19-20.1 are discordant, whilst analyses 19-04.1, 19-21.1, and 20-38.1 are reversed discordant. Discordant analyses plot along a line passing through the origin, which is consistent with recent radiogenic Pb-loss and/or redistribution from the analyses sites. All but one analysis indicate $^{207}Pb/^{206}Pb$ ratios

Figure 3.17 SHRIMP concordia of the samples from the Mixed Zone and the Mt Edgar Gneiss Complex. The corresponding data is listed in appendix 2. Errors of grouped ages are 2s, errors of xenocrysts are 1s. Details of the samples and their structural setting are listed in table 3.1. See text for further interpretation and implications of the ages. Sample CTW-36 is from an undeformed hbl-gabbro boudin in the Mixed zone of the MESZ. Sample P95-gran was taken in a syntectonic leucocratic granite/pegmatite vein in the gneissic footwall of the MESZ. Sample A94-22 is from a grey gneissic granodiorite sheet in the Mt Edgar Gneiss Complex. Sample ME-28 was collected from a biotite-granodiorite sill in the Mixed Zone near the footwall of the MESZ. Sample CTW-1A is from the discordant Cotton Well Pluton of muscovite-granite that intruded the central Mixed Zone.

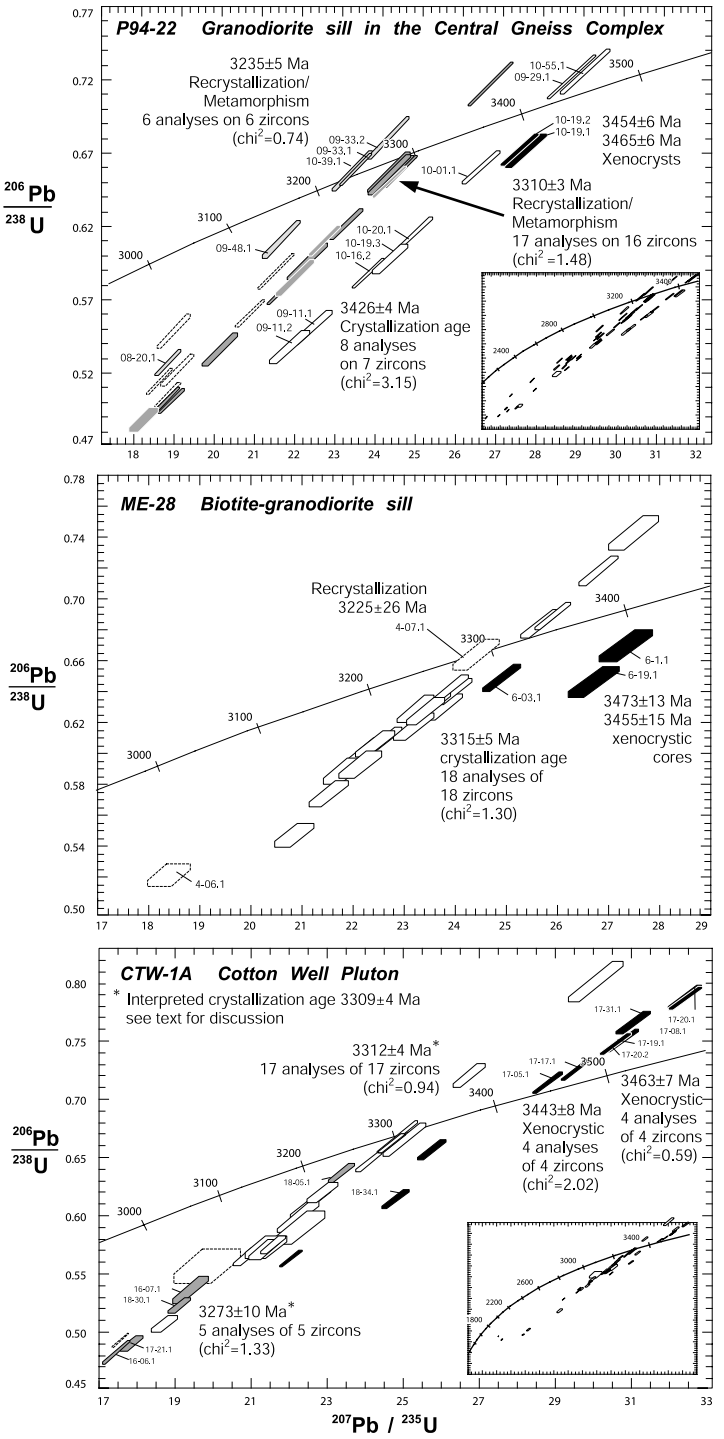

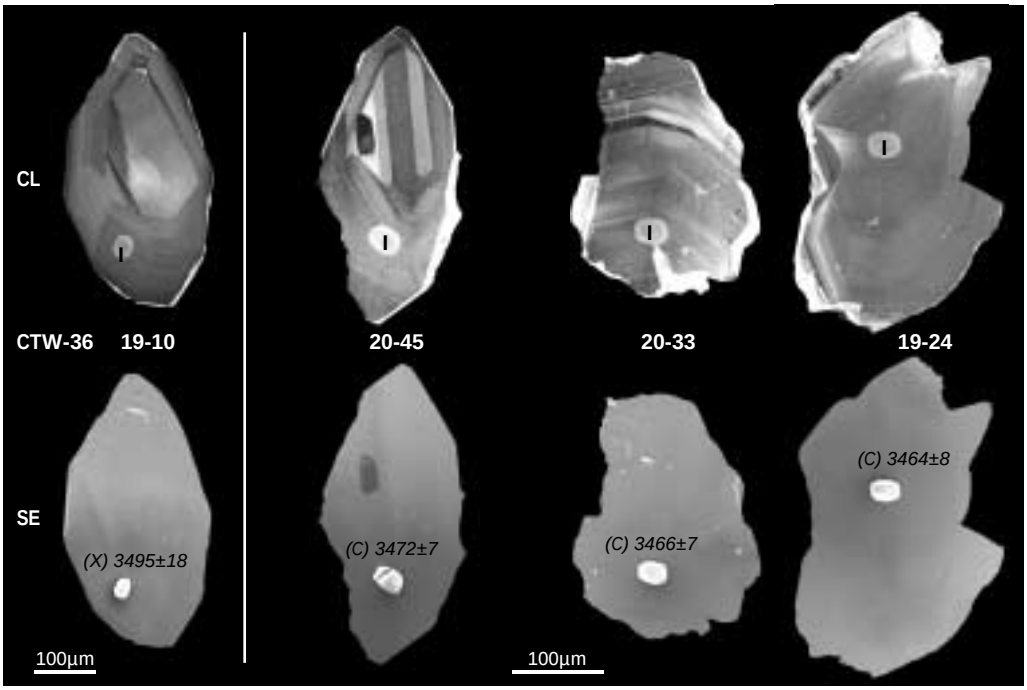

Figure 3.18 Cathodoluminesence (CL) and secondary electron (SE) images of representative zircons from the SHRIMP samples. Grain numbers refer to those in appendix 2. Light-coloured areas mark the areas rastered prior to SHRIMP analyses. These encompass the analyses spots, that are 15 to 20µm in diameter. The analyses spots are marked on the CL-images according to the interpreted origin of the analysed domain (i= igneous growth, m= metamorphic growth, or d= disturbed site) which refers to appendix 2. See text for discussion. The ^{206}Pb-^{207}Pb age of the single analyses are marked on the SE-images (1σ). Capital letters in brackets refer to the interpreted geological significance of its statistical age group (X= xenocrystic zircons, C= crystallization age of sample, D= disturbed/recrystallized event, PM= statistical group formed during a phase of partial melting, M= metamorphic event). (a) sample CTW-36. (b) sample P95-gran. (c) sample A94-22. (d) Sample ME-28. (e) Sample CTW-1A.

defining a single population with a weighted mean date of 3462 ± 4 Ma (chi^2 = 0.95). This is interpreted to correspond to the igneous crystallization age of the hornblende-gabbro/diorite. Analysis 20-35.1 is 93% concordant and has an older ^{207}Pb-^{206}Pb date of 3492 ± 10 Ma. This analysis is interpreted to be of a xenocryst zircon (See also figure 3.19).

Mafic rocks are not likely to contain a large zircon fraction because of the low silica content. Therefore, the question arises whether the zircons have crystallized within the hornblende-gabbro, or whether they are inherited. Rubatto and Gebauer (1999) recognised that zircons of gabbroic rocks are more isometric than those of granitic rocks. Sample CTW-36 contains relatively equidimensional zircons, which are distinctly different from the prismatic zircons from the more felsic samples (See figure 3.18). This supports the interpretation that these zircons were crystallized within a gabbroic/dioritic magma. U and Th contents of the analysed zircons of sample CTW-36 are low and the Th/U ratio is relatively high, ranging from 0.7 to 1.4 (Figure 3.19). This is also characteristic of zircons that crystallized from a magma with intermediate composition (Heaman et

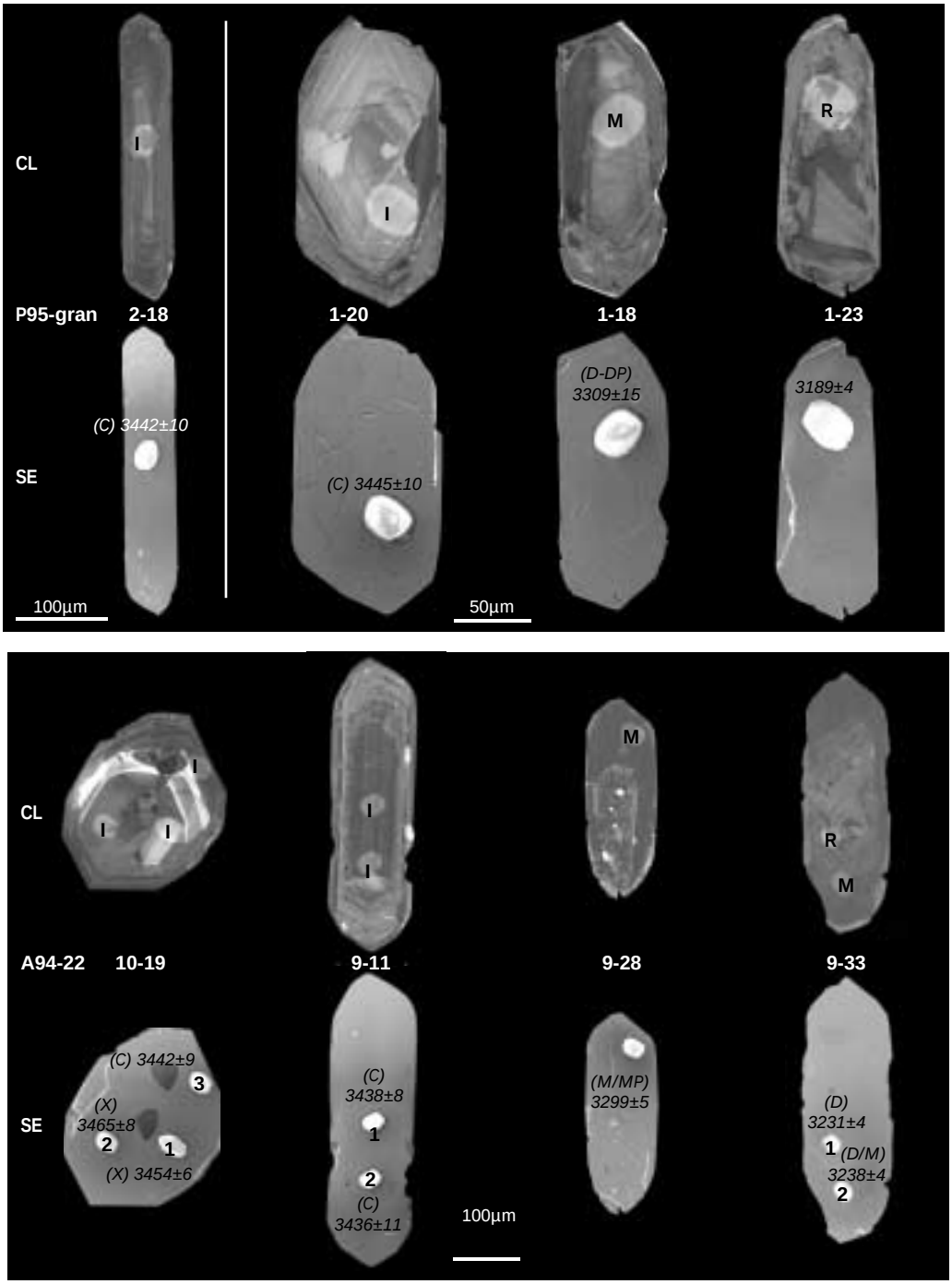

Figure 3.18 (continued)

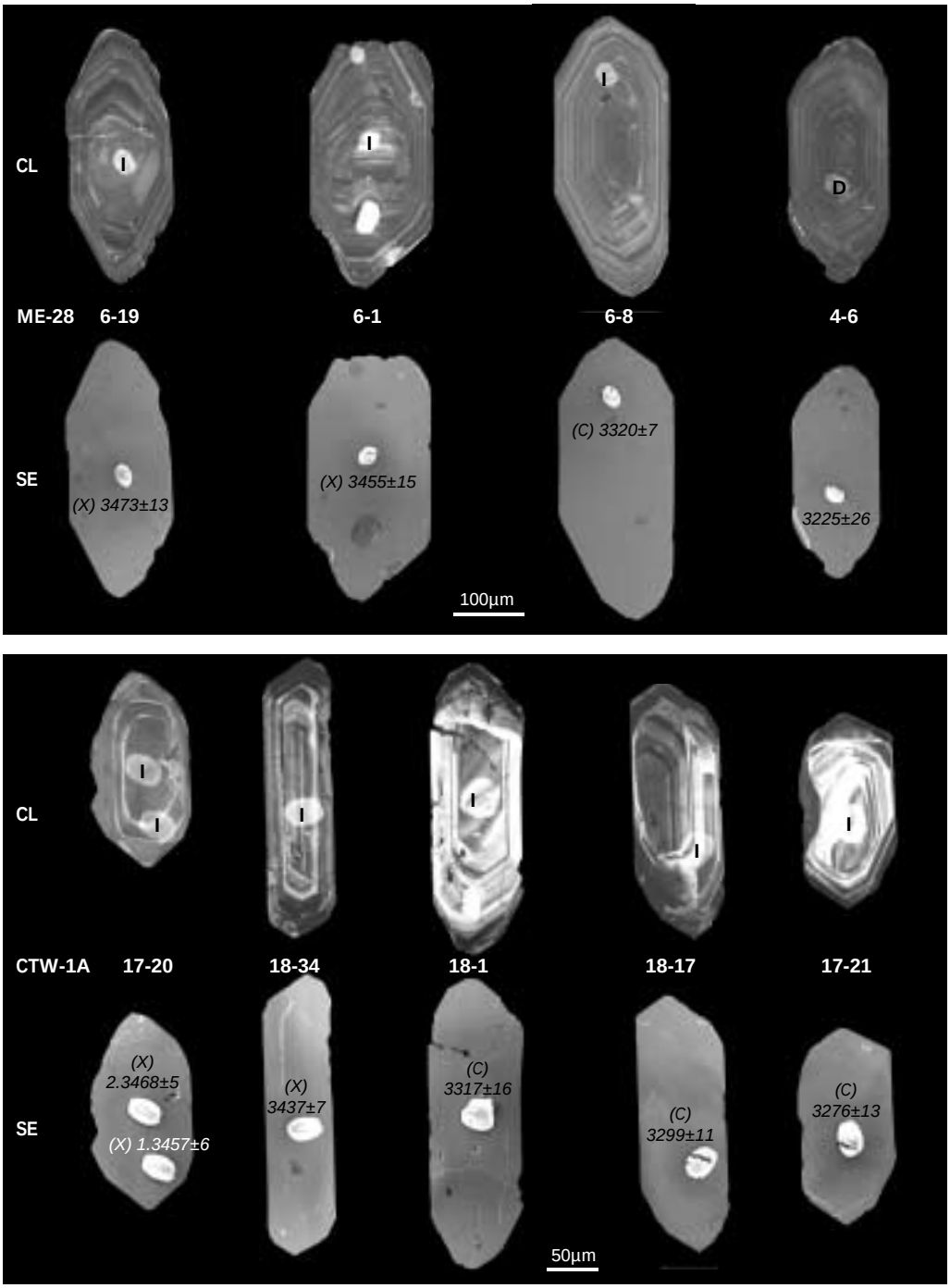

Figure 3.18 (continued)

al., 1990; Rubatto and Gebauer, 1999). Additionally, the observed low contrast of the oscillatory zoning supports the interpretation that the analysed zircons crystallized from an intermediate magma.

3.6.3.2 Leucogranite (P95-gran)

Twenty analyses were obtained from 20 zircons from Sample P95-gran. These were obtained from oscillatory cores, structureless and partly patchy cores and rims, from both long prismatic and equidimensional zircons (Table 3.2). The results are illustrated on a concordia plot in figure 3.17b. Most of the analyses were discordant, with the discordance pattern consistent mostly with recent loss of radiogenic Pb. Seven generally discordant analyses have ^{207}Pb-^{206}Pb ratios that indicate a date of 3447 ± 6 Ma (chi^2=1.51). Four of these (1-20.1, 2-18.1, 2-26.1, 3-03.1) are from oscillatory zoned cores (See grain 1-20 and 2-18 in figure 3.18b), suggesting that the date corresponds to a phase of magmatic zircon growth. Grain 1-20 shows an embayment into its euhedrally-zoned core (See figure 3.18b). This feature has been described for zircons from granite magmas that crystallized within an active shear zone (Van Breemen and Hanmer, 1986). The embayment observed in this sample is consistent with the observation that the leucogranite intruded syntectonically (See figure 4.8) and the embayment may reflect the development of the mylonitic foliation. A low-CL, structureless rim has discordantly overgrown the embayment of grain 1-20 (Figure 3.18b). Two other rims of this type yielded dates of 3309 ± 15 and 3282 ± 6 Ma, and statistically belong to a poorly defined group of five discordant analyses with ages between ca. 3325-3275 Ma (See figure 3.19). These rims may have grown during high-grade metamorphism, and may correspond to a phase of reactivation of the MESZ, possibly during deformation and/or intrusion of later components (components 7 or 8). The date of 3447 ± 6 Ma is interpreted to represent the crystallization age of this syntectonic leucogranite dyke.

Seven younger analyses outside the aforementioned two age groups are less than 75% concordant, have U and Th contents that is higher than the 'threshold' value (See Nelson, 1997) (Figure 3.19) and are from patchy domains (e.g. grain 1-23 in figure 3.18b). In situ radiogenic decay of U and Th, widely held as the principal cause for damage to the crystal structure and Pb loss (Silver, 1963; Pidgeon et al., 1966), is interpreted to have resulted in loss of radiogenic Pb from these analysis sites during both ancient and relatively recent disturbance events.

3.6.3.3 Grey gneissic granodiorite sheets in the Central Gneiss Complex (A94-22)

For sample A94-22, 55 analyses were obtained from 47 zircons of all three morphological groups listed in table 3.2 and from three types of CL-domains (See appendix 2 and figure 3.18c). The results are illustrated on a concordia plot in figure 3.17c. The analyses range from highly discordant to slightly reverse-concordant with a discordance pattern that is consistent with recent Pb-loss and Pb-redistribution. Based on the ^{207}Pb-^{206}Pb ratios, 33 analyses may be assigned to one of four groups. The remaining 25 analyses are mostly strongly discordant (<75%), see inset (See appendix 2 and figure 3.17c) and have not been grouped. Zircons from the largest group, with 17 analyses from 16 grains, have ^{207}Pb-^{206}Pb ratios that indicate a weighted mean date of 3310 ± 3 Ma (chi^2=1.48). Eleven of these analyses are 85 to 100% concordant. Most analyses of this age group were obtained

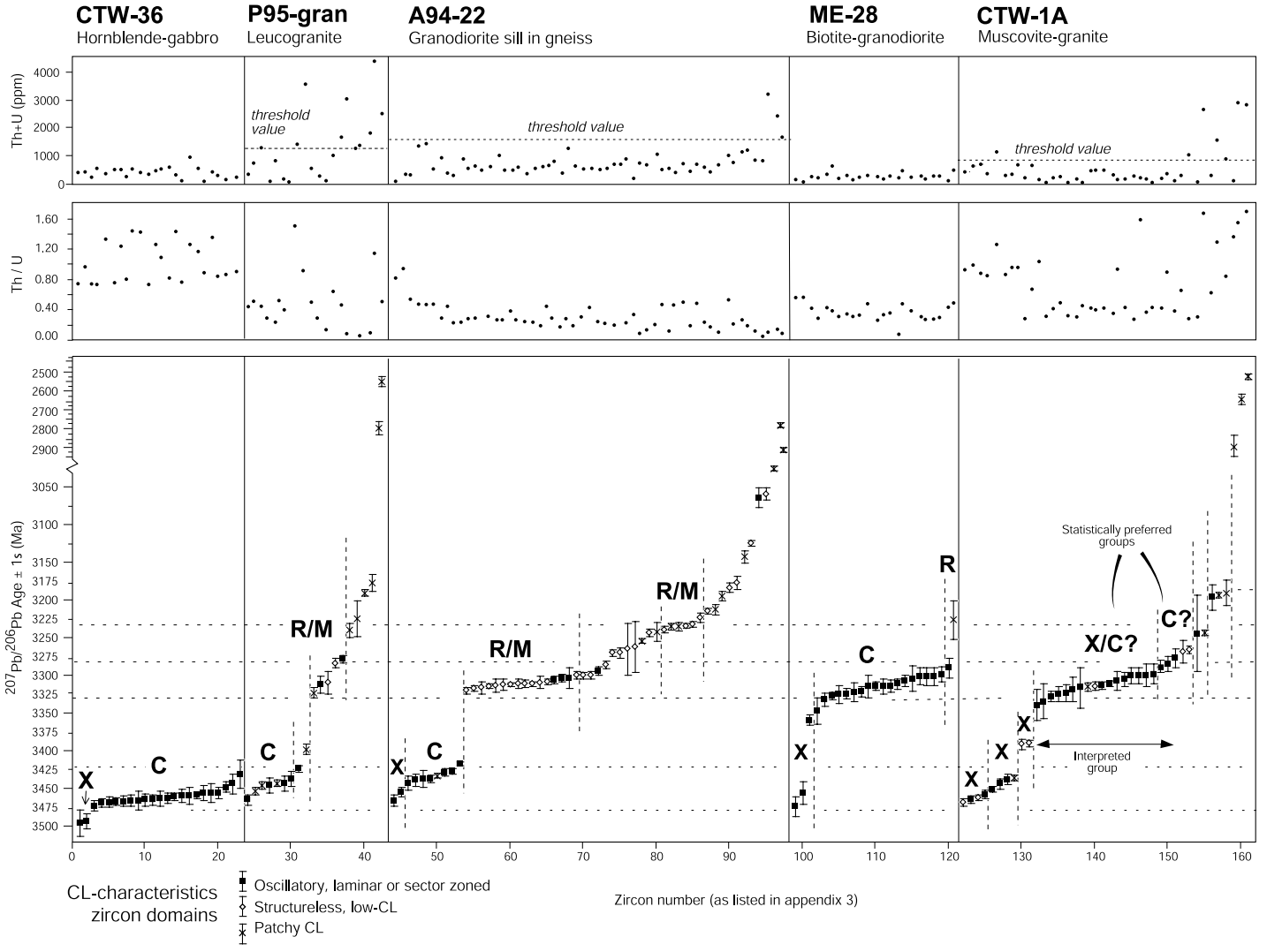
CTW-36
Hornblende-gabbro
P95-gran
Leucogranite
A94-22
Granodiorite sill in gneiss
ME-28
Biotite-granodiorite
CTW-1A
Muscovite-granite
Th+U (ppm)
threshold value
threshold value
threshold value
Th / U
207Pb/206Pb Age ± 1s (Ma)
X
C
C
R/M
X
C
R/M
R/M
X
C
R
X
X
X/C?
C?
Statistically preferred groups
Interpreted group
CL-characteristics zircon domains
Oscillatory, laminar or sector zoned
Structureless, low-CL
Patchy CL
Zircon number (as listed in appendix 3)

from structureless, low-CL rims (See appendix 2 and figure 3.18c), which are characteristic of zircon domains that grew during metamorphism (Rubatto et al., 1999; Vavra et al., 1996, 1999). The Th/U ratios indicated by the analyses of these rims are less than 0.35, generally lower than those of magmatic CL-domains (See figure 3.19), also consistent with a metamorphic origin. Low Th/U ratios (0.1 to <0.05) are commonly found in zircon domains of metamorphic origin (e.g. Kinny et al., 1990; Maas et al., 1992; Vavra et al., 1996, Rubatto and Gebauer, 1999). The ~3310 Ma group is here interpreted as representing the time of a thermal event, possibly related to widespread granite intrusion within the Mt Edgar and Corunna Downs Granitoid Complexes and the MESZ, during which the associated heat and/or fluids may have caused growth or new rim zircon, or the recrystallization of structureless rims.

The oldest spot-ages from this sample were obtained from a high-CL sector zoned core of zircon 10-19 (Figure 3.18c) and yielded ^{207}Pb-^{206}Pb ratios indicating dates of 3465 ± 8 and 3454 ± 6 Ma (1σ), respectively. A third analysis from this grain (10-19.3), obtained on an oscillatory-zoned rim, indicates a date of 3442 ± 9 Ma (1σ). This last date statistically belongs to the second oldest group, which contains eight analyses of seven zircons, with weighted mean ^{207}Pb-^{206}Pb ratios indicating an age of 3426 ± 4 Ma (chi^2=3.51). All analyses of this group are located in high- and low-CL laminar or sector zoned domains (Figure 3.18c). We interpret the above ages to reflect two separate magmatic episodes, of which the 3426 ± 4 Ma group represents the crystallization of the rock. The older two cores are interpreted to be xenocrystic.

A fourth, younger group comprises four near-concordant measurements from four structureless, low CL rims (09-33.1, 09-33.2, 10-39.1, and 09-48.1, figure 3.18c). When grouped with two less concordant analyses from patchy domains (08-20.1, 08-29.1, figure 3.18c), these analyses give a weighted mean ^{207}Pb-^{206}Pb date of 3235 ± 5 Ma (chi^2=0.74). The nature of the domain of the four near-concordant analyses, like those of the 3310-group, suggests a phase of recrystallization and/or metamorphic zircon growth. The near-concordance of these analyses, however, is not what is expected for recrystallized zircon domains, and a metamorphic origin may be more probable.

3.6.3.4 Biotite-granodiorite sill in the MESZ footwall (ME-28)

Twenty-three analyses were obtained from cores and rims of 22 zircons of sample ME-28. The CL-images of the zircons from this sample show oscillatory zoning (See grain 6-8 in figure 3.17d) characteristic of igneous zircons. The results are illustrated on a concordia plot in figure 3.17d. Analyses range from 84% discordant to slightly reverse-discordant (See appendix 2) with a discordance pattern indicating recent redistribution of radiogenic Pb from the analysis sites. The

Figure 3.19 Relationship between the ^{207}Pb-^{206}Pb ages and Th+U and T/U values of all individual analyses. Analyses are ordered with decreasing age per sample. Zircon numbers on the horizontal axis refer to those in appendix 2. The label of each spot indicates the interpreted origin of the analysed domain, either igneous, metamorphic (or disturbed). A positive correlation between younger ages and high Th+U content, suggests that these ages are the effect of disturbance by radiation damage. A threshold value is recognised, above which the analyses are of uncertain geological significance. Analyses between vertical lines define statistical groups, which are marked according to their interpreted geological implication, as marked in the concordia of figure 3.17 and appendix 2. Th/U ratios for all reliable analyses (those with a U+Th content below the threshold value), are plotted against their ^{207}Pb-^{206}Pb age. The highest average Th/U ratio is observed in the hbl-gabbro, as is expected for zircons that crystallized from a more mafic melt. See text for further discussion.

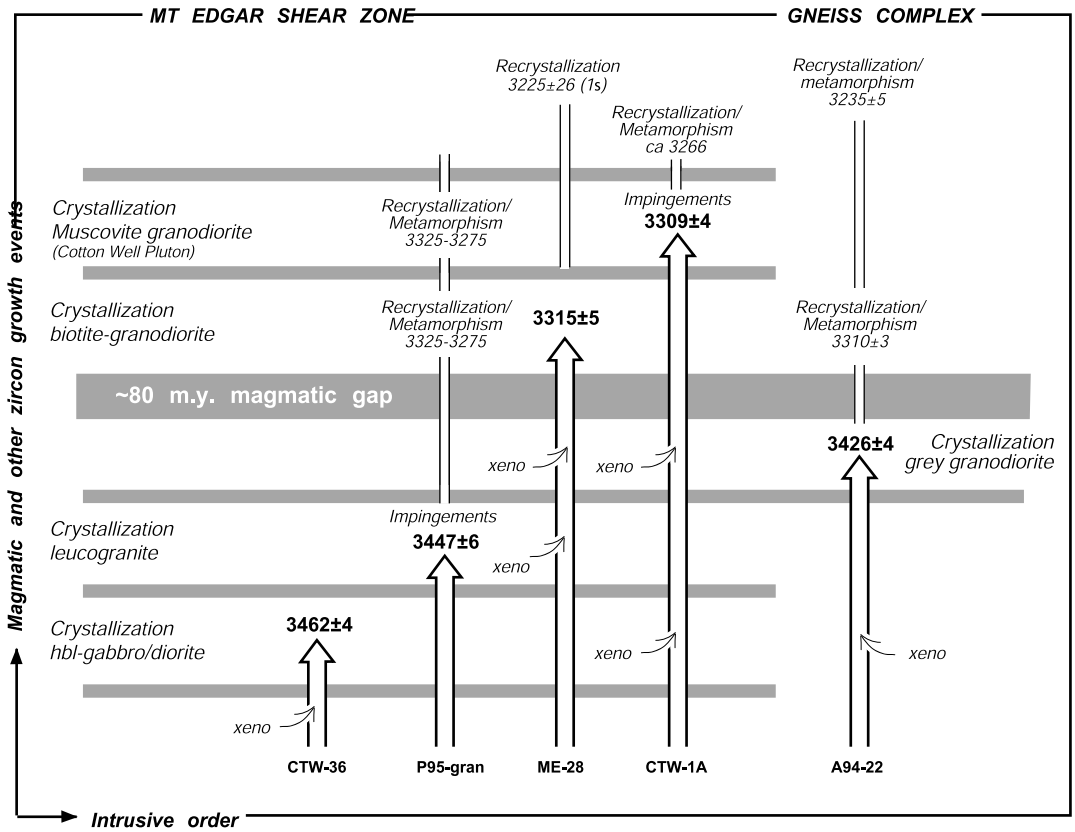

Figure 3.20 Schematic summary of geochronological data illustrating the internal consistency of intrusive relationships, crystallization ages, metamorphic growth of zircon rims and inheritance of xenocrystic zircons (x). See text for discussion.

^{207}Pb-^{206}Pb ratios of 18 analyses belong to a well-defined group (chi^2 = 1.30) corresponding to a date of 3315 ± 5 Ma. This is interpreted to be the igneous crystallization age of the sample. Three of the other five analyses (6-19.1, 6-1.1 and 6-03.1) gave older ^{207}Pb-^{206}Pb dates of 3473 ± 13, 3455 ± 15 and 3358 ± 7 Ma, respectively. The CL-images show that the two oldest dates were from a sector-zoned and an oscillatory-zoned core of grains 6-19 and 6-1, respectively (Figure 3.18d), which were discordantly overgrown by oscillatory-zoned rims. This suggests that the cores are xenocrystic in origin. Their age and their Th/U ratio suggest that these zircons may have been derived either from the leucogranite (P95-gran) or from the grey granodiorite component (A94-22) in the gneiss complex (Figure 3.19).

Analysis 4-07.1 of an oscillatory-zoned zircon indicated a younger ^{207}Pb-^{206}Pb date of 3289 ± 13 Ma. Although this domain is chemically similar to those of the main population (Figure 3.18), statistically it cannot be grouped with these (Figure 3.17). The concordance of this analysis and its U content, which is below the threshold value (Figure 3.19), provides no reason to suspect that its younger age is due to Pb-loss, and the significance of this date is unclear. However, it may be related to the ca. 3.29 – 3.27 Ga event mentioned above (§ 3.5.3.1) In contrast, the discordant 3225

± 26 Ma date of the youngest analysis (4-06.1) is likely to be the result of radiogenic Pb-loss, as the U concentration was above the threshold value (Figure 3.19) and the analysis site was within a domain that shows patchy internal CL structures consistent with recrystallization (Figure 3.18d).

3.6.3.5 Muscovite-rich Cotton Well Pluton (CTW-1A)

Forty analyses were obtained from 38 zircons from all three morphological groups of sample CTW-1A, including elongated prismatic zircons with well-developed crystal faces, and stubby rounded zircons without crystal faces (See table 3.2). The results are illustrated on a concordia plot in figure 3.17e. The majority of analyses are >78% concordant to slightly reverse concordant (See also appendix 2) and define four statistical age groups. Analyses that are more than 78% discordant are not grouped.

The largest statistical group contains 17 analyses with ^{207}Pb-^{206}Pb ratios that define a date of 3312 ± 4 Ma (chi^2=0.94). The CL-images show that all spots were from oscillatory zoned or laminar zoned domains, consistent with a magmatic origin (See appendix 2 and grain 18-1, 18-17 in figure 3.18e) and this date is interpreted as the crystallization age of the pluton. A group of five analyses have ^{207}Pb-^{206}Pb ratios that define an age of 3273 ± 10 Ma (chi^2=1.33). Three of these younger dates were obtained on oscillatory-zoned domains with remarkably high CL emission (e.g. grain 17-21 in figure 3.18e) which have discordantly overgrown the 3312 Ma cores (See figure 3.18e). As the members of the 3312 and 3273-groups have similar Th and U contents and Th/U ratios (apart from the youngest two spot ages, figure 3.19) they may have crystallized from a similar melt. The U and Th concentrations of these five younger analyses are all similar to those of the 3312-group and are well below the 'threshold' value, (apart from analysis 16-6.1, figure 3.19). Therefore, the range in ^{207}Pb-^{206}Pb dates of both groups is unlikely to be the result of ancient or recent radiogenic-Pb loss from a population of zircons that crystallized at 3312 Ma, but it cannot be excluded. Inclusion of the three chemically similar spots (18-05.1, 18-30.1, 17-21.1) in the 3312-group gives a date of 3309 ± 4 Ma (chi^2 = 2.04). This leaves the two low-CL structureless rims dated at 3267 ± 15 (1σ) and 3265 ± 5 Ma (1σ) (See appendix 2) ungrouped, but may reflect the above 3.29 – 2.37 Ga event.

Eight analyses indicating older dates were divided statistically into two groups. The ^{207}Pb-^{206}Pb ratios of the oldest group define an age of 3463 ± 7 Ma (17-8.1, 17-19.1, 17-20.1, 17-20.2) and the younger of 3443 ± 8 Ma (17-5.1, 17-17.1, 17-31.1 and 18-34.1). All but one of the above zircons belonged to the morphological population CTW1A-17, with well-rounded, equidimensional grains with irregular crystal faces (See figure 3.17 and table 3.2). Their shapes, ages and Th/U ratios (Figure 3.19) suggest that they may have been inherited as xenocrysts from the hornblende-gabbro/diorite complex into which the granite has intruded (Figure 3.7). The groups were marked 'X_1' and 'X_2', respectively in appendix 2. To additional dates, analyses 17-3.1 and 17-18.1, have ages of 3390 ± 7 and 3389 ± 4 Ma (1σ), respectively. These analyses are discordant, although U and Th concentrations of these analyses were not above the threshold value. The analysis sites were within low-CL, structureless rims. We interpret these grains (marked 'X_3' in appendix 2) as xenocrysts.

Two interpretations for the crystallization age of this Cotton Well Pluton are feasible. The statistically preferred interpretation is that the pluton has crystallized at 3312 ± 4 Ma and that the five younger spot ages reflect Pb loss. Alternatively, when the CL images and the chemistry are

considered, the three chemically similar zircon domains are included. This then gives a crystallization age of 3309 ± 4 Ma. In the latter interpretation the two ungrouped younger dates of ca. 3266 Ma are interpreted to reflect a phase of recrystallization/metamorphism, possibly during reactivation of the MESZ. The date of 3309 ± 4 Ma is interpreted to provide the best estimate of the crystallization age of the Cotton Well Pluton.

3.7 Discussion

3.7.1 Overview of the new geochronological data

The SHRIMP ages obtained in this study for igneous components from the Mixed Zone and the Gneiss Complex are summarised in figure 3.20. All obtained crystallization ages and dates from xenocrystic zircons are consistent with the observed intrusive inter-relationships, as is schematically illustrated in figure 3.20. Like the available crystallization ages, most of the newly obtained ages fall either within the known time range of the Warrawoona episode (the 3462 ± 4 Ma hornblende-gabbro/diorite, the 3447 ± 6 Ma leucogranite, the 3426 ± 4 Ma granodiorite) or of the Wyman episode (the 3315 ± 5 Ma biotite-granodiorite, the 3309 ± 4 Ma muscovite granite) (Figures 3.21). In addition, some new dates are attributed to phases of metamorphic growth and/or recrystallization in the periods between ca. 3325-3275, ca. 3266 Ma and ca. 3235-3225 Ga, as is discussed in section 3.6 and illustrated in figure 3.20. The implications of these geochronological data for the structural and magmatic history of the MESZ and for the tectonic setting of the Marble Bar Domain are discussed below.

3.7.2 Implications for the timing of activity of the Mt Edgar Shear Zone

3.7.2.1 Timing of the initial tectonomagmatic activity of the MESZ

In chapter 2 the MESZ was recognised as a potentially long-lived detachment that was active at, and prior to, 3.32-3.31 Ga. The exact timing of the early activity, however, was unknown. Based on the crystallization ages reported here, it is evident that the (proto-) MESZ must have existed as some sort of discontinuity at around 3462 Ma, as it has been the locus for intrusion of the hornblende-gabbro/diorite sill of that age. However, active deformation, and development of a mylonitic shear zone, may not have occurred until intrusion of syntectonic dolerite sills (component 5) followed by syn-tectonic leucogranite veins (components 6) at ca. 3447 ± 6 Ma (see figure 3.15).

3.7.2.2 Active or reactive deformation during emplacement of the hornblende-gabbro/diorite complex?

The internal structures within the hornblende-gabbro/diorite complex suggest that the complex formed by multiple intrusions of sheet-like bodies resulting in a total thickness of at least 2.5 km (present thickness). The complex is now situated concordantly along the margin of a steep-sided gneissic dome, at the contact between younger high-grade gneisses and steeply dipping greenschist facies volcanic rocks of the similarly aged Duffer Formation and Salgash Subgroup (See figures 2.8a

and b, 2.13). As the complex intruded at ca. 3462 ± 4 Ma, during deposition of the Duffer Formation, and as the younger central gneisses developed as a dome afterwards, it is interpreted that the complex intruded as subhorizontal sheets (as illustrated in figure 2.18) that were steepened by doming, like the nearby Duffer Formation. The coarse texture of the undeformed parts of the complex indicates that it cooled slowly. This suggests that it intruded relatively hot crust, with an ambient temperature at least equivalent of that currently found at mid-crustal depths. This indicates

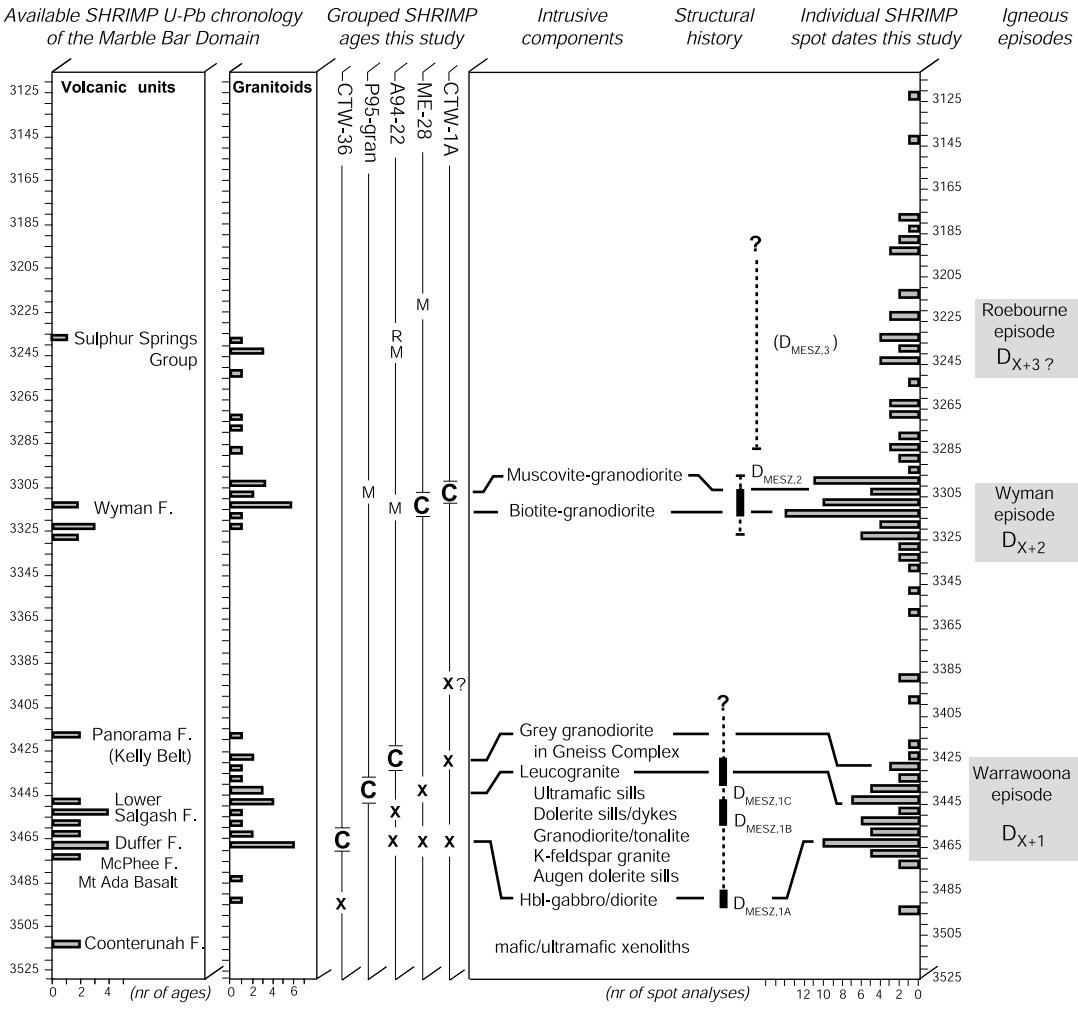

Figure 3.21 Summary of the tectonic and magmatic development of the MESZ with respect to the igneous episodes and the stratigraphy of the Marble Bar Domain. The early development of the MESZ, during intrusion of the hbl-gabbro/diorite (Dx+1), was coeval with deposition of the Duffer Formation. Subsequent extension and intrusion of the dolerite suite was possibly coeval with deposition of the Salgash Group basalts. The granodiorite sheet in the Gneiss Complex is similar in age as the 'young' Duffer, or, McPhee Supersequence in the Kelly Belt. A non-igneous interval occurred in between Dx+1 at 3.46-3.45 Ga and reactivation of the MEGC during Dx+2 at 3.32-3.31 Ga.

that the complex intruded either abnormally hot upper crust or at mid-crustal level.

Mechanisms for intrusion of sills can be regarded by two end-members, with different relationships to deformation. Sills have been described to have forcefully intruded the crust and inflated to form laccoliths that cause uplifting, thermal weakening, and subsequent collapse of the crust (e.g. Parsons and Thompson, 1993). In this model, deformation is merely the result of magmatism and could be regarded as reactive. Alternatively, sills can preferentially use an active extensional shear zone, filling in the created space (Hutton et al., 1990; Lister and Baldwin, 1993). In this model, deformation is active and has allowed for the intrusion of sills. The main difference between these two emplacement mechanisms is, theoretically, reflected in the difference of the relative timing of *initial* extension and *initial* magmatism. This may under favourable circumstances be indicated by field relationships. For the gabbro/diorite complex, it is important to explore and discuss this causal relationship, because it may place constraints on the tectonomagmatic model for this part of the history.

Active deformation that preceded and facilitated intrusion of the hornblende-gabbro/diorite into the MESZ may be supported by the schistose mafic and ultramafic xenoliths observed in undeformed parts of the hornblende-gabbro/diorite complex. The xenoliths provide evidence for the intrusion of hornblende-gabbro/diorite sills into deformed rock (See also chapter 2). The xenoliths may be remnants of a proto-MESZ that directly preceded intrusion of the hornblende-gabbro/diorite complex. However, the exact timing of deformation is unclear and deformation may be much older and hence unrelated to intrusion of the hornblende-gabbro/diorite.

Re-active deformation, i.e. deformation that post-dates intrusion and is merely the result of intrusions, is supported by the following observations. Geochronological data have shown that the emplacement of the hornblende-gabbro/diorite complex was coeval with deposition of the Duffer Formation throughout the Marble Bar Domain (See figure 3.3). The Duffer Formation has been described to display a gradual trend from andesitic at its base to dacitic and rhyodacitic towards the top (Fig. 41 in Hickman, 1983). The andesites in the base may be the extrusive equivalent of the hornblende-gabbro/diorite complex. Extensional growth faults have been recorded in the top of the Duffer Formation (Zegers et al., 1996; Nijman et al., 1998a). As the andesites constitute the base of the Duffer Formation, and if extrusion of the andesites coincided with intrusion of the gabbro/diorite complex, then intrusion of the gabbro/diorite complex preceded extension at upper crustal levels.

The currently known relationships do not resolve the relative timing of *initial* extension and *initial* magmatism at ca. 3.46 Ga in the Marble Bar Domain. Future geochronological data may place additional constraints.

3.7.2.3 NE-SW extension, pre-3447 ± 6 Ma (ultra)mafic dykes and sills, and granite intrusion at ca. 3425 Ma

The structures related to $\mathbf{D_{MESZ,X+1A}}$ (Figure 3.15) are consistent with a model in which a proto-MESZ develops as a mid-crustal detachment (See Chapter 2, figure 2.18) during extension and intrusion of the 3462 ± 4 Ma hornblende-gabbro/diorite complex (CTW-36). Structural relationships indicate that subsequent extension was coeval with intrusion of the main (ultra)mafic sills and dykes (components 5a and b) and doming of the MESZ (See Chapter 2, figure 2.16). The

sills and dykes are intruded by leucogranite sheets throughout the Mixed Zone. A leucogranite dyke in the Mixed Zone is dated at 3447 ± 6 Ma in this study (P95-gran), which provides a minimum age for the (ultra)mafic sills and dykes and thus for the related extension. The time span for the age of the (ultra)mafic sills and dykes is similar to that for the Apex Basalt of the Salgash Subgroup (See figure 3.3) The occurrence of 3426 ± 4 Ma sub-horizontal granodiorite sheets in the central Gneiss Complex of the MEGC (A94-22) indicate ongoing magmatic activity which suggests ongoing tectonism. Felsic volcanic units of similar age have been identified by Barley and Pickard (1999) and Nelson (2000) in the nearby Kelly Belt (See figures 3.3 and 3.4) and are correlated to the Panorama Formation (Nelson, 2000). This shows that mafic and felsic magmatism occurred in the Mixed Zone and gneissic basement at the time of extrusion of the dominantly mafic Apex Basalt and felsic volcanic Panorama Formation, respectively.

3.7.2.4 Development of structures in the Central Gneiss Complex

Three main groups of structures were recognised in the Central Gneiss Complex. They are listed in figure 3.12. The oldest is a strong subhorizontal gneissosity, found both in the banded gneisses and in the concordantly intruded granodiorite sheets, the latter dated at 3426 ± 4. The age of this sheet provides an age for part of the development of the gneissosity, which corresponds to late-stage D_{X+1}. The second group comprises the NNE-trending open subhorizontal folds in the gneisses attributed to F2. A third group contains a set of migmatitic shear bands with a geometry that indicates NE-SW extension. The last two groups are not dated, but a comparison with the structural development of the Warrawoona Greenstone Belt (see figure 2.17) and the MESZ (figure 3.15) leads to the following interpretation. The NE-SW extension direction of the shear bands is similar to that of the MESZ, and the migmatitic nature of the shear bands would be explained by the heat associated with intrusion of the 3.31 Ga granites. Similar shear bands (see photograph figure 2.12a) have been reported for the Beaton Well Zone, the transfer structure to the MESZ (Figure 2.5), ~15 km to the SE (see figure 3.4), which suggests similar cause and timing. For these reasons the NE-SW extensional shear bands are interpreted to be associated with extension and granite intrusion during D_{X+2}.

The NNE-trending folds were interpreted to predate the NE-SW extensional shear bands, as the latter were not folded. It is possible that the folds are associated with the E-W compressional stage of D_{X+2} (see overview in figure 2.17). Possibly, this phase is associated with the formation of the high-P kyanite bearing assemblages, remnants of which were found along the margin with the Warrawoona Belt (see chapter 2 and figure 2.15). Compression followed by extension during granite intrusion and doming of the MEGC would explain the kyanite and sillimanite/andalusite overprint and NE-vergent kinematics. This is consistent with the observed NE-SW extensional shear bands that post date the folding.

3.7.2.4 Granitoid emplacement in the MESZ footwall at ca. 3.31 Ga

The 3315 ± 5 Ma crystallization age of the granodiorite sill from near the footwall of the MESZ (sample ME-28) confirms that the MESZ was active during NE-SW extension ($D_{MESZ, X+2}$) and granite intrusion at that time. The lack of abundant sills of this composition within the rest of the

Mixed Zone (Figure 3.5), and the general lack of MEGC-up kinematics in the older intrusive components of the MESZ (Figure 3.15), is taken to indicate that reactivation of the MESZ was localized at its footwall margin.

Reactivation of the MESZ and intrusion of granitoids at ca. 3.31 Ga is proposed to be the cause for the post-tectonic hornblende and muscovite blastosis in the older intrusive components (See figure 3.15) and zircon overgrowths in sample A95-gran (see figure 3.20). The statistically significant age of 3310 ± 3 Ma obtained from recrystallized/metamorphic zircons from the 3426 ± 4 Ma grey granodiorite from the Central Gneiss Complex (sample A94-22, see figure 3.17c) suggests that the Central Gneiss Complex too has been thermally disturbed at that time.

3.7.2.5 Post-3309 Ma events

Most zircon samples of this study have yielded several individual spot ages younger than ca. 3309 Ma (See figure 3.19). However, in only one sample do they form a statistically significant group (A94-22).

An age of 3235 ± 5 Ma is defined by six spot analyses of sample A94-22 (See figure 3.17c). This age is interpreted to be related to phases of metamorphism and/or recrystallization of zircon domains. A spot analysis from a zircon domain with patchy CL-characteristics has yielded a similar date in sample ME-28 (See figure 3.17d), suggesting that metamorphism/recrystallization is widespread. The dates correspond to the Roebourne episode at 3260-3240 Ma (See figures 3.2 and 3.3). A granitoid of this age has recently been identified in the central MEGC (Nelson, 2000, see figure 3.4) and heat and/or fluids related to the intrusion of granitoid with this age may have disturbed the zircons of rocks within the MESZ. The Roebourne episode involved emplacement of the Strelley Granite and coeval felsic volcanic units of the related Sulphur Springs Group to the west of the Marble Bar Domain. The latter contain extensional structures (Vearncombe et al., 1998). In the MEGC and MESZ no extensional structures have been positively identified as being 3.24 Ga. The structural context of the 3.24 Ga granitoid is unknown.

In addition, the Cotton Well Pluton yielded two spot dates at ca. 3266 Ma (sample CTW-1A). These dates in combination with the ca. 3275 Ma spot dates recorded in sample P95-gran, suggest an additional phase of thermal disturbance. No magmatism of this age has been recognised in the MEGC. But, a phase of pre-3200 Ma (N)NE-(S)SW compression (D_{X+3}) that caused thrusting in the MESZ ($D_{ND,4}$) and thrusting and strike-slip in the Carbana Pool Adamellite near the Kelly Belt ($D_{SD,4}$) (See figures 2.10 and 2.17), may have caused thermal disturbance.

3.7.5 Episodic magmatism in the eastern part of the Pilbara granite-greenstone terrain

Available geochronological coverage of the Marble Bar Domain suggests that magmatic activity was constrained to distinctive time spans. These episodes of magmatic activity interchange with periods of magmatic quiescence, i.e. the ca. 80 m.y. time gap between the Warrawoona and Wyman episodes (See figure 3.2, see also Nelson et al., 1999). Any magmatic phase of intermediate age would have been likely to have exploited the MESZ. Our detailed mapping and zircon study have not identified any of such additional magmatic phases (Figure 3.20). This, in combination with

the lack of components of this age in the neighbouring domains (See figure 3.2), make additional significant magmatic phases in the eastern Pilbara between 3.46 and 3.31 Ga unlikely. However, it can not be ruled out that this age gap is the result of inadequate geochronological coverage.

The distribution of volcanic and plutonic ages in the eastern Pilbara suggests that magmatic activity during the 700 m.y. history (from 3.5 to 2.8 Ga) was not random, but was episodic (See figure 3.2). Magmatic episodes in the Marble Bar Domain ranged in length from ca. 55 ± 5 m.y. (ca 3475-3420 Ma), through ca. 25 ± 5 m.y. (ca 3330-3305 Ma), to approximately 20 ± 5 m.y. (ca 3255-3235 Ma) (see the overview of available SHRIMP ages in the Marble Bar Domain and grouped SHRIMP ages obtained in this study, Figure 3.21). This episodic history and moreover, the ca. 80 m.y. magmatic gap from 3.42 to 3.34 Ga provides extra constraints that must be consistent with a geodynamic model for the development of the area. This is further discussed in chapter 6.

3.8 Conclusions

1. The (proto) Mt Edgar Shear Zone was initially exploited by hornblende-gabbro/diorite sills dated at 3462 ± 4 Ma (CTW-36). Multiple intrusions formed a ca. 2 km thick silled complex. Subsequent intrusion include sills of alkali-feldspar granite, phenocrystic dolerite, and a suite of granodiorite, diorite and tonalite. Deformations structures and kinematics and intrusive relationships suggest synmagmatic extension during the onset of deformation phase D_{X+1}.

2. Subsequent development during D_{X+1} of the Mt Edgar Shear Zone as an extensional mid-crustal detachment occurred during intrusion of (ultra)mafic sills followed by syntectonic intrusion of leucogranite sills at 3447 ± 6 Ma (P95-gran).

3. In the Central Gneiss Complex development of a subhorizontal gneissosity occurred during intrusion of the 3426 ± 4 Ma granodiorite sill (P94-22), interpreted to indicate that extension and doming of the MESZ and MEGC during D_{X+1} was ongoing over an extended period of time.

4. Extension and emplacement of granitoids into the MEGC at 3315 Ma caused reactivation and steepening of the MESZ (D_{X+2}). This caused recrystallization and/or metamorphic growth of zircon in the older components within the MESZ and Central Gneiss Complex.

5. Three zircons from the MESZ recorded recrystallization/metamorphism at ca. 3270 Ma, which is tentatively related to (N)NE-(S)WW compression (D_{X+3}).

6. Zircons from the Central Gneiss Complex have recorded a statistically significant age of 3235 ± 5 Ma, associated with recrystallization/metamorphism. This event may be related to granitoid emplacement at 3240 ± 11 Ma in the centre of the MEGC. A similar date was recorded in zircon rims from the 3315 ± 5 Ma granodiorite in the MESZ. No components of this age have

been identified in the MESZ.

7. Early activity of the MESZ during D_{X+1} was simultaneous with activity of the Split Rock Shear Zone on the margin of the adjacent Shaw Granitoid Complex, indicating that mid-crustal detachments extended over an area that exceeded the scale of the granitoid domes.

8. Ages of igneous rocks in the MESZ and MEGC cluster either around 3.46–3.42 Ga or 3.32–3.31 Ga.

Chapter 4

The mid-Archaean 'Salgash Dyke Swarm': implications for regional crustal extension during emplacement

4.1 Introduction

The timing and the style of deformation of two main tectonomagmatic phases in the eastern Marble Bar Domain have been investigated and described in the previous chapters (see summary in 3.21). The older phase, D_{X+1}, is associated with magmatism of the Warrawoona episode at ca. 3.46-3.42 Ga. It involved intrusion of a 2 km thick hornblende-gabbro/diorite sills complex in a (proto-)MESZ, followed by intrusion of sills with a range of compositions, including alkali-feldspar granite, phenocrystic dolerite, and a suite of granodiorite, diorite and tonalite sills, subsequent syntectonic ultramafic and mafic sills and dykes, followed by syntectonic intrusion of leucogranite sills at 3447 ± 6 Ma. Deformation associated with this stage was attributed to early extension and initial doming of the MEGC (See also figures 3.15 and 2.18a). The younger phase, D_{X+2}, is associated with magmatism of the Wyman episode at ca. 3.32-3.31 Ga. It involved E-W compression and NE-SW extension, doming and granitoid emplacement within the MEGC, reactivation of the Mt Edgar Shear Zone, and felsic volcanism of the Wyman Formation (see chapter 2 and 3).

The time span between D_{X+1} and D_{X+2} is (in part) represented by the Euro Basalt, that forms the upper Salgash Subgroup (See figure 3.3 and 3.21). The upper age for the Salgash Subgroup is generally quoted to be ca 3.42 Ma, which is the age of the youngest unit suitable for U-Pb zircon dating, the felsic volcanic Panorama Formation. However, this formation is overlain by the Euro Basalt, which forms the actual upper unit. In the Kelly Belt a maximoum age for the Euro Basalt is provided by 3417 ± 9 Ma obtained from the underlying Panorama Formation, whereas a minimum age is provided by the ca. 3325 Ma overlying Wyman Formation (McNaughton et al, 1993). A recent finding of a 3346 Ma zircon population in a silicified felsic tuff one kilometer from the top of the Euro Basalt in the Kelly Belt (Nelson, 2001) was interpreted to represent the eruptive age of the tuff (M. Van Kranendonk and L. Bagas, Geological Survey of Western Australia, unpubl. data. In: Van Kranendonk et al., 2002), even though younger zircons of 'Wyman age' also occur in the rock. This, in combination with the age of xenocrystic zircons in overlying units (Nelson, 1998, 1999) led Van Kranendonk et al. (2002) to suggest that deposition of the Euro Basalt has been over a period from at least ca. 3395 to possibly 3325 Ma. If Van Kranendonk et al (op cit.) are correct, and

deposition occurred during this time span, then structures related to deposition of the Salgash Subgroup may help to understand the nature of regional E-W compression and granitoid formation and extension during D_{X+2}. The cause for granitoid emplacement within the MEGC during D_{X+2} is proposed to be a regionally recognised E-W compressional phase, that caused crustal thickening, partial melting of the gneissic basement, collapse and emplacement of the granitoids (chapter 2). Alternatively, if magmatism closely preceded or initiated the Wyman episode, partial melting of a gneissic basement could have been caused by heating due to magmatic injections into the crust.

To date no structural studies in the Marble Bar Domain have focussed on the Salgash Subgroup. The tectonic setting of the Salgash Subgroup has been discussed largely based on geochemical signature, as is further outlined below.

The type sections of the units that form the Salgash Subgroup, all in the Marble Bar Domain, comprise a substantial number of mafic dykes and sills (Hickman, 1977, 1983). In addition, mafic dykes are found in the underlying Talga Talga Subgroup and the Duffer Formation in the Marble Bar Greenstone Belt, and form a semi-radial pattern around the centre of the Mt Edgar Granitoid Complex (See Hickman and Lipple, 1978). Mafic dykes also intruded the 3.43-3.42 Ga felsic volcanic units underlying the Euro Basalt in the Kelly Greenstone Belt (Barley, 1993). Based on chemical similarities of the dykes and the basalts and comparable metamorphic overprint, the dykes in the Kelly Belt have been proposed to be feeders for the basaltic units that overly the felsic units, (Barley, op cit.). Mafic dykes and sills have been reported by Hickman and Gibson (1982) and Nijman et al. (1998a) in the northern Marble Bar Greenstone Belt (Coppin Gap Belt). If the above dykes and sills are related to extrusion of Salgash Subgroup basalts, their geometry and orientation could provide constraints for the tectonic setting of the Salgash Subgroup.

World-wide, Archaean basaltic sequences and their associated mafic dyke swarms have been likened to those that formed in modern settings, including modern continental flood basalt associated with rifting (e.g. Windley, 1973) and those that form at mid-oceanic ridges (e.g. Anhaeusser et al., 1968; De Wit et al., 1987b) or as part of oceanic plateau's (e.g. Kusky and Kid, 1992, Arndt et al., 1997) and continental back-arc basins (e.g. Tarney et al., 1976; Windley, 1977). In contrast, they have also been compared to those that are considered to have formed by typical Archaean processes, such as lunar maria (Green, 1972) (see for an overview: Windley, 1977; Condie, 1981; Kröner, 1981; Hall and Hughes, 1990; Arndt, 1999, and references therein).

The Salgash Subgroup was deposited on the felsic volcanic Duffer Formation (Hickman, 1983). Based on lithological assemblages and geochemical studies, the Salgash Subgroup has been likened to a continental rift sequence, possibly related to a back-arc environment (Barley, 1993; Krapez and Eisenlohr, 1998). Largely subaqueous deposition despite its thickness have been taken to suggest a control on deposition that was either tectonic or tectono-magmatic driven subsidence (Eriksson et al, 1994).

This chapter aims at clarifying the structural setting of the Salgash Subgroup by studying the distribution, orientation and field-relationships of mafic intrusions and structures associated with deposition of the Salgash Subgroup, and the relationships with the underlying rocks, through field mapping and structural analysis. The mapping focussed on two selected greenstone belts in the eastern part of the Marble Bar Domain: the Kelly Greenstone Belt and the Marble Bar Greenstone

Belt. Three selected parts of these belts have been field mapped after interpretation of 1: 50 000 and 1: 40 000 b/w and colour aerial photographs. Each mapped area is restored to Salgash-times, which led to a reconstruction of the original orientation of the dykes and allowed an estimate of the *local* direction of crustal extension during emplacement. Comparison of local palaeo-extension directions of the three mapped areas then forms the basis for a discussion of the geometry and direction of extension at a larger scale, of the Marble Bar Domain. This part of the structural development is then discussed in relation to the nature of regional E-W compression and granitoid formation and extension during D_{X+2}. Dykes associated with the Euro Basalt are subject of an $^{40}Ar - ^{39}Ar$ isotopic dating study in chapter 5.

4.2 Geological setting of the Salgash Subgroup

The Salgash Subgroup has been defined as the upper part of the Warrawoona Group (Lipple, 1975, Hickman, 1977, 1984, Hickman et al.,1990; Van Kranendonk and Morant, 1998). The units of the Salgash Subgroup generally concordantly overlie the 3470-3450 Ma Duffer Formation and are discordantly overlain by the ca. 3315 Ma Wyman Formation. A stratigraphic description of units within the Salgash Subgroup and their available ages is presented in figure 4.1 and is briefly summarised below. The Salgash Subgroup comprises five units, dominantly containing basaltic and felsic volcanic units and sediments, with a total stratigraphic thickness of generally up to 4 km (in the Panorama Greenstone Belt the top unit has been reported to have a thickness of 9.1 km, Van Kranendonk, 2000). Until recently, the only unit that has been dated is the felsic volcanic Panorama Formation. An age of 3457 ± 3 Ma (Thorpe et al., 1992, conventional, U-Pb, zircon) has been obtained from the type section at Panorama Ridge, approximately 16 km south of the North Pole Dome (See figure 2.1). However, an 3434 ± 5 Ma age was obtained in this area using the SHRIMP spot dating method (Nelson, 2000) and is taken to be a better indication of the depositional age of the Panorama Formation. Overlying the Panorama Formation NE of the North Pole Dome is the Strelley Pool Chert. This unit was previously considered to be the equivalent of the Towers Formation (Krapez, 1993) directly overlying the Duffer Formation. But with the 3434 ± 5 Ma age of the underlying Panorama Formation, the Strelley Pool Chert must be younger than the Towers Formation and was recently defined as an additional stratigraphic unit (Van Kranendonk and Morant, 1998). The upper unit of the Salgash Subgroup is formed by the Euro Basalt. It was described by Hickman (1977) in the type area of the Euro Mine in the western Warrawoona Greenstone Belt to comprise tholeiitic pillow basalt with minor felsic volcanic units and dolerites with peridotitic komatiite at the base. The thickness varies from ca. 2 km in the type area to up to 9.4 km in the southwestern flank of the Panorama Greenstone Belt (Van Kranendonk, 2000). Recently, a zircon population (14 zircons) interpreted as xenocrysts, from a vitric tuff/volcaniclastic sediment near the top of the Euro basalt in the Kelly Belt grouped to form an age of 3346 Ma (Nelson, 2001). Other workers interpreted the grouped age of this population to represent the eruptive age of the tuff, whilst another population, that yielded an age of 3363 Ma, was interpreted to be xenocrystic (M. Van Kranendonk and L. Bagas, Geological Survey of Western Australia,

Salgash Subgroup (thickness)	Rock type	Ages	Type section
	Wyman Formation ca 3315 Ma (a, e)		
	Local unconformity		
Euro Basalt 2.0 – 9 km	Tholeiitic pillow basalt with minor chert and felsic volcanic units and dolerites. Peridotitic komatiite at base.		Euro Mine in Warrawoona Belt (Hickman, 1977).
	PM: pillow basalt and chert MCM: pillow tholeiitic basalt and chert CM: Komatiite and high-Mg basalt		(Van Kranendonk and Morant, 1998)
Strelley Pool Chert 20-40 m	Grey and white laminated chert with minor silicified siliciclastics, chemical sedimentary rocks, stromatolitic rocks and carbonate rocks.		Strelley Belt (Lowe, 1983). North Pole Dome (Van Kranendonk and Morant, 1998).
Panorama Formation 0-1.0 km	Dacitic lava, tuff, agglomerate and chert. Local sandstone, conglomerate and ultramafic rocks.	* 3434±5 Ma (d) * # 3457±3 Ma (a) 3417±9 Ma (c) 3433±2 Ma (d) # 3457±3 Ma (a)	Panorama Ridge in southern North Pole Dome (Hickman and Lipple 1975; Lipple, 1975).
Apex Basalt 1.5-2.0 km	Tholeiitic pillow basalt, high-Mg basalt and peridotitic komatiite. Several grey/white banded chert units and minor dolerite and gabbro sills.		From Marble Bar Pool westward (Hickman, 1977)
Towers Formation 0.5 km	Three red/white/grey banded chert members separated by (pillow) basalt, komatiite, felsic volcanics or sediments. Middle member: the Marble Bar Chert Member (100 m.)		Towers Mine in Warrawoona Belt, MB member: Marble Bar Pool (Hickman, 1977).
	Hiatus		
	Duffer Formation ca 3470-3450 Ma (a, b, d, f).		

Figure 4.1 Overview of the stratigraphic units of the Salgash Subgroup. PM= Potkoorok member, MCM= Miralga Creek Member, CM= Cloisters member. References to geochronological data are (a) Thorpe et al. (1992, U-Pb, zircon, conv.), (b) McNaughton et al. (1993, SHRIMP U-Pb, zircon), (c) Barley et al. (1998, SHRIMP U-Pb, zircon), (d) Nelson (2000, SHRIMP U-Pb, zircon), (e) Buick, unpubl. data in Barley et al. (1998), (f) Pidgeon (1978). Data marked with an asterisk (*) are from the type section. Data marked with a (#) are U-Pb dates of zircon using the conventional method.

unpubl. data; in: Van Kranendonk et al., 2002). Nelson (2001) interpreted a pooled age of six zircons at ca 3311 Ma to represent the crystallization age of the rock.

The abundance of shallow water sediment and pillow basalt throughout the Salgash Subgroup indicates a dominantly subaqueous depositional environment (Barley et al., 1979; Lowe, 1982, 1983; Hickman, 1983; DiMarco and Lowe, 1989b; Buick and Dunlop, 1990). Numerous intercalated cherts within the basaltic units are interpreted to represent intervals of volcanic quiescence, representing a cyclicity during deposition (Eriksson et al., 1994). The geochemistry of the basaltic units of the Salgash Group indicate dominantly tholeiitic with MORB, low-K tholeiite or plate margin affinities (Glikson and Hickman, 1981; Hickman, 1983; Barley, 1993; Green et al., 2000). The geochemistry of the upper felsic unit, the Panorama Formation, suggests that magma-genesis involved direct melting of an eclogite residue without crystallization of feldspar (Cullers et al., 1993). Barley (op. cit.) argued that the geochemistry of the Salgash Subgroup basalt is compatible with a near-arc environment, possibly a volcanic arc, or a back-arc setting.

Pre-Salgash Subgroup structures, in units of the underlying 3.47-3.45 Ga Duffer Formation, were reported and discussed by Zegers (1996) and Nijman et al. (1998a) and Zegers et al. (1999). During deposition of the Duffer Formation an extensional growth-fault system was active (Zegers, 1996, Zegers et al., 1999; Nijman et al., 1998a). Related to these upper crustal structures are mid-crustal extensional detachments, including the Split Rock Shear Zone (Zegers et al., 1996) and the Mt Edgar Shear Zone (See chapters 2 and 3). This extension has resulted from a regional stress-field, possibly due to plate-interaction (Chapter 2; Zegers et al., 1996). An alternative view is that the extensional growth-faults in the Duffer Formation may reflect a local stress field that developed during caldera-collapse (Nijman et al., 1998a).

4.3 Results from mapping of the selected areas

The three study areas are indicated in figure 4.2. They include part of the Kelly Greenstone Belt (Figure 4.3), part of the Marble Bar Belt east of Marble Bar (Figure 4.5) and part of this belt near Talga Peak (Figure 4.6). The study focused on the relationships between mafic dykes and the basaltic units of the Salgash Subgroup, the intrusive relationships of the dykes and their host rocks, and relationships to deformation structures. The orientations of bedding within the Salgash Subgroup, mafic dykes and sills, and structural elements are presented in lower hemisphere, equal area stereographic projections.

4.3.1 Mafic dykes in the Kelly Greenstone Belt

4.3.1.1 Observations

The Kelly Greenstone Belt has been selected to establish the geometry and extent of the mafic dykes mentioned by Barley (1993), and to test whether the dykes are feeder dykes to the overlying basaltic units. The study area in the Kelly Greenstone Belt is shown in figure 4.2 and the results are represented in figure 4.3. The western margin of the belt in this area is formed by an intrusive

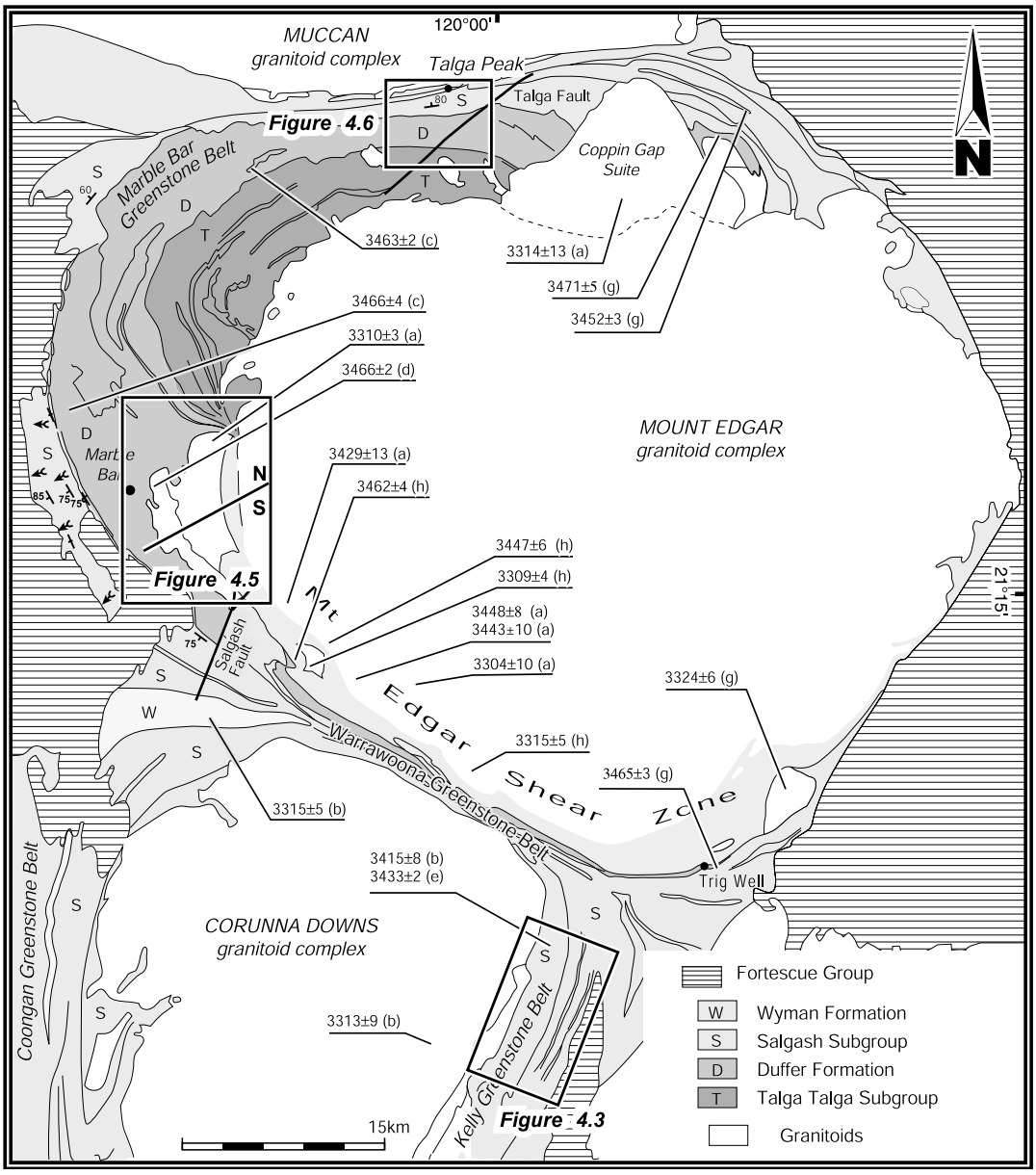

Figure 4.2 Generalised geology of the eastern Marble Bar Domain. Bedding and facing of units in the Salgash Subgroup are after Lipple (1975). The underlying Duffer and Talga Talga Subgroup and younger units are after Lipple (1975) and Hickman (1983). Relevant available geochronological data is included. (a) Williams and Collins (1990, U-Pb, zircon, conv.), (b) Barley et al. (1998), (c) McNaughton et al. (1993), (d) Nelson (1998), (e) Nelson (2000), (f) unpubl. Data in Collins et al., 1998), (g) Thorpe et al. (1992, U-Pb, zircon, conv.), (h) Chapter 3. The locations of the study areas are indicated (Figures 4.3, 4.5 and 4.6).

contact with the 3313 ± 9 Ma Carbana Pool Adamellite and a younger granitoid of unknown age of the Corunna Downs Granitoid Complex (Barley and Pickard, 1999). Adjacent to the granites are felsic volcanic units, generally NNE-trending and 60-80° ESE dipping, dated at 3417 ± 9 Ma and 3433 ± 2 Ma by Barley et al. (1998a) and (Nelson, 2000). This is similar to the age of the Panorama Formation in the type section at Panorama Ridge (See figure 4.1) and therefore will here be referred to as the Panorama Formation. This unit is overlain by a sequence of interlayered basalt and chert. The basaltic units are not dated but, by their concordant position on top of the Panorama Formation, are stratigraphically assigned to the Euro Basalt (Figure 4.3, see also Lipple, 1975). The chert unit immediately deposited on the Panorama Formation would be the stratigraphic equivalent of the Strelley Pool Chert (See figure 4.1). The eastern outcrop margin is formed by the discordantly overlying Mt Roe Basalt of the ca. 2.77 Ga Fortescue Group (Arndt et al., 1991).

ESE-trending dykes were first identified from 1: 40000 b/w aerial photographs. Subsequent field mapping of selected areas within the area covered by figure 4.3 showed a minimum of 70 mafic dykes. These dykes intrude across the Panorama Formation. Some continue into the overlying basalt and chert sequence of the Euro Basalt (Figure 4.3). The dykes and local sills generally form metre-high ridges in the basalt, whilst in the felsic volcanic unit they form minor topographic depressions. The dykes generally have a NW trend and are subvertical or dip steeply to the NE-NNE (See plots in figure 4.3). Several dykes were traced into, or were found to terminate at, pillow basalt in the Euro Basalt (See figure 4.4), which indicates that they are likely feeder dykes to the Euro Basalt. The dykes vary from 0.5 to 25 metres in width, but are generally 5-10 metres. Individual dykes may be over 2 km long (See figure 4.3). Petrographically, the dykes comprise phaneritic gabbro/pyroxenite, ophitic to subophitic dolerite, and aphanitic hornblendite. All show a local greenschist facies metamorphic overprint, which distinguishes them from members of the N to NW-trending 2.77 Ga Black Range Dyke Swarm that lack such an overprint. Locally, the density of the Salgash dykes reaches 50%, but the average density is around 5%. No dykes were found in the Corunna Downs Granitoid Complex, including the Carbana Pool Adamellite, dated at 3313 ± 9 Ma (See figure 4.3). This indicates that the dykes are older than 3313 ± 9 Ma. The available crystallization ages of the felsic volcanic unit and the Carbana Pool Adamellite further constrain the age of mafic dyke swarm to between ca. 3.42 and 3.31 Ga.

Structures in the Euro Basalt of the Kelly Greenstone Belt comprise a conjugate set of generally NW and ENE-trending subvertical faults. Displacement on the faults is best identified by the offset of the interbedded chert units. Offsets are dominantly sinistral for the NW and dextral for the ENE-trending faults. The current fault orientations and the offsets are similar to those for a conjugate strike-slip system resulting from WNW-ESE compression or NNE-SSW extension. However, indications exist that the faults have not formed in their current orientation. Dykes intruded into and across the faults, which indicates that these faults are older than or coeval with intrusion of the dyke. This, in combination with the observation that some of the dykes are feeders to the basaltic units, may appear to be paradoxical. However, the observed relationships can be explained by a system in which volcanism, intrusion of dykes and extension all occur over a period of time. A syn-depositional timing of the faults is indicated by a differential displacement, that may be up to 250 metre in the lower chert units and basalt and zero metre in the upper chert unit (^{08}94E / ^{76}14N,

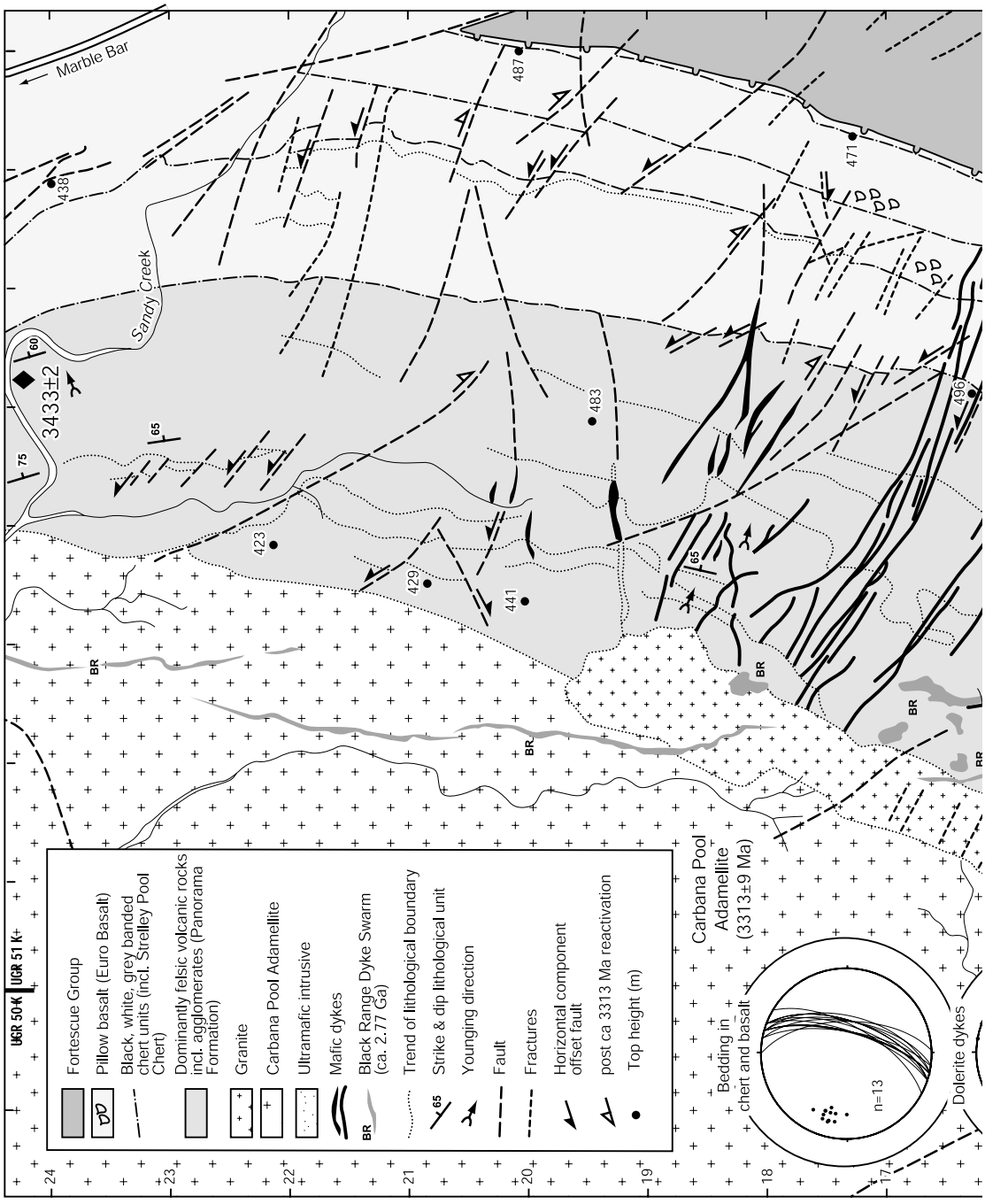

Figure 4.3 Structural and stratigraphic map of the Kelly Greenstone Belt. Reliability diagram: (I) 1:250 000 geological map by Thom et al (1973), (II) aerial photograph interpretation and (III) field mapping (see inset). Lower hemisphere,

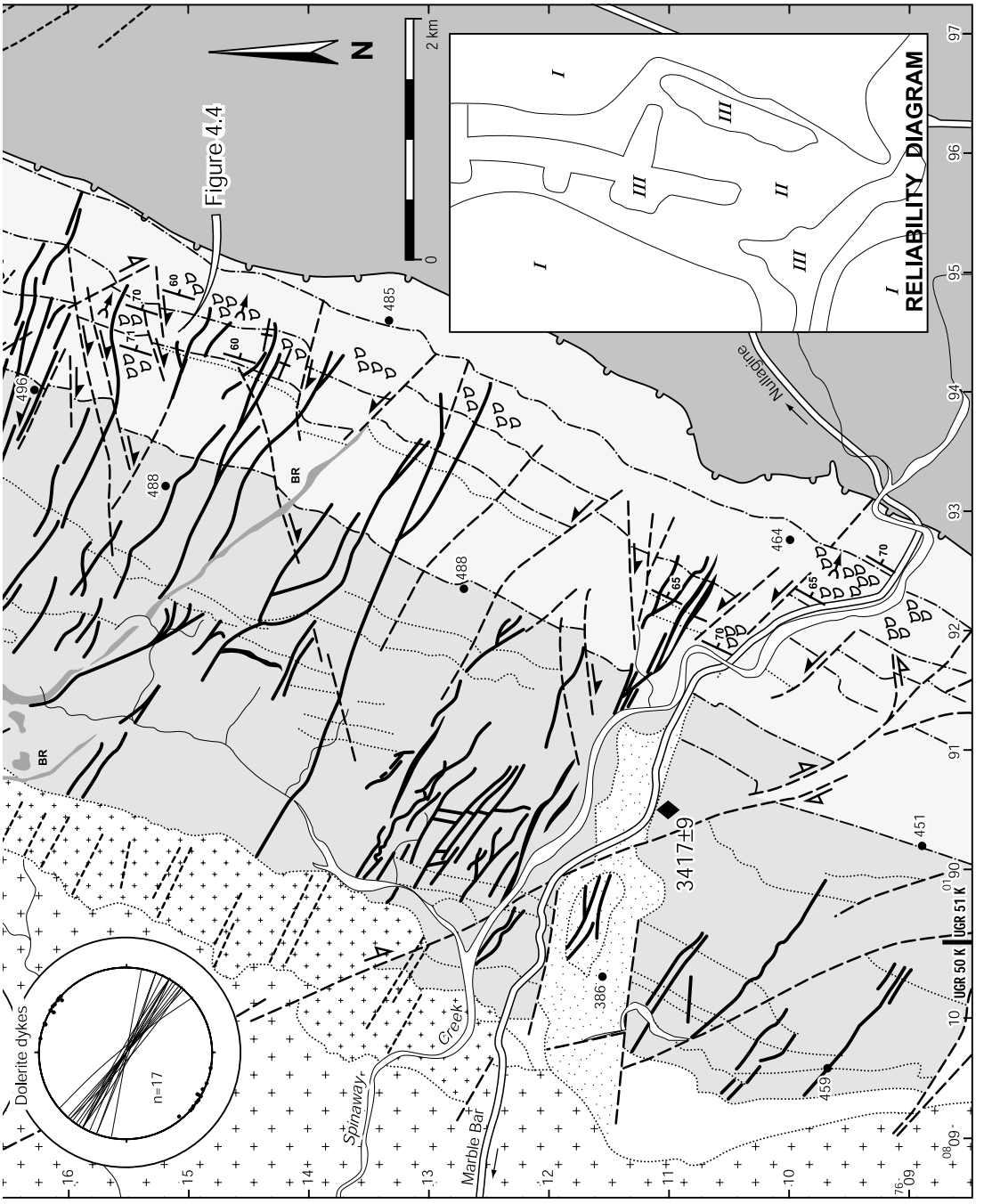

equal area stereographic projections of bedding within the Euro Basalt and mafic dykes.

figure 4.3). Thickness variations of the basaltic units of the Euro Basalt are only minor and are observed across some of the faults. Although a thickness variation due to differential dip across the faults can not be excluded with the available data, the sense of displacement and the thickness variations are consistent with a syn-depositional extensional development. If the faults were active during development of the Euro Basalt, then for a kinematic interpretation of the faults this part of the Kelly Belt must be restored.

Some of the NNW to NW-trending faults show dextral displacement that also offsets the 3313 ± 9 Ma Carbana Pool Adamellite (^{08}10E / ^{76}14N, figure 4.3).

4.3.1.2 Interpretation of the results from the Kelly Greenstone Belt

The observed field relationships between the conjugate faults, the dyke swarm and the available age constraints are compatible with an interpretation in which the dykes in the Kelly Belt are feeders to the Euro Basalt of the upper Salgash Subgroup (See figure 4.1). The observed faults, their conjugate orientation and sense of displacement, in combination with the exploitation of these faults by the mafic dykes indicates that the fault system is extensional. As the dyke swarm contains feeders to the basaltic units, both the units they feed into and the dykes themselves should be restored to palaeo-horizontality to interpret the original orientation of the dykes. The basaltic units can be used to restore the volcano-stratigraphy to horizontal.

The sequence of multiple units of pillow basalt that is interbedded with chert units suggests that the Euro Basalt developed during a series of igneous pulses and intermediate phases of magmatic quiescence. This is consistent with the interpretation that the inter-relationship between intrusion of dykes and fault activity is the result of a longer period of interplay between extension and magmatic activity.

Some of the extensional faults are restricted to the Euro Basalt, and do not cut across the underlying felsic unit (Figure 4.3). This may be explained by the larger amount of mafic dykes in the felsic volcanic unit, which can compensate for part of the extension by the cumulative width of the dykes.

4.3.2 Mafic intrusions in the Marble Bar area

4.3.2.1 Observations

The southern Marble Bar Greenstone Belt was selected to study the mafic dykes mapped by Hickman and Lipple (1978). The greenstones in the Marble Bar Greenstone Belt form part of the hangingwall to the MESZ. A 10 km x 15 km area just east of Marble Bar (See figure 4.2) was

Figure 4.4 Field photographs and sketch of an outcrop in the Kelly Belt (0194.6E /7614.9N). (a) Strike parallel view of part of the Kelly Greenstone Belt, looking to the SSW. (b) Pillow basalt indicating younging direction to the E, with a bedding orientation of ~015/60E. 4c) Schematic field sketch of the relationships of a mafic dyke (290/90) intruding cherts and feeding into overlying pillow basalt. (d) Northward view of the grey-white banded chert with sedimentary structures indicating younging to the E, with a bedding orientation of 015/60E. Intruding dolerite dyke is showing on top of the hill. Note geologist for scale. (e) Detail of bedding in the chert: meter-wide channel with rounded chert clasts fining upwards, overlain by fine-grained laminated grey chert bands. (f) Local columnar jointed basalt below the chert. Pillars are plunging 280/30-45, which is at right angles to bedding. Whether this unit is a sill or a lava flow is not clear.

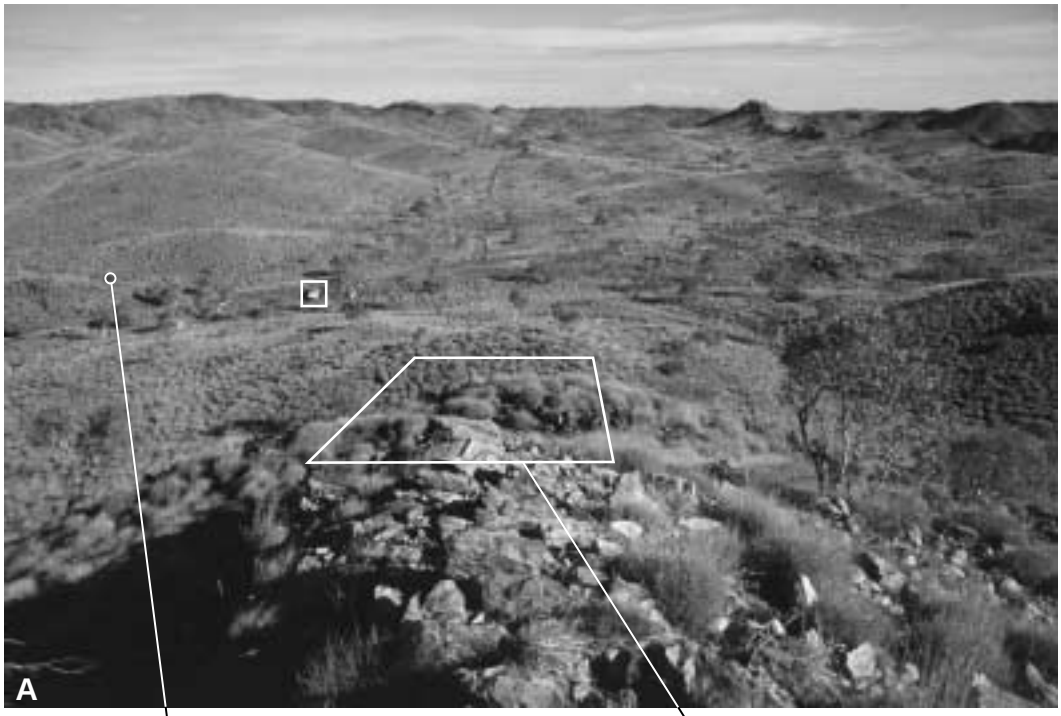
E
W
A

NE
SW
B

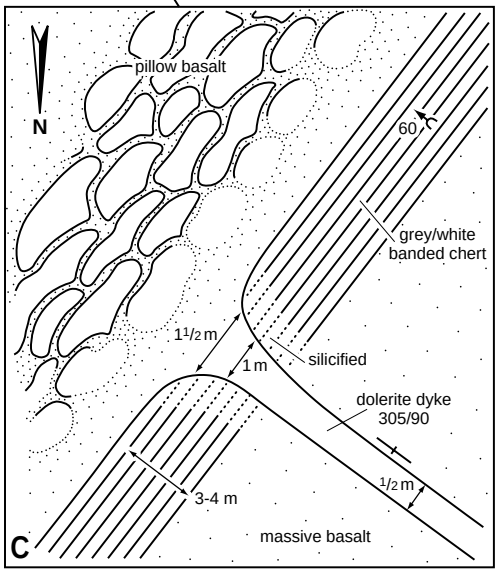
N
pillow basalt
60
grey/white
banded chert
1 1/2 m
1 m
silicified
dolerite dyke
305/90
1/2 m
3-4 m
massive basalt
C

Figure 4.5 Stratigraphic and structural map of part of the Marble Bar Greenstone Belt east of Marble Bar, based on aerial photograph interpretation and numerous traverses. Mapped mafic dykes and sills are plotted in lower hemisphere, equal area stereographic projections. Plots of bedding within the Salgash Subgroup is after Hickman and

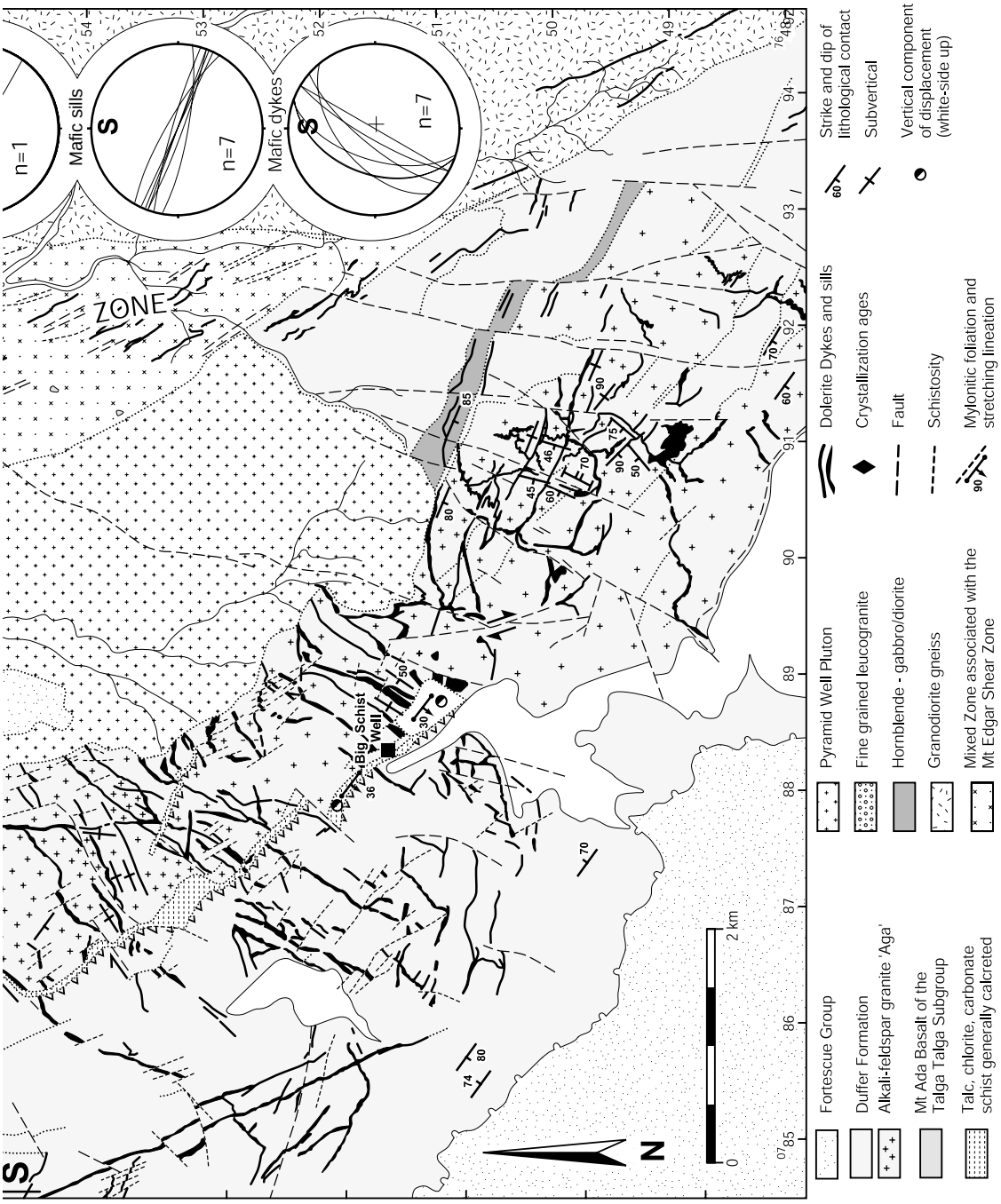

Lipple, 1979 (see figure 4.2 for a map). The bedding and mafic intrusions are plotted separately for the northern and the southern area for reasons discussed in § 4.4.2.2. See figure 4.2 for references to geochronological data.

selected to cover both part of the greenstone belt as well as part of the Mt Edgar Shear Zone (MESZ). Whereas the MESZ hangingwall is generally strongly deformed (see chapter 2), here it is less deformed and has better preserved the intrusive relationships of the mafic dykes. The basaltic units in the north of the area on Figure 4.2 are of the older and stratigraphically underlying Talga Talga Subgroup (Lipple, 1975). The felsic volcanic units are of the Duffer Formation, dated at 3466 ± 4 Ma and 3463 ± 2 Ma (McNaughton et al., 1993). In this area the Duffer Formation is either subvertical, or dips steeply away from the Mt Edgar Granitoid Complex. In the south of the area rocks of the Duffer Formation are discordantly overlain by basalt of the 2.77 Ga Fortescue Group. The footwall of the MESZ is formed by the Gneiss Complex that comprises dominantly 3.46-3.42 granitoids (Chapter 3; Williams and Collins, 1990). The hangingwall of the MESZ contains the 'Aga' alkali-feldspar granite dated at 3466 ± 2 Ma (Lipple, 1975; Nelson, 1998a), and the Pyramid Well Pluton, dated at 3310 ± 3 Ma (Nelson, 2000).

Field mapping of selected parts of the area, following interpretation of 1: 25000 colour aerial photographs, confirmed that mafic intrusions formed an intrusive system of dykes and sills in the Duffer Formation and part of the underlying Mt Ada Basalt of the Talga Talga Subgroup (See figure 4.5). Mafic dykes and sills were mapped in addition to those mapped by Hickman and Lipple (1978). Types of mafic intrusions in both the MESZ and the supracrustal units include gabbro/diorite dykes and sills, dolerite dykes and sills and fine-grained ultramafic sills. Dykes dominantly have a SW trend in the southern part of the mapped area, and a WNW trend more towards the north (See figure 4.5). Sills generally have a WNW trend in the southern part of the area, where bedding of the Duffer Formation dips to the SSW, and a NW to NNW trend more towards the north where bedding dips to the (W)SW (See also figures 4.2). A small number of mafic sills intruded the MESZ. Most dykes are subvertical, although some in the southern part have a steep dip to the NW. On outcrop-scale the dykes form conjugate sets. The width of dykes ranges between 1 to 50 metres, but is generally 5 metres. Individual dykes may be up to 2 km long, and related dyke systems may be up to 3 km long (See figure 4.5). Locally, dykes coalesce to form 50x100 metre patches of fine-grained dolerite within the felsic volcanic rocks of the Duffer Formation. Dyke density can reach 25%, with an average of ca. 4%. When the overall pattern of the dykes in figure 4.5 is compared to the detail, it can be seen that even though the overall trend of the dykes throughout the Marble Bar area defines a sub-radial pattern, they form conjugate sets on outcrop-scale. The implication of this phenomenon is further discussed below. With respect to age, a maximum age for the dykes is provided by the age of the host rock, the Duffer Formation, in this area dated at 3466 ± 4 Ma and 3463 ± 2 Ma (McNaughton et al., 1993). A minimum age follows from the 3310 ± 3 Ma Pyramid Well Granite (Nelson, 2000) that truncates the dykes (^{07}90.0E / ^{76}60.0N, figure 4.5).

The dyke pattern in the Marble Bar area can be used to investigate the local extension direction of the crust during intrusion, but only if the pattern is regarded in its original orientation. As reported in chapters 2 and 3, the area has had a prolonged history with at least three main deformation phases (D_{X+2} to D_{X+4}) between ca. 3.40 and 2.77 Ga. Changes in the orientation of the dyke pattern as a result of any of these deformation phases need to be taken into consideration when interpreting the dyke pattern.

In the mapped area four groups of structures were found to have influenced to varying degrees the

geometry of the dykes and sills. The main structure in the area is the MESZ (See figure 4.5). As outlined in chapters 2 and 3, the MESZ has been active during extension, granitoid emplacement and doming of the MEGC from ca. 3.45 Ga onwards ($D_{MESZ,x+1B}$, see chapter 3, and figure 3.21). The MESZ is located on the contact between the greenstone sequence and the MEGC. Reactivation of the MESZ and doming of the MEGC at ca. 3.32-3.31 Ga ($D_{MESZ,x+2E}$, see chapter 3, and figure 3.21) has caused part of the steepening of the supracrustal hangingwall sequence. Therefore it has changed the orientation of the dykes and sills, being an integral part of the hangingwall. Also, no dykes are found to have intruded across the MESZ. A second group of structures comprise NE-vergent thrusts and related transfer faults (See figure 4.5), which can largely be traced parallel to the trend of the bedding in the area south of Marble Bar, but which consistently cut the stratigraphic sequence in the area to the north (^{07}87E / ^{76}62N, figure 4.5) (cf. Van Haaften and White, 1998). These thrusts are located in strongly calcreted talc-chlorite-carbonate schistose zones that cut across the dolerite sills and dykes and therefore must be younger that the dykes. Dykes and sills show only minor horizontal displacement along the thrusts, which suggests that the thrusts have had no major influence on the outcrop pattern of the dyke swarm as a whole. A third group of structures is intruded by the dykes and sills, and therefore must be older. They comprise km-scale faults with dextral horizontal offsets defining fault blocks in the Duffer Formation near the MESZ (^{07}91-93E / ^{76}49-52N, figure 4.5). The fault pattern bears similarities with an extensional fault array in cross-section, but the orientation of the faults and their kinematics are unknown.

It is noteworthy that mafic sills have exploited strands of the Duffada Shear Zone, a splay off the MESZ along the contact with the Duffer Formation and the Mt Ada Basalt (Van Haaften and White, 1998) (^{07}90E / ^{76}61N, see figure 4.5). This suggests that activity of the Duffada Shear Zone has occurred prior to intrusion of the mafic dykes and sills, the implication of which will be discussed in chapter 6.

4.3.2.2 Interpretation of the results from the Marble Bar area

The intrusive relationships of mafic dykes and the available geochronological data from the area east of Marble Bar are consistent with an interpretation in which these intrusions are the feeders for the Apex and/or Euro Basalt of the Salgash Subgroup. A first impression is that the dykes in the area east of Marble Bar form a sub-radial pattern, radiating from a central point 9-10 km east of Marble Bar. This pattern may at first suggest that the dykes intruded as a radial swarm. However, the map in figure 5.5 shows that the dykes have intruded as conjugate sets on outcrop scale, suggesting that the radial pattern is a secondary feature.

Active extensional doming of the MEGC as is proposed in chapters 2 and 3 has caused steepening of the overlying supracrustal units of the Marble Bar Belt. For an interpretation of the original orientation of the dykes and the geometry of the dyke swarm within these units, the subsequent deformation of the supracrustal sequence must be restored. The supracrustal sequence of this part of the Marble Bar Belt is restored to 'Salgash times' using the current orientation of the units of the Salgash Subgroup in the Marble Bar and the mechanism of extensional doming. This is further discussed after the observations in the Talga Peak area have been presented.

4.3.3 Mafic dykes in the Talga Peak area

4.3.3.1 Observations

The area of interest is an approximately 6 km x 5 km section of the northern Marble Bar Greenstone Belt (also referred to as Coppin Gap Belt) near Talga Peak (See figure 4.2). It comprises steeply north dipping felsic agglomerates that can be correlated with those of the Duffer Formation further to the west, dated at 3463 ± 2 Ma (McNaughton et al., 1993) and to the east, dated at 3471 ± 5 Ma (Thorpe et al., 1992). The felsic volcanic units are interlayered with basaltic units in the southern part of the area (Hickman and Gibson, 1982; Nijman et al., 1998a). Growth-faults have been recognised within the top of the felsic unit (See fig.2 in Nijman et al., 1998a, and references therein). The faults were reported to be filled in with felsic volcanic rocks, with minor basalt and chert in the top (Nijman et al., op. cit.). NNE-trending, 5-10 km long dykes that intruded across the felsic unit and across the granitoids of the Coppin Gap Suite were mapped as members of the 2.77 Ga Black Range Dyke Swarm by Nijman and co-workers (op. cit.). These workers also reported smaller, 1-1.5 km long, mafic dykes. These smaller dykes appear to be cross-cut by the growth-faults and by a mafic and ultramafic hosted shear zone, the lateral equivalent of the Bamboo Creek Shear Zone (See fig.2 in Nijman et al., 1998a). These relationships suggested that the smaller dykes are older than the 2.77 Ga Black Range Dyke Swarm. These dykes have been the focus of the mapping study presented below.

A swarm of at least 35 dykes with a N to NNE-trend was identified after interpretation of 1:25000 colour aerial photographs and field mapping of a selected area, indicated in figure 4.6. The dykes vary between 1 and 10 metres in width and measure up to 2 km in length. They dip subvertically to steeply westward (See plots in figure 4.6). They comprise gabbro, dolerite, which is locally pyrite rich, and pyroxenite. Few dykes were traced into the basaltic fills of the growth-faults (^{08}06.5E / ^{76}83.5N, figure 4.6). These basalts locally contain pillows, which indicates subaqueous flow. A mafic sill occurs throughout the area and has been offset by the growth-fault (See Nijman et al., 1998a; Hickman and Gibson, 1982, and see figure 4.6). The mafic dykes generally intruded across this sill and across the growth-faults, indicating that the dykes are younger. North of the growth-faults, but south of the Bamboo Creek Shear Zone, bedding in a pillow basalt dips steeply to the north. Local dyke density reaches 25%, but on average is ca. 4%.

A maximum age for the dykes is provided by the crystallization age of the felsic volcanic host rock, dated further to the east and west at ca. 3471 ± 5 and 3463 ± 2 Ma, respectively (Thorpe et al., 1992; McNaughton et al, 1993) (see figure 4.2). A minimum age for the dykes may be provided by the 3314 ± 13 Ma (Williams and Collins, 1990) Coppin Gap Suite (See figure 4.2), which intruded the greenstone sequence that hosts the dykes, but which was not intruded by the dykes.

Some of the extensional growth-faults in the Duffer Formation of the Talga Peak area have been reported to have been inverted (See fig. 2 in Nijman et al., 1998a, and see ^{08}04.0E / ^{76}80.5N in figure 4.6). The timing of reactivation of these faults in relation to intrusion of the dykes is unclear. The reversed offset of the faults does not appear to have influenced the overall orientation of the dyke swarm.

4.3.3.2 Interpretation of the results from the Talga Peak area

From the geometry of the dykes, their relationship with the surrounding volcanic units and the structures, the dyke swarm is interpreted to have intruded after extension and deposition of the felsic volcanic units of the Duffer Formation as reported by Nijman et al. (1998a), and prior to intrusion of the Coppin Gap Suite. As the dykes have intruded prior to 3.31 Ga, doming of the MEGC and tilting of the greenstone sequence has been the major influence that led to their current orientation. The stratigraphy of the Marble Bar Domain (See figure 4.1) shows that no major episodes of mafic magmatism other than that of the Salgash Subgroup have been identified for the period after

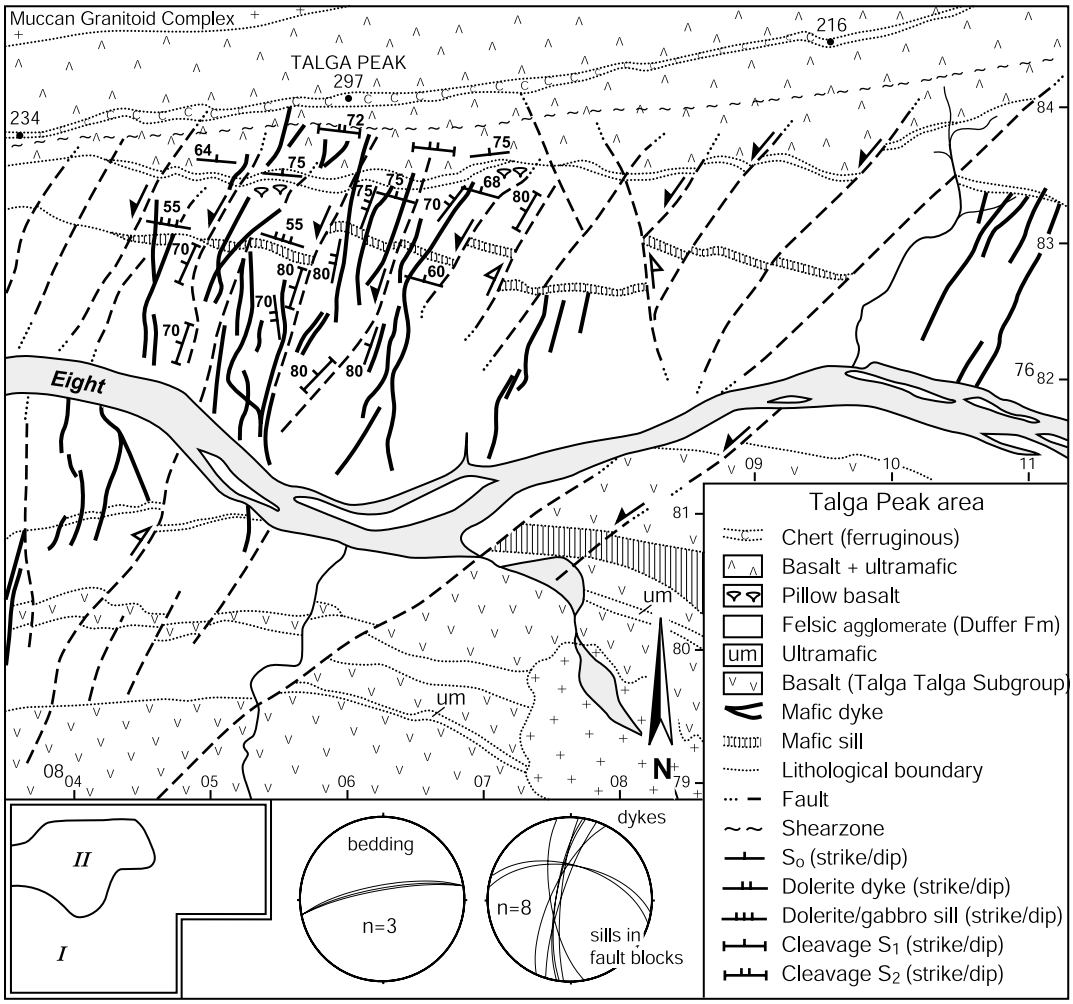

Figure 4.6 Lithological and structural map of the Talga Peak area in the northern Marble Bar Greenstone Belt. Stereographic projections are lower hemisphere, equal area plots of bedding within the basaltic and chert units, and of mafic dykes and sills. Reliability diagram: (I) Lithology and structure of the host rock to the dykes is after Nijman et al. (1998a), (II) Aerial photograph interpretation with near-continuous field mapping.

deposition of the Duffer Formation and prior to intrusion of the Coppin Gap Suite at 3314 ± 13 Ma. The above dyke swarm in the Talga Peak area is therefore likely to be related to deposition of the Salgash Subgroup.

4.4 Discussion

4.4.1 The main findings from field mapping

Mafic to ultramafic dykes and local sills associated with the Salgash Subgroup were identified in the Kelly Greenstone Belt, in the area east of Marble Bar and in the Talga Peak area of the northern Marble Bar Greenstone Belt.

Field relationships and available geochronological data in the Kelly Belt (figure 4.3) suggest a scenario in which mafic and ultramafic dykes and minor sills form a feeder system for the Euro Basalt. Intrusive relationships indicate a minimum age of 3313 ± 9 Ma and a maximum age of 3417 ± 9 Ma for these intrusions. The dykes represent ca. 5% of surface area in cross-section, which is taken to represent 5% of extension, and have a syn-tectonic relationship with a conjugate fault array in the volcanic units. In this area, deposition of the Euro Basalt has largely occurred through fissure-eruptions.

Gabbro/diorite, dolerite and fine-grained ultramafic dykes and sills in the southern (figure 4.5) and northern Marble Bar Belt (figure 4.6) represent a minimum of 4% extension. Based on intrusive relationships with the Duffer Formation and the 3.31 TTG suites of the MEGC, the dykes and sills are interpreted to be associated with the Apex Basalt and/or the Euro Basalt.

4.4.2. The relationship of the Salgash Subgroup and magmatic sequence in the Mt Edgar Shear Zone

The magmatic sequence for the MESZ was reported and constrained in time by dating key components (chapter 3). Intrusion of the 2 km thick hornblende-gabbro/diorite sills complex at 3462 ± 4 Ma (Figure 3.21) was followed by intrusions of alkali-feldspar granite, phenocrystic dolerite, and a suite of granodiorite, diorite and tonalite sills, and syntectonic ultramafic and mafic sills and dykes, a minimum age for which was provided by the 3447 ± 6 Ma crystallization age of a syntectonically intruded leucogranite sill (sample P95-gran).

The 3447 ± 6 Ma minimum age for the syntectonic ultramafic and mafic sills and dykes in the MESZ suggests that they are older than the Panorama Formation, which indicates that they cannot be coeval with deposition of the Euro Basalt but are more likely to be associated with the Apex Basalt. As no mafic components intruded after intrusion of the leucocratic granite at 3447 ± 6 Ma, no intrusive components that relate in age to the Euro Basalt have been identified in the MESZ.

A Panorama-aged syntectonic granodiorite sheet (A94-22) in the Central Gneiss Complex of the MEGC indicates that felsic magmatism was coeval with ongoing doming of the MEGC and MESZ. Growth faults may have developed during deposition of the Panorama Formation, but these were not observed in the Kelly Belt.

4.4.3 Mafic dykes indicating a renewable stress field

The oldest mafic dyke swarm recognised on Earth are of the Ameralik mafic dyke swarm that intruded at ca. 3250 Ma (Friend et al., 1988) into the high-grade Amîtsoq gneisses in south-western Greenland with ca. 3750 Ma protolith ages (McGregor, 1973; Gill and Bridgewater, 1976; Gill, 1979; Chadwick, 1981). The occurrence of mafic dyke swarms indicates that the crust is sufficiently strong to deform as a result of regional imposed stresses, and the presence of the Ameralik dyke swarm has been taken to suggests that the Greenlandic crust has been coherent from at least ca. 3250 Ma onward (Friend et al., 1988).

To develop and preserve a parallel mafic dyke swarm on continental scale, a 'renewable' stress field, i.e. a stress field continuously re-applied over a period of time (Bott and Kuznir, 1984), is needed: without this, magma-filled dilatational cracks would close before the magma crystallized to form a dyke (Pollard and Segall, 1987; Hoek, 1994). The orientation of a dyke swarm may provide information on the direction of regional extension at the time of their intrusion because dykes theoretically form in the plane normal to the least compressional principal stress σ_3 (e.g. Pollard, 1987; Pollard and Segall, 1987; Hoek, 1991).

In modern terrains a relationship between geometries of dyke swarms on various scales and their tectonic setting has been observed (Ernst et al, 1995a; Ernst and Buchan, 1997). Dykes occur as continent-scale radial swarms, associated with mantle plume activity and continental break-up, but they can also form radial swarms on the scale of a volcanic centre. Dykes are observed as parallel swarms on various scales of a rifted margin, of a MOR, and of an orogen or a single ophiolite (See e.g. Ernst et al, 1995a; Ernst and Buchan, 1997). Hence, the geometry of a dyke swarm may place constraints on the tectonic setting that it formed in, but the scale must be considered.

4.4.4 Continental extensional settings with associated mafic magmatism

The stratigraphic position of the Salgash Subgroup, on top of the dominantly felsic volcaniclastic Duffer Formation, has been taken to indicate that the depositional environment is continental (see Barley, 1993 and Eriksson et al., 1994). However, doubt could be raised based on structures in the basal formation of the Salgash Subgroup, the Towers Formation, in the type section near Marble Bar: local breccia and other structures indicate horizontal compression (Oliver and Cawood, 2001), which could indicate that the Salgash Subgroup has been tectonically emplaced onto the Duffer Formation, and that its setting need not have been continental. However, the mafic dykes and sills, that intruded the Duffer Formation in the Marble Bar Belt lends support to the belief that the Salgash Subgroup has been deposited on a felsic crust, and render it unlikely that the Salgash Subgroup has been tectonically emplaced.

Types of continental extensional settings associated with known mafic magmatism are listed in figure 4.7a. This list contains end-members of extensional settings that are related to either a modern day geodynamic behaviour of the crust, or to one regarded as typical for the Archaean. The typical Archaean tectonic regimes are marked with an asterisk(*). Continental extensional settings related to modern plate interaction include a back-arc extensional setting (for an overview see Taylor, 1995),

and an intra-continental rift setting (e.g. Fahrig, 1987). Continental settings that do not require plate-interaction include: (1) extension of the crust as a result of typical Archaean mechanisms of mantle-root drop off 'drip tectonics' (Kröner, 1981; Tarney, 1992; Campbell and Griffiths, 1992; Davies, 1992; Vlaar et al., 1993) or lower crustal delamination (Zegers and Van Keken, 2000), (2) an intra-continental rift system either caused by convection induced thinning, or triggered by an active mantle plume (See overviews by Coffin and Eldholm, 1992; Ernst and Buchan, 1997), (3) local extension due to partial convective overturn of the crust as the proposed effect of a mantle plume beneath a less coherent crust (e.g. Collins et al., 1998). Continental extensional settings have various geometries (figure 4.7a). Extension can either be radial or linear, depending on scale (Figure 4.7b). The geometry of extension can be reflected by the geometry of associated dyke swarms (See also

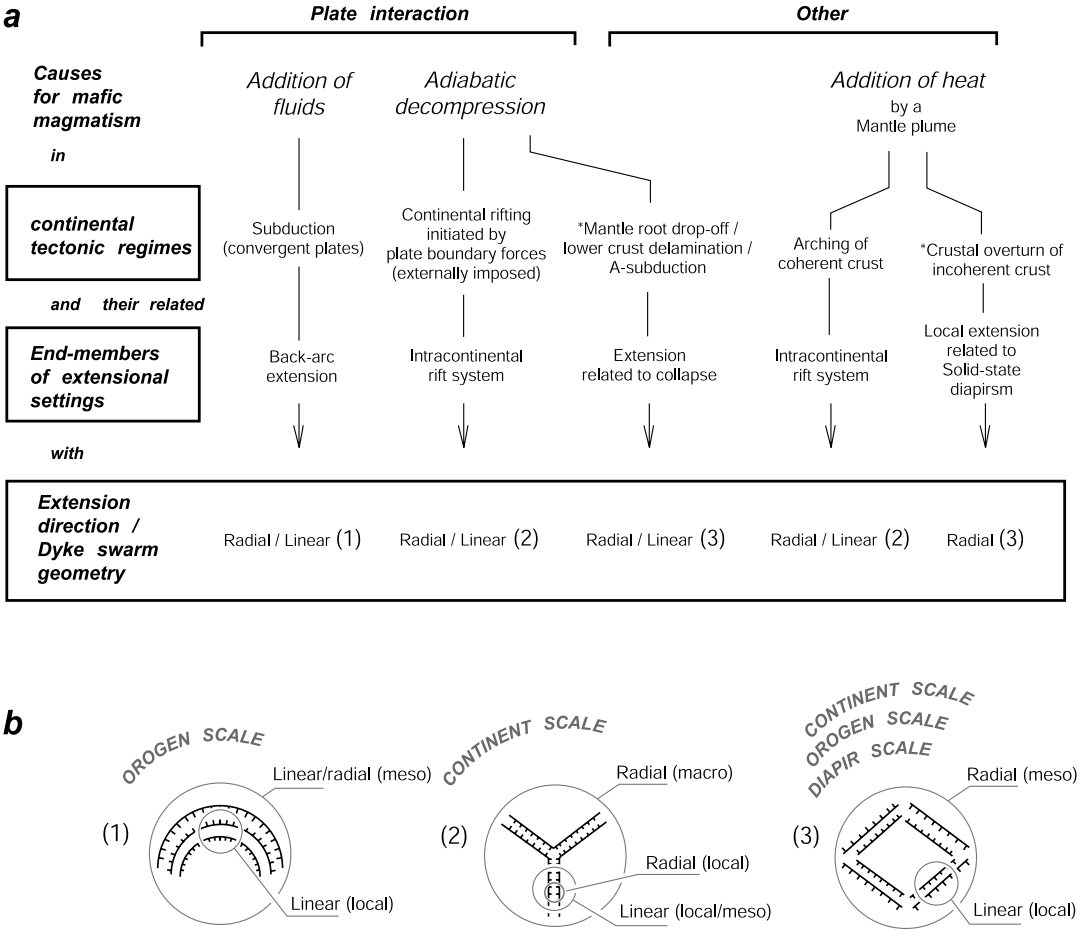

Figure 4.7 (a) An overview of causes for mafic magmatism in extensional continental tectonic regimes with the related end-members of extensional settings (see text for references). Continental tectonic regimes that are typically Archaean are marked with an asterisk*. (b) Illustrating how extension directions and dyke swarm geometries within these end-member extensional settings can be either radial or linear depending on scale of outcrop or area studied.

Ernst et al., 1995b). Hence, the geometry of mafic dykes can be used as a constraint for the extensional setting, but only when scale is taken into account. For example, a linear dyke swarm identified on the 'local' scale of one greenstone belt, could be consistent with either the geometry expected in part of a back-arc extensional setting, part of an intra-continental rift setting, or extension due to delamination or solid state diapirism due to crustal overturn of the crust. But, a linear dyke swarm identified on the 'mesoscopic' scale of a number of greenstone belts, say, at the scale of the Marble Bar Domain, is no longer consistent with extension due to solid-state diapirism.

As palaeo-strain (and indirectly stress) markers, the mafic dykes exposed in the Kelly and the Marble Bar Greenstone Belt provide information on the geometry of extension during deposition of the Salgash Subgroup over an area that exceeds the size of a granitoid complex. However, tilting of the supracrustal units and dykes was caused by tectonism after deposition of the Salgash Subgroup. Hence, to interpret the geometry of extension from the orientation of dykes, the dykes and their host rock must be restored to their original orientation. Below, the geometry of the mafic dykes of the Kelly and the Marble Bar Greenstone Belt is restored and is then used to further discuss the extensional tectonic setting in Salgash times on the basis of the predicted geometrical characteristics summarised in figure 4.7.

4.4.5 Restoration to palaeo-horizontality at Salgash-times

The current geometry of the greenstone sequence of the Salgash Subgroup in the Marble Bar Greenstone Belt and the tilted sequence in the Kelly Greenstone Belt is the result of at least four main deformation phases (D_{X+2} - D_{X+5}, see chapters 2 and 3). An investigation of these greenstone sequences in their original orientation requires restoration of the bedding to the sub-horizontal.

4.4.5.1 Restoration method

Restoration of the Salgash Subgroup to horizontal (the orientation of deposition) influences any directional data within the sequence, such as the orientation of dykes and syn-depositional structures. When selecting the restoration method it is important to consider the local deformation style and history, because different restoration methods may result in different original orientations of directional data.

In the eastern Marble Bar Domain, tilting of the Salgash Subgroup is the result of a combination of deformation phases, including regional E-W compression, NE-SW extension on the MESZ and granite emplacement in the MEGC at 3.32-3.31 Ga (D_{X+2}, chapters 2 and 3 and references therein). In addition, subsequent deformation phases such as the post-3.3 Ga NNE-SSW compression (D_{X+3}) and WNW-ESE compression (D_{X+4}) may have further steepened the Salgash Subgroup, even though these last two are regarded to generally only have caused localised faults and shears in the Marble Bar Greenstone Belt (Van Haaften and White, 1998). This poly-phase deformation history in combination with the lack of quantitative displacement data precludes a step-by-step restoration. Hence, any proposed restoration method is a first order approach. The restoration method proposed hereafter, aims at a simplest, internally consistent solution to restore the units of the Salgash Subgroup to a horizontal position, and is not at a step-by-step restoration.

In previous studies *sections* of greenstone belts have been restored by rotation on *local* horizontal axes that are parallel to the nearest granite margin (See Zegers et al., 1996; Nijman et al., 1998a). Although this may be a suitable method for restoration of *parts* of greenstone belts, in this study concerned with the restoration of the Marble Bar Greenstone Belt *as a whole* a different approach is taken. If the Marble Bar Belt would be restored using the 'local axis' restoration method, space problems would arise, as is illustrated by the cartoon in figure 4.8b.

The Marble Bar Greenstone Belt contains units of the Talga Talga Subgroup, Duffer Formation and Salgash Subgroup that can be traced continuously along strike for ~75 km from the Talga Peak to the southern Marble Bar area (See figure 4.2). The first break in lateral continuity in the north is formed by the Coppin Gap Suite. In the south, the first break in continuity is the Salgash Fault in the Warrawoona Greenstone Belt (See figure 4.2). In between these discontinuities the units are continuous and internally relatively undeformed, except for the strike-parallel Duffada Shear Zone and the McPhee Shear Zone plus smaller shears in the underlying Talga Talga Subgroup (Van Haaften and White, 1998).

The units of the Talga Talga Subgroup dip only 30-45° away from the Mt Edgar Granitoid Complex, whereas the overlying Duffer Formation and the Salgash Subgroup are steeper, dipping 60-90° to locally 80° overturned (Lipple, 1975 and see figure 4.2). From these bedding orientations the Marble Bar Greenstone Belt might be considered to resemble part of a dome with a spherical geometry, in which the dip of the units steadily increases away from the domal crest, as is schematically illustrated in figure 4.8a. Note that the centre of the dome is off-centre from the current outcrop of the MEGC. Spherical geometries have been described in numerical and analogue models of diapirs (e.g. Dixon, 1975). In these models, the volume of a rising diapir is largely accommodated by ductile flattening and shearing of the cover sequence, particularly towards the diapir-interface (Dixon, 1975; Schwerdtner and Tröeng, 1977; Schwerdtner et al., 1978; Dixon and Summers, 1983; Cruden, 1988; Weinberg and Podladchikov, 1995). As the units of the greenstone sequence of the Marble Bar Greenstone Belt lack pervasive internal deformation, steepening of the greenstone sequence is interpreted to have occurred through sliding off the MEGC dome as internally coherent greenstone slabs by localised bedding-parallel slip, rather then pervasive ductile flow and shearing. Localised bedding-parallel slip would have occurred along structures such as the strike-parallel McPhee and Duffada Shear Zones, and also on the MESZ. Bedding parallel slip can have formed steeply dipping, internally relatively undeformed slabs. These slabs are here taken here to be divided by the McPhee and the Duffada Shear Zones, and run in length from the Salgash Fault in the south to the Coppin Gap Suite in the north (See figure 4.8c).

The proposed restoration method for the Marble Bar Greenstone Belt focuses on restoring the Salgash Subgroup and the Duffer Formation as an integral slab. This method considers an antiformal shape of the slab, with a ~60° plunge towards the WNW, conform the current dip of the bedding on the WNW part of the belt (See figure 4.9). The method comprises two steps (see figure 4.9). The first step restores the dip of the 'crestal' Salgash units to subhorizontal by rotating the antiform on an axis parallel to the overall trend of the belt (a 60° NW-up rotation on a 030-trending, horizontal axis). The second step involves 'unfolding' of both limbs to horizontal, along axes that are different for both limbs, and that are further quantified below.

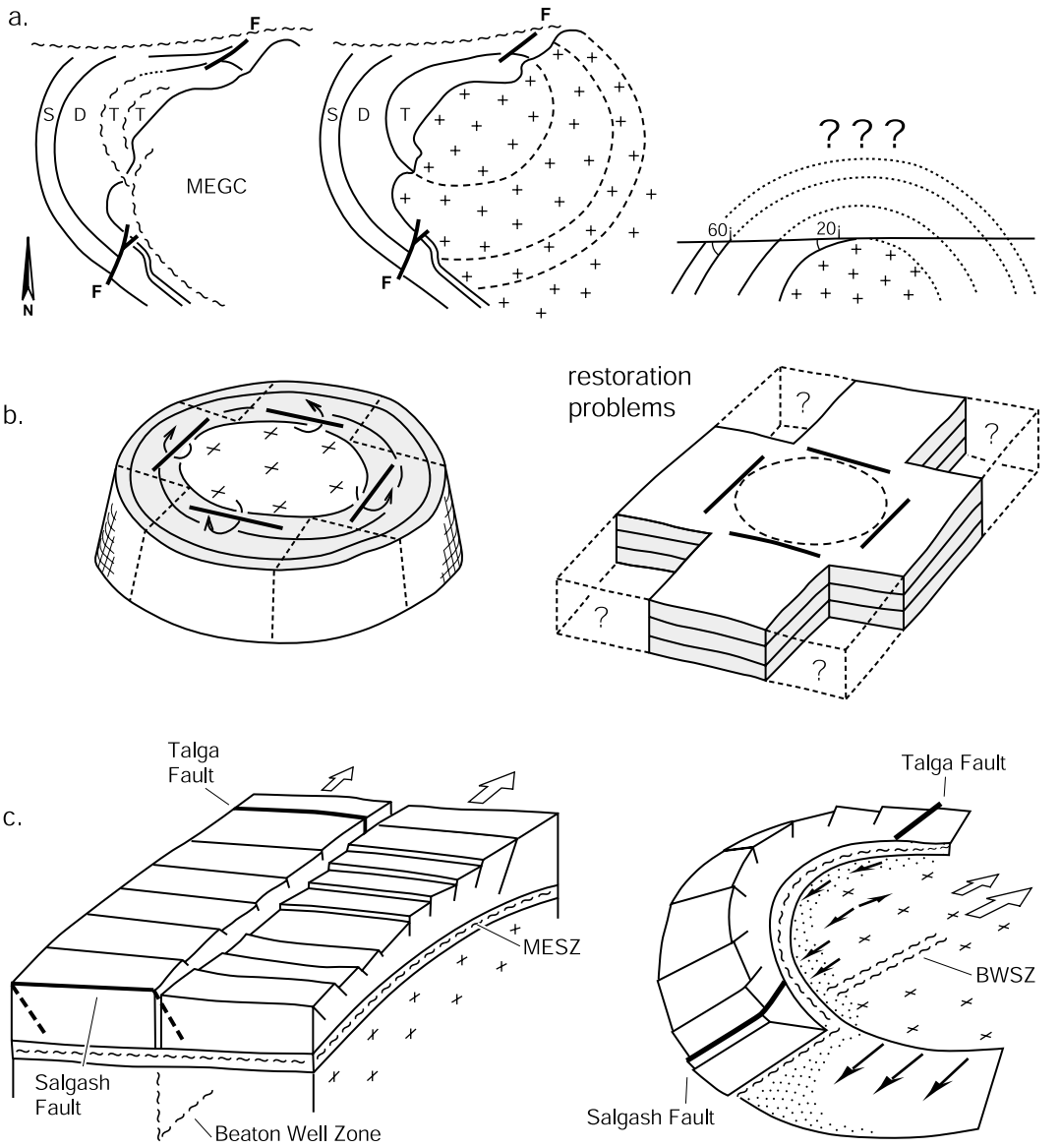

Figure 4.8 Geometrical considerations for restoring the greenstones of the Marble Bar Belt back to palaeo-horizontality in Salgash-times. (a) Overall semi-radial outcrop pattern and inferred conical geometry of the stratigraphy of the Marble Bar Belt. Note the Duffada Shear Zone in between the Talga Talga Subgroup (T) and the Duffer Formation (D). (b) Illustrating space problem after restoration by independent tilting of the internally largely undeformed northern, western and southern parts of the Marble Bar Belt by rotation along local horizontal axes parallel to the MEGC boundary. (c) Proposed mechanism with main detachment faults and shear zone to allow tilting of part of the Marble Bar greenstones as an intergral 'slab'.

4.4.5.2 Restoring the area east of Marble Bar

The bedding in the area east of Marble Bar is restored in two steps (figure 4.10a). The first step involves a rotation of 60° NW-up on a 030/00 axis as outlined above (cf. figure 4.9). After step 1 a second rotation is required to restore the Salgash bedding to horizontal. The orientation of the partly restored bedding (Figure 4.10b) shows that full restoration of the northern part of the area requires a rotation of 60° SW-up on a 330-trending, horizontal rotation axis. The southern area requires an 83° SW-up rotation on a 300°-trending rotation axis (See figure 4.10c). During these rotations the sills and dykes are carried passively. The restored sills are generally subhorizontal and the dykes dip either to the NNE or SSW, as is illustrated in the stereographic projections in figure 4.10c. The dykes throughout the area now form a conjugate set, the orientation of which indicates a local (N)NE-(S)SW extension direction.

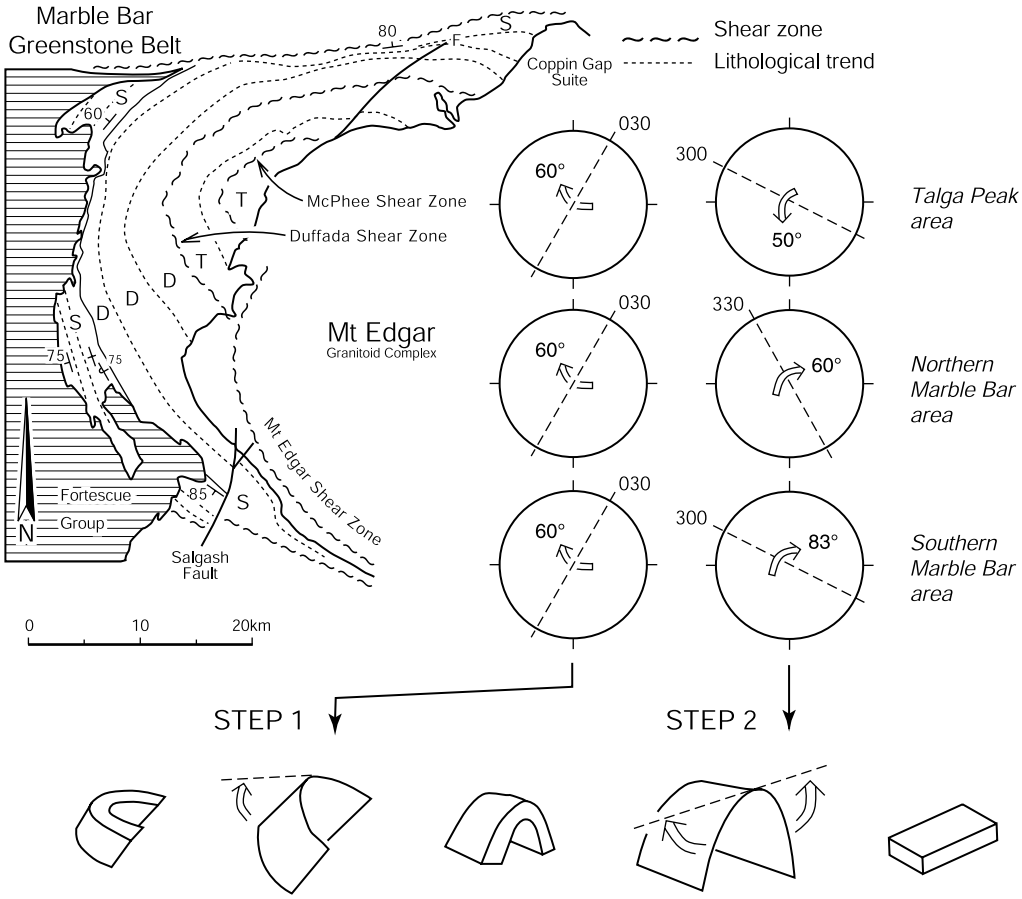

Figure 4.9 Rotational axes of the proposed two-step reconstruction method for restoring to Salgash-times palaeo-horizontality of the Talga Peak and Marble Bar areas (Figures 4.3 and 4.5, respectively). The method is not a stepwise back-stripping exercise, but it does comply with the tilt of the supracrustal units of the Marble Bar Greenstone Belt as one, internally relatively undeformed slab. Letters refer to stratigraphic units as listed in figure 4.2.

4.4.5.3 Restoring the Talga Peak area

In the Talga Peak area the bedding outside the fault bocks, currently subvertical to steeply NNW-dipping (Figure 4.11a), has been restored to palaeo-subhorizontality as part of the Marble Bar Greenstone Belt slab. The first step was identical to that described for the area east of Marble Bar, using a 030/00 axis for rotation of 60° NW-up (cf. figure 4.9). The bedding orientation after STEP-1 is shown in figure 4.11b. Restoration to horizontal required a second step of 50° NE-up rotation on a 300-trending, horizontal rotation axis (Figure 4.11c). These two steps result in subvertical to steeply SW dipping dykes and subhorizontal sills (Figure 4.11c). The restored, SW-dipping dykes suggest a NE-SW extension direction.

4.4.5.4 Restoring the Kelly Greenstone Belt

As the Kelly Greenstone Belt is a ~40 km long, straight greenstone belt with a 015° trend and an overall 60-65°ESE dip (Figure 4.12a), the Euro Basalt and the underlying Panorama Formation are restored to palaeo-subhorizontality by rotating 62° ESE-up on a 015-trending horizontal axis (Figure 4.12b). This rotates the dyke swarm from subvertical to a steeply, dominantly NNE to NE-dipping orientation (Figure 4.12b). This orientation is considered to be the intrusion orientation of the dykes. When the axis of least compressional stress, s_3, is taken normal to the dykes, the inferred extension direction during intrusion is (N)NE-(S)SW.

4.4.5.5 Regional extension during deposition of the Salgash Subgroup

Reconstruction of the three study areas in the Kelly and the Marble Bar Greenstone Belts (See figure 4.10, 4.11 and 4.12) shows that the dykes in all three areas intruded with an original orientation trending WNW to NW. As the dykes line up, they can be regarded as a parallel dyke swarm at this scale.

As mentioned above, the dykes have not been dated directly. Constraints from intrusive relationships date the dykes in the Kelly Belt to post-3417 ± 9 and pre-3313 ± 9 Ma, such that they can conclusively be associated with the Euro Basalt. But, dykes in the Marble Bar Belt were more loosely constrained between post-Duffer and pre-3.31 Ga, and can be interpreted to be related to either the Apex or the Euro Basalt. With these age constraints, it is possible that some of the dykes reported in this study intruded during distinctively different times throughout a period of <140 m.y., from after deposition of the Duffer Formation to intrusion of the granitoids at ca. 3310 Ma. Moreover, the petrographical composition of the different dykes, varying between mafic and ultramafic, suggests that separate phases involved intrusions of separate suites. This is in agreement with the differences in composition observed in the volcanic units of the Salgash Subgroup (e.g. Barley, 1993; Hickman, 1983; Van Kranendonk, 2000).

The available age constraints and orientations of the geometrically restored dykes of the Marble Bar and Kelly Belts are consistent with an interpretation in which crustal extension during emplacement of the Apex and Euro Basalt of the Salgash Subgroup in the eastern Marble Bar Domain was oriented between NNE-SSW and NE-SW (See figure 4.13).

The upper crustal extension direction indicated by the orientation of the dykes is similar to the mid-crustal extension direction on the Mt Edgar Shear Zone at the time of the intrusion of

a. Current orientation	b. Orientation after STEP 1	c. Orientation after STEP 2
N: Northern Marble Bar area **S**: Southern Marble Bar area	**N**: 60° NW-up on 030/00 **S**: 60° NW-up on 030/00	**N**: 60° SW-up on 330/00 **S**: 83° SW-up on 298/00
Bedding	Bedding	Bedding
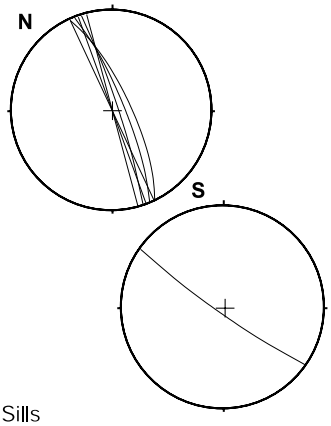	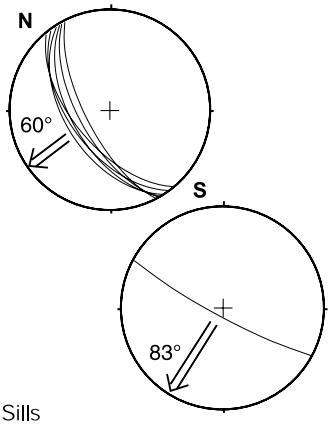	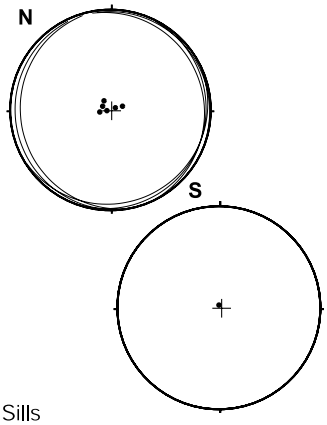
Sills	Sills	Sills
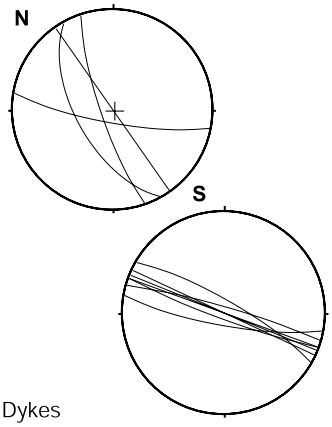	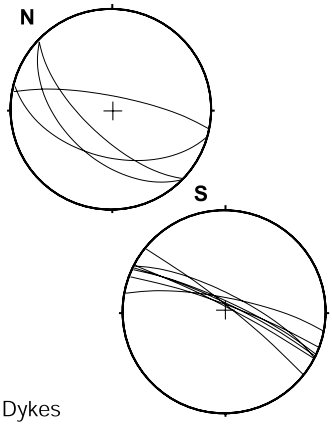	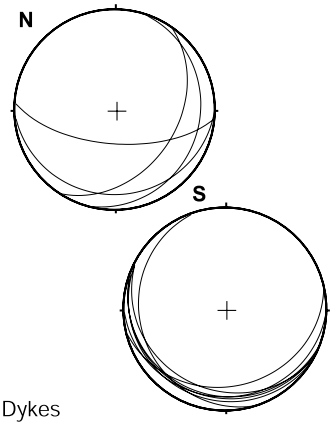
Dykes	Dykes	Dykes
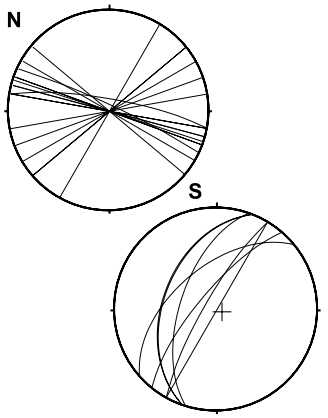	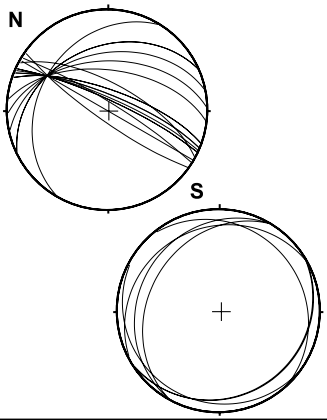	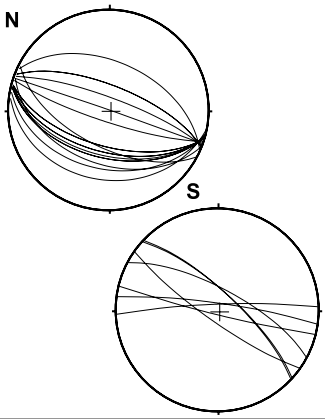

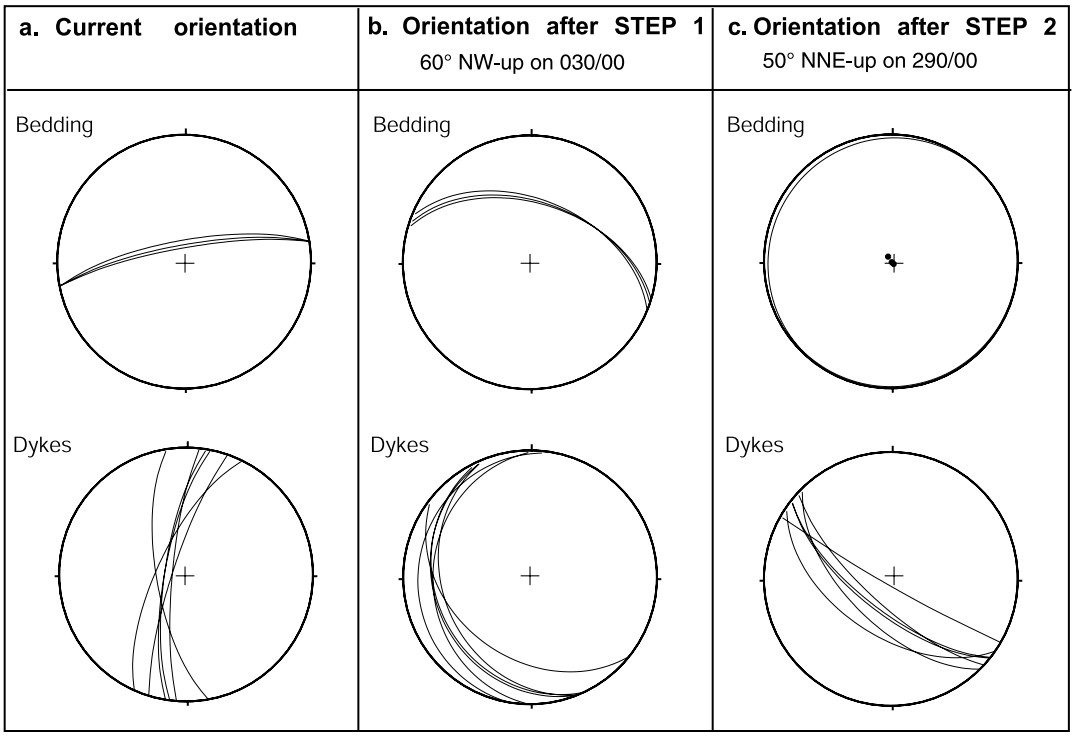

Figure 4.11 Stereographic reconstruction of the Talga Peak area in the Marble Bar Greenstone Belt. (a) Present-day orientation of bedding of the Salgash Subgroup, mafic dykes and sills (see figure 4.5). (b) Orientation of bedding, dykes and sills after STEP 1 of the reconstruction. See text for reconstruction method. (c) Orientation of bedding, dykes and sills after reconstruction to Salgash-times palaeo-horizontality.

Figure 4.10 Stereographic projections of reconstruction steps of the area east of Marble Bar. See figure 4.2 for extend of (N) northern and (S) southern area. (a) Present-day orientation of Salgash Subgroup bedding, mafic dykes and sills in the Marble Bar Greenstone Belt (see figure 4.4). (b) Orientation of bedding, dykes and sills after Step 1 of the reconstruction. See text for reconstruction method. (c) Orientation of bedding, dykes and sills after reconstruction to Salgash-times palaeo-horizontality.

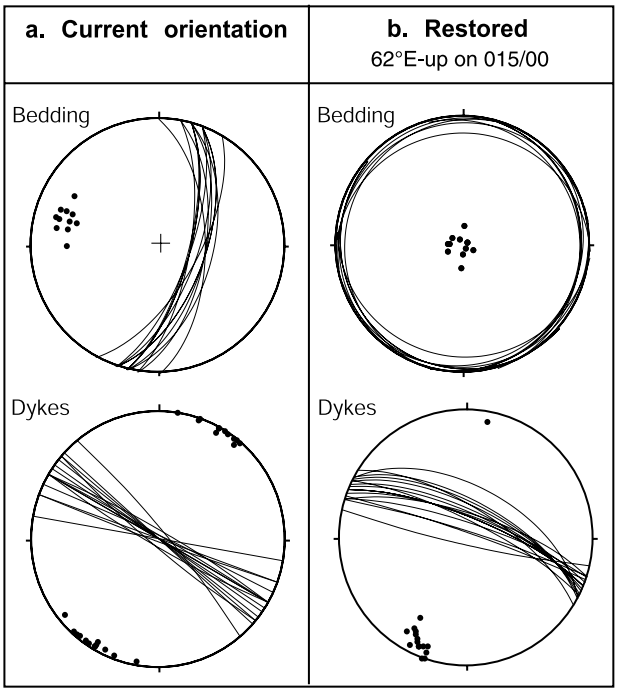

Figure 4.12 Stereographic reconstruction of the Kelly Greenstone Belt. (a) Present-day orientation of Salgash Subgroup bedding and mafic dykes in the Kelly Greenstone Belt (see figure 4.3). (b) Reconstructed orientation of bedding and dykes.

ultramafic and dolerite sills (components 5a and b) at >3447 ± 6 Ma (see figures 3.5, 3.15 and 3.21). This strengthens the interpretation based on structural and intrusive relationships that deformation during D_{X+1} involved (N)NE-(S)SW extension (see chapters 2 and 3).

4.4.6 Implications for the extensional setting of the Salgash Subgroup

The linear geometry of crustal extension during emplacement of the Euro Basalt and possibly the Apex basalt of the Salgash Subgroup on a scale that exceeds that of a granitoid dome can have causes related to processes similar as today's plate-interaction (back-arc extension, intracontinental rifting) or to processes that were characteristic for the Early to Mid Archaean (extensional collapse, intracontinental rifting) as discussed above and illustrated in figure 4.7. Crustal overturn of an incoherent crust due to heating of a mantle plume is unlikely to form a linear extension pattern on the mesoscopic scale of that of the Marble Bar Domain.

The Salgash Subgroup comprises a 2 to locally 9 km thick (Hickman, 1977; Van Kranendonk, 2000) sequence of dominantly mafic and felsic volcanic rocks. Large volumes of continental magmatism and the intrusion of regionally linear mafic dyke swarms in Phanerozoic terrains is generally associated with intracontinental rifting. Intracontinental rifting can either be active, i.e. due to far-field extensional forces associated with plate movement, or reactive, due to mantle plume induced upwellings, as was listed in figure 4.7. One of the differences between active and reactive rift settings is that the first generally results in thinning and subsidence of the crust, forming a subaqueous deposition environment, whereas mantle plume induced upwelling first results in

regional doming of the crust and mostly subaerially deposited basalts. However, the role of rifting and mantle plumes in the formation of large igneous provinces and continental break-up is the subject of ongoing discussions (e.g. Fahrig, 1987; Ernst, 1995a; Sheth, 1999a, 1999b, and references therein).

The largely subaqueous deposition of the Salgash Subgroup would at first sight preclude plume related continental flood basalts as analogues, because the latter are generally extruded subaerially. However, Arndt (1999) remarks that subaqueous mafic magmatism is generally rare: even though

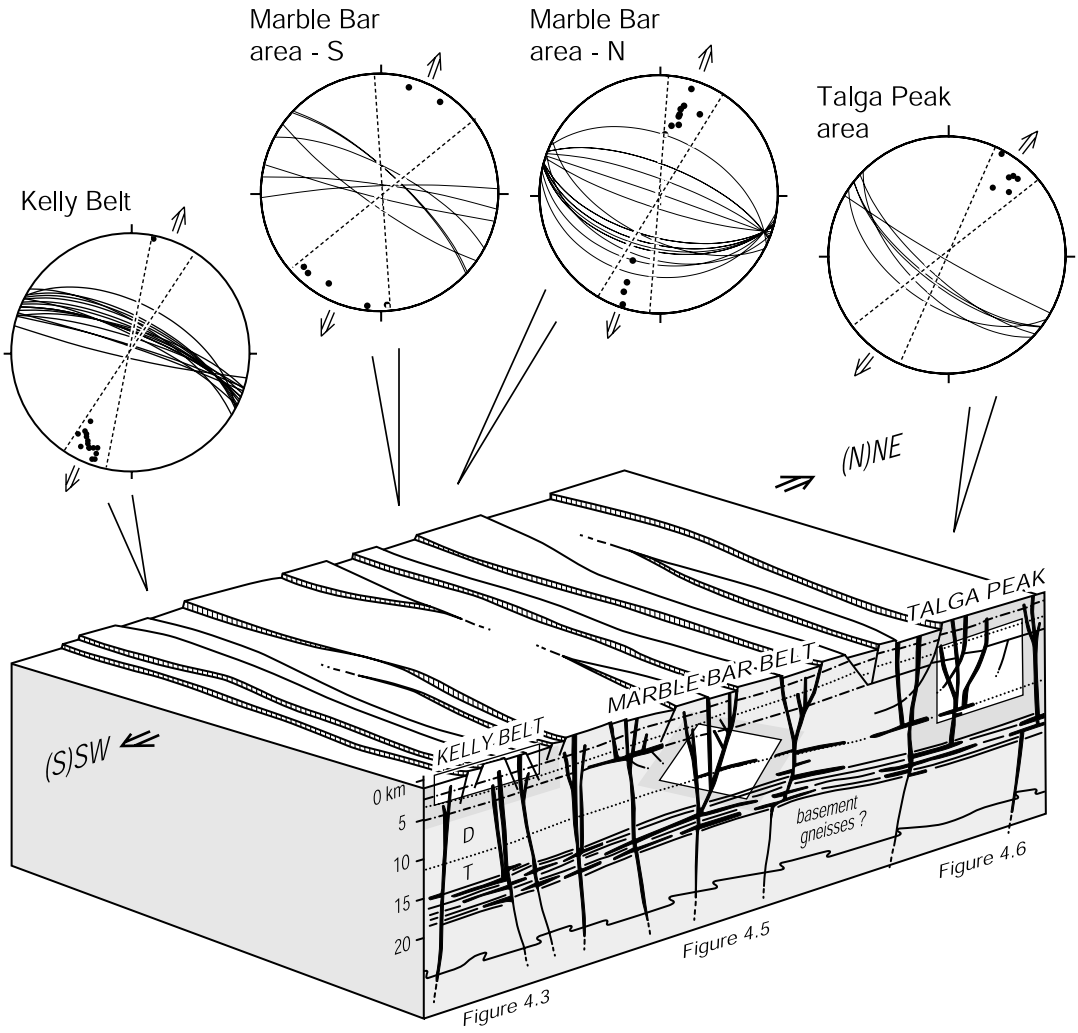

Figure 4.13 Cartoon illustrating crustal section of the crust during intrusion of the Salgash Dyke Swarm, based on the restored orientation of mafic dykes for the Kelly Belt, the Marble Bar and the Talga Peak areas of the Marble Bar Belt. These areas are schematically indicated at their corresponding crustal levels. The mafic dykes indicate overall (N)NE-(S)SW extension during intrusion.

subaqueous mafic magmatism has been observed in modern rifted terrains, such as the North Atlantic Province, it is often related to the final stage only (Arndt, 1999). Arndt (op cit.) recognised that mafic flood volcanism on submerged continental platforms may have been common in the Precambrian, which may have been the effect of typical Precambrian conditions of the mantle and/or the crust that would have promoted high sea levels. Conditions that promote submerged continents include those that cause a relatively high sea level, such as a denser crust, a greater ocean volume, or shallower ocean basins due to a thicker oceanic crust, more active ridges, and periodic bursts of enhanced mantle activity (for an overview and discussion see Arndt, 1999). As the conditions of the Archaean crust and mantle are subject of discussion, and submerged continents may be a typical Precambrian condition, the dominantly subaqueous nature of the Salgash Subgroup cannot not been taken as a constraint in the following discussion on the structural setting and the underlying geodynamic mechanism during development of the Salgash Dyke Swarm.

A mantle plume model was rejected by Zegers (1996) as the underlying geodynamic mechanism for extensional development of a growth-fault array in the 3.47-3.46 Ga felsic volcanic Duffer Formation in the Coongan Greenstone Belt (Figure 4.2). Extension in the upper crustal unit and on the underlying detachment, the Split Rock Shear Zone was recognised to be non-radial on the scale of the Shaw Granitoid Complex. Hence, far-field stresses were implied and a mantle plume was considered unlikely (See Table 9.1 in Zegers, 1996). Their arguments, however, hold a jump in scale as is illustrated in figure 4.7b(2), and should not rule out a plume role, as is discussed below.

As outlined above, the geometry of extension in a particular setting can vary depending on the scale of the area that is considered. The geometry of mafic dykes in a triple junction rift system can be referred to as radial on continental scale, but on the regional scale of one rift-arm, e.g. the East African Rift Valley, extension would be regarded as linear. But, when zooming in at smaller scale, a local dyke system that feeds an associated volcano can, in turn, be radial (See figure 4.7b, see also Ernst et al., 1995). Therefore, scale should be taken into account in any argument based on extension orientation and geometry.

The distance between the Marble Bar and the Talga Peak areas is at least 70 km along strike (See figure 4.2). The reconstructed dyke orientation for both areas suggests that the direction of crustal extension during deposition of the 3.45-3.42 Ga Salgash Subgroup basalt was more or less constant over an area of at least 70 km in the Marble Bar Greenstone Belt alone (See figure 4.13). When the Kelly Belt area is included this could be as much as 85 km along the direction of extension. As the mafic dyke swarm can be referred to as linear at this scale, the cause for extension Salgash-times can be regarded as uni-directional on this scale. The area of linear extension at Salgash-times is larger than the current diameters of the nearby Mt Edgar or Corunna Downs Granitoid Complex. Therefore, the stress-field that caused extension at Salgash-times is likely to have exceeded the scale of the Mt Edgar and Corunna Downs Granitoid Complex. If so, it is unlikely that doming of these granitoid complexes was the dominant cause for extension in the upper crustal sequences. This, however, need not preclude the role of mantle plumes in the Early to Mid Archaean, it may preclude the presence of an incoherent crust in the Marble Bar Domain at Salgash-times.

The limited extent of the study area, and ultimately the limited size of the Pilbara Craton, may preclude a comparison of the extension geometry on a continental scale (Figure 4.7b).

4.4.7 Granitoid genesis during D_{X+2} due to thrusting or magmatism?

Granitoids in the MEGC were generated from partial melts of the gneissic basement during D_{X+2} (Collins, 1989). Based on the structural history of the Warrawoona Belt and surroundings, the cause has been proposed to be E-W compression, thickening of the crust, and radiognic heating leading to partial melting (see chapter 2).

The recently determined 3346 Ma age (Nelson, 2001) of zircons from a tuff of the Euro Basalt near the top of the Salgash Subgroup, interpreted to represent the eruptive age of the tuff (M. Van Kranendonk and L. Bagas, Geological Survey of Western Australia, unpubl. data. In: Van Kranendonk et al., 2002), suggests that the top of the Salgash Subgroup is much closer in age to that of the Wyman episode then previously considered. The possibility that magmatism associated with the Euro Basalt caused partial melting of a gneissic basement, should not be excluded.

Chapter 5 focuses on dating the thermal evolution of the MEGC and the MESZ, using ^{40}Ar - ^{39}Ar isotope systematics. Three samples from mafic dykes from the Kelly Belt are included in dating to investigate the crystallization age.These indicate hornblende cooling ages of 3356 ± 21 Ma and 3440 ± 58 Ma.

4.5 Conclusions

1. Mid Archaean mafic dykes are recognised in the Kelly Greenstone Belt, and in the northern and southern Marble Bar Belt of the Marble Bar Domain.

2. In the Kelly Greenstone Belt dykes are found as feeders to pillow basalt of the Euro Basalt (Salgash Subgroup). These dykes intruded the 3417 ± 9 Ma Ga felsic volcanic Panorama Formation, on top of which the Euro Basalt was deposited. Their cumulative width represents a minimum of 4% of crustal extension in this belt.

3. In the northern and southern Marble Bar Greenstone Belt a system of mafic dykes and sills was found to have intruded the locally 5 km thick, dominantly felsic volcanic Duffer Formation. It is a potential feeder system for the overlying Salgash Subgroup. Here, thickness of the dykes indicate that they represent 5% of crustal extension.

4. After restoration to palaeo-horizontality of the top of the Salgash strata, the dykes in both the Kelly and the Marble Bar Greenstone Belts indicate (N)NE-(S)SW extension at a scale that exceeds the current size of the Mt Edgar Granitoid Complex.

5. The available age constraints and orientations of the reconstructed dykes of the Marble Bar and Kelly Belts are consistent with an interpretation in which crustal extension during emplacement of the Apex and Euro Basalt of the Salgash Subgroup in the eastern Marble Bar Domain was between NNE-SSW and NE-SW.

6. The upper crustal extension direction indicated by the orientation of the dykes is similar to the mid-crustal extension direction on the Mt Edgar Shear Zone at the time of the intrusion of dolerite sills, pre-3347 ± 6 Ma and extension in the Gneiss Complex at ca. 3426±4 Ma. This further strengthens the interpretation that deformation during D_{X+1} was related to crustal scale extension.

7. The scale and parallel pattern of the dykes suggest that the cause for extension was larger than that of an individual granitoid complex. This indicates that solid-state diapirism was not the driving force for extension.

8. Deposition of the largely subaqueous Apex and Euro Basalt on an extending continental crust may represent a phase of continental rifting. Additional constraints are necessary to conclude on the driving force for extension and mafic magmatism.

9. Upper Salgash magmatism may have been responsible for heating and partial melting of a gneissic basement to form granitoids at ca. 3.31 Ga.

Chapter 5

^{40}Ar-^{39}Ar chronology constraints for the development of an extensional detachment in the Marble Bar Domain, Pilbara granite-greenstone terrain, Australia

5.1 Introduction

In the previous chapters new data have been presented on the structure, kinematic evolution and SHRIMP (U-Pb, zircon) chronology of the Mt Edgar and Corunna Downs Granitoid Complexes, and the adjacent Kelly, Warrawoona and Marble Bar Greenstone Belts, in the eastern Pilbara granite-greenstone terrain. It was shown that the area has suffered at least five main deformation phases from as early as 3.46 Ga to after intrusion of the ca. 2.77 Ga Black Range Dyke Swarm.

Two main extensional phases, D_{X+1} and D_{X+2}, dated at 3.46-3.45 Ga and 3.32-3.31 Ga, respectively (See chapter 3), caused extension on an initially mid-crustal shear zone recognised along the southern margin of the Mt Edgar Granitoid Complex, the Mt Edgar Shear Zone (MESZ). This shear zone acted as a master detachment during both phases of extension. Extension caused doming of the Mt Edgar Granitoid Complex (MEGC) during D_{X+2}. During this phase the MEGC has been interpreted to have developed as a steep-sided metamorphic core complex (See figure 2.18) similar to those described by Marshak et al (1992,1997). Earlier extensional activity of the (proto)MESZ occurred at 3.46-3.42 Ga as dated by the age of syn-tectonic intrusions (see chapter 4). An intricate relationship between structural development, syn-tectonic intrusions and related kinematics of the MESZ indicates extension during this early history (See figures 2.16 and 3.9). But the amount of doming and the amount of exhumation of the MEGC and MESZ during D_{X+1} is as yet unclear. It was argued in chapter 2 that a later phase of (N)NE-(S)SW compression (D_{X+3}) and transcurrent movement on the Central Warrawoona Shear Zone during WNW-ESE compression (D_{X+4}) (Chapter 2) may have caused subsequent steepening of the flanks of the MEGC. Hence, questions

Deformation phase (see chapter 2)	Timing (Ma) (see ch.3)	Main structures, kinematics and metamorphic grade (see chapters 2, 3 and 4)		Related Magmatism (see chapters 3 and 5)
D_{X+1A}	ca 3465	MESZ - (E)NE-(W)SW extension	amphibolite	hbl-gabbro/diorite, Kfs-granite.
D_{X+1B}	> 3447	MESZ - (E)NE-(W)SW extension	amphibolite	Dolerite
D_{X+1C}	ca 3447 <3417	MESZ - (E)NE-(W)SW extension Kelly Belt - NE-SW ext. dykes	amphibolite	Leucogranite Salgash Dyke Swarm
D?	> 3340	Warrery Shear Zone - E-W compression (Zegers et al, 1999)	amphibolite (Zegers et al, 1999)	biotite granodiorite
D_{X+2C}	< 3325 > 3315	Camel Creek S.Z. - E-W compression Central Warrawoona S.Z. - strike slip def.	greenschist greenschist	
D_{X+2E}	ca 3315	MESZ - NE-SW extension	amphibolite - greenschist	TTG in MECG and CDGC
D_{X+3}	?	Regional fracture cl., crenulations Local thrusts - (N)NE-(S)SW comp. CPA - 020 transcurrent dextral faults	greenschists	not clear
D_{X+4}	ca 2930 ?	Central Warrawoona S.Z. - dextral transcurrent WNW-ESE compression	greenschist	not clear
D_{X+5}	< 2770	Local faults - ESE-WNW extension Central Warrawoona Shear Zone - dextral		Mt Roe Basalt (Fortescue Group) Black Range Dolerite S.

Figure 5.1 Summary of the structural history of the eastern part of the Marble Bar Domain, as discussed in chapters 2, 3 and 4.

that arose are: what was the relative role of the extensional phases D_{X+1} and D_{X+2} for the geometrical development of the MEGC and MESZ (Figure 3.20), what was the timing of the subsequent deformation phases, and their effect on the steepness of the MESZ?

Additional questions concerning timing arose from the study of the dyke swarms reported in chapter 4. In that chapter it was shown that mafic dykes and sills of pre-3.31 Ga age, collectively referred to as the Salgash Dyke Swarm, intruded the supracrustal rocks of the Marble Bar Belt and Kelly Belt, associated with at least 4% of upper crustal extension. Although they must be older that ca. 3.31 Ga, on the basis of on intrusive relationships, the exact age of the dykes is not known. The dykes in the Kelly Belt were associated with deposition of the Euro basalt. A crystallization age of

the dykes will provide an age for the Euro Basalt and for the associated extension. In chapter 3 is was found that mafic and ultramafic sills exploited the mid-crustal MESZ during the later stages of the first extension phase $D_{MESZ,x+1}$ pre-3447 ± 6 Ma (see figure 3.21). However, the dykes in the Kelly Belt must be younger, because they intruded the Panorama Formation locally dated at 3417 ± 9 Ma (Barley et al., 1998). A recent 3346 Ma age from a population of zircons within a tuff in the upper unit of the Salgash Subgroup (Nelson, 2001) was interpreted to reflect timing of deposition of the Euro Basalt (M. Van Kranendonk and L. Bagas, Geological Survey of Western Australia, unpubl. data. In: Van Kranendonk et al., 2002). If the dykes in the Kelly Belt are of a similar age as suggested for the tuff, then Upper Salgash magmatism and the tectonomagmatic development during D_{X+2} may be genetically related. However, the age of the tuff is uncertain as younger zircons have been identified in this tuff that pool at ca 3311 Ma, which may indicate that the crystallization is ca 3311 Ma (Nelson, 2001).

The work by Wijbrans and McDougall (1987) and subsequently by Davids et al. (1997) and Zegers et al. (1999) has shown that dating of hornblendes and micas using the ^{40}Ar-^{39}Ar method can provide constraints for cooling histories and thereby for deformation that occurred as early as the Mid-Archaean. Therefore, this method was selected to further constrain the timing of the tectonic evolution of the east Pilbara granite greenstone terrain.

The objective of this ^{40}Ar-^{39}Ar study is three-fold: i) To put time constraints on the early development of the MESZ by studying its thermal history. If doming, exhumation/denudation and cooling of the MESZ occurred at 3.45 Ga and was shielded from the effects of subsequent thermal overprinting events (either related to a magmatic episode or tectonic phase), then the ^{40}Ar-^{39}Ar isotopic ages from the MESZ should reflect that thermal history. ii) To further constrain the timing of D_{X+2}, D_{X+3} and D_{X+4} by determining the cooling age of syn-tectonically grown minerals, namely hornblende, muscovite and biotite: if not thermally reset their ages may provide a minimum age for deformation. iii) The third aim is to constrain the age of emplacement of the upper crustal Salgash Dyke Swarm in the Kelly Belt: the ^{40}Ar-^{39}Ar isotopic age of primary hornblendes, if not thermally reset, may provide an estimate of the time of crystallization of the dykes.

To achieve these objectives twenty-one hand specimens were selected from the MESZ, from the dykes in the Kelly Belt and from areas that were affected by deformation related to E-W (western Warrawoona Belt) and to NNE-SSW compression (Carbana Pool Adamellite) (See table 5.1). Microstructural analyses was done for each sample to identify the minerals useful for ^{40}Ar-^{39}Ar dating and to established the relative timing of deformation and mineral growth. Twenty-seven mineral fractions including hornblende, muscovite and biotite were selected for ^{40}Ar-^{39}Ar laser stepwise heating experiments (See table 5.1).

In addition to the age constraints for the tectonic history of the area, the combined results provide a basis for a discussion on the thermal evolution of the currently exposed crust with respect to Ar/Ar systematics in a regional sense. This is done by comparing the results of this study to ^{40}Ar-^{39}Ar isotopic ages within the western part of the Marble Bar Domain, including the Shaw Granitoid Complex and its adjacent greenstone belts as reported by Wijbrans and McDougall (1987), Davids et al. (1997) and Zegers et al. (1999).

Sample	Location	Rock type,	Mineral [b]	Characteristics of mineral i.c.= interference colours p.l.= reflected light	Microstructural context of selected mineral
Argon samples from structures related to D_{x+1} and D_{x+2} in the Mt Edgar Shear Zone					
CTW-36	01 98 500 76 27 500	Hbl-gabbro/diorite	Hornblende <250 (5x)	Dark green, elongate, euhedral to subhedral	Undeformed, magmatic hornblende
			Hornblende >250-400 (3x)	Green, elongate, euhedral to subhedral	Undeformed, magmatic hornblende
P97-366	08 90 300 76 37 200	Undeformed mafic pegmatite/in diorite/ gabbro complex intruded by granite	Hornblende >250 (3x)	Elongate, dark green euhedral	Undeformed, magmatic hornblende
P97-233	01 98 095 76 27 748	Hbl-gabbro/diorite	Hornblende 200x200 (7x)	Dark green fragments	Undeformed, magmatic hornblende
P96-172	02 05 168 76 28 805	Hbl-gabbro/diorite	Hornblende 200x400 (7x)	Dark green, transparent, subhedral	Magmatic fabric
P97-236	02 04 700 76 29 350	Hbl-gabbro/diorite complex	Hornblende 200x250 (8x)	Subhedral, often clusters	Magmatic fabric
P97-237	02 04 700 76 29 350	Schistose mafic xenolith in hbl-gabbro/diorite complex	Hornblende 250x400 (7x)	Dark green, anhedral, semi-transparent, intergrowths with biotite	Undeformed, contact metamorphic fabric
P97-234	01 97 950 76 28 450	Schistose mafic xenolith in hbl-gabbro/diorite complex	Hornblende 150-200 (11x)	Euhedral, lightgreen, transparent, fragments	Undeformed, contact metamorphic fabric
P97-361	07 86 702 76 56 602	Alkali-feldspar granite 'Aga'	Biotite ~250 (4x)	Aggregates,semi-transparent	Random biotite, locally chloritized
			Muscovite <250 (3x)	Yellowish, aggregates	Random Muscovite blasts overgrew chlorite
P96-215	07 95 400 76 42 500	Andalusite-mica quartz schist	Muscovite <150 (14x)	Thin, transparent anhedral flake aggregates	Mylonitic S/C fabric, NE-up kinematics
P96-167	02 05 300 76 27 700	Dolerite dyke, mylonitised	Hornblende <250 (11x)	Elongate, euhedral	Magmatic alignment
			Hornblende >250 (5x)	Equidimensional, aggregates	Undeformed blasts overgrew fabric
P96-100	07 99 800 76 75 800	Mafic mylonite, intruded by granite sills	Hornblende <250 (6x)	Euhedral elongate	Magmatic alignment
		Mafic mylonite, intruded by granite sills	Hornblende >250 (4x)	Euhedral, equidimensional	Undeformed blasts overgrew CPO
CTW-1A	07 97 500 76 43 500	Cotton Well Pluton, muscovite granite	Muscovite ~400 (2x)	Euhedral transparent large crystals	Magmatic foliation
P95-gran	07 99 158 76 43 703	Leucogranite	Muscovite <100 (4x)	Random	Magmatic fabric, undeformed, only unduleuse qtz

Table 5.1 ^{40}Ar-^{39}Ar sample co-ordinates, description of mineral separates, and summarised results of this study.

Sampling reason	Age constraints [a]	**T_1 Plateau age (±2σ, Ma)**	^{39}Ar in plateau	Total fusion age (±2σ, Ma)	Interpretation of T_1 (plateau-age) T_2 (reset ages low temperature domains)
Cooling history, reset?	Dated at 3462±4 Ma (U-Pb, zircon Chapter 4)	**3080±16**	94 %	3107±17	T_1 Reset age
Cooling history, reset?	Dated at 3462±4 Ma (U-Pb, zircon Chapter 4)	**3087±18**	95 %	3090±16	T_1 Reset age
Cooling history / age granite?	< age granite	**3249±15**	96 %	3264±18	T_1 Cooling age / reset age
Cooling history?	< age gabbro (3462±4 Ma, U-Pb, zircon Chapter 4)	**3298±21**	55 %	3250±17	T_1 Cooling age / reset age
Minimum age magmatic fabric	< age gabbro (3462±4 Ma, U-Pb, zircon Chapter 4)	**3309±16**	76 %	3286±18	T_1 Cooling age / reset age
Minimum age magmatic fabric	< age gabbro (3462±4 Ma, U-Pb, zircon Chapter 4)	**3324±18**	79 %	3313±17	T_1 Cooling age / reset age
Minimum cooling age gabbro?	< age gabbro (3462±4 Ma, U-Pb, zircon Chapter 4)	**3315±16**	91 %	3305±18	T_1 Cooling age / reset age
Minimum cooling age gabbro?	< age gabbro (3462±4 Ma, U-Pb, zircon Chapter 4)	**3205±23**	60 %	3273±32	T_1 Cooling age / reset age
Cooling history Aga granite?	3466±2 (Nelson, 1998), intruded by dolerite dikes and 3310±3 Ma granitoid (Nelson, 2000).	**2897±16**	52 %	2851±16	T_1 Growth / reset age. Similar as the age of the first step of the muscovite of this sample. Suggests T_1 is a reset age.
Timing of muscovite blastosis?	Crystallization age 3466±2 (Nelson, 1998)	**3151±16**	79 %	3138±17	T_1 Growth of muscovite during thermal pulse. T_2 2820±64 Ma resetting age.
Minimum age NE-up movement	< 3465±3 crystalization age protolith	**2808±17**	95 %	2807±29	T_1 Thermally reset age associated with the lower Fortescue episode
Age fabric ?		**3249±17**	98 %	3250±22	T_1 Thermally reset ?
Age heat pulse, minimum age fabric		**3325±16**	60 %	3266±22	T_1 Thermally reset ?
Age fabric ? Age T-peak		**2910±16**	66 %	2930±25	T_1 Thermally reset ?
Age granite sills?		**2923±16**	99 %	2913±27	T_1 Thermally reset ?
Age of foliation ?	Crystallization age 3309±6 (Chapter 4)	**2840±15**	73 %	2857±16	T_1 Thermally reset age possibly associated with the lower Fortescue episode.
Cooling history	Crystallization age 3447±6 (Chapter 4)	**2801±19**	29 %	2752±16	T_1 Reset by 2.77 Ga Black Range Dyke Swarm.

	76 43 703		<100 (4x)		undeformed, only unduleuse qtz
P97-282	± 02 05 426 76 31 750	Mafic mylonitic xenolith in granite gneiss	Hornblende <250 (3x)	Euhedral	Has strong CPO, is overgrown by undeformed hbl blasts
A94-22	76 58 800 08 00 600	Grey granodiorite sheet	Muscovite <200 (4x)	Random	Gneissic fabric
Argon samples from E-W compressional structures in the Warrawoona Belt related to D_{x+2}					
P95-7	07 89 644 76 37 432	Sheared basalt Salgash Subgroup?	Actinolite 200-100 (16x)	Aggregates, transparent, light green	Part of mylonitic fabric, W-vergent thrust of Camel Creek Shear Zone
P95-10	07 98 000 76 38 000	Felsic ultra-mylonite, Wyman Formation	Muscovite 80x150 (11x)	Aggregates, anhedral, transparent, yellowish	Part of mylonitic fabric, sl 285/80 on 285/90 mfol S-up kinematics
Argon sample from NNE-SSW compressional structures in the Carbana Pool Adamellite related to D_{x+3}					
P97-339	08 07 000 76 13 000	Carbana Pool Adamellite, monzogranite	Hornblende ~250 (9x)	Fragments, subhedral, non-transparent	Shears indicating NNE - tectonic transport sl 216/50 on 340/50W and 015/75W
			Biotite ~300 (12x)	Subhedral	Shears indicating NNE - tectonic transport sl 216/50 on 340/50W and 015/75W
Argon samples from structures related to dextral transcurrent movement during D_{x+4}					
P97-306	07 95 000 76 37 200	Mafic xenolith in Corunna Downs GC granite	Actinolite 250-400 (12x)	Long prismatic, acicular, lightgreen aggregates	Defines mineral lineation of dextral transcurrent shearing
Argon samples from the mafic dyke swarm in the Kelly Greenstone Belt					
P97-343	01 90 585 76 12 798	Dolerite/pyroxenite dyke, intruded P97-344	Hornblende 300x600 (10x)	Euhedral	Undeformed hornblende, some with px-cores
P97-344	01 90 585 76 12 798	Diorite-gabbro dyke, intruded by P97-343	Hornblende 200x300 (7x)	Equidimensional, subhedral, non-transparent	Undeformed hornblende
			Hornblende ~200 (8x)	Equidimensional, rusty, nonhedral, non-transparent	Undeformed hornblende

[a] Direct age constraints from dating (SHRIMP, U-Pb, zircon), or indirect from relationship with dated rocks

[b] Analysed mineral, grain size and number of grains in the mineral separate

[c] Sample location, easting and northing, Universal Grid Reference, zones 50 and 51.

Table 5.1 Continued.

	3447±6 (Chapter 4)				Swarm.
Minimum age exhumation gneisses	<age granite gneiss	**3341±17**	96 %	3349±21	T_1 Cooling age.
Exhumation gneiss complex ?	Crystallization age 3426±4 (Chapter 4)	**2240±43**	32 %	2235±14	T_1 Thermally reset.
Minimum age thrust fabric	< ~3450 (age Salgash Subgroup).	**No plateau**	---	1997±87	Unknown geological relevance
Minimum age mylonite	<3315±5 Ma (Chapter 4)	**2809±28**	64 %	2711±15	T_1 Thermally reset age associated with the lower Fortescue episode.
Minimum age NNE-tectonic transport ?	< 3313±9 Ma (Barley and Pickard, 1999)	**3281±18**	99 %	3277±17	T_1 Cooling after crystallization granite? Thermally reset age associated with D_{X+3}? T_2 step 2, 2819
Minimum age NNE-tectonic transport ?	< 3313±9 Ma (Barley and Pickard, 1999)	**3210±16**	72 %	3174±17	T_1 Cooling after crystallization granite, or reset age associated with regional phase.
Minimum age dextral shearing, related to W-vergent thrusts?		**2911±366 inverse isochron age**	---	3812±74	T_1 Crystallization age ?
Crystallization age dyke	< 3433±2 Ma < 3417±9 Ma > 3313±9 Ma	**3356±21**	40 %	3338±22	T_1 Cooling after crystallization or reset age.
Crystallization age dyke	< 3433±2 Ma < 3417±9 Ma > 3313±9 Ma	**3440±58**	37 %	3212±38	T_1 Cooling after crystallization
Crystallization age dyke	< 3433±2 Ma < 3417±9 Ma > 3313±9 Ma	**3186±18**	19 %	2980±23	T_1 Reset age.

5.2 Structural history of the marble bar domain and available ^{40}Ar-^{39}Ar ages

The structural history of the eastern part of the Marble Bar Domain has been discussed in Chapters 2, 3 and 4 and is summarised in figure 5.1. The location of the main structures is presented in figure 5.2. The main structures include i) a mid-crustal extensional detachment called the Mt Edgar Shear Zone active during magmatic activity at ca. 3.46-3.42 Ga (D_{X+1}) and reactivated at 3.32-3.31 Ga (D_{X+2E}) (Chapters 2 and 3), ii) a set of faults and mafic dykes in the Kelly Greenstone Belt, that were interpreted to be related to syn-extensional deposition of the upper Salgash Subgroup, during a late stage of D_{X+1} (Chapter 4), iii) W-verging thrusts, including the Hilly Basalt and Brockman Hay Shear Zones, in the western Warrawoona Belt, possibly formed during regional E-W compression (D_{X+2C}) that was related to emplacement of 3.31 granitoids (D_{X+2E}) (Chapter 2), iv) a regional WNW-trending foliation and local thrusts related to (N)NE-(S)SW compression during D_{X+3} (Chapter 2), and v) the dominantly dextral transcurrent Central Warrawoona Shear Zone, D_{X+4}, possibly related to the kinematically compatible 2.95-2.93 Ga strike-slip deformation on the Mulgandinah Shear Zone (Zegers et al., 1998a; Chapter 2).

Deformation activity on the MESZ during D_{X+1} and D_{X+2} was temporally constrained by dating syntectonic intrusions using SHRIMP U-Pb zircon geochronology (Figure 3.20). The subsequent compressional and strike-slip deformation structures could not be further temporally constrained using this method because of lack of identified syntectonic granitoid components. Cross-cutting relationships with stratigraphic units and intrusive rocks of known age has led to an interpretation in which these structures were attributed to deformation phases D_{X+3} and D_{X+4}, both of which are post 3.31 Ga and pre-2.77 Ga (See figure 2.17).

Previous ^{40}Ar-^{39}Ar isotope chronology in the Eastern Pilbara, including spot fusion and whole rock and mineral incremental heating studies, focussed on the Shaw Granitoid Complex and the surrounding Tambourah and Coongan Greenstone Belts in the western part of the Marble Bar Domain (Wijbrans and McDougall, 1987; Davids et al., 1997; Zegers et al., 1996, 1999). Figure 5.3 lists the available ^{40}Ar-^{39}Ar cooling ages, in relation to the igneous ages determined from the then available U-Pb zircon crystallization ages and the structural history of the area (after Zegers et al., 1999). The figure shows the available ^{40}Ar-^{39}Ar ages with respect to the episodes of igneous activity as named by Nelson et al. (1999). Zegers et al. (1996, 1999) related the oldest age to deposition of the ca. 3515 Ma Coonterunah Group. A hornblende cooling age of 3466±13 Ma was attributed to cooling after granitoid intrusion and extension on the Split Rock Shear Zone during the Warrawoona episode (Zegers, 1996). Six cooling-ages cluster at ca. 3.24-3.18 Ga and these were attributed to cooling associated with E-W compression after regional amphibolite facies metamorphism in both the Tambourah Belt (Wijbrans and McDougall, 1987) and in the Coongan Belt (Zegers, 1996; Davids et al., 1997; Zegers et al., 1999). A semi-continuum of ages in the Shaw Granitoid Complex ranges from ca. 3.10 to ca. 2.80 Ga. Zegers et al. (1999) attributed most of these younger ages to a phase of craton-scale sinistral strike-slip deformation on the Mulgandinah Shear Zone and extensive coeval granitoid emplacement, that was dated using U-Pb on zircon at 2.95-2.93 Ga (Zegers et al., 1998a). A hornblende cooling age of the Black Range Dyke Swarm, associated with deposition of the Fortescue Group and dated at 2772 ± 2 Ma using SHRIMP U-Pb

on baddeleyite (Wingate, 1999) was determined at ca. 2800 Ma (Zegers et al., 1999). The only cooling age possibly associated with the Wyman episode is a poorly constrained hornblende cooling age of 3309 ± 118 Ma, from rocks of the Talga Talga Subgroup in the Coongan Greenstone Belt.

5.3 Methodology

5.3.1 Approach

This study was designed to provide age constraints for specific deformation events in the eastern Marble Bar Domain. The deformation history is based on detailed mapping of structures and intrusive relationship, and SHRIMP dating as reported in Chapters 2, 3 and 4. Below, the timing of deformation phases is constrained by determining ^{40}Ar-^{39}Ar isotopic ages of K-bearing minerals with known relationships to deformation fabrics. K-bearing minerals with either a syntectonic or post-tectonic relationship to specific deformation phases were identified, characterised and separated from the specimen. These minerals were then dated to determine their cooling ages using the ^{40}Ar-^{39}Ar stepwise heating method as described by Wijbrans et al. (1995). The obtained cooling ages were then used to constrain the ages for the structure and the associated deformation phase.

5.3.2 The ^{40}Ar - ^{39}Ar method and the meaning of plateau ages

The ^{40}Ar-^{39}Ar method is based on the decay of ^{40}K to ^{40}Ar with a half-live time of 1.72×10^{10} years (Steiger and Jäger, 1977). It can be used to determine the age of K-bearing rocks and single minerals, including muscovite, biotite and hornblende. In this method, a sample is first irradiated by fast neutrons that convert some ^{39}K to ^{39}Ar. The sample is subsequently heated in vacuum and the ^{40}Ar/^{39}Ar ratio of the gas emitted is measured. This ratio is proportional to ^{40}Ar/^{40}K, and thus proportional to the age. The heating of the sample can be done in steps. The advantage of stepwise heating is that argon gas from parts of the crystal that are most susceptible to disturbance of the argon system (causing either argon loss or gain) is extracted in the first steps. Argon derived from crystal sites that are less easily disturbed and therefore more likely to represent the cooling age are extracted in subsequent steps. An undisturbed age is characterised by an argon age plateau, defined as at least three consecutive steps with ages within 2s of their weighted average and representing a considerable amount of the total argon gas (McDougall and Harrison, 1988). True plateau's are relatively rare in Precambrian basement rocks (e.g. Wijbrans and McDougall, 1987; Zegers et al. 1999), but when disturbance of the argon system is minor, still valuable age information can be extracted. Zegers et al. (1999) used the term semi-plateau to characterise these samples that display a minor disturbed system.

A plateau age reflects the moment of final cooling of a particular mineral to below its closure temperature (T_c). T_c in a cooling system is the temperature at which the diffusion of argon gas has become negligibly small (Dodson, 1973). Each mineral species has a specific T_c, reflecting the ease with which Argon can move through the crystal lattice. T_c depends on the type of mineral, but also

on the diffusion parameters grain size and shape, as well as cooling rate (See Dodson, 1973 and McDougall and Harrison, 1988 for a discussion). T_c for commonly used minerals are ~525 ± 25°C (hornblende), ~350 ± 30°C (white mica) and 300 ± 20°C for biotite (Harrison, 1981; Harrison et al., 1985; McDougall and Harrison, 1988; Spear, 1995; Lips, 1998). Hence, a plateau age of a hornblende sample reflects cooling below ~500-550°C, for muscovite it reflects cooling below ~350°C, for biotite cooling below ~300°C. ^{40}Ar-^{39}Ar ages from igneous minerals may represent the time of cooling directly after crystallization of a magma, or cooling due to tectonic uplift and denudation. An ^{40}Ar-^{39}Ar age from a (contact-) metamorphic mineral may represent cooling after contact metamorphism or cooling after regional metamorphism. Because argon is a noble gas, which is extremely mobile compared to for example U and Pb isotopes in zircon, the argon isotope system in a crystal is sensitive to thermal resetting. Both igneous and metamorphic minerals may undergo thermal resetting, either by contact metamorphism, or after a regional prograde metamorphic event related to tectonic activity (Harrison and McDougall, 1980). The temperature interval of closure/resetting of hornblende (500-550 °C, Harrison, 1981; Harrison et al., 1985; McDougall and Harrison, 1988) falls within the range of the metamorphic stability field of hornblende (as illustrated by Lips, 1998). This allows growth of hornblende crystals without disturbing the argon system of older hornblende crystals. The interpretation of ^{40}Ar-^{39}Ar dates is complicated, however, by the observation that the isotope system may be reset at temperatures much lower then those calculated for thermal diffusion when rocks recrystallized under the influence of fluids (Villa, 1998). This means that ages from recrystallized samples, may be erroneously interpreted to reflect cooling below the closure temperature. Therefore, a micro-structural study is necessary to select appropriate rocks and minerals. In addition, micro-structural characterisation of selected minerals is necessary to understand the geological significance of the obtained ^{40}Ar-^{39}Ar age.

A potential pitfall in studying the timing of the early deformation phases in the Marble Bar Domain may be its long tectonic and magmatic history. Villa (1998) has argued that resetting of ^{40}Ar-^{39}Ar systematics can occur in a relatively short period and at temperatures much lower than the T_c by a process that is based on resetting by thermal diffusion. Given the susceptibility of the argon isotopic system to resetting, the emplacement of 3.31 Ga granitoids in the Mt Edgar Granitoid Complex and the Corunna Downs Granitoid Complex during D_{X+2} may have largely reset any older argon signature. It is thus possible that the ^{40}Ar-^{39}Ar ages mainly only reflect late thermal events.

5.3.3 End-member scenarios for the thermal development of the Mt. Edgar Shear Zone

As ^{40}Ar-^{39}Ar ages obtained in this study may reflect late thermal events only, two end member scenarios for the timing of initial cooling of the MESZ are formulated to address the significance of the obtained argon ages.

In the first scenario, a single phase of exhumation and cooling of the MESZ occurred at ca. 3325-3310 Ma. In this model, the domal development and the position of the dome above the ~500°C isograd was largely coeval with extension and emplacement of the granitoids during D_{X+2E}. In this case the hornblende argon isotope signature throughout the MESZ is largely the effect of

closure of the isotope system by exhumation and cooling to below the T_c of hornblende at this stage, and possibly of local new hornblende growth.

In the second scenario, the MESZ may already have been partly exhumed to a position of the dome above the ~500°C isograd before 3325 Ma, during doming as an effect of extension at D_{X+1}. In this case 3.46-3.43 Ga ^{40}Ar-^{39}Ar ages may be preserved, and 3325-3310 Ma ^{40}Ar-^{39}Ar ages may develop by thermal resetting and new hornblende growth.

These models will be tested by dating the 3.46-3.43 Ga intrusive component from the MESZ using the ^{40}Ar-^{39}Ar method: if argon ages corresponding to the timing of D_{X+1} are identified, this indicates that development of the domal geometry of the MESZ and MEGC during D_{X+1} was significant and we can rule out that doming solely occurred at 3.32-3.31 Ga. If, however, argon ages of this age are not identified, both end-member scenarios remain valid.

5.3.3 Sample preparation and analytical methods and conditions

After microscopic investigation of thin sections (See sample description below), the hand specimen were crushed and divided into grain-size fractions of <125 μm, 125-250 μm, and 250-500 μm depending on the size of the minerals of interest. All of the grain size fractions were washed in demineralized water to remove the dirt fraction and dried at 50ffiC. The fractions were passed along a Franz magnet-separator for the separation of hornblende. Hornblende is slightly magnetic, and can be separated from the non-magnetic and the highly magnetic minerals by passing the fractions using the settings of 125, 150, 175 and >175 mA at 5 degrees front and side slope. Hornblende crystals were hand-picked from the purest hornblende fraction(s). For the separation of muscovite and biotite, the washed fractions were transported over a Faul vibration table to select the most platy crystals. All crystals were handpicked under a binocular microscope equipped with both reflected and transmitted light mode. Selection aimed to exclude those grains with inclusions, fractures and/or alterations. The selected grains were ultra-sonically cleaned in water.

Twenty-seven mineral separates with 2 to 16 grains per separate (See table 5.1) were placed in aluminium trays, which were then irradiated as part of batch VU-29 at the ECN/EU high flux research reactor in Petten, The Netherlands, for 150 hours. ANU standard biotite GA-1550 (K/Ar age 97.9 Ma) was used as flux monitor (McDougall and Harrison 1988, Wijbrans et al. 1995). A slight gradient during irradiation caused the irradiation parameter (J) to vary within 2% per tray. The uncertainty of J for each mineral separate was estimated to be in the order of 0.5%. The value of J for each separate is listed in appendix 1

Stepwise heating experiments were conducted using the VULKAAN argon laser-probe facility at the Vrije Universiteit in Amsterdam. Details of argon extraction and purification techniques have been described by Wijbrans et al. (1995). Five argon isotopes (^{40}Ar, ^{39}Ar, ^{38}Ar, ^{37}Ar and ^{36}Ar) were measured using a noble gas mass-spectrometer. Corrections were made for atmospheric argon and argon produced by Ca and K during irradiation (for irradiation batch VU-29: $(^{40}Ar/^{39}Ar)_K$= 0.010240, $(^{39}Ar/^{37}Ar)_{Ca}$= 0.000699, $(^{36}Ar/^{37}Ar)_{Ca}$= 0.000270). The measured amounts of ^{37}Ar and ^{39}Ar were corrected for decay since irradiation. The discrimination factor for the mass spectrometer was determined at 1.0068 from repeated measurement of atmospheric argon during this study.

System blanks were measured after every four steps. Each two succeeding blanks were used for correcting the measured unknowns in between. The raw data was reduced using ArArCalc software developed at the Vrije Universiteit by A. Koppers (Koppers, 2002). The processed data are listed in appendix 3.

5.4 Selected minerals and their relationship to deformation

Twenty-one hand specimen were selected for mineral separation and ^{40}Ar-^{39}Ar dating. The locations of the hand specimen with respect to the main structures in the eastern Marble Bar Domain are shown in figure 5.2. More detailed maps of sample locations are provided by figures 3.6, 3.8 and 4.4 for the areas near Cotton Well, Trig Well and the Kelly Belt, respectively. Hand specimen were taken from components of the Mt Edgar Shear Zone (n=15), from mafic dykes of the Salgash Dyke Swarm within the Kelly Greenstone Belt (n=2) and from areas with structures related to regional deformation phases D_{X+2C}, D_{X+3} and D_{X+4}, in the Corunna Downs Granitoid Complex (n=1) and in the adjacent Marble Bar and Warrawoona Greenstone Belts (n=3).

From these 21 hand specimen, 27 mineral fractions were selected for dating. Of these handspecimen, six samples yielded two mineral fractions, either of different species or of different size. They were selected to represent different stages in the (micro)structural development. Below is a description of the hand specimen, the sample locality, the macro- and microscopic structures and a description of the minerals that are selected for dating and their relationship to the structures in thin section. A summary is presented in table 5.1.

5.4.1 Samples from the Mt Edgar Shear Zone

Fifteen hand specimens were selected from components of the MESZ to put time constraints on the pre-3.31 Ga structural development. Figure 5.2 shows overall sample locations. The samples were collected from the Mixed Zone, the central part of the MESZ, as this is where deformation focussed and where the intricate relationship between deformation and intrusions is most clear. Care was taken to select some samples away from 3.31 Ga granitoids as much as possible, as these may have caused resetting of the argon signature. The structural history of the Mixed Zone has been compiled and discussed in chapter 3 (See figure 3.14 for an overview). This history incorporates the structures, kinematics and metamorphic grade of deformation, the timing of intrusions of the main components and available crystallization ages. The argon samples were selected in this framework. The samples have crystallization ages between 3466 ± 2 Ma and 3309 ± 4 Ma (see chapter 4). In addition to the samples in the Mixed Zone, two samples were selected from the footwall gneisses and the greenstone sequence that forms the hangingwall to the MESZ.

Samples **CTW-36** and **P97-233** were collected from undeformed parts of the oldest recognised intrusive component of the MESZ, the 3462 ± 4 Ma hornblende-gabbro/diorite complex (Figure 3.16a), in the western and eastern Mixed Zone, respectively (see figure 5.2 for sample location and 3.7 for more detail). Both samples showed a coarse-grained isotrope magmatic texture. Sample

CTW-36 yielded two fractions of hornblende crystals of similar elongate, euhedral to subhedral shape, but of different size and colour: one fraction contained dark-green crystals generally smaller that 250 μm, the other contained green crystals, generally 250-400 μm in length. The hornblendes

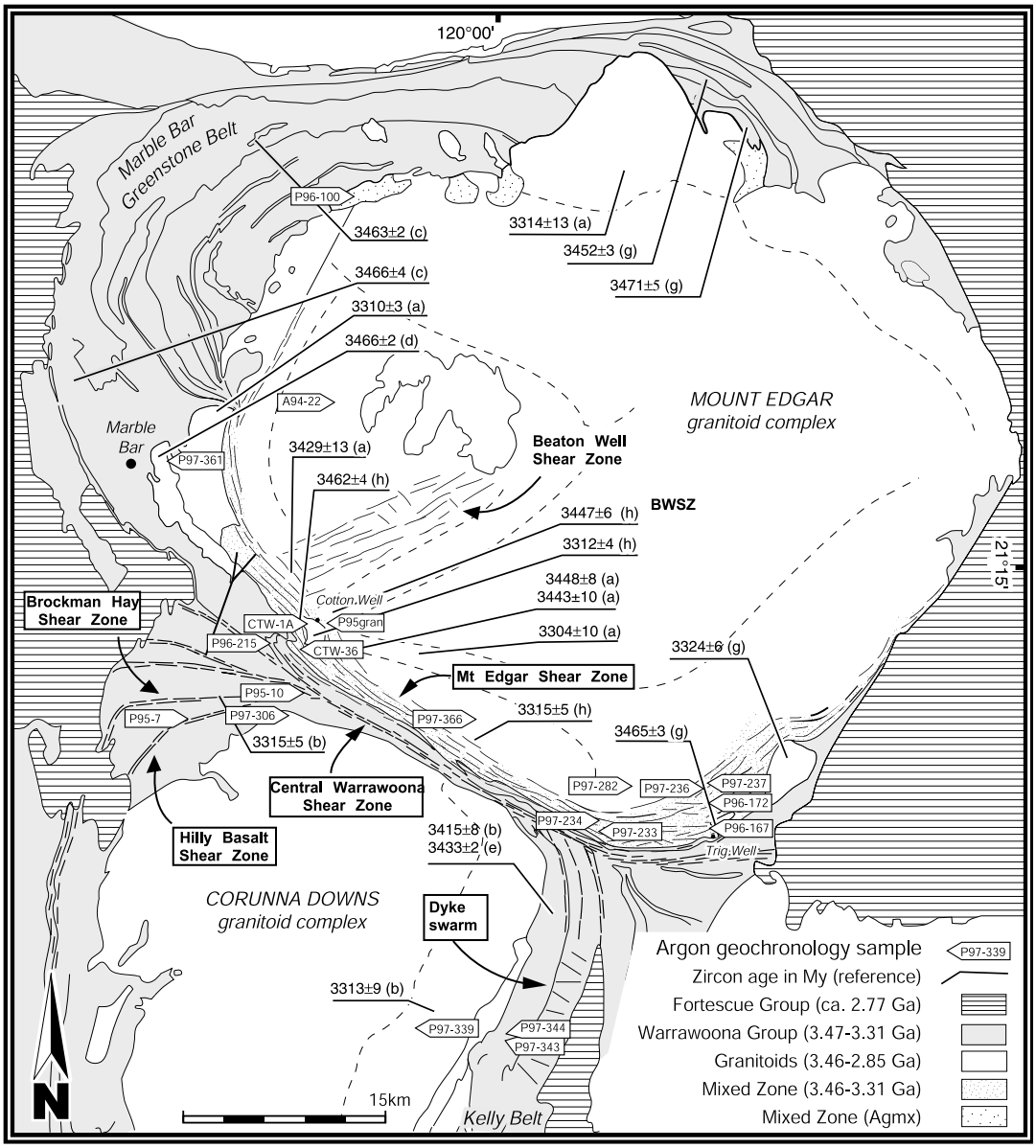

Figure 5.2 Generalised lithological map showing the main shear zones and argon sample localities in the eastern part of the Marble Bar Domain. Available geochronological data is indicated, references as listed in figure 2.2. Coordinates of samples are listed in table 5.1

of sample P97-233 are dark green fragments of ca. 200 μm in diameter. Resulting cooling ages may reflect crystallization of the hornblende-gabbro/diorite complex. Alternatively, they may reflect cooling after exhumation.

Sample **P97-366** comes from an undeformed mafic pegmatite associated with a km-scale raft of hornblende-gabbro/diorite within granitoid gneisses in the area between the Cotton and Trig Well (See figure 5.2 for sample location). Both the gabbro and the gneisses were intruded by granite veins of unknown age. This sample yielded elongate dark-green euhedral magmatic hornblende crystals from a magmatic texture. Resulting cooling ages may reflect crystallization of the undeformed mafic pegmatite.

Samples **P97-234** and **P97-237** are from the eastern Mixed Zone, from schistose ultramafic xenoliths within undeformed parts of the 3462 ± 4 Ma hornblende-gabbro/diorite complex as is described in chapter 2 (See figure 5.2 for sample location and 3.9 for more detail). Thin sections of both samples show randomly orientated, euhedral to anhedral hornblende that was interpreted to be part of a contact metamorphic fabric. Hornblende of sample P97-237 shows local intergrowths with biotite. Eleven light green, 150-200 μm, hornblende fragments were selected from sample P97-234. Seven dark green, 250-400 μm, hornblende crystals were selected from sample P97-237. Resulting cooling ages may reflect cooling after crystallization of the hornblende-gabbro/diorite complex, or cooling after exhumation of that part of the MESZ.

Samples **P96-172** and **P97-236** are from the eastern Mixed Zone, from zones in the hornblende-gabbro/diorite complex with a coarse foliated and lineated fabric defined by hornblende, that was attributed to $D_{MESZ,X+1A}$ as described in chapter 3 (See figure 5.2 for sample location and 3.9 for more detail). Thin sections of both samples confirmed that the fabric is defined by hornblende. Seven 200-400 μm and eight 200-250 μm, dark green subhedral hornblende crystals were selected for dating, respectively. Resulting ages may reflect cooling after crystallization and formation of the fabric within the hornblende-gabbro/diorite complex, or cooling after exhumation of that part of the MESZ.

Sample **P97-361** is from undeformed alkali-feldspar granite, one of the oldest intrusive rocks of the MESZ, attributed to component 3 (See Figure 3.13) near Marble Bar, and designated 'Aga' on the GSWA map (Hickman and Lipple, 1972). The sample was collected using explosives and was dated at 3466 ± 2 Ma by Nelson (1998a). This age confirmed that it is the intrusive equivalent of the Duffer Formation as was proposed on geochemical grounds by Hickman (1983) (See figure 5.2 for sample location and 4.5 for more detail). As can be seen in figure 4.5, the 'Aga' granite was intruded by dolerite dykes of the Salgash Dyke Swarm and by the 3310 ± 3 Ma Pyramid Well Pluton to the east (Nelson, 2000). In thin section the sample is a coarse grained alkali-feldspar granite, with randomly grown magmatic biotite that is locally chloritised, overgrown by randomly orientated muscovite blasts. The muscovite blasts are interpreted to reflect contact metamorphism of either the dolerite dykes or the Pyramid Well Pluton. Four biotite crystals of ca. 250 μm were selected for dating. Their cooling age may reflect cooling after crystallization of the granite. Three <250 μm muscovite crystals were selected. Their cooling age may reflect cooling after muscovite blastesis.

Sample **P96-215** comes from an andalusite-muscovite-quartz mylonite from a partly mylonitised felsic volcanic unit in the hangingwall margin of the Mixed Zone near the Cotton Well area (see

figure 5.2 for sample location and 2.8a for more detailed setting). This felsic volcanic unit was dated in the Trig Well area (along strike to the east, see figure 3.4) at 3465 ± 3 Ma and attributed to the Duffer Formation by Thorpe et al. (1992). Kyanite and sillimanite-bearing assemblages were reported for this unit (Collins and Van Kranendonk, 1999; see also chapter 2). The larger part of the exhumation of these metamorphic assemblages has been related to extension during D_{X+2} (See chapter 2) or to diapirism (Collins and Van Kranendonk, 1999). Thin section analysis of this particular sample shows that the mylonitic fabric is formed by white mica, quartz and andalusite and contains an S/C fabric indicating NE-up kinematics. Fourteen metamorphic (mylonitic) muscovite crystals (<150μm) were selected for dating. Their cooling age may provide a minimum age for the mylonite foliation and hence for the exhumation of this part of the MESZ.

Sample **P96-167** was collected from a dolerite sill that intruded parallel to the mylonitic foliation within felsic mylonites of the MESZ in the Trig Well area (See figure 5.2 for sample location and 3.9 for more detailed setting). This dolerite sill has been attributed to intrusive component 5a in chapter 3 (See figure 3.15). The handspecimen shows an aligned fabric defined by hornblende. Thin section analyses revealed small (<250 μm) blue-green hornblende crystals that are strongly aligned (attributed to $D_{MESZ,X+1B,}$ in chapter 3). These are overgrown by larger (>250 μm) equidimensional hornblende blasts (attributed to $D_{MESZ,X+2}$, see figure 3.14j). In chapter 3 it was shown that hornblende blasts may have overgrown a mylonitic foliation as a result of intrusion of the Boodallana Suite at ca. 3315-3310 Ma (D_{x+2}). Five ca. 250 μm equidimensional hornblende crystals were selected to represent the blast population. Their age may provide an age for the thermal pulse that caused their growth. Eleven <250 μm elongate euhedral hornblende crystals were selected to represent the strongly aligned fabric. Their age may reflect the timing of fabric development or the thermal event that caused the blastesis.

Sample **P96-100** is from an E-W trending mylonitic dolerite on the NW margin of the MEGC, interpreted to be a remnant of the Mixed Zone (See figure 5.2 for sample location). The mylonitic dolerite has intruded granitic gneiss and was intruded along its margin by a granite sill of unknown age. In hand specimen the mylonitic foliation is defined by hornblende and plagioclase, with the hornblendes showing a strong lineation. In thin section two hornblende populations are observed: small prismatic crystals (<250 μm) that lay aligned in the mylonitic fabric, and larger (>250 μm) equidimensional hornblende blasts that overgrow the foliation. Hornblende was selected from both populations. Six <250 μm elongate and euhedral hornblende crystals were selected to represent the mylonitic fabric. Their age may represent the age of the fabric. Four >250 μm equidimensional euhedral hornblende crystals were selected to represent the blasts. Their age may represent the timing of the thermal event that caused blastesis, likely to be the intrusion of the adjacent granite sill.

Sample **CTW-1A** is from the Cotton Well Pluton (See figure 5.2 for sample location and 3.7 for a more detailed map). It was attributed to intrusive component 8 in chapter 3 (See figure 3.13) with a crystallization age of 3309 ± 04 Ma (Figure 3.16e). The muscovite in this pluton defines a magmatic foliation (See § 2.4.3.3.2). The pluton was found to have intruded during the late stages of D_{X+2}. Two cm-scale muscovite crystals were selected for analyses. Their age may reflect the crystallization age of the pluton, or cooling during exhumation.

Sample **P95-gran** was collected from a syntectonic intrusive sheet of leucogranite (Attributed to

intrusive component 6, figure 3.15) near the footwall gneisses of the MESZ in the Cotton Well area (See figure 5.2 for sample location and 3.7 for a more detailed map). The SHRIMP U-Pb zircon age of this particular sheet is 3447 ± 6 Ma (See figure 3.16b). In thin section, the sample shows an isotropic magmatic fabric containing undulose quartz and small, randomly grown muscovite flakes. Four muscovite crystals (<100μm) were selected for analysis. Their age may reflect the timing of cooling associated with exhumation of the footwall gneisses of the MESZ.

P97-282 was taken from a fine-grained mafic xenolith within footwall gneisses of the MESZ, both of unknown age, in the Trig Well area (See figure 5.2 for sample location and 3.9 for a more detailed map). In thin section it contains strongly aligned light to dark green idiomorphic hornblende crystals that are overgrown by larger hornblende porphyroblasts. Three 100-250 μm idiomorphic hornblende crystals were selected to represent the strongly aligned hornblende population. Larger hornblende porphyroblasts all contained inclusions and were not used for analysis. The resulting age may reflect the age of the fabric, the thermal event that caused the blastesis, or the cooling as a result of exhumation of the footwall gneisses.

Sample **A94-22** was collected from the subhorizontal grey granodiorite sheet (component *gn-2*, figure 3.15), dated at 3426 ± 4 Ma (Figure 3.16c) in the Central Gneiss Complex, part of the footwall of the MESZ (see figures 5.2 and 3.10 for sample location and 3.11b for outcrop detail). In thin section it contains a quartz-rich recrystallized fabric with chloritised biotite overgrown by random muscovite crystals, the latter suggesting a post-tectonic thermal event. Four muscovite crystals were selected for analyses. Their age may represent the timing of cooling due to exhumation of the Central Gneiss Complex.

5.4.2 Samples from structures in the Warrawoona Belt related to D_{X+2}

Sample **P95-7** was taken from an actinolite-chlorite-carbonate mylonite zone in the basaltic units of the western Warrawoona Greenstone Belt, south of the Central Warrawoona Shear Zone (See figure 5.2 for sample location, see figure 2.8a for more detail on the structures of the Warrawoona Belt). The mylonite is part of the W-vergent Hilly Basalt Shear Zone (See figure 2.8a and figure 5.2), and transparent light green actinolitic hornblende crystals form an E-plunging mineral lineation. Sixteen 100-200μm actinolitic hornblende crystals were selected for analysis. Their age may provide a minimum age for the W-vergent trusting (D_{X+2C}, figure 2.17). Within the Hilly Basalt Shear Zone, more towards the Central Warrawoona Shear Zone, the stretching lineation is subvertical to steeply SW-plunging. Here, sample **P95-10** was collected from a muscovite-quartz ultra-mylonite (See figure 5.2 for sample location, see figure 2.8a for more detail on the structures of the Warrawoona Belt) in the felsic unit attributed to the Wyman Formation (3315 ± 5 Ma, R.Buick, unpubl. data in: Barley and Pickard, 1999). Eleven 80-150μm muscovite crystals were selected for analyses. Their cooling age may reflect the timing of development of the fabric, which, in combination with that of sample P95-7, may provide additional constraints on the timing of compression and extension associated with D_{X+2} (See chapter 2).

5.4.3 Sample from NNE-SSW compressional structures related to D_{X+3}

Sample **P97-339** is from the 3313 ± 9 Ma Carbana Pool Adamellite (Barley and Pickard, 1999). The handspecimen shows an undeformed, coarse grained magmatic texture, containing primary biotite and hornblende, which were both selected for analyses. On outcrop scale, structures in the Carbana Pool Adamellite comprise cm-wide 030° to 020°-trending subvertical dextral strike-slip shears and associated 310° to 320°-trending subvertical foliations and NNE-vergent thrusts, which have been related to a phase of (N)NE-(S)SW compression (See figure 5.2 for sample location, and figure 2.8b for the geometry of structures). Both 12 biotite crystals (~250 μm) and 9 hornblende crystals (~300 μm) were selected for analyses. The ^{40}Ar-^{39}Ar ages of the hornblende and biotite may provide an age for cooling below the closure temperature of hornblende after crystallization of the CPA. In addition, the biotite may reflect thermal effects of the regional phase of compression (D_{X+3}).

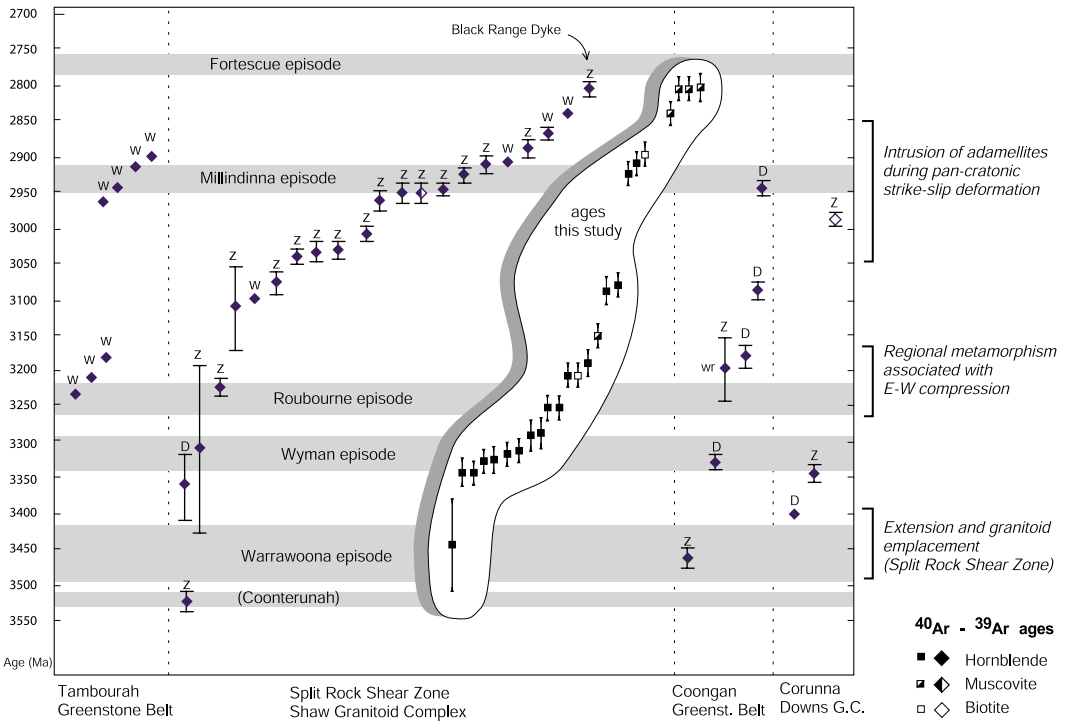

Figure 5.3 An overview of Argon ages obtained in this study and available ^{40}Ar-^{39}Ar chronological data and tectonic interpretation after Zegers (1996), Zegers et al. (1999) for the Pilbara granite-greenstone terrain. W= Wijbrans and McDougall (1987), D= Davids (1997), Z= Zegers et al. (1999). Igneous episodes based on SHRIMP U-Pb zircon ages are summarised in figure 3.2 and are after Nelson et al. (1999).

5.4.4 Sample from a structure related to dextral transcurrent movement during D_{X+4}

Sample **P97-306** was collected from northern margin of the Corunna Downs Granitoid Complex, from a mafic schistose xenolith at the contact of the granite and greenstone belt (See Figure 5.2 for sample location and figure 2.8a for more details on the structures). S/C relationships in the granite and the xenoliths indicated a dextral horizontal component of movement. Actinolitic hornblende crystals in the xenoliths defined a mineral elongation lineation with a pitch of 20-30ffl to the NW. Based on the similarity of structures and kinematics, these minerals were related to deformation phase D_{X+4}. Twelve (>500μm) actinolitic hornblende crystals were selected for analysis. The ^{40}Ar-^{39}Ar age of the actinolite may yield an age for deformation during D_{X+4}.

5.4.5 Argon samples from the mafic dyke swarm in the Kelly Greenstone Belt

Two samples were collected from two mafic dykes to determine the age of the mafic Salgash Dyke Swarm in the Kelly Greenstone Belt (See figure 5.2 for sample locations, and figure 4.3 for more detail on the structures). A summary of the geological setting and the geological implications of the dyke swarm in this area has been presented in chapter 4. Both dykes intruded a felsic volcanic unit dated at 3417 ± 9 and 3433 ± 2 Ma (Barley et al., 1998a; Nelson, 2000). The dyke represented by sample P97-344 is intruded by the one represented by P97-343. Apart from local subvertical 020-trending fractures, the dykes show no evidence for internal deformation.

Sample **P97-344** was collected from a subvertical, 2-3 metre wide WNW-trending internally undeformed coarse grained diorite dyke. The sample shows a dominantly igneous texture with olive to dark-green subhedral hornblende and zoned plagioclase grains, with minor chlorite, epidote and opaques. Two hornblende separates were selected from sample P97-344: both contained equidimensional, non-transparent light to dark-green hornblende, of ~300 μm and ~200 μm, respectively.

Sample **P97-343** was collected from a subvertical, 1-2 metre wide fine-grained mafic dyke. The sample has an igneous texture with pyroxene, hornblende and zoned plagioclase. The hornblende crystals are locally chloritised. Ten 300-600 μm euhedral hornblende crystals were selected for analysis.

Based on the upper crustal setting of the dykes, and on the microstructures, the ages are expected to yield cooling ages that are near their crystallization age. A maximum crystallization age of the dyke swarm is provided by the age of the 3417 ± 9 Ma / 3433 ± 2 Ma felsic volcanic unit that it intruded, and a minimum age is provided by the 3313 ± 9 Ma Carbana Pool Adamellite (See figure 4.3).

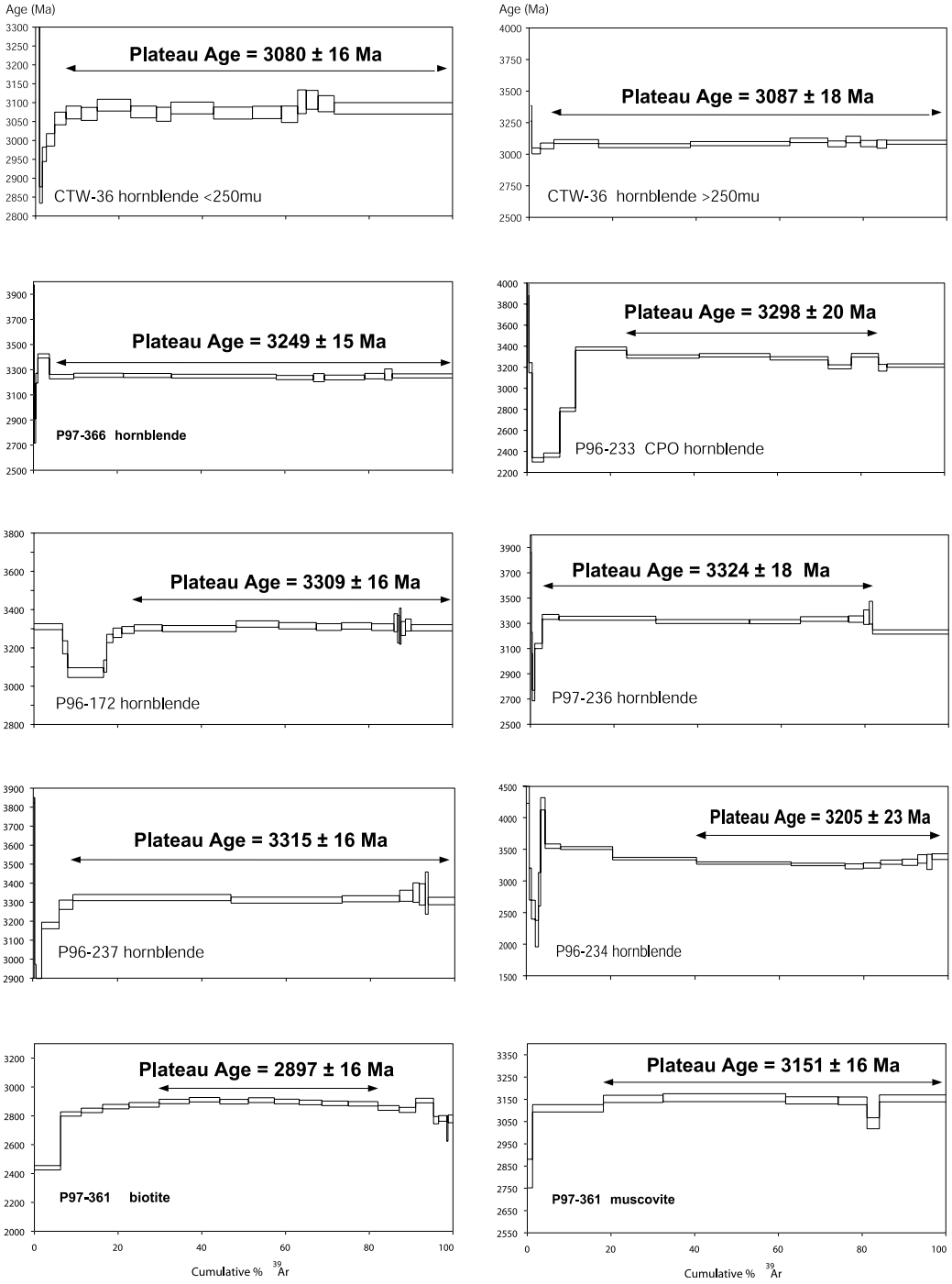

Figure 5.4 ^{40}Ar-^{39}Ar age spectra from samples of the Mt Edgar Shear Zone.

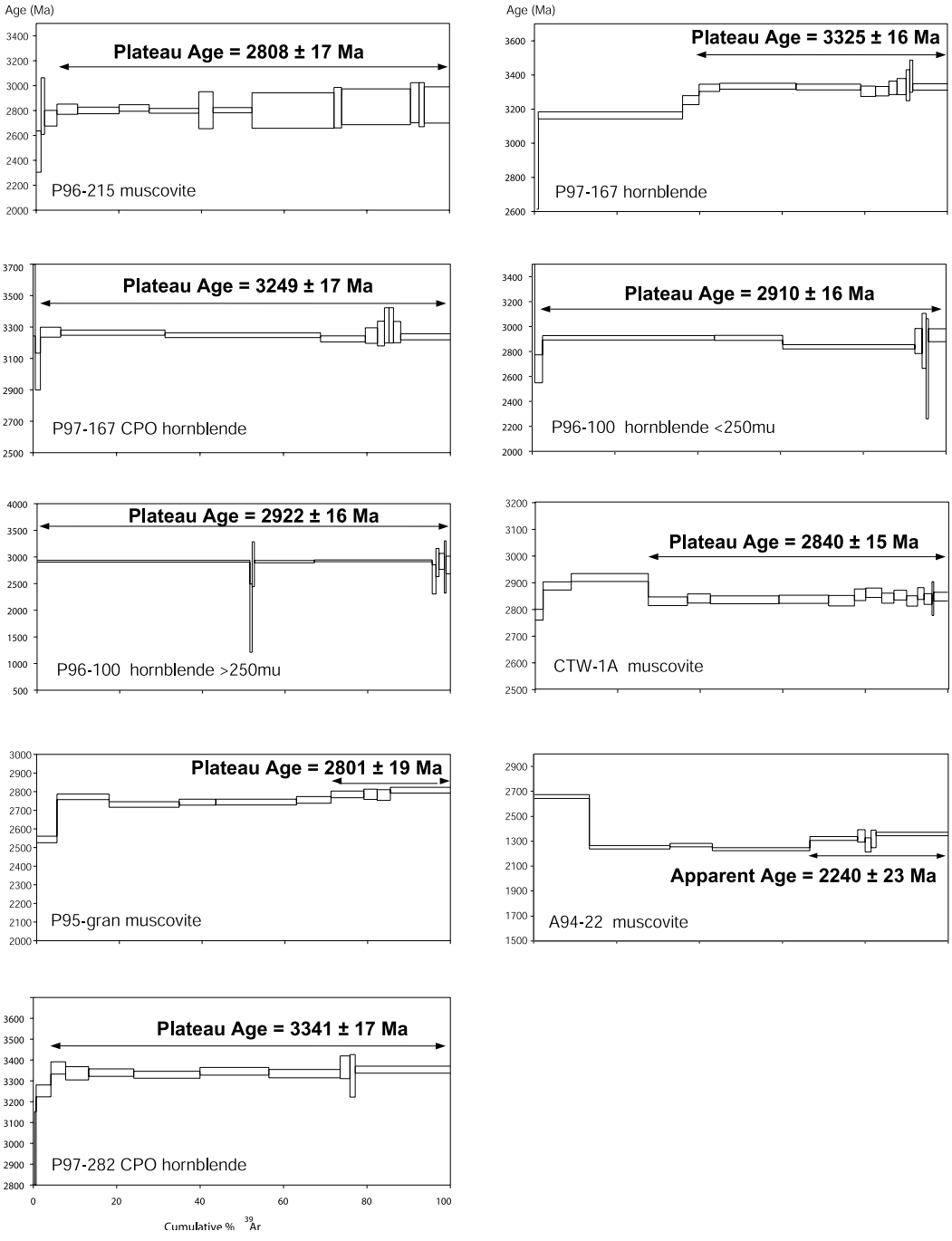

Figure 5.4 Continued.

5.5 Age spectra and interpreted ^{40}Ar-^{39}Ar ages

Figures 5.4, 5.5, 5.6 and 5.7 illustrate the argon release spectra of 24 mineral separates from 21 samples. The data for these spectra is listed in appendix 3.

Of the total of 24, 22 ^{40}Ar-^{39}Ar release spectra show well defined plateau ages. Of these, twenty-one plateau ages range between 3440 ± 58 Ma and ~2800 Ma, with most clustering around 3340-3200 Ma. The obtained ages are consistent with available SHRIMP U-Pb zircon crystallization ages (See chapter 3), i.e. the ^{40}Ar-^{39}Ar isotopic ages are equal or younger than the crystallization ages (See bottom figure 5.9). The ages are listed in tables 5.1 and 5.2. A diagram with the obtained plateau ages with respect to the igneous episodes of the Marble Bar Domain is presented in figure 5.3 and is the basis for further discussion on the implications of the ages for the structural development discussed in §5.6. Below, the results are described and interpreted in the context of their local setting and microstructures.

5.5.1 Age spectra and interpretation related to D_{X+1} or D_{X+2} from the Mt Edgar Shear Zone

Hornblendes from undeformed parts of the oldest recognised intrusive components of the MESZ, the hornblende-gabbro/diorite complex dated at 3462 ± 4 Ma in chapter 3, yield well defined plateaus (94-96% of the released ^{39}Ar). Sample **CTW-36** yields hornblende plateau ages of 3080 ± 16 and 3087 ± 18 Ma, sample **P97-366** is dated at 3249 ± 15 Ma (See appendix 3 for the processed data, figure 5.4 for age spectra). Sample **P96-233** yields an age of 3298 ± 21 Ma (based on 55% of the released ^{39}Ar). The total fusion age of sample P96-233 is ~50 m.y. younger than the plateau age, indicating argon loss in part of the crystal domain, notably of the domains that are tapped in the first heating steps (See spectrum in figure 5.4, and see table 5.1 for a summary). The ages of sample CTW-36 are interpreted to reflect resetting of the argon systematics. The other two ages may either reflect resetting or a cooling age.

Deformed zones within the hornblende-gabbro/diorite complex yielded hornblende plateau ages, with 76% and 79% of the released ^{39}Ar, of 3309 ± 16 and 3324 ± 18 Ma, from aligned hornblendes of samples **P96-172** and **P97-236,** respectively. The ages are interpreted to either reflect the age of resetting of the argon systematics, or of cooling.

Hornblendes from the schistose xenoliths within the hornblende-gabbro/diorite complex yielded hornblende plateau ages of 3315 ± 16 Ma (**P97-237**) based on 91% of the released ^{39}Ar, and 3205 ± 23 Ma (**P97-234**) based on 60% of the released ^{39}Ar. The ages are interpreted to either reflect the age of resetting of the argon systematics, or of cooling.

The alkali-feldspar granite (**P97-361**) dated at 3466 ± 2 Ma (Nelson, 1998a) yielded plateau ages of 3151 ± 16 Ma and 2897 ± 16 Ma from muscovite and biotite, based on 79% and 52% of the released ^{39}Ar, respectively. The first step of the muscovite yielded an age of 2820 ± 64 Ma, within error of that of the biotite plateau age, which suggests that both these ages are due to resetting.

The small (<250μm), magmatically aligned hornblendes from sample **P96-167** of the mylonitised dolerite sill yielded a well defined plateau age of 3249 ± 17 Ma (based on 98% of the released ^{39}Ar). The >250 μm overgrowing hornblende porphyroblasts obtained a plateau age of 3325 ± 16 Ma

(based on 60% of the released ^{39}Ar). The two hornblende populations of sample P97-167 were selected to determine the age of the relative $^{40}Ar/^{39}Ar$ age of the aligned fabric attributed to D_{X+1} (See figure 3.15) and the porphyroblasts proposed to be the contact metamorphic effect of granitoid intrusion at the base of the MESZ during D_{X+2}. The ages of the two corresponding hornblende populations, however, were not consistent with their microstructural relationships (marked 'fabric' and 'blasts' in figure 5.9). The cooling age of the aligned, smaller hornblende crystals is ~75 m.y. younger than the cooling age of the hornblende porphyroblasts. If the ages of both populations are the affect of thermal resetting due to diffusion, at ca. 3250 Ma, then their relative ages could be explained in terms of their relative size: as the larger porphyroblasts have longer diffusion paths, they are more difficult to reset, which would explain their relatively high age with respect to the smaller crystals. Alternatively, the selected crystals may not have been representative for their population. The in-situ spot fusion method (Wijbrans et al., 1995) may provide better grip on the analysed crystal and its structural context.

The small (<250 μm), strongly aligned hornblendes from sample **P96-100** of the mylonitised dolerite sill yields a plateau age of 2910 ± 16 Ma (based on 66% of the released ^{39}Ar). The >250 μm overgrowing hornblende porphyroblasts yield a well-defined plateau age of 2923 ± 16 Ma (based on 99% of the released ^{39}Ar). Like sample P96-167, the relative age of these two populations is opposite to what would be expected from their overprinting relationships. A possible explanation is similar to the one discussed for sample P96-167.

Magmatic muscovite crystals from the Cotton Well Pluton (**CTW-1A**) yield a well defined plateau ages of 2840 ± 15 (based on 73% of the released ^{39}Ar). Randomly overgrown muscovite in the leucogranite (**P95-gran**) yields a poorly defined plateau age of 2801 ± 19 Ma based on 29% of the released ^{39}Ar. In this same area, mylonitic muscovite from the felsic volcanic unit on the hangingwall margin of the MESZ (**P97-215**) yields a well-defined plateau age of 2808 ± 17 Ma (based on 95% of the released ^{39}Ar). All three ages are interpreted to reflect the age of resetting of the argon systematics, possibly associated with the Lower Fortescue episode.

Hornblendes from the mafic mylonitic xenolith in the grey gneisses of the footwall in the Trig Well area (**P97-282**) yield a well-defined plateau age of 3341 ± 17 Ma (based on 96% of the released ^{39}Ar). The age is interpreted as a cooling age.

Randomly grown muscovite crystals from the 3426 ± 4 Ma granodiorite sheet in the Central Gneiss Complex (sample **A94-22**) yield an age of ca. 2240 Ma based on only 32% of the released ^{39}Ar. The age is interpreted to reflect resetting of the argon systematics.

The significance of these ages in terms of the thermal development of the MESZ and MEGC is discussed in §5.6 in combination with the results described below.

5.5.2 Age spectra and interpreted ages from the area with compressional structures related to $D_{X+2}C$

Actinolitic hornblende and muscovite from samples **P95-7** and **P95-10** were analysed to constrain the age of the west-verging movement on the Hilly Basalt Shear Zone, and to time the relationship between E-W compression (D_{X+2C}) and NE-SW extension (D_{X+2E}) (see chapter 2).

Neither the muscovite from P95-10 nor the actinolite from P95-7 yield a well defined plateau

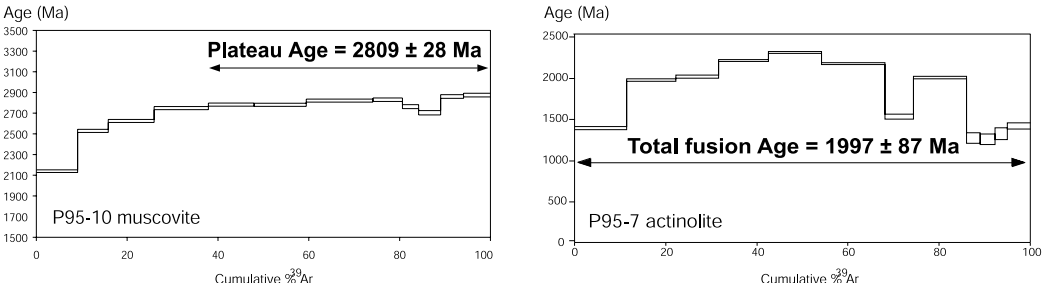

Figure 5.5 ^{40}Ar-^{39}Ar age spectra from minerals related to D_{X+2} structures in the Warrawoona Greenstone Belt.

age (See figure 5.5). During twelve heating steps on the muscovite (P95-10) step ages increased from ca. 2100 Ma in the first step to ca. 2870 in the last two steps, with a total fusion age of 2711 ± 15 Ma (Figure 5.5, appendix 3). A poorly defined plateau of the last 8 steps, with 60% of the total gas, yields an age of 2809 ± 28 Ma. This age is similar to the age of the basal flood basalt unit of the Fortescue Group (Arndt et al., 1991) and the related Black Range Dyke Swarm (Wingate, 1999; Zegers et al., 1999) a member of which intruded approximately 1.5 km to the NW (Figure 2.4a). No plateau age was obtained for the actinolitic hornblende crystals of sample P95-7. The total fusion age is 1997 ± 87 Ma. The geological relevance of this age is unclear.

Most samples from this western part of the Warrawoona Greenstone Belt and MESZ (See figure 5.2) show some indication for thermal resetting at ca. 2.8 Ga. This is further discussed below.

5.5.3 Age spectra and interpreted ages from the Carbana Pool Adamellite with structures related to D_{X+3}

Hornblende and biotite from the 3313 ± 9 Ma (Barley and Pickard, 1999) Carbana Pool Adamellite (CPA, sample **P97-339**) were measured to test whether the argon system would reflect a cooling after crystallization, or if the isotope system was affected by deformation during a phase of regional (N)NE-(S)SW compression.

The hornblende and biotite separates from sample P97-339 both yield well defined plateau ages. The nine hornblende crystals yield an eleven-step plateau age of 3281 ± 18 Ma based on 99% of the

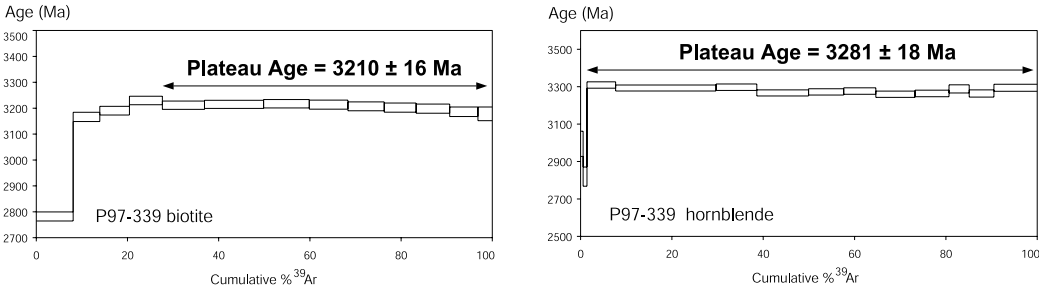

Figure 5.6 ^{40}Ar-^{39}Ar age spectra from minerals related to D_{X+3} structures in the Carbana Pool Adamellite, part of the Corunna Downs Granitoid Complex.

released gas (Figure 5.6). The biotite crystals yielded a nine-step plateau age of 3210 ± 16 Ma corresponding to 72% of the released gas (Figure 5.6). The first steps of both the hornblende and the biotite analyses yielded a date of around 2.80 Ga. This suggests that the isotope system of the most accessible parts of the crystals were reset as the effect of intrusion of the Black Range Dyke Swarm or deposition of the Fortescue group.

Both the 3281 ± 18 Ma and 3210 ± 16 Ma ages can be interpreted as reset ages related to the phase of (N)NE-(S)SW compression, D_{X+3}, associated with deformation in the granite at the sample site. The biotite age of 3210 ± 16 Ma, however, is temporally more consistent with a regional thermal event at ca. 3.20 Ga that has been associated with a phase of E-W compression, folding and thrusting. We tentatively interpret the 3281 ± 18 Ma to reflect resetting of the hornblende associated with deformation during D_{X+3}. An alternative interpretation may be slow cooling after crystallization, which is further discussed in section §5.6.2. The 3210 ± 16 Ma age of the biotite is the oldest ^{39}Ar -^{40}Ar biotite plateau age world-wide reported to date.

5.5.4 Age spectra and interpreted ages from the area with compressional structures related to D_{X+4}

Actinolitic hornblende of sample **P97-306** was collected to determine the age of dextral transcurrent shearing along the northern margin of the Corunna Downs Complex, related to deformation phase D_{X+4}. The argon release spectrum yielded no plateau age (Figure 5.7). The total fusion age was 3812 ± 74 Ma, suggesting excess argon. A poorly defined inverse isochron age of 2911 ± 366 Ma confirms that this sample was affected by excess argon, such that the age is unreliable.

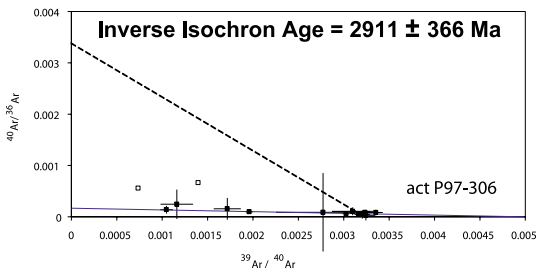

Figure 5.7 ^{40}Ar-^{39}Ar age spectra from actinolitic hornblende related to D_{X+4} structures on the margin of the Warrawoona Greenstone Belt and the Corunna Downs Granitoid Complex.

5.5.5 Age spectra and interpreted ages from the mafic dykes in the Kelly Greenstone Belt

The larger hornblende crystals of the diorite dyke (sample **P97-344)** yield a 5-step plateau age (based on 37% of the released ^{39}Ar) of 3440 ± 58 Ma (Figure 5.8). The eight slightly smaller crystals yielded an argon release spectra of which the last two steps (19% of the released ^{39}Ar) give an age of 3186 ± 18 Ma, which does not qualify as a plateau age. The hornblende crystals of the dolerite dyke (sample **P97-343)** yielded a poorly defined 5-step plateau age based on 40% of the released ^{39}Ar, giving an age of 3356 ± 21 Ma.

We interpret the 3440 ± 58 Ma age to be a cooling age, providing a minimum age for the crystallization of the dyke. However, the dyke cannot be older than the felsic volcanic sequence it intruded, dated at 3417 ± 9 and 3433 ± 2 Ma (Barley et al., 1998a; Nelson, 2000). Yet, the 58 Ma error on the argon date allows an interpretation in which the dyke intruded any time after

deposition of the felsic sequence to up to ~3380 Ma. The other age obtained from this sample, 3186 ± 18 Ma, is unlikely to reflect the crystallization age of this dyke, because this is not consistent with the intrusive relationship with the 3313 ± 9 Ma Carbana Pool Adamellite. As disturbance of the argon system depends on grain size, the smaller grains may preferentially have been reset. Possibly this was associated with deformation that caused the 020-trending fractures.

The 3356 ± 21 Ma age from sample P97-343 is interpreted to be a cooling age, providing a minimum age for the intrusion and crystallization of this dolerite/pyroxenite dyke. This age is consistent with the age of the host rock and the 3440 ± 58 Ma cooling age of the adjacent dyke. It can be concluded that the emplacement of this dyke has not reset the argon system of the adjacent one.

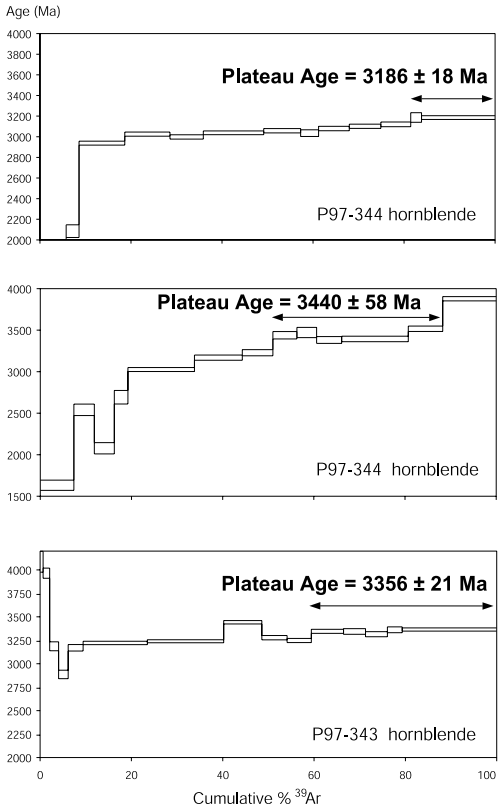

Figure 5.8 ^{40}Ar-^{39}Ar age spectra from hornblende related to crystallization of mafic dykes in the Kelly Greenstone Belt.

5.6 Discussion

The main aims of this ^{40}Ar-^{39}Ar study were three-fold: i) To determine whether the development of the steep domal geometry of the MESZ was initiated during D_{X+1} at ca. 3.45 Ga. ii) To further constrain the timing of the deformation phases D_{X+2}, D_{X+3} and D_{X+4}. iii) To constrain the age of emplacement of the upper crustal Salgash Dyke Swarm in the Kelly Belt.

Twenty-two out of 24 argon release spectra showed well defined plateau ages. The implications of these ages is discussed below. In addition, the thermal evolution of the currently exposed crust with respect to ^{40}Ar -^{39}Ar systematics is discussed in a regional sense.

5.6.1 The thermal history of the Mt Edgar Shear Zone – implications for the timing of doming

Sixteen samples were selected from the MESZ to test if their argon age would reflect any cooling of the MESZ corresponding to the timing of the early development of the MESZ and extension during D_{X+1} between ca. 3462-3410 Ma (See figure 3.21). None of them has. The total of

ages obtained from the MESZ span ~85% of its history, ca. 550 m.y., between 3350 Ma and 2800 Ma (Figure 5.9). The oldest ages clustered around 3341-3290 Ma. These ages indicates that the eastern MESZ had largely cooled below ~500°C (the lower margin of the T_c range, see §5.3) at 3341/3290 Ma, and did not experience temperatures in excess of ~500°C after this time. This age range corresponds in time with compression, extension and felsic magmatism of D_{X+2} at ca. 3315 Ma, which confirms the interpretation that by the end of this phase the MESZ was a well established upper crustal structure (chapter 2).

Two younger ages of 3249 ± 15 Ma and 3249 ± 17 Ma have been obtained from hornblendes of a mafic pegmatite in the hornblende-gabbro/diorite complex (P97-366) and from a mylonitic fabric in a dolerite dyke (P96-167), respectively. These ages could be explained to reflect the last stages of doming of the MESZ, and final upward movement of the MESZ into upper crustal levels. Alternatively, the ages could reflect resetting due to granite intrusion. In chapter 3, zircon recrystallization and resetting was found to correspond in age to the 3260-3240 Ma Roebourne episode (See figures 3.2 and 3.3). A granitoid of this age has recently been identified in the central MEGC (Nelson, 2000, see figure 3.4). Even though this particular granitoid is too far away to have had direct influence, magmatism associated with this phase may have been more wide-spread, and related heat and/or fluids of yet unidentified granitoids may have disturbed the hornblende isotopic signature.

Nine samples from the MESZ show younger plateau ages of ca. 3150, 3080, 2930, 2850 Ma, and ca. 2800 Ma (See figure 5.9). These were interpreted to indicate resetting. Yet, no tectonomagmatic events corresponding to these ages have been reported for the MESZ, apart from mafic magmatism of the Fortescue Group, which makes it difficult to discuss potential causes for resetting. Therefore, the significance of the younger ages is discussed in the larger context of the history of the Marble Bar Domain in §5.6.4. Notably, seven of these younger ages are from the western MESZ (See figure 5.2), whereas all of the older, 3.3 Ga, ages have been obtained from samples in the eastern part of the MESZ. Apparently, resetting was locally induced and focussed on the western MESZ. It must be noted, however, that all of the older argon ages were obtained from hornblende, whereas the younger ages are from hornblende, muscovite and biotite, the latter with lower closure temperatures which makes them more susceptible to resetting.

Two potential pitfalls should be regarded when the implications of the absence of argon ages related to D_{X+1} are discussed. Firstly, the sampling density may not have been sufficient to sample potential older ages. Secondly, as mentioned in the introduction, K-bearing minerals are susceptible to fluid and deformation assisted recrystallization and resetting of $^{40}Ar - ^{39}Ar$ systematics. As the MESZ is a shear zone that has acted as a preferential site for the emplacement of granitoid sheets at ~3.31 Ga (See chapter 3), it is possible that the granitoids have caused resetting of the isotope system.

In summary, no evidence has been found that the MESZ moved through the 500°C isograd (the closure temperature of hornblende) during D_{X+1}. Therefore, there is no basis to conclude that doming, coupled with exhumation/denudation and cooling was substantial during this phase. Based on the observations to date, it is concluded that the eastern part of the MESZ was situated at upper crustal levels, above the 500°C isograd, from ca. 3341 Ma, and has remained there from 3290 Ma onwards.

5.6.2 Timing of compressional phases D_{X+2}, D_{X+3}, and D_{X+4}

For the timing of E-W compression related to NE-SW extension, D_{X+2C}, no additional constraints were obtained. The samples P95-7 and P95-10 did not yield plateau ages, and the significance of their unreliable total fusion ages of 1997 ± 87 Ma and 2711 ± 15 Ma is unclear.

For the timing of NE-SW compression, D_{X+3}, ages were obtained from hornblende and biotite from the Carbana Pool Adamellite (sample P97-339). Both the 3281 ± 18 Ma (hbl) and 3210 ± 16

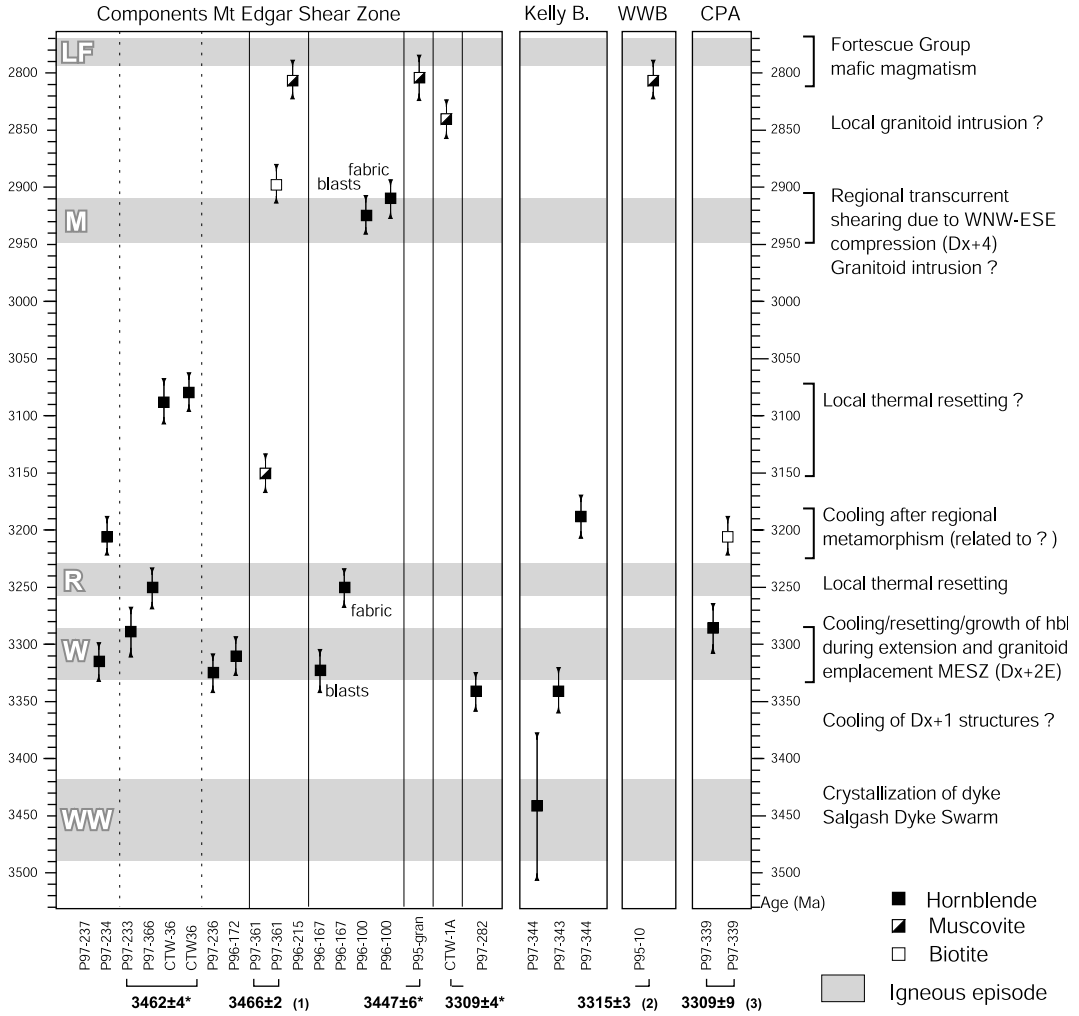

Figure 5.9 Overview of the obtained Argon data and interpreted relationship to the igneous episodes (after Nelson et al., 1999, see also figure 3.2) and to the tectonic history (see figure 3.3) of the eastern Pilbara. WW= Warrawoona episode, W= Wyman episode, M= Millindinna episode, R= Roebourne episode, LF= Lower Fortescue episode. * SHRIMP U-Pb zircon ages, this study (Chapter 3); 1= Nelson (1998), 2= Buick, unpublished data, in: Collins et al. (1998); 3= Barley and Pickard (1999).

Ma (biotite) ages can be interpreted as reset ages related to the phase of (N)NE-(S)SW compression, D_{X+3}, associated with deformation in the granite at the sample site. Alternatively, the magmatic nature of the hornblende and the biotite, in combination with the lack of evidence for recrystallization, may be taken to suggest that the ages reflect cooling after crystallization of the granite. In this interpretation the granite cooled to below 500-550°C (Tc of hornblende) at 3281 ± 18 Ma, and ~300°C (T_c of biotite) at 3210 ± 16 Ma (McDougall and Harrison, 1988; Spear, 1995). In a conservative interpretation of the time-span between the ages, the time from intrusion at 3313 ± 9 Ma (Barley and Pickard, 1999) to cooling below 500-550°C at 3281 ± 18 Ma is >5 m.y. Cooling from the temperature of a granitic melt in de upper crust of ca. ~1000°C (Philpotts, 1990) to below Tc of hornblende of 500°C in 5 m.y. infers a minimum cooling rate of 100°C/m.y., or $0.001x10^{-1}$°C/y. This rate appears to be low compared to cooling rates expected for granites that intrude high crustal levels. We tentatively interpret 3281 ± 18 Ma to reflect resetting of the hornblende associated with deformation during D_{X+3}.

For the timing of strike-slip deformation related to NW-SE compression, D_{X+4}, a poorly defined inverse isochron age of 2911 ± 366 Ma (sample P97-306) was obtained. This age is consistent with an interpretation that the dextral transcurrent shearing on the southern margin of the Warrawoona Belt was related to regional strike-slip deformation at 2950-2930 Ma, however, due to the large uncertainty this age does not provide any realistic constraint.

5.6.3 Timing of intrusion of the Salgash Dykes in the Kelly Belt

Two mafic dykes in the Kelly Belt were dated: a 3440 ± 58 Ma diorite/gabbro dyke (P97-344) and a 3356 ± 21 Ma dolerite/pyroxenite dyke (P97-343) (See figure 5.9). These ages were interpreted as cooling ages after intrusion and crystallization of the dykes. These dykes are associated with mafic magmatism and deposition of basalts of the Euro Basalt on top of the Panorama Formation. The Panorama Formation has been dated at ca. 3415 ± 8 Ma (Barley et al., 1998) in this area, which provides a direct minimum age for the Euro Basalt and which is consistent with the age of the dykes.

The ages indicate a difference in age between the two dykes, which suggests that the Salgash Dyke Swarm was emplaced over a prolonged period of time: the Dyke Swarm may comprise multiple suites. The occurrence of multiple suites is consistent with the observations in the Mixed Zone, where two different suites of dykes/sills have been recorded: doleritic (component 5a) and ultramafic (component 5b) (see Figure 3.13). These components cannot be temporally related to the dykes in the Kelly Belt because they are older: a maximum age for these components is provided by the 3447 ± 6 Ma leucocratic granite vein that intruded them (See figures 3.20 and 3.21) and are similar in age to the Apex Basalt.

The 3356 ± 21 Ma age obtained from the dolerite/pyroxenite dyke is younger than the 3.42 to 3.41 Ga upper age bracket generally quoted for the Warrawoona Group and for the Warrawoona igneous episode (see figure 3.2). A recent finding, however, has suggested that mafic magmatism of the Euro Basalt was more prolonged than previously assumed: a zircon population of 3346 Ma in a silicified felsic tuff one kilometer from the top of the Euro Basalt in the Kelly Belt (Nelson, 2001)

was interpreted to represent the eruptive age of the tuff (M. Van Kranendonk and L. Bagas, Geological Survey of Western Australia, unpubl. data. In: Van Kranendonk et al., 2002). Irrespective of the interpretation of the age of the felsic unit that yielded this zircon population, the fact that this 3346 Ma population exists, together with another population dated at 3363 Ma in the same sample indicates that zircons were crystallizing at this period in time. This, combined with xenocrystic zircons of similar age as well as Wyman age both in the felsic tuff and in the overlying sedimentary units (Nelson, 1998, 1999) leads us to interpret these data to indicate that deposition of the Euro Basalt has been over a period from at least 3395 to at least 3346, possibly but not necessarily to ca. 3310 Ma. The preserved 3356 ± 21 Ma argon age obtained for the dolerite/pyroxenite is more consistent with an interpretation in which the upper Euro Basalt was deposited during or shortly after 3356 ± 21 Ma, otherwise this age would have been reset.

5.6.4 Significance of ^{40}Ar-^{39}Ar ages unrelated to magmatism in the Marble Bar Domain

Most of the ^{40}Ar-^{39}Ar ages in this study relate to known igneous episodes within the Marble Bar Domain (See figure 5.9) and can either be related to cooling after crystallization or thermal resetting. Other ages cluster around ca. 3200, 3150, 3080, and 2850 Ma (Figure 5.9). The significance of these ages is discussed here in the context of the tectonomagmatic history of the Marble Bar Domain.

Three argon ages were found to cluster around 3200 Ma: from hornblende of a schistose mafic xenolith within the MESZ, from hornblende in the Kelly Belt and from biotite in the Carbana Pool Adamellite (CPA) (See figure 5.9). The first two ages were interpreted to reflect resetting of the argon signature, the biotite from the CPA age may reflect slow cooling. Regionally, ages that cluster around 3200 Ma have been been related to regional amphibolite facies metamorphism associated with E-W compression. This thermal event was first recognised in the Tambourah Belt (Wijbrans and McDougall, 1987) and subsequently in the Coongan Belt (Davids et al., 1997; Zegers et al., 1999). The relationship between this thermal event and the areas from which the three associated ages were obtained in this study is unclear. The structural relationship between E-W compression and the ~3200 Ma age from the MESZ may be explained by local strike-slip reactivation of the MESZ at that stage (See chapter 2). For the Kelly Belt and the Carbana Pool Adamellite, however, a relationship is not clear as E-W compressional structures have not been documented in these areas. A similar date for a thermal event was reported based on whole-rock Rb-Sr work by Williams and Collins (1989). These workers attributed the age to either a thermal resetting or a late closure of the isotope system.

Argon ages of ca. 3150 and 3080 Ma were found in the MESZ (See figure 5.9). These ages cannot be linked to any igneous episode in the Marble Bar Domain. However, igneous rocks of this age have been identified in the area to the west, Domain 3 (See figure 3.2) and are abundant in the West Pilbara (Nelson et al., 1999). These igneous episodes may have had a thermal effect on the rocks in the Marble Bar Domain.

A 2840 ± 15 Ma muscovite cooling age was found for the Cotton Well Pluton (See figure 5.9). This age is similar to the age of late granites such as the crystallization age of the Cooglegong Adamellite in the Shaw Granitoid Complex, dated at 2851 ± 2 Ma (Nelson, 1998a) and the

Moolyella Adamellite (Nelson, 2000) in the centre of the Mt Edgar Granitoid Complex (See figure 5.3). Possibly, the ~2840 Ma age is related to a thermal pulse associated with this phase.

Three ca. 2810 Ma ages were obtained from three muscovite separates, one from the MESZ basement gneisses, one from the mylonitised felsic volcanic rocks in the hangingwall, and one from the undeformed 'Aga' K-feldspar granite in the hangingwall (See figure 5.9). These ages are within error of the age of the onset of the Fortescue episode (Nelson et al., 1999), that involved intrusion of the Black Range Dyke Swarm and deposition of mafic flood basalt of the lower Fortescue Group throughout the Pilbara Craton at ca. 2.77 Ga (Arndt et al, 1991; Wingate, 1999, Zegers et al., 1999). Dykes belonging to this dyke swarm observed in the vicinity of the samples may have caused local thermal overprinting. Additionally, as the basal unit of the Fortescue Group largely filled a relief at a level that is only metres removed from the present day outcrop level (Hickman, 1983), the deposition of the flood basalt may also have had a thermal effect on the directly underlying rocks.

5.6.6 Implications for the overall thermal history of the eastern part of the Pilbara granite-greenstone terrain

The ^{40}Ar-^{39}Ar ages of hornblende and micas in the Pilbara granite-greenstone terrain span the 700 m.y. history of the area, as is illustrated in figures 5.3 and 5.9, covering the time-span during which this terrain formed. Therefore it may be concluded that, considering the susceptibility of the argon isotope system for thermal overprinting, conditions during the development of the crust were such that older ^{40}Ar-^{39}Ar ages have been preserved. Therefore, it must be concluded that these conditions were of relatively low to medium ambient temperatures and pressures, which is consistent with general field observations. As this wide range in ages is also observed within the local sections of the study area, it can be concluded that resetting and thermal overprinting occurred at conditions not above low to medium T and P and over (at present) relatively short distances. This has previously been noted by Zegers et al. (1999) for the data available around the Shaw Granitoid Complex. These workers argued that a wide range in ages is due to localised resetting of the argon isotope system. This is considered to be the effect of preferential intrusion of granites, a difference in heat conductivity between granite and greenstones, and localisation of fluids in shear zones.

In contrast to this matching range of argon ages, a discrepancy between time-spans of SHRIMP U-Pb zircon ages and ^{40}Ar-^{39}Ar ages is observed in the Late Archaean Superior Province of Canada. Whereas the crystallization ages in this Late Archaean terrain vary between 2.75 Ga and 2.65 Ga (U-Pb, zircon), the ^{40}Ar-^{39}Ar ages are largely younger, between 2.57 Ga to 2.0 Ga (Lee et al., 1990; Lopez Martinez and York, 1990; Hanes et al., 1992, 1994). This has been attributed to resetting as the result of a regionally active fluid and thermal events (Lopez Martinez and York, 1990; Kerrich and Keyser, 1994). In the Pilbara, flood basalt erupted and a dyke swarm intruded as part of the Mount Bruce Supergroup of the Hamersley Province (Blake, 1993) during the lower Fortescue igneous episode starting at ca. 2.77 Ga (Arndt et al, 1991; Wingate, 1999; Zegers et al., 1999) Ages throughout the area covered by ^{40}Ar-^{39}Ar dating have been interpreted to reflect local resetting by this thermal event (See figures 5.3 and 5.9). The ages from the Cotton Well area and those from the Carbana Pool Adamellite are examples of this. Yet, magmatism of this episode apparently only

affected the argon system at a local scale, leaving many older argon isotope systems undisturbed. The picture that emerges is that of rocks which locally preserve a thermal and tectonic record of the early, *essentially from 3.4 Ga,* stabilisation of the continental crust.

The preservation of Warrawoona Episode-age thermal signature in the Marble Bar Domain has implications for the interpretation of recent geophysical data. Wellman (2000) interpreted gravity and magnetic data to show that the base of the granitoid complexes and greenstone belts throughout the Pilbara granite-greenstone terrain is subhorizontal and located at ~14 km depth. One of the consequences of this interpretation is that, when the average diameter and the depth of the granitoid complexes are compared, the granitoid complexes are flat, tabular bodies. This may have implications for the emplacement mechanism of the granitoids that constitute the granitoid complexes. Namely, the tabular geometry of the granitoid complexes is not easily compatible with models of solid-state diapirism and partial convective overturn, models that are generally illustrated with equidimensional granitoid bodies (e.g. fig. 13 in Van Kranendonk et al. 2002). Collins et al. (1998), however, argued that the age of this mid-crustal discontinuity is not known and that this basal boundary could have developed at a relatively late stage in the history of the Pilbara Craton. The forming of such a boundary after development of the granite-greenstone terrain would require removal or thermal reorganisation of a substantial part of the base of the granite-greenstone terrain. This would have a profound regional thermal effect on the overlying crust. The preservation of the relatively old ^{40}Ar-^{39}Ar ages, and the spread of ^{40}Ar-^{39}Ar ages throughout the 700 m.y. history of the Marble Bar Domain indicates that such dramatic thermal effect has not occurred in the history of the area. The complex thermal signature suggests that the 14 km boundary developed progressively as the result of a tectonic and magmatic history, stretched out over more than 700 million years.

5.7 Conclusions

1. The obtained ^{40}Ar-^{39}Ar ages define a 640 m.y. time span, from ca. 3440 to ca. 2800 Ma, indicating that the eastern Marble Bar Domain of the Pilbara granite-greenstone terrain contains a well preserved record of thermal and tectonic events dating back to the age of deposition of the Warrawoona Group. The ^{40}Ar-^{39}Ar ages of this study provide constraints for the timing of development of the Marble Bar Domain.

2. ^{40}Ar-^{39}Ar isotopic ages show that the eastern part of the MESZ was situated at upper crustal levels from ca. 3341 Ma, and has remained there from 3290 Ma onwards. This suggests that compression, extension, doming and granitoid emplacement during D_{X+2} caused the MESZ to leave the mid-crust. No argon ages correspond with the timing of D_{X+1}. Therefore, there is no basis to conclude that doming of the Mt Edgar Granitoid Complex and the MESZ was substantial during D_{X+1}.

3. No ^{40}Ar -^{39}Ar isotopic constraints were obtained for the timing of compressional structures

associated with D_{X+2}. Selected samples yielded no plateau ages.

4. A 3281 ± 18 Ma hornblende plateau age from the Carbana Pool Adamellite of the Corunna Downs Granitoid Complex was interpreted to reflect resetting as the result of (N)NE-(S)SW compression during $D_{X+3.}$, and provides a minimum age for this phase.

5. A poorly defined 2911 ± 366 Ma inverse isochron age for actinolitic hornblende (P97-306) is consistent with an interpretation that dextral transcurrent shearing on the southern margin of the Warrawoona Belt (D_{X+4}) was part of regional WNW-ESE compression at ca. 2.91 Ga. Two hornblende samples from the eastern MESZ have reset ages in the same range.

6. A diorite/gabbro and dolerite/pyroxenite dyke of the Salgash Dyke Swarm in the Kelly Belt, associated with deposition of the Euro Basalt, yielded ^{40}Ar -^{39}Ar ages of 3440 ± 58 Ma and 3356 ± 21 Ma, respectively. These ages were interpreted to reflect cooling after crystallization and are consistent with timing of deposition of the Euro Basalt. The ages indicate the occurrence of multiple suites within the Salgash Dyke Swarm.

7. Other findings include: i) Two ~3250 Ma hornblende ages from the MESZ are taken to represent cooling after local thermal resetting, possibly as the result of granitoids this age in the MESZ footwall. ii) Two ~3200 Ma hornblende ^{40}Ar-^{39}Ar ages in the eastern MESZ and the Kelly Belt, and one biotite of similar age in the Carbana Pool Adamellite are interpreted to represent resetting, tentatively attributed to E-W compression, dated at ca. 3200 Ma in the western part of the Marble Bar Domain. iii) ages of ~3150 Ma (biotite) and ~3080 Ma (hornblende) are obtained from the MESZ, but the significance of these ages is unclear iv) A 2840 ± 15 Ma muscovite age from the 3312 ± 4 Ma Cotton Well Pluton was interpreted to reflect thermal resetting. v) Three ~2810 Ma muscovite ages were obtained from the footwall and the hangingwall of the MESZ. These ages are interpreted to reflect resetting associated with mafic magmatism of the Lower Fortescue Group throughout the Pilbara Craton, dated at ca. 2.77 Ga (Arndt et al, 1991; Wingate, 1999, Zegers et al., 1999).

8. The preservation of argon ages in the eastern part of the Pilbara granite-greenstone terrain ranging from Early to Mid Archaean strongly suggests that the geological history of this area affected rocks that at that time, and since, represented the upper levels of the continental crust.

Chapter 6

Synthesis, discussion and conclusions

6.1 Introduction

The objective of the present study was to provide insight into the relative importance of horizontal tectonic processes and diapiric processes in the development of Early and Mid Archaean terrains world-wide. The specific aim of this study was to determine the relationship between horizontal and vertical tectonics during the development of the Early to Mid Archaean structural architecture of the Marble Bar Domain, by identifying and studying the main structures, the deformation history, and the role of associated magmatism. Time constraints on deformation, crystallization and cooling/denudation were provided by combined SHRIMP U-Pb zircon chronology and ^{40}Ar-^{39}Ar isotope chronology (VULKAAN laser-probe).

In this chapter, after a summary of the main findings of this study, the structural and magmatic development of the study area is integrated with the tectono-magmatic history of the Marble Bar Domain as a whole.The tectonomagmatic history then serves as a basis for further discussion of the causal relationship between deformation and magmatism, and the possible tectonic settings and underlying geodynamic behaviour of the Earth throughout the ~800 m.y. history of the Marble Bar Domain.

6.2 Main findings of this study

1. The main deformation structures in the Mt Edgar Granitoid Complex and selected parts of the surrounding greenstone belts include the Mt Edgar Shear Zone, an originally mid-crustal detachment, mainly preserved along the SW half margin of the Mt Edgar Granitoid Complex; the Beaton Well Zone, which acted as a transfer zone to the Mt Edgar Shear Zone within high-grade gneisses of the Mt Edgar Granitoid Complex; the Central Warrawoona Shear Zone with a complex deformation history, located along the central axis of the Warrawoona Greenstone Belt; the Brockman Hay and Fieldings Find Shear Zones that dominantly show W-vergent thrusting, and regional foliations, crenulations and minor thrusts that indicate (N)NE-(S)SW compression (see chapter 2).

2. The main structure, the mid-crustal Mt Edgar Shear Zone has been the locus of shearing (localization) and magma infiltration, as was described in chapter 3. It has recorded a complex structural history. Most significant is the uni-directional pattern of well developed stretching lineations in combination with kinematics that show initial layer parallel extension followed by

dominantly NE-tectonic transport. Structures and kinematics of the Mt Edgar Shear Zone indicated that if diapirism played a role in the development of the domes it was a minor one.

3. The Mt Edgar Shear Zone has been active during five deformation phases (D_{x+1} to D_{x+5}), but most of its development was associated with extension and magmatic intrusions dated at 3.47-3.42 Ga (D_{X+1}) and 3315-3309 Ma (D_{X+2E}) as determined by the crystallization age of syn- and post-tectonic granitoids, using SHRIMP U-Pb zircon chronology (see chapter 3).

4. The period preceding the 3.32-3.31 Ga granitoid genesis and doming of the Mt Edgar Granitoid Complex, involved regional (N)NE-(S)SW extension and intrusion of multiple mafic to ultramafic dyke suites associated with deposition of the Salgash Subgroup (chapter 4), followed by a phase of regional E-W compression (D_{X+2C}) (see chapter 2). $^{40}Ar/^{39}Ar$ cooling ages (Chapter 5) indicate an intrusion age prior to 3356 ± 21 Ma.

5. The period following the 3.32-3.31 Ga granitoid genesis and doming of the Mt Edgar Granitoid Complex involved a phase of (N)NE-(S)SW compression and (N)NE-vergent thrusting (D_{X+3}) that caused regional brittle-ductile fracture cleavages, crenulation cleavages and local thrusts. This phase post-dated 3.32-3.31 Ga granitoid intrusions, but the absolute age is not clear (see chapters 2 and 5).

6. Pre-2.77 Ga dextral transcurrent shearing, largely localised on the Central Warrawoona Shear Zone along the axis of the Warrawoona Belt (D_{X+4}), was attributed to a phase of regional WNW-ESE compression at 2.95-2.93 Ga (chapter 2).

7. The cooling history of the Mt Edgar Shear Zone as measured by ^{40}Ar-^{39}Ar isotope chronology (VULKAAN laser-probe) indicates it developed as an upper crustal dome at 3341-3290 Ma (chapter 5). Local younger reset ages suggests that the steep domal geometry may have been partly caused by late deformation and/or granite intrusion. Despite local resetting, the many preserved 3341-3290 Ma ages indicated that the crustal and lithospheric structure of the Marble Bar Domain is at least of that age and has not suffered regional resetting afterwards.

6.3 A new model for the structural evolution of the Marble Bar Domain - integrating new and published data and implications for tectonic setting

6.3.1 The basement to the Warrawoona Group

A schematic section of the pre-Warrawoona Group crust of the Marble Bar Domain is presented in figure 6.1. Various components that are older than ~3.49 Ga have been recognised, and are potentially basement to the Warrawoona Group, but most rocks are only locally observed and most are strongly deformed. This makes it difficult to establish a stratigraphic relationship, and to identify

Figure 6.1 Schematic cross-section through the crust of the Marble Bar Domain at >3465 Ma.

the oldest basement (see also Green, 2000).

The oldest supracrustal rock sequence has been recognised as the 3515 Ma Coonterunah Formation (Buick et al., 1995), now referred to as the Coonterunah Group (Van Kranendonk and Morant, 1998). Folds and foliations have been recognised in the type-section, which have been taken to indicate that a compressional deformation occurred prior to erosion and deposition of the overlying strata of the Salgash Subgroup (Buick et al., 1995). Geochemical studies on basaltic units of the Coonterunah Group have suggested that they are crustally contaminated (Green et al., 2000), rendering an oceanic origin unlikely. The recent discovery of a 3660 Ma granitoid component in the gneisses of the Warrawagine Granitoid Complex (Nelson, 1999) proves that an older granitoid basement existed in the Eastern Pilbara craton. This would provide an explanation for the crustal contamination of the Coonterunah Group. Xenocrystic zircons with a similar age have been found in granitoids of the Split Rock Shear Zone (Zegers, 1996) and in the gneisses of the Mt Edgar Granitoid Complex (Williams and Collins, 1990), suggesting that rocks of Coonterunah age have been widespread in the Marble Bar Domain.

One stratigraphic unit that is potentially older than the Coonterunah Group is the North Star Basalt, dated at 3560 ± 32 Ma (Sm/Nd, whole rock isochron) (see figure 1.1, chapter 1). This dominantly basaltic unit has been defined as the basal unit of the Warrawoona Group, but, if correct, the age difference with the McPhee Formation and the Mt Ada Formation is too large to include this unit in the Warrawoona Group or in the Coonterunah Group, and it may be considered as a separate unit (see figure 1.1, chapter 1). The depositional environment of the upper Talga Talga Subgroup has been regarded in terms of a shallow marine marginal setting (Barley et al., 1979). In contrast, the lower Talga Talga Subgroup has been proposed to have developed as an oceanic island or plateau (Krapez, 1993; Eriksson et al., 1994).

A structural and geochemical study in the type section of the North Star Basalt has been conducted by Van Koolwijk (1997, unpublished MSc Thesis) and Beintema (1997, unpublished

MSc Thesis, see also Beintema, 2003). These workers concluded that the North Star Basalt does not resemble a modern ophiolite: although it contains several components of modern oceanic crust (pillow basalts, cherts, mafic dykes), critical components such as a sheeted dyke complex underlain by gabbro are lacking. Also, the trace element geochemistry of the basalts, dykes and pyroxenite lenses is not similar to that of modern-day MOR- or OI-basalt, but it shows indications of crustal contamination similar to the finding of Green et al. (2001) for the Coonterunah Group (Beintema 2003).

6.3.2 The tectonic setting of the Marble Bar Domain during the Warrawoona episode

6.3.2.1 The development of the study area

Key indications for the tectonomagmatic history of the area come from the main structure, the MESZ (see Chapter 2). Initial development of the MESZ involved (E)NE-(W)SW layer-parallel extension during intrusion of hornblende-gabbro and hornblende-diorite sills (Chapter 3). These sills formed a hornblende-gabbro/diorite complex, part of which is dated at 3462 ± 4 Ma (Chapter 4). The MESZ developed at mid-crustal depth during deposition of the Duffer Formation and activity along growth faults in Coppin Gap and Coongan Belts (discussed in chapter 3), as is illustrated in figure 6.2.

Extrusion of the Salgash Subgroup followed that of the Duffer Formation. The most striking feature associated with the development of the Salgash Subgroup is a regional parallel mafic dyke swarm, part of which is observed in the Kelly and Marble Bar Belt (Chapter 4, figure 4.13). It

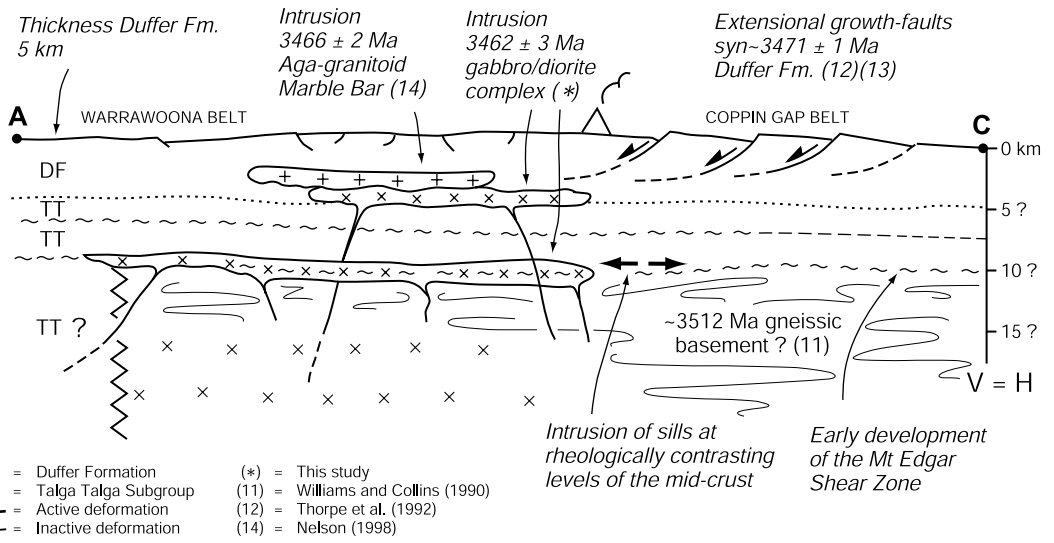

Figure 6.2 Schematic cross section through the crust during extrusion and deposition of the Duffer Formation, growth fault development on the supracrustal rocks and layer parallel extension on the MESZ, at mid crustal levels, at 3470-3450 Ma. For section location see figure 2.18 on p. 71.

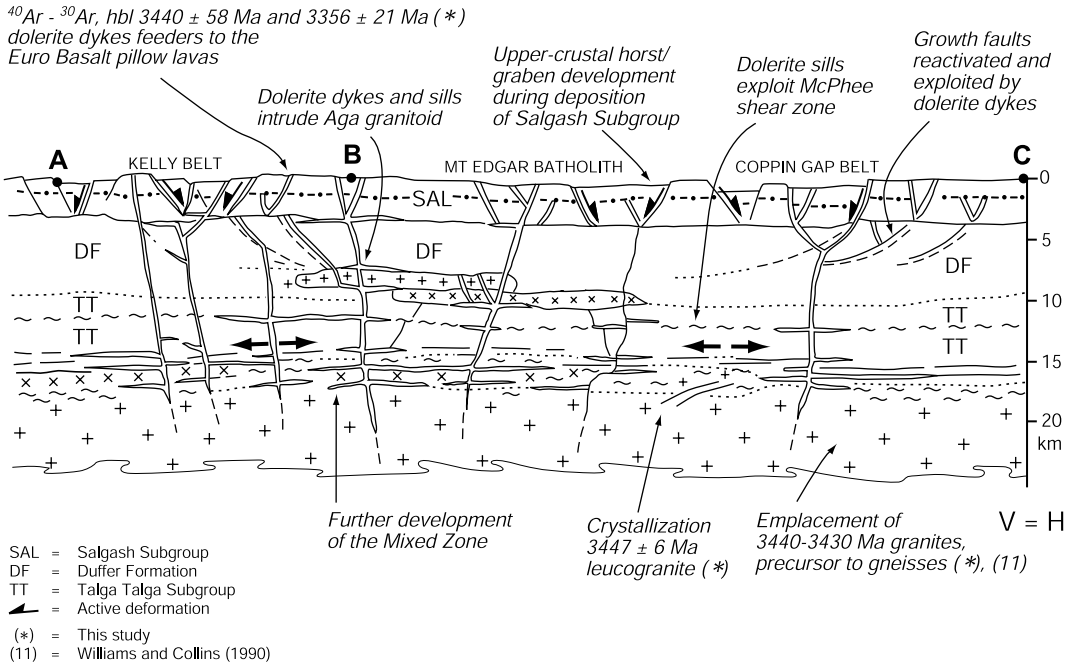

Figure 6.3 Schematic cross section through the crust at 3450-3420 Ma

comprises feeder dykes to the Euro Basalt, and possibly to the Apex Basalt, of the Salgash Subgroup. The reconstructed orientation of the dyke swarm indicates a (N)NE-(S)SW extension direction over an area of ~80 km by 50 km during emplacement. Structural and kinematic analysis of the MESZ indicates that the extension direction at the time of dolerite intrusion was NE-SW (D_{X+1B}). This is comparable to extension at upper crustal levels during emplacement of the Salgash Dyke Swarm. The coeval mid-crustal sill emplacement and the dyke intrusions in the upper crust are likely to be related, as is schematically illustrated in figures 4.13 and 6.3.

As for the timing of the Salgash Dyke Swarm, minimum ages of two dykes in the Kelly Greenstone Belt are provided by ^{40}Ar-^{39}Ar hornblende cooling ages of 3440 ± 58 Ma and 3356 ± 21 Ma from a dolerite and pyroxenite dyke, respectively (Chapter 5). The difference in age suggests that the Salgash Dyke Swarm has been formed during several pulses of magmatism, which is also indicated by the variable compositions of the dykes. Pulses of magmatism may correspond to the stratigraphic alternation of basalt and chert within the Euro Basalt, and on a larger scale, within the Salgash Subgroup.

In the MESZ, the dolerite sills have not been dated directly, but a minimum age is provided by the intrusive relationship with the 3447 ± 6 Ma leucogranite sills (Chapter 3). Dolerite sills that are older than ca. 3447 ± 6 Ma could be associated with the extrusion of the Apex Basalt. If so, the (N)NE-(S)SW extension may have occurred over a period from at least 3447 ± 6 Ma to extrusion of the Euro Basalt, between 3417 ± 9 Ma and 3356 ± 21 Ma (Figure 6.3).

6.3.2.2. Constraints from structures in the Duffer Formation in the Marble Bar Domain

Evidence of the oldest recognised deformation phase in the Marble Bar Domain has been identified within the mostly andesitic, dacitic and volcaniclastic rocks of the 3.47-3.45 Ga Duffer Formation and the syn-tectonic intrusion of the oldest recognised TTG suites (Zegers, 1996; Zegers et al., 1996; Nijman et al, 1998a). Extrusion of these volcanic rocks and deposition of the volcaniclastic sediments of the Duffer Formation may have occurred in growth faults in the Coongan Greenstone Belt (Zegers et al., 1996) and the Coppin Gap Greenstone Belt (Nijman et al., 1998a). Coeval ENE-WSW extension initiated shearing in the Split Rock Shear Zone, which runs along the interface between the Shaw Granitoid Complex and the supracrustal sequence of the Coongan Belt (Zegers, 1996; Zegers et al., 1996). This extensional shear zone was syntectonically intruded by TTG suites.

Zegers et al. (1996) have emphasised that growth fault development at 3.46-3.45 Ga was coeval with felsic volcanism of the Duffer Formation. Their data, however, also show that the development of growth faults preceded the extrusion/deposition of the Duffer Formation. These structures can be traced into the underlying basalt and high-Mg basalt conformable below the Duffer Formation. Recent geochronological data from volcanic units below the Duffer Formation (3477 $\pm$ 2 Ma McPhee Formation, 3469 $\pm$ 3 Ma Mt Ada Formation, Nelson, 2000) have shown that mafic volcanism has preceded deposition of the Duffer Formation by about 5-10 m.y. Additionally, initial extension on the (proto-)MESZ was accompanied by mafic intrusions, including the hornblende-gabbro/diorite complex (Chapter 3, figure 3.15). These data, in combination with those of Zegers et al. (1996), suggest that felsic volcanism initiated during extension, after mafic extrusive magmatism (upper Talga Talga Subgroup). This indicates that the role of mafic magmatism was more important at the onset of this deformation phase then previously recognised, the possible implications of which are discussed below.

6.3.2.3 Constraints from the Salgash Subgroup in the Marble Bar Domain

An extensional, dominantly subaqueous setting, possibly a submerged continental platform, has been proposed for the extrusion of the 4-5 km thick Salgash Subgroup (Barley, 1993; Krapez, 1993; Eriksson et al., 1994). Geochemistry has shown that the felsic volcanic Panorama Formation in the Kelly Belt was formed by partial melting of garnet-bearing mafic rocks, that possibly were part of subducted mafic crust (Barley et al., 1984; Barley et al., 1998a).

In summary, from the above discussion it follows that the main tectonomagmatic events in the Marble Bar domain during the Warrawoona episode are:

i) A pulse of mafic magmatism of the McPhee and Mt Ada Basalt during possible upper crustal extension at 3.48-3.47 Ga.
ii) Deposition of a regional 4-5 km thick andesitic and dacitic igneous sequence with a calc-alkaline trend, a phase of clastic sedimentation (Duffer Formation); possibly during ongoing uni-directional extension at upper and mid-crustal levels at 3.47-3.45 (D_{X+1A}) and hornblende-gabbro/diorite, and TTG suite intrusion.
iii) Activity of the Duffada Shear Zone pre-dating the intrusion of dykes of the Salgash Subgroup.

iv) Extrusion of a 4-5 km thick subaqueous dominantly tholeiitic (bimodal) magmatic sequence and intrusion of the parallel mafic Salgash Dyke Swarm during extension from 3.45 to 3.42 Ga ($D_{X+1B \text{ and } C}$), possibly to prior to 3356 Ma.

6.3.2.4.1 Proposed tectonic setting(s) for the Warrawoona episode

Felsic magmatism at 3.46-3.45 Ga is the oldest phase of felsic magmatism in the Marble bar Domain that led to the preservation of a considerable volume of felsic supracrustal units (Duffer Formation) and TTGs. Based on the calc-alkaline geochemistry of the felsic volcanic rocks of the Duffer Formation and because of the coeval TTG suites the petrogenetic process has been related to either subduction of mafic crust, or melting at the base of a thickened crust (Barley et al., 1984; Bickle et al., 1993; Smithies, 2000). Because of this geochemical signature in combination with the type of volcanoclastic sediments, these rocks are believed to have formed near volcanic centres similar to those observed in and around present day volcanic arcs, or back-arc settings (Hickman, 1983; Barley et al., 1984; DiMarco and Lowe, 1989a). The geochemical signature of the Duffer Formation in combination with (i) the possibly uni-directional extension on the Split Rock Shear Zone, (ii) the presence of a continental basement and (iii) the possibly syn-extensional deposition, led Zegers (1996) to consider a continental rift setting (induced by either plate-interaction or collapse), or a back-arc basin setting as the tectonic environment for the Duffer Formation.

Several scenarios for the generation of the McPhee Formation, the Mt Ada Basalt, the Duffer Formation and the coeval TTG melts are possible (see chapter 1). Archaean TTGs have been noted to bear similarities with Adakites (for an overview see Defant and Kapezhinskas, 2001). However, the Pilbara TTGs differ from Phanerozoic Adakites in their lower Mg-number and their higher Si-content: the Pilbara TTGs provide no evidence for subduction (Smithies, 2000). Smithies (2000) has emphasised that the composition of the 3.45 Ga TTG suites from the Shaw Granitoid Complex does not allow to distinguish between modern-style subduction processes and melting at the base of a thickened crust. The latter may be a more appropriate setting to form Archaean TTG suites.

Without conclusive evidence for modern style subduction, an alternative scenario for generating TTGs could involve stacking of hydrated basaltic slabs of (parts of) oceanic crust and/or top-slices of oceanic plateaus: 'flake tectonics' (see chapter 1). This model predicts genesis of TTGs by partial melting at the base of the stack due to heating. Melting of the base of a thick mafic crust is consistent with the geochemical data of the Pilbara (see Smithies, 2000) and stacking has been recognised in other Archaean terrains (e.g. De Wit, 1982; De Wit et al., 1987a; Dirks and Jelsma, 1998; De Ronde and De Wit, 1994; Kusky and Vearncombe, 1997).

If early stacking occurred in the Marble Bar Domain, candidates for the facilitating structures are found in the stratigraphically lower Talga Talga Subgroup. The upper and lower formations of the Talga Talga Subgroup, the North Star Basalt and the Mt Ada Basalt, are internally mostly undeformed (Hickman, 1977). However, the 50-200 metre thick McPhee Formation coincides largely with a shear zone (Van Haaften and White, 1998). The possibility of horizontal transport along these largely layer parallel shear zones early in the history of the area has been raised by Van Haaften and White (1998) for the Marble Bar Greenstone Belt. As ^{40}Ar-^{39}Ar data confirm that the MEGC had fully developed as an upper crustal dome at ca. 3.32-3.31 Ga (Chapter 5), possibly large

horizontal transport on layer-parallel shear zones (décollements), is most likely to have occurred before 3.32 Ga, i.e. at the time that supracrustal units were still largely horizontal.

An alternative mechanism for the construction of a thick crust of hydrated basaltic rocks to form TTG melts is magmatic thickening (e.g. Saunders et al., 1996). The North Star Basalt may have developed partly by magmatic thickening, as indicated by abundant mafic dykes and sills in its type section (Hickman, 1983). Plume activity appears to be a likely cause for a magmatically thickened mafic/ultramafic crust. Modern-day Large Igneous Provinces (LIP) are often associated with plume activity (for an overview see Mahoney and Coffin, 1997, cf. Sheth, 1999). Comparison of the volcanic sequences of the McPhee Formation, the Mt Ada Basalt and Duffer units with the sequence predicted for a mantle plume shows that the order is similar (Hill, 1991). However, the relative volume of the felsic Duffer Formation in the Marble Bar Domain is much larger than expected for the volume of felsic volcanic rocks in modern plume-related LIPs. Also, it has been noted from seismological data that currently the crust under the Pilbara lacks a basal high velocity zone, i.e. it has no mafic underplate (Drummond and Collins, 1986), which further questions the role of a mantle plume during this stage.

A different cause for partial melting of the base of the crust has been proposed. Cooling of the base of the crust, after which metamorphic phase-changes cause gravitational destabilisation, may be followed by A-subduction, i.e. the drop-off of the entire mantle root (e.g. Kröner, 1981; Davies, 1992; Vlaar et al., 1994). The drop off would require replacement by hotter mantle, which would cause heating and melting of the remaining crust. However, as noted by De Wit (1998), removal of mantle roots is unlikely to have caused tectonic events of which evidence is exposed at the surface of cratons, because roots appear to have led to their survival at the Earth's surface.

Alternatively, and on a smaller scale, *lower* crust may delaminate without removal of the mantle root (Zegers and Van Keken, 2000). In this model, a phase change of the lower basaltic crust to high density garnet-eclogite or granulite may be associated with partial melting (forming high-Al TTG melts) and delamination of part of the crust. Delaminating lower crust is replaced by mantle material. Partial melting of this upwelling mantle forms (high-Mg) basaltic melts, and also causes melting of remaining lower crustal amphibolites to form a second suite of TTG suites. As the largely mafic and ultramafic McPhee Formation and the Mt Ada Basalt have preceded deposition of the Duffer Formation, it is possible that these units may represent the first melts formed by this process. The Duffer Formation and the coeval TTG suites are proposed to represent the partial melts from the lower crustal amphibolites (Zegers and Van Keken, 2000). Delamination causes extension of the crust by doming and uplift, consistent with the subaerial deposition of the Duffer Formation and the syn-depositional faults (Zegers and Van Keken, 2000).

In chapter 4 the development of the Salgash Subgroup and the Salgash Dyke Swarm has been compared to that of various Phanerozoic and Archaean continental extensional settings. Mechanisms responsible for continental extension and coeval, dominantly mafic magmatism are listed as either mantle plume-induced rifting, plate-induced rifting (including a back-arc setting), A-subduction, or 'delamination' of the lower crust (Chapter 4, Figure 4.7). The results of this study provide only limited constraints for the possible setting, but indicate that extension of the crust due to a diapiric

passive rise of granitoids is an unlikely cause for the reconstructed unidirectional extension of the crust over an area of ~80-50 km (Chapter 4, figure 4.13). Hickman (1983), Barley and Pickard (1999) and Green et al. (2000) noted that the basalts of the Salgash Subgroup in the Marble Bar Domain are largely tholeiitic, although crustally contaminated, rendering an oceanic setting unlikely. The extrusion of large quantities of continental tholeiitic flood basalt is consistent with both plume and plate-induced rifting, and less consistent with a continental back-arc setting (e.g. Lambert et al., 1992).

In contrast to the depositional environment of the Duffer Formation, that of the Salgash Subgroup was largely subaqueous. As both an active mantle plume, and delamination of the lower crust would cause uplift of the crust, a largely subaqueous development of the Salgash Subgroup indicates that both processes are unlikely causes for this part of the tectonomagmatic development. McKenzie and Bickle (1988) have argued that in the Archaean limited extension may have produced a significant amount of mafic melt because of a hotter mantle (see also Blake, 1993). Based on the abundant subaqueous mafic magmatism in combination with the extensional setting indicated by the Salgash Dyke Swarm, the Salgash Subgroup may represent a phase of crustal extension, destabilisation, and possibly rifting, as found in modern volcanic rifted margins.

The development of the crust during extrusion of the Salgash Subgroup may not have led to rifting *within* the Marble Bar Domain, but it may have formed its *margins*. If the margins of the Pilbara Craton rifted, it may have led to the break-up of an early Archaean continent, as has been tested for the Pilbara and the Kaapvaal Craton (Zegers et al., 1998c). If the Salgash Subgroup represents a rifting stage that led to oceanization, the role of fragmentation and reassembly of smaller continents may have played a bigger role in the 800 m.y. development of the Pilbara granite-greenstone terrain than previously thought (see also Myers, 1993).

6.3.3 The structural development of the Marble Bar Domain during the Wyman episode (3325 – 3290 Ma)

6.3.3.1 The development of the study area

The main development of the area involved NE-SW extension and granitoid emplacement in the Mt Edgar Granitoid Complex at 3325-3310 Ma (Chapter 2, see figure 2.18b). Based on structural overprinting relationships and absolute age dating in the Warrawoona Greenstone Belt it is found that E-W compression structures were temporally closely related to extension. However, whereas compression structures occur in the upper crustal rocks, including the 3315 Ma Wyman Formation, none were found in the MESZ with rocks of similar age (figure 6.4). In contrast, the MESZ is dominated by NE-SW extensional structures.

How NE-SW extension was associated with E-W compression is discussed in chapter 2. Thickening of the upper crust led to heating and partial melting of the basal gneisses to form the TTG granitoids of the Mt Edgar and Corunna Downs Granitoid Complex. A thickened, partly migmatitic crust may result in sideways expulsion of the most mobile parts of the crust (See figure 6.5). The MESZ is proposed to have detached the upper and the lower parts of the crust, allowing different transport directions (chapter 2), as has been proposed for parts of the Zimbabwe Craton (Dirks and Jelsma, 1998), the Wawa Gneiss Domain of the Superior Province (Moser, 1994, Moser

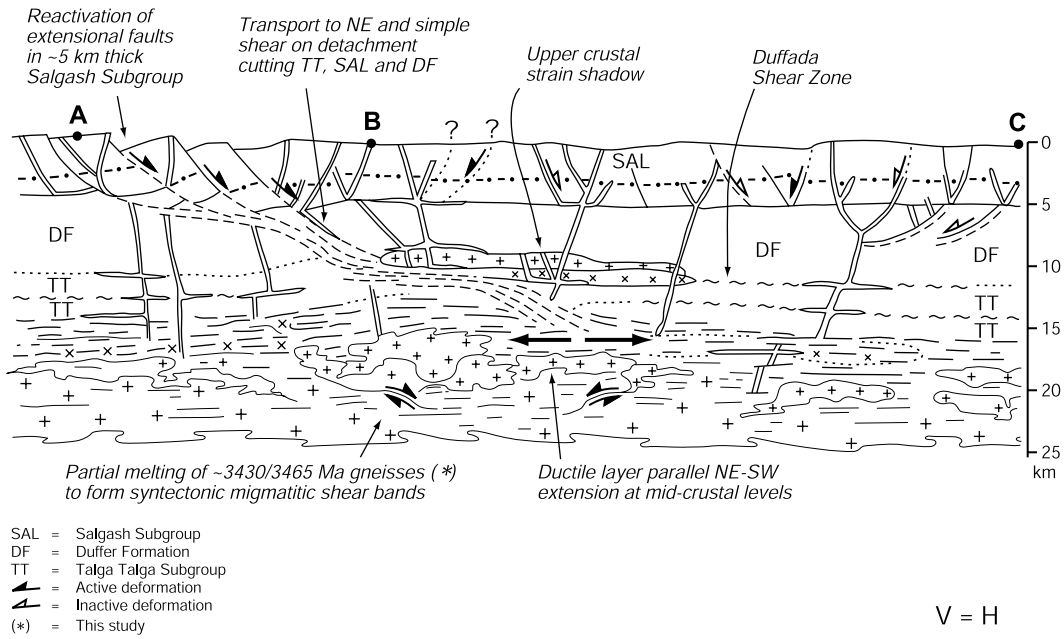

Figure 6.4 Development of the Mt Edgar Shear Zone as a crustal detachment (at 3325 ?).

et al., 1996) and in Western Greenland (Manatshal et al., 1998). At the end of this phase granitoid emplacement in the footwall of the MESZ caused the development of the MEGC as a steep, Marshak-type metamorphic core complex (Figure 6.6 and 6.7), prior to ca. 3.30 Ga (see chapter 5). Its steep sides are the effect of the rheology of the hotter and more mobile Palaeoproterozoic crust (see Marshak et al., 1992, 1997; Marshak, 1999). A relatively weak crust with a reversed density profile would also promote solid-state diapirs. But the difference is that in the scenario presented here for the 3.31 Ga development of the MEGC initial granitoid-genesis and vertical tectonics (doming) are caused by horizontal rather than vertical tectonics.

Although some effect of post D_{X+2E} deformation can not be ruled out, the ^{40}Ar-^{39}Ar geochronology of the MESZ indicates that the MEGC developed as an upper crustal structure prior to ca. 3.30 Ma, and has remained in a thermally stable upper crustal domain since this time.

6.3.3.2 Additional constraints for doming during the Wyman episode from the Marble Bar Domain

The timing of E-W compressional structures throughout the Marble Bar Domain varies between 3.34 Ga and 3.20 Ga (Chapter 2). The range in timing of the E-W compression structures suggests a prolonged phase of compression. In contrast, granitoid emplacement occurred in relatively short intervals and was localised. TTG suites and monzo-granites were emplaced in the MEGC and the CDGC between ca. 3315-3305 Ma (Chapter 3, Williams and Collins, 1990; Barley and Pickard, 1999). Petrogenesis of the 3.31 Ga TTGs and monzogranite may have occurred over a range of crustal depths with sources including both garnet-bearing eclogite and granitoid gneisses (Barley and Pickard, 1999).

The main events during the Wyman episode in the Marble Bar Domain are:

i) A phase of regional E-W compression possibly from 3350 Ma to prior to ca. 3.20 Ga (D_{x+2C}).
ii) Granitoid genesis by partial melting of the gneissic basement at 3.32-3.31 Ga, during unidirectional NE-SW extension (D_{x+2E}) on the MESZ.

An important finding is the apparent long period of regional compression (ca 3.34 - 3.20 Ga) in combination with relatively short periods of granitoid genesis and extension. Compression and the associated development of fold and thrust belts on the scale of the Marble Bar Domain, is not readily explained by gravity-driven gliding that is thought to be associated with diapirism (Hickman, 1983). Rather, it is likely to require externally imposed compressional forces like those associated with modern continental convergent margins (Bickle et al., 1985).

The driving force for the evolution of the Marble Bar Domain during the Wyman episode is interpreted here to be (some form of) convergent plate interaction. Barley and Pickard (1999) have noted that the 3.32-3.31 Ga granitoids only occur in the area east of the Mulgandinah Shear Zone Complex, i.e. east of the western margin of the Marble Bar Domain, which was taken to suggests that this structure has formed some sort of collision boundary. Noteworthy, this margin is near one of the two areas with kyanite-bearing rocks, that indicate conditions of tectonically depressed geotherms (Bickle et al., 1980, 1985). Two phases of folding and thrusting prior to doming of the Shaw Granitoid Complex have been recognised in this area (Bickle et al., 1980, 1985; Boulter et al., 1987).

In the model that emphasises solid-state diapirism, kyanite/sillimanite occurrences have been explained to have formed in the relatively cool keel that sinks in between two diapirs (Collins and Van Kranendonk, 1999). This model, however, does not provide a mechanism for exhumation and denudation of these assemblages. Active extension and doming of the MESZ as proposed for the development of the MEGC, rather that passive diapirism, can more readily explain the kyanite/sillimanite occurrences.

Even though a continental fore-arc/arc setting, associated with a convergent plate margin, could explain the close relationship between compression and extension described for the MEGC, evidence of subduction, such as a regional linear trend, accretionary melanges, paired metamorphic belts with HP-LT blueschists, has not been observed in the eastern Pilbara granite-greenstone terrain.

Regarding the timing of the development of the steep domes, magnetic and gravity anomaly data were used to determine the shape, slope and depth of the granitoid bodies. This was partly done by modelling the location and orientation of high magnetic units in the greenstone belts. It was found that most granitoid complexes comply to a starting model, in which the granitoids are assumed to be 14 km deep cylindrical bodies with subvertical sides (Wellman, 1999). The subvertical sides are based on the orientation of the high magnetic units of the Gorge Creek Group (see Blewett, 2000). Blewett (2002) argues that, as these magnetic units are ca 3250 ma in age, the doming occurred relatively late, i.e. post-3250 Ma.

6.3.3.3 Constraints from regional activity of mid-crustal detachments in the Marble Bar Domain

Similarities occur between the Mt Edgar Shear Zone and the Split Rock Shear Zone, that crops out on the (north)eastern margin of the Shaw Granitoid Complex (Zegers, 1996; Zegers et al.,

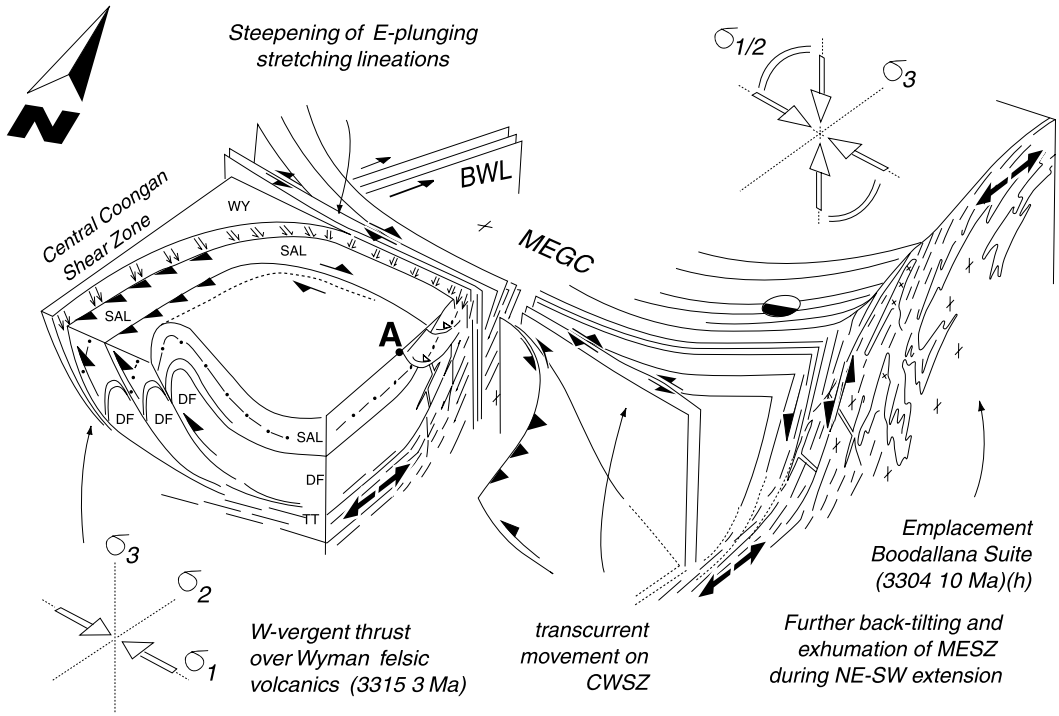

Figure 6.5 Schematic cross section through the crust at 3340-3310 Ma, illustrating the relationship between the upper crustal compressional structures and the NE-SE extension in the granitoid-rich crust below the MESZ.

1999). Both are km-wide shear zones that form the steeply dipping contact zone between high grade gneisses and supracrustal rocks, dipping away from the granitoid complex. Both have well developed mylonitic foliations and stretching lineations that show a uni-directional pattern. Both have been exploited by magmatic intrusion.

The Split Rock Shear Zone was recognised as a mid-crustal shear zone that may have been active during extension and development of half-graben extensional growth faults in the Coongan Greenstone Belt (Zegers et al., 1996; Zegers et al., 1999). Coeval ENE-WSW extension was envisaged to have caused shearing in the Split Rock Shear Zone during granite sheet intrusion at the interface between the Shaw Granitoid Complex and the supracrustal sequence of the Coongan Belt (Zegers, 1996; Zegers et al., 1996). Zegers and co-workers (1996) have related deposition of the Duffer Formation and activity of the Split Rock Shear Zone to regional unidirectional extension, whereas Nijman and co-workers (1998a) envisaged a caldera collapse type setting.

Timing of activity on the Split Rock Shear Zone was determined to be syn-Duffer at ca. 3452 Ma, the age of the Duffer Formation in the Coongan Belt (Pidgeon, 1978) associated with the growth faults (Zegers et al., 1996). Further constraints were obtained from the 3469 ± 3 Ma age of a syntectonic granitoid sheet that has intruded along the contact with the greenstones (Zegers, 1996; Zegers et al., 1999). Based on these ages it can be argued that the two (proto)shear zones have been active coevally. In addition, an enclave of hornblende-diorite within the high-grade gneissic core of

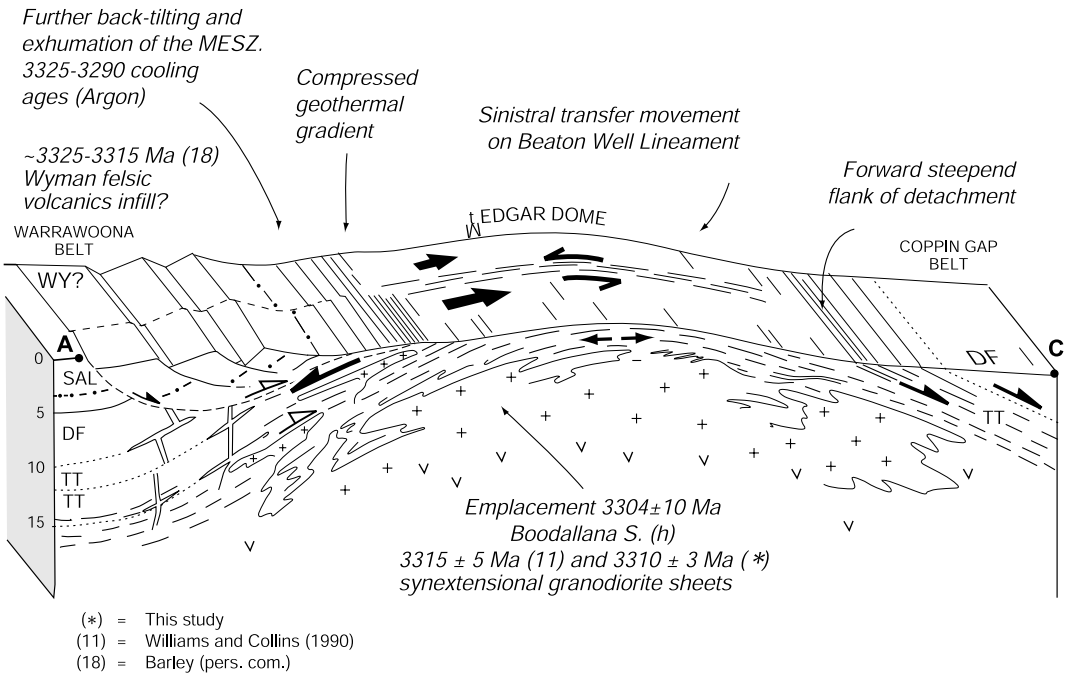

Figure 6.6 Schematic cross section through the crust during extension at doming of the Mt Edgar Shear Zone and Mt Edgar Granitoid Complex.

the Shaw Granitoid Complex has been dated at 3464 ± 3 Ma (Zegers, 1996), which is within error of that of the diorite/gabbro complex of the MESZ, which indicates that both have developed during coeval magmatic episodes.

The significance of recognising these two coevally active shear zones is that it allows investigation of the transport directions on a scale that exceeds the size of single domes. This is particularly important when studying the cause for doming and doming mechanisms. As mentioned in chapter 2, two end-member models for development of the granitoid domes in the eastern Pilbara granite-greenstone terrain have been proposed: passive, gravity driven solid-state diapirism, and extensional, core-complex type doming. As mentioned in chapter 2, one of the key observations in the MESZ was that the constant SW-plunging stretching lineations in the MESZ form a uni-directional pattern that cannot be explained by diapiric doming of the Mt Edgar Granitoid Complex. A similar observation was done by Zegers (1996) who reported constantly ENE plunging stretching lineations in the Split Rock Shear Zone. Now that it is known that the MESZ has an early history, coeval with the Split Rock Shear Zone, their extension directions can be compared. ENE-WSW extension in the Split Rock Shear Zone and NE-SW extension in the Mt Edgar Shear Zone is co-linear within ca 22°. This supports a model in which regional deformation, rather then local diapirism, was involved in the development of the domes.

A marked difference, however, between the Split Rock Shear Zone and the Mt Edgar Shear

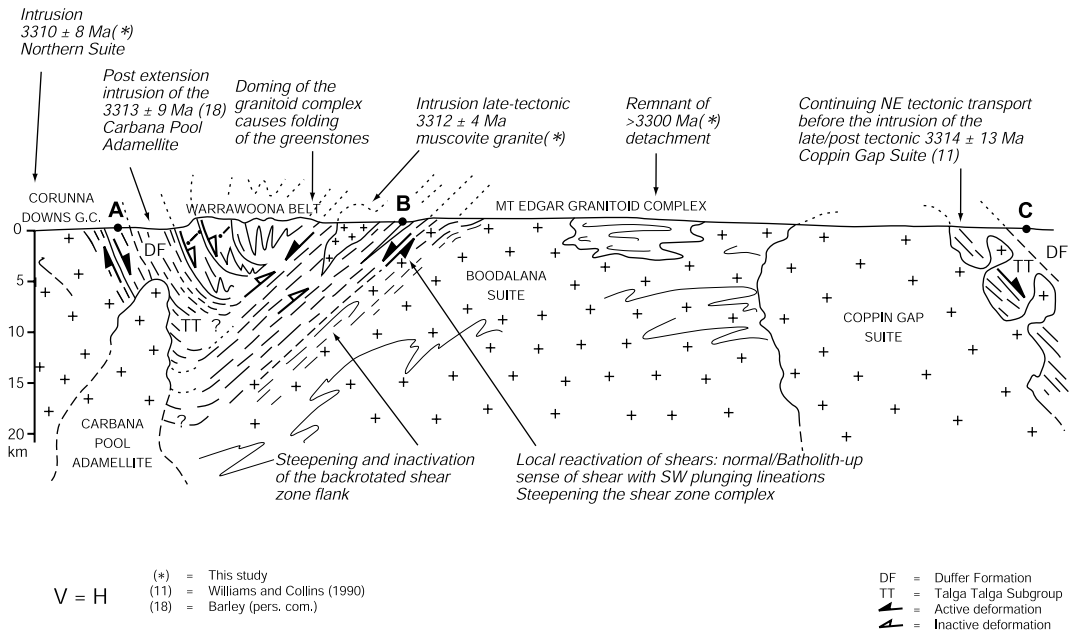

Figure 6.7 Schematic cross section through the crust at 3315-3310 Ma, illustrating the late-stage development of the Mt Edgar Shear Zone and Mt Edgar Granitoid Complex as a steep, Marshak-type dome.

Zone is that the MESZ contains a variety of intrusive components that constitute the Mixed Zone. Such a mixed zone is absent in the Split Rock Shear Zone. Absence, or weak development, could either be explained by doming from a shallower detachment level of the crust, i.e. one that was less affected by intrusions, or from one at a similar level, but one that locally lacks magma-infiltration: the presence of a Mixed Zone in the MESZ may reflect proximity of the MEGC to a magma centre. An additional difference between the Split Rock Shear Zone and the Mt Edgar Shear Zone is that the former encompasses a granitoid complex (Shaw Granitoid Complex) that generally lacks 3.3 Ga granitoid components. Granitoid of this age in the MEGC have been proposed to have been derived from partial melting of the 3.45 Ga basal gneisses based on geochemical signature (Collins, 1993; Barley and Pickard, 1999). Gneisses can partially melt by thickening of the crust and subsequent radiothermal heating. Thickening of the crust as a cause for partial meting during D_{X+2} has already been discussed in the previous chapter and is feasible in terms of timing. However, it has been noted that even though well developed E-W compressional structures occur in the Tambourah Belt on the western margin of the Shaw Granitoid Complex, (Bickle et al., 1980), no associated granitoids have been reported for the Shaw Granitoid Complex (see also §2.6.2). An alternative cause for melting of gneissic basement is heating of the crust as a result of addition of hot magma (such as mafic dykes). Substantial mafic additions to the crust have been recorded in the MESZ in the form of the hornblende-gabbro/diorite complex and the (ultra)mafic dykes and sills, components 1 and 5, respectively (see figure 3.13). Yet, intrusive relationships and SHRIMP dating has indicated that these mafic components intruded the MESZ before 3447 ± 6 Ma (as determined

by the intrusive relationship with the crystallization age of the leucogranite, component 6), which is >120 m.y. before intrusion of the 3.31 Ga granitoids, such that this mafic component cannot be responsible the genesis of these granitoids. In general, as is illustrated in figure 3.2, few crystallization ages have been recorded for the period between the end of the Warrawoona episode at ca. 3420 Ma and the start of the Wyman episode at ca. 3325 Ma. However, granitoid genesis and doming of the eastern Pilbara granitoid complexes at ~3.31 Ga has recently been proposed to be associated with mantle plume impingement at the base of a continental crust (Collins et al., 1998; Van Kranendonk et al., 2002). Van Kranendonk et al. (2002) propose that deposition of the Salgash Subgroup may have been ongoing to ca. 3325 Ma in the Marble Bar Domain. However, apart from a zircon population in a silicified felsic tuff in the Euro Basalt of the Kelly Belt dated at 3346 Ma (Nelson, 2001) that was interpreted to represent the eruptive age of the tuff (M. Van Kranendonk and L. Bagas, Geological Survey of Western Australia, unpubl. data. In: Van Kranendonk et al., 2002) but is likely to be xenocrystic, and the poorly defined 3356±21 Ma ^{40}Ar-^{39}Ar hornblende age of the pyroxenite dyke (chapter 5), no ages are available to indicate that mafic magmatism caused melting of the granitic gneisses at ca 3.31 Ga.

6.3.4 The tectonic setting of the Marble Bar Domain during the Roebourne episode

Evidence for magmatic activity during the Roebourne episode is found in the form of a monzogranite that has recently been identified in the centre of the MEGC and has been dated at 3241 ± 11 Ma (Nelson, 2000). Nelson (op cit.) noted that the monzogranite is foliated, but the structural significance is not clear. The SHRIMP zircon results show recrystallized zircon domains and metamorphic rims with spot dates varying from ca. 3325 to 3180 Ma (Chapter 3, figure 3.18), suggesting some magmatic and/or tectonic reactivation of the MESZ and the Central Gneiss Complex. In sample A94-22 they form a statistically significant group at ca. 3235 ± 5 Ma (See chapter 3, figure 3.19). Two ^{40}Ar-^{39}Ar isotopic ages of 3249 ± 17 Ma and 3249 ± 15 Ma are obtained from hornblendes in the central and eastern MESZ as discussed in chapter 5 (see figure 5.9). These are interpreted to be the result of local resetting, possibly associated with intrusion of a 3.24 Ga granitoids.

On the western margin of the Marble Bar Domain, the Roebourne episode involved extrusion of felsic volcanic units, minor komatiites and deposition of sediments in the Strelley Greenstone Belt (Van Kranendonk and Morant, 1998). Granitoids of this age, which are biotite-monzogranites, have been found in the Muccan and Warrawagine Granitoid Complex (Nelson, 1998a, 1999). Extrusion of a felsic volcanic unit has been associated with intrusion of the Strelley Pool Granite and the development of an extensional fault array and formation of VMS-type deposits (Vearncombe et al., 1995). The development of the Strelley area has been interpreted as an extensional tectonic setting in a convergent continental margin, possibly a back-arc setting (Vearncombe et al, 1995; Krapez, 1993, Vearncombe and Kerrich, 1999). This episode has been proposed to be the continuation of extension during 3.31 Ga (Krapez, 1993; Barley and Pickard, 1999).

Rocks associated with the Roebourne episode are abundant in the western part of the Pilbara granite-greenstone terrain (see Blewett, 2002; Van Kranendonk et al., 2002; Beintema 2003). They

form the first units that occur in the east as well as in the west of the Pilbara granite-greenstone terrain, and have been interpreted to reflect a minimum age for amalgamation of the eastern and the western part of the Pilbara Granite-greenstone terrain (Nelson et al., 1999).

6.3.5 Tectonic setting of the the study area during (N)NE-(S)SW compression (D_{x+3})

A phase of (N)NE-(S)SW compression is recognised to have formed regional crenulation cleavages, fracture cleavages and dominantly (N)NE-vergent thrusts (see figure 6.8). The timing for this deformation is loosely constrained at between 3.30 Ga and 2.95 Ga (see chapters 2, 3).

Indirect evidence for the timing of this phase may come from the disturbance of isotope systems used for geochronology. Collins and Gray (1990) have reported a ca. 3200 Ma Rb-Sr age for all components of the MEGC including the ca. 3.31 TTG suites and the older Central Gneiss Complex. They have attributed this to either slow cooling of the 3.31 Ga granitoids, or to a phase of thermal resetting. Only two ^{40}Ar-^{39}Ar cooling ages of ca. 3200 Ma were determined in the MESZ and the CDGC, indicating that the MESZ was only locally reset at 3200 Ma. The Carbana Pool Adamellite in the CDGC, from which the biotite yielded a cooling ages of ca. 3200 Ma, contained structures of with (N)NE-vergent thrusting and strike-slip shearing (Chapter 5). Possibly the 3200 Ma resetting was caused by the phase of (N)NE-(S)SW compression.

One of the structures within the Marble Bar Domain that kinematically fit (N)NE-(S)SW compression include the NNE-trending Lionel Fault. This structure forms the eastern margin of the Marble Bar Domain. Dextral strike-slip movement along this fault occurred after deposition of the <3.24 Ga Gorge Creek sediments of the Mosquito Creek Block and before emplacement of the ca. 2.77 Ga Fortescue Group (Zegers, 1996). The kinematics are consistent with the (N)NE-(S)SW compression and may provide an upper limit for the age of this phase. A late NW to NNW-trending crenulation cleavage throughout the N-S trending Coongan Greenstone Belt has been recorded by Zegers (1996). In terms of kinematics and overprinting relationships, this crenulation foliation may be related to the phase of NE-SW compression (Zegers, pers.com). As the crenulations overprint the E-W thrust foliation in the Coongan Belt, they must be younger. Regional trending foliations and craton-scale strike slip faults require some form of far-field compression.

6.3.6 Tectonic setting of the study area during ESE-WNW compression (D_{x+4})

Dextral shearing on the Central Warrawoona Shear Zone (Figure 6.9) occurred after (N)NE-(S)SW compression and prior to intrusion of the W-dyke, member of the 2.77 Ga Black Range Dyke Swarm (D_{x+4}) (Chapter 2). It is attributed to a regional phase of (W)NW-(E)SE compression, based on the consistent order of deformation events in the Warrawoona Greenstone Belt and the compatible kinematics.

Craton-scale transcurrent fault systems have been active during regional ESE-WNW compression in the eastern part of the Pilbara Craton at ca. 2.95-2.93 Ga, during the Millindinna episode (Zegers, 1996; Van Kranendonk and Collins, 1998; Zegers et al., 1998a). Transcurrent

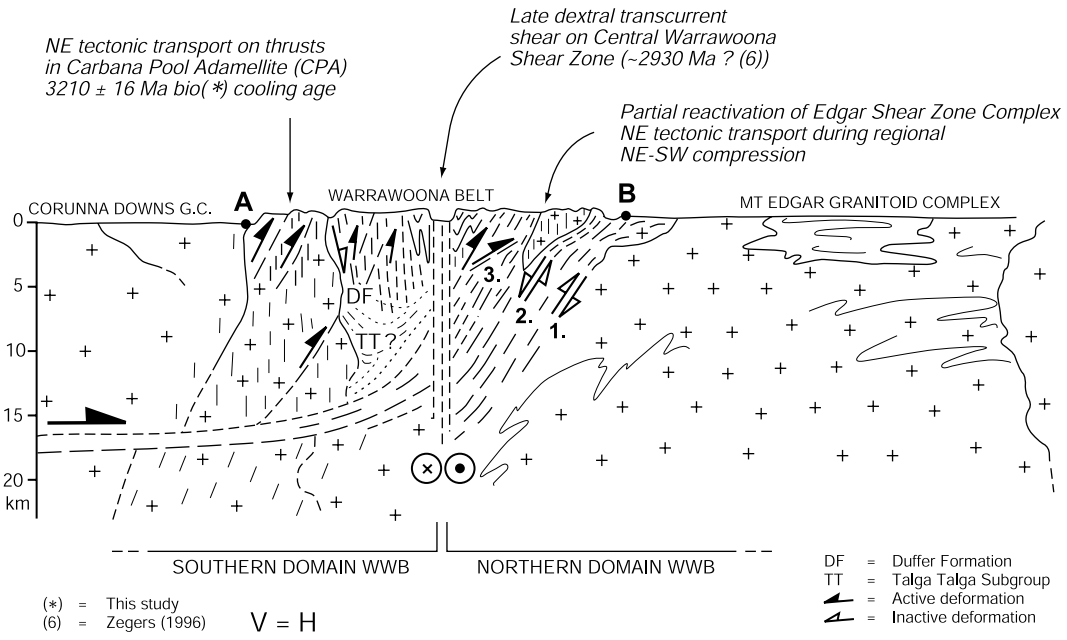

Figure 6.8 Schematic cross section through the crust illustrating (N)NE-(S)SW compression (D_{X+3}).

movement during this phase is responsible for the development of the Lalla Rookh Basin and Whim Creek Greenstone Belt (Krapez and Barley, 1987). These workers noted that craton-wide strike-slip deformation indicates that externally imposed horizontal stresses were applied at a regional scale (see also Sleep, 1992). The movement along these craton-wide shears reflects minor intra-craton reorganisation during cratonization, rather than interaction of (micro)plates and terrane accretion (Krapez and Barley, 1987).

In this study, no direct evidence has been found for deformation during the Millindinna episode, and no granitoids of this age have been recognised. However, dextral shearing on the Central Warrawoona Shear Zone (D_{x+4}) is attributed to this phase, based on the compatibility of the order of deformation events in the area and the compatible kinematics with (W)NW-(E)SE compression (see chapter 2). In the NW margin of the MEGC, two hornblende ^{40}Ar-^{39}Ar cooling ages are recorded, suggesting thermal resetting during the Millindinna episode.

6.4 Conclusions

1. The observations in this study have fine-tuned the tectonomagmatic history of the Marble Bar Domain. The Early to Mid Archaean tectonomagmatic history included the following phases:

- Deposition of the Coonterunah Group at ~3515 Ma. (on continental crust) followed by folding /Extrusion of the North Star Basalt on continental crust (age unconstrained).

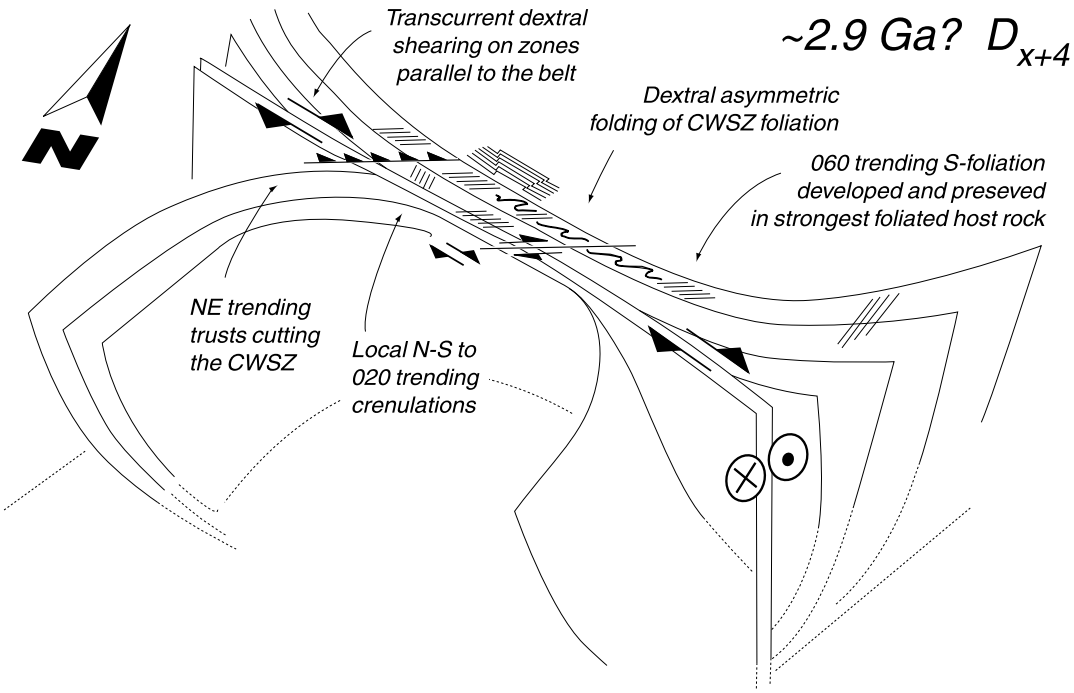

Figure 6.9 Schematic cross section through the crust at 2950-2930 Ma, illustrating a phase of dextral strike-slip deformation (D_{X+4}) with the main activity on the Central Warrawoona Shear Zone.

- Deposition of the Warrawoona Group at ~3480 Ma – 3450 Ma, on continental crust, during possible extension, development of mid-crustal detachments, the Mt Edgar Shear Zone and Split Rock Shear Zone, and initial doming of the early granitoid complexes.
- Deposition of the upper Warrawoona Group: the Salgash Subgroup (>3450 Ma - >3325 Ma) associated with the development of a regional parallel mafic Salgash Dyke Swarm (partly) during (N)NE-(S)SW extension. (Ongoing?) development of the Mt Edgar Shear Zone. Doming of the Gneiss Complex during granitoid sheet intrusion at ~3420 Ma.
- A prolonged period of regional E-W compression, possibly from 3.34 to 3.20 Ga.
- Granitoid magmatism and doming of the granitoid complexes of the Marble Bar Domain at ca. 3325-3300 Ma, reactivation of the Mt Edgar Shear Zone and deposition of the Wyman Formation.
- A phase of (N)NE-(S)SW compression and (N)NE-vergent thrusting (D_{X+3}) causing regional brittle-ductile fracture cleavages, crenulation cleavages and local thrusts.
- A phase of regional WNW-ESE compression at 2.95-2.93 Ga causing dextral transcurrent shearing on the Central Warrawoona Shear Zone along the axis of the Warrawoona Belt (D_{X+4}).

2. The relationship between horizontal and vertical tectonics in the development of the Marble Bar Domain follows from the structures and kinematics of regionally recognised mid-crustal

detachments, such as the Mt Edgar Shear Zone and the Split Rock Shear Zone, and the spatial and temporal relationship between those and structures in the supracrustal sequences. The tectonomagmatic history of the Mt Edgar Granitoid Complex and adjoining greenstone belts indicate that doming was the consequence of horizontal deformation including extension and compression, not the cause. Solid-state diapirism only played a minor role in the development of the Mt Edgar Granitoid Complex.

3. Mid-crustal detachments such as the Mt Edgar Shear Zone and the Split Rock Shear Zone played a central role in doming of the granitoid complexes. Intrusive sheets of ultramafic, mafic and felsic rocks that exploited the mid-crustal Mt Edgar Shear Zone facilitated displacement and may have enhanced doming, possibly by inflating the structure and by heating and weakening the crust.

4. Magmatic thickening of the crust and possibly 'vertical tectonics' is considered to have been a probable mechanism for the formation of the pre-3.46 Ga crust, possibly by a combination of mantle plumes and lower crustal delamination. From at least the development of the upper Salgash Subgroup onwards, the structural history of the Marble Bar Domain provides indications for 'horizontal tectonics'. The first regional compressional phase occurred between 3.34 Ga and 3.20 Ga, indicating regionally imposed stresses, suggesting some form of plate-interaction at this stage.

6.5 Suggestions for future research

Additional studies of the Pilbara granite-greenstone terrain may comprise:

- Further studies on the role of mid-crustal detachments by studying the structures and kinematics of identified mixed zones in the southern margin of the Muccan Granitoid Complex, in the Warrawagine Granitoid Complex, the southern margin of the Mosquito Creek Block and the western Corunna Downs Granitoid Complex.
- Better characterization of the nature of the phase of E-W compression (D_{X+2c}) by constraining the timing of the onset, the regional occurrence, possibly by obtaining more far-field information from windows in the Hamersley Basin to the south.
- Further investigation of the Salgash Dyke Swarm, to test regional occurrence, regional extension direction, the age of various dykes suites, and the geochemical constraints on petrogenesis. The Salgash Dyke Swarm may also be a potential site for paleomagnetic studies, to extend the pole path of the Marble Bar Domain and of the Pilbara granite-greenstone terrain, to compare to other domains, and other Mid-Archaean terrains (e.g. of the Kaapvaal Craton) to test for proximity, domain re-arrangement, and to test for horizontal plate motion in the Early-Mid Archaean.
- Quantification of 'mid-crustal' depth by determining the pressure conditions during crystallization of 3465 Ga hornblende-gabbro-diorite in the proto-MESZ, for a better understanding of the crustal thicknesses, thermal gradient, and crustal strength profiles.
- Further testing of the proposed scheme for the history of the Marble Bar Domain in the light of petrogenetic processes by conducting geochemical studies on temporally and structurally constrained samples.

Appendix 1. Analytical procedures and conditions during zircon analysis using SHRIMP

U, Th, and Pb analyses of zircons were made at the Perth Consortium sensitive high-resolution ion microprobe (SHRIMP II) located at Curtin University of Technology, Perth, Australia. Operating procedures follow those of described by Compston et al. (1984) and Williams et al. (1984). Data reduction and construction of conventional concordia plots was done using software written by D.R. Nelson of the G.S.W.A. During four analytical sessions, using the Sri Lankan zircon SL-2 standard, a calibration error was determined between 1.2391 and 2.0571 %, see below. During the first session, one of 13 analyses of the standard was treated as an outlier. Typically, the primary ion beam would be 15-20 μm in diameter (See figures 18a-e). Lead isotopes measurements were corrected for common lead (204Pb) using the method of Compston et al. (1984). When the average common-lead value of the 'unknowns' was similar to the average common-lead values of the standard, a correction was made assuming Broken Hill isotopic composition. Those that were higher than six times the average value of the standard were corrected assuming Cumming and Richards (1975) isotopic composition. These are marked with an asterisk in appendix 2.

Session		*1 standard deviation*	*measured samples*
1	12(-1) analyses on three SL-2 grains	2.0571 %	A94-22
2	10 analyses on one SL-2 grain	1.6567 %	A94-22, CTW-1A
3	14 analyses on two SL-2 grains	1.2391 %	ME-28, CTW-1A
4	13 analyses on two SL-2 grains	1.4834 %	CTW-36, P95-gran

Appendix 2. Common-lead corrected data from SHRIMP analysis. The internal structure of the domain refers to the CL-characteristics. The interpreted origin of the zircon domain is either igneous (i), metamorphic (m) or disturbed (d), and is interpreted in terms of the zircon growth stratigraphy as summarised for each sample in table 1. The interpreted geological significance of the (grouped) analyses is discussed in the text. Abbreviations follow those in figure 3.19.

CTW-36 Hornblende-gabbro/diorite in the Mixed Zone, central Mt Edgar Shear Zone

	Spot	Internal structure	U (ppm)	Th/U	Pb (ppm)	f206%	$^{207}Pb/^{206}Pb$	±1σ	$^{208}Pb/^{206}Pb$	±1σ	$^{206}Pb/^{238}U$	±1σ	$^{207}Pb/^{235}U$	±1σ	Conc. %	$^{206}Pb/^{207}Pb$ Age±1σ(Ma,		Interpretation Origin domain (Strat.)	Interpretation Geological interpretation
1.	19-10.1	sector z. r.	240	0,76	181	0,142	0,30490	0,00360	0,19297	0,00453	0,58304	0,01014	24,511	0,544	85	3495	18	i (1)	C
2.	20-35.1	sector z. c.	235	0,97	207	0,344	0,30433	0,00187	0,25039	0,00259	0,65287	0,01053	27,395	0,492	93	3492	10	i (1)	X
3.	20-45.1	sector.z. r.	174	0,74	168	0,071	0,30035	0,00141	0,19051	0,00160	0,74932	0,01179	31,032	0,526	104	3472	7	i (1)	C
4.	20-39.1	sector z.	314	0,75	298	0,022	0,29954	0,00109	0,19754	0,00128	0,73541	0,01131	30,372	0,493	102	3468	6	i (1)	C
5.	19-22.1	sector z.	181	1,34	194	0,254	0,29930	0,00137	0,34999	0,00217	0,74760	0,01170	30,851	0,520	104	3467	7	i (1)	C
6.	19-29.1	sector z. c.	297	0,76	294	0,016	0,29911	0,00100	0,20092	0,00105	0,76604	0,01176	31,592	0,509	106	3466	5	i (1)	C
7.	20-33.1	oscill.z.c.	237	1,25	231	0,033	0,29909	0,00137	0,31229	0,00189	0,70097	0,01106	28,907	0,491	99	3466	7	i (1)	C
8.	19-23.1	sector z. r.	171	0,81	170	0,167	0,29907	0,00138	0,20413	0,00171	0,76262	0,01195	31,447	0,531	105	3465	7	i (1)	C
9.	19-26.1	sector z. c.	226	1,45	223	-0.037	0,29901	0,00235	0,38082	0,00366	0,68159	0,01112	28,100	0,533	97	3465	12	i (1)	C
10.	19-24.1	sector z. c.	186	1,43	198	0,004	0,29884	0,00161	0,37347	0,00236	0,73909	0,01183	30,453	0,533	103	3464	8	i (1)	C
11.	20-34.1	sector z. c.	229	0,74	209	0,015	0,29878	0,00141	0,19444	0,00149	0,70913	0,01117	29,213	0,497	100	3464	7	i (1)	C
12.	19-25.1	sector z. c.	213	1,27	215	0,057	0,29857	0,00189	0,33038	0,00285	0,72053	0,01158	29,662	0,533	101	3463	10	i (1)	C
13.	20-37.1	sector z.	274	1,09	254	0,006	0,29848	0,00144	0,27773	0,00178	0,68484	0,01080	28,184	0,481	97	3462	7	i (1)	C
14.	20-47.1	sector z. r.	357	0,82	353	0,023	0,29807	0,00087	0,21429	0,00095	0,75981	0,01156	31,226	0,495	105	3460	5	i (1)	C
15.	19-28.1	sector z. c.	157	1,45	171	0,064	0,29782	0,00179	0,37752	0,00271	0,75162	0,01221	30,864	0,556	104	3459	9	i (1)	C
16.	20-41.1	laminar z.	89	0,76	86	0,202	0,29783	0,00205	0,19458	0,00261	0,75041	0,01258	30,815	0,582	104	3459	11	i (1)	C
17.	19-11.1	sector z. r.	431	1,27	466	0,031	0,29767	0,00084	0,33079	0,00119	0,76989	0,01167	31,598	0,498	106	3458	4	i (1)	C
18.	19-03.1	oscill.z.	267	1,17	242	0,091	0,29714	0,00192	0,29681	0,00259	0,65789	0,01075	26,953	0,493	94	3455	10	i (1)	C
19.	19-04.1	oscill.z.	71	0,90	76	0,186	0,29702	0,00247	0,21992	0,00316	0,80979	0,01406	33,163	0,669	111	3455	13	i (1)	C
20.	19-12.1	oscill.z.	194	1,36	203	0,101	0,29704	0,00163	0,34175	0,00242	0,73946	0,01182	30,285	0,531	103	3455	8	i (1)	C
21.	20-38.1	sector.z.	185	0,84	204	0,058	0,29547	0,00134	0,21218	0,00157	0,84666	0,01333	34,492	0,583	115	3447	7	i (1)	C
22.	19-21.1	sector z. c.	114	0,88	122	0,453	0,29474	0,00241	0,20528	0,00365	0,81724	0,01391	33,212	0,657	112	3443	13	i (1)	C
23.	19-20.1	sector.z.	150	0,91	126	0,176	0,29231	0,00350	0,23329	0,00439	0,63422	0,01144	25,561	0,584	92	3430	19	i (1)	C

P95-gran Syntectonic leucogranite/pegmatite vein in footwall gneisses of Mt Edgar Shear Zone

	Spot	Internal structure	U (ppm)	Th/U	Pb (ppm)	f206%	$^{207}Pb/^{206}Pb$	±1σ	$^{208}Pb/^{206}Pb$	±1σ	$^{206}Pb/^{238}U$	±1σ	$^{207}Pb/^{235}U$	±1σ	Conc. %	$^{206}Pb/^{207}Pb$ Age±1σ (Ma)		Interpretation: Origin domain (Strat.)	Interpretation: Geological interpretation
24.	2-26.1	oscill.c.	261	0,46	199	0,174	0,29881	0,00133	0,13881	0,00152	0,61132	0,00940	25,186	0,416	89	3464	7	i (1)	C
25.	1-25.1	patchy zr.	533	0,51	373	0,384	0,29665	0,00102	0,16320	0,00133	0,55024	0,00833	22,506	0,359	82	3453	5	d (4)	C
26.	1-10.1	patchy c.	919	0,44	725	0,191	0,29520	0,00096	0,11601	0,00103	0,64514	0,00976	26,258	0,417	93	3445	5	d (4)	C
27.	1-20.1	oscill.c.	98	0,30	86	-0.021	0,29514	0,00198	0,08461	0,00146	0,74181	0,01238	30,187	0,566	104	3445	10	i (1)	C
28.	1-24.1*	patchy	698	0,24	547	0,245	0,29463	0,00072	0,04903	0,00071	0,67262	0,01011	27,324	0,424	96	3442	4	d (4)	C
29.	2-18.1	oscill.c.	130	0,52	117	0,932	0,29463	0,00193	0,13707	0,00294	0,71202	0,01135	28,925	0,520	101	3442	10	i (1)	C
30.	3-03.1	oscill.c.	98	0,41	81	0,860	0,29352	0,00198	0,11146	0,00296	0,66603	0,01071	26,955	0,490	96	3436	10	i (1)	C
31.	1-21.1	oscill.c.	577	1,51	554	0,177	0,29093	0,00083	0,37949	0,00136	0,66442	0,01005	26,652	0,420	96	3423	4	i (1)	
32.	2-15.1*	patchy c.	1862	0,92	555	0,574	0,28621	0,00129	0,11485	0,00180	0,24247	0,00363	9,568	0,155	41	3397	7	d (4)	
33.	2-05.1*	patchy c.	387	0,50	244	0,468	0,27282	0,00115	0,12978	0,00162	0,51416	0,00785	19,341	0,316	80	3322	7	d (4)	R/M
34.	1-09.1	oscill.c.	244	0,30	171	0,058	0,27082	0,00193	0,07921	0,00165	0,60365	0,00968	22,540	0,413	92	3311	11	i (1)	R/M
35.	1-18.1	str.less. c.	134	0,14	86	-0.053	0,27048	0,00264	0,03653	0,00229	0,56907	0,00978	21,223	0,441	88	3309	15	m (3)	R/M
36.	3-01.1*	str.less. c.	633	0,65	373	1,403	0,26583	0,00109	0,17799	0,00196	0,45177	0,00678	16,559	0,266	73	3282	6	m (3)	R/M
37.	2-25.1	oscill.c.	1151	0,46	589	0,068	0,26501	0,00091	0,11606	0,00085	0,42985	0,00647	15,706	0,249	70	3277	5	i (1)	R/M
38.	2-04.1*	str.less. c.	494	5,16	287	0,968	0,25870	0,00150	0,17807	0,00256	0,45533	0,00691	16,242	0,275	75	3239	9	d (4)	
39.	1-12.1	patchy zr.	1205	0,08	486	0,335	0,25612	0,00397	0,02598	0,00547	0,36200	0,00560	12,784	0,297	62	3223	24	d (4)	
40.	1-23.1*	patchy r.	1319	0,06	635	0,632	0,25073	0,00070	0,02718	0,00097	0,42793	0,00638	14,794	0,229	72	3189	4	d (4)	
41.	3-04.1	patchy zr.	1665	0,09	471	0,247	0,24855	0,00166	0,04364	0,00184	0,25242	0,00375	8,650	0,147	46	3176	11	d (4)	
42.	2-03.1*	patchy	2034	1,15	576	3,112	0,19687	0,00180	0,06020	0,00361	0,23413	0,00352	6,355	0,118	48	2800	15	d (4)	
43.	1-13.1	patchy zr.	1672	0,51	480	0,634	0,16825	0,00113	0,07768	0,00187	0,26183	0,00394	6,074	0,105	59	2540	11	d (4)	

A94-22 Syntectonic grey gneissic granodiorite sheet in Central Gneiss Complex

	Spot	Internal structure	U (ppm)	Th/U	Pb (ppm)	f206%	$^{207}Pb/^{206}Pb$	±1σ	$^{208}Pb/^{206}Pb$	±1σ	$^{206}Pb/^{238}U$	±1σ	$^{207}Pb/^{235}U$	±1σ	Conc. %	$^{206}Pb/^{207}Pb$ Age±1σ(Ma,		Interpretation Origin domain (Strat.)	Interpretation Geological interpretation
44.	10-19.1	sector z.c.	79	0,84	70	0,001	0,29900	0,00157	0,21641	0,00191	0,66913	0,01193	27,585	0,530	95	3465	8	i (1)	X
45.	10-19.2	sector z.c.	188	0,95	168	0,001	0,29693	0,00105	0,25027	0,00134	0,67000	0,01148	27,431	0,492	96	3454	6	i (1)	X
46.	10-19.3*	oscill.r.	239	0,53	202	0,034	0,29464	0,00178	0,17656	0,00348	0,59585	0,01014	24,206	0,454	88	3442	9	i (2)	C
47.	09-11.1	str.less. c.	950	0,47	634	0,000	0,29377	0,00158	0,11720	0,00121	0,54962	0,01157	22,262	0,498	82	3438	8	i (2)	C
48.	09-11.2	str.less. c.	989	0,48	645	0,000	0,29343	0,00203	0,11851	0,00153	0,53617	0,01135	21,692	0,500	81	3436	11	i (2)	C
49.	10-20.1	sector z.c.	362	0,47	273	0,002	0,29353	0,00089	0,12483	0,00101	0,61364	0,01038	24,835	0,436	90	3436	5	i (1)	C
50.	10-16.2*	patchy c.	754	0,29	525	0,001	0,29271	0,00064	0,08055	0,00058	0,58627	0,00983	23,662	0,406	87	3432	3	d (2)	C
51.	10-01.1	laminar c.	256	0,45	205	0,001	0,29177	0,00085	0,11551	0,00079	0,65794	0,01118	26,469	0,465	95	3427	5	i (1)	C
52.	10-55.1	laminar c.	285	0,22	239	0,000	0,29151	0,00068	0,05926	0,00044	0,72290	0,01503	29,056	0,616	102	3426	4	i (1)	C
53.	09-29.1	laminar c.	734	0,24	615	0,000	0,28967	0,00049	0,06198	0,00031	0,71938	0,01488	28,732	0,602	102	3416	3	i (1)	C
54.	09-10.1	str.less. r.	490	0,26	282	0,000	0,27233	0,00072	0,06773	0,00055	0,49975	0,00839	18,765	0,325	79	3319	4	m (3)	M/PM
55.	10-22.1	str.less. r.	531	0,29	355	0,001	0,27164	0,00068	0,07529	0,00056	0,57456	0,00964	21,519	0,372	88	3316	4	m (3)	M/PM
56.	10-45.1	str.less. r.	406	0,31	277	0,001	0,27157	0,00134	0,08122	0,00125	0,58348	0,01230	21,848	0,486	89	3315	8	m (3)	M/PM
57.	09-30.1	str.less. r.	519	0,25	427	0,000	0,27121	0,00050	0,06600	0,00036	0,71449	0,01479	26,718	0,561	105	3313	3	m (3)	M/PM
58.	09-26.1	str.less. r.	787	0,32	490	0,001	0,27105	0,00150	0,08023	0,00132	0,53459	0,01121	19,979	0,446	83	3312	9	m (3)	M/PM
59.	09-15.1	str.less. c.	406	0,26	194	0,005	0,27094	0,00121	0,07116	0,00160	0,40823	0,00689	15,250	0,274	67	3311	7	m (3)	M/PM
60.	10-41.1	str.less. r.	407	0,27	308	0,000	0,27089	0,00060	0,07020	0,00044	0,65520	0,01101	24,472	0,421	98	3311	3	m (3)	M/PM
61.	09-09.1*	str.less. r.	454	0,39	240	0,003	0,27072	0,00104	0,09981	0,00119	0,44287	0,00746	16,531	0,293	71	3310	6	m (3)	M/PM

A94-22 Syntectonic grey gneissic granodiorite sheet in Central Gneiss Complex

Spot	Internal structure	U (ppm)	Th/U	Pb (ppm)	f206%	$^{207}Pb/^{206}Pb$	±1σ	$^{208}Pb/^{206}Pb$	±1σ	$^{206}Pb/^{238}U$	±1σ	$^{207}Pb/^{235}U$	±1σ	Conc. %	$^{206}Pb/^{207}Pb$ Age±1σ(Ma)		Interpretation: Origin domain (Strat.)	Interpretation: Geological interpretation
10-19.1	sector z.c.	79	0,84	70	0,001	0,29900	0,00157	0,21641	0,00191	0,66913	0,01193	27,585	0,530	95	3465	8	i (1)	X
10-19.2	sector z.c.	188	0,95	168	0,001	0,29693	0,00105	0,25027	0,00134	0,67000	0,01148	27,431	0,492	96	3454	6	i (1)	X
10-19.3*	oscill.r.	239	0,53	202	0,034	0,29464	0,00178	0,17656	0,00348	0,59585	0,01014	24,206	0,454	88	3442	9	i (2)	C
09-11.1	str.less. c.	950	0,47	634	0,000	0,29377	0,00158	0,11720	0,00121	0,54962	0,01157	22,262	0,498	82	3438	8	i (2)	C
09-11.2	str.less. c.	989	0,48	645	0,000	0,29343	0,00203	0,11851	0,00153	0,53617	0,01135	21,692	0,500	81	3436	11	i (2)	C
10-20.1	sector z.c.	362	0,47	273	0,002	0,29353	0,00089	0,12483	0,00101	0,61364	0,01038	24,835	0,436	90	3436	5	i (1)	C
10-16.2*	patchy c.	754	0,29	525	0,001	0,29271	0,00064	0,08055	0,00058	0,58627	0,00983	23,662	0,406	87	3432	3	d (2)	C
10-01.1	laminar c.	256	0,45	205	0,001	0,29177	0,00085	0,11551	0,00079	0,65794	0,01118	26,469	0,465	95	3427	5	i (1)	C
10-55.1	laminar c.	285	0,22	239	0,000	0,29151	0,00068	0,05926	0,00044	0,72290	0,01503	29,056	0,616	102	3426	4	i (1)	C
09-29.1	laminar c.	734	0,24	615	0,000	0,28967	0,00049	0,06198	0,00031	0,71938	0,01488	28,732	0,602	102	3416	3	i (1)	C
09-10.1	str.less. r.	490	0,26	282	0,000	0,27233	0,00072	0,06773	0,00055	0,49975	0,00839	18,765	0,325	79	3319	4	m (3)	M/PM
10-22.1	str.less. r.	531	0,29	355	0,001	0,27164	0,00068	0,07529	0,00056	0,57456	0,00964	21,519	0,372	88	3316	4	m (3)	M/PM
10-45.1	str.less. r.	406	0,31	277	0,001	0,27157	0,00134	0,08122	0,00125	0,58348	0,01230	21,848	0,486	89	3315	8	m (3)	M/PM
09-30.1	str.less. r.	519	0,25	427	0,000	0,27121	0,00050	0,06600	0,00036	0,71449	0,01479	26,718	0,561	105	3313	3	m (3)	M/PM
09-26.1	str.less. r.	787	0,32	490	0,001	0,27105	0,00150	0,08023	0,00132	0,53459	0,01121	19,979	0,446	83	3312	9	m (3)	M/PM
09-15.1	str.less. c.	406	0,26	194	0,005	0,27094	0,00121	0,07116	0,00160	0,40823	0,00689	15,250	0,274	67	3311	7	m (3)	M/PM
10-41.1	str.less. r.	407	0,27	308	0,000	0,27089	0,00060	0,07020	0,00044	0,65520	0,01101	24,472	0,421	98	3311	3	m (3)	M/PM
09-09.1*	str.less. r.	454	0,39	240	0,003	0,27072	0,00104	0,09981	0,00119	0,44287	0,00746	16,531	0,293	71	3310	6	m (3)	M/PM
10-36.2	str.less. r.	326	0,28	235	0,002	0,27072	0,00081	0,07174	0,00081	0,61948	0,01047	23,123	0,405	94	3310	5	m (3)	M/PM
10-52.1	str.less. r.	460	0,25	343	0,000	0,27067	0,00054	0,06583	0,00042	0,64825	0,01086	24,192	0,414	97	3310	3	m (3)	M/PM
09-46.1	str.less. r.	519	0,24	354	0,000	0,27042	0,00138	0,06399	0,00079	0,59415	0,01251	22,153	0,493	91	3308	8	m (3)	M/PM
10-50.1*	str.less. r.	569	0,19	339	0,011	0,27014	0,00072	0,06063	0,00114	0,50107	0,00837	18,663	0,322	79	3307	4	m (3)	M/PM
09-49.1*	oscill.r.	611	0,45	498	0,010	0,26984	0,00091	0,13296	0,00148	0,65247	0,01355	24,276	0,521	98	3305	5	i (2)	M/PM
10-34.1*	oscill.r.	326	0,28	232	0,004	0,26928	0,00084	0,07098	0,00106	0,60820	0,01024	22,581	0,395	93	3302	5	i (2)	M/PM
10-47.1	oscill.r.	1057	0,19	608	0,013	0,26923	0,00245	0,04750	0,00396	0,48711	0,00818	18,082	0,363	77	3302	14	i (2)	M/PM
09-28.1	str.less. r.	516	0,29	391	0,001	0,26888	0,00088	0,07643	0,00085	0,65222	0,01357	24,180	0,519	98	3299	5	m (3)	M/PM
10-17.1*	str.less. r.	484	0,20	310	0,002	0,26877	0,00070	0,05478	0,00067	0,55922	0,00940	20,723	0,359	87	3299	4	m (3)	M/PM
09-25.1	str.less. r.	440	0,31	259	0,003	0,26858	0,00080	0,07375	0,00087	0,50404	0,00847	18,665	0,326	80	3298	5	m (3)	
09-49.2*	oscill.r.	388	0,40	311	0,010	0,26784	0,00108	0,10299	0,00172	0,65469	0,01364	24,178	0,525	99	3293	6	i (2)	
09-03.1	str.less. r.	472	0,25	245	0,001	0,26642	0,00091	0,06352	0,00069	0,45154	0,00762	16,587	0,292	73	3285	5	m (3)	
09-31.1	str.less. r.	576	0,23	389	0,002	0,26363	0,00064	0,06152	0,00068	0,58779	0,01218	21,365	0,452	91	3269	4	m (3)	
09-35.1	str.less. r.	615	0,21	370	0,005	0,26364	0,00111	0,05632	0,00148	0,52065	0,01084	18,926	0,412	83	3269	7	m (3)	
09-36.1	str.less. r.	716	0,24	333	0,012	0,26291	0,00570	0,06973	0,00931	0,38973	0,00867	14,128	0,465	65	3264	34	m (3)	
10-33.1*	str.less. r.	183	0,34	84	0,090	0,26243	0,00572	0,16332	0,01212	0,27996	0,00493	10,130	0,301	49	3261	34	m (3)	
10-36.1*	patchy c.	705	0,09	403	0,002	0,26112	0,00058	0,02546	0,00054	0,51317	0,00857	18,476	0,316	82	3253	3	d (3)	
10-31.1	str.less. r.	617	0,15	311	0,002	0,25923	0,00079	0,03909	0,00081	0,44729	0,00750	15,987	0,278	74	3242	5	m (3)	
08-06.1*	patchy	865	0,20	299	0,030	0,25912	0,00221	0,06281	0,00423	0,27298	0,00458	9,753	0,193	48	3241	13	d (3)	
09-33.2	str.less. r.	367	0,47	297	0,000	0,25856	0,00070	0,12515	0,00067	0,67797	0,01411	24,170	0,515	103	3238	4	m (3)	R/M

08-20.1*	patchy	512	0,12	309	0,008	0,25787	0,00071	0,03942	0,00105	0,52566	0,00879	18,690	0,323	84	3234	4	d (3)	R/M
08-29.1	patchy	308	0,47	161	0,001	0,25792	0,00100	0,14385	0,00121	0,43335	0,00730	15,411	0,273	72	3234	6	d (3)	R/M
10-39.1	str.less. r.	501	0,49	393	0,000	0,25769	0,00052	0,12909	0,00051	0,65694	0,01101	23,341	0,400	101	3233	3	m (3)	R/M
09-33.1	str.less. r.	402	0,20	300	0,003	0,25738	0,00069	0,05262	0,00077	0,65568	0,01361	23,268	0,495	101	3231	4	m (3)	R/M
09-48.1	str.less. r.	470	0,50	342	0,001	0,25597	0,00102	0,12856	0,00105	0,60951	0,01274	21,512	0,468	95	3222	6	m (3)	R/M
09-47.1*	str.less. r.	523	0,23	265	0,003	0,25451	0,00069	0,05884	0,00083	0,44384	0,00742	15,575	0,269	74	3213	4	m (3)	
08-08.1*	patchy	412	0,17	164	0,013	0,25418	0,00108	0,06553	0,00182	0,33495	0,00560	11,739	0,209	58	3211	7	d (3)	
10-48.1*	patchy c.	648	0,11	343	0,018	0,25126	0,00097	0,03713	0,00171	0,44644	0,00923	15,467	0,332	75	3193	6	d (3)	
10-54.1	str.less. c.	679	0,53	441	0,000	0,24951	0,00102	0,12716	0,00099	0,54713	0,01134	18,822	0,407	88	3182	6	m (3)	
10-37.1	str.less	669	0,22	321	0,003	0,24864	0,00143	0,08643	0,00170	0,41262	0,00864	14,146	0,317	70	3176	9	m (3)	
10-16.1*	patchy r.	931	0,26	294	0,016	0,24317	0,00122	0,07372	0,00214	0,26327	0,00439	8,827	0,159	48	3141	8	d (3)	
09-12.1	str.less. r.	1020	0,19	496	0,001	0,24044	0,00066	0,05126	0,00058	0,43608	0,00903	14,457	0,307	75	3123	4	m (3)	
10-14.1*	oscill.r.	816	0,12	266	0,019	0,23160	0,00181	0,08045	0,00333	0,26981	0,00452	8,616	0,167	50	3063	13	i (?)	
10-30.2*	str.less. r.	820	0,06	224	0,008	0,23082	0,00117	0,02100	0,00181	0,24595	0,00410	7,827	0,141	46	3058	8	m (3)	
09-27.1*	patchy c.	2907	0,10	1182	0,004	0,22604	0,00049	0,03746	0,00064	0,36809	0,00759	11,472	0,241	67	3024	3	d (3)	
10-38.1*	patchy c.	2080	0,15	717	0,004	0,20979	0,00036	0,04324	0,00047	0,31539	0,00524	9,123	0,154	61	2904	3	d (3)	
08-16.1*	patchy	1540	0,10	419	0,019	0,19557	0,00067	0,03707	0,00124	0,23895	0,00397	6,443	0,112	50	2790	6	d (3)	

ME-28 Syntectonic biotite-granodiorite sill near footwall margin of Mt Edgar Shear Zone

Spot	Internal structure	U (ppm)	Th/U	Pb (ppm)	f206%	$^{207}Pb/^{206}Pb$	± 1σ	$^{208}Pb/^{206}Pb$	± 1σ	$^{206}Pb/^{238}U$	± 1σ	$^{207}Pb/^{235}U$	± 1σ	Conc. %	$^{206}Pb/^{207}Pb$ Age±1σ(Ma)		Interpretation: Origin domain (Strat.)	Interpretation: Geological interpretation
6-19.1	sector z. c.	101	0,56	82	0,565	0,30059	0,00258	0,14162	0,00362	0,64713	0,01008	26,821	0,502	93	3473	13	i (1)	X
6-01.1*	oscill.c.	71	0,56	62	1,407	0,29699	0,00283	0,15420	0,00477	0,67065	0,01051	27,463	0,531	96	3455	15	i (2)	X
6-03.1	oscill.c.	195	0,43	152	0,102	0,27915	0,00124	0,10723	0,00126	0,64952	0,00884	25,000	0,371	96	3358	7	i (2)	X
4-19.1	oscill.r.	194	0,30	125	0,644	0,27703	0,00296	0,07279	0,00420	0,54693	0,00780	20,891	0,394	84	3346	17	i (3)	C
4-16.1*	oscill.c.	279	0,42	220	1,134	0,27435	0,00162	0,11991	0,00265	0,63075	0,00845	23,860	0,365	95	3331	9	i (3)	C
4-17.1*	oscill.c.	464	0,39	383	0,298	0,27340	0,00094	0,10078	0,00106	0,69003	0,00902	26,011	0,362	102	3326	5	i (3)	C
4-20.1	oscill.r.	182	0,33	132	0,208	0,27319	0,00201	0,08443	0,00201	0,61754	0,00900	23,261	0,398	93	3324	12	i (3)	C
4-04.1	oscill.r.	241	0,35	194	0,125	0,27290	0,00123	0,08931	0,00117	0,68490	0,00934	25,771	0,383	101	3323	7	i (3)	C
4-31.1	oscill.r.	160	0,33	107	0,058	0,27253	0,00230	0,08237	0,00213	0,57405	0,00839	21,571	0,383	88	3321	13	i (3)	C
6-08.1	oscill.r.	224	0,34	169	0,223	0,27239	0,00124	0,08363	0,00130	0,64057	0,00872	24,058	0,358	96	3320	7	i (3)	C
4-30.1	oscill.r.	208	0,48	148	0,066	0,27146	0,00268	0,12423	0,00259	0,59292	0,00899	22,193	0,424	91	3314	15	i (3)	C
4-05.1	oscill.c.	231	0,28	193	0,093	0,27118	0,00105	0,07077	0,00087	0,71996	0,00957	26,919	0,385	106	3313	6	i (3)	C
6-06.1	oscill.r.	164	0,34	123	0,634	0,27126	0,00168	0,09455	0,00234	0,62803	0,00872	23,489	0,373	95	3313	10	i (3)	C
6-11.1	oscill.r.	238	0,35	176	0,022	0,27123	0,00140	0,09069	0,00122	0,63163	0,00873	23,621	0,362	95	3313	8	i (3)	C
6-07.1	oscill.r.	232	0,07	166	0,199	0,27065	0,00126	0,02030	0,00125	0,64279	0,00862	23,988	0,353	97	3310	7	i (3)	C
4-34.1	oscill.r.	341	0,49	252	0,192	0,27005	0,00137	0,12898	0,00156	0,60913	0,00824	22,681	0,341	93	3306	8	i (3)	C
4-21.2	oscill.c.	199	0,40	143	1,158	0,26949	0,00297	0,09692	0,00475	0,58887	0,00854	21,881	0,422	90	3303	17	i (3)	C
4-21.1	oscill.r.	223	0,31	156	0,027	0,26898	0,00195	0,08019	0,00196	0,60147	0,00870	22,306	0,379	92	3300	11	i (3)	C
4-32.1	oscill.r.	209	0,29	147	0,035	0,26904	0,00207	0,07463	0,00261	0,60644	0,00866	22,496	0,384	93	3300	12	i (3)	C
6-02.1	oscill.r.	232	0,29	200	0,327	0,26891	0,00212	0,06627	0,00247	0,74465	0,01100	27,610	0,486	109	3300	12	i (3)	C
4-15.1	oscill.r.	223	0,31	164	0,199	0,26846	0,00168	0,07669	0,00168	0,62932	0,00874	23,295	0,371	95	3297	10	i (3)	C
4-07.1	oscill.r.	115	0,43	92	0,354	0,26713	0,00229	0,11057	0,00288	0,66503	0,01010	24,494	0,449	100	3289	13	i (3)	
4-06.1*	patchy c.	332	0,49	288	9,712	0,25647	0,00422	0,16204	0,00898	0,52064	0,00724	18,411	0,420	84	3225	26	d (4)	

CTW1A Discordant Cotton Well Pluton muscovite-granite post Mixed Zone and main development Mt Edgar Shear Zone

Spot	Internal structure	U (ppm)	Th/U	Pb (ppm)	f206%	$^{207}Pb/^{206}Pb$	±1σ	$^{208}Pb/^{206}Pb$	±1σ	$^{206}Pb/^{238}U$	±1σ	$^{207}Pb/^{235}U$	±1σ	Conc. %	$^{206}Pb/^{207}Pb$ Age±1σ(Ma)		Interpretation Origin domain (Strat.)	Interpretation Geological interpretation
17-20.1	str.less c.	228	0,93	239	0,001	0,29954	0,00101	0,23825	0,00123	0,78725	0,01043	32,514	0,458	108	3468	5	m (1)	X-1
17-08.1	sector z. c.	318	0,99	337	0,001	0,29880	0,00087	0,25424	0,00109	0,78878	0,01025	32,496	0,444	108	3464	5	i (1)	X-1
17-19.1	str.less r.	385	0,88	383	0,001	0,29815	0,00074	0,23559	0,00091	0,75048	0,00962	30,852	0,412	104	3461	4	m (2)	X-1
17-20.2	oscill.r.	213	0,85	210	0,004	0,29752	0,00115	0,21829	0,00166	0,74749	0,00991	30,664	0,438	104	3457	6	i (2)	X-1
17-17.1	laminar c.	517	1,26	526	0,001	0,29619	0,00068	0,32658	0,00097	0,72548	0,00926	29,628	0,393	102	3450	4	i (1)	X-2
17-31.1	oscill.r.	182	0,87	187	0,007	0,29472	0,00138	0,23267	0,00225	0,76621	0,01022	31,136	0,457	107	3443	7	i (2)	X-2
18-34.1*	oscill.c.	194	0,96	159	0,005	0,29361	0,00142	0,23050	0,00217	0,61383	0,00816	24,850	0,365	90	3437	7	i (2)	X-2
17-05.1	str.less.c.	358	0,96	342	0,002	0,29330	0,00082	0,25130	0,00110	0,71405	0,00919	28,877	0,390	101	3435	4	d (1)	X-2
17-03.1	str.less.r.	200	0,28	154	0,005	0,28493	0,00135	0,05901	0,00172	0,65691	0,00875	25,807	0,379	96	3390	7	m (5?)	X-3
17-18.1	str.less r.	419	0,67	302	0,002	0,28480	0,00076	0,19596	0,00095	0,56255	0,00715	22,090	0,294	85	3389	4	m (5?)	X-3
18-24.1	oscill.c.	81	1,04	40	0,017	0,27560	0,00371	0,12773	0,00675	0,39067	0,00853	14,845	0,401	64	3338	21	i (3)	X/C?
16-18.1	oscill.r.	82	0,33	57	0,001	0,27476	0,00405	0,08168	0,00357	0,58928	0,01425	22,324	0,667	90	3333	23	i (3)	X/C?
18-33.1	oscill.c.	184	0,43	146	0,001	0,27362	0,00126	0,10700	0,00147	0,66530	0,01407	25,099	0,557	99	3327	7	i (3)	X/C?
18-32.1*	oscill.c.	195	0,50	146	0,019	0,27294	0,00170	0,15174	0,00312	0,57451	0,00757	21,620	0,330	88	3323	10	i (3)	X/C?
16-12.1	oscill.r.	76	0,33	71	0,001	0,27281	0,00198	0,08852	0,00211	0,80159	0,01777	30,152	0,729	114	3322	11	i (3)	X/C?
18-01.1	laminar c.	152	0,32	101	0,001	0,27195	0,00284	0,08535	0,00381	0,57053	0,00872	21,393	0,418	88	3317	16	i (1?)	X/C?
18-26.1	oscill.c.	77	0,45	53	0,002	0,27151	0,00472	0,11582	0,00509	0,57263	0,00983	21,437	0,555	88	3315	27	i (3)	X/C?
18-16.1	str.less.c.	347	0,43	276	0,004	0,27135	0,00101	0,10583	0,00132	0,66225	0,00863	24,777	0,347	99	3314	6	m (5?)	X/C?
18-20.1*	str.less.c.	396	0,41	305	0,003	0,27118	0,00096	0,09605	0,00119	0,64607	0,00837	24,156	0,335	97	3313	6	m (5?)	X/C?
18-31.1	oscill.r.	368	0,43	290	0,002	0,27108	0,00083	0,10230	0,00095	0,66231	0,00852	24,755	0,337	99	3312	5	i (3)	X/C?
18-04.1	oscill.r.	274	0,36	215	0,001	0,27072	0,00064	0,08852	0,00060	0,66745	0,01386	24,914	0,528	100	3310	4	i (3)	X/C?
18-02.1	laminar c.	109	0,94	81	0,005	0,27003	0,00223	0,13831	0,00339	0,59843	0,01327	22,281	0,548	91	3306	13	i (1?)	X/C?
17-22.1	oscill.r.	148	0,44	127	0,002	0,26971	0,00153	0,10112	0,00177	0,72070	0,00996	26,801	0,417	106	3304	9	i (3)	X/C?
18-03.1	oscill.r.	239	0,27	170	0,005	0,26874	0,00181	0,06800	0,00238	0,61043	0,01313	22,619	0,528	93	3299	11	i (3)	X/C?
18-17.1	oscill.r.	104	1,59	72	0,007	0,26878	0,00186	0,12109	0,00292	0,56438	0,00777	20,916	0,338	87	3299	11	i (3)	X/C?
18-22.1	oscill.c.	157	0,38	94	0,004	0,26868	0,00249	0,08816	0,00312	0,50638	0,00726	18,759	0,338	80	3298	15	i (3)	X/C?
17-04.1	oscill.r.	71	0,44	53	0,004	0,26842	0,00219	0,09706	0,00298	0,61960	0,00908	22,931	0,404	94	3297	13	i (3)	X/C?
18-05.1*	oscill.c.	179	0,43	136	0,006	0,26676	0,00129	0,09371	0,00179	0,63670	0,00844	23,418	0,343	97	3287	8	i (3)	C ?
18-30.1*	oscill.c.	206	0,90	138	0,019	0,26604	0,00176	0,13368	0,00320	0,52240	0,00690	19,163	0,297	83	3283	10	i (3)	C ?
17-21.1	oscill.c.	111	0,39	65	0,009	0,26492	0,00211	0,09357	0,00330	0,48983	0,00678	17,892	0,301	78	3276	13	i (3)	C ?
16-07.1	str.less.c.	200	0,66	132	0,018	0,26336	0,00246	0,09016	0,00436	0,53559	0,01151	19,449	0,476	85	3267	15	m (5?)	R ?
16-06.1	str.less.c.	823	0,30	467	0,002	0,26309	0,00085	0,09370	0,00094	0,48207	0,01002	17,487	0,375	78	3265	5	m (5?)	R ?
18-06.1	laminar c.	78	0,32	53	0,023	0,25943	0,00833	0,05378	0,01563	0,55616	0,01485	19,894	0,880	88	3243	51	i (1?)	
17-09.1	patchy c.	1003	1,68	722	0,000	0,25917	0,00058	0,43494	0,00104	0,49246	0,00620	17,598	0,230	80	3242	4	d (6)	
18-05.2*	oscill.r.	180	0,63	64	0,024	0,25160	0,00273	0,11256	0,00514	0,28060	0,00375	9,734	0,177	50	3195	17	i (3)	
17-06.1*	patchy c.	693	1,29	420	0,003	0,25119	0,00068	0,31883	0,00116	0,44465	0,00562	15,400	0,204	74	3192	4	d (6)	
18-28.1	patchy r.	508	0,84	198	0,033	0,25060	0,00268	0,09816	0,00528	0,30363	0,00639	10,491	0,260	54	3189	17	d (6)	
18-18.1	patchy c.	60	1,35	10	0,067	0,20910	0,00740	-0,00827	0,01568	0,12979	0,00288	3,742	0,165	27	2899	57	d (6)	
17-13.1	patchy c.	1138	1,55	403	0,002	0,18940	0,00112	0,39640	0,00237	0,25797	0,00328	6,737	0,099	54	2737	10	d (6)	

Appendix 3. Processed ^{40}Ar-^{39}Ar incremental heating data

Sample CTW-36 / hornblende >250 µm (irradiation batch VU29)

Steps	$^{36}Ar(a)$	$^{37}Ar(Ca)$	$^{38}Ar(Cl)$	$^{39}Ar(K)$	$^{40}Ar(a+r)$	Age ± 2σ	$^{40}Ar(r)$	Fraction	K/Ca
98M0258B	0,00664	0,23149	0,00229	0,03496	26,90313	4783,9 32,0	92,71%	0,30%	0,074
98M0258C	0,00056	0,03670	0,00038	0,00692	4,03260	4378,7 52,5	95,87%	0,06%	0,092
98M0258D	0,00100	0,10846	0,00086	0,02612	9,19560	3584,7 32,8	96,79%	0,23%	0,118
98M0258E	0,00147	0,24912	0,00134	0,04189	13,18082	3409,9 29,5	96,71%	0,36%	0,082
98M0258G	0,00032	0,46955	0,00210	0,07748	16,32402	2855,6 21,6	99,42%	0,67%	0,081
98M0258H	0,00017	0,83218	0,00339	0,11260	25,45906	2963,2 19,1	99,80%	0,98%	0,066
98M0258I	0,00048	1,80042	0,00703	0,22881	53,15531	3001,7 16,5	99,73%	1,98%	0,062
98M0258J	0,00089	2,47600	0,00928	0,31420	75,91756	3058,1 16,7	99,65%	2,72%	0,062
98M0258L	0,00011	3,13810	0,01237	0,41766	101,68686	3074,0 17,0	99,96%	3,62%	0,065
98M0258M	0,00073	3,90185	0,01312	0,44429	108,06524	3070,1 17,2	99,80%	3,85%	0,056
98M0258N	0,00280	6,74439	0,02719	0,92708	229,43639	3093,3 15,6	99,64%	8,04%	0,067
98M0258O	0,00326	5,67540	0,02109	0,70977	173,87143	3075,3 15,6	99,44%	6,16%	0,061
98M0258Q	0,00000	3,08143	0,01167	0,40027	97,10784	3069,2 18,7	100,00%	3,47%	0,064
98M0258R	0,00162	8,76895	0,03456	1,18197	290,49802	3086,0 15,6	99,83%	10,25%	0,066
98M0258S	0,00140	8,45264	0,03122	1,07362	261,45971	3072,5 15,8	99,84%	9,31%	0,062
98M0258T	0,00175	5,85243	0,02175	0,80203	195,74301	3074,1 16,3	99,73%	6,96%	0,067
98M0258V	0,00000	3,53959	0,01222	0,44901	108,93081	3069,2 21,8	100,00%	3,89%	0,062
98M0258W	0,00000	1,79963	0,00516	0,23543	58,41193	3102,4 31,3	100,00%	2,04%	0,064
98M0258X	0,00000	2,36758	0,00827	0,32698	81,40870	3107,5 24,9	100,00%	2,84%	0,068
98M0258Y	0,00000	4,03271	0,01295	0,44727	110,58544	3097,2 21,3	100,00%	3,88%	0,054
98M0258Z	0,00570	29,86724	0,09590	3,27221	804,03012	3084,9 15,1	99,79%	28,38%	0,054

Irrediation values		*Results*	40*/39K ± 2σ	Age	2σ
J	= 0,018470	Weighted Mean of Plateau	244,4570 ± 0,8585	3080	16
sd-J (1σ)	= 0,000092	Total Fusion	246,0301 ± 1,2139	3090	16

Sample CTW-36 / hornblende <250 µm (irradiation batch VU29)

Steps	$^{36}Ar(a)$	$^{37}Ar(Ca)$	$^{38}Ar(Cl)$	$^{39}Ar(K)$	$^{40}Ar(a+r)$	Age ± 2σ	$^{40}Ar(r)$	Fraction	K/Ca
98M0271C	0,00135	0,04869	0,00058	0,00523	8,27997	6096,2 66,2	95,16%	0,19%	0,053
98M0271D	0,00061	0,02774	0,00031	0,00429	3,94014	5160,9 73,7	95,39%	0,15%	0,076
98M0271E	0,00036	0,05648	0,00018	0,00838	2,47506	3323,6 61,1	95,65%	0,30%	0,073
98M0271F	0,00053	0,46741	0,00178	0,05722	13,39766	3026,4 23,4	98,82%	2,05%	0,060
98M0271H	0,00000	0,72286	0,00280	0,09036	21,47720	3065,9 22,6	100,00%	3,24%	0,061
98M0271I	0,00000	2,50719	0,00915	0,29868	72,66870	3100,4 15,8	100,00%	10,70%	0,058
98M0271J	0,00110	5,07765	0,01772	0,61376	146,38056	3067,7 15,4	99,77%	21,99%	0,059
98M0271K	0,00089	5,20315	0,01889	0,66435	160,12149	3084,0 16,5	99,83%	23,80%	0,063
98M0271M	0,00000	1,90758	0,00712	0,25379	62,15148	3110,1 17,7	100,00%	9,09%	0,065
98M0271N	0,00000	1,18507	0,00354	0,12087	29,04553	3082,1 23,4	100,00%	4,33%	0,050
98M0271O	0,00000	0,85288	0,00275	0,09793	24,09234	3116,9 25,7	100,00%	3,51%	0,056
98M0271P	0,00000	1,07513	0,00303	0,10939	26,32648	3084,3 24,7	100,00%	3,92%	0,050
98M0271R	0,00000	0,62441	0,00148	0,06492	15,58010	3080,2 32,7	100,00%	2,33%	0,051
98M0271S	0,00000	3,69180	0,01134	0,40168	97,36312	3094,9 15,7	100,00%	14,39%	0,053

Irrediation values		*Results*	40*/39K ± 2σ	Age	2σ
J	= 0,018810	Weighted Mean of Plateau	241,1511 ± 1,7014	3087	18
sd-J (1σ)	= 0,000094	Total Fusion	244,3208 ± 1,5249	3107	17

Sample P96-233 / hornblende 250 µm (irradiation batch VU29)

Steps	^{36}Ar(a)	^{37}Ar(Ca)	^{38}Ar(Cl)	^{39}Ar(K)	^{40}Ar(a+r)	Age ± 2σ	^{40}Ar(r)	Fraction	K/Ca
98M0278B	0,00206	0,06294	0,00063	0,01117	13,57838	5792,2 65,8	95,52%	0,46%	0,087
98M0278C	0,00060	0,02802	0,00046	0,01893	4,68188	3195,4 48,4	96,20%	0,78%	0,331
98M0278D	0,00090	0,07780	0,00103	0,06732	8,86566	2320,3 20,9	97,00%	2,76%	0,424
98M0278E	0,00020	0,14377	0,00126	0,09404	12,48502	2364,7 20,1	99,53%	3,86%	0,320
98M0278F	0,00026	0,56657	0,00140	0,09168	16,68508	2797,2 17,5	99,54%	3,76%	0,079
98M0278H	0,00100	4,25832	0,00609	0,29832	80,31804	3376,6 15,9	99,63%	12,24%	0,034
98M0278I	0,00044	6,07737	0,00816	0,42416	108,44479	3301,8 15,7	99,88%	17,41%	0,034
98M0278J	0,00080	5,90638	0,00836	0,41256	106,45084	3314,1 16,4	99,77%	16,93%	0,034
98M0278K	0,00081	3,65098	0,00621	0,33901	85,83265	3284,6 15,6	99,72%	13,91%	0,045
98M0278L	0,00051	2,12495	0,00241	0,13539	32,54234	3203,5 19,4	99,53%	5,56%	0,031
98M0278N	0,00000	2,84651	0,00310	0,15846	40,79977	3314,3 17,3	100,00%	6,50%	0,027
98M0278O	0,00000	0,81888	0,00075	0,04924	11,71336	3194,9 31,8	100,00%	2,02%	0,029
98M0278P	0,00047	5,67770	0,00630	0,33601	81,18897	3215,8 15,8	99,83%	13,79%	0,029

Irrediation values		*Results*	40*/39K ± 2σ	Age	2σ
J	= 0,020500	Weighted Mean of Plateau	254,6793 ± 2,3141	3298	20
sd-J (1σ)	= 0,000103	Total Fusion	246,7735 ± 1,2037	3250	17

Sample P97-366 / hornblende 100-500 (irradiation batch VU29)

Steps	^{36}Ar(a)	^{37}Ar(Ca)	^{38}Ar(Cl)	^{39}Ar(K)	^{40}Ar(a+r)	Age ± 2σ	^{40}Ar(r)	Fraction	K/Ca
98M0277B	0,00130	0,01316	0,000204	0,001880	4,763481	6899,1 217,2	91,94%	0,10%	0,070
98M0277C	0,00018	0,00348	0,000097	0,002020	0,938767	4043,4 144,5	94,21%	0,11%	0,284
98M0277D	0,00013	0,01836	0,000195	0,006520	1,312068	2812,4 96,5	97,13%	0,34%	0,174
98M0277E	0,00000	0,08551	0,000172	0,009680	2,520104	3232,1 39,7	99,99%	0,50%	0,055
98M0277F	0,00028	0,95534	0,001170	0,053036	15,604407	3409,6 16,8	99,46%	2,76%	0,027
98M0277H	0,00000	2,05807	0,002130	0,111756	29,337047	3244,5 18,0	100,00%	5,82%	0,027
98M0277I	0,00006	3,34637	0,004680	0,226908	60,014891	3255,4 16,6	99,96%	11,82%	0,033
98M0277J	0,00008	3,19022	0,004560	0,220188	58,188631	3253,9 16,1	99,95%	11,47%	0,034
98M0277K	0,00156	5,27852	0,010936	0,479788	126,729549	3248,3 15,5	99,63%	25,00%	0,045
98M0277L	0,00067	2,08618	0,003660	0,170035	44,620163	3237,3 16,9	99,55%	8,86%	0,040
98M0277N	0,00000	0,69351	0,000572	0,050442	13,171553	3236,6 32,5	100,00%	2,63%	0,036
98M0277O	0,00000	2,61230	0,003700	0,184726	48,279726	3237,9 19,1	100,00%	9,63%	0,035
98M0277P	0,00000	1,44236	0,001760	0,091222	24,011588	3248,6 22,1	100,00%	4,75%	0,031
98M0277Q	0,00000	0,51006	0,000164	0,034495	9,159393	3261,7 44,4	100,00%	1,80%	0,033
98M0277R	0,00034	4,00530	0,005720	0,276348	72,938060	3250,6 16,6	99,86%	14,40%	0,034

Irrediation values		*Results*	40*/39K ± 2σ	Age	2σ
J	= 0,019200	Weighted Mean of Plateau	263,2366 ± 0,6254	3249	15
sd-J (1σ)	= 0,000096	Total Fusion	265,8755 ± 1,6126	3264	18

Sample P96-234 / hornblende 125-250 µm (irradiation batch VU29)

Steps	^{36}Ar(a)	^{37}Ar(Ca)	^{38}Ar(Cl)	^{39}Ar(K)	^{40}Ar(a+r)	Age ± 2σ	^{40}Ar(r)	Fraction	K/Ca
98M0266C	0,00165	0,04187	0,00022	0,00399	2,41983	4362,0 134,3	79,89%	0,72%	0,047
98M0266D	0,00018	0,00736	0,00007	0,00274	0,59052	2950,3 254,0	90,80%	0,50%	0,182
98M0266E	0,00023	0,01895	0,00015	0,00508	0,81332	2545,2 149,9	91,67%	0,92%	0,131
98M0266F	0,00011	0,03920	0,00010	0,00413	0,48811	2167,3 209,2	93,20%	0,75%	0,052
98M0266H	0,00000	0,06693	0,00006	0,00282	0,52080	2867,8 265,6	99,99%	0,51%	0,021
98M0266I	0,00014	0,30787	0,00000	0,00585	2,64166	4219,6 97,1	98,40%	1,06%	0,009
98M0266J	0,00013	1,58812	0,00041	0,02024	5,94422	3550,2 35,2	99,33%	3,67%	0,006
98M0266K	0,00030	5,27424	0,00171	0,06811	19,57233	3519,6 22,6	99,54%	12,34%	0,006
98M0266M	0,00052	8,45898	0,00263	0,10979	28,32060	3352,6 20,2	99,46%	19,89%	0,006
98M0266N	0,00040	9,98367	0,00274	0,12371	30,42677	3282,6 17,9	99,60%	22,41%	0,006
98M0266O	0,00023	5,64128	0,00174	0,07056	17,09987	3260,2 20,4	99,59%	12,78%	0,006
98M0266P	0,00024	1,86936	0,00044	0,02408	5,76867	3230,5 39,0	98,79%	4,36%	0,006
98M0266R	0,00009	1,75761	0,00051	0,02236	5,36664	3243,8 41,1	99,49%	4,05%	0,006
98M0266S	0,00071	2,21203	0,00069	0,02827	7,19940	3296,3 33,1	97,07%	5,12%	0,006
98M0266T	0,00030	1,76259	0,00043	0,02029	5,10031	3295,1 49,2	98,26%	3,68%	0,006
98M0266U	0,00000	1,08550	0,00029	0,01212	3,09955	3347,2 66,2	100,00%	2,20%	0,005
98M0266W	0,00000	0,56058	0,00007	0,00668	1,65657	3300,8 119,3	99,99%	1,21%	0,006
98M0266X	0,00017	1,78206	0,00050	0,02109	5,57266	3383,4 44,5	99,07%	3,82%	0,006

Irrediation values		*Results*	40*/39K ± 2σ	Age	2σ
J = 0,020110		Weighted Mean of Plateau	244,1677 ± 2,8217	3205	23
sd-J (1σ) = 0,000101		Total Fusion	255,4674 ± 4,7626	3273	32

Sample P96-237 / hornblende 250-400 µm (irradiation batch VU29)

Steps	^{36}Ar(a)	^{37}Ar(Ca)	^{38}Ar(Cl)	^{39}Ar(K)	^{40}Ar(a+r)	Age ± 2σ	^{40}Ar(r)	Fraction	K/Ca
98M0270C	0,00160	0,11918	0,00077	0,00934	4,35374	3978,4 59,6	89,15%	0,33%	0,038
98M0270D	0,00073	0,07381	0,00021	0,01008	2,28645	2900,8 69,5	90,56%	0,36%	0,067
98M0270E	0,00056	0,17076	0,00074	0,03746	7,71491	2872,8 22,9	97,86%	1,32%	0,108
98M0270F	0,00074	1,06949	0,00302	0,11720	29,22998	3174,3 17,4	99,25%	4,13%	0,054
98M0270H	0,00000	1,03810	0,00302	0,09256	24,63896	3283,5 24,5	100,00%	3,26%	0,044
98M0270I	0,00159	12,34694	0,03608	1,06461	290,99605	3321,2 15,6	99,83%	37,52%	0,042
98M0270J	0,00257	8,42861	0,02624	0,74819	203,04806	3307,1 15,9	99,62%	26,37%	0,043
98M0270K	0,00165	4,84015	0,01296	0,38715	105,69819	3314,8 16,0	99,53%	13,64%	0,039
98M0270M	0,00000	1,06277	0,00315	0,09008	24,73697	3330,8 28,9	100,00%	3,17%	0,042
98M0270N	0,00000	0,54898	0,00160	0,04243	11,77862	3347,1 51,2	100,00%	1,50%	0,038
98M0270O	0,00000	0,47913	0,00121	0,04085	11,26900	3337,6 55,8	100,00%	1,44%	0,042
98M0270P	0,00000	0,21049	0,00039	0,01844	5,10783	3344,1 111,4	100,00%	0,65%	0,043
98M0270Q	0,00000	2,23104	0,00671	0,17942	48,37402	3302,9 19,9	100,00%	6,32%	0,039

Irrediation values		*Results*	40*/39K ± 2σ	Age	2σ
J = 0,019430		Weighted Mean of Plateau	271,8696 ± 0,9138	3315	16
sd-J (1σ) = 0,000097		Total Fusion	270,0832 ± 1,5588	3305	17

Sample P96-172 / hornblende 250-500 µm (irradiation batch VU29)

Steps	^{36}Ar(a)	^{37}Ar(Ca)	^{38}Ar(Cl)	^{39}Ar(K)	^{40}Ar(a+r)	Age ± 2σ	^{40}Ar(r)	Fraction	K/Ca
98M0265C	0,00317	1,451333	0,00782	0,25373	68,22508	3310,9 15,6	98,62%	6,85%	0,086
98M0265D	0,00069	0,253804	0,00125	0,04537	11,40769	3203,3 33,9	98,20%	1,22%	0,088
98M0265E	0,00770	1,750954	0,00977	0,31774	74,04571	3070,9 25,5	96,92%	8,58%	0,089
98M0265F	0,00025	0,135501	0,00073	0,02677	6,26244	3105,1 31,7	98,80%	0,72%	0,097
98M0265H	0,00002	0,305187	0,00162	0,05603	14,26853	3249,1 21,6	99,95%	1,51%	0,090
98M0265I	0,00009	0,427225	0,00222	0,07758	20,17041	3279,0 24,5	99,87%	2,09%	0,089
98M0265J	0,00011	0,608610	0,00339	0,10979	28,81339	3293,5 18,2	99,89%	2,96%	0,088
98M0265K	0,00047	1,431458	0,00761	0,24930	66,00580	3305,3 15,9	99,78%	6,73%	0,085
98M0265M	0,00108	3,824186	0,02073	0,65388	172,58973	3301,0 16,0	99,81%	17,65%	0,084
98M0265N	0,00115	2,121717	0,01192	0,37684	101,19435	3324,8 16,6	99,66%	10,17%	0,087
98M0265O	0,00043	1,802288	0,01073	0,33283	88,66749	3315,7 16,5	99,85%	8,98%	0,090
98M0265P	0,00048	1,239399	0,00758	0,22233	59,03017	3309,1 17,5	99,75%	6,00%	0,088
98M0265R	0,00031	1,508975	0,00849	0,26712	71,12485	3315,1 16,7	99,87%	7,21%	0,087
98M0265S	0,00000	1,141858	0,00680	0,19776	52,35421	3308,4 17,5	100,00%	5,34%	0,085
98M0265T	0,00000	0,185006	0,00087	0,03104	8,34438	3331,6 46,9	100,00%	0,84%	0,082
98M0265U	0,00000	0,100520	0,00042	0,01803	4,74017	3297,8 71,9	100,00%	0,49%	0,088
98M0265W	0,00000	0,064267	0,00037	0,01333	3,54209	3313,7 94,7	100,00%	0,36%	0,102
98M0265X	0,00000	0,207572	0,00107	0,03927	10,34821	3301,2 36,6	100,00%	1,06%	0,093
98M0265Y	0,00000	0,279478	0,00133	0,04966	13,24432	3319,6 31,4	100,00%	1,34%	0,087
98M0265Z	0,00028	2,121495	0,01173	0,36692	97,01496	3305,1 16,3	99,91%	9,90%	0,085

Irrediation values		*Results*	40*/39K ± 2σ	Age	2σ
J	= 0,019860	Weighted Mean of Plateau	264,8901 ± 0,7408	3309	16
sd-J (1σ)	= 0,000099	Total Fusion	260,8663 ± 1,6503	3286	18

Sample P96-236 / hornblende 200-250 µm (irradiation batch VU29)

Steps	^{36}Ar(a)	^{37}Ar(Ca)	^{38}Ar(Cl)	^{39}Ar(K)	^{40}Ar(a+r)	Age ± 2σ	^{40}Ar(r)	Fraction	K/Ca
98M0261B	0,00312	0,03460	0,00061	0,00992	11,19312	5450,1 65,3	91,75%	0,22%	0,141
98M0261C	0,00046	0,01495	0,00016	0,00980	2,58965	3146,5 82,8	94,79%	0,22%	0,321
98M0261D	0,00058	0,06076	0,00058	0,02638	5,11950	2727,5 41,6	96,63%	0,60%	0,213
98M0261E	0,00014	0,47136	0,00169	0,07995	19,71192	3120,2 20,3	99,79%	1,80%	0,083
98M0261G	0,00051	1,28635	0,00421	0,17681	50,85304	3350,5 19,6	99,70%	3,99%	0,067
98M0261H	0,00166	6,12300	0,02480	1,02705	293,06624	3340,4 15,8	99,83%	23,18%	0,082
98M0261I	0,00322	5,80846	0,02409	0,99096	278,37154	3313,9 15,5	99,65%	22,36%	0,084
98M0261J	0,00345	3,13858	0,01142	0,54049	152,20750	3312,7 16,4	99,33%	12,20%	0,084
98M0261L	0,00000	2,89654	0,01136	0,50875	144,30729	3333,9 18,6	100,00%	11,48%	0,086
98M0261M	0,00000	0,98991	0,00373	0,16158	45,81033	3333,1 25,3	100,00%	3,65%	0,080
98M0261N	0,00000	0,35033	0,00056	0,05926	16,97508	3348,8 57,9	100,00%	1,34%	0,083
98M0261O	0,00000	0,20946	0,00016	0,03521	10,32393	3384,2 90,7	100,00%	0,79%	0,082
98M0261P	0,00452	5,13537	0,02150	0,80503	214,68362	3231,1 16,7	99,37%	18,17%	0,077

Irrediation values		*Results*	40*/39K ± 2σ	Age	2σ
J	= 0,018850	Weighted Mean of Plateau	281,8480 ± 1,8758	3324	18
sd-J (1σ)	= 0,000094	Total Fusion	279,8338 ± 1,5312	3313	17

Sample P97-361 / muscovite (irradiation batch VU29)

Steps	$^{36}Ar(a)$	$^{37}Ar(Ca)$	$^{38}Ar(Cl)$	$^{39}Ar(K)$	$^{40}Ar(a+r)$	Age ± 2σ	$^{40}Ar(r)$	Fraction	K/Ca
98M0275A	0,00000	0,00000	0,00038	0,03255	6,71660	2816,4 64,4	99,99%	1,25%	3274,739
98M0275B	0,00051	0,00000	0,00591	0,44005	111,24786	3109,6 16,5	99,86%	16,92%	44276,496
98M0275C	0,00029	0,02478	0,00532	0,37095	96,44551	3151,9 16,4	99,91%	14,26%	7,336
98M0275D	0,00120	0,03642	0,01116	0,76190	198,96769	3157,2 17,9	99,82%	29,30%	10,252
98M0275G	0,00027	0,02797	0,00451	0,32624	84,43321	3145,1 16,2	99,90%	12,54%	5,716
98M0275H	0,00000	0,00000	0,00255	0,17903	46,22067	3142,8 17,4	100,00%	6,88%	17757,690
98M0275I	0,00032	0,00000	0,00100	0,07712	18,69690	3042,4 24,9	99,49%	2,97%	7649,512
98M0275J	0,00176	0,00000	0,00480	0,41290	107,91858	3153,9 15,7	99,51%	15,88%	40873,013

Irrediation values		*Results*	40*/39K ± 2σ	Age	2σ
J = 0,018240		Weighted Mean of Plateau	259,5355 ± 0,8181	3151	16
sd-J (1σ) = 0,000091		Total Fusion	257,3731 ± 1,4449	3138	17

Sample P97-361 / biotite (irradiation batch VU29)

Steps	$^{36}Ar(a)$	$^{37}Ar(Ca)$	$^{38}Ar(Cl)$	$^{39}Ar(K)$	$^{40}Ar(a+r)$	Age ± 2σ	$^{40}Ar(r)$	Fraction	K/Ca
98M0290C	0,01803	0,00001	0,00881	0,47149	73,78312	2440,2 14,8	92,77%	6,26%	37622,010
98M0290D	0,00121	0,00001	0,00722	0,37058	70,80720	2812,8 14,9	99,49%	4,92%	29541,740
98M0290E	0,00072	0,00001	0,00781	0,38442	74,57210	2837,5 15,5	99,71%	5,10%	30635,220
98M0290F	0,00075	0,02962	0,00942	0,47644	94,07786	2863,6 15,5	99,76%	6,33%	7,883
98M0290G	0,00114	0,07401	0,01076	0,54360	108,34363	2876,0 15,9	99,68%	7,22%	3,599
98M0290I	0,00007	0,00001	0,00998	0,54069	109,20672	2899,3 15,5	99,98%	7,18%	43034,016
98M0290J	0,00000	0,00001	0,01034	0,54780	111,56999	2911,6 15,5	99,99%	7,27%	43584,534
98M0290K	0,00000	0,00001	0,01003	0,51557	104,02141	2898,0 15,8	99,99%	6,85%	41007,684
98M0290L	0,00030	0,04480	0,00943	0,46696	95,01173	2908,9 16,6	99,90%	6,20%	5,107
98M0290M	0,00016	0,01742	0,00909	0,44709	90,32981	2899,3 16,0	99,94%	5,94%	12,577
98M0290O	0,00000	0,00552	0,00758	0,40797	82,00636	2892,7 16,1	99,99%	5,42%	36,208
98M0290P	0,00014	0,02391	0,00934	0,47456	95,01601	2886,4 15,8	99,95%	6,30%	9,725
98M0290Q	0,00020	0,01853	0,00975	0,53416	106,71913	2883,1 15,5	99,94%	7,09%	14,125
98M0290R	0,00000	0,01328	0,00727	0,38190	74,75744	2854,6 16,4	99,99%	5,07%	14,093
98M0290S	0,00000	0,01106	0,00573	0,29788	57,75060	2840,8 17,5	99,99%	3,96%	13,192
98M0290U	0,00023	0,02691	0,00623	0,32038	65,05350	2905,7 16,2	99,89%	4,25%	5,834
98M0290V	0,00000	0,01782	0,00178	0,09187	16,94533	2769,8 25,3	99,99%	1,22%	2,526
98M0290W	0,00003	0,02721	0,00289	0,14633	27,22996	2781,9 19,4	99,96%	1,94%	2,635
98M0290X	0,00000	0,01979	0,00056	0,02160	3,82414	2711,9 87,7	99,99%	0,29%	0,535
98M0290Y	0,00000	0,00001	0,00168	0,08998	16,70369	2779,0 26,7	99,99%	1,19%	7122,579

Irrediation values		*Results*	40*/39K ± 2σ	Age	2σ
J = 0,019750		Weighted Mean of Plateau	201,6381 ± 1,0177	2897	16
sd-J (1σ) = 0,000099		Total Fusion	195,3111 ± 0,9717	2851	16

Sample P96-215 / muscovite (irradiation batch VU29)

Steps	^{36}Ar(a)	^{37}Ar(Ca)	^{38}Ar(Cl)	^{39}Ar(K)	^{40}Ar(a+r)	Age ± 2σ	^{40}Ar(r)	Fraction	K/Ca
98M0287A	0,00006	0,00001	0,00012	0,00690	1,18140	2470,7 165,8	98,43%	1,18%	607,002
98M0287B	0,00000	0,00001	0,00001	0,00492	1,08007	2836,2 227,3	99,99%	0,84%	432,043
98M0287C	0,00000	0,00001	0,00022	0,01757	3,59690	2738,4 63,0	99,99%	3,00%	1542,665
98M0287D	0,00000	0,00001	0,00039	0,02929	6,31113	2810,6 40,9	99,99%	5,00%	2572,171
98M0287E	0,00000	0,00001	0,00130	0,05895	12,61422	2800,7 26,1	99,99%	10,07%	5177,038
98M0287G	0,00000	0,00001	0,00048	0,04245	9,21046	2820,6 26,1	99,99%	7,25%	3721,028
98M0287H	0,00007	0,00001	0,00078	0,07029	15,02870	2797,7 19,1	99,85%	12,00%	6161,193
98M0287I	0,00000	0,00001	0,00024	0,02026	4,34111	2802,7 148,7	99,99%	3,46%	1775,951
98M0287J	0,00000	0,00001	0,00066	0,05509	11,80872	2803,3 20,6	99,99%	9,41%	4829,106
98M0287K	0,00008	0,00174	0,00170	0,11626	24,88598	2800,1 142,5	99,90%	19,85%	32,739
98M0287M	0,00000	0,00001	0,00011	0,01073	2,33189	2823,1 162,7	99,99%	1,83%	938,751
98M0287N	0,00000	0,00001	0,00144	0,09765	21,33434	2830,3 143,7	99,99%	16,68%	8544,651
98M0287O	0,00000	0,00001	0,00024	0,01207	2,69725	2863,0 160,9	99,99%	2,06%	1055,955
98M0287P	0,00000	0,00001	0,00009	0,00745	1,64746	2847,1 177,2	99,99%	1,27%	651,875
98M0287Q	0,00011	0,00001	0,00045	0,03573	7,92008	2845,1 145,5	99,57%	6,10%	3126,353

Irradiation values		*Results*	40*/39K ± 2σ	Age	2σ
J	= 0,017400	Weighted Mean of Plateau	215,0111 ± 1,2844	2808	17
sd-J (1σ)	= 0,000087	Total Fusion	214,9752 ± 3,8890	2807	29

Sample P97-167 / hornblende ~150µm (irradiation batch VU29)

Steps	^{36}Ar(a)	^{37}Ar(Ca)	^{38}Ar(Cl)	^{39}Ar(K)	^{40}Ar(a+r)	Age ± 2σ	^{40}Ar(r)	Fraction	K/Ca
98M0263B	0,00036	0,005510	0,00005	0,00357	1,26613	3485,0 242,1	91,50%	0,52%	0,317
98M0263C	0,00000	0,073641	0,00039	0,00850	2,02017	3016,6 117,4	99,99%	1,23%	0,057
98M0263D	0,00000	0,434814	0,00236	0,03369	9,47727	3267,4 31,7	100,00%	4,88%	0,038
98M0263E	0,00017	2,317368	0,01322	0,17247	48,46696	3264,2 16,7	99,89%	24,98%	0,036
98M0263G	0,00045	3,550928	0,01937	0,25741	71,62748	3248,1 15,5	99,81%	37,28%	0,036
98M0263H	0,00056	1,023721	0,00554	0,07413	20,43430	3224,5 19,3	99,18%	10,74%	0,035
98M0263I	0,00012	0,299442	0,00157	0,02014	5,62253	3245,6 49,2	99,34%	2,92%	0,033
98M0263J	0,00000	0,150859	0,00091	0,01151	3,21738	3258,4 78,6	100,00%	1,67%	0,037
98M0263L	0,00000	0,101972	0,00059	0,00750	2,16991	3310,6 112,1	100,00%	1,09%	0,036
98M0263L	0,00000	0,101972	0,00059	0,00750	2,16991	3310,6 112,1	100,00%	1,09%	0,036
98M0263M	0,00000	0,158890	0,00101	0,01193	3,35655	3267,7 67,6	100,00%	1,73%	0,037
98M0263N	0,00012	1,112945	0,00613	0,08217	22,70295	3238,0 19,4	99,85%	11,90%	0,036

Irradiation values		*Results*	40*/39K ± 2σ	Age	2σ
J	= 0,018190	Weighted Mean of Plateau	277,9547 ± 1,2511	3249	17
sd-J (1σ)	= 0,000091	Total Fusion	278,0605 ± 3,0080	3250	22

Sample P97-167 / hornblende ~250µm (irradiation batch VU29)

Steps	$^{36}Ar(a)$	$^{37}Ar(Ca)$	$^{38}Ar(Cl)$	$^{39}Ar(K)$	$^{40}Ar(a+r)$	Age ± 2σ	$^{40}Ar(r)$	Fraction	K/Ca
98M0264B	0,00093	0,018906	0,00018	0,00426	2,06907	3989,8 110,2	86,77%	0,41%	0,110
98M0264C	0,00000	0,010770	0,00002	0,00450	0,63832	2378,5 231,7	99,99%	0,43%	0,205
98M0264D	0,01133	4,484756	0,02404	0,36316	92,96285	3159,7 20,9	96,40%	34,90%	0,040
98M0264E	0,00029	0,544730	0,00294	0,04157	10,97219	3248,9 26,3	99,22%	3,99%	0,037
98M0264G	0,00008	0,700054	0,00393	0,05215	14,35095	3321,0 21,1	99,83%	5,01%	0,037
98M0264H	0,00037	2,671597	0,01473	0,19243	53,30470	3330,6 17,1	99,79%	18,49%	0,035
98M0264I	0,00051	2,257096	0,01224	0,16291	45,03890	3325,6 17,0	99,66%	15,65%	0,035
98M0264J	0,00027	0,495895	0,00255	0,03735	10,20475	3301,1 30,2	99,22%	3,59%	0,037
98M0264L	0,00033	0,459716	0,00261	0,03352	9,18496	3301,2 27,6	98,95%	3,22%	0,036
98M0264M	0,00005	0,284045	0,00173	0,02057	5,66520	3321,0 39,4	99,74%	1,98%	0,035
98M0264N	0,00021	0,328871	0,00183	0,02292	6,38971	3328,4 47,2	99,03%	2,20%	0,034
98M0264O	0,00000	0,121719	0,00071	0,00921	2,55509	3336,4 90,7	100,00%	0,89%	0,037
98M0264P	0,00000	0,108645	0,00064	0,00756	2,17255	3388,9 94,3	100,00%	0,73%	0,034
98M0264Q	0,00022	1,265708	0,00666	0,08857	24,48237	3326,3 18,6	99,73%	8,51%	0,034

Irradiation values		*Results*	40*/39K ± 2σ	Age	2σ
J = 0,019300		Weighted Mean of Plateau	275,5028 ± 0,9272	3325	16
sd-J (1σ) = 0,000097		Total Fusion	264,9089 ± 2,8083	3266	22

Sample P96-100 / hornblende <250 (irradiation batch VU29)

Steps	$^{36}Ar(a)$	$^{37}Ar(Ca)$	$^{38}Ar(Cl)$	$^{39}Ar(K)$	$^{40}Ar(a+r)$	Age ± 2σ	$^{40}Ar(r)$	Fraction	K/Ca
98M0256A	0,00035	0,00567	0,00000	0,00197	2,69106	5970,2 273,3	96,16%	0,60%	0,170
98M0256B	0,00000	0,06605	0,00008	0,00618	1,03908	2661,2 112,1	99,99%	1,88%	0,046
98M0256D	0,00042	1,76693	0,00330	0,13618	27,41183	2909,9 17,3	99,54%	41,53%	0,038
98M0256E	0,00040	0,63915	0,00156	0,05415	10,96429	2909,4 20,2	98,93%	16,51%	0,042
98M0256F	0,00063	1,10622	0,00212	0,10475	20,14974	2837,9 17,1	99,07%	31,94%	0,046
98M0256G	0,00018	0,07892	0,00023	0,00576	1,18783	2883,9 100,1	95,44%	1,76%	0,036
98M0256I	0,00000	0,04554	0,00000	0,00314	0,61879	2885,6 220,5	99,88%	0,96%	0,034
98M0256J	0,00000	0,02196	0,00000	0,00182	0,30531	2661,7 401,9	99,98%	0,55%	0,041

Irradiation values		*Results*	40*/39K ± 2σ	Age	2σ
J = 0,020050		Weighted Mean of Plateau	200,3835 ± 1,0789	2910	16
sd-J (1σ) = 0,000100		Total Fusion	203,1633 ± 2,9048	2929,85	25,27

Sample P96-100 / hornblende >250 (irradiation batch VU29)

Steps	$^{36}Ar(a)$	$^{37}Ar(Ca)$	$^{38}Ar(Cl)$	$^{39}Ar(K)$	$^{40}Ar(a+r)$	Age ± 2σ	$^{40}Ar(r)$	Fraction	K/Ca
98M0257A	0,00054	1,53104	0,00276	0,13284	27,45666	2920,1 16,9	99,42%	51,47%	0,043
98M0257B	0,00016	0,01008	0,00003	0,00142	0,17733	1852,9 641,6	72,90%	0,55%	0,069
98M0257C	0,00000	0,01529	0,00006	0,00136	0,26927	2863,9 421,7	99,98%	0,53%	0,044
98M0257D	0,00013	0,42746	0,00077	0,03748	7,70097	2912,9 21,5	99,49%	14,52%	0,043
98M0257F	0,00019	0,85831	0,00158	0,07361	15,26883	2928,5 16,6	99,63%	28,52%	0,042
98M0257G	0,00016	0,03678	0,00003	0,00231	0,42011	2579,0 273,7	88,52%	0,89%	0,031
98M0257H	0,00002	0,02885	0,00009	0,00191	0,39167	2895,5 264,0	98,29%	0,74%	0,032
98M0257I	0,00000	0,05359	0,00005	0,00337	0,69073	2916,3 149,1	99,99%	1,31%	0,031
98M0257K	0,00009	0,01643	0,00004	0,00099	0,21488	2812,1 491,1	87,83%	0,38%	0,030
98M0257L	0,00004	0,05410	0,00016	0,00282	0,56285	2849,2 165,6	97,92%	1,09%	0,026

Irradiation values		*Results*	40*/39K ± 2σ	Age	2σ
J = 0,019690		Weighted Mean of Plateau	205,8727 ± 1,0653	2923	16
sd-J (1σ) = 0,000098		Total Fusion	204,4173 ± 3,2155	2913	27

Sample CTW1A / muscovite (irradiation batch VU29)

Steps	^{36}Ar(a)	^{37}Ar(Ca)	^{38}Ar(Cl)	^{39}Ar(K)	^{40}Ar(a+r)	Age ± 2σ	^{40}Ar(r)	Fraction	K/Ca
98M0272C	0,00179	0,00000	0,00148	0,12965	25,18490	2780,5 20,0	97,90%	1,94%	13634,584
98M0272D	0,00116	0,00000	0,00612	0,45412	93,46105	2888,1 15,3	99,63%	6,81%	47740,551
98M0272E	0,00249	0,10334	0,01756	1,24475	261,60562	2919,6 14,8	99,71%	18,66%	5,902
98M0272F	0,00093	0,04071	0,00872	0,63351	125,08435	2830,8 16,2	99,78%	9,50%	7,625
98M0272H	0,00000	0,00000	0,00489	0,37035	73,49915	2841,2 17,1	99,99%	5,55%	38882,261
98M0272I	0,00034	0,03136	0,01527	1,10831	219,29639	2836,3 14,7	99,95%	16,62%	17,319
98M0272J	0,00175	0,04519	0,01182	0,80118	159,18132	2838,2 15,3	99,67%	12,01%	8,686
98M0272K	0,00080	0,04906	0,00605	0,41833	82,78187	2833,0 19,6	99,71%	6,27%	4,179
98M0272L	0,00013	0,01918	0,00291	0,18259	36,62876	2855,1 21,6	99,89%	2,74%	4,665
98M0272N	0,00000	0,00966	0,00349	0,25877	52,13242	2862,8 17,5	99,99%	3,88%	13,130
98M0272O	0,00000	0,00413	0,00265	0,19620	38,96671	2842,3 18,9	99,99%	2,94%	23,281
98M0272P	0,00000	0,00050	0,00284	0,20673	41,39346	2853,9 18,1	99,99%	3,10%	202,655
98M0272Q	0,00000	0,00000	0,00245	0,17656	34,81419	2832,0 19,4	99,99%	2,65%	18480,660
98M0272S	0,00000	0,00000	0,00148	0,10441	20,99043	2859,8 22,1	99,99%	1,57%	10921,775
98M0272T	0,00000	0,00000	0,00176	0,12866	25,49642	2839,2 20,2	99,99%	1,93%	13817,957
98M0272U	0,00000	0,00000	0,00013	0,02693	5,34382	2841,0 63,3	99,99%	0,40%	2815,385
98M0272V	0,00015	0,00000	0,00378	0,22820	45,55043	2848,2 16,3	99,90%	3,42%	23846,651

Irradiation values		*Results*	40*/39K ± 2σ	Age	2σ
J	= 0,019300	Weighted Mean of Plateau	198,2895 ± 0,6109	2840	15
sd-J (1σ)	= 0,000097	Total Fusion	200,7112 ± 0,9837	2857	16

Sample P95-gran / muscovite (irradiation batch VU29)

Steps	^{36}Ar(a)	^{37}Ar(Ca)	^{38}Ar(Cl)	^{39}Ar(K)	^{40}Ar(a+r)	Age ± 2σ	^{40}Ar(r)	Fraction	K/Ca
98M0274B	0,00011	0,00000	0,00163	0,11259	18,42191	2543,5 17,4	99,83%	4,91%	11385,118
98M0274C	0,00000	0,01333	0,00398	0,28872	55,58992	2772,1 14,9	99,99%	12,59%	10,616
98M0274D	0,00011	0,00738	0,00520	0,38902	72,79137	2731,1 15,0	99,95%	16,96%	25,840
98M0274E	0,00016	0,00024	0,00282	0,20291	38,33523	2743,6 15,8	99,87%	8,85%	408,182
98M0274F	0,00050	0,00030	0,00615	0,44710	84,54576	2744,2 15,5	99,82%	19,49%	728,929
98M0274H	0,00000	0,00000	0,00270	0,19109	36,36999	2755,7 17,8	99,99%	8,33%	19283,196
98M0274I	0,00000	0,00271	0,00236	0,18279	35,52702	2785,4 17,9	99,99%	7,97%	33,092
98M0274J	0,00000	0,00000	0,00103	0,07373	14,33141	2785,6 27,6	99,99%	3,21%	7434,578
98M0274K	0,00000	0,00000	0,00098	0,07278	14,10850	2781,7 28,6	99,99%	3,17%	7336,491
98M0274L	0,00000	0,00000	0,00459	0,33279	65,70618	2807,8 15,4	99,99%	14,51%	33535,530

Irradiation values		*Results*	40*/39K ± 2σ	Age	2σ
J	= 0,018950	Weighted Mean of Plateau	196,4965 ± 1,6685	2801	19
sd-J (1σ)	= 0,000095	Total Fusion	189,8695 ± 1,0537	2752	16

Sample P97-282 / hornblende 100-250 µm (irradiation batch VU29)

Steps	^{36}Ar(a)	^{37}Ar(Ca)	^{38}Ar(Cl)	^{39}Ar(K)	^{40}Ar(a+r)	Age ± 2σ	^{40}Ar(r)	Fraction	K/Ca
98M0262A	0,00115	0,00602	0,00006	0,00403	4,42948	5311,3 179,8	92,33%	0,32%	0,328
98M0262B	0,00000	0,00000	0,00006	0,00453	1,03935	2928,9 223,1	99,99%	0,36%	693,656
98M0262C	0,00000	0,29267	0,00087	0,04520	12,91158	3251,9 28,6	100,00%	3,54%	0,076
98M0262E	0,00000	0,33131	0,00099	0,04522	13,89032	3361,8 29,5	100,00%	3,55%	0,067
98M0262F	0,00012	0,50710	0,00142	0,07034	21,27963	3336,2 31,9	99,83%	5,51%	0,068
98M0262G	0,00031	0,99299	0,00310	0,13796	41,85477	3339,6 17,9	99,77%	10,82%	0,068
98M0262H	0,00060	1,44333	0,00456	0,20252	61,07409	3329,4 16,6	99,71%	15,88%	0,069
98M0262J	0,00000	1,54941	0,00490	0,21068	64,04527	3346,0 18,5	100,00%	16,52%	0,067
98M0262K	0,00000	1,60650	0,00516	0,21779	65,71623	3334,7 19,9	100,00%	17,08%	0,066
98M0262L	0,00000	0,20458	0,00055	0,02998	9,22748	3365,1 54,4	100,00%	2,35%	0,072
98M0262M	0,00000	0,11381	0,00027	0,01619	4,85048	3324,2 101,9	100,00%	1,27%	0,070
98M0262N	0,00007	2,25250	0,00774	0,29103	88,94673	3353,8 16,8	99,97%	22,82%	0,063

Irradiation values		*Results*	40*/39K ± 2σ	Age	2σ
J	= 0,017730	Weighted Mean of Plateau	303,0385 ± 1,4566	3341	17
sd-J (1σ)	= 0,000089	Total Fusion	304,6725 ± 2,9370	3349	21

Sample A94-22 / muscovite (irradiation batch VU29)

Steps	$^{36}Ar(a)$	$^{37}Ar(Ca)$	$^{38}Ar(Cl)$	$^{39}Ar(K)$	$^{40}Ar(a+r)$	Age ± 2σ	$^{40}Ar(r)$	Fraction	K/Ca
98M0289B	0,00021	0,00001	0,00243	0,19339	33,78324	2658,7 14,9	99,81%	13,48%	16371,186
98M0289C	0,00006	0,00719	0,00374	0,27775	35,79865	2253,1 13,5	99,94%	19,36%	18,933
98M0289D	0,00011	0,02297	0,00215	0,14642	19,12751	2268,8 15,1	99,82%	10,21%	3,123
98M0289E	0,00023	0,01254	0,00485	0,33780	43,01801	2236,2 13,4	99,84%	23,55%	13,199
98M0289F	0,00015	0,00228	0,00236	0,16602	22,60607	2322,2 14,7	99,79%	11,57%	35,619
98M0289H	0,00000	0,00001	0,00020	0,02493	3,44010	2342,5 48,5	99,99%	1,74%	2103,972
98M0289I	0,00000	0,00001	0,00012	0,02132	2,78363	2270,3 57,0	99,99%	1,49%	1798,903
98M0289J	0,00000	0,00001	0,00010	0,01703	2,30796	2318,5 71,1	99,99%	1,19%	1436,668
98M0289K	0,00006	0,00378	0,00396	0,24997	34,92533	2358,0 14,1	99,95%	17,42%	32,370

Irrediation values		*Results*	40*/39K ± 2σ	Age	2σ
J = 0,017800		Weighted Mean of Plateau	138,2561 ± 2,0908	2240	23
sd-J (1σ) = 0,000089		Total Fusion	137,7013 ± 0,7621	2235	15

Sample P97-343 / hornblende (irradiation batch VU29)

Steps	$^{36}Ar(a)$	$^{37}Ar(Ca)$	$^{38}Ar(Cl)$	$^{39}Ar(K)$	$^{40}Ar(a+r)$	Age ± 2σ	$^{40}Ar(r)$	Fraction	K/Ca
98M0269C	0,00288	0,16319	0,00100	0,00522	6,73940	5664,9 111,2	87,37%	0,65%	0,016
98M0269D	0,00207	0,37403	0,00124	0,01149	5,30424	3964,5 54,0	88,47%	1,44%	0,015
98M0269E	0,00122	0,31522	0,00094	0,01569	4,23913	3185,7 47,9	91,49%	1,96%	0,024
98M0269F	0,00062	0,49675	0,00146	0,01677	3,56297	2886,0 45,2	94,87%	2,10%	0,017
98M0269H	0,00029	1,40711	0,00376	0,02618	6,48619	3169,4 34,7	98,70%	3,27%	0,009
98M0269I	0,00133	8,53000	0,02180	0,11261	28,90739	3221,4 18,2	98,64%	14,07%	0,006
98M0269J	0,00162	11,52535	0,02822	0,13375	34,75297	3239,3 16,4	98,62%	16,71%	0,006
98M0269K	0,00111	6,39767	0,01525	0,06689	19,91066	3441,8 17,8	98,35%	8,36%	0,005
98M0269M	0,00043	4,17098	0,00950	0,04430	11,76852	3277,3 23,5	98,93%	5,54%	0,005
98M0269N	0,00038	3,85569	0,00990	0,04246	11,05148	3247,4 22,2	98,97%	5,31%	0,005
98M0269O	0,00069	5,42303	0,01329	0,05637	15,69377	3345,0 21,6	98,70%	7,04%	0,005
98M0269P	0,00050	3,59149	0,00867	0,03865	10,75494	3343,0 30,1	98,63%	4,83%	0,005
98M0269R	0,00005	3,73890	0,00840	0,03827	10,32092	3314,4 26,7	99,86%	4,78%	0,005
98M0269S	0,00000	2,74678	0,00584	0,02603	7,22962	3361,4 31,4	100,00%	3,25%	0,005
98M0269T	0,00138	18,73589	0,03973	0,16557	46,49001	3364,4 17,1	99,12%	20,69%	0,004

Irrediation values		*Results*	40*/39K ± 2σ	Age	2σ
J = 0,019600		Weighted Mean of Plateau	276,7065 ± 2,6988	3356	21
sd-J (1σ) = 0,000098		Total Fusion	273,5601 ± 2,9222	3338	22

Sample P97-344 / hornblende (irradiation batch VU29)

Steps	$^{36}Ar(a)$	$^{37}Ar(Ca)$	$^{38}Ar(Cl)$	$^{39}Ar(K)$	$^{40}Ar(a+r)$	Age ± 2σ	$^{40}Ar(r)$	Fraction	K/Ca
98M0267E	0,00362	0,43439	0,00050	0,01660	2,28315	1632,3 61,9	53,14%	7,37%	0,019
98M0267F	0,00144	0,82857	0,00073	0,01011	1,97619	2540,7 69,1	78,46%	4,49%	0,006
98M0267G	0,00066	0,20955	0,00069	0,00987	1,25569	2077,8 68,0	84,39%	4,38%	0,023
98M0267H	0,00025	0,24500	0,00076	0,00672	1,22322	2692,4 81,3	94,05%	2,98%	0,013
98M0267J	0,00059	1,34501	0,00618	0,03289	7,27439	3026,0 24,3	97,62%	14,60%	0,012
98M0267K	0,00037	1,36128	0,00455	0,02361	5,72605	3169,0 31,6	98,09%	10,48%	0,008
98M0267L	0,00028	1,40971	0,00315	0,01514	3,82707	3228,3 36,7	97,86%	6,72%	0,005
98M0267M	0,00020	1,98715	0,00234	0,01186	3,43090	3439,1 44,6	98,27%	5,27%	0,003
98M0267O	0,00000	1,09211	0,00229	0,00971	2,81862	3471,8 61,8	100,00%	4,31%	0,004
98M0267P	0,00015	0,64438	0,00265	0,01238	3,43561	3381,7 41,4	98,68%	5,50%	0,009
98M0267Q	0,00031	1,77283	0,00647	0,03295	9,18725	3394,0 33,2	98,99%	14,63%	0,009
98M0267R	0,00033	1,46224	0,00324	0,01701	5,18587	3517,2 32,8	98,09%	7,55%	0,006
98M0267S	0,00144	4,11272	0,00574	0,02641	10,36406	3878,5 25,8	95,89%	11,72%	0,003

Irrediation values		*Results*	40*/39K ± 2σ	Age	2σ
J = 0,020150		Weighted Mean of Plateau	284,3517 ± 10,2961	3440	58
sd-J (1σ) = 0,000101		Total Fusion	244,7936 ± 5,6208	3212	38

Sample P97-344 / hornblende-II (irradiation batch VU29)

Steps	^{36}Ar(a)	^{37}Ar(Ca)	^{38}Ar(Cl)	^{39}Ar(K)	^{40}Ar(a+r)	Age ± 2σ	^{40}Ar(r)	Fraction	K/Ca
98M0288B	0,00399	0,20205	0,00063	0,01946	2,15386	1150,5 61,3	45,3%	3,80%	0,047
98M0288C	0,00132	0,25011	0,00025	0,00995	1,07458	1442,7 114,7	63,7%	1,95%	0,019
98M0288D	0,00064	0,26146	0,00096	0,01446	1,95693	2084,8 61,5	90,3%	2,83%	0,027
98M0288E	0,00050	1,21931	0,00879	0,05149	11,99686	2937,8 19,2	98,8%	10,07%	0,021
98M0288F	0,00036	1,29662	0,00941	0,05073	12,50500	3025,6 20,2	99,1%	9,92%	0,019
98M0288G	0,00008	1,10386	0,00650	0,03752	9,02028	2998,0 21,1	99,7%	7,34%	0,017
98M0288I	0,00028	1,89290	0,01254	0,06781	16,79319	3038,0 18,0	99,5%	13,26%	0,018
98M0288J	0,00022	1,50103	0,00780	0,04152	10,43828	3058,0 20,9	99,4%	8,12%	0,014
98M0288K	0,00008	0,77580	0,00337	0,02021	4,99607	3035,2 32,4	99,5%	3,95%	0,013
98M0288L	0,00002	1,13124	0,00629	0,03446	8,74356	3079,8 21,1	99,9%	6,74%	0,015
98M0288M	0,00014	1,01239	0,00606	0,03547	9,16783	3101,6 20,1	99,6%	6,94%	0,017
98M0288O	0,00005	0,95207	0,00651	0,03360	8,77022	3120,4 22,8	99,8%	6,57%	0,017
98M0288P	0,00000	0,39669	0,00238	0,01206	3,28560	3186,7 46,7	100,0%	2,36%	0,015
98M0288Q	0,00061	3,56118	0,01597	0,08271	22,69682	3185,5 18,3	99,2%	16,17%	0,011

Irradiation values		*Results*	40*/39K ± 2σ	Age	2σ
J	= 0,017800	Weighted Mean of Plateau	272,2417 ± 1,8631	3186	18
sd-J (1σ)	= 0,000089	Total Fusion	236,8742 ± 2,8173	2980	23

Sample P95-7 / actinolite (irradiation batch VU29)

Steps	^{36}Ar(a)	^{37}Ar(Ca)	^{38}Ar(Cl)	^{39}Ar(K)	^{40}Ar(a+r)	Age ± 2σ	^{40}Ar(r)	Fraction	K/Ca
98M0268B	0,00138	0,19080	0,000834	0,037503	2,606639	1402,0 20,2	84,32%	11,36%	0,096
98M0268C	0,00010	0,05918	0,000521	0,035836	3,605315	1982,6 14,6	99,19%	10,85%	0,297
98M0268D	0,00004	0,00610	0,000411	0,030598	3,168488	2022,9 17,0	99,63%	9,27%	2,456
98M0268E	0,00006	0,03193	0,000467	0,036139	4,380032	2218,8 14,4	99,61%	10,95%	0,555
98M0268G	0,00028	0,06710	0,000442	0,038814	5,130710	2315,1 12,7	98,41%	11,76%	0,283
98M0268H	0,00003	0,22893	0,000652	0,045875	5,396562	2183,5 11,7	99,82%	13,90%	0,098
98M0268J	0,00031	0,12600	0,000221	0,020301	1,457746	1540,9 30,3	93,70%	6,15%	0,079
98M0268I	0,00024	0,12474	0,000460	0,038508	4,010433	2012,6 13,4	98,23%	11,66%	0,151
98M0268L	0,00023	0,11038	0,000141	0,010181	0,593027	1278,3 64,5	88,28%	3,08%	0,045
98M0268M	0,00000	0,14995	0,000134	0,010539	0,535558	1267,4 64,1	99,97%	3,19%	0,034
98M0268N	0,00012	0,11190	0,000205	0,008868	0,519501	1334,1 71,1	93,20%	2,69%	0,039
98M0268O	0,00016	0,23764	0,000239	0,016982	1,068126	1427,1 35,0	95,59%	5,14%	0,035

Irradiation values		*Results*	40*/39K ± 2σ	Age	2σ
J	= 0,020050	Weighted Mean of Plateau	101,0013 ± 7,2910	1997	87
sd-J (1σ)	= 0,000100	Total Fusion	95,7234 ± 1,4435	1933	19

Sample P95-10 / muscovite (irradiation batch VU29)

Steps	^{36}Ar(a)	^{37}Ar(Ca)	^{38}Ar(Cl)	^{39}Ar(K)	^{40}Ar(a+r)	Age ± 2σ	^{40}Ar(r)	Fraction	K/Ca
98M0273B	0,00151	0,01034	0,00846	0,58624	72,86572	2139,1 12,9	99,38%	9,09%	27,774
98M0273E	0,00006	0,00000	0,00577	0,43497	72,41751	2529,0 15,1	99,97%	6,74%	44827,818
98M0273F	0,00069	0,01803	0,00870	0,65231	116,62969	2624,8 14,7	99,82%	10,11%	17,727
98M0273G	0,00056	0,02259	0,01140	0,77045	150,45524	2748,9 14,9	99,88%	11,94%	16,708
98M0273H	0,00078	0,06425	0,00965	0,65066	130,19924	2782,5 15,0	99,82%	10,08%	4,962
98M0273I	0,00089	0,00000	0,01012	0,73995	147,91134	2780,9 15,1	99,82%	11,47%	76157,308
98M0273K	0,00126	0,05767	0,01346	0,94763	194,91567	2821,4 14,7	99,80%	14,69%	8,052
98M0273L	0,00026	0,01903	0,00533	0,41949	86,72807	2830,2 16,7	99,91%	6,50%	10,799
98M0273M	0,00000	0,00000	0,00323	0,22935	45,20705	2763,6 19,2	99,99%	3,55%	23572,993
98M0273N	0,00000	0,00000	0,00454	0,31302	59,13187	2703,8 20,7	99,99%	4,85%	32162,729
98M0273O	0,00000	0,01932	0,00451	0,32570	68,74537	2861,1 18,2	100,00%	5,05%	8,260
98M0273Q	0,00000	0,00680	0,00529	0,38226	81,45541	2874,7 17,9	100,00%	5,92%	27,551

Irradiation values		*Results*	40*/39K ± 2σ	Age	2σ
J	= 0,018400	Weighted Mean of Plateau	203,5570 ± 3,3740	2809	28
sd-J (1σ)	= 0,000092	Total Fusion	189,8446 ± 0,8442	2711	15

Sample P97-339 / hornblende (irradiation batch VU29)

Steps	$^{36}Ar(a)$	$^{37}Ar(Ca)$	$^{38}Ar(Cl)$	$^{39}Ar(K)$	$^{40}Ar(a+r)$	Age ± 2σ	$^{40}Ar(r)$	Fraction	K/Ca
98M0293B	0,00192	0,03143	0,00043	0,01400	3,61398	2994,8 67,3	84,30%	0,55%	0,218
98M0293C	0,00003	0,07181	0,00057	0,02149	4,15129	2819,4 51,3	99,76%	0,84%	0,147
98M0293D	0,00017	0,78390	0,00516	0,15959	42,94899	3309,2 17,0	99,88%	6,27%	0,100
98M0293E	0,00143	2,68503	0,01795	0,55949	149,19924	3292,8 16,0	99,71%	21,99%	0,102
98M0293F	0,00032	1,08778	0,00729	0,22756	60,78257	3297,2 17,3	99,84%	8,94%	0,103
98M0293H	0,00000	1,34918	0,00845	0,28834	75,35848	3266,6 16,4	100,00%	11,33%	0,105
98M0293I	0,00000	0,88194	0,00584	0,19529	51,22398	3272,1 16,9	100,00%	7,68%	0,109
98M0293J	0,00000	0,84718	0,00556	0,17943	47,20286	3276,5 17,3	100,00%	7,05%	0,104
98M0293K	0,00000	1,08361	0,00721	0,21807	56,73271	3259,7 16,8	100,00%	8,57%	0,099
98M0293L	0,00000	1,02884	0,00599	0,18937	49,40246	3263,9 17,5	100,00%	7,44%	0,090
98M0293N	0,00000	0,58875	0,00347	0,11286	29,91882	3288,1 21,8	100,00%	4,44%	0,094
98M0293O	0,00000	0,75223	0,00434	0,13742	35,84259	3263,5 19,3	100,00%	5,40%	0,090
98M0293P	0,00000	1,43348	0,00768	0,24128	64,21903	3294,2 18,9	100,00%	9,48%	0,082

Irradiation values		*Results*	40*/39K ± 2σ	Age	2σ
J	= 0,019570	Weighted Mean of Plateau	263,8026 ± 1,7654	3281	18
sd-J (1σ)	= 0,000098	Total Fusion	263,1311 ± 1,4700	3277	17

Sample P97-339 / biotite (irradiation batch VU29)

Steps	$^{36}Ar(a)$	$^{37}Ar(Ca)$	$^{38}Ar(Cl)$	$^{39}Ar(K)$	$^{40}Ar(a+r)$	Age ± 2σ	$^{40}Ar(r)$	Fraction	K/Ca
98M0295A	0,28699	0,09631	0,011698	0,738453	228,374525	2782,1 17,5	62,86%	8,08%	3,757
98M0295B	0,01627	0,00001	0,008950	0,533543	139,862591	3166,4 17,8	96,56%	5,84%	39195,795
98M0295C	0,00659	0,00001	0,008340	0,593769	154,669944	3190,2 16,7	98,74%	6,50%	43620,240
98M0295D	0,00448	0,04658	0,010715	0,660406	175,698877	3229,6 16,4	99,24%	7,23%	6,947
98M0295E	0,00203	0,11332	0,012836	0,843240	220,588093	3211,5 16,1	99,72%	9,23%	3,646
98M0295G	0,00198	0,06011	0,018702	1,183751	310,064887	3214,7 15,8	99,81%	12,96%	9,649
98M0295H	0,00269	0,06912	0,014846	0,915986	240,668784	3217,2 16,2	99,67%	10,03%	6,493
98M0295I	0,00180	0,08392	0,010937	0,773381	202,570801	3213,6 17,5	99,73%	8,47%	4,515
98M0295J	0,00085	0,05397	0,011512	0,727926	189,589998	3207,1 17,1	99,86%	7,97%	6,609
98M0295K	0,00000	0,07847	0,010880	0,638980	165,661999	3202,2 17,7	100,00%	6,99%	3,990
98M0295M	0,00000	0,13963	0,010349	0,672092	173,782392	3198,2 17,5	100,00%	7,36%	2,359
98M0295N	0,00015	0,10108	0,006830	0,566676	145,391300	3186,1 18,4	99,97%	6,20%	2,747
98M0295O	0,00020	0,03320	0,003960	0,286987	73,280457	3178,2 26,3	99,92%	3,14%	4,236

Irradiation values		*Results*	40*/39K ± 2σ	Age	2σ
J	= 0,018900	Weighted Mean of Plateau	260,5409 ± 1,0791	3210	16
sd-J (1σ)	= 0,000095	Total Fusion	254,4508 ± 1,3666	3174	17

Sample P97-306 / actinolite (irradiation batch VU29)

Steps	$^{36}Ar(a)$	$^{37}Ar(Ca)$	$^{38}Ar(Cl)$	$^{39}Ar(K)$	$^{40}Ar(a+r)$	Age ± 2σ	$^{40}Ar(r)$	Fraction	K/Ca
98M0276A	0,00186	0,09708	0,00049	0,00246	3,34293	5713,1 199,0	83,56%	1,39%	0,012
98M0276B	0,00026	0,05077	0,00027	0,00121	1,04188	5115,7 308,7	92,77%	0,68%	0,012
98M0276C	0,00049	0,05885	0,00024	0,00103	0,73731	4567,8 731,8	80,40%	0,58%	0,009
98M0276D	0,00003	0,07115	0,00007	0,00103	0,37151	3767,4 447,2	97,41%	0,58%	0,007
98M0276E	0,00023	0,37049	0,00039	0,00254	1,47920	4503,1 160,9	95,40%	1,43%	0,003
98M0276G	0,00056	1,22429	0,00047	0,00424	4,04785	5344,5 92,6	95,92%	2,39%	0,002
98M0276H	0,00094	8,22632	0,00140	0,01881	9,59811	4314,5 30,7	97,11%	10,60%	0,001
98M0276I	0,00042	5,09968	0,00061	0,01224	3,94883	3576,8 82,0	96,82%	6,89%	0,001
98M0276J	0,00043	9,61973	0,00125	0,02160	7,13617	3635,9 25,7	98,22%	12,17%	0,001
98M0276K	0,00050	8,44936	0,00110	0,01913	5,91333	3520,7 29,6	97,49%	10,78%	0,001
98M0276M	0,00018	5,71044	0,00067	0,01266	3,95131	3553,6 41,4	98,65%	7,14%	0,001
98M0276N	0,00053	8,97718	0,00120	0,02147	6,40032	3465,9 33,9	97,55%	12,10%	0,001
98M0276O	0,00009	4,56162	0,00057	0,01036	3,19325	3542,8 49,3	99,16%	5,84%	0,001
98M0276P	0,00077	22,46588	0,00289	0,04871	15,39131	3571,1 21,6	98,52%	27,44%	0,001

Irradiation values		*Results*	40*/39K ± 2σ	Age	2σ
J	= 0,020040	Weighted Mean of Plateau	309,7560 ± 8,0957	3563	43
sd-J (1σ)	= 0,000100	Total Fusion	362,8521 ± 12,9538	3812	59

References

Abbott, D. H., 1996. Plumes and hotspots as sources for greenstone belts., Lithos, 37: 113-237.

Abbott, D. H. and Mooney, W., 1995. The structural and geochemical evolution of the continental crust: Support for the oceanic plateau model of continental growth. Rev.Geoph. Supplement: 231-242.

Anhaeusser, C. R., 1975. Precambrian tectonic environments. Ann. Rev. Earth Planet. Sci., 3: 31-53.

Anhaeusser, C. R., Mason, R., Viljoen, M. J., and Viljoen, R. P., 1969. Reappraisal of some aspects of Precambrian shield geology. Bull. Geol. Soc. America, 80: 2175-2200.

Armstrong, 1981. Radiogenic isotopes: the case for crustal recycling on a near steady-state no continent growth. Earth Phil. Trans. Royal Soc. London, 301: 443-472.

Arndt, N. T., 1994. Archaean komatiites. In: Archaean crustal evolution. Developments in Precambrian Geology., 11., K. C. Condie (Editor) . Elsevier, 11-40.

Arndt, N. T., 1999. Why was flood volcanism on submerged continental platforms so common in the Precambrian. Precambrian Res., 97: 155-164.

Arndt, N. T., Nelson, D. R., Compston, W., Trendall, A. F., and Thorne, A. M., 1991. The age of the Fortescue Group, Hamersley basin, Western Australia, from ion microprobe zircon U-Pb results. Aust. J. Earth Sci., 38: 261-281.

Arndt, N. T., and Nisbet, E.G., 1982. Komatiites. Allen & Unwin, London.

Arndt, N. T., Albarede, F., Nisbet, E.G., 1997. Mafic and Ultramafic magmatism., In: De Wit, M. J. and Ashwal. D., Greenstone Belts. Oxford Monogr. Geol. Geoph. 35: 233-254.

Bailey, R. C., 1999. Gravity-driven continental overflow and Archaean tectonics. Nature, 398: 413-415.

Barley, M. E., 1993. Volcanic, sedimentary and tectonostratigraphic environments of the ~3.46 Ga Warrawoona Megasequense: a review. Precambrian Res., 60: 47-67.

Barley, M. E., 1997. The Pilbara Craton. In: Wit, M. D., and Ashwal, L. D. (Editors), Greenstone Belts. Oxford Monogr. Geol. Geoph. 35: 657-664.

Barley, M. E., 1999. Growth and recycling of Archaean continental crust in the Pilbara Craton. Terra Abstracts, 11: 142.

Barley, M. E., Dunlop, J. S. R., Glover, J. E., and Groves, D. I., 1979. Sedimentary evidence for an Archean shallow-water volcanic-sedimentary facies, Eastern Pilbara Block, Western Australia. Earth Planet. Sci. Lett., 43: 74.

Barley, M. E., Loader, S. E., and McNaughton, N. J., 1998. 3430 to 3417 Ma calc-alkaline volcanism in the McPhee Dome and Kelly Belt, and growth of the eastern Pilbara Craton. Precambrian Res., 88: 3-24.

Barley, M. E., and Pickard, A. L., 1999. An extensive, crustally derived, 3325 to 3310 Ma silicic volcanoplutonic suite in the eastern Pilbara Craton: evidence from the Kelly Belt, McPhee Dome and Corunna Downs Batholith. Precambrian Res., 96: 41-62.

Barley, M. E., Sylvester, G. C., and Groves, D. I., 1984. Archaean calc-alkaline volcanism in the

Pilbara Block, Western Australia. Precambrian Res., 24: 285-319.

Beintema, K., 1997. Unpublished Thesis, Utrecht University.

Beintema, K. 2003.

Beghoul, N. and Meren, R. 1992. Pn and mantle lid thickness of major Archean and Proterozoic provinces on Earth., Eos Trans. AGU, 73: 43.

Bickle, M. J., 1978. Heat loss from the earth: a constraint on Archean tectonics from the relation between geothermal gradients and the rate of plate production. Earth Planet. Sci. Lett, 40: 301-315.

Bickle, M. J., 1986. Global thermal histories. Nature, 319: 13-14.

Bickle, M.J., Bettenay, L.F., Boultier, C.A., Groves, D. I., and Morant, P., 1980. Horizontal tectonic interaction of an Archean gneiss belt and greenstones, Pilbara block, Western Australia. Geology, 8: 525-529.

Bickle, M. J., Bettenay, L. F., Chapman, H. J., Groves, D. I., McNaughton, N. J., Campbell, I. H., and De Laeter, J. R. D., 1989. The age and origin of younger granitic plutons of the Shaw Batholith in the Archaean Pilbara Block, Western Australia. Contrib. Mineral Petrol., 101: 361-376.

Bickle, M. J., Bettenay, L. F., Chapman, H. J., Groves, D. I., McNaughton, N. J., Campbell, I. H., and De Laeter, J. R. D., 1993. Origin of the 3500-3300 Ma calc-alkaline in the Pilbara Archaean; Isotopic and geochemical constraints from the Shaw Batholith. Precambrian Res., 60: 117-149.

Bickle, M. J., Morant, P., Bettenay, L. F., Boulter, C. A., Blake, T. S., and Groves, D. I., 1985. Archean tectonics of the Shaw Batholith, Pilbara Block, Western Australia: structural and metamorphic tests of the batholith concept. In: Ayres, L. D., Thurston, P. C., Card, K. D., and Weber, W. (Editors), Evolution of Archean Supracrustal Sequences. v. 28. Geological Association of Canada Special Paper, 325-341.

Blake, T. S., 1993. Late Archaean crustal extension, sedimentary basin formation, flood basalt volcanism and continental rifting: The Nullagine and Mt Jope Supersequences, Western Australia. Precambrian Res, 60: 185-242.

Blewett, R. S., 2002. Archaean tectonic processes: a case for horizontal shortening in the North Pilbara Granite-Greenstone Terrane, Western Australia. Precambrian Res., 113: 87-120.

Blewett, R. S., and Huston, D.L., 1999a. Deformation and gold mineralization of the Archaean Pilbara Craton, Western Australia. AGSO Res. Newsletter, 30: 12-15.

Blewett, R. S., and Huston, D., 1999b. Structural controls of Archaean gold in the North Pilbara Craton, Western Australia, In: Jessell, M., (Editor), Halls Gap SGTSG, Vol. 53: Geological Society of Australia Abstract Series: Halls Gap, Victoria, Australia, p. 15-16.

Bott, M. H. P., and Kusznir, N. J., 1984. The origin of tectonic stress in the lithosphere. Tectonophysics, 105: 1-13.

Bouhallier, H., Choukroune, P., and Ballèvre, M., 1993. Diapirism, bulk homogeneous shortening and transcurrent shearing in the Archaean Dharwar craton: the Holenarsipur area, southern India. , 63: 43 - 58.

Boulter, C.A., Bickle, M.J., Gibson, B., and Wright, R.K., 1987. Horizontal tectonics pre-dating

upper Gorge Creek Group sedimentation Pilbara Block, Western Australia. Precambrian Res., 36: 241-258.

Buick, R., Brauhart, C., Morant, P., Thornett, J. R., Maniw, J., Archibald, N. J., Doepel, M. G., A. L., Fletcher, Pickard, I. R., Smith, J. B., Barley, M. E., McNaughton, N. J., and Groves, D. I., 2002. Geochronology and stratigraphic relationships of the Sulphur Springs Group and Strelley Granite: a temporally distinct province in the Archaean Pilbara Craton, Australia., Precambrian Res., 114: 87-120.

Buick, R., and Dunlop, J. S. R., 1990. Evaporitic sediments of early Archean age from the Warrawoona Group, North Pole, W.A. Sedimentology, 37: 247-277.

Buick, R., Thornett, J. R., McNaughton, N. J., Smith, J. B., Barley, M. E., and Savage, M., 1995. Record of emergent continental crust ~3.5 billion years ago in the Pilbara craton of Australia. Nature, 375: 574-577.

Byerly, G. R., Kröner, A., Lowe, D. L., Todt, W., and Walsh, M. M., 1996. Prolonged magmatism and time constraints for sediment deposition in the Early Archean Barberton greenstone belt: evidence from the upper Onverwacht and Fig Tree groups. Precambrian. Res, 78: 125-138.

Calvert, A. J., Sawyer, E. W., Davis, W. J., and Ludden, J. W., 1995. Archean subduction inferred from seismic images of a mantle suture in the Superior Province. Nature, 375: 670-674.

Campbell, I. H., and Griffiths, R. W., 1992. The changing nature of mantle hotspots through time: implications for the chemical evolution of the mantle. J. Geol., 100: 497-523.

Campbell, I. H., Griffiths, R. W., and Hill, R. I., 1989. Melting in an Archaean mantle plume: heads its basalt, tails its komatiites. Nature, 339: 697-699.

Campbell, I. H., and Hill, R. I., 1988. A two-stage model for the formation of the granite-greenstone terrains of the Kalgoorlie-Norseman area, Western Australia. Earth Planet. Sci. Lett., 90: 11-25.

Chadwick, B., 1981. Field relations Petrography and Geochemistry of Archean Amphibolite Dykes and Malene Supracrustal Amphibolites, Northwest Buksefjorden, Southern West Greenland. Precambrian Res., 14: 221-259.

Chardon, D., Choukroune, P., and Jayananda, M., 1996. Strain patterns, décollement and incipient sagducted greenstone terrains in the Archaean Dharwar craton (south India). J. Struct. Geol., 18: 991-1004.

Chardon, D., Choukroune, P., and Jayananda, M., 1998. Sinking of the Dharwar Basin (South India): implications for Archaean tectonics. Precambrian Res., 91: 15-39.

Choukroune, P., Bouhallier, H., and Arndt, N. T., 1995. Soft lithosphere during periods of Archean crustal growth or crustal reworking. In: Coward, M. P., and Ries, A. C. (Editors), Early Precambrian Processes. v. 95. Geol. Soc. London. Spec. Publ., London, p. 67-86.

Coffin, M. F., and Eldholm O., 1994. Large igneous provinces: crustal structure, dimensions and external consequences., Reviews in Geophysics, 32: 1-36.

Collins, W. J., 1989. Polydiapirism of the Archaean Mount Edgar Batholith, Pilbara, Western Australia. Precambrian Res., 43: 41-62.

Collins, W. J., 1993. Melting of Archaean sialic crust under high aH2O conditions: genesis of 3300 Ma Na-rich granitoids in the Mount Edgar Batholith, Pilbara Block, Western Australia.

Precambrian Res., 60: 151-174.
Collins, W. J., and Gray, C. M., 1990. Rb-Sr isotopic systematics of an Archaean granite-gneiss terrain: The Mount Edgar Batholith, Pilbara Block, Western Australia. Austr. J. Earth Sci., 37: 9-22.
Collins, W. J., and Van Kranendonk, M. J., 1999. Model for the development of kyanite during partial convective overturn of Archaean granite-greenstone terrains: the Pilbara Craton, Australia. J. Metamorphic Geol., 17: 145-156.
Collins, W. J., Van Kranendonk, M. J., and Teyssier, C., 1998. Partial convective overturn of Archaean crust in the east Pilbara Craton, Western Australia: driving mechanisms and tectonic implications. J. Struct. Geology, 200: 1405-1424.
Collins, W. J., and Teyssier, C., 1990. Mount Edgar Batholith and Warrawoona Syncline., In: Ho, S. E., Glover, J. E., Myers, J. S., and Muhling, J. R., (Editors), Third International Archean Symposium, Vol. 21: Perth, Geol. Dept. & Univ. Extension, Univ. of Western Australia, p. 36-45.
Condie, K. C. (Editor), 1981. Archean Greenstone Belts. Elsevier, Amsterdam, 434 pp.
Condie, K. C. (Editor), 1994. Archean Crustal evolution. Elsevier, Amsterdam, 528 pp.
Condie, K. C., 1997. Plate Tectonics and Crustal Evolution., Butterworth-Heinemann, Bath, pp. 492.
Condie, K. C., 2000. Episodic continental growth models: afterthoughts and extensions. Tectonophysics, 322: 153-162.
Courtillot, V., Jaupart, C., Monighetti, I., Tapponnier, P., and Besse, J., 1999. On causal links between flood basalts and continental breakup. Earth Planet. Sci. Lett., 166: 177-195.
Cruden, A. R., 1988. Deformation around a rising diapir modelled by creeping flow past a sphere. Tectonics, 7: 1091 - 1101.
Cullers, R. L., DiMarco, M. J., Lowe, D. R., and Stone, J., 1993. Geochemistry of a silicified, felsic volcaniclastic suite from the early Archean Panorama Formation, Pilbara Block, Western Australia: an evaluation of depositional and post-depositional processes with special emphasis on the rare-earth elements. Precambrian Res., 60: 99-116.
Davids, C., Wijbrans, J. R., and White, S. H., 1997. $^{40}Ar/^{39}Ar$ laser probe ages of metamorphic hornblendes from the Coongan Belt, Pilbara, Western Australia. Precambrian Res., 83: 221-242.
Davies, G. F., 1992. On the emergence of plate tectonics. Geology, 20: 963-966.
Davies, G. F., 1993. Conjectures on the thermal and tectonic evolution of the earth. Lithos, 30: 281 - 289.
Davies, G. F., and Richard, M. A., 1992. Mantle Convection. , 100: 151-206.
Davy, R., and Lewis, J. D., 1981. The geochemistry of the Mount Edgar Batholith, Pilbara area, Western Australia. Spec. Publ. Geol. Soc. Aust., 7: 373-383.
De Ronde, C. E. J., and De Wit, M. J., 1994. Tectonic history of the Barberton greenstone belt, South Africa: 490 million years of Archean evolution., Tectonics, 13: 983-1005.
De Wit, M. J., 1982. Gliding and overthrust nappes in the Barberton greenstone belt., J. Struct. Geol., 4: 117-136.
De Wit, M. J., 1998. On Archean granites, greenstones, cratons and tectonics: does the evidence

demand a verdict? Precambrian Res., 91: 181-226.
De Wit, M. J., Armstrong, R., Hart, R., and Wilson, A., 1987a. Felsic igneous rocks with in the 3.3-3.5 Ga Barberton Greenstone Belt: high level crustal equivalents of the surrounding tonalite-trondhjemite terrain, emplaced during thrusting. Tectonics, 6: 529-549.
De Wit, M. J., and Ashwal, L. D., 1997. Greenstone Belts. Oxford Monogr. Geol. Geoph. 35: p. 803.
De Wit, M. J., and Hart, R. A., 1993. Earth's earliest continental lithosphere, hydrothermal flux and crustal recycling. Lithos, 30: 309-335.
De Wit, M. J., Hart, R. A., and Hart, R. J., 1987b. The Jamestown ophiolite complex, Barberton Mountain Belt: a section through 3.5 Ga oceanic crust. J. Afr. Earth Sci., 6: 681-730.
De Wit, M. J., and Hynes, A., 1995. The onset of interaction between the hydrosphere and oceanic crust, and the origin of the first continental lithosphere. In: Coward, M. P., and Ries, A. C. (Editors), Early Precambrian Processes. v. 95. Geol. Soc. Spec. Publ., p. 1-9.
Defant, M. J., and Kapezhinskas, P., 2001. Evidence suggests slab melting in arc magmas. Eos, 82: 65-69.
Délor, C., Burg, J.-P., and Clarke, G. L., 1991. Diapirism-Metamorphism relationships in the Pilbara Province (Western Australia): implications for thermal and tectonic regimes in the Archaean., Acad. Sci. Paris, 312: 257-263.
Desrocher, J.-P., Hubert, C., Ludden, J. N., and Pilote, P., 1993. Accretion of Archaean oceanic plateau fragments in the Abitibi greenstone belt, Canada. Geology, 21: 451-454.
Dewey, J. F., 1988. Extensional collaps of orogens. Tectonics, 7: 1123-1139.
DiMarco, M. J., and Lowe, D. R., 1989. Shallow-water volcaniclastic deposition in the Early Archaean Panorama Formation, Warrawoona Group, eastern Pilbara Block, Western Australia. Sediment. Geol., 64: 43-63.
Dirks, P. H. G. M., and Jelsma, H. A., 1998a. Continental extensional setting for the Archaean Belingwe Greenstone Belt, Zimbabwe. Geology, 26: 11-14.
Dirks, P. H. M. G., and Jelsma, H. A., 1998b. Horizontal accretion and stabilization of the Archean Zimbabwe Craton. Geology, 26: 11-14.
Dixon, J. M., 1975. Finite strain and progressive deformation in models of diapiric structures. Tectonophysics, 28: 89-124.
Dixon, J. M., and Summers, J. M., 1983. Patterns of total and incremental strain in subsiding troughs: experimental centrifuged models of inter-diapir synclines. Can. J. Earth Sc., 20: 1843-1861.
Dodson, M. H., 1973. Closure temperature in cooling geochronological and petrological systems. Contrib. Mineral. Petrol., 40: 259-274.
Dokka, R. K., 1993. Original dip and subsequent modification of a Cordilleran detachment fault, Mojave extensional belt, California. Geology, 21: 711-714.
Drummond, B. J., 1983. Detailed seismic velocity/depth models of the upper lithosphere of the Pilbara Craton, northwest Australia. BMR J. Austr. Geol. & Geoph., 8: 35-51.
Drummond, B. J., 1988. A review of crust/upper mantle structure in the Precambrian areas of Australia and implications for Precambrian crustal evolution. , 40/41: 101-116.

Drummond, B. J., and Collins, C. D. N., 1986. Seismic evidence for underplating of the lower continental crust of Australia. Earth Planet. Sci. Lett., 79: 361-372.

Drummond, B. J., Goleby, B. R., Swager, C. P., and Williams, P. R., 1993. Constraints on Archean crustal composition and structure provided by deep seismic sounding in the Yilgarn Block. Ore Geology Review, 8: 117-124.

Drury, S. A., Harris, N. B., Holt, R. W., Reeves-Smith, G. J., and Wightman, R. T., 1984. Precambrian tectonics and crustal evolution in South India. J. of Geol., 92:3-20.

Durrheim, R. J., and Mooney, W. D., 1991. Archaen and Proterozoic crustal evolution: evidence from crustal seismology., Geology, 19: 606-609.

Durrheim, R. J., and Mooney, W. D., 1994. Evolution of the Precambrian Lithosphere: Seismological and geochemical constraint., 99: 15,359-15,374.

Easton, R. M., 1985. The nature and significance of pre-Yellowknife Supergroup rocks in the Point Lake area, Slave structural province, Canada. In: Evolution of Archean supracrustal sequences. Ayers, L. D., Thurston, P. C., Crad, K. D., Weber, W., Geological Assoc. Canada Spec. Papers. 28: 153-167.

Eriksson, K. A., Krapez, B., and Fralick, P. W., 1994. Sedimentology of Archaean greenstone belts: signatures of tectonic evolution. Earth-Sc. Rev., 37: 1-88.

Ernst, R. E., and Buchan, K. L., 1997. Giant radiating dyke swarms: their use in identifying pre-mesozoic large igneous provinces and mantle plumes. In: Mahoney, J. J., and Coffin, F. (Editors), Large Igneous Provinces. Continental, Oceanic and Planetary Flood Volcanism. Geophysical Monograph Series. v. 100. American Geophysical Union, Washington, p. 438.

Ernst, R. E., Buchan, K. L., and Palmer, H. C., 1995b. Giant Dyke Swarms: characteristics, distribution and geotectonic applications. In: Baer, G., and Heimann, A. (Editors), Physics and Chemistry of Dykes. Balkema, Rotterdam, p. 3-21.

Ernst, R. E., Head, J. W., Parfitt, E., Grosfils, E., and Wilson, L., 1995a. Giant radiating dyke swarms on Earth and Venus. Earth Sci. Rev., 39: 1-58.

Evans, O. C., and Hanson, G. H., 1992. Most late Archaean tonalites, trondhjemites and granodiorites (TTG) in the SW Superior Province were derived from mantle melts, not by melting of basalt., EOS, Transactions of the Am. Geoph. Union, 22D-3: 330.

Friend, C. R. L., Nutman, A. P., and McGregor, V. R., 1988. Late Archean terrane accretion in the Godthab region, southern West Greenland. Nature, 335: 535-538.

Froude, D. O., Wijbrans, J. R., and Williams, I. S., 1984. 3400-3430 Ma ages from U-Pb analyses in the Western Shaw belt, Pilbara Block.. Aust. Nation. Univ. Res. School, Earth Sci. Ann. Rep. 1983: 126-128.

Fyfe, W. S., 1978. Evolution of earth's crust: modern plate tectonics to ancient hot spot tectonics? Chemical Geology, 23: 89-114.

Gee, R. D., Baxter, J. L., Wilde, S. A., and Williams, I. R., 1981. Crustal development in the Yilgarn Block., In: Glover, J. E., and Groves, D. I., (Editors), 2nd International Archean Symposium, Vol. 7: Perth, W.A., Geological Society of Australia, Special Publication, p. 43-56.

Gill, R. C. O., 1979. Comparative Petrogenesis of Archean and Modern Low-K Tholeiites, a Critical Review of some Geochemical Aspects., Phys. Chem. Earth, 11: 431-447.

Glikson, A.Y. 1999. Geology, 27:387-341.

Glikson, A. Y., and Hickman, A. H., 1981. Geochemistry of Archaean volcanic sequences, eastern Pilbara Block, Western Australia, Australia. Bur. Mineral Res. Geol. Geoph. Australia., Record No. 1981/36.

Green, D. H., 1972. Archean greenstone belts may include terrestrial equivalents of lunar maria ? Earth Planet. Sci. Lett., 15: 263-270.

Green, M. G., Sylvester, P. J., and Buick, R., 2000. Growth and recycling of continental crust: geochemical evidence from the Coonterunah and Warrawoona Groups, Pilbara Craton, Australia. Tectonophysics, 322: 69-88.

Griffin, T. J., 1990. North Pilbara granite- greenstone terrane. In: Survey, W. A. G., (Editor), in: Geology and Mineral Resources of Western Australia, Vol. Memoir 3, p. 77-119.

Grove, T. L., and De Wit, M. J., 1995. Wet komatiites and Archean mantle conditions, Conference Proceeding. Precambrian '95: Montreal, Canada, p. 29.

Groves, D. I., Archibald, N. J., Bettenay, L. F. and Binns, R. A., 1978. Greenstone belts as ancient marginal basins or ensialic rift zones., Nature, 273: 460-461.

Guérin, G., Brun, J. P., and Driessche, J. V. D., 1990. Kinematics of pre-Miocene ductile deformation in the Santa Catalina core complex and adjacent regions. Tectonics, 9: 1305-1326.

Hall, R. P., and Hughes, D. J., 1990. Early Precambrian Basic Magmatism: New York, Blackie, p. 486.

Hamilton, P. J., Evensen, N. M., Nions, R. K. O., Glikson, A. Y. and Hickman, A. H., 1981. Sm-Nd dating of the North Star Basalt, Warrawoona Group, Pilbara Block, Western Australia. Spec. Publs. Geol. Soc. Austr., 7: 187-191.

Hamilton, W. B., 1998. Archaean magmatism and deformation were not products of plate tectonics. Precambrian Res., 91: 143-179.

Hanes, J. A., Archibald, D. A., Hodgson, C. J., and Robert, F., 1992. Dating of Archean auriferous quartz vein deposits in the Abitibi Greenstone Belt, Canada: ^{40}Ar-^{39}Ar evidence for a 70-100 m.y. time gap between plutonism-metamorphism and mineralization. Economic Geology, 87: 1849-1861.

Hanes, J. A., Archibald, D. A., Queen, M., and Farrar, M., 1994. Constraints from ^{40}Ar-^{39}Ar geochronology on the tectonothermal history of the Kapuskasing uplift in the Canadian Superior Province. Can. J. Earth Sci., 31: 1146-1171.

Hargraves, R. B., 1986. Faster spreading or greater ridge length in the Archean ? Geology, 14: 750-752.

Harrison, T. M., 1981. Diffusion of ^{40}Ar in Hornblende. Contrib. Mineral. Petrol., 78: 324-331.

Harrison, T. M., Duncan, I., and McDougall, I., 1985. Diffusion of ^{40}Ar in biotite: Temperature, pressure and compositional effects. Geoch. Cosmoch. Act., 49: 2461-2468.

Harrison, T. M., and McDougall, I., 1980. Investigations of an intrusive contact, northwest Nelson, New Zealand - Thermal, chronological and isotopic constraints. Geoch. Cosmoch. Act., 44: 1985-2003.

Heaman, L. M., Bowins, R., and Crocket, J., 1990. The chemical composition of igneous zircon suites: Implications for geochemical tracer studies. Geochim. Cosmochim. Acta, 54: 1597-1607.

Henderson, J. B., 1981. Archean basin evolution in the Slave Province, Canada. In: Kröner, A. (Editor), Precambrian Plate Tectonics. Elsevier, Amsterdam, p. 213-235.

Henderson, J. B., 1985. Geology of the Yellowknife – Hearne Lake area, district of McKenzie: a segment across an Archean basin. Geological Survey of Canada Memoir nr. 14.

Hickman, A.H., 1975. Precambrian Structural Geology of part of the Pilbara Region. Western Australia Geol. Survey Ann. Rpt., 1974: 68-73.

Hickman, A. H., 1977. New and revised definitions of rock units in the Warrawoona Group, Pilbara Block. Western Australia Geol. Survey Ann Rep, 1976: 53.

Hickman, A. H., 1980. Crustal evolution of the Pilbara Block in 'Archaean Geology", In: Glover, J. E., and Groves, D. I., (Editors), Second International Archean Symposium: Perth, p. 57-69.

Hickman, A.H., 1981. Crustal evolution of the Pilbara Block, Western Australia. Spec. Publs. Geol. Soc. Aust., 7: 57-69.

Hickman, A.H., 1983. Geology of the Pilbara Block and its environs. Geol. Surv. Australia Bull., 127: P. 268.

Hickman, A. H., 1984. Archaean diapirism in the Pilbara Block, Western Australia. In: Kröner, A., and Greiling, R. (Editors), Precambrian Tectonics Illustrated. p. 113-127.

Hickman, A. H., and Gibson, D. L., 1982. Explanatory notes on the Port Hedland-Bedout Island Geological Sheet: Perth, Geological Survey of Western Australia.

Hickman, A. H., and Lipple, S. L., 1978. Explanatory notes on the Marble Bar Geological Sheet: Perth, Geological Survey of Western Australia.

Hickman, A. H., Thorne, A. M., and Trendall, A. F., 1990. Geology of the Pilbara Craton, In: Ho, S. E., Glover, J. E., Myers, J. S., and Muhling, J. R., (Editors), 3IAS - Third International Archaean Symposium, Excursion Guidebook, Vol. 21: Perth, Geol. Dept. & Univ. Extensions University of Western Australia, p. 2-56.

Hill, R. I., Campbell, I. H., Compston, W., 1989. Age and origin of granitic rocks in the Kalgoorlie-Norseman region of Western Australia: implications for the origin of the Archean crust., Geochim. Cosmochim. Acta., 53: 1259-1275.

Hill, E. J., 1994. Geometry and kinematics of shear zones formed during continental extension in eastern Papua New Guinea. J. Struct. Geol., 16: 1093-1105.

Hill, R. I., 1991. Starting plumes and continental break-up. Earth Planet. Sci. Lett., 104: 389-416.

Hill, R. I., Campbell, G. F., Davies, G. F., and Griffiths, R. W., 1992a. Mantle plumes and continental tectonics. Science, 256: 186-193.

Hoek, J. D., 1991. A classification of dyke-fracture geometry with examples from Precambrian dyke swarms in the Vestfold Hills, Antarctica. Geol. Runds., 80: 233-248.

Hoek, J. D., 1994. Mafic dykes of the Vestfold Hills, East Antarctica. An analysis of the emplacement mechanism of tholeiitic dyke swarms and of the role of dyke emplacement during crustal extension. Ph.D. Thesis, University of Utrecht.

Hoffman, P. F., 1991. On accretion of granite-greenstone terranes. In: Robert, F. (Editors), Greenstone gold and crustal evolution. St. John's, Geological Association of Canada, Newfoundland, p. 32-45.

Hoffman, P. F., and Ranalli, G., 1988. Archean oceanic flake tectonics., Geoph. Res. Letters, 15:

1077-1080.

Horwitz, R. C., 1990. Paleogeographic and tectonic evolution of the Pilbara Craton, Northwestern Australia. Precambrian Res., 48: 327-340.

Hurley, P. M., 1968. Absolute abundance and distribution of Rb, K and Sr in the Earth., Geochim Cosmochim. Acta, 32: 19-22.

Hutton, D. H. W., Dempster, T. J., Brown, P. E., and Beckers, S. D., 1990. A new mechanism of granite emplacement: intrusion in active extensional shear zones. Nature, 343: 452-455.

Jackson, M. J., and Pollack, H. N., 1984. On the sensitivity of parameterized convection to the rate of decay of internal heat sources., J. Geoph. Res., 89: 10,103-10,108.

Jackson, S. L., and Cruden, A. R., 1995. Formation of the Abitibi greenstone belt by arc-trench migration. Geology, 23: 471-474.

James, D. T., and Mortensen, J. K., 1992. An Archean metamorphic core complex in the southern Slave Province: basement-cover structural relations between the Sleepy Dragon Complex and the Yellowknife Supergroup., Can. J. Earth Sci., 29: 2133-2145.

Jelsma, H. A., and Van Den Beek, P. A., 1993. Tectonic evolution of the Bindura - Shamva greenstone belt (northern Zimbabwe): progressive deformation around diapiric batholiths. J. Struct. Geol., 15: 163 - 176.

Karato, S. I. and Wu, P. 1993. Rheology of the upper mantle; a synthesis. Science, 260: 5109, 771-778.

Kent, R. W., Hardarson, B. S., Saunders, A. D., and Storey, M., 1996. Plateaux ancient and modern: Geochemical and sedimentological perspectives on Archean oceanic magmatism. Lithos, 37: 1229-142.

Kerr, A. C., Marriner, G. F., Arndt, N. T., Tarney, J., Nivia, A., Saunders, A. D. and Duncan, R. A., 1996. The petrogenesis of Gorgona komatiites, picrites and basalts: new field, petrographic and geochemical constraints., Lithos 37: 245-260.

Kerrich, R., and Keyser, T. K., 1994. 100 Ma timing paradox of Archean gold, Abitibi greenstone belt (Canada): New evidence from U-Pb and Pb-Pb evaporation ages of hydrothermal zircons. Geology, 22: 1131 - 1134.

Kinny, P. D., Wijbrans, J. R., Froude, D. O., Williams, I. S., and Compston, W., 1990. Age constraints on the geological evolution of the Narryer Gneiss Complex, Western Australia. Earth Planet. Sci. Lett., 37: 51-69.

Kiyokawa, S., and A. Taira, 1998. The Cleaverville Group in the West Pilbara Coastal Granitoid-Greenstone Terrain of Western Australia: an example of a Mid-Archaean immature oceanic island-arc succession. Precambrian Res., 88: 109-142.

Koppers, A. A. P., 2002. ArArCALC-software for $^{40}Ar/^{39}Ar$ age calculations, Computers & Geosciences, 28: 605-619. 2002.

Krapez, B., 1984. Sedimentation in a small, fault-bounded basin: the Lalla Rookh Sandstone, east Pilbara Block. Geology dept. and Univ. Extension, U.W.A, 9: 89-110.

Krapez, B., 1993. Sequence stratigraphy of the Archaean supracrustal belts of the Pilbara Block, Western Australia. Precambrian Res., 60: 1-45.

Krapez, B., and Barley, M. E., 1987. Archaean strike-slip faulting and related ensialic basins:

evidence from the Pilbara Block, Australia. Geol. Mag., 124: 555-567.
Krapez, B., and Eisenlohr, B., 1998. Tectonic settings of Archaean (3325-2775 Ma) crustal-supracrustal belts in the West Pilbara Block. Precambrian Res., 88: 173-205.
Kröner, A., 1981. Precambrian Plate Tectonics. Elsevier, Amsterdam.
Kröner, A., 1982. Archean to early Proterozoic tectonics and crustal evolution: a review. Revista Brasileira de Geociencias, 12: 15-31.
Kröner, A., 1984. Evolution, growth and stabilization of the Precambrian lithosphere. Phys. Chem. Earth, 15: 69-106.
Kröner, A., 1991. Tectonic evolution in the Archaean and Proterozoic. Tectonophysics, 187: 393-410.
Kusky, T. M., and Vearncombe, J. R., 1997. Structural aspects. In: De Wit, M. J. and Ashwal, L. D. (Editors), Greenstone Belts., Oxford Monogr. Geol. Geoph., 35: 91-124.
Kusky, T. M., 1993. Collapse of Archean orogens and the origin of late granitoids., Geology, 10: 925-935.
Kusky, T. M., and Kidd, W. S. F., 1992. Remnants of an Archean oceanic plateau, Belingue greenstone belt, Zimbabwe. Geology, 20: 43-46.
Kyte, F. T., Shykolyukov, A., Lugmair, G.W., Lowe, D.R., Byerly, G.R., 1999. Early Archean spherule beds; confirmation of impact origin. In: Geological Society of America, 1999 annual meeting. Abstr. With Progr. Geol. Soc. Am. 31, 7: 64-65.
Lambert, M. B., Ernst, R. E., and Dudas, F. O. L., 1992. Archaean mafic dyke swarms near the Cameraon River and Beaulieu River volcanic belts and their implications for tectonic modelling of the Slave Province, Northwest Territories. Can. J. Earth Sci., 29: 2226-2248.
Lee, J. K. W., Onstott, T. C., and Hanes, J. A., 1990. An $^{40}Ar/^{39}Ar$ investigation of the contact effects of a dyke intrusion, Kapuskasing Structural Zone, Ontario. Contrib. Mineral. Petrol., 105: 87 - 105.
Lipple, S. L., 1975. Definitions of new and revised stratigraphic units of the eastern Pilbara Region., Western Australia Geol. Surv. Ann. Report 1974., p.58-63.
Lips, A. L. W., 1998. Temporal constraints on the kinematics of the destabilization of an orogen. Geologica Ultraiectina, 166: p. 224.
Lister, G. S., and Baldwin, S. L., 1993. Plutonism and the origin of metamorphic core complexes. Geology, 21: 607-610.
Lister, G. S., and Davis, G. A., 1989. The origin of metamorphic core complexes and detachment faults formed during Tertiary continental extension in the Northern Colorado River region, U.S.A., J. Struct. Geol., 11: 65-94.
Lopez-Martinez, M., and York, D., 1990. A comparative ^{40}Ar-^{39}Ar study of the Kapuskasing structural zone and the Wawa gneiss terrain: thermal and tectonic implications. Can. J. Earth Sci., 27: 787-793.
Lowe, D. R., 1982. Comparative sedimentology of the principal volcanic sequences of Archean greenstone belts in South Africa, Western Australia, and Canada: implications for crustal evolution. Precambrian Res., 17: 1-29.
Lowe, D. R., 1983. Restricted shallow-water sedimentation of early Archean stromatolitic and

evaporitic strata of the Strelley Pool Chert, Pilbara block, Western Australia. Precambrian Res., 19: 239-283.

Ludden, J. N., Hubert, C. and Gariepy, C., 1986. The tectonic evolution of the Abitibi Belt, Canada., Geological Magazine, 123: 153-166.

Maas, R., Kinny, P. D., Williams, I. S., Froude, D. O., and Compston, W., 1992. The earth's oldest known crust: A geochronological and geochemical study of 3900-4200 Ma old detrital zircons from Mt Narryer and Jack Hills, Western Australia. Geochim. Cosmochim. Acta, 56: 1281-1300.

Mahoney, J. J., and Coffin, M. F., 1997. Large Igneous Provinces: Continental, Oceanic, and Planetary Flood Volcanism, Geophysical Monograph Series, Vol. 100: Washington, American Geophysical Union.

Manatschal, G., Ulfbeck, D., and Van Gool, J., 1998. Change from thrusting to syncollisional extension at a mid-crustal level: an example from the Palaeoproterozoic Nagssugtoqidian Orogen (West Greenland). Can. J. Earth Sci., 35: 802-819.

Marshak, S., 1999. Deformation style way back when: thoughts on the contrasts between Paleoproterozoic and contemporary orogens. J. Struct. Geol., 21: 1175-1182.

Marshak, S., Alkmim, F. F., and Jordt-Evangelista, H., 1992. Proterozoic crustal extension and the generation of dome-an-keel structure in an Archaean granite-greenstone terrain. Nature, 357: 491-493.

Marshak, S., Tinkham, D., Alkmim, F., Brueckner, H., and Bornhorst, T., 1997. Dome-and-keel provinces formed during Paleoproterozoic orogenic collapse - core complexes, diapirs or neither ? Examples from the Quadrilátero Ferrífero and the Penokean Orogen. Geology, 25: 415-418.

Martin, H., 1994. The Archaean grey gneisses and the genesis of continental crust. In: Condie, K. C. (Editor), Archaean Crustal Evolution, Elsevier, Amsterdam. 205-259.

McDonough, W.F. and Ireland, T. R., 1993. Intraplate origin of komatiites inferred from trace elements in glass inclusions., Nature, 365: 432-434.

McDougall, I., and Harrison, T. M., 1988. Geochronology and Thermochronology by the $^{40}Ar/^{39}Ar$ Method. Oxford University Press, New York, p. 212.

McGregor, V. R., 1973. Further rubidium-strontium age determinations on the very early Precambrian rocks of the Godthaab District, West Greenland. In: Europaeisches Kolloquium fuer Geochronologie, II, Referate., Moorbath, S, O'Nions, R.K., Pankhurst, R.J., Gale, N.H. (Editors). Forschritte der Mineralogie, 50: 111-112.

McGregor, A. M., 1951. Some milestones in the Precambrian of southern Africa., Proc. Geol. Soc. S. Afr., 54: 27-71.

McKenzie, D. P., 1984. The generation and compaction of partially molten rock., J. Petrology, 25: 713-765.

McKenzie, D., and Bickle, M. J., 1988. The volume and composition of melt generated by extension of the lithosphere. J. Petr., 29: 625-679.

McNaughton, N. J., Compston, W., and Barley, M. E., 1993. Constraints on the age of the Warrawoona Group, eastern Pilbara Block, Western Australia. Precambrian Res., 60: 69-98.

McNaughton, N. J., Green, M. D., Compston, W., and Williams, I. S., 1988. Are anorthositic

rocks basement to the Pilbara Craton ? Geol. Soc. Austr. Abstr., 21: 272-273.
Moser, D. E., 1994. The geology and structure of the mid-crustal Wawa gneiss domain: a key to understanding tectonic variation with depth and time in the late Archean Abitibi-Wawa orogen. Can. J. Earth Sci., 31: 1064-1080.
Moser, D. E., Heaman, L. M., Krogh, T. E., and Hanes, J. A., 1996. Intracrustal extension of an Archean orogen revealed using single-grain U-Pb zircon geochronology. Tectonics, 15: 1093-1109.
Myers, J. S., 1993. Precambrian history of the West Australian Craton and adjacent orogens. Annu. Rev. Earth Planet. Sci., 21: 453-485.
Myers, J. S., 1995. The generation and assembly of an Archean super continent: evidence from the Yilgarn Craton, Western Australia. In: Coward, M. P., and Ries, A. C. (Editors), Early Archean Processes. Geol. Soc. Lond. Spec. Publ. v. 95.
Nelson, D. R., 1996. Compilation of SHRIMP U-Pb zircon geochronology data, 1995. Geol. Surv. Western Australia, Record 1996/5: 168 p.
Nelson, D. R., 1997. Compilation of SHRIMP U-Pb zircon geochronology data, 1996. Geol. Surv. Western Australia, Record 1997/2: 189 p.
Nelson, D. R., 1998a. Compilation of SHRIMP U-Pb zircon geochronology data, 1997. Geol. Surv. Western Australia, Record 1998/2: 242 p.
Nelson, D. R., 1998b. Granite-greenstone crust formation on the Archaean Earth: a consequence of two superimposed processes. Earth Planet. Sci. Lett., 158: 109-119.
Nelson, D. R., 1999. Compilation of SHRIMP U-Pb zircon geochronology data, 1998. Geol. Surv. Western Australia, Record 1999/2: 222 p.
Nelson, D. R., 2000. Compilation of SHRIMP U-Pb zircon geochronology data, 1999. Geol. Surv. Western Australia, Record 2000/2: 251 p.
Nelson, D. R., 2001. Compilation of SHRIMP U-Pb zircon geochronology data, 2000. Geol. Surv. Western Australia, Record 2001/2: 205 p.
Nelson, D. R., 2002. Compilation of SHRIMP U-Pb zircon geochronology data, 2001. Geol. Surv. Western Australia, Record 2002/2: 282 p.
Nelson, D. R., Trendall, A. F., and Altermann, W., 1999. Chronological correlations between the Pilbara and Kaapvaal cratons. Precambrian Res., 97: 165-189.
Nijman, W., Bruijne, C. H. D., and Valkering, M., 1998b. Growth fault control on early Archaean cherts, barite mounds and chert-barite veins, North Pole, East Pilbara. Precambrian Res., 88: 25-52.
Nijman, W., Willigers, B. J. A., and Krikke, A., 1998a. Tensile and compressive growth structures: the relation between sedimentation, deformation and granite intrusion in the Archean Coppin Gap Greenstone Belt, East Pilbara, W. Australia. Precambrian Res., 88: 83-108.
Nisbet, E. G., 1987. The Young Earth., Allen and Unwin, London, 402 pp.
Nisbet, E. G., Cheadle, M. J., Bickle, M. J., and Arndt, N. T., 1993. Constraining the potential temperature of the Archaean mantle: A review of the evidence from komatiites., Lithos, 30: 291-308.
Nisbet, E. G., and Fowler, C. M. R., 1983. Model for Archean plate tectonics., Geology, 11: 376-

379.
Nutman, A. P., Kinny, C. R. L., and McGregor, V. R., 1993. Anatomy of an early Archaean gneiss complex: 3900-3600 Ma crustal evolution in southern West Greenland., Geology, 21: 415-418.
Nutman, A. P., and Myers, J. S., 1996. The Itsag Gneiss Complex of southern West Greenland: the world's most extensive record of early crustal evolution (3900 - 3600 Ma). Precambrian Res., 78: 1-39.
O'Nions, R. K., Evensen, N. M., Hamilton, P. J., and Carter, S. R., 1978. Melting of the mantle past and present: isotopic and trace element evidence. Philos. Trans. Soc. Lond., A258: 547-559.
O'Nions, R. K., and Pankhurst, R. J., 1978. Early Archaean rocks and geochemical evolution of the earth's crust. Earth Planet Sci. Lett., 38: 211-236.
Oliver, N. H. S., and Cawood, P. A., 2001. Early tectonic dewatering and brecciation on the overturned sequence at Marble Bar, Pilbara Craton, Western Australia: dome-related of not ? Precambrian Res., 105: 1-15.
Park, R. G., 1982. Archean Tectonics., Geol. Rundschau, 71: 22-37.
Parsons, T. and Thompson, G. A., 1993. Does magmatism influence low-angle normal faulting ? Geology, 21: 247-250.
Passchier, C. W., 1995. Precambrian orogenesis: was it really different ? Geol. Mijnbouw, 74: 141-150.
Paterson, S. R., Vernon, R. H., and Fowler-Jr., T. K., 1991. Aureole Tectonics. In: Kerrick, D. M. (Editors), Contact Metamorphism. Reviews in Mineralogy. v. 26. Min. Soc. Am., p. 673-722.
Pavlis, T. L., 1996. Fabric development in syn-tectonic intrusive sheets as a consequence of melt-dominated flow and thermal softening of the crust. Tectonophysics, 253: 1-31.
Pawley, M. J., Collins, W. J., Van Kranendonk, M.. J., 2002. Origin of fine-scale sheeted granites by incremental injection of magma into active shear zones: examples from the Pilbara Craton, NW Australia., Lithos 61: 127-139.
Philpotts, A. R., 1990. Principles of igneous and metamorphic petrology. Prentice Hall, New Jersey, 498 p.
Pidgeon, R. T., 1978a. 3450-m.y.-old volcanics in the Archaean layered greenstone succession of the Pilbara Block, Western Australia. Earth Planet. Sci. Lett., 37: 421-428.
Pidgeon, R. T., 1978b. Geochronological investigations of granite batholiths of the Archaean granite greenstone terrain of the Pilbara Block, Western Australia, In: I. E. M. Smith (Editor), Archaean Geochemistry Conference: Toronto, p. 360-362.
Pidgeon, R.T., 1984. Geochronological constraints on early volcanic evolution of the Pilbara Block, Western Australia. Aust. J. Earth Sci., 31: 237-242.
Pidgeon, R. T., and Aftalion, M., 1978. Co-genetic and inherited zircon U-Pb systems in granites: Palaeozoic granites of Scotland and England. Geol. J. Spec. Issue, 10: 183-248.
Pidgeon, R. T., O'Neill, J. R., and Silver, L. T., 1966. Uranium and lead isotopic stability in a metamict zircon under experimental hydrothermal conditions. Science, 154: 1538-1540.
Polat, A., Kerrich, R., Wyman, D. A., 1998. The Late-Archean Schreiber-Hemlo and White River-Dayohessarah greenstone belts, Superior Province: collages of oceanic plateaus, oceanic arcs, and subduction-accretion provinces. Tectonophysics, 289: 295-326.

Pollack, 1997. Thermal characteristics of the Archaean. In: De Wit, M and Ashwal, L. D. (Editors) Greenstone Belts, Oxford Monogr. Geol. Geoph. 35: 223-232.

Pollack, H.N., 1986. Cratonization and thermal evolution of the mantle. Earth Planet. Sci. Lett., 80: 175-182.

Pollard, D. D., 1987. Elementary fracture mechanics applied to the structural interpretation of dykes. Geol. Assoc. Can. Spec. Paper, 34: 5-24.

Pollard, D. D., and Segall, P., 1987. Theoretical displacements and stresses near fractures in rock: with applications to faults, joints, veins, dikes, and solution surfaces. Academic Press, London, 277-349 p.

Rapp, R. P. and Watson, R. B., 1995. Dehydration melting of metabasalt at 8-32 kbar: implications for continental growth and crust-mantle recycling., J. Petrol., 36: 891-931.

Reymer, A. and Schubert, G., 1986. Rapid growth of some major segments of continental crust. Geology, 14: 299-302.

Reynolds, S. J., and Lister, G. S., 1990. Folding of mylonitic zones in Cordilleran metamorphic core complexes: Evidence from near the mylonitic front. Geology, 18: 216-219.

Richards, M. A., Duncan, R. A. and Courtillot, V. E., 1989. Flood basalts and hot-spot tracks: plume heads and tails., Science, 246: 103-107.

Richardson, 1985. . : .

Richter, F. M., 1984. Regionalized models for thermal evolution of the earth., Earth Planet. Sci. Lett., 68: 471-484.

Rubatto, D., and Gebauer, D., 1999. Use of Cathodoluminescence for U-Pb Zircon Dating by Ion Microprobe: Some Examples from the Western Alps. In: Pagel, M., Barbin, V., Blanc, P., and Ohnestetter, D. (Editors), Cathodoluminescence in Geosciences., Springer Verlag, p. 373-400.

Rubatto, D., Gebauer, D., and Compagnoni, R., 1999. Dating of eclogite-facies zircons: the age of Alpine metamorphism in the Sesia-Lanze Zone (Western Alps). Earth Planet. Sci. Lett., 167: 141-158.

Sandiford, 1989. Secular trends in the thermal evolution of metamorphic terains., Earth Planet. Sci. Lett., 95, 1-2: 85-96.

Saunders, A. D., Tarney, J., Kerr, A. C., and Kent, R. W., 1996. The formation and fate of large oceanic igneous provinces., Lithos , 37: 81-95.

Schwerdtner, W. M., Sutcliffe, R. H., and Tröeng, B., 1978. Patterns of total strain in the crestal region of immature diapirs., Can. J. Earth Sci., 15: 1437 - 1447.

Schwerdtner, W. M., and Tröeng, B., 1977. Strain distribution within arcuate diapiric ridges of silicone putty., Tectonophysics, 50: 13 - 28.

Sheth, H. C., 1999a. Flood basalts and large igneous provinces from deep mantle plumes: fact, fiction and fallacy., Tectonophysics, 311: 1-29.

Sheth, H. C., 1999b. A historical approach to continental flood basalt volcanism: insights into pre-volcanic rifting, sedimentation, and early alkaline magmatism., Earth Planet. Sci. Lett., 168: 19-26.

Silver, L. T., and Deutsch, S., 1963. Uranium-lead isotopic variations in zircons: a case study., J. Geol., 71: 721-758.

Sleep, N. H. and Windley, B. F., 1982. Archaean plate tectonics: constraints and inferences., J. Geology, 90: 363-379.

Sleep, N. H., 1979. Thermal history and degassing of the Earth: some simple calculations., J. Geol., 87: 671-686.

Sleep, N. H., 1992. Archean plate tectonics: what can be learned from continental geology ?, Can. J. Earth Sci., 29: 2066-2071.

Smith, J. B., Barley, M. E., Groves, D. I., Krapez, B., and McNaughton, N. ., 1998. The Sholl Shear Zone, Western Pilbara: Evidence for a domain boundary structure from integrated tectonostratigraphic analyses, SHRIMP U-Pb dating and isotopic and geochemical data of granitoids., Precambrian Res., 88: 143-171.

Smithies, R. H., 2000. The Archaean tonalite-trondhjemite-granodiorite (TTG) series is not an analogue of Cenozoic adakite., Earth Planet. Sci. Lett., 182: 115-125.

Spear, F. S., 1995. Temperature-time histories, Metamorphic Phase equilibria and Pressure-Temperature-Time Paths. Monograph., Mineralogical Society of America, Washington, p. 711-745.

Spencer, J. E., 1984. Role of tectonic denudation in warping and uplift of low-angle normal faults., Geology, 12: 95-98.

Spray, J. G., 1985. Dynamothermal transition between Archean greenstone and granite-gneiss at lake Dundas, Western Australia., Geology, 7: 187-203.

Steiger, R. H., and Jager, E., 1977. Subcommission on Geochronology: convention on the use of decay constants in geo- and cosmochronology., Earth Planet. Sci. Lett., 36: 359-362.

Storey, M., Mahoney, J. J., Kroenke, L. W. and Saunders, A. D., 1991. Are oceanic plateaus sites of komatiite formation?, Geology, 19: 376-379.

Streckeisen, A., 1974. Classification and Nomenclature of Plutonic Rocks Recommendations., N. Jahrbuch für Mineralogie, 4: 149-164.

Streckeisen, A., 1976a. To each plutonic rock its proper name. Earth Sc. Review, 12: 1-33.

Sylvester, E., 1987. Post-subduction granites and their Proterozoic occurrence., Geol. Soc. Am., Abstr. With Progr. 19-7: 862-863.

Tarney, J., 1992. Geochemistry and significance of mafic dyke swarms in the Proterozoic. In: Condie, K. C. (Editor), Proterozoic Crustal Evolution. Developments in Precambrian Geology 10. Elsevier, Amsterdam, p. 151-180.

Tarney, J., Dalziel, I. W. D., and De Wit, M. J., 1976. Marginal basin "Rocas Verdes" complex from S. Chile: a model for Archean greenstone belt formation. In: Windley, B. F. (Editor), The Early History of the Earth. Wiley, London, p. 131-146.

Taylor, B., 1995. Backarc Basins - Tectonics and Magmatism: New York, Plenum Press, p. 524.

Taylor, S. R., and McLennan, S. M., 1995. The geochemical evolution of the continental crust., Rev. Geophysics, 33: 241-265.

Teyssier, C., 1988. Structures in greenstone belts (Pilbara Block, Western Australia)-diapirism and extensional tectonics, a cart and a horse problem. Geol. Soc. Am. Abstr. with Prog., 20: 391-392.

Thorpe, R. I., Hickman, A. H., Davis, D. W., Mortensen, J. K., and Trendall, A. F., 1990.

Constraints to models for Archaean lead evolution from precise zircon U-Pb zircon geochronology for the Marble Bar region, Pilbara Craton, Western Australia., Geol. Dept. & University Extensions, 22: 395-407.

Thorpe, R. I., Hickman, A. H., Davis, D. W., Mortensen, J. K., and Trendall, A. F., 1992. U-Pb zircon geochronology of Archaean felsic units in the Marble Bar region, Pilbara Craton, Western Australia., Precambrian Res., 56: 169-189.

Van Breemen, O., and Hanmer, S., 1986. Zircon morphology and geochronology in active shear zones: studies on syntectonic intrusions along the northwest boundary of the Central Metasedimentary Belt, Grenville Province, Ontario., Paper / Geol. Surv. Can., 86-1B: 776-784.

Van Haaften, W. M., and White, S. H., 1998. Evidence for multiphase deformation in the Archean basal Warrawoona Group in the Marble Bar area, east Pilbara, Western Australia., Precambrian Res., 88: 53-66.

Van Koolwijk, M., 1998. Study of the Talga Talga Subgroup, the lowermost part of the Archean Marble Bar greenstone Belt: Implications for petrogenesis of mafic and ultramafic volcanism with use of petrography, geochemistry and field relationships: oceanic or not? Unpublished report of fieldwork and geochemical laboratory work, Vrije Universiteit, Amsterdam, 46 pp, 6 appendices.

Van Kranendonk, M. J., 1998. Litho-tectonic and structural components of the North Shaw 1:100 000 sheet, Archaean Pilbara Craton., West. Austr. Geol. Surv. Ann. Rev., 1997-98: 63-70.

Van Kranendonk, M. J., 1999, North Shaw W.A., Sheet 2755: Perth, Western Australia Geological Survey.

Van Kranendonk, M. J., Hickman, A. H., Smithies, R. H., Nelson, D. R., Pike, G., 2002. Geology and tectonic evolution of the Archaean North Pilbara Terrain, Pilbara Craton, Western Australia., Economic Geology, 97: 695-732.

Van Kranendonk, M. J., and Collins, W. J., 1998. Timing and tectonic significance of Late Archaean, sinistral strike-slip deformation of the Central Pilbara Structural Corridor, Pilbara Craton, Western Australia., Precambrian Res., 88: 207-232.

Van Kranendonk, M. J., and Morant, P., 1998. Revised Archaean stratigraphy of the North Shaw 1:100 000 sheet, Pilbara Craton., West. Austr. Geol. Surv. Ann. Rev., 1997-98: 55-62.

Vavra, G., Gebauer, D., and Schmid, R., 1994. Unravelling the growth 'stratigraphy' in granulite zircons for SHRIMP dating of the lower crust: A case study from the Ivrea Zone (Southern Alps)., ICOG-8, Vol. 1107: Berkeley, USA, U.S. Geological Survey Circular, p. 337.

Vavra, G., Gebauer, D., Schmid, R., and Compston, W., 1996. Multiple zircon growth and recrystallization during polyphase Late Carboniferous to Triassic metamorphism in granulites of the Ivrea Zone (Southern Alps): an ion microprobe (SHRIMP) study., Contrib. Mineral. Petrol., 122: 337-358.

Vavra, G., Schmid, R., and D. Gebauwer, 1999. Internal morphology, habit, U-Th-Pb microanalysis of amphibolite-to-granulite facies zircons: geochronology of the Ivrea Zone (Southern Alps). Contrib. Mineral. Petrol., 134: 380-404.

Vearncombe, S., Barley, M. E., Groves, D. I., McNaughton, N. J., Mikucki, E. J., and Vearncombe, J. R., 1995. 3.26 Ga Black smoker-type mineralization in the Strelley Belt, Pilbara

Craton, Western Australia., J. Geol. Soc. London, 152: 587-590.
Vearncombe, S., and Kerrich, R., 1999. Geochemistry and geodynamic setting of volcanic and plutonic rocks associated with early Archaean volcanic massive sulphide mineralization, Pilbara Craton., Precambrian Res., 98: 243-270.
Vearncombe, S., Vearncombe, J. R., and Barley, M. E., 1998. Fault and stratigraphic controls on volcanogenic massive sulphide deposits in the Strelley Belt, Pilbara Craton, Western Australia., Precambrian Res., 88: 67-82.
Veizer, J. and Jansen, S. L., 1979. Basement and sedimentary recycling and continental evolution., J. Geology 87: 341-370.
Vervoort, J. D., Patchett, P. J., Gehrels, G. E., and Nutman, A. P., 1996. Constraints on early earth differentiation from hafnium and neodymium isotopes., Nature, 379: 624-627.
Viljoen, M. J., and Viljoen, R. P., 1969. Evidence of the existence of mobile extrusive peridotitic magma from the Komati formation of the Onverwacht Group., Spec. Publ. Geol. Soc. S. Afr., 2: 87-112.
Villa, I. M., 1998. Isotopic closure., Terra Nova, 10: 42-47.
Vlaar, N. J., 1986. Archaean global dynamics., Geologie en Mijnbouw, 65: 91-101.
Vlaar, N. J., 2000. Continental emergence and growth on a cooling earth., Tectonophysics, 322: 191-202.
Vlaar, N. J., van Keken, P. E., and van den Berg, A. P., 1994. Cooling of the Earth in the Archaean: consequences of pressure-release melting in a hotter mantle., Earth Planet. Sci. Lett., 121: 1-18.
Weinberg, R. F., and Podladchikov, Y. Y., 1995. The rise of solid-sate diapirs., J. Struct. Geol., 17: 1183-1195.
Wellman, P., 1998. Mapping of a granite batholith using geological and remotely sensed data: the Mount Edgar Batholith, Pilbara Craton., Exploration Geoph., 29: 643-648.
Wellman, P., 1999. Granitoid complexes and greenstone belts in the Pilbara Craton interpreted to extend down to the mid-crustal boundary at 14 km., AGSO Res. Newsletter, 30: 15-17.
Wellman, P., 2000. Upper crust of the Pilbara Craton, Australia; 3D geometry of a granite-greenstone terrain., Precambrian Res., 104: 175-186.
White, R. S., and McKenzie, D., 1989. Magmatism at rift zones: The generation of volcanic continental margins and flood basalts., J. Geophys. Res., 94: 7685-7729.
White, S. H., Bretan, P. G., and Rutter, E. H., 1986. Fault-zone reactivation: kinematics and mechanisms., Phil. Trans. R. Soc. Lond., A317: 81-97.
White, S. H., Zegers, T. E., Van Haaften, W. M., Kloppenburg, A., and Wijbrans, J. R., 1998. Tectonic evolution of the eastern Pilbara, Australia., Geologie en Mijnbouw, 76: 343-347.
Wijbrans, J. R., and McDougall, I., 1987. On the metamorphic history of an Archaean granitoid greenstone terrane, East Pilbara, Western Australia, using the $^{40}Ar/^{39}Ar$ age spectrum technique. Earth Planet. Sci. Lett., 84: 226-242.
Wijbrans, J. R., Pringle, M. S., Koppers, A. A. P., and Schevers, R., 1995. Argon geochronology of small samples using the Vulkaan argon laserprobe. Proc. Kon. Ned. Akad. v. Wetensch., 98: 185 - 218.
Williams, I. S., and Collins, W. J., 1990. Granite-greenstone terranes in the Pilbara Block, Australia,

as coeval volcano-plutonic complexes; evidence from U-Pb zircon dating of the Mount Edgar Batholith., Earth Planet. Sci. Lett., 97: 41-53.

Williams, I. S., Page, R. W., Froude, D. O., Fosters, J. J., and Compston, W., 1983. Early crustal components in the western Australian Archaean: zircon U-Pb ages by ion microprobe analysis from the Shaw Batholith and Narryer metamorphic belt., Geol. Soc. Austr. Abstr., 9: 169.

Williams, P. R., and Whitaker, A. J., 1993. Gneiss domes and extensional deformation in the highly mineralised Archean Eastern Goldfields Province, Western Australia., Ore Geol. Rev., 8: 141-162.

Wilson, M., 1989. Igneous Petrogenesis: a Global Approach. Chapman and Hall, London, 466 pp.

Windley, 1984. The Evolving Continents (2nd edition)., Wiley and Sons, New York, 399 p.

Windley, B.F., 1973. Crustal development in the Precambrian., Phil. Trans. R. Soc. Lond., A273: 321-341.

Windley, B. F., 1977. The Evolving Continents., Wiley and Sons, New York, 526 p.

Wingate, M. T. D., 1999. Ion microprobe baddeleyite and zircon ages for Late Archaean mafic dykes of the Pilbara Craton, Western Australia., Austr. J. Earth Sc., 46: 493-500.

Wyllie, P.J., Wolf, M. B. and Van Der Laan, S.G., 1997. In: De Wit, M and Ashwal, L. D. (Editors) Greenstone Belts, Oxford Monogr. Geol. Geoph. 35: 256-266.

Zegers, T. E., 1996. Structural, kinematic and metallogenic evolution of selected domains of the Pilbara granitoid-greenstone terrain., Geologica Ultraiectina, 146: 208.

Zegers, T. E., Keijzer, M.. D., Passchier, C. W., and White, S. H., 1998a. The Mulgandinnah Shear Zone Complex; an Archean crustal scale strike-slip zone, eastern Pilbara, Western Australia. Precambrian Res., 88: 233-248.

Zegers, T. E., Wijbrans, J.R., Nelson, D. R. and White, S H., 1998b. $^{40}Ar/^{39}Ar$ and U-Pb dating in the eastern Pilbara, Australia; temporal constraints on structural and metamorphic events between 3.5 and 2.8 Ga. Schurmann symposium on the early Archaean; extended abstracts. Geology en Mijnbouw, 76-4: 353-355.

Zegers, T. E., De Wit, M. J., Dann, J. and White, S., 1998c.Vaalbara, Earth's oldest assembled continent? A combined structural, geochemical, and palaeomagnetic test. Terra Nova, 10-5: 250.

Zegers, T. E., and Van Keken, P. E., 2000. Mid Archean continent formation by crustal delamination, AGU Fall Meeting.

Zegers, T. E., White, S. W., Keijzer, M. D., and Dirks, P., 1996. Extensional structures during deposition of the 3460 Ma Warrawoona Group in the eastern Pilbara Craton, Western Australia., Precambrian Res., 80: 89-105.

Zegers, T. E., Wijbrans, J. R., and White, S. H., 1999. $^{40}Ar/^{39}Ar$ age constraints on tectonothermal events in the Shaw area of the eastern Pilbara granite-greenstone terrain (W. Australia): 700 Ma of Archean tectonic evolution., Tectonophysics, 311: 45-81.

Acknowledgements/dankbetuiging

Dit proefschrift is to stand gekomen met de hulp van velen.

First of all I would like to thank my advisor, Stan White. He had given me the opportunity to undertake this project. His experience in Australian Archaean geology was a benefit to the project. In addition, he introduced me to Australia and australian bush-practice. I thoroughly enjoyed our days out it the field, the cold cans of beer at the end of the day, and your many stories around the camp fire. Mijn co-promotor Jan Wijbrans ben ik, naast zijn continue support, vooral dankbaar voor de begeleiding bij het geochronologische deel van het onderzoek. Zowel bij het analytische deel als bij het gesteente bemonsteren in de Pilbara is zijn jarenlange ervaring van onmeetbare waarde. Onmisbaar voor de goede afloop van dit onderzoek is Tanja Zegers, een goeie vriendin en mijn voorganger promovenda in het Utrecht Pilbara Project. Niet alleen voor de vele discussies – geologische en niet-geologische - en inspiratie, maar ook voor haar ondersteuning en geduld bij het leesbaar maken van het belangerijkste hoofdstuk van dit proefschrift.

The Utrecht Pilbara Project, of which this study is part, was initiated by Stan White and Wout Nijman in 1992. It has since involved many people without whom this project and hence this study would not have been the same. Apart from Stan, Wout, and Jan, participation of scientists from in (and outside) the department has moved the work presented here forward in different ways; Mark Barley, Paul Dirks, Dave Nelson, Cees Passchier, Maarten de Wit, Hugo de Boorder. I would also like to thank the many people that were part of the Pilbara Project as students; Bart Willigers, Martin de Keijzer, Marielle Valkering, Karin de Bruine, Corine Davids, Willem Maarten van Haaften, Fernando Guerreiro, Geert, Bas 'sledgehammer' Bossers, Yvonne Smit, Yvette Kuiper, Willem Fliervoet, Kike Beintema en Marije van Koolwijk. Their participation in the project, particularly during the field expeditions in the Pilbara, made it all very enjoyable.

The SHRIMP zircon geochronology study would not have been possible without Dave Nelson. His knowledge and support are an inspiration. Thanks Dave! Also for your valuable comments on earlier drafts of chapter 3. The - always heavy - zircon samples were collected with the help of many participants of the Utrecht Pilbara Project, including Dave Nelson, Stan White, Cees Passchier, Willem Maarten, Yvonne, Yvette, Willem and Bas. Zircon preparation was done at the mineral separation laboratory at the Free University of Amsterdam, directed by Lodewijk van IJlst, and with assistance of Roel van Elzas and Wijnanda Root. Cathodoluminescence images of the zircons were made at the Electron Microscope facilities at Utrecht University with the help of Herman van Roermund. Evert Jan Kloppenburg compiled cathodoluminescence maps of the zircon mounts, invaluable for navigation during SHRIMP analysis sessions. The Perth SHRIMP Consortium, comprising Curtin University of Technology, University of Western Australia and the Geological Survey of Western Australia, facilitated the analyses. Jon Gregory has been very

helpful with instructions and assistance during SHRIMP sessions. Simon Wilde kept me up to date with the latest zircon geochronology publications, introduced me to the Yilgarn greenstone belts, and often made me laugh out loud when reading his fantastic stories and latest gossip. The SHRIMP analyses was funded by The Netherlands Organisation for Scientific Research (NWO).

Jan Wijbrans and Laurence Page provided helpful instructions and discussions during argon analyses using the laser VULKAAN microprobe facilities at the Vrije University in Amsterdam. Argon sample preparation was done at the mineral separation laboratory at the Free University of Amsterdam, directed by Lodewijk van IJlst, with assistance of Roel van Elzas and Wijnanda Root. The step-wise argon analyses would not have been as effective without the preparational 'Argon Dance' training by Andor Lips and Bart Willigers during the Argon Workshop in Lausanne..

At the very first stages of this study, Arjan Dijkstra en Ernst Schetselaar have kindly helped me with producing Pilbara satelite images. Also Andy Glikson has been very helpful in getting the 'recipies' for the remote sensing images right.

An important part of the work presented here is based on field studies in the Pilbara granite greenstone terrain, a remote and desolate place in Western Australia. Many Pilbarians contributed to make these trips possible and memorable experiences and make our base camp in Marble Bar 'home away from home'. Denis O'Meara kindly offered us a place at the Old Hospital during the first years of the project. Then, our base camp moved to the Marble Bar Caravan Park, run by Fred and Anne. Central in any trip was the Toyota truck, your life-line out in the field. Alec of the Marble Bar Garage took good care of them, and reparing many many tires.. Lenny Lever kindly offered us his historical knowledge of old mine sites and pit outcrops. Gary and Monica Mullen are thanked for taking me to see the old Klondyke gold workings in the Warrawoona greenstone belt, and also for endless supply of Minties that at some stage even made it to Utrecht! Dave and Carmen Taylor are thanked for their friendship, delicious curries and cold VBs. And last but not least, Jeremy 'little ozzie' Peters, Marble Bar would not have been the same without you!

During my travels in the Pilbara I have met many geologists, who contributed to the thesis in different ways, including Arthur Hickman, Martin van Kranendonk, Ian Williams. John Martin kindly discussed with me his findings in the Kelly Belt and provided me with copies of his maps. John Sims of Geoverde Pty Ltd joined me in the field and kindly discussed with me the aspects of the high metamorphic grade parts of the granitoid gneisses of the Mt Edgar Granitoid Complex. Ian Williams kindly provided updates on track routes and conditions to the far north of the Pilbara. Chris Spooner of the Stockdales team bush-bashed his way to collect Argon sample P97-366. Judy McKenzie, Jock Keene and Cris Vasconcelos joined us for an expedition to Dolomite Creek, and explained all about dolomite as an indication of early live on Earth.

CRA-Exploration kindly funded field transport in the Pilbara in the form of the best ever equiped Toyota truck. They also shared their knowledge of the Klondyke gold prospect, located

in the middle of my studie area, and provided access to aerial photographs and in-house reports of this area. Special thanks goes to Barry Davis, Naomi Wall, Tracey, and Robby Kruger, also for many good times, and sharing many cold ones.Nomes, thanks for your hospitality during my stay in Karratha. Marg, thanks for your daily safety radio sceds.

At the institute back in Utrecht, a group of geologists, friends, were always there to welcome me back and provide appreciated distractions - of various kinds - from work.. Fraukje, Tanja, Rachel, Andor, Arjan, Coen, Marga, Rene, Kike en Bernard, Marije, Sieze, Bart, Rob, Julie and Will, Herman, Martyn and Gill, Hans and Kim. Thanks guys for making it a memorable time. Gedurende alle jaren, maar vooral tijdens het afronden van deze promotie op afstand vanuit Glasgow, zijn Magda 'Steunpilaar' Martens en Marnella van der Tol onmisbaar geweest voor de logistieke support. En over onmisbaar gesproken.. Fraukje, bedankt voor het delen van onze kamer gedurende serieuze en minder serieze tijden..haha!.. Bedankt voor het proeflezen van hoofdstukken van dit proefschrift, het screenen van publicaties tijdens mijn verblijf in Glasgow, en voor al je steun, vooral tegen het einde van het project.

De layout van dit proefschrift en de basis voor vele tekeningen is gedaan door Fred Trappenburg, Jaco Van Bergenhenegouwen en Paul van Oudenallen van de Audio-Visuele dienst Aardwetenschappen. Bedankt voor jullie altijd vriendelijke en proffesionele hulp!

At present I am working with Midland Valley in Glasgow and I would like to thank my colleagues for providing an inspiring scientific environment and a refreshing perspective on structural geology. Thank you, Ros and Alan, for giving me the opportunity and support to actually finish this project. And thank you all for lots of fun!

Many old and new friends have supported and inspired me throughout the years in many ways, Monique, Tanja, Danie, Ria en Harry, Hans en Els, Rob Coli, Elizabeth, Marc, Evelyn, Marco and Ali, Marielle, Erwin and Karen, Karel en Wilma, Elly en Luuk, Liz, Jan Kees, Delphine, Massimo, Susan, Lina, Juan Carlos, Germán, and many more. Thanks for your friendschip, your support and for putting finishing this project in a wider perspective.

Maar zonder de liefdevolle opvoeding van mijn ouders, Herma and Evert Jan Kloppenburg, zou dit onderzoek nooit mogelijk zijn geweest. Zij hebben me altijd gesteund in alles, en doen dat nog steeds, wat ik ook bedenk.. En ook Ondine, mijn 'rare' zusje – zakenvrouw die ook bergen beklimt – en Valette, mijn kleine zusje - die helicopter vliegt en zelfs mee is geweest als fieldy in Australie – en ook Ruud en Meneer Ei, hebben me en geven me nog steeds veel plezier en inspiratie. Mary and Martin Hols, en Anita, Maarten, Nils, Timo en Marjean zorgen altijd voor veel vriendschap en gezelligheid. Maar centraal in het succesvol afronden van dit onderzoek, en centraal in mijn leven, staat Rob. Zijn liefde, vertrouwen en steun zijn onontbeerlijk geweest voor het afronden van dit project. Hij is meerdere malen meegeweest naar Australie, en naar Canada, Frankrijk, Spanje.. 'waar gaan we nu weer heen?' Scotland?.. hmm.. ook wel leuk!

The fieldwork for this project was partly supported by the Dr. Schürmann Foundation for Precambrian Research (grant nrs 1995/14, 1996/14, 1997/14, and 1998/14).

Curriculum Vitae

Armelle Kloppenburg werd geboren op 23 april 1970 in Den Haag. Na het succesvol doorlopen van het VWO aan de Dalton Scholengemeenschap te Den Haag – en na twee jaar in het bankwezen te hebben gewerkt – studeerde zij Geologie aan de Universiteit Utrecht. In 1995 behaalde zij het doktoraal diploma Geologie bij Prof. Stan H. White in de vakgoep Structurele Geologie en Tektoniek, waar zij in september 1995 aan haar promotie onderzoek is begonnen.

Sinds mei 2001 werkt zij als structureel geoloog bij Midland Valley Exploration in Glasgow, Schotland.

foto; E.J. Kloppenburg